NBSIR 83-2742 (R)

Photonuclear Data - Abstract Sheets 1955 - 1982 Volume XI (Silver - Barium)

U.S. DEPARTMENT OF COMMERCE
National Bureau of Standards
National Measurement Laboratory
Center for Radiation Research
Gaithersburg, MD 20899

August 1985

U.S. DEPARTMENT OF COMMERCE
NATIONAL BUREAU OF STANDARDS

NBSIR 83-2742

PHOTONUCLEAR DATA - ABSTRACT SHEETS
1955 - 1982
VOLUME XI (SILVER - BARIUM)

E. G. Fuller, Henry Gerstenberg

U.S. DEPARTMENT OF COMMERCE
National Bureau of Standards
National Measurement Laboratory
Center for Radiation Research
Gaithersburg, MD 20899

August 1985

U.S. DEPARTMENT OF COMMERCE, Malcolm Baldrige, *Secretary*
NATIONAL BUREAU OF STANDARDS, Ernest Ambler, *Director*

TABLE OF CONTENTS

Photonuclear Data-Abstract Sheets
1955-1982

I. Introduction

As used in connection with this collection of data-abstract sheets, the term photonuclear data is taken to mean any data leading to information on the electromagnetic matrix element between the ground state and excited states of a given nuclide. The most common types of reactions included in this compilation are: (e,e'), (γ,γ), (γ,γ'), (γ,n), (γ,p), etc. as well as ground-state particle capture reactions, e.g. (α,γ_0). Two reactions which fit the matrix element criterion are not included in the compilation because of their rather special nature. These are heavy particle Coulomb excitation and the thermal neutron capture reaction (n,γ_0). While the energy region of particular interest extends from 0 to 150 MeV, papers are indexed which report measurements in the region from 150 MeV to 4 GeV. Most of the experiments listed are concerned with the excitation energy range from 8 to 30 MeV, the region of the photonuclear giant resonance.

The hierarchical grouping of the photonuclear data-abstract sheets within the file is by: 1. Target Element, 2. Target Isotope, and 3. by the Bibliographic Reference Code assigned to the paper from which the data on the sheet were abstracted. In this file, colored pages are used to mark the beginning and end of the sheets for each chemical element. A brief historical sketch of the element is given on the divider sheet marking the start of each section; the information for this sketch was derived from references such as the Encyclopaedia Britannica. In those cases where the sheets for a given element make up a major part of a volume, colored pages are also used to delineate sections pertaining to the individual isotopes of the element. Each of the sections of the file, as delineated by two colored divider sheets, represents a 27 year history of the study of electromagnetic interactions in either a specific nuclide or a specifc element.

The data-abstract sheets are filed under the element and/or isotope in which the ground-state electromagnetic transition takes place. For example, the abstract sheet for a total neutron yield measurement for a naturally occurring copper sample would appear in the elemental section of the copper file. On the other hand, a measurement of the ^{62}Cu 9.73 minute positron activity produced in the same sample by photons with energies below the three-neutron separation energy for ^{65}Cu (28.68 MeV) would be filed with the sheets for ^{63}Cu. Similarly a measurement of the ground-state neutron capture cross section in ^{12}C would be filed under ^{13}C while the corresponding ground-state alpha-particle capture cross section would be filed under ^{16}O.

At the end of this volume there is a master list of the abbreviations that have been used in the index section of the abstract sheets. The listings are those used in the final published index, Photonuclear Data Index, 1973-1981, NBSIR 82-2543, issued in August 1982 by the U. S. Department of Commerce, National Bureau of Standards, Washington, DC 20234. In some cases two notations are entered for the same quantity. The second entry is the abbreviation that was used in one or more of the earlier published editions of the index.

GERMANUIM
Z=32

Germanuim—the element noted for its remarkable electrical properties has a metalic silver-gray color with properties somewhere between a metal and a nonmetal. D. I. Mendeleyev (1834-1907) predicted the existence and properties of a hypothetical element beween silicon and tin which he called eka-silicon. Clemens Winkler (1838-1904), in 1886, analyzed the sulphide mineral argyrodite and found a previously unknown constituent to which he gave the name germanium after his native country. The argyrodite was a recently discovered mineral from an old silver mine near Freiberg. Winkler had determined that the argyrodite consisted of 75% silver and 18% sulfur; this left an unknown substance of about 7%. After toiling incessantly for four months, Winkler managed to precipitate the sulfide of the new element.

GE

CE

REF. NO.

Synchrotron; $C^{12}(\gamma,n)$ monitor 64 Co 2 JOC

REACTION	RESULT	EXCITATION ENERGY	SOURCE		DETECTOR		ANGLE
			TYPE	RANGE	TYPE	RANGE	
G,XN	ABY	THR - 80	C	80	BF3-I		4 PI

Table 1

Element	Yield ($\int_0^{80}$) eV cm^2 mol MeV	60 NZ/A (mb MeV)	Σ_0^{30}	Σ_0^{80}	$\Sigma_0^{30} / \Sigma_0^{80}$	E_m (MeV)	σ_m (mb)
$_{24}Cr$	83 x10^{-5}	777	1.21	2.1	0.53	18.5	97
$_{25}Mn$	108 x10^{-5}	813	1.52	2.02	0.55	18.5	114
$_{26}Fe$	68 x10^{-5}	832	0.88	1.40	0.60	17.5	75
$_{27}Co$	89 x10^{-5}	878	1.03	1.52	0.59	17.5	92
$_{28}Ni$	44 x10^{-5}	879	0.55	1.07	0.51	16.5	56
$_{29}Cu$	95 x 10^{-5}	947	1.06	1.99	0.53	17.5	98
$_{30}Zn$	58 x 10^{-5}	975	0.94	1.65	0.56	17.3	86
$_{31}Ga$	130 x 10^{-5}	1034	1.29	2.18	0.59	17.5	151
$_{32}Ge$	139 x 10^{-5}	1084	1.25	2.29	0.59	17.5	158
$_{33}As$	127 x 10^{-5}	1109	1.22	2.18	0.56	17.5	127

$$\Sigma_0^{30} = \frac{\int_0^{30} \sigma(\gamma,xn)dE}{60\ NZ/A}$$

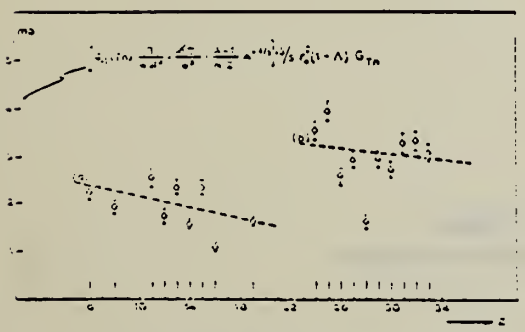

Fig. 2. Bremsstrahlung-weighted cross sections, $\sigma_{-1}(Tm)$, conventionally normalized, versus Z.

Table 2

Element	maximum yield (x 10^{-5})	$\sigma_{-1}(Tm)$	$\sigma_{-1}(Tm) \times \left[\frac{3}{4\pi^2}\frac{\hbar c}{e^2}\left(\frac{A-1}{NZ}\right)A^{-\frac{1}{3}}\right]$
$_6C$	4.0	3.54	2.18
$_8O$	5.2	4.05	1.92
$_{11}Na$	13.6	11.60	2.45
$_{12}Mg$	10.0	8.81	1.73
$_{13}Al$	15.0	13.02	2.50
$_{14}Si$	11.0	9.56	1.53
$_{15}P$	19.8	17.36	2.82
$_{16}S$	9.5	8.35	1.37
$_{19}K$	19.6	17.00	1.91
$_{20}Ca$	12.1	11.08	1.92
$_{24}Cr$	86	81.6	8.60
$_{25}Mn$	115	70.1	8.00
$_{26}Fe$	71	60.5	2.55
$_{27}Co$	84	00.3	2.04
$_{28}Ni$	46	00.2	1.50
$_{29}Cu$	102	72.6	3.00
$_{30}Zn$	93	05.7	2.06
$_{31}Ga$	140	00.6	3.01
$_{32}Ge$	150	101.5	3.06
$_{33}As$	131	00.8	3.12

REF. G. Kraft, R. Kosiek, R. Mundhenke and J. Winter
Nucl. Phys. A118, 25 (1968)

ELEM. SYM.	A	Z
Ge		32

METHOD

REF. NO. 68 Kr 2 egf

REACTION	RESULT	EXCITATION ENERGY	SOURCE		DETECTOR		ANGLE
			TYPE	RANGE	TYPE	RANGE	
G,A	ABX	THR-33	C	33	SCD-D	4-11	90
				(32.5)			

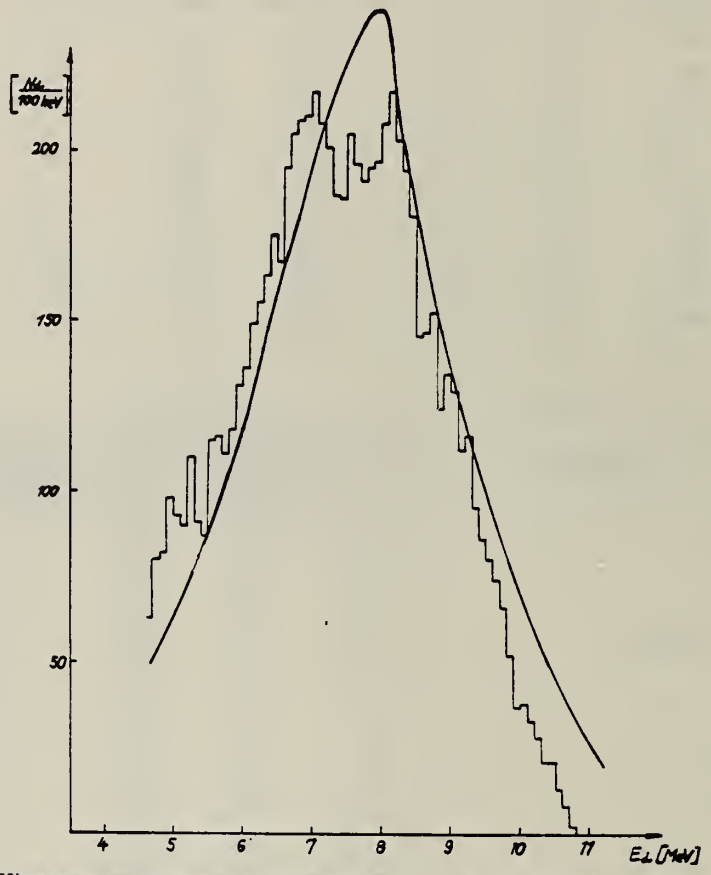

Fig. 3. Histogram: energy distribution of α-particles from Ge. Curve: statistical-model calculation.

GE
A=70

REF. O.A. Borello, J. Goldemberg, M.D.S. Santos
An. Acad. Brasil. Cienc. 27, 413 (1955)

ELEM. SYM.	A	Z
Ge	70	32

METHOD: Betatron

REF. NO.: 55 Bo 1 NVB

REACTION	RESULT	EXCITATION ENERGY	SOURCE TYPE	SOURCE RANGE	DETECTOR TYPE	DETECTOR RANGE	ANGLE
G,N	ABX	12-21	C	12-21	ACT-I		4PI

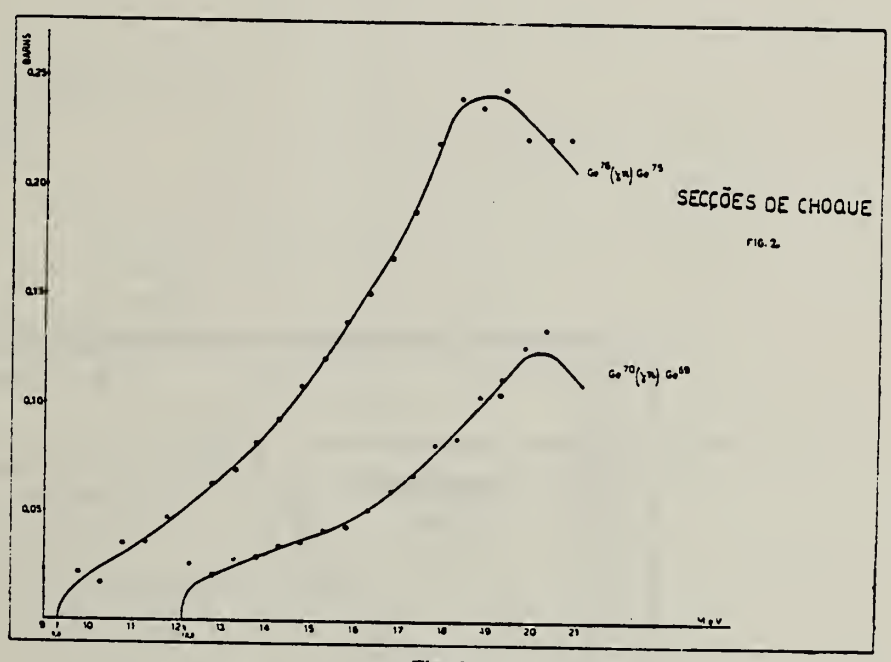

Fig. 2

Elemento	Threshold Limiar	E_{max}	σ max	σ int até 21 Mev
Ge^{70}	12,1 ± 0,20 Mev	20 Mev	0,125 barn	0,59 Mev × barn
Ge^{76}	9,3 ± 0,10 Mev	18,9 Mev	0,243 barn	1,5 Mev × barn

M.D. DeSouza Santos, J. Goldemberg, R.R. Pieroni, E. Silva,
O.A. Borello, S.S. Villaca, J.L. Lopes
Int. Conf. Peaceful Uses of Atomic Energy II (UN, NY), 169 (1955)

ELEM. SYM.	A	Z
Ge	70	32

METHOD: Betatron; neutron yield; radioactivity; r-chamber

REF. NO.: 55 De 1 | EGF

REACTION	RESULT	EXCITATION ENERGY	SOURCE		DETECTOR		ANGLE
			TYPE	RANGE	TYPE	RANGE	
G,N	ABX	9-21	C	9-21	ACT-I		4PI

(γ,n) threshold = 12.1±0.2 MeV

THRESHOLD

$\int \sigma dE$ = 0.59 MeV-b

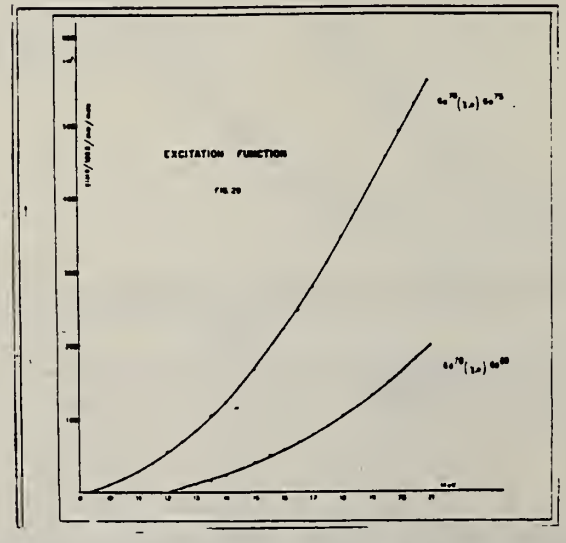

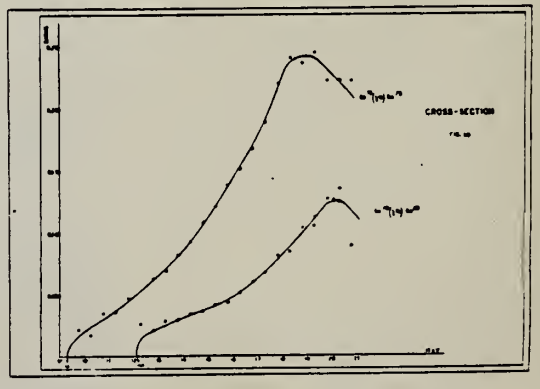

Ref. F. Ferrero, S. Ferroni, R. Malvano, S. Menardi, E. Silva
Nuclear Phys. 15, 436 (1960)

Elem. Sym.	A	Z
Ge	70	32

Method 31 MeV betatron; activation; NaI

Ref. No. 60 Fe 1 JHH

Reaction	E or ΔE	E_o	Γ	$\int \sigma dE$	Jπ	Notes
	Bremss.					
(γ,n)	31					Annihilation radiation of β^+ from Ge^{69}
(γ,np)						Annihilation radiation of β^+ from Ga^{68}

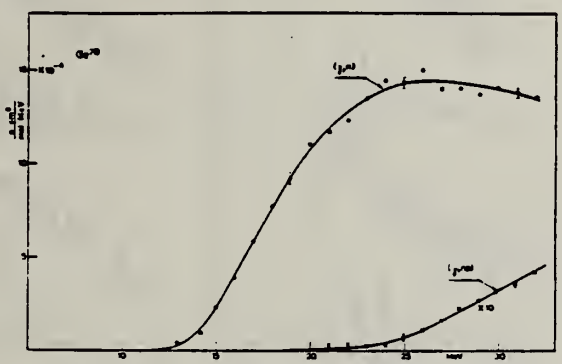

Fig. 8. (γ, n), (γ, np) excitation functions for Ge^{70}.

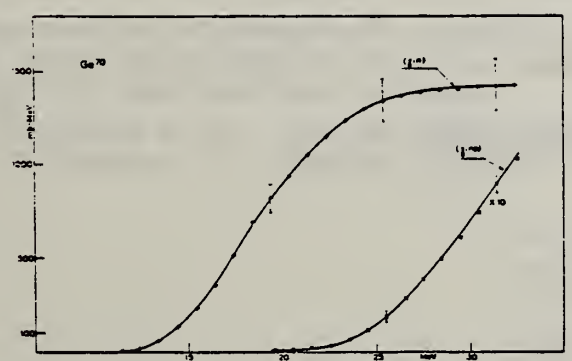

Fig. 9. Integrated cross section deduced from the excitation functions of fig. 8.

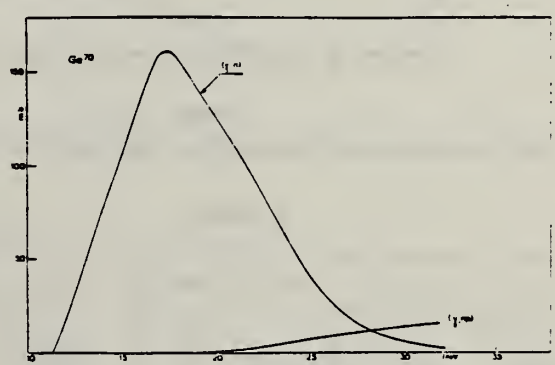

Fig. 10. Cross section for the two photonuclear processes of fig. 8.

REF. J.J. McCarthy, R.C. Morrison and H.J. Vander Molen
Nucl. Phys. A213, 371 (1973)

ELEM. SYM.	A	Z
Ge	70	32

METHOD

REF. NO. 73 Mc 10 egf

REACTION	RESULT	EXCITATION ENERGY	SOURCE		DETECTOR		ANGLE
			TYPE	RANGE	TYPE	RANGE	
G,NP	ABX	17- 40	C	12- 42	ACT-I		4PI

$\int_{(\gamma,np)}^{40} \sigma dE = 39.3 \pm 5$ MeV • mb

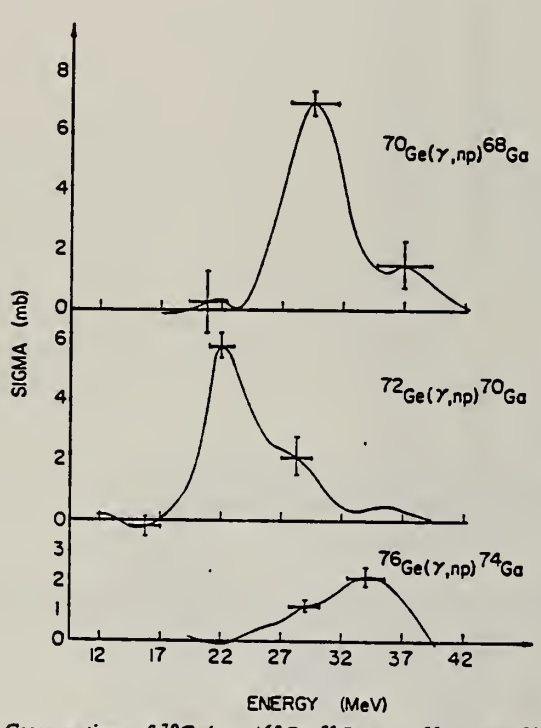

Fig. 5. Cross sections of $^{70}Ge(\gamma, np)^{68}Ga$, $^{72}Ge(\gamma, np)^{70}Ga$, and $^{76}Ge(\gamma, np)^{74}Ga$.

REF.		EL.EM. SYM.	A	Z
	A.M. Goryachev, G.N. Zalesnyi, and B.A. Tulupov Izv. Akad. Nauk SSSR. Ser. Fiz. 39, 134 (1975) Bull. Acad. Sci. USSR Phys. Ser. 39, 116 (1975)	Ge	70	32
METHOD		REF. NO.		
		75 Go 1		hmg

REACTION	RESULT	EXCITATION ENERGY	SOURCE		DETECTOR		ANGLE
			TYPE	RANGE	TYPE	RANGE	
G,XN	ABX	11- 25	C	9- 25	BF3-I		4PI

σ(G,SN). Statistical theory used to obtain SN cross section from XN cross section.

Table 2

Nuclide	β_n	E_2, MeV	E_1, MeV	Nuclide	β_n	E_2, MeV	E_1, MeV
^{61}Zn	0.25	0.99	18	^{74}Ge	0.25	0.562	18
^{65}Zn	0.23	1.04	18	^{75}Se	0.33	0.559	18
^{69}Zn	0.2	1.08	18	^{79}Se	0.3	0.618	18
^{73}Ge	0.23	1.04	18	^{80}Se	0.25	0.654	18
^{72}Ge	0.27	0.835	18	^{82}Se	0.2	0.655	18
^{71}Ge	0.3	0.6	18				

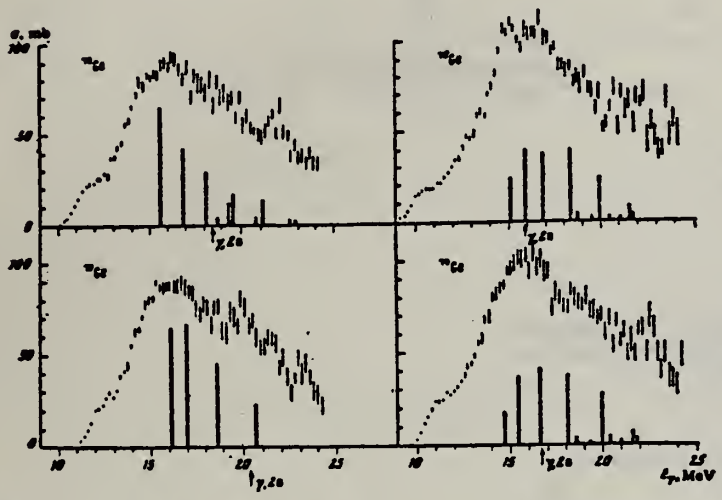

Fig. 2. The same as in Fig. 1, but for ^{70,72,74,76}Ge.

Cross sections of photoneutron reactions. The dipole photoabsorption forces are taken from [6,7] (the solid black columns).

[6] M.G.Huber et al., Phys.Rev.155,1073(67)
[7] M.G.Huber et al., Phys.Rev.192,223(66.

Table 3

Nuclide	σ, mb	Nuclide	σ, mb	Nuclide	σ, mb
^{61}Zn	397±15	^{74}Ge	760±37	^{78}Se	1021±52
^{65}Zn	579±27	^{75}Ge	872±41	^{80}Se	1029±50
^{69}Zn	718±35	^{76}Ge	911±43	^{82}Se	1067±53
^{73}Ge	731±37	^{79}Se	930±50		

*Mean - square errors

Values given are for σ_0(24.2 MeV).

REF. F. J. Kline, I. P. Auer, J. C. Bergstrom, and H. S. Caplan
Nucl. Phys. A255, 435 (1975)

ELEM. SYM.	A	Z
Ge	70	32

METHOD

REF. NO. 75 K1 9 egf

REACTION	RESULT	EXCITATION ENERGY	SOURCE		DETECTOR		ANGLE
			TYPE	RANGE	TYPE	RANGE	
E,E/	LFT	1, 2	D	84-120	MAG-D		DST

1.04, 2.562 MEV

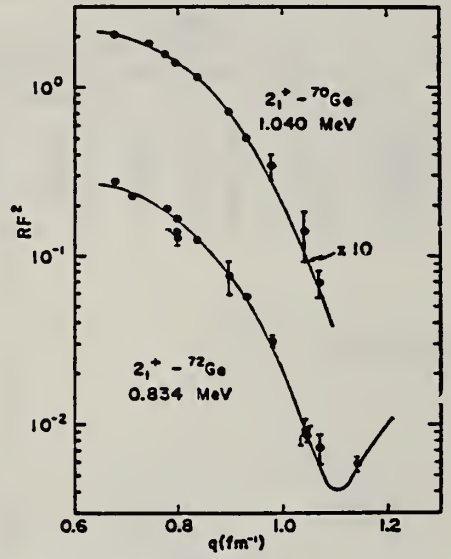

Fig. 4. Plot of the converted form factors squared versus q for the 2_1^+ states in $^{70,72}Ge$. The solid lines are the results of fitting to the data with a DWBA program. Note that both the data and the curve for ^{70}Ge have been multiplied by a factor of ten.

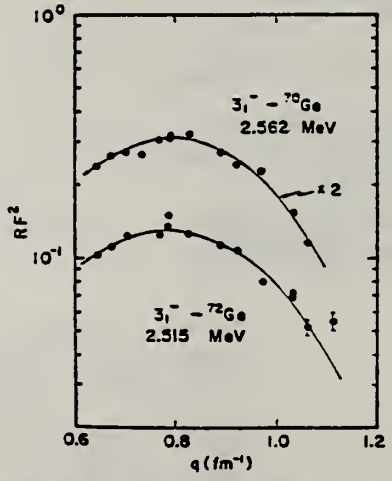

Fig. 5. Plot of the converted form factors squared versus q for the 3_1^- states in $^{70,72}Ge$. The solid lines are the results of fitting to the data with a DWBA program. Note that both the data and the curve for ^{70}Ge have been multiplied by a factor of two.

(over)

TABLE 3

Parameters obtained from fits to the inelastic data

State	Nucleus	c_{tr} (fm)	t_{tr} (fm)	$B(EL, \omega\uparrow)$ (W.u.) [a,b]	χ^2_{pot}
2_1^+	^{70}Ge	4.22±0.14	2.41±0.26	19.7±1.2	0.56
	^{72}Ge	4.32±0.02	2.49±0.05	26.8±2.0	5.2
3_1^-	^{70}Ge	4.34±0.09	2.23±0.11	36±5	12.4
	^{72}Ge	3.84±0.12	2.80±0.11	37±7	12.3

[a]) W.u. are Weisskopf single-particle units.
[b]) Uncertainties have been multiplied by $\sqrt{\chi^2_{pot}}$.

TABLE 4

Reduced transition probabilities

State	$B(EL, \omega\uparrow)$ (W.u.) [a]		Work
	^{70}Ge	^{72}Ge	
2_1^+	19.7±1.2	26.8±2.0	present
	20.5±1.1	22.3±1.4	compilation [b,c])
3_1^-	36±5	37±7	present
	21	22	Kregar and Elbek [d])
	32	27	Curtis *et al.* [e])
	27	23	Perey *et al.* [f])
	21	17	Perey *et al.* [f])

[a]) W.u. are Weisskopf single-particle units.
[b]) Ref. [12]). [c]) Ref. [13]). [d]) Ref. [10]). [e]) Ref. [9]). [f]) Ref. [14]).

[9] T.H. Curtis et al., Phys. Rev. C1, 1418 (1970).

[10] M. Kregar et al., Nucl. Phys. A93, 49 (1967).

[12] K.R. Alvar et al., Nucl. Data Sheets 8, 1 (1972).

[13] K.R. Alvar, Nucl. Data Sheets 11, 121 (1972).

[14] C.M. Perey et al., Phys. Rev. C2, 468 (1970).

REF.

J.J. McCarthy, R.C. Morrison, and H.J. Vander Molen
Phys. Rev. C11, 772 (1975)

ELEM. SYM.	A	Z
Ge	70	32

METHOD

REF. NO. 75 Mc 1 hmg

REACTION	RESULT	EXCITATION ENERGY	SOURCE		DETECTOR		ANGLE
			TYPE	RANGE	TYPE	RANGE	
G,N	ABX	11- 40	C	10- 40	MOD-I		4PI
G,2N	ABX	20- 40	C	10- 40	MOD-I		4PI
G,NP	ABI	18- 40	C	10- 40	ACT-I		4PI

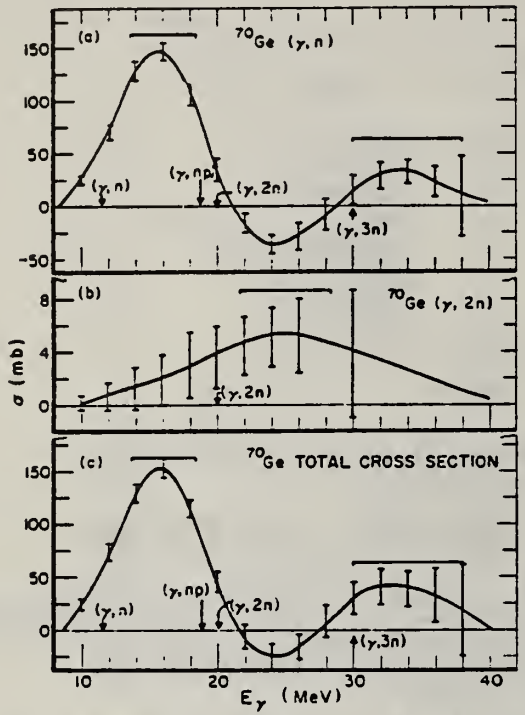

FIG. 4. (a) The (γ, n) cross section for ^{70}Ge. (b) The $(\gamma, 2n)$ cross section for ^{70}Ge. (c) The total cross section $\sigma[(\gamma, n) + (\gamma, 2n) + (\gamma, np) + (\gamma, p)]$ for ^{70}Ge. The thresholds (arrows) are taken from Ref. 26.

TABLE II. Integrated cross sections.

Isotope	(γ, n)	$(\gamma, 2n)$	(γ, p) (MeV mb)	(γ, np)	Total
^{70}Ge	1273(127) [a] 1464(290) [b]	60(6)		40(6)	1463(129)
^{72}Ge	1140(110)	420(40)		40(14)	1690(118)
^{74}Ge	1320(130)	360(40)	90(10)	35(3) [c]	1805(136)
^{76}Ge	1077(54) [a] 1067(106) [b]	710(70)		15(3)	1892(89)

[a] Result of the activation measurements.
[b] Result of the neutron counting measurements.
[c] Includes the contribution from the ^{73}Ge(γ, p) reaction.

TABLE III. Lorentz fit parameters and integrated cross sections for total cross sections.

Isotope	σ_0 (mb)	Γ (MeV)	E_0 (MeV)	σ_{LF} $(\frac{1}{2}\pi)\sigma_0\Gamma$ (MeV mb)	σ_{Int} (MeV mb)	$\sigma_{Int} - \sigma_{LF}$ (MeV mb)	$D = 60\frac{NZ}{A}$ (MeV mb)	$\frac{\sigma_{Int}}{D}$	$\frac{\sigma_{Int} - \sigma_{LF}}{\sigma_{Int}}$
^{70}Ge	150	5.85	15.5	1380	1463	83	1040	1.41	0.06
^{72}Ge	150	5.90	17.9	1390	1690	300	1070	1.58	0.18
^{74}Ge	144	6.96	16.5	1580	1805	225	1090	1.66	0.12
^{76}Ge	120	8.20	16.7	1550	1892	342	1110	1.70	0.18

REF.		ELEM. SYM.	A	Z
	P. Carlos, H. Beil, R. Bergere, J. Fagot, A. Lepretre, A. Veyssiere, G. V. Solodukhov Nucl. Phys. A258, 365 (1976)	Ge	70	32

METHOD	REF. NO.	
	76 Ca 1	egf

REACTION	RESULT	EXCITATION ENERGY	SOURCE		DETECTOR		ANGLE
			TYPE	RANGE	TYPE	RANGE	
G,N	ABX	11- 26	D	11- 26	MOD-I		4PI
G,2N	ABX	19- 26	D	11- 26	MOD-I		4PI

975+

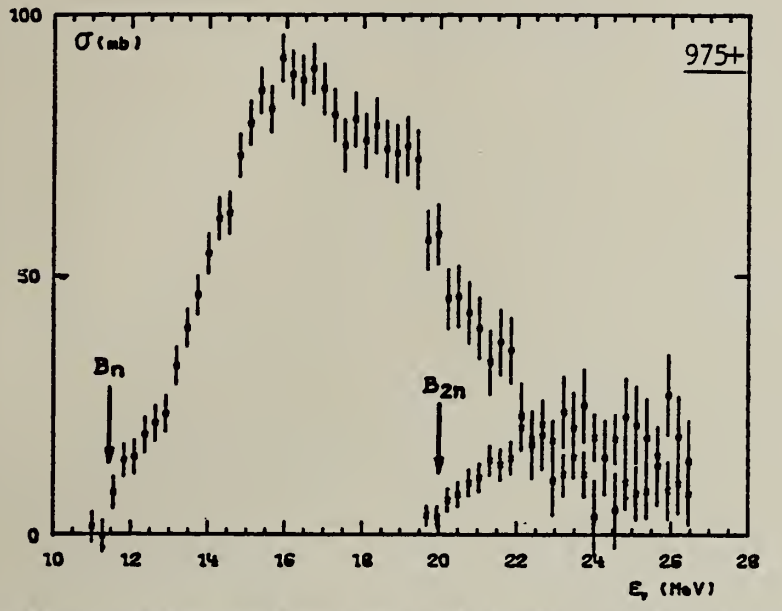

Fig. 3. Partial photoneutron cross sections $[\sigma(\gamma, n)+\sigma(\gamma, pn)]$ and $\sigma(\gamma, 2n)$ for ^{70}Ge. Arrows B_n and B_{2n} indicate theoretical threshold values for (γ, n) and $(\gamma, 2n)$ reactions respectively. Data were not corrected for impurities.

TABLE 3

Integrated photoneutron cross sections and comparison with sum rules

Nucleus	^{64}Zn	^{69}Ga / ^{71}Ga	^{70}Ge	^{72}Ge	^{74}Ge	^{76}Ge	^{75}As	^{76}Se	^{78}Se	^{80}Se	^{82}Se
E_M (MeV)	29	26.5	26.5	26.5	26.5	26.5	26.5	26.5	26.5	26.5	26.5
σ_{0a} (MeV · b)	0.75	0.91	0.78	0.94	1.02	1.12	1.09	1.01	1.06	1.11	1.13
$\frac{\sigma_{0a}A}{0.06\,NZ}$	0.78	0.87	0.75	0.88	0.94	1	0.98	0.90	0.92	0.94	0.95
$B_n - B_p$ (MeV)	4.2	3.7 / 1.4	3	1	− 0.8	−2.6	3.3	1.7	0.1	−1.5	−3
σ_{-1a} (mb)	38	52	44	54	59	64	63	58	62	65	67
$\sigma_{-1a}A^{-\frac{1}{2}}$ (mb)	0.15	0.18	0.15	0.18	0.19	0.20	0.20	0.18	0.19	0.19	0.19
σ_{-2a} (mb · MeV^{-1})	2.0	3.1	2.5	3.2	3.6	3.9	3.7	3.4	3.8	3.9	4.2
$\sigma_{-2a}A^{-\frac{1}{2}}$ (μb · MeV^{-1})	1.9	2.6	2.1	2.6	2.8	2.9	2.8	2.5	2.7	2.6	2.7

The notation used is defined in the text. The average experimental errors $\Delta\sigma_{0a}/\sigma_{0a}$, $\Delta\sigma_{-1a}/\sigma_{-1a}$ and $\Delta\sigma_{-2a}/\sigma_{-2a}$ are approximately 8 %.

GE
A=72

GE
A=72

Ref. F.R. Metzger
Phys. Rev. 101, 286 (1956)

Elem. Sym.	A	Z
Ge	72	32

Method Radioactive source; photon scattering; NaI spectrometer

Ref. No. 56 Me 1 NVB

Reaction	E or ΔE	E_o	Γ	$\int \sigma dE$	Jπ	Notes
$Ge^{72}(\gamma,\gamma)$	835 keV	835 keV			2 (excited)	Mean life: $\tau = (4.6 \pm 1.2)\ 10^{-12}$ sec.
					0 (ground)	

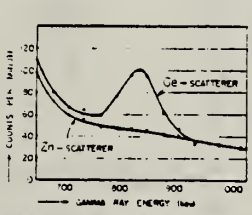

FIG. 2. Resonance fluorescence in Ge^{72}. Pulse-height distributions of the radiation scattered from zinc and germanium rings.

REF. J. J. McCarthy, R. C. Morrison and H. J. Vander Molen
Nucl. Phys. A213, 371 (1973)

ELEM. SYM.	A	Z
Ge	72	32

METHOD

REF. NO. 73 Mc 10 egf

REACTION	RESULT	EXCITATION ENERGY	SOURCE		DETECTOR		ANGLE
			TYPE	RANGE	TYPE	RANGE	
G,NP	ABX	17- 40	C	12- 42	ACT-I		4PI

$$\int_{(\gamma,np)}^{40} \sigma dE = 38.9 \pm 14 \text{ MeV}\cdot\text{mb}$$

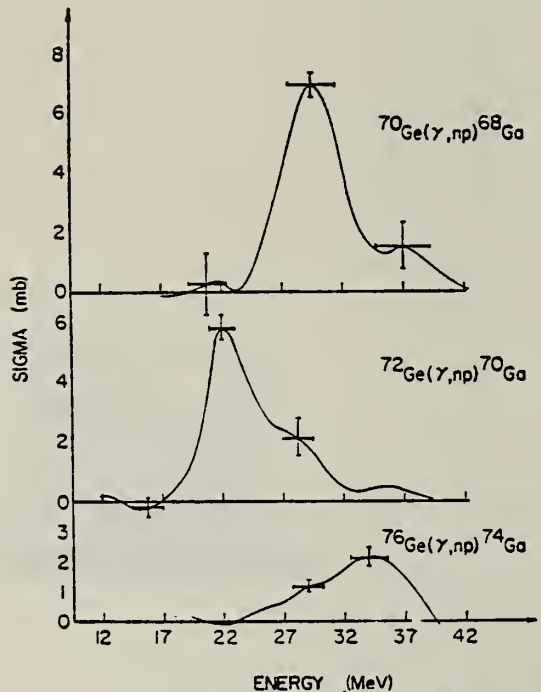

Fig. 5. Cross sections of $^{70}Ge(\gamma, np)^{68}Ga$, $^{72}Ge(\gamma, np)^{70}Ga$, and $^{76}Ge(\gamma, np)^{74}Ga$.

REF.		ELEM. SYM.	A	Z
	A.M. Goryachev, G.N. Zalesnyi, and B.A. Tulupov Izv. Akad. Nauk SSSR. Ser. Fiz. 39, 134 (1975) Bull. Acad. Sci. USSR Phys. Ser. 39, 116 (1975)	Ge	72	32
METHOD		REF. NO.		
		75 Go 1		nmg

REACTION	RESULT	EXCITATION ENERGY	SOURCE		DETECTOR		ANGLE
			TYPE	RANGE	TYPE	RANGE	
G,XN	ABX	11- 25	C	9- 25	BF3-I		4PI

σ(G,SN). Statistical theory used to obtain SN cross section from XN cross section.

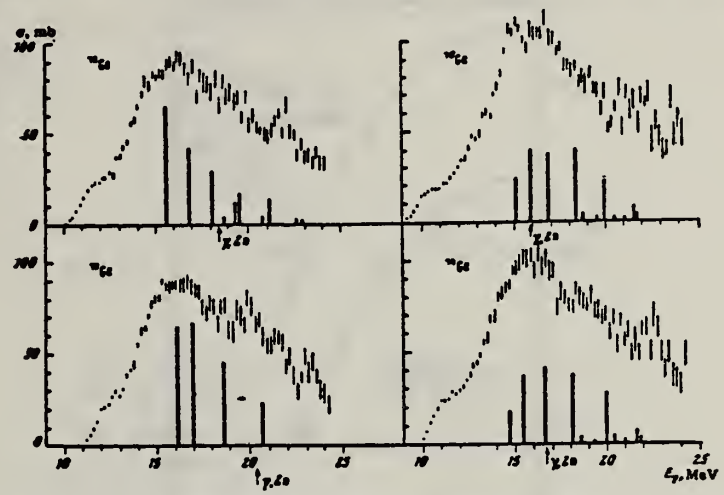

Fig. 2. The same as in Fig. 1, but for ^{70,72,74,76}Ge.

Cross sections of photoneutron reactions. The dipole photoabsorption forces are taken from [6,7] (the solid black columns).

[6] M.G.Huber et al., Phys.Rev.155,1073(67)
[7] M.G.Huber et al., Phys.Rev.192,223(66.

Table 2

Nuclide	β_0	E_2, MeV	E_1, MeV	Nuclide	β_0	E_2, MeV	E_1, MeV
^{64}Zn	0.25	0.99	18	^{70}Ge	0.25	0.562	18
^{66}Zn	0.23	1.04	18	^{70}Se	0.33	0.559	18
^{68}Zn	0.2	1.08	18	^{76}Se	0.3	0.616	18
^{70}Ge	0.23	1.04	18	^{80}Se	0.25	0.654	18
^{72}Ge	0.25	0.835	18	^{82}Se	0.2	0.655	18
^{74}Ge	0.3	0.6	18				

Table 3

Nuclide	σ, mb	Nuclide	σ, mb	Nuclide	σ, mb
^{64}Zn	397±19 *	^{72}Ge	760±37	^{76}Se	1021±52
^{66}Zn	579±27	^{73}Ge	872±41	^{80}Se	1029±50
^{68}Zn	718±35	^{76}Ge	911±43	^{82}Se	1067±53
^{70}Ge	751±37	^{76}Se	930±50		

* Mean - square errors

Values given are for σ_0(24.2 MeV).

REF. F. J. Kline, I. P. Auer, J. C. Bergstrom, and H. S. Caplan
Nucl. Phys. A255, 435 (1975)

ELEM. SYM.	A	Z
Ge	72	32

METHOD

REF. NO. 75 Kl 9 egf

REACTION	RESULT	EXCITATION ENERGY	SOURCE TYPE	SOURCE RANGE	DETECTOR TYPE	DETECTOR RANGE	ANGLE
E,E/	LFT	1, 2	D	84-120	MAG-D		DST

0.835, 2.515 MEV

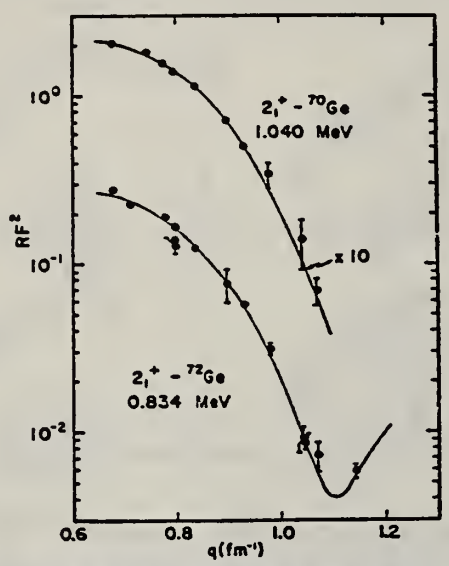

Fig. 4. Plot of the converted form factors squared versus q for the 2_1^+ states in $^{70,72}Ge$. The solid lines are the results of fitting to the data with a DWBA program. Note that both the data and the curve for ^{70}Ge have been multiplied by a factor of ten.

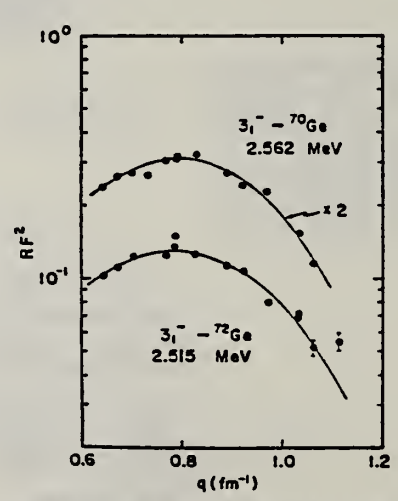

Fig. 5. Plot of the converted form factors squared versus q for the 3_1^- states in $^{70,72}Ge$. The solid lines are the results of fitting to the data with a DWBA program. Note that both the data and the curve for ^{70}Ge have been multiplied by a factor of two.

(over)

TABLE 3

Parameters obtained from fits to the inelastic data

State	Nucleus	c_w (fm)	t_w (fm)	$B(EL, \omega\uparrow)$ (W.u.) [a,b]	χ^2_{pot}
2_1^+	^{70}Ge	4.22±0.14	2.41±0.26	19.7±1.2	0.56
	^{72}Ge	4.32±0.02	2.49±0.05	26.8±2.0	5.2
3_1^-	^{70}Ge	4.34±0.09	2.23±0.11	36±5	12.4
	^{72}Ge	3.84±0.12	2.80±0.11	37±7	12.3

[a]) W.u. are Weisskopf single-particle units.
[b]) Uncertainties have been multiplied by $\sqrt{\chi^2_{pot}}$.

TABLE 4

Reduced transition probabilities

State	$B(EL, \omega\uparrow)$ (W.u.) [a]		Work
	^{70}Ge	^{72}Ge	
2_1^+	19.7±1.2	26.8±2.0	present
	20.5±1.1	22.3±1.4	compilation [b,c])
3_1^-	36±5	37±7	present
	21	22	Kregar and Elbek [d])
	32	27	Curtis *et al.* [e])
	27	23	Perey *et al.* [f])
	21	17	Perey *et al.* [f])

[a]) W.u. are Weisskopf single-particle units.
[b]) Ref. [12]). [c]) Ref. [13]). [d]) Ref. [10]). [e]) Ref. [9]). [f]) Ref. [14]).

[9] T.H. Curtis et al., Phys. Rev. C1, 1418 (1970).

[10] M. Kregar et al., Nucl. Phys. A93, 49 (1967).

[12] K.R. Alvar et al., Nucl. Data Sheets 8, 1 (1972).

[13] K.R. Alvar, Nucl. Data Sheets 11, 121 (1972).

[14] C.M. Perey, R.J. Silva et al., Phys. Rev. C2, 468 (1970).

REF.

J.J. McCarthy, R.C. Morrison, and H.J. Vander Molen
Phys. Rev. C11, 772 (1975)

ELEM. SYM.	A	Z
Ge	72	32

METHOD

REF. NO. 75 Mc 1 hmg

REACTION	RESULT	EXCITATION ENERGY	SOURCE		DETECTOR		ANGLE
			TYPE	RANGE	TYPE	RANGE	
G,N	ABX	10- 40	C	10- 40	MOD-I		4PI
G,2N	ABX	18- 40	C	10- 40	MOD-I		4PI
G,NP	ABI	19- 40	C	10- 40	ACT-I		4PI

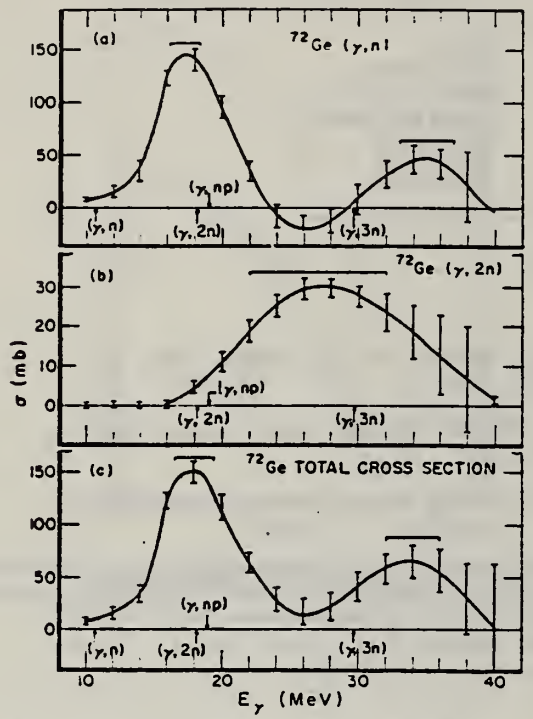

FIG. 5. The (γ, n) cross section for ^{72}Ge. (b) The (γ, 2n) cross section for ^{72}Ge. (c) The total cross section σ[(γ, n) + (γ, 2n) + (γ, np) + (γ, p)] for ^{72}Ge.

TABLE II. Integrated cross sections.

Isotope	(γ, n)	(γ, 2n)	(γ, p) (MeV mb)	(γ, np)	Total
^{70}Ge	1273(127) [a] 1464(290) [b]	60(6)		40(6)	1463(128)
^{72}Ge	1140(110)	420(40)		40(14)	1690(118)
^{74}Ge	1320(130)	360(40)	90(10)	35(3) [c]	1805(136)
^{76}Ge	1077(54) [a] 1067(106) [b]	710(70)		15(3)	1892(89)

[a] Result of the activation measurements.
[b] Result of the neutron counting measurements.
[c] Includes the contribution from the ^{73}Ge(γ, p) reaction.

TABLE III. Lorentz fit parameters and integrated cross sections for total cross sections.

Isotope	σ_0 (mb)	Γ (MeV)	E_0 (MeV)	σ_{LF} $(\frac{1}{2}\pi)\sigma_0\Gamma$ (MeV mb)	σ_{Int} (MeV mb)	$\sigma_{Int}-\sigma_{LF}$ (MeV mb)	$D=60\frac{NZ}{A}$ (MeV mb)	$\frac{\sigma_{Int}}{D}$	$\frac{\sigma_{Int}-\sigma_{LF}}{\sigma_{Int}}$
^{70}Ge	150	5.55	15.5	1380	1463	83	1040	1.41	0.06
^{72}Ge	150	5.90	17.9	1390	1690	300	1070	1.58	0.18
^{74}Ge	144	6.96	16.5	1580	1805	225	1090	1.66	0.12
^{76}Ge	120	8.20	16.7	1550	1892	342	1110	1.70	0.18

REF.		ELEM. SYM.	A	Z
	P. Carlos, H. Beil, R. Bergere, J. Fagot, A. Lepretre, A. Veyssiere, G. V. Solodukhov Nucl. Phys. A258, 365 (1976)	Ge	72	32
METHOD		REF. NO.		
		76 Ca 1		egf

REACTION	RESULT	EXCITATION ENERGY	SOURCE		DETECTOR		ANGLE
			TYPE	RANGE	TYPE	RANGE	
G,N	ABX	10- 26	D	10- 26	MOD-I		4PI
G,2N	ABX	18- 26	D	10-26	MOD-I		4PI

978+

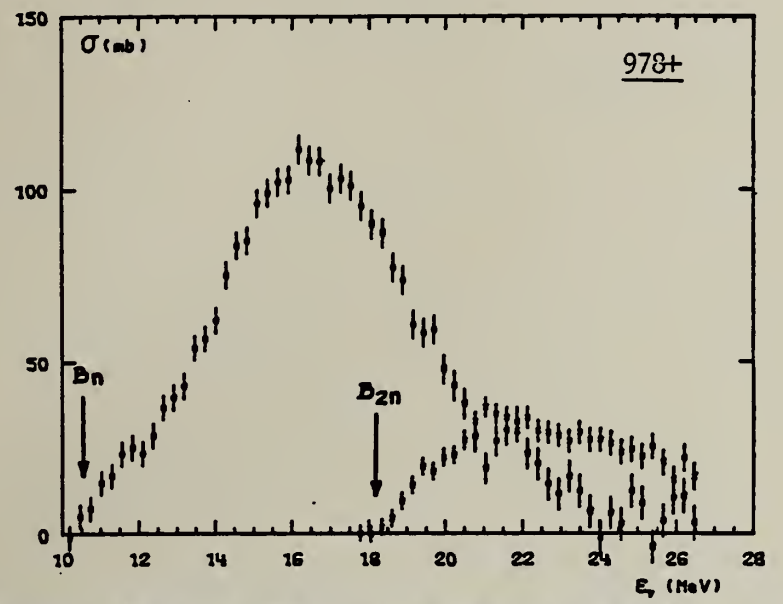

Fig. 4. Partial photoneutron cross sections $[\sigma(\gamma, n)+\sigma(\gamma, pn)]$ and $\sigma(\gamma, 2n)$ for ^{73}Ge. Arrows B_n and B_{2n} indicate theoretical threshold values for (γ, n) and $(\gamma, 2n)$ reactions respectively.

TABLE 3

Integrated photoneutron cross sections and comparison with sum rules

Nucleus	^{64}Zn	^{69}Ga / ^{71}Ga	^{70}Ge	^{72}Ge	^{74}Ge	^{76}Ge	^{75}As	^{76}Se	^{78}Se	^{80}Se	^{82}Se
E_M (MeV)	29	26.5	26.5	26.5	26.5	26.5	26.5	26.5	26.5	26.5	26.5
σ_{0n} (MeV · b)	0.75	0.91	0.78	0.94	1.02	1.12	1.09	1.01	1.06	1.11	1.13
$\frac{\sigma_{0n}A}{0.06\,NZ}$	0.78	0.87	0.75	0.8[illegible]	0.94	1	0.98	0.90	0.92	0.94	0.95
B_n-B_p (MeV)	4.2	3.7 / 1.4	3	1	−0.8	−2.6	3.3	1.7	0.1	−1.5	−3
σ_{-1n} (mb)	38	52	44	54	59	64	63	58	62	65	67
$\sigma_{-1n}A^{-1}$ (mb)	0.15	0.18	0.15	0.18	0.19	0.20	0.20	0.18	0.19	0.19	0.19
σ_{-2n} (mb · MeV^{-1})	2.0	3.1	2.5	3.2	3.6	3.[illegible]	3.7	3.4	3.8	3.9	4.2
$\sigma_{-2n}A^{-1}$ (μb · MeV^{-1})	1.9	2.6	2.1	2.6	2.8	2.[illegible]	2.8	2.5	2.7	2.6	2.7

The notation used is defined in the text. The average experimental errors $\Delta\sigma_{0n}/\sigma_{0n}$, $\Delta\sigma_{-1n}/\sigma_{-1n}$ and $\Delta\sigma_{-2n}/\sigma_{-2n}$ are approximately 8 %.

GE
A=73

GE
A=73

REF.

F. Heinrich, H. Wäffler, and M. Walter
Helv. Phys. Acta 29, 3 (1956)

ELEM. SYM.	A	Z
Ge	73	32

METHOD

REF. NO.	
56 He 2	EGF

REACTION	RESULT	EXCITATION ENERGY	SOURCE		DETECTOR		ANGLE
			TYPE	RANGE	TYPE	RANGE	
G,A	RLY	THR - 31	C	31	ACT-I		

Yield measured relative to (γ,n) yield in ^{63}Cu.

31 MeV bremsstrahlung yields

$$\frac{^{73}Ge(\gamma,a)}{^{63}Cu(\gamma,n)} = (1.5\pm0.8) \times 10^{-2}$$

Ref. R. Tobin, J. McElhinney, L. Cohen
Phys. Rev. 110, 1388 (1958)

Elem. Sym.	A	Z
Ge	73	32

Method: 22 MeV betatron; neutron counters

Ref. No.: 58 To 1 | EH

Reaction	E or ΔE	E_o	Γ	$\int \sigma dE$	Jπ	Notes
$Ge^{73}(\gamma,n)$	Bremss 22					E_{th} = 6.5±0.16

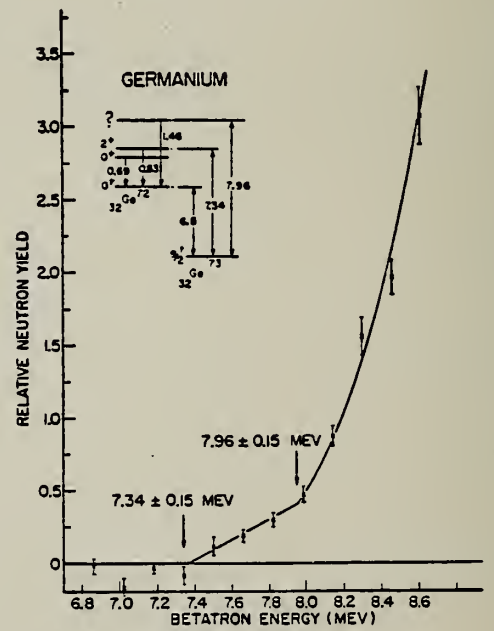

FIG. 4. Photoneutron yield from germanium as a function of betatron energy.

REF.	ELEM. SYM.	A	Z
Y. Oka, T. Kato, K. Nomura, T. Saito and H. T. Tsai Bull. Chem. Soc. Japan 41, 2660 (1968)	Ge	73	32

METHOD	REF. NO.	
	68 Ok 1	egf

REACTION	RESULT	EXCITATION ENERGY	SOURCE		DETECTOR		ANGLE
			TYPE	RANGE	TYPE	RANGE	
G,A	ABY	THR-20	C	20	ACT-I		4PI

TABLE 1. SUMMARY OF DATA ON (γ, α) REACTIONS WITH 20 MeV BREMSSTRAHLUNG

Nuclide		E_{th}	Observed gamma-ray			Results obtained	
Parent (Natural abundance, %)	Product (Half-life)	$(-Q, MeV)$	Energy (MeV)	Branching ratio (%)	Type of multipole transition	$\mu Ci/mg^{a)}$	Yield $(mol^{-1} \cdot R^{-1})$
$^{51}V(99.75)$	$^{47}Sc(3.4\,d)$	10.27	0.160	100	$M1+E2$	1.99×10^{-3}	2.8×10^{3}
$^{63}Cu(30.9)$	$^{61}Co(99\,min)$	6.75	0.068	99	$M1+E2$	7.23×10^{-3}	9.7×10^{3}
$^{71}Ga(39.6)$	$^{67}Cu(61\,hr)$	5.15	0.184	41	$M1$	2.70×10^{-3}	9.6×10^{3}
$^{73}Ge(7.67)$	$^{69m}Zn(14\,hr)$	5.89	0.435	100	$M4$	1.11×10^{-2}	5.0×10^{3}
$^{81}Br(49.48)$	$^{77}As(39\,hr)$	6.46	0.246	2.81	$M1+E2$	1.97×10^{-4}	4.3×10^{2}
$^{109}Ag(48.65)$	$^{105}Rh(36\,hr)$	3.28	0.319+0.306	24.8	$M1+E2$	8.29×10^{-4}	3.7×10^{1}
$^{115}In(95.77)$	$^{111}Ag(7.6\,d)$	3.78	0.340	6	$M1+E2$	5.70×10^{-5}	4.3×10^{1}

a) The value corrected at the end of 1 hr irradiation (9.4×10^{6} R/min).

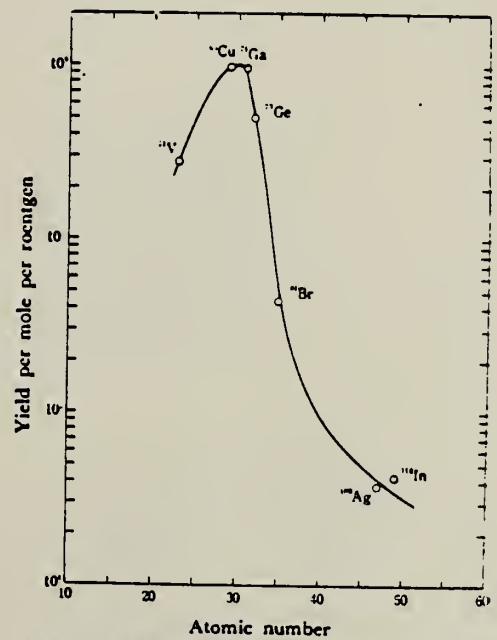

Fig. 1. The yield curve for (γ, α) reaction with 20 MeV bremsstrahlung.

GE
A=74

GE
A=74

GE
A=74

Ref. F.R. Metzger
Phys. Rev. 101, 286 (1956)

Elem. Sym.	A	Z
Ge	74	32

Method: Radioactive source; photon scattering; NaI spectrometer

Ref. No.: 56 Me 1 | NVB

Reaction	E or ΔE	E_o	Γ	$\int \sigma dE$	Jπ	Notes
$Ge^{74}(\gamma,\gamma)$	596 keV	596 keV			2 (excited)	Mean life: $\tau = (1.9 \pm 0.3)\ 10^{-11}$ sec.
					0 (ground)	

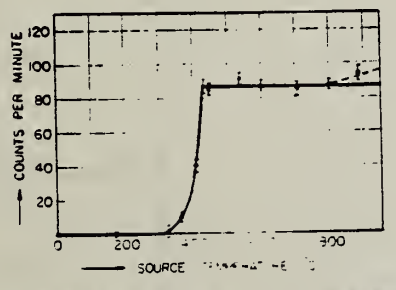

FIG. 3. Resonance fluorescence in Ge^{74}. Dependence of the resonance effect on the temperature of the arsenic source. The solid line represents the temperature dependence of the density of the As_4-vapor calculated on the basis of vapor pressure data,[13] and normalized to give the experimental value of the plateau. Above 800°C the dissociation of the As_4 vapor causes an increase (dashed line) of the resonance fluorescence effect (see discussion in the last chapter).

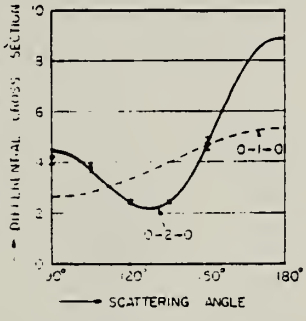

FIG. 4. Angular distribution of the resonance radiation from the 596-kev level in Ge^{74}. The solid line represents the theoretical angular distribution for an excited state with spin 2 and a ground state with spin 0, corrected for the finite angular resolution. The differential cross section is given in arbitrary units.

TABLE I. Observed and predicted ratios of the differential cross sections at 90° and 121°.

Spin of the 835-kev level	Theoretical ratio $d\sigma(90°)/d\sigma(120°)$	Experimental ratio
1	0.79	
2	2.04	2.2±0.3
3	0.08	

REF.

S. Costa, F. Ferrero, S. Ferroni and R. Malvano
Proc. Paris Conference 1034 (1964)

ELEM. SYM.	A	Z
Ge	74	32

METHOD

100 MeV synchrotron

REF. NO.	
64 Co 3	JDM

REACTION	RESULT	EXCITATION ENERGY	SOURCE		DETECTOR		ANGLE
			TYPE	RANGE	TYPE	RANGE	
G,N	ABX	THR-80	C	10-80	BF3-I		4PI

TABLE

ELEMENT	Yield (36 MeV) $\left(\frac{\text{n. cm}^2}{\text{mol. MeV}} \times 10^5\right)$	Σ_0^{30}	Σ_0^{80}	$\Sigma_0^{30}/\Sigma_0^{80}$	σ_{-1} (mb)
$_{24}$Cr	83	1.21	2.1	0.58	62
$_{25}$Mn	108	1.52	2.33	0.65	76
$_{26}$Fe	68	0.88	1.46	0.60	50
$_{27}$Co	89	1.08	1.82	0.59	64
$_{28}$Ni	44	0.55	1.07	0.51	34
$_{29}$Cu	95	1.06	1.99	0.53	72
$_{30}$Zn	88	0.94	1.68	0.56	66
$_{31}$Ga	130	1.29	2.18	0.59	94
$_{32}$Ge	139	1.35	2.29	0.59	101
$_{33}$As	137	1.22	2.18	0.56	100

$\sum_a^b = \frac{A}{60\,NZ}\int_a^b \sigma(E)\,dE$ is the integrated cross section measured in units of the classical dipole $60\,NZ/A$ mb. MeV.

REF. Y. Oka, T. Kato, K. Nomura, T. Saito, Hui-Tuh Tsai
Bull. Chem. Soc. Japan 41, 380 (1968)

ELEM. SYM.	A	Z
Ge	74	32

METHOD

REF. NO. 68 Ok 3 egf

REACTION	RESULT	EXCITATION ENERGY	SOURCE		DETECTOR		ANGLE
			TYPE	RANGE	TYPE	RANGE	
G,P	ABY	THR-20	C	20	ACT-I		4PI

TABLE 1. SUMMARY OF DATA ON (γ, p) REACTIONS WITH 20 MeV BREMSSTRAHLUNG

Nuclide: Parent (Natural abundance, %)	Nuclide: Residual (Half-life)	S_p (MeV)	Observed γ-ray: Energy (MeV)	Observed γ-ray: Branching ratio (%)	Observed γ-ray: Type of multipole transition	Yield determined: μCi/mg[a]	Yield determined: Yield/mol·R
^{25}Mg (10.11)	^{24}Na (15 hr)	12.06	1.37	100	$E2$	1.48×10^{-1}	1.7×10^{5}
^{29}Si (4.71)	^{28}Al (2.27 min)	12.33	1.78	100	$E2$	1.91	2.8×10^{5}
^{30}Si (3.12)	^{29}Al (6.56 min)	13.59	1.28	93.8	$E2+M1$	6.51×10^{-1}	1.5×10^{5}
^{44}Ca (2.06)	^{43}K (22.4 hr)	12.17	0.374	85	$E2+M1$	7.86×10^{-3}	1.3×10^{5}
^{47}Ti (7.32)	^{46}Sc (84.1 d)	10.47	0.887	100	$E2$	7.11×10^{-4}	3.1×10^{5}
^{48}Ti (73.99)	^{47}Sc (3.4 d)	11.44	0.160	100	$E2+M1$	6.83×10^{-3}	1.2×10^{5}
^{49}Ti (5.46)	^{48}Sc (1.8 d)	11.35	1.31	100	$E2$	4.40×10^{-3}	5.8×10^{4}
^{52}Cr (9.55)	^{52}V (3.8 min)	11.15	1.43	100	$E2$	5.01×10^{-1}	6.6×10^{4}
^{57}Fe (2.17)	^{56}Mn (2.58 hr)	10.57	1.81	23.5	$E2+M1$	8.10×10^{-2}	2.1×10^{5}
^{74}Ge (36.74)	^{73}Ga (4.8 hr)	10.92	0.295	97	($E2$)	3.70×10^{-1}	1.3×10^{5}
^{77}Se (7.58)	^{76}As (26.5 hr)	9.61	0.559	41	$E2$	1.48×10^{-2}	1.3×10^{5}
^{87}Sr (7.02)	^{86}Rb (19 d)	9.41	1.08	9	$E2$	5.15×10^{-4}	9.9×10^{4}
^{116}Cd (12.26)	^{115}Ag (3.2 hr)	9.74	1.39	35	$E2$	1.91×10^{-2}	2.1×10^{4}
^{117}Sn (7.57)	^{116m}In (54 min)	9.58	1.27	84	$E2$	9.80×10^{-3}	6.9×10^{5}
^{137}Ba (11.32)	^{136}Cs (13 d)	8.67	0.830	100	$E2$	1.68×10^{-4}	2.2×10^{4}
^{199}Hg (16.84)	^{198}Au (2.7 d)	7.27	0.412	100	$E2$	8.43×10^{-4}	2.2×10^{4}

a) The value corrected at the end of 1 hr irradiation (9.4×10^{6} R/min).

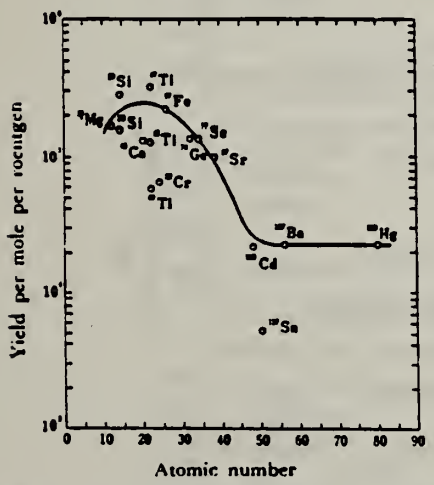

Fig. 2. The yield curve for the (γ, p) reaction with 20 MeV bremsstrahlung.

REF. R. Moreh, S. Shlomo, and A. Wolf
Phys. Rev. C2, 1144 (1970)

ELEM. SYM.	A	Z
Ge	74	32

METHOD

REF. NO. 70 Mo 2 hmg

REACTION	RESULT	EXCITATION ENERGY	SOURCE TYPE	SOURCE RANGE	DETECTOR TYPE	DETECTOR RANGE	ANGLE
G,G	ABX	6	D	6	SCD-D		DST
		(6.018)		(6.018)			

6 = 6.018, LFT

TABLE III. Summary of the results of spins, parities, and total widths of resonance levels excited by γ rays obtained from neutron capture in iron. Parities in parantheses are uncertain.

Isotope	Energy (MeV)	$\delta = \lvert E_r - E_c \rvert$ (eV)	J^π_0	J^π_r	Transition	Γ_0/Γ_γ (±8%)	Γ_γ (10^{-3} eV)
^{50}Cr	8.888	18 ±1	0^+	1	···	0.90	750 ± 200
^{62}Ni	7.646	14 ±1	0^+	1^-	$E1$	0.64	480 ± 50
^{74}Ge	6.018	4.5 ± 0.5	0^+	1^-	$E1$	0.19	120 ± 15
^{75}As	7.646	7.4 ± 0.3	$3/2^-$	$1/2^{(+)}$	···	0.11	360 ± 100
^{109}Ag	7.632	9 ±1	$1/2^-$	3/2	···	0.7	2 ± 1
^{112}Cd	7.632	4.8 ± 0.4	0^+	1^-	$E1$	0.55	86 ± 15
^{139}La	6.018	8.2 ± 0.6	$7/2^+$	$7/2^-$	$E1$	0.50	51^{+14}_{-8}
^{141}Pr	7.632	$11.4^{+0.3}_{-0.9}$	$5/2^+$	$5/2^+$	$M1$	0.46	72^{+24}_{-8}
^{205}Tl	7.646	9.3 ± 0.3	$1/2^+$	$1/2^{(-)}$	···	0.58	980 ± 90
^{208}Pb	7.279	7.1 ± 0.3	0^+	1^+	$M1$	1.00	780 ± 60

TABLE IV. Effective elastic scattering cross section $\langle\sigma_r\rangle = \sigma_0^m (\Gamma_0/\Gamma_\gamma)\Psi(x_0, t_0)$, where δ, J, Γ_0, Γ_γ were taken from Table III. The temperature of the scatterer was 300°K, while that of the iron γ source was 640°K.

Target	Resonance energy (MeV)	$\langle\sigma_r\rangle$ (mb)
^{50}Cr	8.888	905
^{62}Ni	7.646	569
^{74}Ge	6.018	61
^{75}As	7.646	4.4
^{109}Ag	7.632	3.5
^{112}Cd	7.632	198
^{139}La	6.018	39
^{141}Pr	7.632	20
^{205}Tl	7.646	574
^{208}Pb	7.279	5560

REF. R. Moreh and O. Shahal
Phys. Rev. C2, 2217 (1970)

ELEM. SYM.	A	Z
Ge	74	32

METHOD

REF. NO. 70 Mo 4 hmg

REACTION	RESULT	EXCITATION ENERGY	SOURCE		DETECTOR		ANGLE
			TYPE	RANGE	TYPE	RANGE	
G,G	LFT	6	D	6	SCD-D		DST
		(6.018)		(6.018)			

Γ_γ= 0.12 eV, $\Gamma_\sigma/\Gamma_\gamma$= 0.19, $\langle\sigma_r\rangle$ = 61 mb,

δ = 4.5 eV

6=6.018,J-PI,LFT

TABLE II. Most probable spins and parities of levels in ^{74}Ge as found in the present work. Also listed are angular distribution coefficients A of the corresponding γ lines together with $M2/E1$ mixing ratio.

Level energy (MeV)	J^π	γ-line energy (MeV)	A	$\frac{x^2}{\frac{M2}{E1}}$
0.596	2^+	5.422	0.044 ± 0.010	$(1^{+1}_{-1})\times 10^{-4}$
1.206	2^+	4.812	0.041 ± 0.029	$(0.2^{+1}_{-0.2})\times 10^{-4}$
1.486	0^+	4.532	0.506 ± 0.076	0
2.200	2^+	3.818	0.140 ± 0.040	$(1.7^{+\infty}_{-1.7})\times 10^{-4}$
2.229	0^+	3.789	0.514 ± 0.102	0
6.018	1^-	6.018	0.506 ± 0.023	0

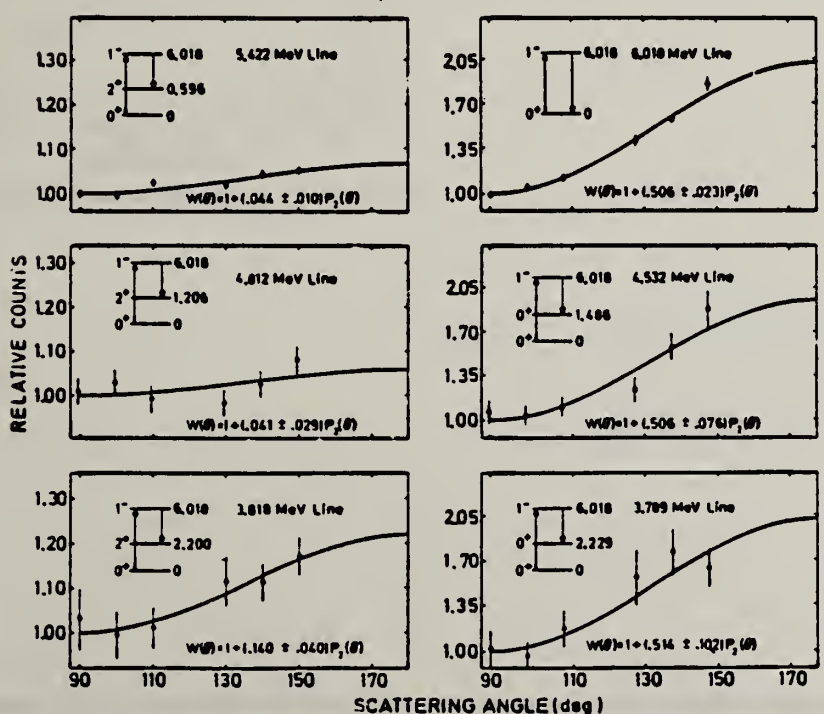

FIG. 4. Angular distribution of the elastic and some intense inelastic lines in ^{74}Ge as measured using a 20-cc Ge(Li) detector. The solid lines have the form $W(\theta) = 1 + AP_2(\cos\theta)$ and are least-square fits to the experimental distribution. In each case the corresponding γ-γ cascade is indicated.

R. Moreh, A. Nof, O. Shahal and A. Wolf
Phys. Letters 36B, 71 (1971)

Ge	74	32

METHOD

REF. NO. 71 Mo 2 egf

REACTION	RESULT	EXCITATION ENERGY	SOURCE		DETECTOR		ANGLE
			TYPE	RANGE	TYPE	RANGE	
G,G/	LFT	6,8	D	6,8	SCD-D		DST

6.018,7.632 MEV

Table 1
Summary of the experimental and theoretical decay properties of the resonance levels excited by nuclear photo-excitation.

Scatterer	Transition $1^- \rightarrow 2^+$ (keV)	A $(1^- \rightarrow 2^+)$	Γ_γ (meV)	$\Gamma(M2)$ (μeV)	$\Gamma(M2)$ (W.u.)	$\delta^2(M2/E1)$ ($\times 10^3$)	$\delta^2(M2/E1)$ Weisskopf estimate ($\times 10^6$)
^{74}Ge	6018 → 2200	0.14 ± 0.04	120 ± 15	190	0.89	17^{+23}_{-12}	3.2
^{100}Mo	6418 → 1064	0.20 ± 0.08	50 ± 45	110	0.079	46^{+53}_{-33}	6.3
^{112}Cd	7632 → 617	0.09 ± 0.02	86 ± 15	36	0.006	$3.6^{+4.5}_{-2.7}$	10.8
^{186}W	6418 → 122	-0.011 ± 0.014	46 ± 35	110	0.023	$9.0^{+5.4}_{-4.1}$	8.7

REF. J.J. McCarthy, R.C. Morrison and H.J. Vander Molen
Nucl. Phys. A213, 371 (1973)

ELEM. SYM.	A	Z
Ge	74	32

METHOD

REF. NO. 73 Mc 10 egf

REACTION	RESULT	EXCITATION ENERGY	SOURCE		DETECTOR		ANGLE
			TYPE	RANGE	TYPE	RANGE	
G,P	ABX	9- 40	C	9- 40	ACT-I		4PI

$$\int_{(\gamma,p)}^{40} \sigma dE = 92 \pm 10 \text{ MeV}\cdot\text{mb}$$

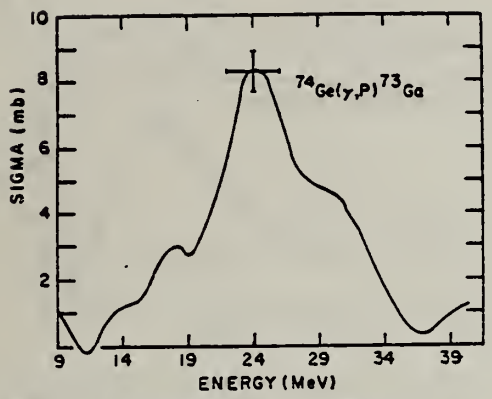

Fig. 3. Total cross section for the reaction $^{74}Ge(\gamma, p)^{73}Ga$.

REF.

A.M. Goryachev, G.N. Zalesnyi, and B.A. Tulupov
Izv. Akad. Nauk SSSR. Ser. Fiz. 39, 134 (1975)
Bull. Acad. Sci. USSR Phys. Ser. 39, 116 (1975)

ELEM. SYM.	A	Z
Ge	74	32

METHOD

REF. NO.: 75 Go 1 | hmg

REACTION	RESULT	EXCITATION ENERGY	SOURCE TYPE	SOURCE RANGE	DETECTOR TYPE	DETECTOR RANGE	ANGLE
G,XN	ABX	10- 25	C	9- 25	BF3-I		4PI

σ(G,SN). Statistical theory used to obtain SN cross section from XN cross section.

Table 2

Nuclide	β_0	E_2, MeV	E_1, MeV	Nuclide	β_0	E_2, MeV	E_1, MeV
^{61}Zn	0.25	0.99	18	^{70}Ge	0.25	0.562	18
^{66}Zn	0.23	1.04	18	^{72}Se	0.33	0.579	18
^{68}Zn	0.2	1.08	18	^{74}Se	0.3	0.618	18
^{70}Ge	0.23	1.04	18	^{76}Se	0.25	0.654	18
^{72}Ge	0.25	0.835	18	^{82}Se	0.2	0.655	18
^{74}Ge	0.3	0.8	18				

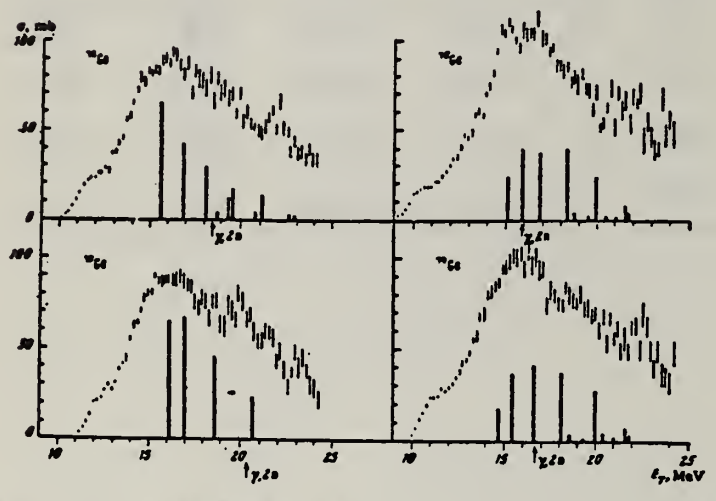

Fig. 2. The same as in Fig. 1, but for ^{70,72,74,76}Ge.

Cross sections of photoneutron reactions. The dipole photoabsorption forces are taken from [6,7] (the solid black columns).

[6] M.G.Huber et al., Phys.Rev.155,1073(67)
[7] M.G.Huber et al., Phys.Rev.192,223(66.

Values given are for σ_0(24.2 MeV).

Table 3

Nuclide	σ, mb	Nuclide	σ, mb	Nuclide	σ, mb
^{64}Zn	307±19 *	^{72}Ge	760±37	^{76}Se	1021±52
^{66}Zn	579±27	^{74}Ge	872±41	^{80}Se	1029±50
^{67}Zn	718±35	^{76}Ge	911±43	^{82}Se	1067±53
^{70}Ge	731±37	^{78}Se	930±50		

* Mean - square errors

REF.

J.J. McCarthy, R.C. Morrison, and H.J. Vander Molen
Phys. Rev. C11, 772 (1975)

ELEM. SYM.	A	Z
Ge	74	32

METHOD

REF. NO.: 75 Mc 1 | hmg

REACTION	RESULT	EXCITATION ENERGY	SOURCE		DETECTOR		ANGLE
			TYPE	RANGE	TYPE	RANGE	
G,N	ABX	10- 40	C	10- 40	MOD-I		4PI
G,2N	ABX	17- 40	C	10- 40	MOD-I		4PI
G,P	ABI	11- 40	C	10- 40	ACT-I		4PI
G,NP	ABI	20- 40	C	10- 40	ACT-I		4PI

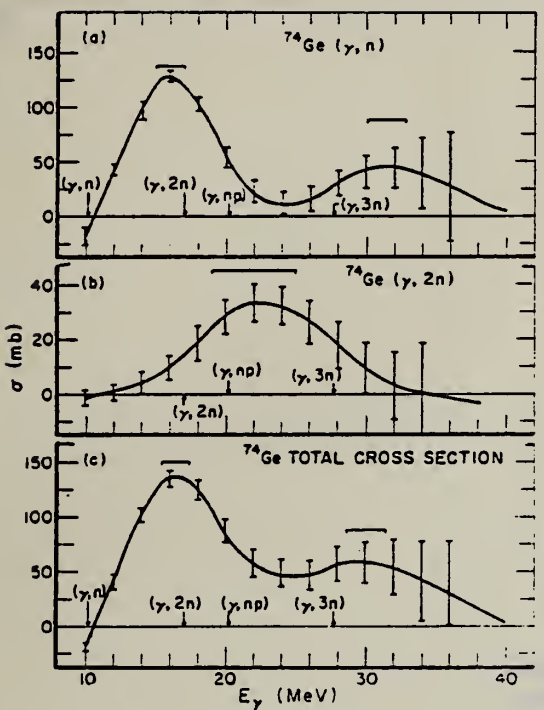

FIG. 6. (a) The (γ, n) cross section for ^{74}Ge. (b) The $(\gamma, 2n)$ cross section for ^{74}Ge. (c) The total cross section $\sigma[(\gamma, n) + (\gamma, 2n) - (\gamma, np) + (\gamma, p)]$ for ^{74}Ge.

TABLE II. Integrated cross sections.

Isotope	(γ, n)	$(\gamma, 2n)$	(γ, p) (MeV mb)	(γ, np)	Total
^{70}Ge	1273(127) [a]	60(6)		40(6)	1463(128)
	1464(290) [b]				
^{72}Ge	1140(110)	420(40)		40(14)	1690(119)
^{74}Ge	1320(130)	360(40)	90(10)	35(3) [c]	1805(136)
^{76}Ge	1077(54) [a]	710(70)		15(3)	1892(89)
	1067(106) [b]				

[a] Result of the activation measurements.
[b] Result of the neutron counting measurements.
[c] Includes the contribution from the ^{73}Ge(γ, p) reaction.

TABLE III. Lorentz fit parameters and integrated cross sections for total cross sections.

Isotope	σ_0 (mb)	Γ (MeV)	E_0 (MeV)	$\frac{\sigma_{Lf}}{(\frac{1}{2}\pi)\sigma_0\Gamma}$ (MeV mb)	σ_{Int} (MeV mb)	$\sigma_{Int} - \sigma_{Lf}$ (MeV mb)	$D = 60\frac{NZ}{A}$ (MeV mb)	$\frac{\sigma_{Int}}{D}$	$\frac{\sigma_{Int} - \sigma_{Lf}}{\sigma_{Int}}$
^{70}Ge	150	5.85	15.5	1380	1463	83	1040	1.41	0.06
^{72}Ge	150	5.90	17.9	1390	1690	300	1070	1.58	0.18
^{74}Ge	144	6.96	16.5	1580	1805	225	1090	1.66	0.12
^{76}Ge	120	8.20	16.7	1550	1892	342	1110	1.70	0.18

REF.

P. Carlos, H. Beil, R. Bergere, J. Fagot, A. Lepretre,
A. Veyssiere, G. V. Solodukhov
Nucl. Phys. A258, 365 (1976)

ELEM. SYM.	A	Z
Ge	74	32

METHOD

REF. NO.: 76 Ca 1 egf

REACTION	RESULT	EXCITATION ENERGY	SOURCE		DETECTOR		ANGLE
			TYPE	RANGE	TYPE	RANGE	
G,N	ABX	10- 26	D	10- 26	MOD-I		4PI
G,2N	ABX	16- 26	D	10- 26	MOD-I		4PI

981+

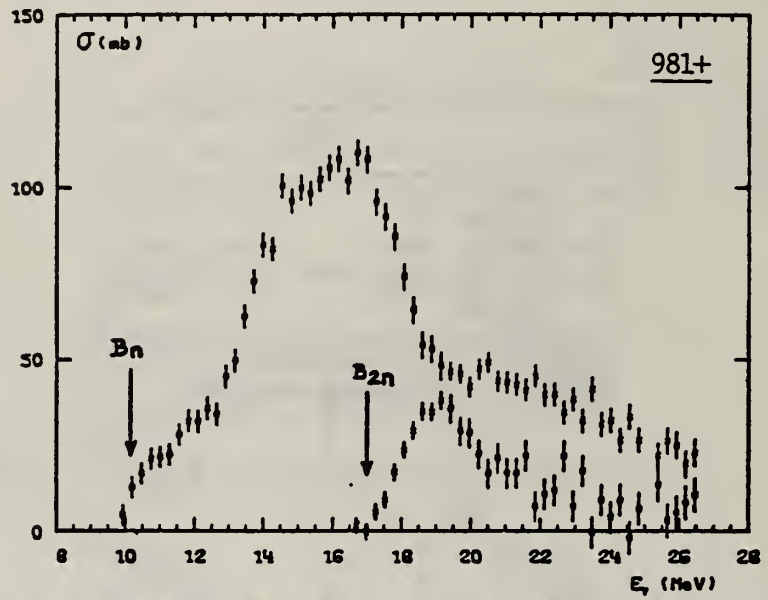

Fig. 5. Partial photoneutron cross sections $[\sigma(\gamma, n)+\sigma(\gamma, pn)]$ and $\sigma(\gamma, 2n)$ for ^{74}Ge. Arrows B_n and B_{2n} indicate theoretical threshold values for (γ, n) and $(\gamma, 2n)$ reactions respectively.

TABLE 3

Integrated photoneutron cross sections and comparison with sum rules

Nucleus	^{64}Zn	^{69}Ga / ^{71}Ga	^{70}Ge	^{72}Ge	^{74}Ge	^{76}Ge	^{75}As	^{76}Se	^{78}Se	^{80}Se	^{82}Se
E_M (MeV)	29	26.5	26.5	26.5	26.5	26.5	26.5	26.5	26.5	26.5	26.5
σ_{0a} (MeV · b)	0.75	0.91	0.78	0.94	1.02	1.12	1.09	1.01	1.06	1.11	1.13
$\frac{\sigma_{0a}A}{0.06\,NZ}$	0.78	0.87	0.75	0.88	0.94	1	0.98	0.90	0.92	0.94	0.95
$B_a - B_p$ (MeV)	4.2	3.7 / 1.4	3	1	−0.8	−2.6	3.3	1.7	0.1	−1.5	−3
σ_{-1a} (mb)	38	52	44	54	59	64	63	58	62	65	67
$\sigma_{-1a}A^{-\frac{1}{3}}$ (mb)	0.15	0.18	0.15	0.18	0.19	0.20	0.20	0.18	0.19	0.19	0.19
σ_{-2a} (mb · MeV^{-1})	2.0	3.1	2.5	3.2	3.6	3.9	3.7	3.4	3.8	3.9	4.2
$\sigma_{-2a}A^{-\frac{1}{3}}$ (μb · MeV^{-1})	1.9	2.6	2.1	2.6	2.8	2.9	2.8	2.5	2.7	2.6	2.7

The notation used is defined in the text. The average experimental errors $\Delta\sigma_{0a}/\sigma_{0a}$, $\Delta\sigma_{-1a}/\sigma_{-1a}$ and $\Delta\sigma_{-2a}/\sigma_{-2a}$ are approximately 8 %.

GE
A=76

GE
A=76

GE
A=76

REF. O.A. Borello, J. Goldemberg, M.D.S. Santos
An. Acad. Brasil. Cienc. 27, 413 (1955)

ELEM. SYM.	A	Z
Ge	76	32

METHOD: Betatron

REF. NO.: 55 Bo 1 NVB

REACTION	RESULT	EXCITATION ENERGY	SOURCE TYPE	SOURCE RANGE	DETECTOR TYPE	DETECTOR RANGE	ANGLE
G,N	ABX	9-21	C	9-21	ACT-I		4PI

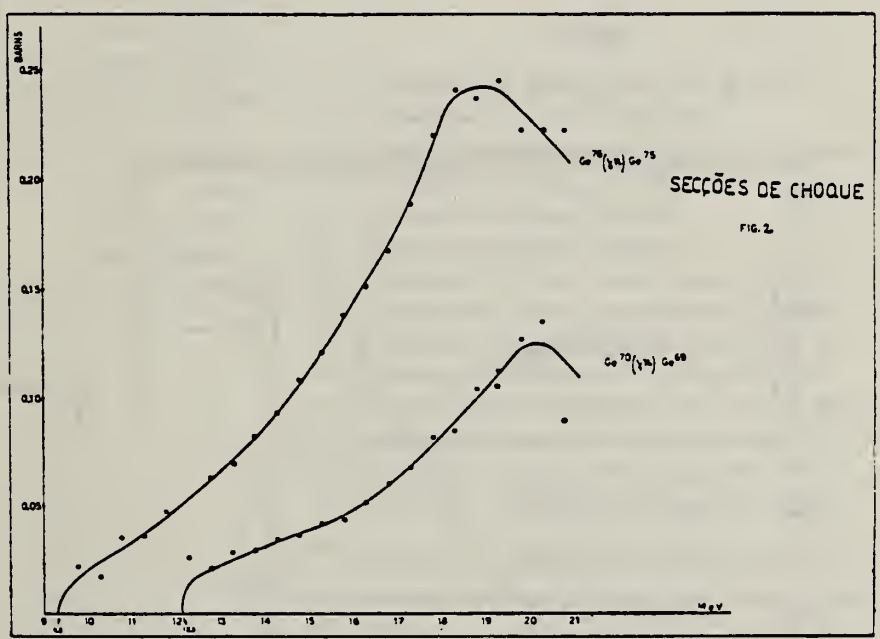

Fig. 2

Elemento	(Threshold) Limiar	E_{max}	σ max	σ int até 21 Mev
Ge^{70}	12,1 ± 0,20 Mev	20 Mev	0,125 barn	0,59 Mev × barn
Ge^{76}	9,3 ± 0,10 Mev	18,9 Mev	0,243 barn	1,5 Mev × barn

M.D. DeSouza Santos, J. Goldemberg, R.R. Pieroni, E. Silva,
O.A. Borello, S.S. Villaca, J.L. Lopes
Int. Conf. Peaceful Uses of Atomic Energy II (UN, NY), 169 (1955)

ELEM. SYM.	A	Z
Ge	76	32

METHOD: Betatron; neutron yield; radioactivity; r-chamber

REF. NO.: 55 De 1 EGF

Reaction	RESULT	EXCITATION ENERGY	SOURCE		DETECTOR		ANGLE
			TYPE	RANGE	TYPE	RANGE	
G,N	ABX	9-21	C	9-21	ACT-I		4PI

$\int \sigma dE$ = 0.59 MeV-b

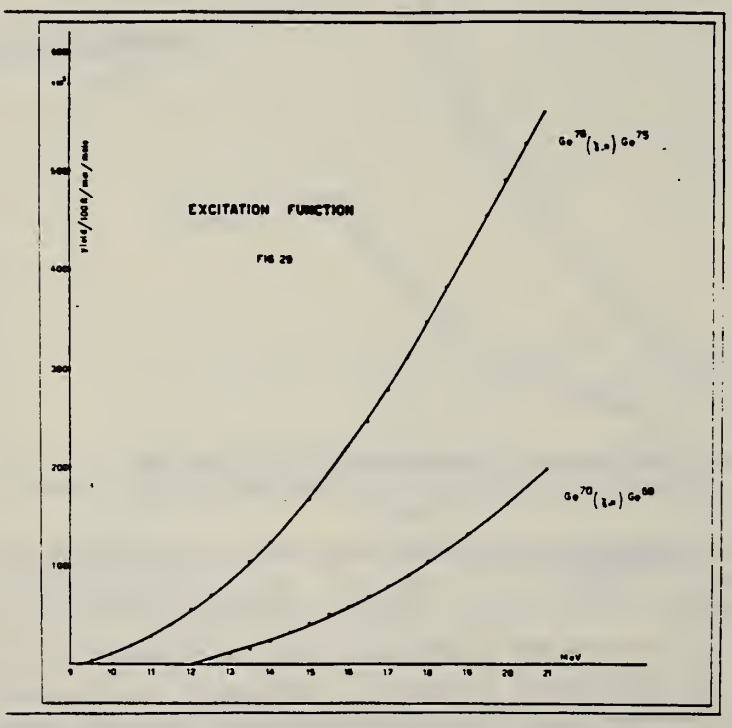

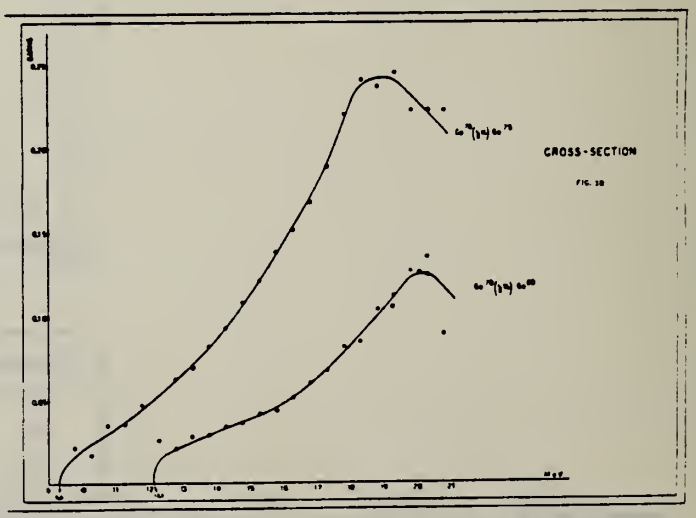

Ref. J.H. Carver, G.E. Coote, T.R. Sherwood
Nuclear Phys. 37, 449 (1962)

Elem. Sym.	A	Z
Ge	76	32

Method: 30 MeV electron synchrotron; activation; NaI

Ref. No.: 62 Ca 1 JHH

Reaction	E or ΔE	E_0	Γ	$\int \sigma dE$	Jπ	Notes
$Ge^{76}(\gamma,n)$	Bremss. 30					

TABLE 1

Isomeric Ratios from (γ,n) reactions

Target Nucleus	J_0	Residual Nucleus:	Ground state: Spin	Ground state: Half-life	Metastable state: Spin	Metastable state: Half-life	Interm. state: Spin	Isomer ratio $Y_1/(Y_1+Y_2)$	σ
Co^{59}	$7/2^-$	Co^{58}	2^+	71.3d	5^+	9.2h		0.44 ±0.02	3.2 ±0.2
Ge^{76}	0^+	Ge^{75}	$1/2^-$	82m	$7/2^+$	49s		0.48 ±0.07	2.8 ±0.5
Br^{81}	$3/2^-$	Br^{80}	1^+	18m	5^-	4.4h	2^-	0.32 ±0.02	6.5 ±1.0
Sr^{86}	0^+	Sr^{85}	$9/2^+$	64d	$1/2^-$	70m	$7/2^+$	0.36 ±0.07	2.2 ±0.4
Zr^{90}	0^+	Zr^{89}	$9/2^+$	79h	$1/2^-$	4.4m		0.33 ±0.10	2.8 ±0.7
Mo^{92}	0	Mo^{91}	$9/2^+$	15.7m	$1/2^-$	66s		0.46 ±0.04	6^{+4}_{-2}
Ag^{107}	$1/2^-$	Ag^{106}	1^+	24m	6	8.3d		0.04 ±0.02	2.0 ±0.3
In^{113}	$9/2^+$	In^{112}	1^+	14.5m	4^+	20.7m	7^-	0.8 ±0.1	3.1 ±0.7
Cd^{116}	0^+	Cd^{115}	$1/2^+$	53h	$11/2^-$	43d		≤ 0.2	≤ 3
Ce^{140}	0^+	Ce^{139}	$3/2^+$	140d	$11/2^-$	55s		0.08 ±0.01	2.5 ±0.2
Hg^{198}	0^+	Hg^{197}	$1/2^-$	65h	$13/2^+$	24h	$3/2^-$ $5/2^-$	0.05 ±0.01	3.4 ±0.5
Previous work									
Br^{81} [10]	$3/2^-$	Br^{80}	1^+	18m	5^-	4.4h	2^-	0.33	6.5
Se^{82} [12]	0^+	Se^{81}	$1/2^-$	18m	$7/2^+$	57m		0.5	3.0
Zr^{90} [11]	0^+	Zr^{89}	$9/2^+$	79h	$1/2^-$	4.3m		0.44 ±0.06	4.5 ±1
In^{115} [23]	$9/2^+$	In^{114}	1^-	72s	5^+	50d	8 ($T_{\frac{1}{2}}$ = 2.5s)	0.85	5.0

REFERENCES

1) J. R. Huizenga and R. Vandenbosch, Phys. Rev. 120 (1960) 1305
2) T. Ericson, Advances in Physics, 9 (1960) 425
3) D. L. Allan, Nuclear Physics 24 (1961) 274
4) C. T. Hibdon, Phys. Rev. 114 (1959) 179
5) C. T. Hibdon, Phys. Rev. 122 (1961) 1235
6) T. Ericson, Nuclear Physics 11 (1959) 481
7) J. H. Carver and G. A. Jones, Nuclear Physics 19 (1960) 184
8) A. C. Douglas and N. Macdonald, Nuclear Physics 13 (1959) 382
9) T. Ericson and V. M. Scrutinski, Nuclear Physics 8 (1958) 284
10) L. Katz, L. Pssas and H. Moody, Can. J. Phys. 30 (1952) 476
11) L. Katz, R. G. Baker and R. Montalbetti, Can. J. Phys. 31 (1953) 250
12) E. Silva and J. Goldemberg, An. Acad. Brasil Ciance 28 (1956) 275
13) J. H. Carver and D. C. Peaslee, Phys. Rev. 120 (1960) 2155
14) J. M. Blatt and V. F. Weisskopf "Theoretical Nuclear Physics" New York: Wiley (1952)
15) S. H. Vegors, L. L. Marsden and R. L. Heath, U.S. Atomic Energy Commission Report IDO-16370 (1958)
16) Nuclear Data Sheets, National Research Council, Washington (1960, up to and including Set 5)
17) R. Vandenbosch and J. R. Huizenga, Phys. Rev. 120 (1960) 1313
18) E. Weigold and R. Glover, Nuclear Physics (in press)
19) K. J. Le Couteur and D. W. Lang, Nuclear Physics 13 (1959) 32
20) T. D. Newton, Can. J. Phys. 34 (1956) 804
21) D. W. Lang, Nuclear Physics 26 (1961) 434
22) M. E. Rose, "Internal Conversion Coefficients", Amsterdam: North Holland Publishing Co. (1958)
23) J. Goldemberg and L. Katz, Phys. Rev. 90 (1953) 308

REF. Y. Oka, T. Kato and A. Yamadera
Bull. Chem. Soc. Japan 41, 1606 (1968)

ELEM. SYM.	A	Z
Ge	76	32

METHOD

REF. NO.	
68 Ok 2	egf

REACTION	RESULT	EXCITATION ENERGY	SOURCE		DETECTOR		ANGLE
			TYPE	RANGE	TYPE	RANGE	
G,N	ABY	THR-20	C	20	ACT-I		4PI

ISOMERIC YIELD

TABLE 1. THE PARTICULARS OF THE (γ,n) REACTION PRODUCTS AND THE DATA OBTAINED WITH 20 MeV BREMSSTRAHLUNG

Nuclide		Half-life of product (sec)	Gamma-ray determined			Limit of detection (μg)	Yield ($mol^{-1} \cdot R^{-1}$)
Parent (Natural abundance, %)	Residual		Energy (MeV)	Branching ratio (%)	Photopeak activity (cpm/mg)[a]		
$^{24}Mg(78.60)$	^{23}Mg	9.9	0.511	200	2.04×10^{6}	0.49	8.1×10^{4}
$^{76}Ge(7.67)$	^{75m}Ge	48	0.139	100	6.37×10^{5}	1.6	1.1×10^{6}
$^{78}Se(23.52)$	^{77m}Se	17	0.162	100	1.82×10^{6}	0.55	1.2×10^{6}
$^{92}Mo(15.86)$	^{91m}Mo	65	0.650	57	2.22×10^{5}	4.5	2.7×10^{6}
$^{140}Ce(88.48)$	^{139m}Ce	58	0.745	100	1.06×10^{6}	0.95	1.3×10^{6}
$^{142}Nd(27.13)$	^{141m}Nd	64	0.760	100	3.19×10^{5}	3.1	1.4×10^{6}
$^{159}Tb(100)$	^{158m}Tb	11	0.111	100	2.56×10^{6}	3.8	2.2×10^{6}

a) The value corrected at the end of one-minute irradiation with the dose rate of 10^{7} R/min; Counting geometry is 20% with a 3"dia.×3"NaI(Tl) detector.

REF. J.J. McCarthy, R.C. Morrison and H.J. Vander Molen
Nucl. Phys. A213, 371 (1973)

ELEM. SYM.	A	Z
Ge	76	32

METHOD

REF. NO. 73 Mc 10 egf

REACTION	RESULT	EXCITATION ENERGY	SOURCE		DETECTOR		ANGLE
			TYPE	RANGE	TYPE	RANGE	
G,NP	ABX	17- 40	C	12- 42	ACT-I		4PI

$$\int_{(\gamma,np)}^{40} \sigma dE = 15.2 \pm 3 \text{ MeV}\cdot\text{mb}$$

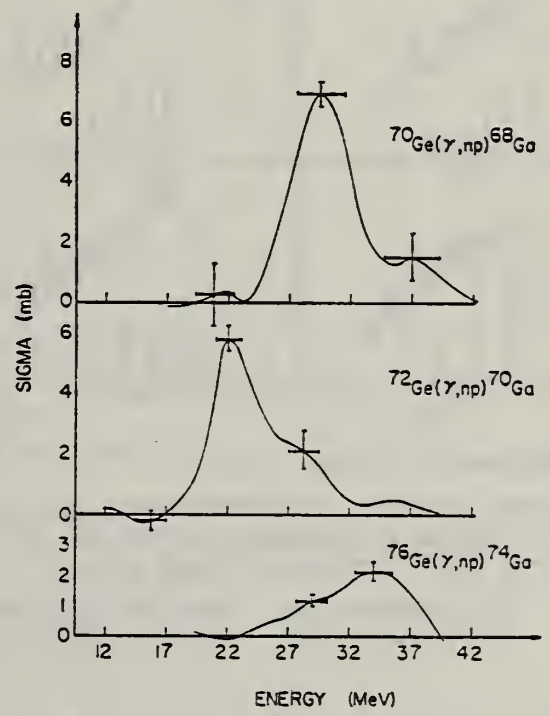

Fig. 5. Cross sections of $^{70}Ge(\gamma, np)^{68}Ga$, $^{72}Ge(\gamma, np)^{70}Ga$, and $^{76}Ge(\gamma, np)^{74}Ga$.

REF.	A.M. Goryachev, G.N. Zalesnyi, and B.A. Tulupov Izv. Akad. Nauk SSSR. Ser. Fiz. 39, 134 (1975) Bull. Acad. Sci. USSR Phys. Ser. 39, 116 (1975)	ELEM. SYM.	A	Z
		Ge	76	32

METHOD	REF. NO.	
	75 Go 1	hmg

REACTION	RESULT	EXCITATION ENERGY	SOURCE		DETECTOR		ANGLE
			TYPE	RANGE	TYPE	RANGE	
G,XN	ABX	9 - 25	C	9- 25	BF3-I		4PI

σ(G,SN). Statistical theory used to obtain SN cross section from XN cross section.

Table 2

Nuclide	β_0	E_2, MeV	E_1, MeV	Nuclide	β_0	E_2, MeV	E_1, MeV
^{61}Zn	0.25	0.99	18	^{70}Ge	0.25	0.562	18
^{66}Zn	0.23	1.04	18	^{72}Se	0.33	0.559	18
^{68}Zn	0.2	1.08	18	^{74}Se	0.3	0.616	18
^{70}Ge	0.23	1.04	18	^{76}Se	0.25	0.654	18
^{72}Ge	0.25	0.835	18	^{82}Se	0.2	0.655	18
^{74}Ge	0.3	0.6	18				

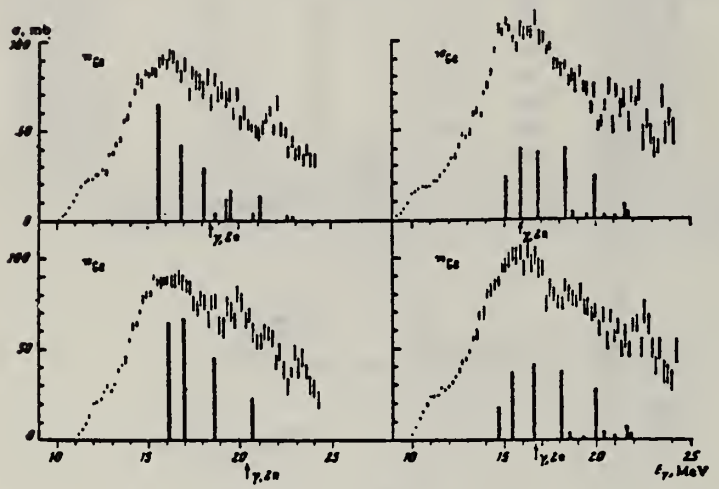

Fig. 2. The same as in Fig. 1, but for ^{70,72,74,76}Ge.

Cross sections of photoneutron reactions. The dipole photoabsorption forces are taken from [6,7] (the solid black columns).

[6] M.G.Huber et al., Phys.Rev.155,1073(67)
[7] M.G.Huber et al., Phys.Rev.192,223(66.

[over]

Table 3

Nuclide	σ, mb	Nuclide	σ, mb	Nuclide	σ, mb
^{67}Zn	367±19	^{72}Ge	760±37	^{76}Se	1021±52
^{68}Zn	379±27	^{73}Ge	872±41	^{80}Se	1029±50
^{69}Zn	718±35	^{76}Ge	911±43	^{82}Se	1067±53
^{70}Ge	753±37	^{76}Se	930±50		

*Mean - square errors

Values given are for σ_0(24.2 MeV).

REF.

J.J. McCarthy, R.C. Morrison, and H.J. Vander Molen
Phys. Rev. C11, 772 (1975)

ELEM. SYM.	A	Z
Ge	76	32

METHOD

REF. NO.	
75 Mc 1	hmg

REACTION	RESULT	EXCITATION ENERGY	SOURCE		DETECTOR		ANGLE
			TYPE	RANGE	TYPE	RANGE	
G,N	ABX	9- 40	C	10- 40	MOD-I		4PI
G,2N	ABX	15- 40	C	10- 40	MOD-I		4PI
G,NP	ABI	20- 40	C	10- 40	ACT-I		4PI

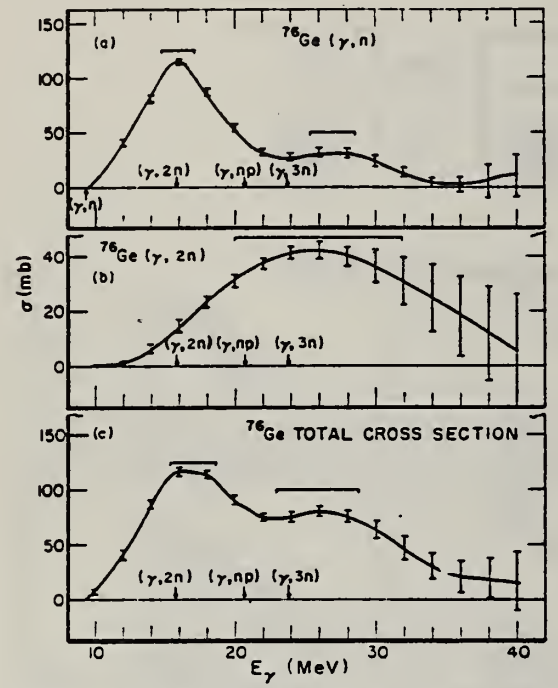

FIG. 7. (a) The (γ,n) cross section for ^{76}Ge. (b) The $(\gamma,2n)$ cross section for ^{76}Ge. (c) The total cross section $\sigma[(\gamma,n)+(\gamma,2n)+(\gamma,np)+(\gamma,p)]$ for ^{76}Ge.

TABLE II. Integrated cross sections.

Isotope	(γ,n)	$(\gamma,2n)$	(γ,p) (MeV mb)	(γ,np)	Total
^{70}Ge	1273(127) [a]	60(6)		40(6)	1463(123)
	1464(290) [b]				
^{72}Ge	1140(110)	420(40)		40(14)	1690(118)
^{74}Ge	1320(130)	360(40)	90(10)	35(3) [c]	1805(136)
^{76}Ge	1077(54) [a]	710(70)		15(3)	1992(89)
	1067(106) [b]				

[a] Result of the activation measurements.
[b] Result of the neutron counting measurements.
[c] Includes the contribution from the ^{73}Ge(γ,p) reaction.

TABLE III. Lorentz fit parameters and integrated cross sections for total cross sections.

Isotope	σ_0 (mb)	Γ (MeV)	E_0 (MeV)	σ_{LF} $(\frac{1}{2}\pi)\sigma_0\Gamma$ (MeV mb)	σ_{Int} (MeV mb)	$\sigma_{Int}-\sigma_{LF}$ (MeV mb)	$D=60\frac{NZ}{A}$ (MeV mb)	$\frac{\sigma_{Int}}{D}$	$\frac{\sigma_{Int}-\sigma_{LF}}{\sigma_{Int}}$
^{70}Ge	150	5.85	15.5	1380	1463	83	1040	1.41	0.06
^{72}Ge	150	5.90	17.9	1390	1690	300	1070	1.58	0.18
^{74}Ge	144	6.96	16.5	1580	1805	225	1090	1.66	0.12
^{76}Ge	120	8.20	16.7	1550	1992	342	1110	1.70	0.18

REF.		ELEM. SYM.	A	Z
	P. Carlos, H. Beil, R. Bergere, J. Fagot, A. Lepretre, A. Veyssiere, G. V. Solodukhov Nucl. Phys. A258, 365 (1976)	Ge	76	32

METHOD	REF. NO.	
	76 Ca 1	egf

REACTION	RESULT	EXCITATION ENERGY	SOURCE		DETECTOR		ANGLE
			TYPE	RANGE	TYPE	RANGE	
G,N	ABX	8- 26	D	8- 26	MOD-I		4PI
G,2N	ABX	16- 26	D	8- 26	MOD-I		4PI

984+

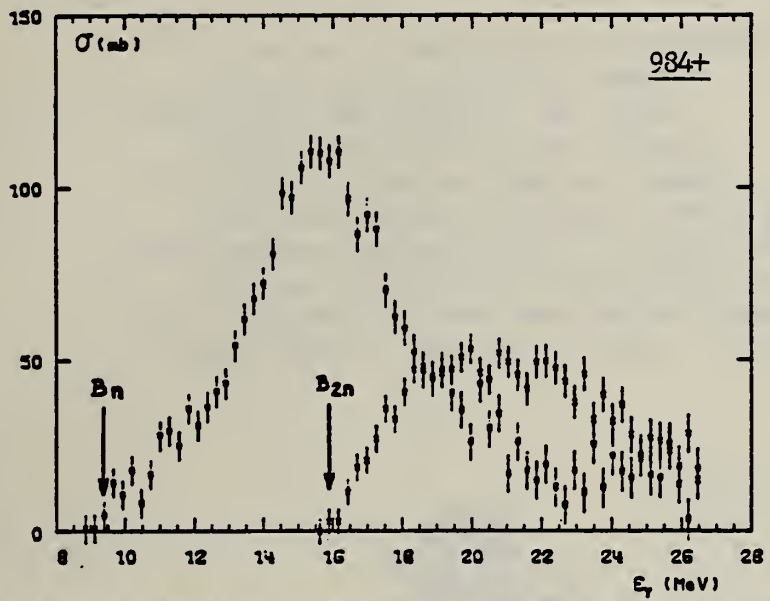

Fig. 6. Partial photoneutron cross sections $[\sigma(\gamma, n)+\sigma(\gamma, pn)]$ and $\sigma(\gamma, 2n)$ for ^{76}Ge. The rough data have been corrected for the presence of oxygen in the target but not for the 30 % impurities of other Ge isotopes. Arrows B_n and B_{2n} indicate theoretical threshold values for (γ, n) and $(\gamma, 2n)$ reactions respectively.

TABLE 3

Integrated photoneutron cross sections and comparison with sum rules

Nucleus	^{64}Zn	^{69}Ga / ^{71}Ga	^{70}Ge	^{72}Ge	^{74}Ge	^{76}Ge	^{75}As	^{76}Se	^{78}Se	^{80}Se	^{82}Se
E_{th} (MeV)	29	26.5	26.5	26.5	26.5	26.5	26.5	26.5	26.5	26.5	26.5
σ_{0n} (MeV · b)	0.75	0.91	0.78	0.94	1.02	1.12	1.09	1.01	1.06	1.11	1.13
$\frac{\sigma_{0n}A}{0.06\,NZ}$	0.78	0.87	0.75	0.88	0.94	1	0.98	0.90	0.92	0.94	0.95
$B_n - B_p$ (MeV)	4.2	3.7 / 1.4	3	1	−0.8	−2.6	3.3	1.7	0.1	−1.5	−3
σ_{-1n} (mb)	38	52	44	54	59	64	63	58	62	65	67
$\sigma_{-1n}A^{-1}$ (mb)	0.15	0.18	0.15	0.18	0.19	0.20	0.20	0.18	0.19	0.19	0.19
σ_{-2n} (mb · MeV^{-1})	2.0	3.1	2.5	3.2	3.6	3.9	3.7	3.4	3.8	3.9	4.2
$\sigma_{-2n}A^{-1}$ (μb · MeV^{-1})	1.9	2.6	2.1	2.6	2.8	2.9	2.8	2.5	2.7	2.6	2.7

The notation used is defined in the text. The average experimental errors $\Delta\sigma_{0n}/\sigma_{0n}$, $\Delta\sigma_{-1n}/\sigma_{-1n}$ and $\Delta\sigma_{-2n}/\sigma_{-2n}$ are approximately 8 %.

As
A=75

# ARSENIC
Z=33

"For smelter fumes have I been named.
  I am an evil, poisonous smoke . . .
But when from poison I am freed,
  Through art and sleight of hand,
Then can I cure both man and beast,
  From dire disease ofttimes direct them;
But prepare me correctly, and take great care
  That you faithfully keep watchful guard over me;
For else am I poison, and poison remain,
  That pierces the heart of many a one." (1)

As
A=75

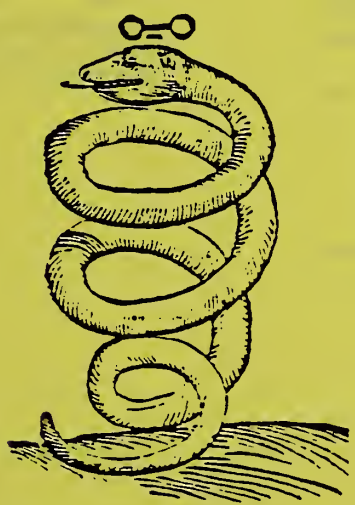

(2)

(1) Fr. Basilli Valentini chymische Schriften, Gottfried Liebezeit, Hamburg, 1694, part 2, p. 156.

(2) Seventeen-Century alchemistic symbol for arsenic.

As
A=75

REF.

T. T. Sugihara and I. Halpern
Phys. Rev. 101, 1768 (1956)

ELEM. SYM.	A	Z
As	75	33

METHOD

REF. NO. 56 Su 1 JOC

REACTION		RESULT	EXCITATION ENERGY	SOURCE TYPE	SOURCE RANGE	DETECTOR TYPE	DETECTOR RANGE	ANGLE
G,N	G,5N5P	RLY	THR-320	C	140,320	ACT-I		4PI
G,3N	G,7N2P	ditto	ditto	ditto		ditto		ditto
G,N2P	G,7N4P							
G,3N2P	G,8N6P							
G,3N4P	G,10N4P							
G,4N5P	G,14N6P							
G,5N2P	G,2P							

TABLE I. Relative yields of observed radionuclides from the irradiation of arsenic with x-ray spectra at 140 Mev and 320 Mev.[a]

Separated nuclide	Half-life[b]	Yield at 140 Mev (arbitrary units)	Yield at 320 Mev (arbitrary units)
As^{74}	17.5 days	1050	1050
As^{73}	26 hr	110	110
Ga^{72}	5.0 hr	0.3	0.5
Ga^{72}	14.3 hr	0.9	1.2
Ga^{70}	20.3 min	8.4	9.5
Ga^{68}	68 min	4.2	7.6
Ga^{66}	9.45 hr	0.2	0.7
Cu^{67}	58.5 hr	0.1	0.2
Cu^{64}	12.80 hr	0.3	2.5
Cu^{61}	3.33 hr	<0.1	0.6
Ni^{66}	56 hr	<0.02	0.05
Ni^{65}	2.56 hr	0.08	0.1
Co^{61}	99.0 min	0.09	0.2
Co^{60}	18.2 hr	<0.02	0.1

[a] The yields at both energies are normalized to the same flux of resonance-energy (17 Mev) photons.
[b] Hollander, Perlman, and Seaborg, Revs. Modern Phys. 25, 469 (1953).

TABLE III. Average cross sections. Average cross sections for the production of a number of nuclides from arsenic by photons from 140 Mev to 320 Mev.

Nuclide	$\bar{\sigma}$ (mb)	Integrated cross section (Mev-mb)
Ga^{72}	0.02	3.6
Ga^{66}	0.3	54
Ga^{66}	0.05	9
Cu^{67}	0.01	1.8
Cu^{64}	0.2	36
Cu^{61}	0.05	9
Ni^{66}	0.002	0.4

TABLE II. Ratios of yields of some gallium isotopes from arsenic to the (γ,n) yield.

Isotope	Reaction	50 Mev[a]	140 Mev	320 Mev
Ga^{70}	(γ,an)	46 $\times 10^{-4}$	80×10^{-4}	90×10^{-4}
Ga^{72}	$(\gamma,n2p)$	2.4×10^{-4}	9×10^{-4}	12×10^{-4}
Ga^{72}	$(\gamma,2p)$	1.7×10^{-4}	3×10^{-4}	5×10^{-4}

[a] See reference 17.

[17] R. B. Holtzman and N. Sugarman, Phys. Rev. 87, 633 (1952).

[18] H. H. Hopkins, Jr., Phys. Rev. 77, 717 (1950).

Ref. F. Ferrero, R. Malvano, C. Tribuno
Nuovo Cimento 6, 385 (1957)

Elem. Sym.	A	Z
As	75	33

Method: Betatron; neutron yield; threshold detector

Ref. No.: 57 Fe 2 NB

Reaction	E or ΔE	E_o	Γ	$\int \sigma dE$	Jπ	Notes
$As^{75}(\gamma,n!)$	Bremss. 14-30					R - ratio between area of second maximum in cross section and first maximum. R = 0.6±0.12

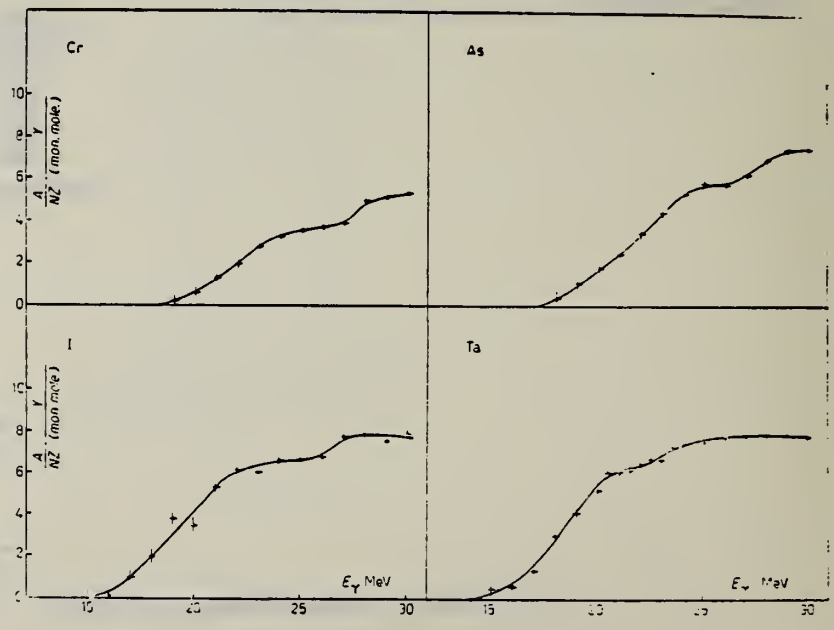

Fig. 1.

B.G. Chidley, L. Katz, S. Kowalski
Can. J. Phys. 36, 407 (1958)

ELEM. SYM.	A	Z
As	75	33

METHOD
Betatron

REF. NO.
58 Ch 2 NVB

REACTION	RESULT	EXCITATION ENERGY	SOURCE		DETECTOR		ANGLE
			TYPE	RANGE	TYPE	RANGE	
G,N	RLY	THR	C	THR	BF3-I		4PI

See 58 Ka 1 for cross sections.

THRESHOLD

TABLE I

MEASURED PHOTONEUTRON THRESHOLDS

Reaction	Measured Q value, Mev.	Other Q values, Mev.	Method	Reference
$As^{75}(\gamma, n)As^{74}$	10.24±0.08 (10.14±0.10)			
		10.18 ±0.19	Mass data	Wapstra (1955)
		10.3 ±0.2	Threshold	Ogle *et al.* (1950)
		10.10 ±0.20	Threshold	Sher *et al.* (1951)
		9.92 ±0.07*	Mass data	Duckworth (unpublished)
			Q^+ value	Way *et al.* (1955)
		10.14 ±0.07*	Mass data	Duckworth (unpublished)
			Q^- value	Way *et al.* (1955)

*Errors given are from mass values only, those of Q^+ and Q^- values are not known.

L. Katz, G.B. Chidley
Nuclear Reactions at Low and Medium Energies (Academy of Science, USSR: 1958) 371

As	75	33

METHOD: Betatron; neutron cross section; BF_3 counters; ion chamber monitor

REF. NO.: 58 Ka 1 | NVB

REACTION	RESULT	EXCITATION ENERGY	SOURCE		DETECTOR		ANGLE
			TYPE	RANGE	TYPE	RANGE	
G,XN	ABX	10-22	C	10-22	BF3-I		4PI

THRESHOLDS

Таблица 2

Пороги испускания фотонейтронов

Изотоп	B_n, *Мэв*	$B_{эм}$, *Мэв*	Изотоп	B_n, *Мэв*	$B_{эм}$, *Мэв*
V^{51}	11,16	20,5	L^{139}	8,81	16,1
Mn^{55}	10,14	19,2	Pr^{141}	9,46	17,6
Co^{59}	10,44	18,6	Tb^{159}	8,16	14,8
As^{75}	10,24	18,1	Ho^{165}	8,10	14,6
Y^{89}	11,82	20,7	Tm^{169}	8,00	14,7
Nb^{93}	8,86	17,1	Lu^{175}	7,77	14,2
Rh^{103}	9,46	16,8	Ta^{181}	7,66	13,8
J^{127}	9,14	16,2	Au^{197}	7,96	13,3
Cs^{133}	9,11	16,5	Bi^{209}	7,43	14,5

не приведены, поскольку они превышают 22 *Мэв* во всех случаях, кроме золота, для которого $B_{эм}=21$ *Мэв*. Свойства сечений $\sigma_C(\gamma)$ сведены в табл. 3.

Таблица 1

Изотоп	$E_{макс}$, *Мэв*	$\sigma_n(E_\gamma)$, *барн*	Γ, *Мэв*	$\int\sigma d\varepsilon$, *Мэв·барн*	Y(22), 10^6 *нейтрон/100 р·мин*
V^{51}	18,4	0,062	5,2	0,33	1,62
Mn^{55}	20,2	0,060	7,0	0,39	2,01
Co^{59}	18,3	0,068	6,3	0,44	2,30
As^{75}	16,4	0,090	9,5	0,74	4,25
Y^{89}	17,1	0,172	5,2	0,93	5,33
Nb^{93}	18,0	0,156	7,5	1,17	6,80
Rh^{103}	17,5	0,160	9,4	1,40	8,28
J^{127}	15,2	0,273	6,8	1,76	11,9
Cs^{133}	16,5	0,238	7,7	1,59	10,7
La^{139}	15,5	0,325	3,8	1,55	11,2
Pr^{141}	15,0	0,320	4,9	1,93	13,1
Tb^{159}	15,6	0,274	9,8	2,49	18,1
Ho^{165}	13,5	0,305	8,9	2,52	18,7
Tm^{169}	16,4	0,250	8,4	1,91	14,9
Lu^{175}	16,0	0,225	8,4	1,90	23,0
Ta^{181}	14,5	0,380	8,5	3,15	22,0
Au^{197}	13,8	0,475	4,7	3,04	22,6
Bi^{209}	13,2	0,455	5,9	2,89	23,2

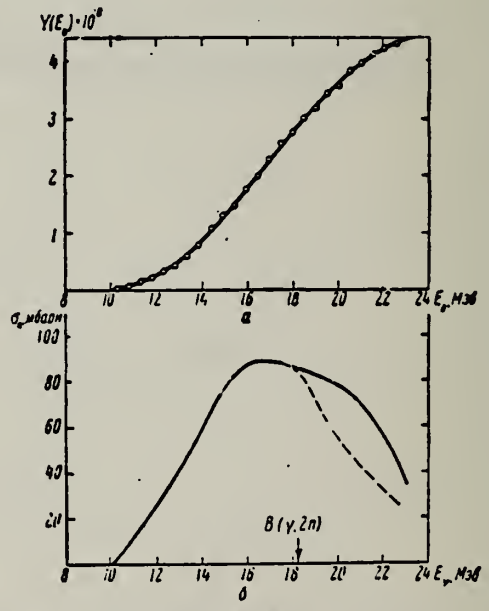

Рис. 4.

а — Выход фотонейтронов для As; б — $\sigma_n(\delta_\gamma)$ и $\sigma_C(\gamma)$ для As

R. N. Geller, J. Halpern, and E. G. Muirhead
Phys. Rev. 118, 1302-12 (1960)

ELEM. SYM.	A	Z
As	75	33

METHOD
Betatron; neutron threshold; ion chamber

REF. NO.
60 Ge 3

NVB

REACTION	RESULT	EXCITATION ENERGY	SOURCE		DETECTOR		ANGLE
			TYPE	RANGE	TYPE	RANGE	
G,N	NØX	THR	C THR		BF3-I		4 PI

THRESHØLD

TABLE I. Summary and comparison of neutron separation energies inferred from present threshold measurements with values predicted from mass data and reaction energies. All energies are expressed in the center-of-mass system in Mev.

Reaction	No. runs	Present results	Other results	Method	Reference
$As^{75}(\gamma,n)As^{74}$	4	10.259±0.031	10.11 ±0.16	mass data $Q(\beta^+)$	m o
			10.14 ±0.13	mass data $Q(\beta^-)$	m o
			10.24 ±0.08	threshold	f

[m] Henry E. Duckworth, *Mass Spectroscopy* (Cambridge University Press, New York, 1958), p. 177.
[o] L. J. Lidofsky, Revs. Modern Phys. 29, 773 (1957).
[f] R. W. King, Revs. Modern Phys. 26, 327 (1954).

R.G. Baker, K.G. McNeill
Can. J. Phys. 39, 1158(1961)

As	75	33	

METHOD: betatron; fast neutron yield; angular distribution; Al and Si threshold detectors; ion chamber

REF. NO.: 61 Ba 2 NVB

REACTION	RESULT	EXCITATION ENERGY	SOURCE TYPE	SOURCE RANGE	DETECTOR TYPE	DETECTOR RANGE *	ANGLE
G,XN	ABY	THR-22	C	22	THR-I	3-+	DST
G,XN	ABY	THR-22	C	22	THR-I	5-+	DST

In Tables 2 and 4:

$\bar{\sigma}$ = average cross section of detector weighted with neutron spectrum

Φ = neutrons/100 roentgen/mole

$$W(\theta) = a_o \sum_{n=1}^{\infty} [1 + A_n P_n (\cos \theta)]$$

* "3-+" is the detector range of Aluminum and "5-+" of Silicon.

TABLE II

Normalized yields for aluminum detectors

	Al(n,γ) reaction				Al(n,p) reactions						
Element	30°	90°	150°	a_0	30°	60°	90°	a_0	a_1	a_2	$(\bar{\sigma}\Phi)^*\times10^3$
Bismuth	399	567±130	620	541±83	3032	5139±200	3168	4306±185	0.06±0.06	−0.35±0.1	17.76
	478	423±130	641	484±85	2562	5353±290	2955	4144±185	−0.05±0.06	−0.53±0.1	16.87
Lead	426	312±120	725	429±77	3123	5754±260	3154	4591±166	−0.004±0.05	−0.51±0.07	18.63
Tantalum	378	367±190	688	441±122	2757	3024±425	2088	2757±275	0.14±0.14	−0.19±0.17	11.22
Lanthanum	208	222±110	330	243±70	2139	3371±250	1891	2768±160	0.05±0.07	−0.43±0.10	11.27
Arsenic	77	100±50	108	97±32	788	937±115	764	865±74	0.02±0.11	−0.16±0.14	3.52
Copper	13	65±30	70	55±20	710	748±70	569	700±45	0.11±0.08	−0.14±0.11	2.85

*$(\bar{\sigma}\Phi) = 4.07\times10^{4}$ millibarn-neutron.

TABLE IV

I Element	II a_0	III a_1	IV a_2	V $(\bar{\sigma}\Phi)\times10^{26}$	VI Φ_{fast}(22 Mev)$\times10^{3}$	VII Φ_{fast}/Φ_{total}
Vanadium	245(1±0.06)	0.01±0.08	−0.00±0.10	6.05	0.21	0.12
Chromium	164(1±0.03)	0.04±0.04	−0.05±0.05	4.05	0.17	0.10
Manganese	308(1±0.02)	0.07±0.02	−0.09±0.04	7.61	0.25	0.12
Iron	200(1±0.03)	0.05±0.04	−0.17±0.05	4.94	0.18	0.11
Cobalt	390(1±0.02)	0.08±0.03	−0.22±0.04	9.63	0.26	0.15
Nickel	145(1±0.05)	0.07±0.07	−0.23±0.00	3.58	0.12	0.12
Copper	347(1±0.02)	0.05±0.03	−0.29±0.04	8.57	0.30	0.12
Arsenic	482(1±0.03)	0.11±0.04	−0.24±0.05	11.91	0.33	0.15
Rubidium	638(1±0.05)	0.13±0.06	−0.14±0.08	15.76		
Strontium	409(1±0.05)	0.10±0.06	−0.17±0.08	10.10		
Yttrium	290(1±0.10)	0.08±0.12	−0.12±0.15	7.16		
Silver	590(1±0.04)	0.10±0.06	−0.22±0.08	14.57	0.87	0.07
Cadmium	905(1±0.02)	0.02±0.02	−0.26±0.03	22.35		
Iodine	1133(1±0.03)	0.04±0.04	−0.29±0.05	27.99	1.42	0.08
Barium	1048(1±0.04)	0.10±0.06	−0.38±0.08	25.89		
Lanthanum	1595(1±0.02)	0.02±0.03	−0.42±0.04	39.40	1.04	0.15
Cerium	1316(1±0.05)	0.05±0.06	−0.39±0.08	32.50		
Dysprosium	1652(1±0.03)	0.04±0.10	−0.34±0.13	40.80		
Tantalum	1558(1±0.02)	0.04±0.03	−0.22±0.04	38.48	2.50	0.06
Tungsten	1365(1±0.02)	0.07±0.03	−0.24±0.04	33.71		
Mercury	1345(1±0.02)	0.04±0.03	−0.31±0.04	33.22		
Lead	2274(1±0.01)	0.02±0.02	−0.42±0.03	56.17	2.72	0.08
Bismuth	2162(1±0.02)	0.05±0.03	−0.45±0.04	53.40	3.36	0.06
Thorium	3031(1±0.04)	0.06±0.05	−0.32±0.07	74.87		
Uranium	4630(1±0.02)	0.05±0.03	−0.17±0.04	114.36		

*$(\bar{\sigma}\Phi) = 2.47\times10^{3}$ millibarn-neutron. Errors are standard errors due to counting statistics only.

Ref. F. Tagliabue, J. Goldemberg
Nuclear Phys. 23, 144 (1961)

Elem. Sym.	A	Z
As	75	33

Method 22 MeV betatron; $Si^{28}(n,p)Al^{28}$ threshold detector.

Ref. No. 61 Ta 1 JHH

Reaction	E or ΔE	E_o	Γ	∫σdE	Jπ	Notes
$As^{75}(\gamma,n)$	Bremss. 22					$E_n > 6$ MeV. $W(\theta_n) = A + B \sin^2\theta$ where B/A = 0.52±0.21

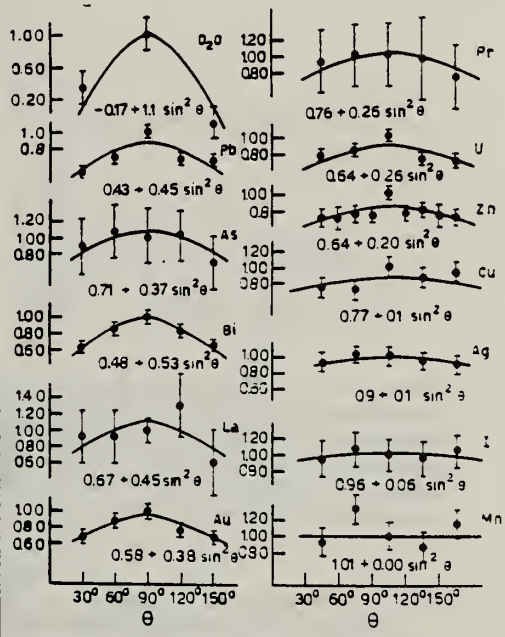

Figure 4: Angular distributions of fast photoneutron as observed with the $Si^{28}(n,p)Al^{28}$ detector. Data normalized at 90° in each case.

F.R. Metzger
Phys. Rev. 127, 220 (1962)

As	75	33

METHOD: Radioactive source; total absorption

REF. NO.: 62 Me 2 | NVB

REACTION	RESULT	EXCITATION ENERGY	SOURCE TYPE	SOURCE RANGE	DETECTOR TYPE	DETECTOR RANGE	ANGLE
G,G	LFT	1	D	1	NAI-D		0
		(265 keV)		(265 keV)			

LIFETIME

Mean life:

$\tau = (1.57 \pm 0.10)\ 10^{-11}$ sec.

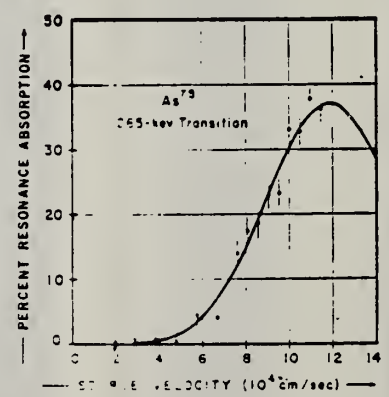

Fig. 3. Cur... [illegible] ... experimental absorption points ... with ... [illegible] ... calculated for ... $\Gamma = 4.07 \times 10$

TABLE I. Experimental results of the transmission experiments carried out with the 16.05 g cm² arsenic absorber. The absorptions expected for $\Gamma_\gamma = 4.07 \times 10^{-3}$ eV are tabulated for comparison purposes. In the last column, the widths calculated from the observed absorptions are listed.

Source velocity (10^4 cm/sec)	Absorption in %: Experiment	Absorption in %: Calculated for $\Gamma = 4.07 \times 10^{-3}$ eV	Width Γ_γ from experimental absorption (10^{-3} eV)
1.89	0.0 ± 2.0	0.07	≤ 120
2.94	0.7 ± 1.4	0.24	12 +6 −5
3.70	0.9 ± 2.0	0.7	5.4 ± 1.2
4.74	0.4 ± 1.4	1.7	1.0 ± 3.4
5.69	4.4 ± 2.1	3.7	4.8 ± 2.4
6.65	4.1 ± 1.6	7.4	2.1 ± 0.9
7.60	14.1 ± 1.9	12.6	4.2 ± 0.8
8.08	17.4 ± 2.1	16.0	4.5 ± 0.7
8.56	18.6 ± 2.1	19.6	3.8 ± 0.6
9.04	23.0 ± 2.1	23.4	4.0 ± 0.4
9.53	25.3 ± 2.1	27.2	3.3 ± 0.4
10.01	33.0 ± 1.9	30.5	4.5 ± 0.3
10.49	32.7 ± 1.9	33.4	4.0 ± 0.3
10.97	37.8 ± 1.9	35.6	4.4 ± 0.3
11.46	36.2 ± 1.9	36.8	4.0 ± 0.3
11.93	...	37.3	...
12.41	...	36.5	...
13.37	...	42.4	...

Ref. M. Sugawara, S. Mori, A. Ono, A. Hotta, M. Kimura
J. Phys. Soc. Japan 18, 17 (1963)

Elem. Sym.	A	Z
As	75	33

Method
≈ 25 MeV betatron; photon scattering; NaI spectrometer; NBS chamber

Ref. No. 63 Su 1 | NVB

Reaction	E or ΔE	E_o	Γ	$\int \sigma dE$	Jπ	Notes
$As^{75}(\gamma,\gamma)$	Bremss. 4-14					Detector at 120°. σ_{max} = 0.6 mb [Corrects results in J. Phys. Soc. Japan 16, 1657 (1961)]

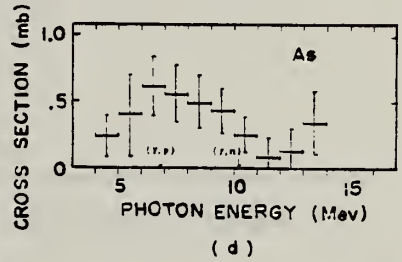

Fig. 2. The elastic scattering cross sections for Mg, Fe, Zn, As, Cd, Sb and Bi. The indicated spread in energy is the width of the sum-up channels, and the vertical lines are the statistical errors including background counts. The arrows represent the positions of the threshold energies of (γ, p) or (γ, n) reaction taken from Ref. 16. The open squares at 7 Mev are Reibel and Mann's data[9]. In Fig. 2(c), the cross section values, which are analyzed by displacing the sum-up channels by five channels to lower energy side than the positions generally used, are indicated by the closed triangles.

9) K. Reibel and A. K. Mann: Phys. Rev. **118** (1960) 701.
10) J. S. Pruitt and S. R. Domen: NBS Monograph 48 (1962).
11) E. G. Fuller and E. Hayward: J. Research 1857.
15) J. A. Stratton: *Electromagnetic Theory* (McGraw-Hill Book Co., New York, 1941).
16) *Nuclear Data Sheets*, National Academy of Sciences (N. R. C.).

REACTION	RESULT	EXCITATION ENERGY	SOURCE TYPE	SOURCE RANGE	DETECTOR TYPE	DETECTOR RANGE	ANGLE
C.XN	ABY	THR - 80	C	80	BF3-I		4 PI

Table 1

Element	Yield (36) eV cm^2 mol MeV	60 NZ/A (mb MeV)	Σ_0^{30}	Σ_0^{60}	$\Sigma_0^{30}/\Sigma_0^{60}$	E_m (MeV)	σ_m (mb)
$_{24}Cr$	83×10^{-5}	777	1.21	2.1	0.58	18.5	97
$_{25}Mn$	108×10^{-5}	813	1.52	2.33	0.65	18.5	114
$_{26}Fe$	68×10^{-5}	832	0.88	1.46	0.60	17.5	75
$_{27}Co$	89×10^{-5}	873	1.06	1.82	0.59	17.5	92
$_{28}Ni$	44×10^{-5}	879	0.55	1.07	0.51	18.5	56
$_{29}Cu$	95×10^{-5}	947	1.06	1.99	0.53	17.5	98
$_{30}Zn$	88×10^{-5}	975	0.94	1.68	0.56	17.5	86
$_{31}Ga$	130×10^{-5}	1034	1.29	2.18	0.59	17.5	151
$_{32}Ge$	139×10^{-5}	1084	1.35	2.29	0.59	17.5	158
$_{33}As$	137×10^{-5}	1109	1.22	2.18	0.56	17.5	127

$$\Sigma_0^{30} = \frac{\int_0^{30} \sigma(\gamma,xn)dE}{60\ NZ/A}$$

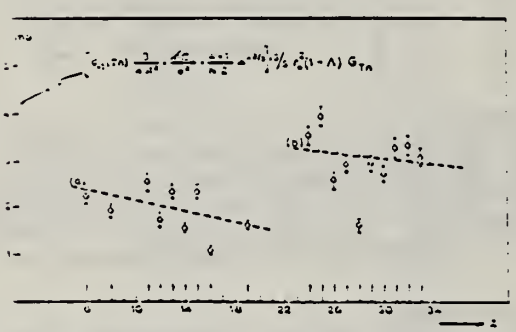

Fig. 2. Bremsstrahlung weighted cross sections, $\sigma_{-1}(Zn)$, conveniently normalized, versus Z.

Table 2

Element	maximum yield ($\times 10^{-5}$)	$\sigma_{-1}(Zn)$	$\sigma_{-1}(Zn) \times \left[\frac{3}{4\pi^2}\frac{Ne}{c^2}\left(\frac{A-1}{NZ}\right)A^{-\frac{1}{3}}\right]$
$_6C$	4.0	3.54	2.13
$_8O$	5.2	4.05	1.92
$_{11}Na$	13.6	11.60	2.49
$_{12}Mg$	10.0	8.81	1.73
$_{13}Al$	15.9	13.92	2.30
$_{14}Si$	11.6	9.96	1.55
$_{15}P$	19.3	17.56	2.32
$_{16}S$	9.5	8.35	1.07
$_{19}K$	19.3	17.90	1.81
$_{20}Ca$	12.1	11.68	1.02
$_{24}Cr$	86	81.6	3.56
$_{25}Mn$	116	78.1	3.96
$_{26}Fe$	71	80.6	2.56
$_{27}Co$	94	83.6	2.94
$_{28}Ni$	46	34.2	1.39
$_{29}Cu$	102	72.6	2.93
$_{30}Zn$	93	85.7	2.63
$_{31}Ga$	140	93.6	3.81
$_{32}Ge$	150	101.6	3.86
$_{33}As$	151	99.8	3.12

REF.

S. Costa, F. Ferroni, S. Ferroni and C. Molino
Phys. Letters 11, 324 (1964)

ELEM. SYM.	A	Z
As	75	33

METHOD

Synchrotron; $C^{12}(\gamma,n)$ monitor

REF. NO. 64 Co 2 JOC

REACTION	RESULT	EXCITATION ENERGY	SOURCE		DETECTOR		ANGLE
			TYPE	RANGE	TYPE	RANGE	

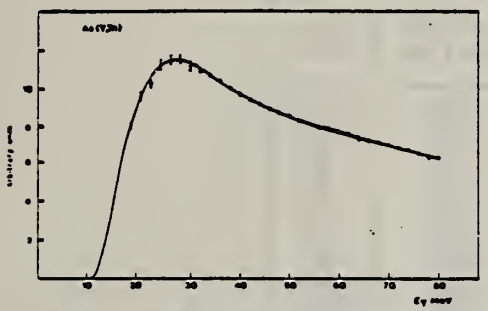

Fig. 1. A typical yield curve (As(γ, Tn)).

REF.

S. Costa, F. Ferrero, S. Ferroni and R. Malvano
Proc. Paris Conference 1034 (1964)

ELEM. SYM.	A	Z
As	75	33

METHOD

100 MeV synchrotron

REF. NO.	
64 Co 3	JDM

REACTION	RESULT	EXCITATION ENERGY	SOURCE		DETECTOR		ANGLE
			TYPE	RANGE	TYPE	RANGE	
G,N	ABΣ	THR-80	C	10-80	BF3-I		4PI

TABLE

ELEMENT	Yield (36 MeV) $\left(\frac{\text{n. cm}^2}{\text{mol. MeV}}\right) \times 10^5$	Σ_0^{30}	Σ_0^{80}	$\Sigma_0^{30}/\Sigma_0^{80}$	σ_{-1} (mb)
$_{24}$Cr	83	1.21	2.1	0.58	62
$_{25}$Mn	108	1.52	2.33	0.65	76
$_{26}$Fe	68	0.88	1.46	0.60	50
$_{27}$Co	89	1.08	1.82	0.59	64
$_{28}$Ni	44	0.55	1.07	0.51	34
$_{29}$Cu	95	1.06	1.99	0.53	72
$_{30}$Zn	88	0.94	1.68	0.56	66
$_{31}$Ga	130	1.29	2.18	0.59	94
$_{32}$Ge	139	1.35	2.29	0.59	101
$_{33}$As	137	1.22	2.18	0.56	100

$\sum_a^b = \frac{A}{60\,NZ}\int_a^b \sigma(E)\,dE$ is the integrated cross section measured in units of the classical dipole $60\,NZ/A$ mb. MeV.

REF.

Yu. K. Shubnyĭ, D. K. Kaipov, and R.B. Begzhanov
J. Exptl. Theoret. Phys. (USSR) 47, 16 (1964)
Soviet Phys. JETP 20, 11 (1965)

ELEM. SYM.	A	Z
As	75	33

METHOD

Resonance scattering; high temperature source

REF. NO.	
64 Sh 5	JOC

REACTION	RESULT	EXCITATION ENERGY	SOURCE		DETECTOR		ANGLE
			TYPE	RANGE	TYPE	RANGE	
G,G	LFT	1	D	1	NAI-D		122

$\tau_\gamma(M1) = (1.7 \pm 0.3) \times 10^{-11}$ sec for 0.265 MeV level.

REF.

D.S. Fielder, J. Le Tourneux, K. Min, and W. D. Whitehead
Phys. Rev. Letters 15, 33 (1965)

ELEM. SYM.	A	Z
As	75	33

METHOD

REF. NO.: 65 Fi 1 JOC

REACTION	RESULT	EXCITATION ENERGY	SOURCE		DETECTOR		ANGLE
			TYPE	RANGE	TYPE	RANGE	
G,XN	ABX	10 - 25	C	10-25	BF3 - I		4 PI

$$\int_{10}^{23} \sigma(xn) = 744 \pm 56 \text{ MeV-mb}$$

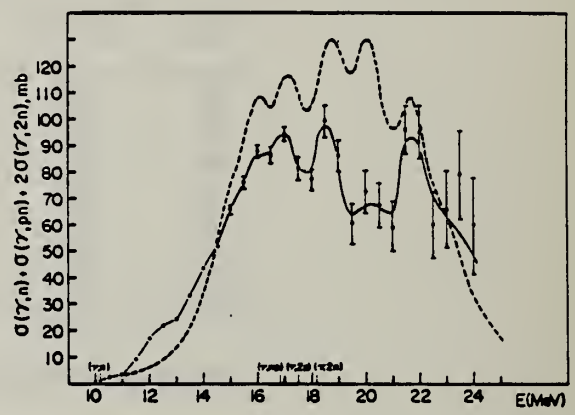

See: Phys. Rev. Letters 15, 530 (1965) for Danos et al. fit.

FIG. 1. Solid line: photoneutron production cross section of As^{75}; dashed line: total photoabsorption cross section.

U. Amaldi, Jr., G. Campos Venuti, G. Cortellessa, E. De Sanctis, S. Frullani, R. Lombard, P. Salvadori
Lincei-Rend.Sc.fis.mat. e nat. 41, 494 (1966)

As	75	33

METHOD

REF. NO. 66 Am 2 hmg

REACTION	RESULT	EXCITATION ENERGY	SOURCE TYPE	SOURCE RANGE	DETECTOR TYPE	DETECTOR RANGE	ANGLE
E,E/P	SPC	105-365	D	560-880	MAG-D	475	62

ANGLE OF E/ is 51

TABLE I.

	A	B	C
E_M (MeV)	27 ± 8	58 ± 14	111 ± 12
σ (MeV)	28 ± 12	32 ± 25	52 ± 20

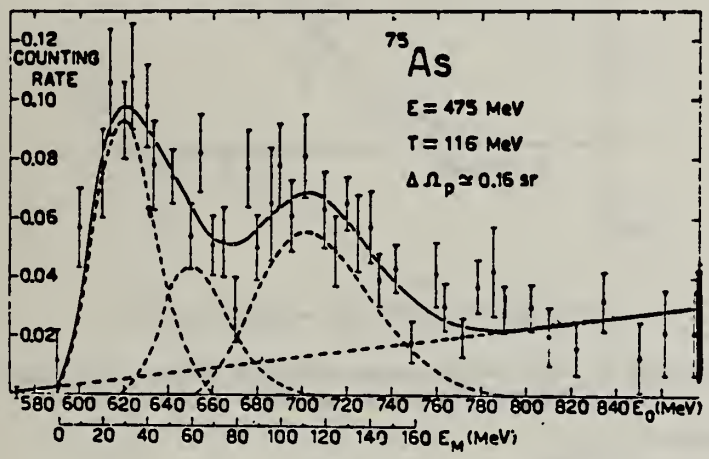

Fig. 1.

REF. R. R. Hurst and D. J. Donahue
Nucl. Phys. A91, 365 (1967)

ELEM. SYM.	A	Z
As	75	33

METHOD: Neutron capture gamma rays

REF. NO.: 67 Hu 1 EGF

REACTION	RESULT	EXCITATION ENERGY	SOURCE TYPE	SOURCE RANGE	DETECTOR TYPE	DETECTOR RANGE	ANGLE
G,N	ABX	11	D	11	BF3-I		4PI

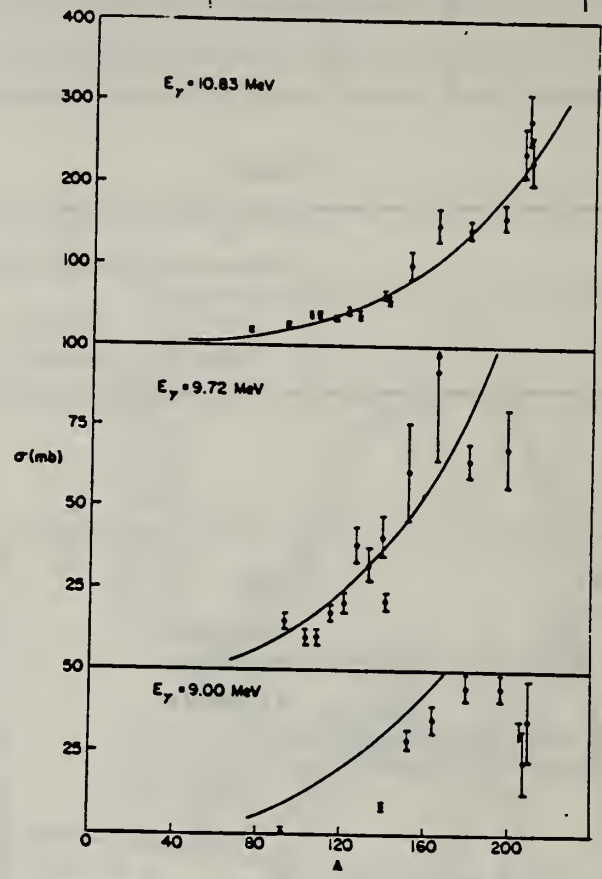

Fig. 1. Cross section (in mb) versus mass number of the target for gamma-ray energies of 9.00, 9.72 and 10.83 MeV. The solid lines are plots of eq. (1) in the text.

TABLE I
Photoneutron cross sections (mb)

Target	7.72 MeV	9.00 MeV	9.72 MeV	10.83 MeV
^{59}Co				9.0± 0.8
^{75}As				20.4± 1.7
^{93}Nb		0.53± 0.10	14.6± 2.2	25.8± 2.1
^{103}Rh			10.6± 1.7	38.8± 3.1
^{107}Ag, ^{109}Ag			10.0± 1.5	37.6± 2.9
^{115}In			17.1± 2.6	33.3± 2.7
^{121}Sb, ^{123}Sb			20.7± 3.1	42.5± 3.6
^{127}I			38.7± 5.8	38.8± 3.1
^{133}Cs			31.7± 4.8	52.5± 3.8
^{139}La		8.61± 0.86	40.8± 6.5	63.0± 5.0
^{141}Pr			21.5± 3.2	58.3± 4.1
^{151}Eu, ^{153}Eu		28.9 ± 3.2	61.3±14.7	102 ±18
^{165}Ho		35.6 ± 4.3	92.2±27.6	150 ±20
^{181}Ta	4.14±0.36	45.4 ± 3.7	65.0± 5.5	146 ±12
^{197}Au		44.5 ± 3.6	68.4±13.5	160 ±15
^{206}Pb		<34.3		238 ±29
^{208}Pb		22.6 ±11.3		280 ±31
^{209}Bi		36.1 ±12.0		226 ±27

REF.

H. Langhoff and M. Schumacher
Phys. Rev. 155, 1246 (1967)

ELEM. SYM.	A	Z
As	75	33

METHOD

Resonance Fluorescence

REF. NO.	
67 La 1	JDM

REACTION	RESULT	EXCITATION ENERGY	SOURCE		DETECTOR		ANGLE
			TYPE	RANGE	TYPE	RANGE	
G,G	LFT	1	D	1	NAI-D		DST

$$d\sigma/d\Omega = \sigma_0[1+A_2 P_2(\cos\theta)].$$

TABLE I. Results of the present investigation.

E_γ (keV)	Spin	A_2	$\delta_{E2/M1}$	$(g_2/g_1)\Gamma_0^2/\Gamma$ (eV)	Γ_0/Γ	τ_{level} (sec)
265	$\frac{3}{2}$	0.14±0.05	−0.01±0.04	$(3.62\pm0.20)\times10^{-5}$	0.97	$(1.71\pm0.10)\times10^{-11}$
280	$\frac{5}{2}$	0.92±0.12	−0.42±0.08	$(2.40\pm0.18)\times10^{-6}$	0.99	$(4.02\pm0.30)\times10^{-10}$

REF.
W. J. Alston III, H. H. Wilson and E. C. Booth
Nucl. Phys. A116, 281 (1968)

ELEM. SYM.	A	Z
As	75	33

METHOD

REF. NO.: 68 Al 1 egf

REACTION	RESULT	EXCITATION ENERGY	SOURCE TYPE	SOURCE RANGE	DETECTOR TYPE	DETECTOR RANGE	ANGLE
G,G	LFT	0 - 1	C	4	SCD-D	0-3	130
		(1.35)					

Angle greater than 90° for all measurements.

SELF-ABSORPTION

TABLE 1
Direct and absorption measurements of resonance fluorescence

Nucleus	E_r (MeV)	J_r	Γ_0/Γ	$gW\Gamma_0\Gamma_0/\Gamma$ (meV)	Error (%)	This work Γ_0 (meV)	Other work Γ_0
^{55}Mn	0.000	$\frac{5}{2}^-$					
	1.527	$(\frac{3}{2}^-)$	0.9	5.2	25	8–12	
				abs [a]	40	8.0	
	1.884	?	0.82 [b]	41	25	$50/gW'$	
				abs [a]	10	$55/g$	
	2.197	?	(0.8) [c]	17	25	$21/gW$	
				abs	20	$17/g$	
	2.252	?	(0.9) [c]	17	25	$19/gW$	
				abs	20	$13/g$	
	2.365	?	?	3.5	36	$(2–6)\Gamma/\Gamma_0$	
	2.564	?	(1.0)	50	25	$50/gW$	
				abs [a]	20	$61/g$	
	2.751	?	?	6.7	42	$6.7(\Gamma/\Gamma_0)/gW$	
^{59}Co	0.000	$\frac{7}{2}^-$					
	1.187	$(\frac{7}{2}^-)$	(1.0)	6.8	25	7.5	0.33(E2) [d]
				abs	25 [a]	12	
		$(\frac{3}{2}^-)$	(1.0)	6.8	25	(5.4–6.5)	0.27(E2)
				abs	25 [a]	9.6	
^{63}Cu	0.000	$\frac{3}{2}^-$					
	1.414	$\frac{1}{2}^-$	?	1.6	30	$(1.1–1.7)\Gamma/\Gamma_0$	
	1.551	$\frac{3}{2}^-$	?	1.7	37	$(1.7–2.5)\Gamma/\Gamma_0$	0.1(E2) [e]
^{69}Ga	0.000	$\frac{3}{2}^-$					
	0.872	$(\frac{1}{2}^-)$	0.95	1.1	35	$0.8/W$	
	1.107	$(\frac{1}{2}^-)$	0.95	8.0	20	$8.4/W$	
^{75}As	0.000	$\frac{3}{2}^-$					
	0.86	?	?	1.7	20	$1.7\ \Gamma/gW\Gamma_0$	
	1.07	?	?	2.6	30	$2.6\ \Gamma/gW\Gamma_0$	
	1.35	?	?	3.6	20	$3.6\ \Gamma/gW\Gamma_0$	
^{89}Y	0.000	$\frac{1}{2}^-$					
	1.51	$\frac{3}{2}^-$	(1.0)	52 [a]	30	28	0.37(E2) [f]
				abs [a]	15	22	

[a] Measured with NaI.
[b] Ref. [24]).
[c] Measured with a Ge(Li) detector to ±10 %.
[d] Ref. [13]). [e] Ref. [14]). [f] Ref. [23]).

[13] D.G. Alkhazov, K.I. Erokhina and I.K. Lemberg, Izv. Akad.Nauk.SSSR(ser.fiz.) 28 (1964) 1667.
[14] B.G. Harvey, J.R. Meriwether and A.Bussiere, Nucl. Phys. 70 (1965) 305.
[23] G.A. Peterson and J.Alster, Phys. Rev. 166 (1968) 136.
[24] N. Nath, M.A. Rothman, D.M. Van Patter and C.E. Mandeville, Nucl. Phys. 13 (1959) 74 .

REF.	ELEM. SYM.	A	Z
B. L. Berman, R. L. Bramblett, J. T. Caldwell, H. S. Davis, M. A. Kelly and S. C. Fultz Phys. Rev. 177, 1745 (1969)	As	75	33

METHOD	REF. NO.
	69 Be 1 hmg

REACTION	RESULT	EXCITATION ENERGY	SOURCE		DETECTOR		ANGLE
			TYPE	RANGE	TYPE	RANGE	
G,N	ABX	THR-30	D	10-30	BF3-I		4PI
G,2N	ABX	THR-30	D	18-30	BF3-I		4PI

TABLE VI. Integrated cross sections.

Nucleus	$\sigma_{int}[(\gamma,n)+(\gamma,pn)]$ (MeV-b)[a]	$\sigma_{int}(\gamma,2n)$ (MeV-b)[a]	$\frac{\sigma_{int}(\gamma,2n)}{\sigma_{int}(\gamma,\text{total})}$[b]	$\frac{1}{2}\pi\sigma_m\Gamma$ (MeV-b)[c]	$0.06(NZ/A)$ (MeV-b)
As^{75}	0.69	0.22	0.24	1.13	1.11
Ag^{107}	1.09	0.26	0.19	1.56	1.58
Cs^{133}	1.48	0.50	0.25[d]	2.27	1.94

[a] All measured integrated cross-section values are given for an energy region from threshold to 29.5 MeV.

[b] The word "total" in this table refers to the total photoneutron cross section $\sigma[(\gamma,n)+(\gamma,pn)+(\gamma,2n)+(\gamma,3n)]$, and excludes the (γ,γ) and (γ,p) cross sections.

[c] For As^{75} and Ag^{107}, the quantity tabulated is $\frac{1}{2}\pi[\sigma_m(1)\Gamma(1)+\sigma_m(2)\Gamma(2)]$.

[d] This value includes the contribution of $\sigma_{int}(\gamma,3n)$, which equals 0.01 MeV-b from threshold to 29.5 MeV.

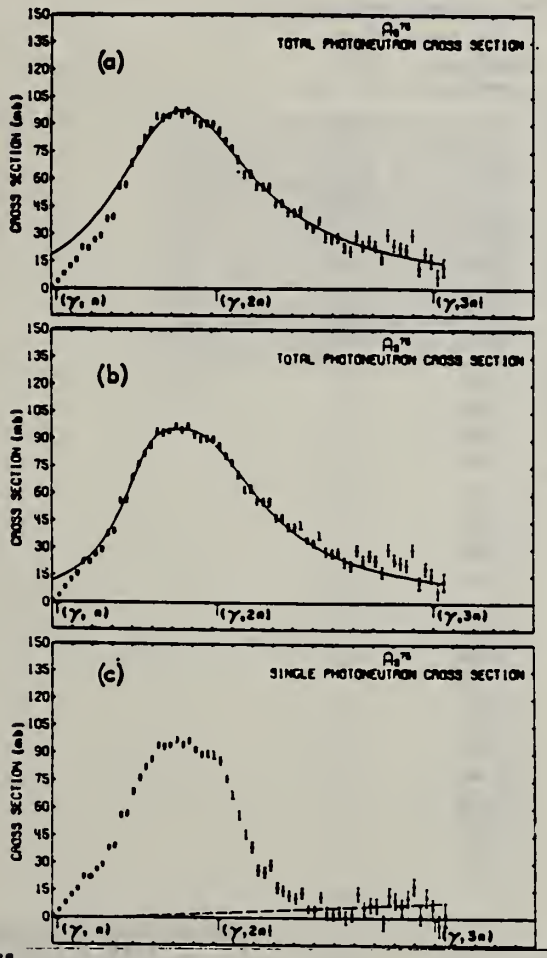

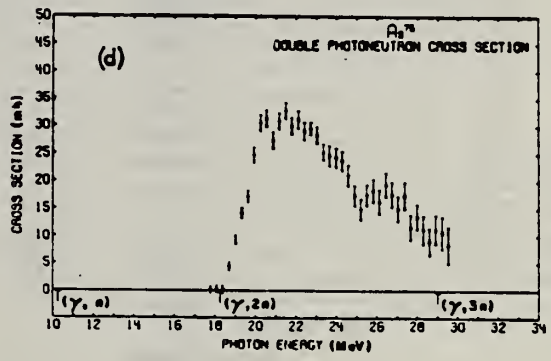

FIG. 5. Photoneutron cross sections for As^{75}. (a) Total photoneutron cross section $\sigma[(\gamma,n)+(\gamma,pn)+(\gamma,2n)]$. The solid line is a single-component Lorentz-curve fit to the giant-resonance data (13.6 to 21.3 MeV). (b) Total photoneutron cross section, repeated. The solid line is a two-component Lorentz-curve fit to the giant-resonance data. (c) Single photoneutron cross section $\sigma[(\gamma,n)+(\gamma,pn)]$. The dashed line represents the maximum systematic error owing to the uncertainty in the normalization of the positron bremsstrahlung subtraction. (d) Double photoneutron cross section $\sigma(\gamma,2n)$.

REF.

R. Moreh and O. Shahal
Phys. Rev. 188, 1765 (1969)

ELEM. SYM.	A	Z
As	75	33

METHOD

REF. NO. 69 Mo 3 hmg

REACTION	RESULT	EXCITATION ENERGY	SOURCE		DETECTOR		ANGLE
			TYPE	RANGE	TYPE	RANGE	
G,G	ABX	8	D	8	SCD-D	0-8	DST

J-PI, G-WIDTH, 7.646

Elastic and inelastic nuclear resonant scattering of monochromatic photons from ^{75}As have been studied using a 47-cc Ge(Li) detector. The γ source was provided by thermal-neutron capture in iron. The energy of the resonance level in ^{75}As was found to be 7.646 MeV. Assuming the high-energy lines to be primary transitions deexciting the resonance level, 25 energy levels were found from the ground state up to 2.6 MeV, seven of which may be identified with recently reported levels. By measuring the angular distribution of the scattered radiation, the spin of the scattering level was determined to be $\frac{1}{2}$ and the spins of 14 low-lying levels were thus found to be either $\frac{1}{2}$ or $\frac{3}{2}$. The total radiative width of the resonance level was determined and was found to be $\Gamma = 0.36 \pm 0.10$ eV and $\Gamma_0/\Gamma = 0.11$. The ^{75}As levels are compared with the predictions of the Coriolis coupling model.

TABLE I. γ energies and level energies in ^{75}As from (γ, γ') reaction. The level energies are obtained by assuming that the γ lines are emitted in primary transitions. The branching ratios of the decay of the 7.646-MeV level are given. Line energies are accurate to ±4 keV. Branching ratios of the strong intensity lines are accurate to ±8%. The existence of γ lines and levels in parentheses is uncertain.

γ energy (MeV)	Branching ratio (%)	Level energies (MeV) Present work	Ref. 5
7.646	11.3	0	0
7.447	1.5	0.199	0.199
7.381	40.9	0.265	0.265
...	...	...	0.280
...	...	...	0.304
(7.242)	...	(0.404)	0.401
7.178	9.7	0.468	0.469
(7.078)	...	(0.568)	0.572
7.028	2.9	0.618	0.618
...	...	...	0.822
...	...	...	1.021
6.570	5.7	1.076	...
6.512	6.8	1.134	...
6.443	2.1	1.203	...
6.384	1.4	1.262	...
...	...	...	1.3
6.291	0.9	1.355	...
6.214	7.1	1.432	...
6.141	1.2	1.505	...
6.039	1.2	1.607	1.6
...	...	...	1.8
(5.803)	0.1	(1.843)	...
5.774	2.5	1.872	...
5.582	0.5	2.064	...
5.549	1.8	2.097	...
5.470	0.9	2.176	...
5.413	1.0	2.233	...
(5.176)	...	(2.470)	...
(5.074)	...	(2.572)	...
5.050	0.5	2.596	...
(4.959)	...	(2.687)	...
2.596	...	...	...
1.911	...	...	...
1.799	...	...	...
1.432	...	...	...
1.028	...	...	...

[over]

TABLE II. Partial radiation widths Γ_γ and $E1$ and $M1$ radiation strengths of intense transitions from the 7.646-MeV resonance state; the most probable spins and parities are also given where values in parentheses indicate uncertain determinations. The level spacing D was taken to be 750 eV.

Transition energy (MeV)	Level energy (MeV)	Spin and parity	$\Gamma_\gamma \times 10^3$ (eV)	$k_{E1} \times 10^9$ $(\text{MeV})^{-3}$	$k_{M1} \times 10^9$ $(\text{MeV})^{-3}$
7.646	0	$\frac{3}{2}^-$	41	6.8	121
7.381	0.265	$(\frac{1}{2}^-, \frac{3}{2}^-)$	147	27.5	488
7.178	0.468	$(\frac{1}{2}^-, \frac{3}{2}^-)$	35	7.1	126
7.028	0.618	$(\frac{1}{2}, \frac{3}{2})$	10	2.3	40
6.570	1.076	$(\frac{1}{2}^-, \frac{3}{2}^-)$	21	5.4	97
6.512	1.134	$(\frac{1}{2}^-, \frac{3}{2}^-)$	25	6.6	118
6.443	1.203	$(\frac{1}{2}, \frac{3}{2})$	8	2.1	38
6.384	1.262	$(\frac{1}{2}, \frac{3}{2})$	5	1.5	26
6.214	1.432	$(\frac{1}{2}^-, \frac{3}{2}^-)$	26	8.0	142
6.141	1.505	$(\frac{1}{2}, \frac{3}{2})$	4	1.4	25
6.039	1.607	$(\frac{1}{2}, \frac{3}{2})$	4	1.5	26
5.774	1.872	$(\frac{1}{2}, \frac{3}{2})$	9	3.5	62
5.549	2.097	$(\frac{1}{2}, \frac{1}{2})$	7	2.8	51
5.470	2.176	$(\frac{1}{2}, \frac{3}{2})$	3	1.5	26
5.413	2.233	$(\frac{1}{2}, \frac{3}{2})$	4	1.7	30
	7.646	$\frac{1}{2}^{(+)}$			

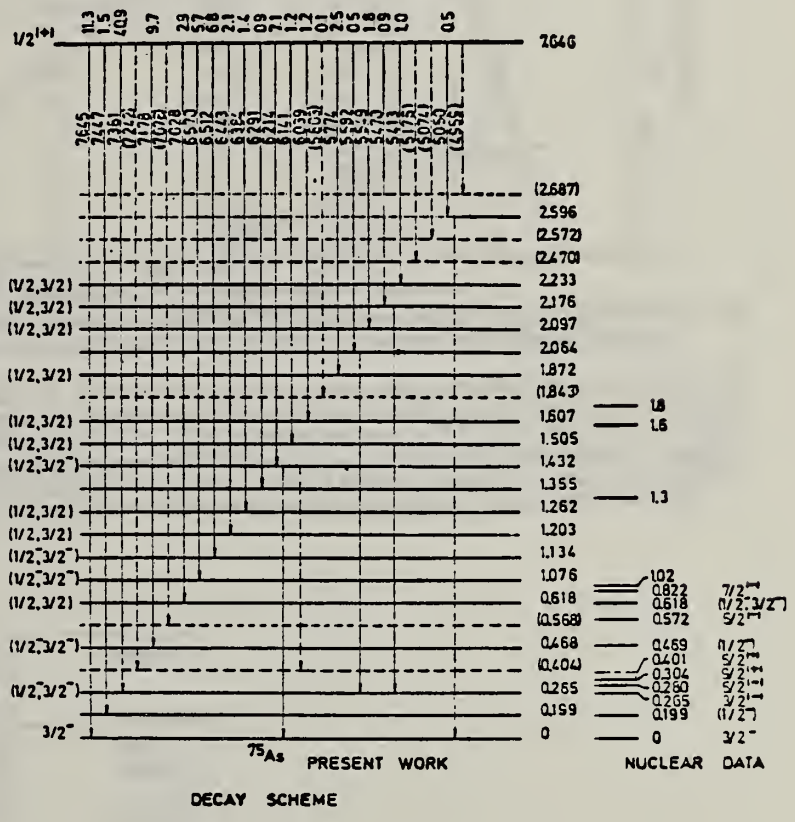

FIG. 4. Decay scheme of 7.646-MeV level of ^{75}As showing level energies and corresponding branching ratios as constructed by assuming that all high-energy γ lines in the scattered spectrum are emitted in primary transitions; broken lines indicate uncertain transitions and hence uncertain levels. Most probable spin and parities for some levels, assigned in the present work, are given where assignements in parentheses are uncertain. For comparison, the energy-level diagram as reported in Ref. 5 is also shown.

REF. H. Arenhovel, J. M. Maison
Nucl. Phys. A147, 305 (1970)

ELEM. SYM.	A	Z
As	75	33

METHOD

REF. NO. 70 Ar 1 egf

REACTION	RESULT	EXCITATION ENERGY	SOURCE		DETECTOR		ANGLE
			TYPE	RANGE	TYPE	RANGE	
G,G	ABX	12-30	C	32	NAI	12-30	DST

GETS G,G/ TO 2+

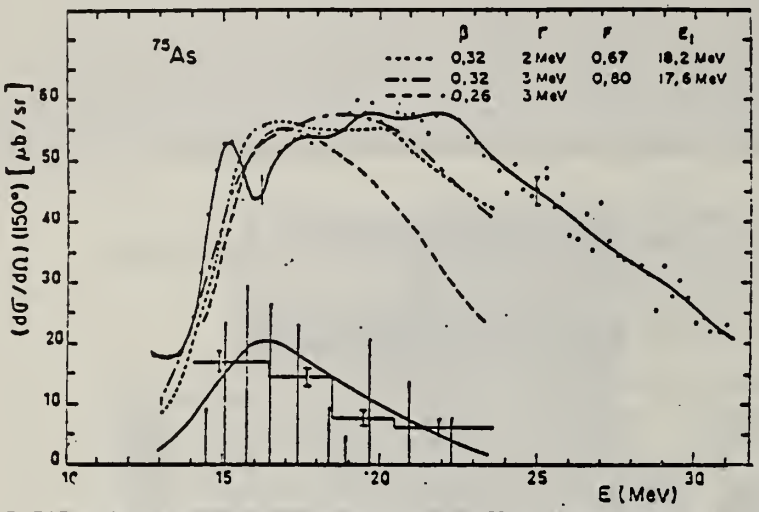

Fig. 7. Differential total scattering cross section at 150° for ^{75}As. See caption for fig. 4. In particular is shown the influence of parameter β on the shape of the scattering cross section.

Fig. 4. Differential total scattering cross section at 150° for natural Ti. The full curve through experimental points is only a guide for the eyes. The vertical bars represent the relative strength of dipole levels calculated by the D.C.M. with parameters of table 1. Theoretical elastic plus inelastic scattering is computed from these levels with a common width Γ (dashed curve). Experimental inelastic scattering (histogram) and theoretical inelastic scattering to the first 2^+ (full curve) are shown in the lower part of the figure. Open circles give the cross section after background subtraction.

TABLE 4

Integrated inelastic scattering cross section

Nucleus	Limits of integration (in MeV)	Experimental [a]) $\int \sigma_i(E)dE$ (MeV · μb)	Theoretical [a]) 2^+	$2^{-\prime}$ (MeV · μb)	Total
Ti(^{48}Ti)	16 −24	250 ± 50	425	109	534
^{51}V(^{52}Cr)	16.4−24.9	492 ± 50	509	116	579
Cr	16.4−23.4	431 ± 60	509	116	579
^{75}As(^{76}Se)	14.1−23.6	1254 ± 120	1373	414	1787
Se(^{80}Se)	14.1−24.6	1035 ± 100	1066	353	1419
^{89}Y					364
Cd(^{112}Cd)	13.6−23.3	3264 ± 240	1894	370	2264
In(^{114}Cd)	13.6−23.6	2840 ± 220	2173	388	2561
Sn(^{110}Sn)	14.2−24.2	2363 ± 220			643

[a]) We assume an angular distribution of the form $1 + \frac{1}{13}\cos^2\theta$.

REF. R. Moreh, S. Shlomo, and A. Wolf
Phys. Rev. C2, 1144 (1970)

ELEM. SYM.	A	Z
As	75	33

METHOD

REF. NO. 70 Mo 2 hmg

REACTION	RESULT	EXCITATION ENERGY	SOURCE		DETECTOR		ANGLE
			TYPE	RANGE	TYPE	RANGE	
G,G	ABX	8	D	8	SCD-D		DST
		(7.646)		(7.646)			

8 = 7.646, LFT

TABLE III. Summary of the results of spins, parities, and total widths of resonance levels excited by γ rays obtained from neutron capture in iron. Parities in parantheses are uncertain.

Isotope	Energy (MeV)	$\delta = \lvert E_r - E_e \rvert$ (eV)	J^π_0	J^π_r	Transition	Γ_0/Γ_γ (±8%)	Γ_γ (10^{-3} eV)
^{50}Cr	8.888	18 ±1	0^+	1	···	0.90	750 ± 200
^{62}Ni	7.646	14 ±1	0^+	1^-	*E*1	0.64	480 ± 50
^{74}Ge	6.018	4.5 ± 0.5	0^+	1^-	*E*1	0.19	120 ± 15
^{75}As	7.646	7.4 ± 0.3	$3/2^-$	$1/2^{(+)}$	···	0.11	360 ± 100
^{109}Ag	7.632	9 ±1	$1/2^-$	3/2	···	0.7	2 ± 1
^{112}Cd	7.632	4.8 ± 0.4	0^+	1^-	*E*1	0.55	86 ± 15
^{139}La	6.018	8.2 ± 0.6	$7/2^+$	$7/2^-$	*E*1	0.50	51^{+14}_{-6}
^{141}Pr	7.632	$11.4^{+0.3}_{-0.9}$	$5/2^+$	$5/2^+$	*M*1	0.46	72^{+24}_{-6}
^{205}Tl	7.646	9.3 ± 0.3	$1/2^+$	$1/2^{(-)}$	···	0.58	980 ± 90
^{208}Pb	7.279	7.1 ± 0.3	0^+	1^+	*M*1	1.00	780 ± 60

TABLE IV. Effective elastic scattering cross section $\langle\sigma_r\rangle = \sigma_0^m (\Gamma_0/\Gamma_\gamma)\Psi(x_0, t_0)$, where δ, *J*, Γ_0, Γ_γ were taken from Table III. The temperature of the scatterer was 300°K, while that of the iron γ source was 640°K.

Target	Resonance energy (MeV)	$\langle\sigma_r\rangle$ (mb)
^{50}Cr	8.888	905
^{62}Ni	7.646	569
^{74}Ge	6.018	61
^{75}As	7.646	4.4
^{109}Ag	7.632	3.5
^{112}Cd	7.632	198
^{139}La	6.018	39
^{141}Pr	7.632	20
^{205}Tl	7.646	574
^{208}Pb	7.279	5560

REF. G. J. Kumbartzki, Ung Kim and Ch. K. Kwan
Nucl. Phys. A160, 237 (1971)

ELEM. SYM.	A	Z
As	75	33

METHOD

REF. NO. 71 Ku 2 egf

REACTION	RESULT	EXCITATION ENERGY	SOURCE		DETECTOR		ANGLE
			TYPE	RANGE	TYPE	RANGE	
G,SPL	ABY	THR-999	C	900	ACT-I		4PI

$\sigma_q(A,Z) = K\exp\left[PA-R(A-SZ+TZ^2)^2\right]$, cross section per equivalent quantum. 999 = 1.5 GEV

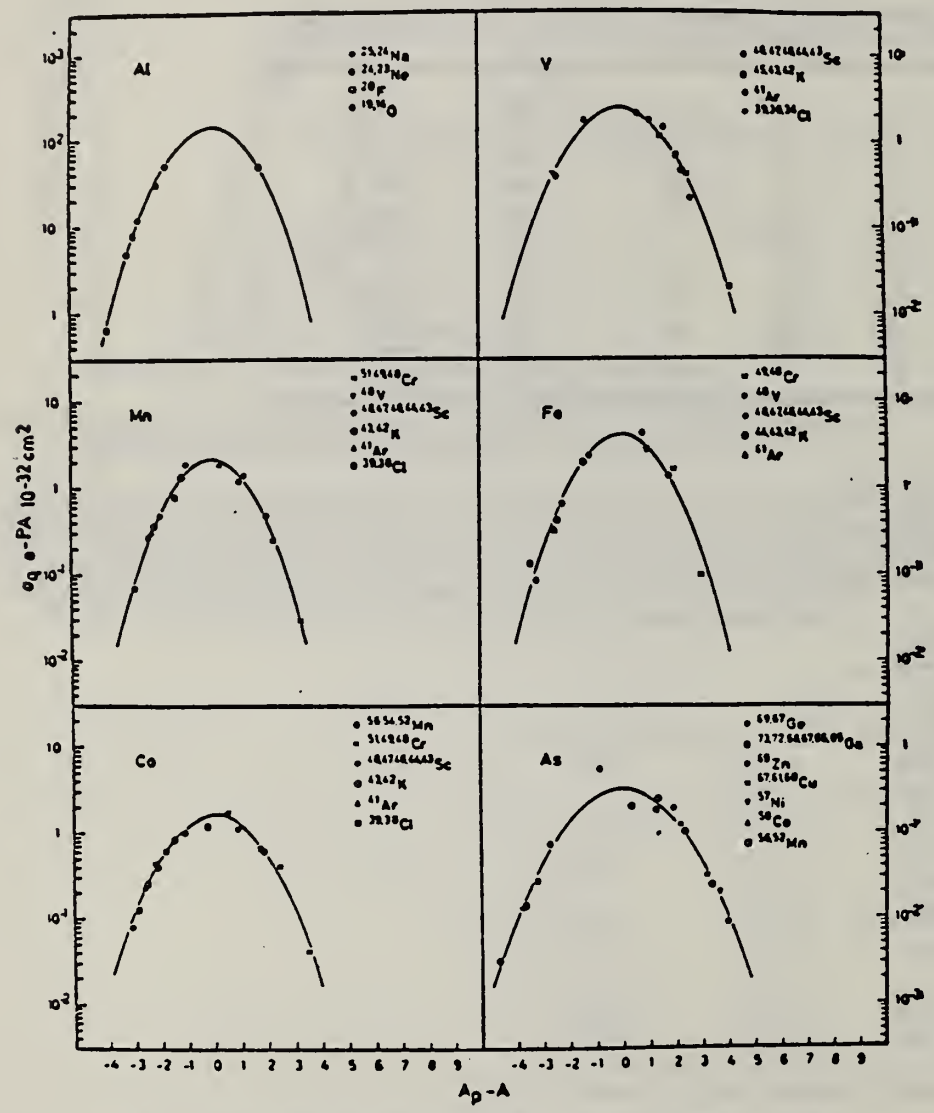

Fig. 4. Yield distributions from various targets with bremsstrahlung of 1.5 GeV.

[over]

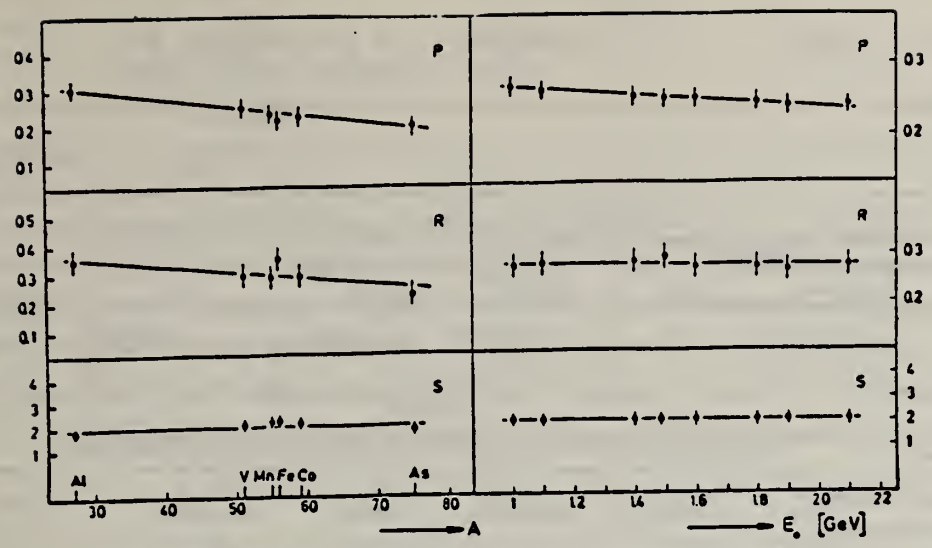

Fig. 6. Behaviour of the parameters P, R and S as functions of A and E_0.

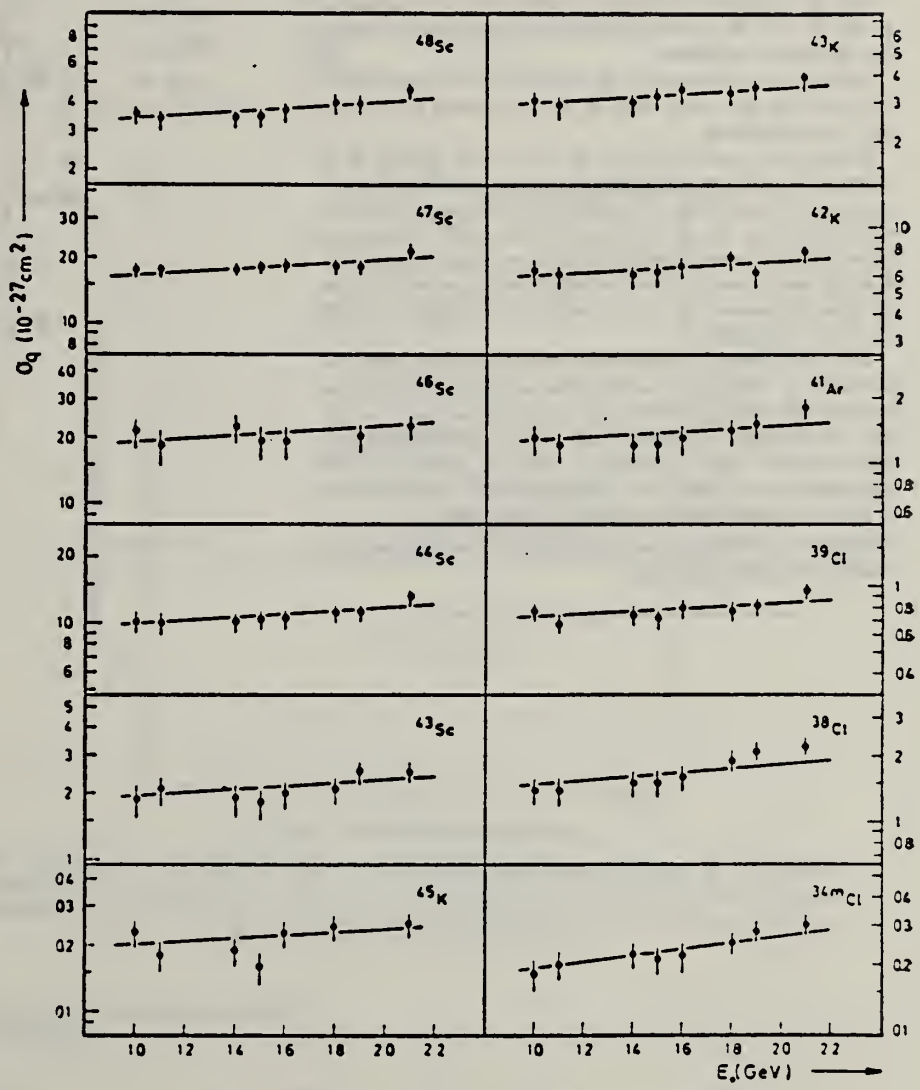

Fig. 5. Yields of spallation products using vanadium targets.

REF.

Tatsuya Saito
Nippon Kagaku Zasshi 92, 164 (1971)

ELEM. SYM.	A	Z
As	75	33

METHOD

REF. NO.	
71 Sa 1	egf

REACTION	RESULT	EXCITATION ENERGY	SOURCE		DETECTOR		ANGLE
			TYPE	RANGE	TYPE	RANGE	
G,N	ABY	10-68	C	10-68	ACT-I		4PI

Nippon Kagaku Zasshi. 92. 164~168(1971)

The Yields of Radioactivities Induced by (γ, n) Reactions with Bremsstrahlung up to 68 MeV

by Tatsuya SAITO

The (γ, n) yields of 12 target nuclides have been measured at 10, 13, 16, 30, 45 and 68 MeV bremsstrahlung by observing the induced activities.

The energy dependence of the yields has been investigated extensively in the same way as in the previous work at 20 MeV bremsstrahlung.

In the case of heavy nuclides, the yields rise greatly as a function of maximum bombarding energy up to 20 MeV, and rise gradually from 20 MeV up to 68 MeV. However, in the case of light nuclides, the yields rise greatly up to 30 MeV, because the neutron separation energies of light ones are larger than those of heavy ones, and the bremsstrahlung spectrum covers the giant resonance and so the yields rise gradually from 30 MeV up to 68 MeV.

The yields have approximately been estimated from the parameter of the giant resonance, that is the peak cross section and the half width, in order to compare with the experimental data. As a result, the experimental data of light nuclides and heavy ones are nearly in agreement with the estimated data of Nathans et al., Johns et al. and Montalbetti et al., but those of medium weight ones are relatively lower values.

Department of Chemistry, Faculty of Science, Tohoku University; Katahira-cho, Sendai-shi, Japan

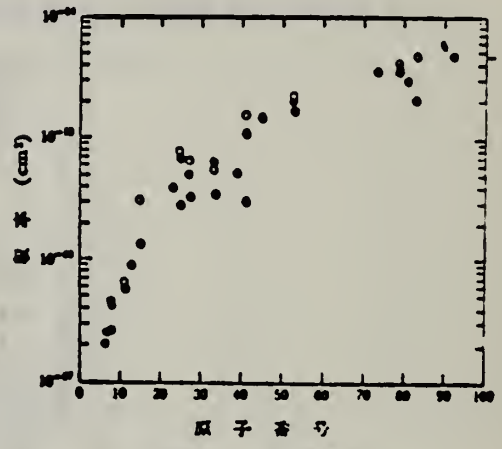

図 4 (γ, n)反応の収率の比較

REF. M. Eriksson and G. G. Jonsson
Nucl. Phys. A242, 507 (1975)

ELEM. SYM.	A	Z
As	75	33

METHOD

REF. NO. 75 Er 2 egf

REACTION	RESULT	EXCITATION ENERGY	SOURCE TYPE	SOURCE RANGE	DETECTOR TYPE	DETECTOR RANGE	ANGLE
G,SC44	ABY	THR-800	C	250-800	ACT-I		4PI

ISOMER RATIO

TABLE 2

Comparison between experimental and calculated cross sections and isomeric ratios

Target	$\bar{\sigma}_{exp}$ (mb) 250–800 MeV	σ_{MC} (mb) 400 MeV	$\bar{\sigma}_{SE}$ (mb) 250–800 MeV	$\sigma(m)/\sigma(g)_{exp}$ 250–800 MeV	$\sigma(m)/\sigma(g)_{calc}$ 400 MeV
^{45}Sc	≈ 0.5	0.58 ± 0.05		≈ 0	0.05
^{51}V	≈ 0.5	0.48 ± 0.05	0.47	0.7	0.72
^{55}Mn	0.40 ± 0.14	0.59 ± 0.05	0.28	1.08 ± 0.04	1.04
Fe	0.40 ± 0.14		0.26	1.00 ± 0.05	
^{59}Co	0.26 ± 0.10	0.34 ± 0.04 0.65 ± 0.07 [a])	0.18	1.26 ± 0.06	1.12 1.15 [a])
^{75}As		0.01 ± 0.01	0.044	1.9 ± 0.3	

[a]) 325 MeV.

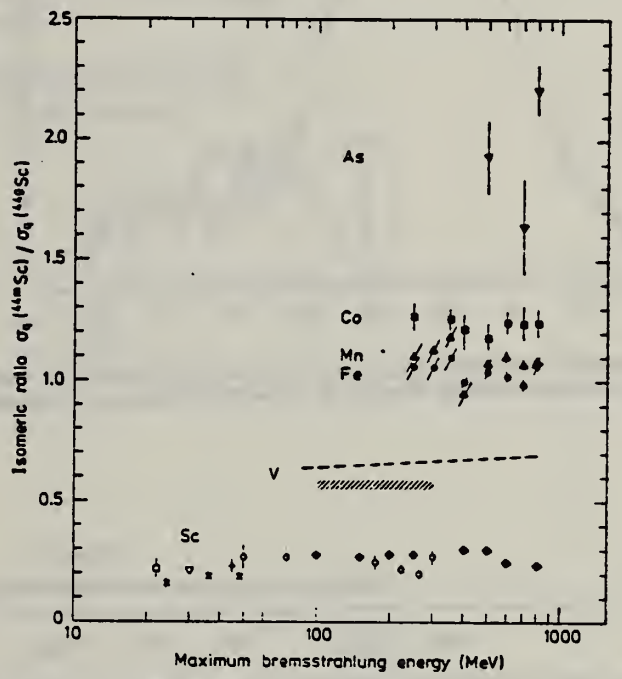

Fig. 6. Isomeric ratio $\sigma_q(^{44m}Sc)$ $\sigma_q(^{44g}Sc)$ versus bremsstrahlung end-point energy for the different targets. Sc target: ◆ – this work, □ – ref. [15]), × – ref. [16]), ▽ – ref. [17]), + – ref. [18]), ○ – ref. [19]); V target: dashed curve – ref. [20]), dashed area – ref. [21]); Fe target: ⊙ – this work; Mn target: ▲ – this work; Co target: ■ – this work: As target: ▼ – this work.

15) S. A. Steinberg, B. Sc. thesis, Univ. of Illinois, 1963, unpublished (value taken from ref. [19]))
16) J. R. Tatarczuk and H. A. Medicus, Phys. Rev. 143 (1966) 818
17) T. Kato and Y. Oka, Talanta 19 (1972) 515
18) R. Völpel, Nucl. Phys. A182 (1972) 411
19) W. B. Walters and J. P. Hummel, Phys. Rev. 150 (1966) 867
20) B. Bülow, Lund, private communication (preliminary results)
21) R. A. Meyer, thesis, Univ. of Illinois, 1963, unpublished

REF.		ELEM. SYM.	A	Z
	P. Carlos, H. Beil, R. Bergere, J. Fagot, A. Lepretre, A. Veyssiere, G. V. Solodukhov Nucl. Phys. A258, 365 (1976)	As	75	33

METHOD	REF. NO.
	76 Ca 1 egf

REACTION	RESULT	EXCITATION ENERGY	SOURCE		DETECTOR		ANGLE
			TYPE	RANGE	TYPE	RANGE	
G,N	ABX	10- 26	D	10- 26	MOD-I		4PI
G,2N	ABX	18- 26	D	10- 26	MOD-I		4PI

987+

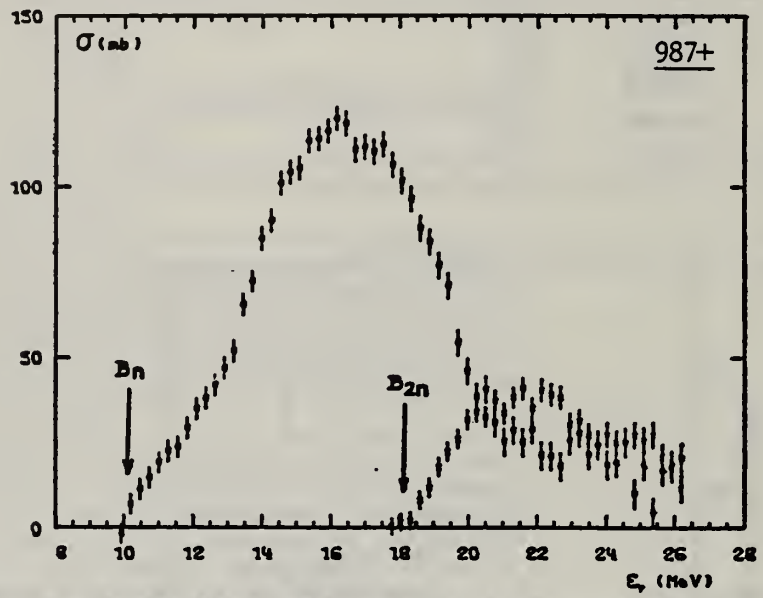

Fig. 7. Partial photoneutron cross sections $[\sigma(\gamma, n)+\sigma(\gamma, pn)]$ and $\sigma(\gamma, 2n)$ for ^{75}As. Arrows B_n and B_{2n} indicate theoretical threshold values for (γ, n) and $(\gamma, 2n)$ reactions respectively.

TABLE 3

Integrated photoneutron cross sections and comparison with sum rules

Nucleus	^{64}Zn	^{69}Ga / ^{71}Ga	^{70}Ge	^{72}Ge	^{74}Ge	^{76}Ge	^{75}As	^{76}Se	^{78}Se	^{80}Se	^{82}Se
E_M (MeV)	29	26.5	26.5	26.5	26.5	26.5	26.5	26.5	26.5	26.5	26.5
σ_{0a} (MeV · b)	0.75	0.91	0.78	0.94	1.02	1.12	1.09	1.01	1.06	1.11	1.13
$\frac{\sigma_{0a}A}{0.06\,NZ}$	0.78	0.87	0.75	0.88	0.94	1	0.98	0.90	0.92	0.94	0.95
$B_n - B_p$ (MeV)	4.2	3.7 / 1.4	3	1	−0.8	−2.6	3.3	1.7	0.1	−1.5	−3
σ_{-1a} (mb)	38	52	44	54	59	64	63	58	62	65	67
$\sigma_{-1a}A^{-\frac{1}{3}}$ (mb)	0.15	0.18	0.15	0.18	0.19	0.20	0.20	0.18	0.19	0.19	0.19
σ_{-2a} (mb · MeV^{-1})	2.0	3.1	2.5	3.2	3.6	3.9	3.7	3.4	3.8	3.9	4.2
$\sigma_{-2a}A^{-\frac{1}{3}}$ (μb · MeV^{-1})	1.9	2.6	2.1	2.6	2.8	2.9	2.8	2.5	2.7	2.6	2.7

The notation used is defined in the text. The average experimental errors $\Delta\sigma_{0a}/\sigma_{0a}$, $\Delta\sigma_{-1a}/\sigma_{-1a}$ and $\Delta\sigma_{-2a}/\sigma_{-2a}$ are approximately 8 %.

REF. Y. Cauchois, H. Ben Abdelaziz, R. Khérouf, C. Schloesing-Möller
J. Phys. G7, 1539 (1981)

ELEM. SYM.	A	Z
As	75	33

METHOD

REF. NO. 81 Ca 2 hg

REACTION	RESULT	EXCITATION ENERGY	SOURCE		DETECTOR		ANGLE
			TYPE	RANGE	TYPE	RANGE	
G,G	LFT	0 - 2	C	0 - 2	SCD-D		
		(.572 - 1.370)					

7 LEVELS, .57-1.37MEV

Abstract. Lifetimes of 49 excited states below 1.65 MeV have been measured in ^{24}Mg, ^{27}Al, ^{48}Ti, ^{58}Ni, ^{59}Co, ^{61,62}Ni, ^{63,65}Cu, ^{64,66,68}Zn, ^{75}As, ^{103}Rh, ^{113,115}In, ^{116,118,120}Sn and ^{121,123}Sb by means of nuclear resonance fluorescence experiments. The levels are excited by bremsstrahlung x-ray photons. The self-absorption technique applied to suitable cases provides nuclear absorption cross sections, widths and lifetimes from which the x-ray spectral distributions are also obtained. Scattering experiments are performed for all other cases in order to obtain widths and lifetimes from these x-ray photon curves. The Compton effect in the sample is taken into account. Self-absorption provides $g\Gamma_0$ from which Γ is deduced using adopted J^π and Γ_0/Γ values; scattering provides $u = g(\Gamma_0^2/\Gamma)W(\theta)$ from which Γ is also deduced with J, Γ_0/Γ and mixing ratios taken from the literature. Thanks to simultaneous determination of the x-ray spectra all the lifetimes as given by our programs with their statistical errors form an unusually coherent set of values.

NUCLEAR REACTIONS (γ, γ), bremsstrahlung excitation; natural isotopes: ^{24}Mg, ^{27}Al, ^{48}Ti, ^{58}Ni, ^{59}Co, ^{61,62}Ni, ^{63,65}Cu, ^{64,66,68}Zn, ^{75}As, ^{103}Rh, ^{113,115}In, ^{116,118,120}Sn and ^{121,123}Sb; $E \simeq 0.5$–1.65 MeV; measured $g\Gamma_0$ or $g(\Gamma_0^2/\Gamma)W(\theta)$; deduced $T_{1/2}$.

(OVER)

Tableau 3. Résultats des mesures des niveaux étudiés par diffusion.

Table 3. Results obtained using the diffusion method.

Isotope	Energie (keV)	J^π	J_0^π	Γ_0/Γ	δ	$u=g(\Gamma_0^2/\Gamma)W(\theta)$ (meV)	τ (ps) ce travail	τ_{ref} (ps)	Références†
^{24}Mg	1368.59(4)	2^+	0^+	1	E2	1,08(13)	1,76(21)	1,98(4)	Endt et van der Leun (1978)
^{27}Al	1014,45(3)	$\frac{1}{2}^+$	$\frac{1}{2}^+$	0,971	+0.351(12)	0,186(13)	2.20(16)	2,12(8)	Endt et van der Leun (1978)
^{46}Ti	983.512(3)	2^+	0^+	1	E2	0.282(23)	6,74(55)	6.1(13)	Been (1978)
^{58}Ni	1454,45(15)	2^+	0^+	1	E2	2,11(26)	0,90(11)	0.92(3)	Kocher et Auble (1976)
^{59}Co	1099,224(25)	$\frac{1}{2}^-$	$\frac{7}{2}^-$	1	(E2)	0,069(8)	4,79(55)	3,17(58)	Kim (1976)
^{59}Co	1458.8(3)	$\frac{9}{2}^-$	$\frac{7}{2}^-$	0.91	(E2)	0,68(8)	1,17(14)	1.52(16)	Kim (1976)
^{59}Co	1480.9(3)	$\frac{3}{2}^-$	$\frac{7}{2}^-$	0.8	$<0.35^a$	1,23(15)	0,254(31)	0.31(3)	Kim (1976)
^{61}Ni	1185.7(6)	$\frac{3}{2}^-$	$\frac{1}{2}^-$	0,77(8)[i]	|0,14|	1,88(49)	0,21(5)	0,16(3)	Andreev *et al* (1974)
^{62}Ni	1172,91(9)	2^+	0^+	1	E2	0,88(17)	2,15(42)	2,09(3)	Halbert (1979a)
^{63}Cu	1327.00(7)	$\frac{7}{2}^-$	$\frac{3}{2}^-$	0.84	(E2)	1,04(14)	0,84(11)	0,88(4)	Auble (1979b)
^{63}Cu	1412.05(4)	$\frac{5}{2}^-$	$\frac{1}{2}^-$	0,72	$+0.61\{^{+29}_{-8}\}$	0.260(38)	1,90(28)	1,61(3)	Auble (1979b)
^{64}Zn	991.54(7)	2^+	0^+	1	E2	0,640(54)	2,97(25)	2,60(13)[j]	Halbert (1979b)
^{65}Cu	1481.83(5)	$\frac{7}{2}^-$	$\frac{3}{2}^-$	0,85	(E2)	1,13(19)	0,79(13)	0,49(5)	Auble (1975a)
^{66}Zn	1039,37(6)	2^+	0^+	1	E2	0,70(6)	2,71(23)	2.25(15)	Auble (1975b)
^{68}Zn	1077.38(5)	2^+	0^+	1	E2	0,70(6)	2,71(23)	2,34(23)	Lewis (1975)
^{73}As	572.5(10)	$\frac{3}{2}^-$	$\frac{3}{2}^-$	1[d]	0,39[b]	0,236(26)	4,14(46)	3,5(9)	Horen et Lewis (1975)
^{73}As	823.0(10)	$\frac{7}{2}^-$	$\frac{3}{2}^-$	0,86[d]	(E2)	0,214(22)	4,27(43)	3.5(3)	Robinson *et al* (1967)
^{73}As	865.5(10)	$\frac{5}{2}^+$	$\frac{3}{2}^-$	0,83[d]	—[c]	0,78(6)	0,863(68)	0,60(12)	Celliers *et al* (1977)
^{73}As	1076.0(10)	$\frac{1}{2}^-$	$\frac{3}{2}^-$	0,94[d]	0,38[d]	1,97(13)	0,287(19)	0,32(7)	Celliers *et al* (1977)
^{73}As	1128.5(10)	$\frac{1}{2}^+$	$\frac{3}{2}^-$	1	E1[d]	0,224(24)	1,47(16)	—	
^{75}As	1349.0(10)	$\frac{1}{2}^-$	$\frac{3}{2}^-$	0.67[d]	0.20[d]	1.61(29)	0,180(32)	0.12(3)	Wilson (1970)
^{75}As	1370.0(10)	$\frac{1}{2}^-$	$\frac{3}{2}^-$	0.47[d]	0.47[d]	0,64(13)	0,218(44)	—	
^{103}Rh	803.1(2)	$\frac{1}{2}^-$	$\frac{1}{2}^-$	0.70	M1	1,85(16)	0,174(15)	—	Harmatz (1979)
^{103}Rh	1277.0(2)	$\frac{3}{2}^-$	$\frac{1}{2}^-$	0.75	$-0.62(30)^e$	0,81(9)	0.87(10)	1.3(9)	Harmatz (1979)
^{113}In	1177(1)	$\frac{9}{2}^+$	$\frac{9}{2}^+$	1	+0.5(2)	9.1(8)	0,086(8)	0.10(6)	Tuttle *et al* (1976)
^{113}In	1510(1)	$\frac{7}{2}^+$	$\frac{9}{2}^+$	0.935	$-0.5\{^{+1}_{-3}\}$	6,4(9)	0.071(10)	$0.11\{^{+4}_{-3}\}$	Tuttle *et al* (1976)
^{115}In	1077.7(10)	$\frac{3}{2}^+$	$\frac{9}{2}^+$	0.81[j]	(E2)	0.159(24)	1.61(24)	1.23(7)	Tuttle *et al* (1976)
^{115}In	1290.59(3)	$\frac{11}{2}^+$	$\frac{9}{2}^+$	0.98[j]	(E2)	1,31(11)	0.66(6)	0.55(4)	Tuttle *et al* (1976)
^{115}In	1448.78(3)	$\frac{5}{2}^+$	$\frac{9}{2}^+$	0.86	-8^f	0,90(11)	0.50(6)	0.52(20)	Tuttle *et al* (1976)
^{115}In	1486.1(1)	$\frac{9}{2}^-$	$\frac{9}{2}^+$	0.787	-0.8^f	0,63(9)	0.63(9)	0.4(3)	Tuttle *et al* (1976)
^{115}In	1497.2(4)	$(\frac{5}{2}^+)$	$\frac{9}{2}^+$	<1	(E2)	1.33(16)	$<0.30(4)$	—	
^{115}In	1607.8(15)	$(\frac{5}{2}^+)$	$\frac{9}{2}^+$	$\leqslant 1$	(E2)	1.54(24)	$\leqslant 0.26(4)$	—	
^{116}Sn	1293.54(2)	2^+	0^+	1	E2	3,58(37)	0,53(6)	0.522(14)[k]	Carlson *et al* (1975)
^{118}Sn	1229.64(4)	2^+	0^+	1	E2	2,75(28)	0,69(7)	0.67(2)	Carlson *et al* (1976)
^{120}Sn	1171.6(2)	2^+	0^+	1	E2	1.83(16)	1.04(9)	0.91(2)	Kocher (1976)
^{121}Sb	1023.5(10)	$\frac{7}{2}^-$	$\frac{5}{2}^-$	1	|0.57|[g]	3.69(34)	0.228(21)	0.20(7)[h]	Tamura *et al* (1979)
^{121}Sb	1105.5(10)	$\frac{9}{2}^+$	$\frac{7}{2}^+$	0.4	—	0,47(4)	0.42(4)	—	
^{121}Sb	1142.5(10)	$\frac{9}{2}^+$	$\frac{5}{2}^+$	0.6	(E2)	0.85(8)	0.449(40)	0.41(8)[h]	Booth *et al* (1973)
^{121}Sb	1384.0(10)	$\frac{3}{2}^+$	$\frac{5}{2}^+$	1	|0.45|[g]	4,7(5)	0.092(10)	0.088(14)[h]	Booth *et al* (1973)
^{123}Sb	1029.5(10)	$\frac{9}{2}^+$	$\frac{7}{2}^+$	1	|0.57|[g]	2.96(27)	0.272(25)	0.26(4)[h]	Booth *et al* (1973)
^{123}Sb	1086.5(10)	$\frac{9}{2}^+$	$\frac{7}{2}^+$	1	$\|\delta\|>1.26^g$	1.06(9)	0.67(6)	0.72(15)[h]	Booth *et al* (1973)

† Références pour les colonnes 3, 4, 5, 6 et 9 de chaque ligne, sauf indication appelée au bas de ce tableau. Pour les autres données se reporter au texte.

Remarque. Pour calculer δ^2 quand nous ne disposons que de $B(E2)$, pour un mélange (E2) + (M1), nous déduisons $g\Gamma_0(E2) \propto B(E2)E_\gamma^5$; en admettant $W(\theta)=1$ et connaissant Γ_0/Γ, notre détermination de u donne une première approximation de $g\Gamma_0$ d'où une valeur de $\delta^2=(g\Gamma_0(E2))/(g\Gamma_0-g\Gamma_0(E2))$ qui permet d'améliorer $W(\theta)$ et $g\Gamma_0$ de proche en proche.

[a] Swann (1971); [b] Robinson *et al* (1967); [c] $W(\theta)=0.99$ calculé d'après la formule de Celliers *et al* (1977); [d] Abbondanno *et al* (1978); [e] Sayer *et al* (1972); [f] Tuttle *et al* (1976); [g] d'après $B(E2)$ de Barnes *et al* (1966); [h] calculé d'après Booth *et al* (1973); [i] Williams *et al* (1975); [j] Dietrich *et al* (1970).

SELENIUM

Z=34

Selenium was identified as an element in 1817 by J. J. Berzelius a professer of chemistry in Stockholm, Sweden. While looking for a method of producing sulfuric acid, he observed a sediment with an offensive odor — an indicator of the scarce element tellurium discovered thirty-five years earlier. Further analysis showed it to be a new element with chemical properties similar to tellurium. Because these elements were so closely related, Berzelius named the new substance selenium, from the Greek word *selene*, meaning the moon since tellurium was named from the Latin word *tellus*, meaning the earth.

REF.
T. Kaminishi, C. Kojima
Jap. J. Appl. Phys. 2, 399 (1963)

ELEM. SYM.	A	-
Se		34

METHOD
Linac; isomer yield; activity

REF. NO.	
63 Ka 2	NVB

REACTION	RESULT	EXCITATION ENERGY	SOURCE		DETECTOR		ANGLE
			TYPE	RANGE	TYPE	RANGE	
G,G/	RLY	1	C5		ACT-I		4PI
		(0.16)					

Table II. The isomers observed

Isomer	Observed value		Referenced value[1][13]	
	Half-life	Energy (MeV)	Half-life	Energy (MeV)
Se-77m	17.5 sec	0.160	17.5 sec	0.161
Br-79m	4.80 sec	0.209	4.8 sec	0.208
Sr-87m	2.3 hr	0.390	2.8 hr	0.388
Y-89m	15.0 sec	0.920	14 sec	0.915
Rh-103m	58 min	*	57 min	0.040
Ag-107m	42 sec	0.95	44 sec	0.094
Ag-109m			40 sec	0.088
Cd-111m	47 min	0.150,0.255	49 min	0.150,0.247
In-115m	4.5 hr	0.335	4.5 hr	0.335
Sn-117m	17 day	0.160	14 day	0.159,0.161
Ba-137m	2.6 min	0.660	2.6 min	0.662
Er-167m	2.10 sec	0.209	2.5 sec	0.208
Hf-179m	18.5 sec	0.157,0.215	19 sec	0.161,0.217
W-183m	5.4 sec	0.200,0.170,0.115	5.5 sec	0.1025,0.2915 others
Ir-191m	4.90 sac	0.129, <0.07	4.9 sec	0.042-0.129
Pt-195m	4.5 day	0.065**	4.1 day	0.031-0.130
Au-197m	7.0 sec	0.10,0.27,0.40	7.2 sec	0.130,0.270,0.407
Hg-199m	43 min	0.160,0.370	42 min	0.158,0.368

* This isomer was measured with a G-M flow counter.
** This value corresponds to Pt-K X-ray energy.

Table III. Induced activation rate

Element	Beam energy (MeV)	Counting rate (×10000 cpm)	Sample form
Se	5	1300	metallic pellet
Br	4	1600	NaBr grain
Sr	6	0.3	$SrCO_3$ powder
Y	5	90	metallic grain
Rh	5	(0.2)*	$RhCl_3$ grain
Ag	5	180	metallic plate
Cd	6	0.5	$CdCl_2$ grain
In	6	8	metallic plate
Sn	6	0.0005	metallic plate
Ba	5	0.6	BaS powder
Er	4	4900	Er_2O_3 powder
Hf	5	1600	metallic plate
W	5	120	metallic powder
Ir	5	2100	metallic powder
Pt	5	0.3	metallic plate
Au	4	4300	metallic plate
Hg	6	0.09	metallic liquid

* The value measured with a G-M flow counter.

REF.

A. Veres
Acta Phys. Acad. Sci.Hung. 16, 261-73 (1963)

ELEM. SYM.	A	Z
Se		34

METHOD

Radioactive source

REF. NO. 63 Ve 2 NVB

REACTION	RESULT	EXCITATION ENERGY	SOURCE		DETECTOR		ANGLE
			TYPE	RANGE	TYPE	RANGE	
G,G/	ABX	0-1	D	0-1	NAI-D		

ISØMERS

Таблица II

Измеренные значения после облучения, сравниваемые с другими литературными данными

Элемент	Активность облучения после первого измерения (имп/мин.)	Активн. экстрп. в конце облуч. (имп/мин.)	Литературные данные		Данные измерений		σ_m (10^{-28} см^2)	Γ_{ym} (10^{-3} эв)
			$T_{1/2}$	E (кэв)	$T_{1/2}$	E (кэв)		
Se-77m	3842±96	5400	17,5 сек.	160	18,1±1 сек.	160±10	9,5	1,75
Sr-87m	191±5	200	2,8 ч.	390	2,9±0,1 ч.	365±25	0,85	0,2
У-89m	96±20	170	16 сек.	910	16,7±5 сек.		0,08	0,02
Rh-103m	28±5	31	57 мин.	40	58±2 мин.	20,5±0,5	0,08	0,01
Ag-107m	220±14	250	44 сек.	93	43,8±0,6 сек	91±10	0,8	0,2
Ag-109m			39 сек.	88				
Hf-179m	80±18	155	19 сек.	160; 215	19±2 сек.		1	0,2
Ir-191m	90±20	250	4,9 сек.	42; 130	5±2 сек.		5,6	1
Pt-195m	90±9	100	3,5 д.	31; 100; 130;	3,5±0,2 д.	32±3 67,5±5 96±5 130±10	0,2	0,04
Au-197m	240±16	520	7,2 сек.	130; 277; 407	7,2±1 сек.	68:130: 280±20 390±20	0,07	0,01
Hg-199m	9,6±3,2		42 мин.	160; 370			0,005	0,001

REF. G. Ben-David, B. Arad, J. Balderman, and Y. Schlesinger
Phys. Rev. 146, B852 (1966)

ELEM. SYM.	A	Z
Se		34

METHOD

Nuclear Resonance Scattering using N,G reactions.

REF. NO. 66 Be 3 JDM

REACTION	RESULT	EXCITATION ENERGY	SOURCE TYPE	SOURCE RANGE	DETECTOR TYPE	DETECTOR RANGE	ANGLE
G,G	RLX	5 - 10	D	5 - 10	NAI-D	5 - 10	135

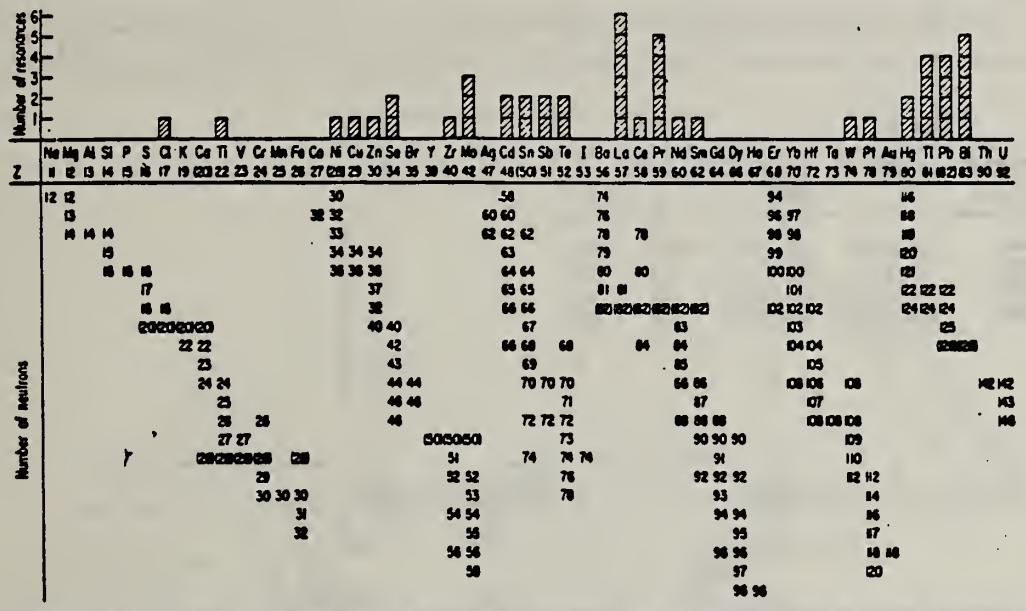

FIG. 3. Histogram of distribution of observed resonances among the different targets. The atomic number is given directly beneath the chemical symbol followed by the neutron numbers of the naturally occurring isotopes. Magic numbers are shown in brackets.

TABLE III. List of effective cross sections.

Scatterer	Energy (MeV)	Gamma source	σ (mb)	Scatterer	Energy (MeV)	Gamma source	σ (mb)
Sm^{144}	8.997	Ni	100	Sn	7.01	Cu	110
Pr^{141}	8.881	Cr	9	Nd	6.867	Co	30
La	8.532	Ni	6	Pr^{141}	6.867	Co	3
Te	8.532	Ni	3[a]	Te	6.7	Ni	...
Cu	8.499	Cr	24	La	6.54	Ag	12
Zr	8.496	Se	3050	Cd	6.474	Co	110
Zn	8.119	Ni	13	Mo	6.44	Hg	25[e]
Se	7.817	Ni	50	La	6.413	Ti	72
Se	7.76	K	90	Mo	6.413	Ti	10
Sb	7.67	V	...[b]	Ti	6.413	Ti	25
Cd	7.64	Fe	40[a]	W	~6.3	Ti	...[b]
Ni	7.64	Fe	7[a]	Sb	6.31	Hg	6[a]
Pr^{141}	7.64	Fe	12[a]	Ti	6.31	Hg	2[a]
Ti	7.64	Fe	370[a]	Sn	6.27	Ag	75
La	7.634	Cu	7	Pb^{206}	6.15	Gd	...[g]
Mo	7.634	Cu	11	Te	5.8	Ni	...[f]
Bi^{209}	7.634	Cu	4	La	6.12	Cl	35
Te	7.528	Ni	66[d]	Pr^{141}	6.12	Cl	110
Bi^{209}	7.416	Se	100	Pt	5.99	Hg	40[a,e]
Bi^{209}	7.300	As	80[a]	Ti	5.99	Hg	5[e]
Pb^{206}	7.285	Fe	4100	Pb^{206}	5.9	Sr	...[b]
Cl	7.285	Fe	34	Ce	5.646	Co	17
Pr^{141}	7.185	Se	80	Bi^{209}	5.646	Co	55
Tl	7.16	Cu	120	Pb^{206}	5.53	Ag	70
La	7.15	Mn	50	Hg	5.44	Hg	75[e]
Bi^{209}	7.149	Tl	2000	Hg	4.903	Co	385

[a] High-energy component of a complex spectrum.
[b] A broad scattered spectrum with no observable peak structure.
[c] There are actually two lines of energies 7.647 and 7.633 MeV having equal intensities in the iron capture gamma spectrum. The cross section has therefore been corrected, although there is no possibility at present of deciding which line is responsible for each resonance.
[d] Is probably an independent level in the complex spectrum of Ni γ rays on Te.
[e] Rough estimate.
[f] May be inelastic component from 7.528 level in Te.
[g] The relative line intensities in this case are due to Groshev and co-workers.
[h] No line is known for the source at this energy.
[i] Difficult to resolve among the many source lines present at this energy.

REF.

R. Wendling and R. Kosiek
Z. fur Physik 192, 502 (1966)

ELEM. SYM.	A	Z
Se		34

METHOD

REF. NO.	
66 We 2	EGF

REACTION	RESULT	EXCITATION ENERGY	SOURCE		DETECTOR		ANGLE
			TYPE	RANGE	TYPE	RANGE	
G,A	ABX	6-33	C	33	SCD-D	4-16	90
				(32.5)			

Tabelle

Element	Dicke (mg/cm²)	Gesamt-auflösung (keV)	Gesamtzahl gemessener α-Teilchen	Ausbeute (μb/MeV · ster)	Ausbeute $\frac{10^6 N\alpha}{Mol \cdot r}$	$E_{\gamma\,max}$ (exp) (MeV)	$E_{\gamma\,min}$ (MeV)
Al	2,35	770	14600	1,3 ± 0,2	3,5 ± 0,6	(≈3,5)	3,5
Ar	200 Torr	480	5200	3,0 ± 0,5	8,3 ± 1,3	5,2	3,5
Se	3,72	790	12200	0,28 ± 0,04	0,76 ± 0,12	9,2	4,5
Ag	3,12	670	3150	0,12 ± 0,02	0,33 ± 0,05	11,8	6,5

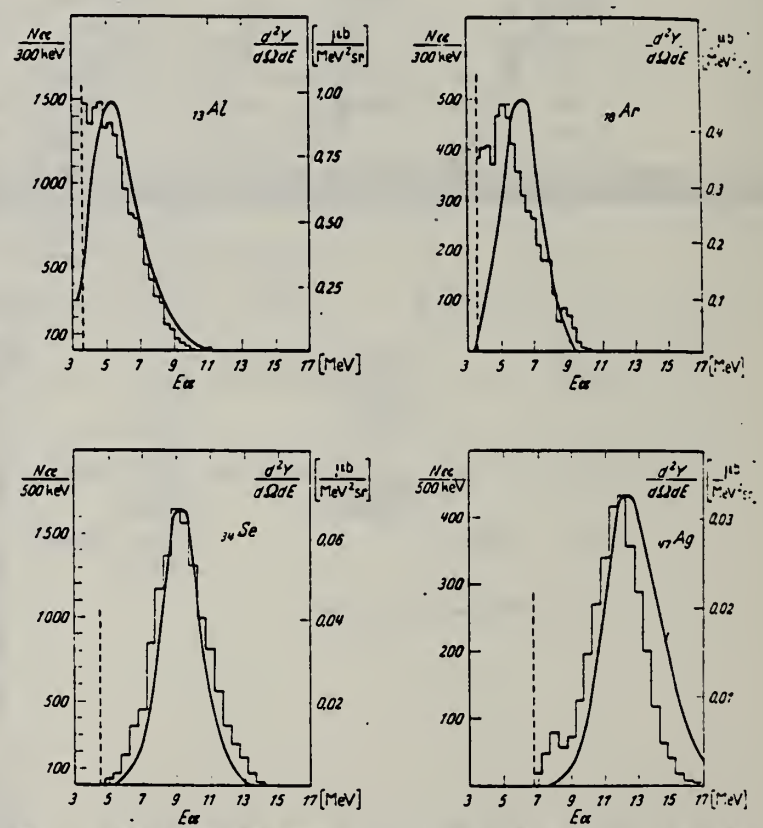

Fig. 1. a Histogramm: Gemessene Energieverteilung und differentielle Ausbeute der Photo-α-Teilchen.
b Kurve: Berechnetes Spektrum. Nähere Angaben im Text

REF.

S. Costa, F. Ferrero, C. Manfredotti, L. Pasqualini, G. Piragino, and H. Arenhovel
Nuovo Cimento 51B, 199 (1967)

ELEM. SYM.	A	Z
Se		34

METHOD

REF. NO.	
67 Co 2	EGF

REACTION	RESULT	EXCITATION ENERGY	SOURCE		DETECTOR		ANGLE
			TYPE	RANGE	TYPE	RANGE	
G,XN	ABX	THR- 24	C	11-24	BF3-I		4PI

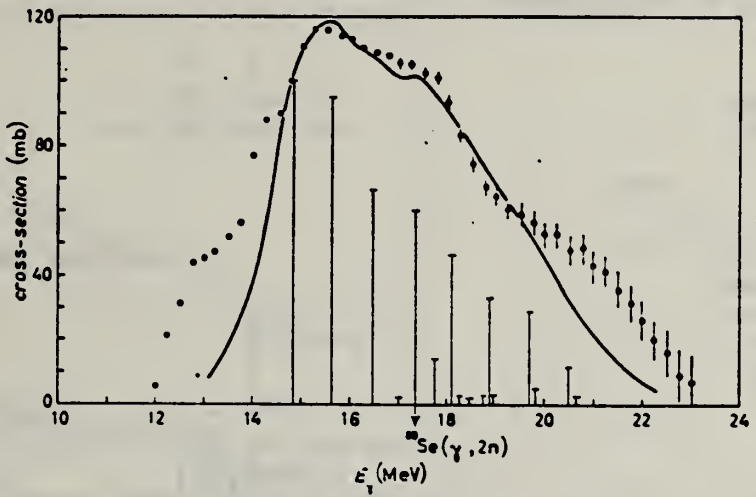

Fig. 1. – Corrected (γ, Tn) cross-section for Se. The dipole strengths, calculated for ^{80}Se, are indicated by the vertical bars.

REF. S. M. Hussain and K. G. McNeill
Can. J. Phys. 45, 2851 (1967)

ELEM. SYM.	A	Z
Se		34

METHOD

REF. NO. 67 Hu 2 EGF

REACTION	RESULT	EXCITATION ENERGY	SOURCE		DETECTOR		ANGLE
			TYPE	RANGE	TYPE	RANGE	
G,N	ABY	THR-22	C	22	THR	4-	DST

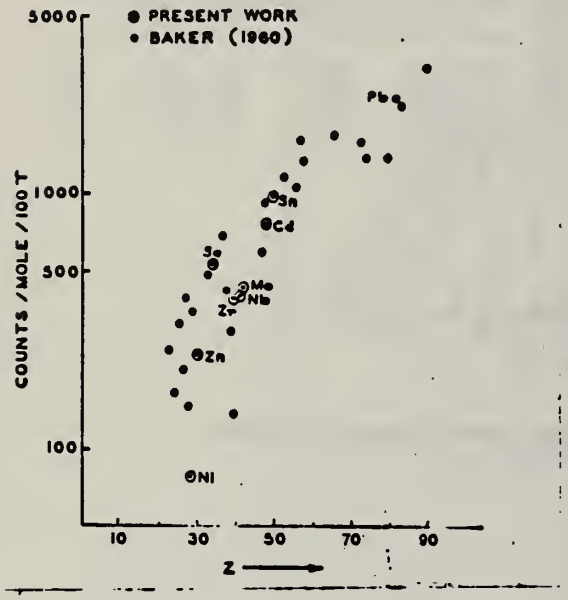

FIG. 3. The yields of fast photoneutrons from various elements as measured in the present work and by Baker. The present results have been normalized to Baker's measurements for lead.

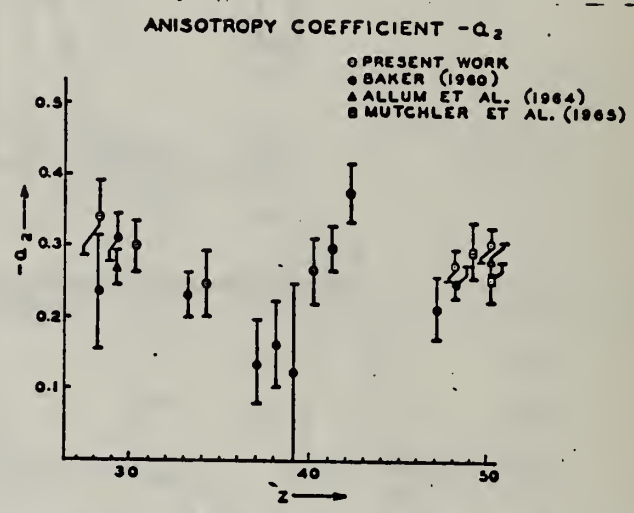

FIG. 2. The anisotropy coefficients a_2, in the formula $W(\theta) = a_0(1 + a_1P_1 + a_2P_2)$, obtained in the present work, and those obtained by other workers in the same part of the Periodic Table.

TABLE I

Element	a_0*	a_1	a_2
Nickel	77 (1.0±0.05)	0.14±0.04	−0.34±0.06
Zinc	236 (1.0±0.04)	0.06±0.03	−0.30±0.04
Selenium	525 (1.0±0.05)	0.10±0.04	−0.25±0.05
Zirconium	380 (1.0±0.05)	0.03±0.04	−0.27±0.05
Niobium	392 (1.0±0.03)	0.01±0.02	−0.30±0.03
Molybdenum	410 (1.0±0.03)	0.05±0.03	−0.41±0.04
Cadmium	755 (1.0±0.02)	0.05±0.01	−0.28±0.02
Tin	955 (1.0±0.02)	0.08±0.02	−0.30±0.02
Lead	2274 (1.0±0.02)	0.06±0.02	−0.48±0.02

*For comparison purposes the experimental value of a_0 for Pb has been normalized to coincide with that obtained by Baker and McNeill (1961) and is the yield per mole per 100 roentgen. All other values of a_0 have also been quoted with the same normalization.

REF. H. Arenhovel, J. M. Maison
Nucl. Phys. A147, 305 (1970)

ELEM. SYM.	A	Z
Se		34

METHOD

REF. NO.	
70 Ar 1	egf

REACTION	RESULT	EXCITATION ENERGY	SOURCE		DETECTOR		ANGLE
			TYPE	RANGE	TYPE	RANGE	
G,G	ABX	12-30	C	32	NAI	12-30	DST

GETS G,G/ TO 2+

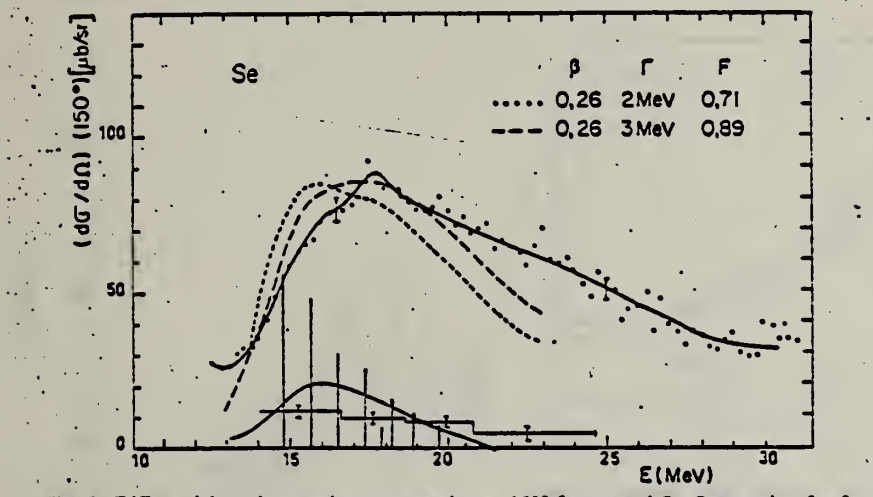

Fig. 8. Differential total scattering cross section at 150° for natural Se. See caption for fig. 4.

Fig. 4. Differential total scattering cross section at 150° for natural Ti. The full curve through experimental points is only a guide for the eyes. The vertical bars represent the relative strength of dipole levels calculated by the D.C.M. with parameters of table 1. Theoretical elastic plus inelastic scattering is computed from these levels with a common width Γ (dashed curve). Experimental inelastic scattering (histogram) and theoretical inelastic scattering to the first 2^+ (full curve) are shown in the lower part of the figure. Open circles give the cross section after background subtraction.

TABLE 4
Integrated inelastic scattering cross section

Nucleus	Limits of integration (in MeV)	Experimental [a]) $\int \sigma_i(E)dE$ (MeV · μb)	Theoretical [a]) 2^+	$2^{+\prime}$ (MeV · μb)	Total
Ti(^{48}Ti)	16 −24	250 ± 50	425	109	534
^{51}V(^{52}Cr)	16.4−24.9	492 ± 50	509	116	579
Cr	16.4−23.4	431 ± 60	509	116	579
^{75}As(^{76}Se)	14.1−23.6	1254 ± 120	1373	414	1787
Se(^{80}Se)	14.1−24.6	1035 ± 100	1066	353	1419
^{89}Y					364
Cd(^{112}Cd)	13.6−23.3	3264 ± 240	1894	370	2264
In(^{114}Cd)	13.6−23.6	2840 ± 220	2173	388	2561
Sn(^{110}Sn)	14.2−24.2	2363 ± 220			643

[a]) We assume an angular distribution of the form $1 + \frac{1}{13}\cos^2\theta$.

S. Costa, L. Ferrero, L. Pasqualini, and E. Mancini
Lettere al Nuovo Cimento 2, 665 (1971)

	Se		34
METHOD	REF. NO.		
	71 Co 2		egf

REACTION	RESULT	EXCITATION ENERGY	SOURCE		DETECTOR		ANGLE
			TYPE	RANGE	TYPE	RANGE	
G,XN	ABI	36-64	C	10-64	BF3-I		4PI

431 FAST N YIELD

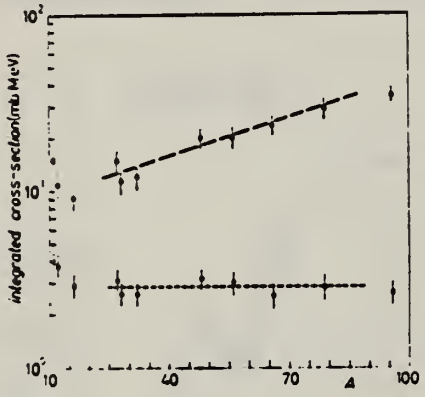

Fig. 2.

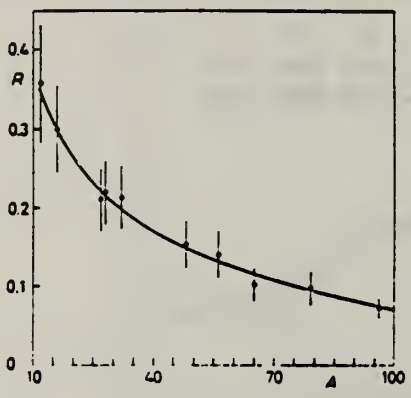

Fig. 3.

Fig 2. – Experimental photoneutron cross-sections integrated over photon energy between 36 and 64 MeV and divided by NZ/A are plotted as a function of the mass number. Black dots are total cross-sections not corrected for neutron multiplicity; open circles represent fast neutron cross-sections (see text). The dashed lines are drawn only to guide the eye.

Fig. 3. – The ratio between «fast» and total photoneutron integrated cross-sections as a function of the mass number A. The solid line represents a fit of the ratios calculated for some nuclei by taking into account the theoretical neutron energy spectra given by GABRIEL and ALSMILLER (*) and the efficiencies of our detector (see Fig. 1).

REF.

R.F. Barrett, J.R. Birkelund, B.J. Thomas, K.S. Lam, and H.H. Thies
Nucl. Phys. A210, 355 (1973)

ELEM. SYM.	A	Z
Se		34

METHOD

REF. NO. 73 Ba 20 egf

REACTION	RESULT	EXCITATION ENERGY	SOURCE		DETECTOR		ANGLE
			TYPE	RANGE	TYPE	RANGE	
G,N	NOX	THR- 27	C	10- 27	BF3-I		4PI

MEAN NEUT ENERGY

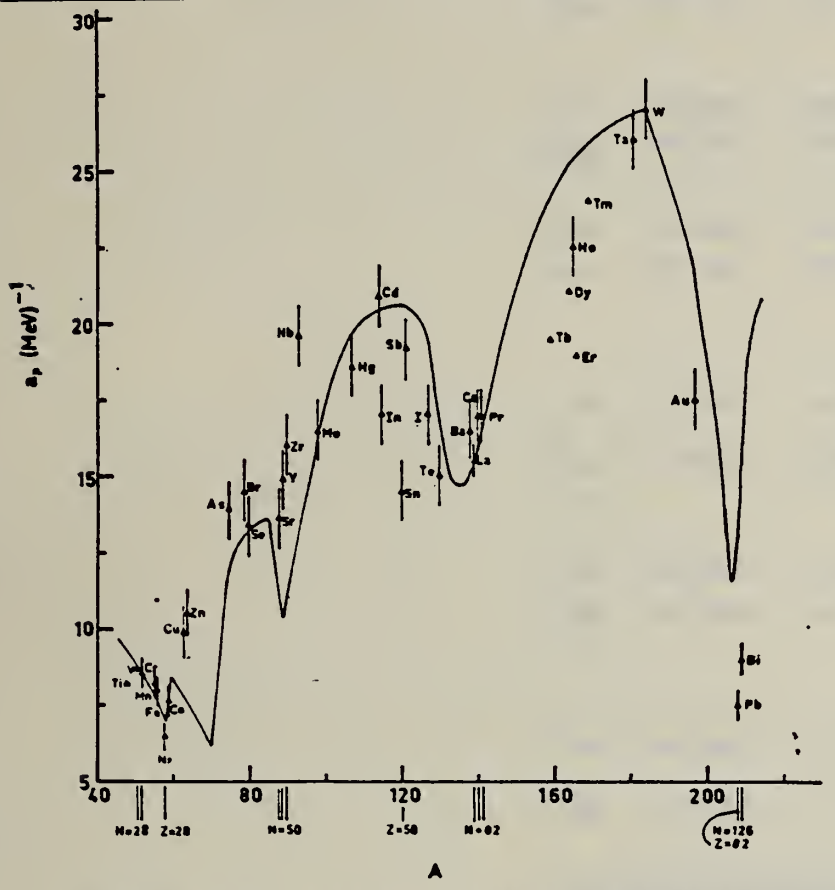

Fig. 12. Experimental values of the level density parameter a_p (Fermi gas formula plus pairing correction) versus atomic number A. The continuous curve is a least-squares fit to the data of a theoretical calculation from Newton [15]).

1
H. Baba and S. Baba, Japan Atomic Energy Research Institute report JAERI-1183 (1969).

2
H. Baba, Nucl. Phys. A159, 625 (1970).

15
T.D. Newton, Can. J. Phys. 34, 804 (1956).

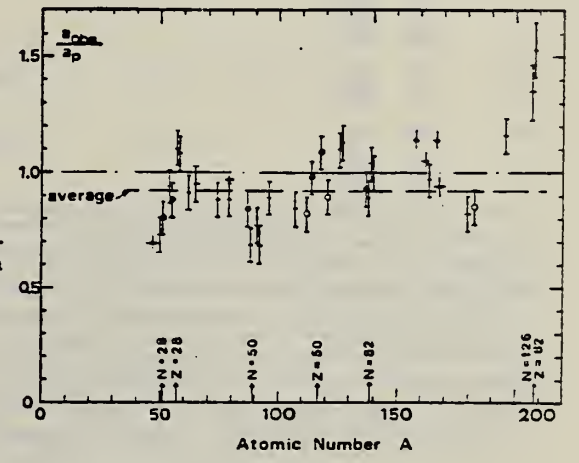

Fig. 15. Ratio a_{obs}/a_p versus atomic number A. Here a_{obs} is the level density parameter taken from the neutron resonance work of refs. [1,2]), and a_p is the level density parameter derived from the present (γ, n) work. Filled circles represent points where nuclei in the neutron resonance and in the (γ, n) experiment were the same. Open circles represent points where the respective nuclei were approximately matched. Triangles represent points which are based on measurement of neutron mean energies at two bremsstrahlung energies only.

(over)

TABLE 3

Comparison of experimental and theoretical data on nuclear level densities with Fermi gas formulae, and comparison of nuclear level density parameters from (γ, n) and n-resonance absorption experiments

Target	N (residual nucleus) [a]		Goodness of fit [b]		$\hat{E}_0(24)$ (MeV) [c]	T (MeV) [d]	a_p (MeV^{-1}) [e]	a_{obs} (MeV^{-1}) [f]	a_{obs}/a_p
			no p.c.	with p.c.					
Ti [g]	23	8%			1.93		8.1–^{47}Ti	6.41–^{47}Ti	0.79
	24	8%							
	25	73%							
	26	5%							
	27	5%							
V [g]	27	100%			1.96		8.7–^{50}V	6.35–^{51}V	0.73
Cr	25	4%	P	G	1.89		8.6–^{51}Cr	6.9 –^{51}Cr	0.80
	27	84%							
	28	10%							
	29	2%							
Mn	29	100%	V.P.	G	2.1		8.2–^{54}Mn	7.82–^{56}Mn	0.94
Fe	27	6%	F	G	1.96		8.0–^{55}Fe	7.06–^{55}Fe	0.88
	29	92%							
	30	2%							
Co	31	100%	P	F	2.12		7.7–^{58}Co	8.35–^{60}Co	1.08
Ni	29	68%	V.P.	P	2.04	1.4	6.5–$^{57.7}$Ni	7.19–^{59}Ni	1.10
($Z = 28$)	31	26%							
	32	1%							
	33	4%							
	35	1%							
Cu	33	69%	V.P.	P	1.78	1.0	9.8–^{62}Cu	8.90–^{64}Cu	0.91
	35	31%							
Zn	33	49%	F	F	1.61		10.5–$^{64.4}$Zn	10.0–^{65}Zn	0.95
	35	28%							
	36	4%							
	37	19%							
As	41	100%	V.P.	F	1.44		14.5–^{74}As	12.81–^{76}As	0.88
Se [g]	41	9%			1.39		13.3–^{78}Se	12.8 –^{78}Se	0.97
	42	8%							
	43	24%							
	45	50%							
	47	9%							
Br	43	45%	V.P.	V.P.	1.41		14.5–^{79}Br	12.69–^{80}Br	0.88
	45	49%							
Sr	47	10%	F	G	1.31		13.6–^{87}Sr	11.4 –^{87}Sr	0.84
	48	7%							
	49	83%							

[a]) Neutron numbers and abundances of respective residual nuclei in (γ, n) experiments.

[b]) These give an assessment of the goodness of fit of a calculated $\hat{E}_n$ versus E_0 curve to the observed data, using the Fermi gas level density formula both without and with pairing corrections.

[c]) Bremsstrahlung photoneutron mean energies $\hat{E}_n$ for peak bremsstrahlung energy $E_0 = 24$ MeV.

[d]) Nuclear temperature from fit with constant-temperature formula.

[e]) Level density parameter a_p derived from the present (γ, n) experiment, using a Fermi gas formula plus pairing correction, and corresponding residual nucleus (the atomic weight shown is the weighted average of atomic weights of the respective isotopes present).

[f]) As column 7, but using data on n-resonance absorption from refs. [1,2]).

[g]) Measurements of $\hat{E}_n(E_0)$ for these nuclei were made only for $E_0 = 21$, 23 and 24 MeV.

Se
A=74

Se
A=74

REF. F.Z. Khien N.K. Zui, N.T. An
Yad. Fiz. 35, 257 (1982)
Sov. J. Nucl. Phys. 35, 145 (1982)

ELEM. SYM.	A	Z
Se	74	34

METHOD

REF. NO. 82 Kh 2 egf

REACTION	RESULT	EXCITATION ENERGY	SOURCE		DETECTOR		ANGLE
			TYPE	RANGE	TYPE	RANGE	
G,N	NOX	12-14	C	14	ACT-I		4PI

ISOMERIC RATIO

The method is developed for calculation of the isomeric ratio for the case of low excitation energy of the residual nucleus, and the isomeric ratio is measured in the $(n, 2n)$ and (γ, n) reactions in the neutron-deficient nuclei ^{92}Mo, ^{90}Zr, ^{86}Sr, and ^{74}Se. The good agreement between the experimental and theoretical results on the (γ, n) reaction has confirmed the reliability of the characteristics of the residual nuclei, the transmission coefficients of the emitted neutrons, etc., used in the calculations. From study of the $(n, 2n)$ reaction we have obtained values of the parameters of the spin dependence of the level density of the nucleus in the excitation-energy region ~14 MeV.

PACS numbers: 25.20. + y, 25.40.Gr, 27.50. + e, 27.60. + j

TABLE III. Isomeric ratio in the (γ, n) reaction.

Target nucleus	σ_{exp}	σ_{theor}	Published data[1]
^{92}Mo	1.34±0.15	1.36	1.82±0.15 (70) [3] 1.03±0.21 [10] 0.85±0.07 (30) [15]
^{90}Zr	1.52±0.04	1.49	0.50±0.15 (30) [15]
^{86}Sr	0.70±0.07	0.86	0.68±0.14 (30) [15]
^{74}Se	7.5±1.0	10.5[2] 8.8[3]	

[1] In parentheses we have given the values of the bremsstrahlung maximum energy.
[2] In the calculations we used the ^{73}Se level scheme of Ref. 2, $I_g = 7/2^+$ and $I_m = 1/2^-$.
[3] In the calculations we used the level scheme of ^{73}Se in Ref. 3, $I_g = 9/2^+$ and $I_m = 3/2^-$.

Se
A=76

Se
A=76

N. N. Delyagin
J. Exptl. Theoret. Phys. (USSR) 38, 1111 (1960)
Soviet Phys. JETP 11, 303 (1960)

Se	76	34

METHOD

REF. NO. 60 De 2 EGF

REACTION	RESULT	EXCITATION ENERGY	SOURCE		DETECTOR		ANGLE
			TYPE	RANGE	TYPE	RANGE	
G,G	LFT	.56	D	.56			

Cascade transition used to supply recoil energy.
No data given on detector
LFT $(1.3\pm0.2) \times 10^{-11}$ sec

REF. J. R. Pruett
Phys. Rev. 129, 2583 (1963).

ELEM. SYM.	A	Z
Se	76	34

METHOD
Radioactive source; photon scattering; NaI spectrometer

REF. NO. 63 Pr 2 NVB

REACTION	RESULT	EXCITATION ENERGY	SOURCE		DETECTOR		ANGLE
			TYPE	RANGE	TYPE	RANGE	
G,G	LFT	1	D	1	NAI-D		
		(0.559 MeV)		(0.559 MeV)			

Lifetime:

$$\tau_{0.559} = (1.55^{+0.13}_{-0.19}) \times 10^{-11} \text{ sec.}$$

$$\tau_{1.216} > 3 \times 10^{-12} \text{ sec.}$$

REF. A.M. Goryachev, G.N. Zalesnyi, and B.A. Tulupov
Izv. Akad. Nauk SSSR. Ser. Fiz. 39, 134 (1975)
Bull. Acad. Sci. USSR Phys. Ser. 39, 116 (1975)

ELEM. SYM.	A	Z
Se	76	34

METHOD

REF. NO. 75 Go 1 hmg

REACTION	RESULT	EXCITATION ENERGY	SOURCE TYPE	SOURCE RANGE	DETECTOR TYPE	DETECTOR RANGE	ANGLE
G,XN	ABX	11- 25	C	9- 25	BF3-I		4PI

σ(G,SN). Statistical theory used to obtain SN cross section from XN cross section.

Table 2

Nuclide	β_2	E_2, MeV	E_1, MeV	Nuclide	β_2	E_2, MeV	E_1, MeV
^{64}Zn	0.27	0.99	18	^{76}Ge	0.25	0.562	18
^{66}Zn	0.23	1.04	18	^{76}Se	0.33	0.559	18
^{68}Zn	0.2	1.08	18	^{78}Se	0.3	0.616	18
^{74}Ge	0.23	1.04	18	^{80}Se	0.25	0.654	18
^{72}Ge	0.25	0.835	18	^{82}Se	0.2	0.655	18
^{73}Ge	0.3	0.8	18				

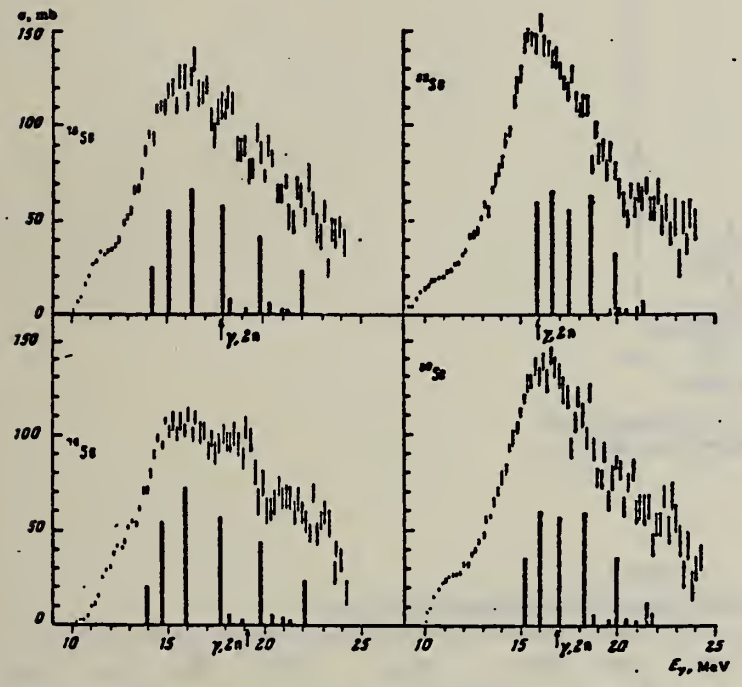

Fig. 3. The same as in Fig. 1, but for ^{76,78,80,82}Se.

Cross sections of photoneutron reactions. The dipole photoabsorption forces are taken from [6,7] (the solid black columns).

6 M.G.Huber et al., Phys.Rev.155,1073(67)
7 M.G.Huber et al., Phys.Rev.192,223(66.

Table 3

Nuclide	σ, mb	Nuclide	σ, mb	Nuclide	σ, mb
^{64}Zn	397±19*	^{74}Ge	760±37	^{76}Se	1021±52
^{66}Zn	579±27	^{76}Ge	872±41	^{80}Se	1029±50
^{68}Zn	718±35	^{78}Ge	911±43	^{82}Se	1067±53
^{70}Ge	739±37	^{78}Se	930±50		

*Mean - square errors

REF.		ELEM. SYM.	A	Z
	P. Carlos, H. Beil, R. Bergere, J. Fagot, A. Lepretre, A. Veyssiere, G. V. Solodukhov Nucl. Phys. A258, 365 (1976)	Se	76	34

METHOD	REF. NO.
	76 Ca 1 egf

REACTION	RESULT	EXCITATION ENERGY	SOURCE		DETECTOR		ANGLE
			TYPE	RANGE	TYPE	RANGE	
G,N	ABX	10- 26	D	10- 26	MOD-I		4PI
G,2N	ABX	17- 26	D	10- 26	MOD-I		4PI

990+

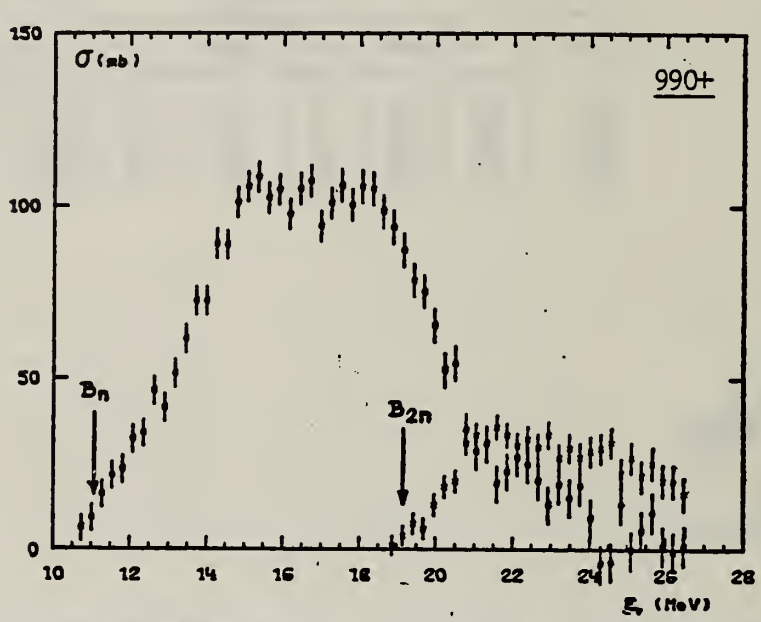

Fig. 8. Partial photoneutron cross section $[\sigma(\gamma, n)+\sigma(\gamma, pn)]$ and $\sigma(\gamma, 2n)$ for ^{76}Se. Arrows B_n and B_{2n} indicate theoretical threshold values for (γ, n) and $(\gamma, 2n)$ reactions respectively. Data were not corrected for impurities.

TABLE 3

Integrated photoneutron cross sections and comparison with sum rules

Nucleus	^{64}Zn	^{69}Ga / ^{71}Ga	^{70}Ge	^{72}Ge	^{74}Ge	^{76}Ge	^{75}As	^{76}Se	^{78}Se	^{80}Se	^{82}Se
E_M (MeV)	29	26.5	26.5	26.5	26.5	26.5	26.5	26.5	26.5	26.5	26.5
σ_{0n} (MeV · b)	0.75	0.91	0.78	0.94	1.02	1.12	1.09	1.01	1.06	1.11	1.13
$\frac{\sigma_{0n}A}{0.06\,NZ}$	0.78	0.87	0.75	0.88	0.94	1	0.98	0.90	0.92	0.94	0.95
$B_n - B_p$ (MeV)	4.2	3.7 / 1.4	3	1	−0.8	−2.6	3.3	1.7	0.1	−1.5	−3
σ_{-1n} (mb)	38	52	44	54	59	64	63	58	62	65	67
$\sigma_{-1n}A^{-\frac{1}{3}}$ (mb)	0.15	0.18	0.15	0.18	0.19	0.20	0.20	0.18	0.19	0.19	0.19
σ_{-2n} (mb · MeV^{-1})	2.0	3.1	2.5	3.2	3.6	3.9	3.7	3.4	3.8	3.9	4.2
$\sigma_{-2n}A^{-\frac{1}{3}}$ (μb · MeV^{-1})	1.9	2.6	2.1	2.6	2.8	2.9	2.8	2.5	2.7	2.6	2.7

The notation used is defined in the text. The average experimental errors $\Delta\sigma_{0n}/\sigma_{0n}$, $\Delta\sigma_{-1n}/\sigma_{-1n}$ and $\Delta\sigma_{-2n}/\sigma_{-2n}$ are approximately 8 %.

Se
A=77

Se
A=77

REF. Y. Oka, T. Kato, K. Nomura, T. Saito, Hui-Tuh Tsai
Bull. Chem. Soc. Japan 41, 380 (1968)

ELEM. SYM.	A	Z
Se	77	34

METHOD

REF. NO. 68 Ok 3 egf

REACTION	RESULT	EXCITATION ENERGY	SOURCE		DETECTOR		ANGLE
			TYPE	RANGE	TYPE	RANGE	
G,P	ABY	THR-20	C	20	ACT-I		4PI

TABLE 1. SUMMARY OF DATA ON (γ, p) REACTIONS WITH 20 MeV BREMSSTRAHLUNG

Nuclide: Parent (Natural abundance, %)	Nuclide: Residual (Half-life)	S_p (MeV)	Observed γ-ray: Energy (MeV)	Observed γ-ray: Branching ratio (%)	Observed γ-ray: Type of multipole transition	Yield determined: μCi/mg[a]	Yield determined: Yield/mol·R
^{25}Mg (10.11)	^{24}Na (15 hr)	12.06	1.37	100	$E2$	1.48×10^{-1}	1.7×10^{5}
^{29}Si (4.71)	^{29}Al (2.27 min)	12.33	1.78	100	$E2$	1.91	2.8×10^{5}
^{30}Si (3.12)	^{29}Al (6.56 min)	13.59	1.28	93.8	$E2+M1$	6.51×10^{-1}	1.5×10^{5}
^{44}Ca (2.06)	^{43}K (22.4 hr)	12.17	0.374	85	$E2+M1$	7.86×10^{-3}	1.3×10^{5}
^{47}Ti (7.32)	^{46}Sc (84.1 d)	10.47	0.887	100	$E2$	7.11×10^{-4}	3.1×10^{5}
^{48}Ti (73.99)	^{47}Sc (3.4 d)	11.44	0.160	100	$E2+M1$	6.83×10^{-3}	1.2×10^{5}
^{49}Ti (5.46)	^{48}Sc (1.8 d)	11.35	1.31	100	$E2$	4.40×10^{-3}	5.8×10^{4}
^{53}Cr (9.55)	^{52}V (3.8 min)	11.15	1.43	100	$E2$	5.01×10^{-1}	6.6×10^{4}
^{57}Fe (2.17)	^{56}Mn (2.58 hr)	10.57	1.81	23.5	$E2+M1$	8.10×10^{-3}	2.1×10^{5}
^{76}Ge (36.74)	^{73}Ga (4.8 hr)	10.92	0.295	97	$(E2)$	3.70×10^{-1}	1.3×10^{5}
^{77}Se (7.58)	^{76}As (26.5 hr)	9.61	0.559	41	$E2$	1.48×10^{-2}	1.3×10^{5}
^{87}Sr (7.02)	^{86}Rb (19 d)	9.41	1.08	9	$E2$	5.15×10^{-4}	9.9×10^{4}
^{113}Cd (12.26)	^{112}Ag (3.2 hr)	9.74	1.39	35	$E2$	1.91×10^{-2}	2.1×10^{4}
^{117}Sn (7.57)	^{116m}In (54 min)	9.58	1.27	84	$E2$	9.80×10^{-3}	6.9×10^{3}
^{137}Ba (11.32)	^{136}Cs (13 d)	8.67	0.830	100	$E2$	1.68×10^{-4}	2.2×10^{4}
^{199}Hg (16.84)	^{199}Au (2.7 d)	7.27	0.412	100	$E2$	8.43×10^{-4}	2.2×10^{4}

a) The value corrected at the end of 1 hr irradiation (9.4×10^{8} R/min).

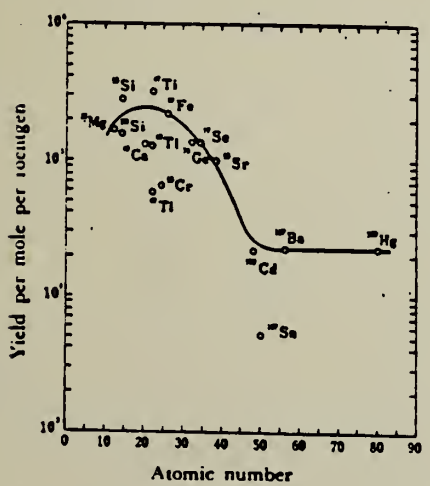

Fig. 2. The yield curve for the (γ, p) reaction with 20 MeV bremsstrahlung.

M. Boivin, Y. Cauchois and Y. Heno
Nucl. Phys. A137, 520 (1969)

Se	77	34

METHOD

REF. NO. 69 Bo 3 egf

REACTION	RESULT	EXCITATION ENERGY	SOURCE		DETECTOR		ANGLE
			TYPE	RANGE	TYPE	RANGE	
G,G	ABX	0-2	C	0-2	ACT-I		4PI

8 LEVELS

TABLEAU I

Energie des niveaux excités, sections efficaces intégrées et $u = g\Gamma_\gamma\Gamma_n/\Gamma$ pour le ^{77}Se

E(keV)	σ (μb · MeV)	u(eV)
250±10	$8\ ^{+7}_{-2.5}\times10^{-4}$	$1.3^{+1}_{-0.4}\times10^{-8}$
440±10	$1.8^{+1.2}_{-0.4}\times10^{-3}$	$9.1^{+5}_{-2}\times10^{-8}$
520±10	$5.7^{+5}_{-1.5}\times10^{-3}$	$4.1^{+3.5}_{-1}\times10^{-8}$
825±10	$4.6^{+4}_{-1}\times10^{-3}$	$8.0^{+7}_{-2}\times10^{-7}$
932±10	$3.5^{+3}_{-1}\times10^{-2}$	$7.8^{+6.5}_{-2}\times10^{-6}$
1000±10	$3.2^{+3}_{-1}\times10^{-2}$	$8.4^{+8}_{-2.5}\times10^{-6}$
1190±10	$0.18^{+0.12}_{-0.04}$	$6.7^{+4.5}_{-1.5}\times10^{-5}$
1600±10	$0.52^{+0.4}_{-0.1}$	$3.5^{+2.5}_{-0.5}\times10^{-5}$

Indirect Activation of 17.38s 162.0 keV level by .5-2.0 MeV bremsstrahlung.

Se
A=78

Se
A=78

Se
A=73

REF. Y. Oka, T. Kato and A. Yamadera
Bull. Chem. Soc. Japan 41, 1606 (1968)

ELEM. SYM.	A	Z
Se	78	34

METHOD

REF. NO. 68 0k 2 egf

REACTION	RESULT	EXCITATION ENERGY	SOURCE		DETECTOR		ANGLE
			TYPE	RANGE	TYPE	RANGE	
G,N	ABY	THR-20	C	20	ACT-I		4PI

ISOMERIC YIELD

TABLE 1. THE PARTICULARS OF THE (γ,n) REACTION PRODUCTS AND THE DATA OBTAINED WITH 20 MeV BREMSSTRAHLUNG

Nuclide		Half-life of product (sec)	Gamma-ray determined			Limit of detection (μg)	Yield ($mol^{-1} \cdot R^{-1}$)
Parent (Natural abundance, %)	Residual		Energy (MeV)	Branching ratio (%)	Photopeak activity (cpm/mg)[a]		
^{26}Mg(78.60)	^{25}Mg	9.9	0.511	200	2.04×10^{6}	0.49	8.1×10^{4}
^{76}Ge(7.67)	^{75m}Ge	48	0.139	100	6.37×10^{5}	1.6	1.1×10^{4}
^{78}Se(23.52)	^{77m}Se	17	0.162	100	1.82×10^{6}	0.55	1.2×10^{5}
^{92}Mo(15.86)	^{91m}Mo	65	0.650	57	2.22×10^{5}	4.5	2.7×10^{6}
^{140}Ce(88.48)	^{139m}Ce	58	0.745	100	1.06×10^{6}	0.95	1.3×10^{5}
^{142}Nd(27.13)	^{141m}Nd	64	0.760	100	3.19×10^{5}	3.1	1.4×10^{6}
^{159}Tb(100)	^{159m}Tb	11	0.111	100	2.56×10^{5}	3.8	2.2×10^{6}

a) The value corrected at the end of one-minute irradiation with the dose rate of 10^{7} R/min; Counting geometry is 20% with a 3"dia.×3"NaI(Tl) detector.

Values given are for σ_0 (24.2 MeV).

REF. A.M. Goryachev, G.N. Zalesnyi, and B.A. Tulupov
Izv. Akad. Nauk SSSR. Ser. Fiz. 39, 134 (1975)
Bull. Acad. Sci. USSR Phys. Ser. 39, 116 (1975)

ELEM. SYM.	A	Z
Se	78	34

METHOD

REF. NO. 75 Go 1 hmg

REACTION	RESULT	EXCITATION ENERGY	SOURCE TYPE	SOURCE RANGE	DETECTOR TYPE	DETECTOR RANGE	ANGLE
G,XN	ABX	10- 25	C	9- 25	BF3-I		4PI

σ(G,SN). Statistical theory used to obtain SN cross section from XN cross section.

Table 2

Nuclide	β_0	E_2, MeV	E_1, MeV	Nuclide	β_0	E_2, MeV	E_1, MeV
^{64}Zn	0,25	0,99	18	^{76}Ge	0,25	0,562	18
^{66}Zn	0,23	1,04	18	^{76}Se	0,33	0,559	18
^{68}Zn	0,2	1,08	18	^{78}Se	0,3	0,616	18
^{70}Ge	0,23	1,04	18	^{80}Se	0,25	0,654	18
^{72}Ge	0,25	0,835	18	^{82}Se	0,2	0,655	18
^{74}Ge	0,3	0,8	18				

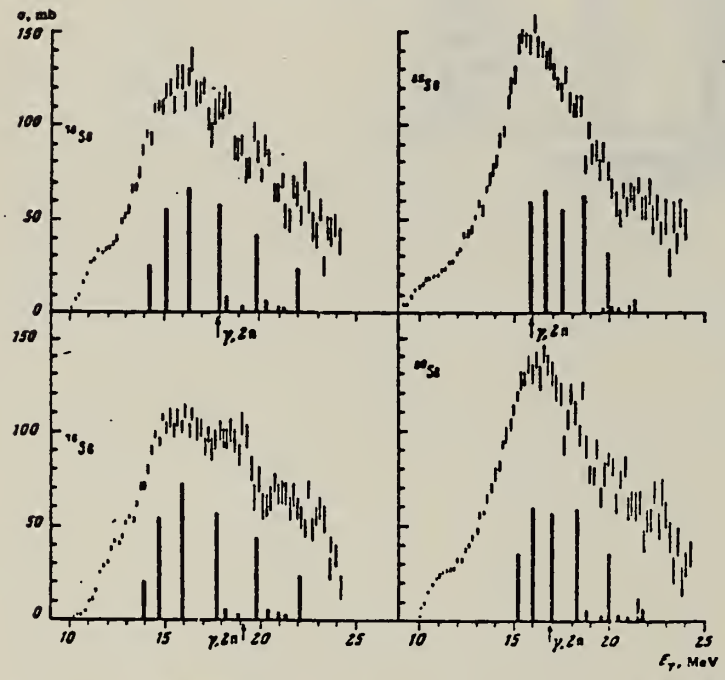

Fig. 3. The same as in Fig. 1, but for ^{76,78,80,82}Se.

Cross sections of photoneutron reactions. The dipole photoabsorption forces are taken from [6,7] (the solid black columns).

[6] M.G.Huber et al., Phys.Rev.155,1073(67)
[7] M.G.Huber et al., Phys.Rev.192,223(66).

Values given are for σ_0(24.2 MeV).

Table 3

Nuclide	σ, mb	Nuclide	σ, mb	Nuclide	σ, mb
^{64}Zn	397±19*	^{74}Ge	760±37	^{76}Se	1021±52
^{66}Zn	579±27	^{76}Ge	872±41	^{80}Se	1029±50
^{68}Zn	718±35	^{78}Ge	911±43	^{82}Se	1067±53
^{70}Ge	783±37	^{78}Se	930±50		

*Mean - square errors

REF. P. Carlos, H. Beil, R. Bergere, J. Fagot, A. Lepretre, A. Veyssiere, G. V. Solodukhov
Nucl. Phys. A258, 365 (1976)

ELEM. SYM.	A	Z
Se	78	34

METHOD

REF. NO. 76 Ca 1 egf

REACTION	RESULT	EXCITATION ENERGY	SOURCE		DETECTOR		ANGLE
			TYPE	RANGE	TYPE	RANGE	
G,N	ABX	10- 26	D	10- 26	MOD-I		4PI
G,2N	ABX	18- 26	D	10- 26	MOD-I		4PI

993+

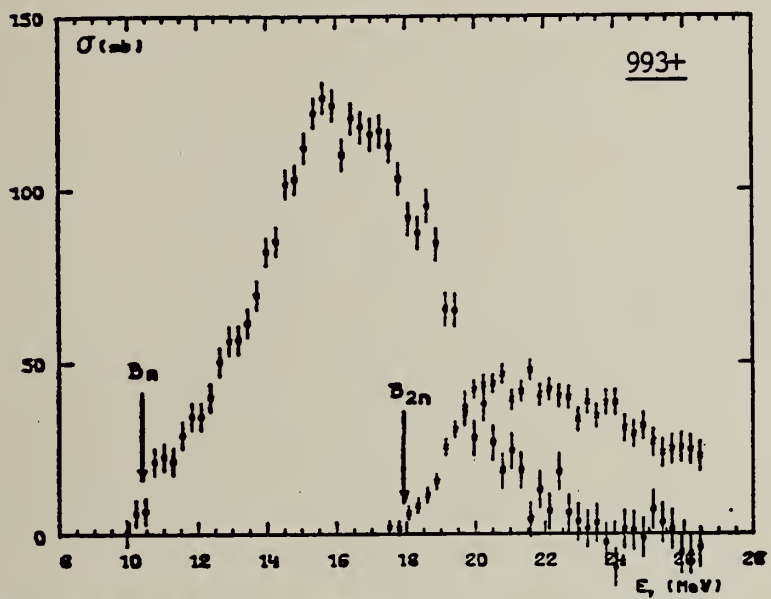

Fig. 9. Partial photoneutron cross sections [$\sigma(\gamma, n)+\sigma(\gamma, pn)$] and $\sigma(\gamma, 2n)$ for ^{78}Se. Arrows B_n and B_{2n} indicate theoretical threshold values for (γ, n) and $(\gamma, 2n)$ reactions respectively.

TABLE 3

Integrated photoneutron cross sections and comparison with sum rules

Nucleus	^{64}Zn	^{69}Ga / ^{71}Ga	^{70}Ge	^{72}Ge	^{74}Ge	^{76}Ge	^{75}As	^{76}Se	^{78}Se	^{80}Se	^{82}Se
E_M (MeV)	29	26.5	26.5	26.5	26.5	26.5	26.5	26.5	26.5	26.5	26.5
σ_{0n} (MeV · b)	0.75	0.91	0.78	0.94	1.02	1.12	1.09	1.01	1.06	1.11	1.13
$\frac{\sigma_{0n}A}{0.06\,NZ}$	0.78	0.87	0.75	0.88	0.94	1	0.98	0.90	0.92	0.94	0.95
$B_n - B_p$ (MeV)	4.2	3.7 / 1.4	3	1	−0.8	−2.6	3.3	1.7	0.1	−1.5	−3
σ_{-1n} (mb)	38	52	44	54	59	64	63	58	62	65	67
$\sigma_{-1n}A^{-1}$ (mb)	0.15	0.18	0.15	0.18	0.19	0.20	0.20	0.18	0.19	0.19	0.19
σ_{-2n} (mb · MeV^{-1})	2.0	3.1	2.5	3.2	3.6	3.9	3.7	3.4	3.8	3.9	4.2
$\sigma_{-2n}A^{-1}$ (μb · MeV^{-1})	1.9	2.6	2.1	2.6	2.8	2.9	2.8	2.5	2.7	2.6	2.7

The notation used is defined in the text. The average experimental errors $\Delta\sigma_{0n}/\sigma_{0n}$, $\Delta\sigma_{-1n}/\sigma_{-1n}$ and $\Delta\sigma_{-2n}/\sigma_{-2n}$ are approximately 8 %.

Se
A=80

Se
A=80

REF.

A. Hofmann, P. Stoll
Helv. Phys. Acta 31, 591 (1958)

ELEM. SYM.	A	Z
Se	80	34

METHOD

REF. NO.

58 Ho 1 egf

REACTION	RESULT	EXCITATION ENERGY	SOURCE		DETECTOR		ANGLE
			TYPE	RANGE	TYPE	RANGE	
G,NP	ABI	20- 32	C	32	ACT-I		4PI

(γ,np) yields include (γ,d).

Tabelle I

Reaktion	Q-Wert MeV	I.W.Q. $\bar{\sigma}$ MeV barn	σ_{max} mb	E_{max} MeV	Γ MeV
$Ca^{40}(\gamma, pn)\ K^{39}$	− 24,3	0,005	2,4	30 ± 1	2,1
$Zn^{64}(\gamma, pn)\ Cu^{63}$	− 18,36	0,03			
$Zn^{66}(\gamma, pn)\ Cu^{65}$	− 18,65	0,031	7,2	28 ± 1	4
$Zn^{68}(\gamma, p)\ Cu^{67}$	− 10,01	0,19	11,4	22,7 ± 1	6
$Sc^{89}(\gamma, pn)\ As^{78}$	− 20,43	0,02			
$Zn^{64}(\gamma, 2n)\ Zn^{62}$	− 20,82	0,08			
$Mo^{92}(\gamma, pn)\ Nb^{90}$	− 19,5	0,02			
$Sb^{123}(\gamma, pn)\ Sn^{121}$	− 18,2	0,0006			

REF.

H. Szichman
Phys. Rev. C8, 1429 (1973)

ELEM. SYM.	A	Z
Se	80	34

METHOD

REF. NO. 73 Sz 17 hmg

REACTION	RESULT	EXCITATION ENERGY	SOURCE TYPE	SOURCE RANGE	DETECTOR TYPE	DETECTOR RANGE	ANGLE
G,G	LFT	8	D	8	SCD-D		DST
		(7.819)		(7.819)			

8=7.819 MEV

TABLE I. Reduced partial radiation widths of the 7818.9-keV resonance level in ^{80}Se.

Energy of transitions (keV)	Energy of final state (keV)	Relative intensity (%)	Reduced widths (eV MeV^{-4} × 10^3) $k(E1)$	$k(M1)$	Most likely character
7818.9	0	100±0.5	6±1	117±22	$E1$
6369.4	1449.5±0.3	8.4±0.2	1.0±0.2	18±4	$E1$ or $M1$
6339.4	1479.5±0.1	9.4±0.2	1.1±0.2	21±4	$E1$ or $M1$
5944.7	1874.2±0.8	1.1±0.2	0.2	3±1	$E1$ or $M1$
5858.4	1960.5±0.2	27.3±0.3	4±1	78±14	$E1$
5507.2	2311.3±0.7	4.2±0.5	0.8±0.2	14±3	$E1$ or $M1$
5304.4	2514.5±0.3	6.4±0.3	1.3±0.2	24±5	$E1$ or $M1$
5191.6	2627.3±0.4	1.0±0.3	0.3±0.1	4±2	$E1$ or $M1$
5004.3	2814.6±0.5	3.5±0.3	0.8±0.2	16±3	$E1$ or $M1$
4991.4	2827.5±0.2	12.4±0.4	3±1	56±10	$E1$
4692.4	3126.5±0.2	12.5±0.3	4±1	68±13	$E1$
4619.1	3199.8±0.3	5.5±0.3	1.6±0.3	30±6	$E1$ or $M1$
4570.1	3248.8±0.5	7.3±0.3	2.2±0.4	43±8	$E1$
4502	3317 ±1	2.2±0.4	0.7±0.2	14±3	$E1$ or $M1$
4468.2	3350.7±0.2	9.2±0.4	3±1	58±11	$E1$
4427.1	3391.3±0.3	8.5±0.3	3±1	55±10	$E1$
4376.8	3442.1±0.3	5.2±0.4	1.9±0.3	35±7	$E1$ or $M1$
4212.0	3606.9±0.4	3.7±0.3	1.5±0.3	28±6	$E1$ or $M1$
4199.1	3619.8±0.5	2.8±0.3	1.1±0.2	21±5	$E1$ or $M1$
4163	3656 ±1	1.3±0.3	0.5±0.1	10±3	$E1$ or $M1$
3949.1	3869.8±0.5	3.0±0.4	1.5±0.3	27±6	$E1$ or $M1$
3866.9	3952.0±0.4	3.0±0.5	1.6±0.4	30±7	$E1$ or $M1$
3756.1	4062.8±0.4	4.3±0.4	3±1	50±10	$E1$

(over)

TABLE II. Experimental A_{22} coefficients compared with theory, assuming pure dipole.

Energy of transition (keV)	Energy of final state (keV)	Transitions in ^{80}Se Theoretical A_{22} coefficients for various assumed spin sequences 0—1—0 0.500	0—1—1 −0.250	0—1—2 0.050
7818.9	0	+0.500		
6369.4	1449.5			+0.15±0.13
6339.4	1479.5	+0.58±0.06		
5944.7	1874.2	+0.62±0.58		+0.62±0.58
5858.4	1960.5			+0.06±0.03
5507.2	2311.8			−0.03±0.17
5304.4	2514.5			+0.17±0.09
5004.3	2814.6	+0.37±0.37		+0.37±0.37 [a]
4991.4	2827.5			+0.13±0.07
4692.4	3126.5			+0.14±0.08
4619.1	3199.8			+0.21±0.10
4570.1	3248.8			+0.01±0.09
4502	3317	+1.2 ±0.7		
4468.2	3350.7		−0.25±0.08	
4427.1	3391.8			+0.11±0.07
4376.8	3442.1	+0.40±0.18		
4212.0	3606.9			+0.19±0.19
4199.1	3619.8	+0.46±0.28		
3949.1	3869.8		−0.25±0.30	−0.25±0.30
3866.9	3952.0		−0.30±0.38	−0.30±0.38
3756.1	4062.8	+0.39±0.24		

[a] Only spin assignment of 2 is valid for the final state, since the transition to the ground state was observed (see Fig.

REF. A.M. Goryachev, G.N. Zalesnyi, and B.A. Tulupov
Izv. Akad. Nauk SSSR. Ser. Fiz. 39, 134 (1975)
Bull. Acad. Sci. USSR Phys. Ser. 39, 116 (1975)

ELEM. SYM.	A	Z
Se	80	34

METHOD

REF. NO. 75 Go 1 hmg

REACTION	RESULT	EXCITATION ENERGY	SOURCE TYPE	SOURCE RANGE	DETECTOR TYPE	DETECTOR RANGE	ANGLE
G,XN	ABX	9- 25	C	9- 25	BF3-I		4PI

σ(G,SN). Statistical theory used to obtain SN cross section from XN cross section.

Table 2

Nuclide	β_0	E_2, MeV	E_1, MeV	Nuclide	β_0	E_2, MeV	E_1, MeV
^{64}Zn	0.25	0.99	18	^{76}Ge	0.25	0.562	18
^{66}Zn	0.23	1.04	18	^{76}Se	0.33	0.559	18
^{68}Zn	0.2	1.08	18	^{78}Se	0.3	0.616	18
^{70}Ge	0.23	1.04	18	^{80}Se	0.25	0.634	18
^{72}Ge	0.25	0.835	18	^{82}Se	0.2	0.655	18
^{74}Ge	0.3	0.6	18				

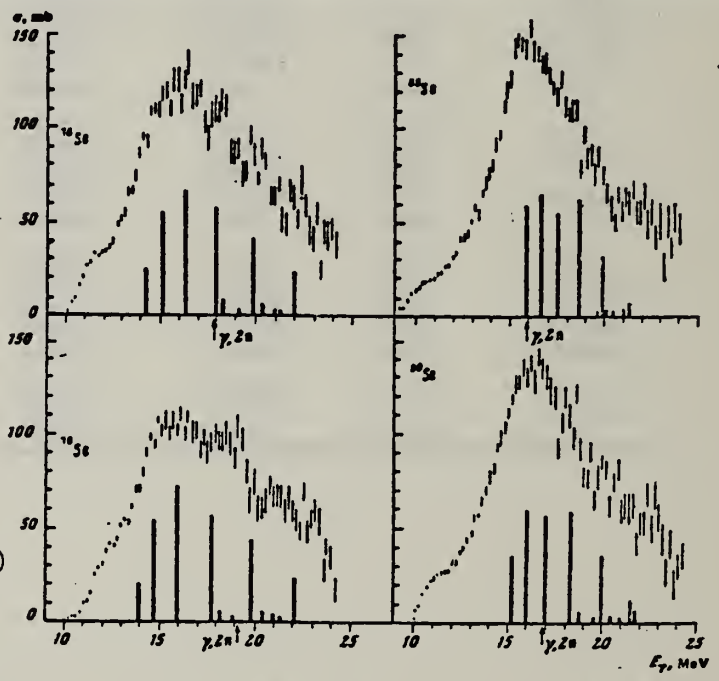

Fig. 3. The same as in Fig. 1, but for ^{76,78,80,82}Se.

Table 3

Nuclide	σ, mb	Nuclide	σ, mb	Nuclide	σ, mb
^{64}Zn	397±19*	^{72}Ge	760±37	^{76}Se	1021±52
^{66}Zn	579±27	^{73}Ge	872±41	^{80}Se	1029±50
^{68}Zn	718±35	^{76}Ge	911±43	^{82}Se	1067±53
^{70}Ge	731±37	^{78}Se	930±50		

*Mean - square errors

Cross sections of photoneutron reactions. The dipole photoabsorption forces are taken from [6,7] (the solid black columns).

Values given are for σ_0(24.2 MeV).

[6] M.G.Huber et al., Phys.Rev.155,1073(67)
[7] M.G.Huber et al., Phys.Rev.192,223(66.

REF. P. Carlos, H. Beil, R. Bergere, J. Fagot, A. Lepretre, A. Veyssiere, G. V. Solodukhov
Nucl. Phys. A258, 365 (1976)

ELEM. SYM.	A	Z
Se	80	34

METHOD

REF. NO.: 76 Ca 1 egf

REACTION	RESULT	EXCITATION ENERGY	SOURCE		DETECTOR		ANGLE
			TYPE	RANGE	TYPE	RANGE	
G,N	ABX	10- 28	D	10- 28	MOD-I		4PI
G,2N	ABX	16- 28	D	10- 28	MOD-I		4PI

996+

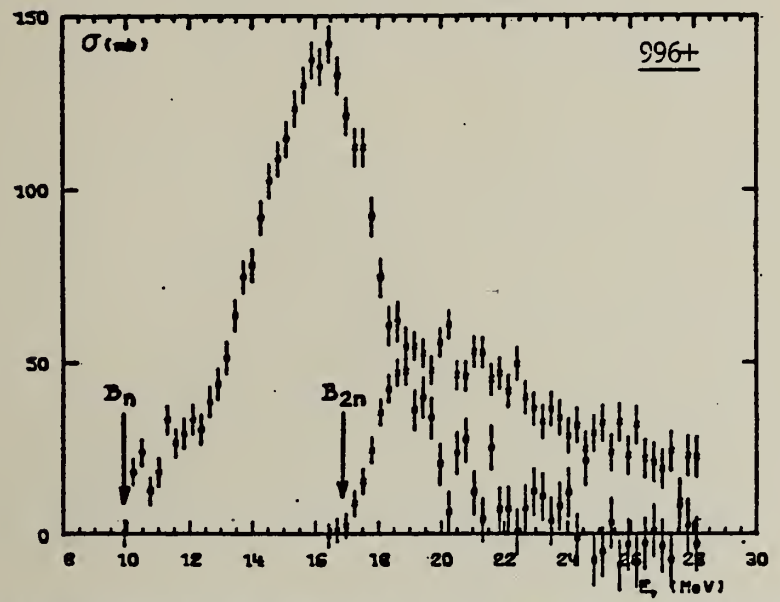

Fig. 10. Partial photoneutron cross section $[\sigma(\gamma, n)+\sigma(\gamma, pn)]$ and $\sigma(\gamma, 2n)$ for ^{80}Se. Arrows B_n and B_{2n} indicate theoretical threshoid values for (γ, n) and $(\gamma, 2n)$ reactions respectively.

TABLE 3

Integrated photoneutron cross sections and comparison with sum rules

Nucleus	^{64}Zn	^{69}Ga / ^{71}Ga	^{70}Ge	^{72}Ge	^{74}Ge	^{76}Ge	^{75}As	^{76}Se	^{78}Se	^{80}Se	^{82}Se
E_M (MeV)	29	26.5	26.5	26.5	26.5	26.5	26.5	26.5	26.5	26.5	26.5
σ_{0n} (MeV · b)	0.75	0.91	0.78	0.94	1.02	1.12	1.09	1.01	1.06	1.11	1.13
$\frac{\sigma_{0n}A}{0.06\,NZ}$	0.78	0.87	0.75	0.88	0.94	1	0.98	0.90	0.92	0.94	0.95
$B_n - B_p$ (MeV)	4.2	3.7 / 1.4	3	1	−0.8	−2.6	3.3	1.7	0.1	−1.5	−3
σ_{-1n} (mb)	38	52	44	54	59	64	63	58	62	65	67
$\sigma_{-1n}A^{-\frac{1}{3}}$ (mb)	0.15	0.18	0.15	0.18	0.19	0.20	0.20	0.18	0.19	0.19	0.19
σ_{-2n} (mb · MeV^{-1})	2.0	3.1	2.5	3.2	3.6	3.9	3.7	3.4	3.8	3.9	4.2
$\sigma_{-2n}A^{-\frac{1}{3}}$ (μb · MeV^{-1})	1.9	2.6	2.1	2.6	2.8	2.9	2.8	2.5	2.7	2.6	2.7

The notation used is defined in the text. The average experimental errors $\Delta\sigma_{0n}/\sigma_{0n}$, $\Delta\sigma_{-1n}/\sigma_{-1n}$ and $\Delta\sigma_{-2n}/\sigma_{-2n}$ are approximately 8 %.

SE
A=82

SE
A=82

REF.
E. Silva, J. Goldemberg
An. Acad. Brasil. Cienc. 28, 275 (1956)

ELEM. SYM.	A	Z
Se	82	34

METHOD
Betatron

REF. NO.
56 Si 2 | NVB

REACTION	RESULT	EXCITATION ENERGY	SOURCE		DETECTOR		ANGLE
			TYPE	RANGE	TYPE	RANGE	
G,N	ABX	9-22	C	9-22	ACT-I		4PI

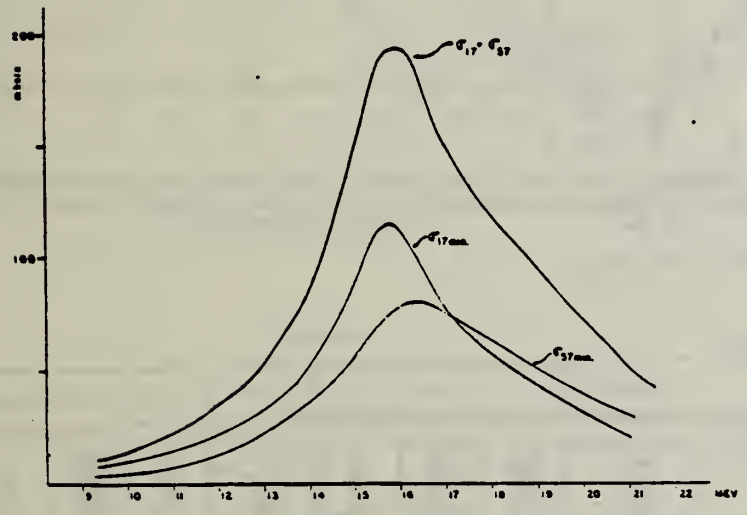

Fig. 5

TABELA I

REAÇÃO	σ max (barns)	Γ (largura) (Mev)	∫σdE Experimental	∫σdE teórico x = 0	∫σdE teórico x = 0,55
$Se^{82}(\gamma,n)Se^{81}$ e Se^{81*}	0,19	4,6	0,87 Mev-barn	1,23 Mev-barn	1,77 Mev-barn

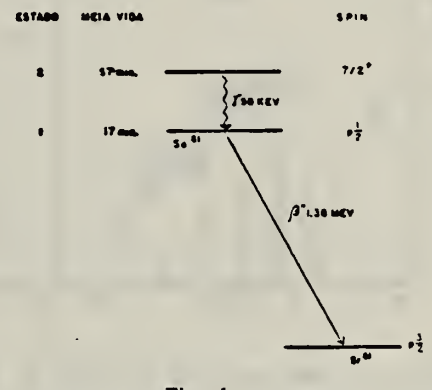

Fig. 1

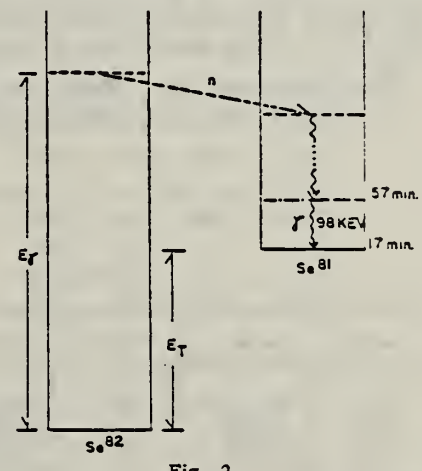

Fig. 2

REF. A.M. Goryachev, G.N. Zalesnyi, and B.A. Tulupov
Izv. Akad. Nauk SSSR. Ser. Fiz. 39, 134 (1975)
Bull. Acad. Sci. USSR Phys. Ser. 39, 116 (1975)

EL EM. SYM.	A	Z
Se	82	34

METHOD

REF. NO. 75 Go 1 hmg

REACTION	RESULT	EXCITATION ENERGY	SOURCE TYPE	SOURCE RANGE	DETECTOR TYPE	DETECTOR RANGE	ANGLE
G,XN	ABX	9- 25	C	9- 25	BF3-I		4PI

σ(G,SN). Statistical theory used to obtain SN cross section from XN cross section.

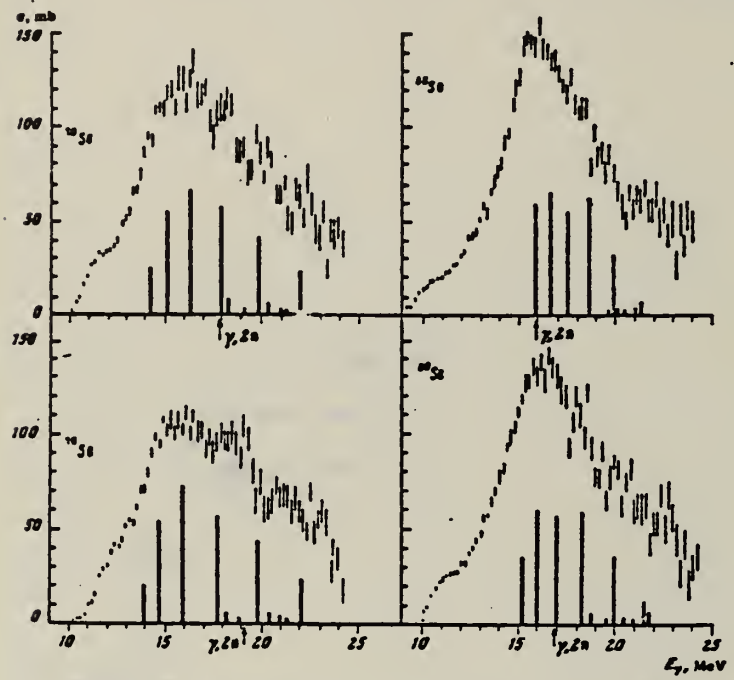

Fig. 3. The same as in Fig. 1, but for ^{76,78,80,82}Se.

Cross sections of photoneutron reactions. The dipole photoabsorption forces are taken from [6,7] (the solid black columns).

[6] M.G.Huber et al., Phys.Rev.155,1073(67)
[7] M.G.Huber et al., Phys.Rev.192,223(66.

Table 2

Nuclide	β_0	E_2, MeV	E_1, MeV	Nuclide	β_0	E_2, MeV	E_1, MeV
^{64}Zn	0.25	0.99	18	^{76}Ge	0.25	0.562	18
^{66}Zn	0.23	1.01	18	^{76}Se	0.33	0.559	18
^{68}Zn	0.2	1.08	18	^{78}Se	0.3	0.616	18
^{70}Ge	0.21	1.04	18	^{80}Se	0.25	0.654	18
^{72}Ge	0.25	0.835	18	^{82}Se	0.2	0.655	18
^{74}Ge	0.3	0.6	18				

Table 3

Nuclide	σ, mb	Nuclide	σ, mb	Nuclide	σ, mb
^{64}Zn	397±19*	^{74}Ge	760±37	^{76}Se	1021±52
^{66}Zn	579±27	^{76}Ge	872±41	^{80}Se	1029±50
^{68}Zn	718±35	^{78}Ge	911±43	^{82}Se	1067±53
^{70}Ge	751±37	^{78}Se	930±50		

*Mean - square errors

Values given are for σ_0(24.2 MeV).

REF.		ELEM. SYM.	A	Z
	P. Carlos, H. Beil, R. Bergere, J. Fagot, A. Lepretre, A. Veyssiere, G. V. Solodukhov Nucl. Phys. A258, 365 (1976)	Se	82	34
METHOD		REF. NO.		
		76 Ca 1		egf

REACTION	RESULT	EXCITATION ENERGY	SOURCE		DETECTOR		ANGLE
			TYPE	RANGE	TYPE	RANGE	
G,N	ABX	9- 26	D	9- 26	MOD-I		4PI
G,2N	ABX	16- 26	D	9- 26	MOD-I		4PI

999+

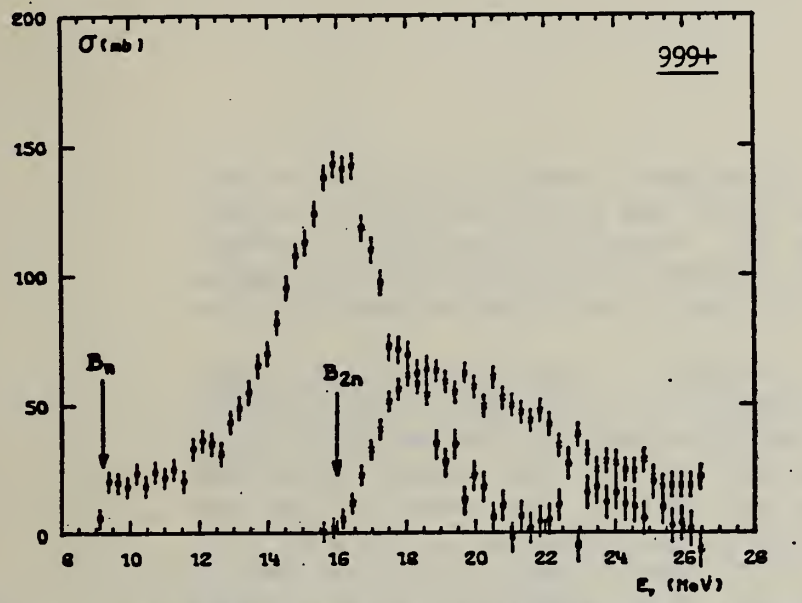

Fig. 11. Partial photoneutron cross sections $[\sigma(\gamma, n)+\sigma(\gamma, pn)]$ and $\sigma(\gamma, 2n)$ for ^{82}Se. Arrows B_n and B_{2n} indicate theoretical threshold values for (γ, n) and $(\gamma, 2n)$ reactions respectively. Data were not corrected for impurities.

TABLE 3

Integrated photoneutron cross sections and comparison with sum rules

Nucleus	^{64}Zn	^{69}Ga / ^{71}Ga	^{70}Ge	^{72}Ge	^{74}Ge	^{76}Ge	^{75}As	^{76}Se	^{78}Se	^{80}Se	^{82}Se
E_M (MeV)	29	26.5	26.5	26.5	26.5	26.5	26.5	26.5	26.5	26.5	26.5
σ_{0a} (MeV · b)	0.75	0.91	0.78	0.94	1.02	1.12	1.09	1.01	1.06	1.11	1.13
$\frac{\sigma_{0a}A}{0.06\,NZ}$	0.78	0.87	0.75	0.88	0.94	1	0.98	0.90	0.92	0.94	0.95
$B_a - B_p$ (MeV)	4.2	3.7 / 1.4	3	1	−0.8	−2.6	3.3	1.7	0.1	−1.5	−3
σ_{-1a} (mb)	38	52	44	54	59	64	63	58	62	65	67
$\sigma_{-1a}A^{-\frac{1}{3}}$ (mb)	0.15	0.18	0.15	0.18	0.19	0.20	0.20	0.18	0.19	0.19	0.19
σ_{-2a} (mb · MeV^{-1})	2.0	3.1	2.5	3.2	3.6	3.9	3.7	3.4	3.8	3.9	4.2
$\sigma_{-2a}A^{-\frac{1}{3}}$ (μb · MeV^{-1})	1.9	2.6	2.1	2.6	2.8	2.9	2.8	2.5	2.7	2.6	2.7

The notation used is defined in the text. The average experimental errors $\Delta\sigma_{0a}/\sigma_{0a}$, $\Delta\sigma_{-1a}/\sigma_{-1a}$ and $\Delta\sigma_{-2a}/\sigma_{-2a}$ are approximately 8 %.

BROMINE

Z=35

Tyrian purple (an organic compound of bromine) was used as a rich and costly dye centuries before the element bromine was discovered. It was prepared from a white juice secreted by the Mediterranean mollisk that was mentioned in the Bible (Ezek. 27:7,16).

Credit for the discovery of bromine is given to Antoine-Jérôme Balard (1802-1876), a Frenchman and an obscure young assistant at the chemistry department of the College of Montpellier. At the time of his discovery he was only 23 years old. In 1824, while studying the flora of a salt marsh, Balard noticed a deposit of sodium sulfate which had crystallized out in a pan containing mother liquid from common salt. In an attempt to find a use for these waste liquors he made a series of observations which led to the discovery of bromine. He suggested the name "muride" for the new element to the French Academy of Science. They, in turn, proposed the name "brome" from the Greek word *bromos* meaning stench, to indicate its strong irritating odor.

T. Kaminishi, C. Kojima
Jap. J. Appl. Phys. 2, 399 (1963)

Br		55

METHOD: Linac; isomer yield; activity

REF. NO.: 63 Ka 2 | NVB

REACTION	RESULT	EXCITATION ENERGY	SOURCE TYPE	SOURCE RANGE	DETECTOR TYPE	DETECTOR RANGE	ANGLE
G,G/	RLY	1	C4		ACT-I		4PI
		(0.21)					

Table II. The isomers observed

Isomer	Observed value		Referenced value[1)13)]	
	Half-life	Energy (MeV)	Half-life	Energy (MeV)
Se-77m	17.5 sec	0.160	17.5 sec	0.161
Br-79m	4.80 sec	0.209	4.8 sec	0.208
Sr-87m	2.3 hr	0.390	2.8 hr	0.388
Y-89m	15.0 sec	0.920	14 sec	0.915
Rh-103m	58 min	*	57 min	0.040
Ag-107m	42 sec	0.95	44 sec	0.094
Ag-109m			40 sec	0.088
Cd-111m	47 min	0.150,0.255	49 min	0.150,0.247
In-115m	4.5 hr	0.335	4.5 hr	0.335
Sn-117m	17 day	0.160	14 day	0.159,0.161
Ba-137m	2.6 min	0.660	2.6 min	0.662
Er-167m	2.10 sec	0.209	2.5 sec	0.208
Hf-179m	18.5 sec	0.157,0.215	19 sec	0.161,0.217
W-183m	5.4 sec	0.200,0.170,0.115	5.5 sec	0.1025,0.2915 others
Ir-191m	4.90 sac	0.129, <0.07	4.9 sec	0.042-0.129
Pt-195m	4.5 day	0.065**	4.1 day	0.031-0.130
Au-197m	7.0 sec	0.10,0.27,0.40	7.2 sec	0.130,0.270,0.407
Hg-199m	43 min	0.160,0.370	42 min	0.158,0.368

* This isomer was measured with a G-M flow counter.
** This value corresponds to Pt-K X-ray energy.

Table III. Induced activation rate

Element	Beam energy (MeV)	Counting rate (×10000 cpm)	Sample form
Se	5	1300	metallic plate
Br	4	1600	NaBr grain
Sr	6	0.3	$SrCO_3$ powder
Y	5	90	metallic grain
Rh	5	(0.2)*	$RhCl_3$ grain
Ag	5	180	metallic plate
Cd	6	0.5	$CdCl_2$ grain
In	6	8	metallic plate
Sn	6	0.0005	metallic plate
Ba	5	0.6	BaS powder
Er	4	4900	Er_2O_3 powder
Hf	5	1600	metallic plate
W	5	120	metallic powder
Ir	5	2100	metallic powder
Pt	5	0.3	metallic plate
Au	4	4300	metallic plate
Hg	6	0.09	metallic liquid

* The value measured with a G-M flow counter.

REF.

J. W. Jury, J. S. Hewitt, and K. G. McNeill
Can. J. Phys. 46, 1823 (1968)

ELEM. SYM.	A	Z
Br		35

METHOD

REF. NO.	
68 Ju 1	EGF

REACTION	RESULT	EXCITATION ENERGY	SOURCE		DETECTOR		ANGLE
			TYPE	RANGE	TYPE	RANGE	
G,N	NOX	THR - 27	C	27	THR	5-	DST

$$W(\theta) = a_o + a_1 P_1 + a_2 P_2$$

TABLE I

Target element	Z	Energy	a_0*	a_1/a_0	a_2/a_0
Vanadium	23	32	640 ± 50	0.11 ± 0.10	−0.09 ± 0.11
Chromium	24	22	365 ± 39	0.02 ± 0.08	0.00 ± 0.10
Manganese	25	22	450 ± 33	0.07 ± 0.05	−0.11 ± 0.06
Bromine	35	27	874 ± 54	0.05 ± 0.06	−0.15 ± 0.08
Molybdenum	42	22	610 ± 60	0.09 ± 0.05	−0.35 ± 0.06
Ruthenium	44	27	1100 ± 25	0.12 ± 0.02	−0.29 ± 0.03
Rhodium	45	27	1270 ± 47	0.06 ± 0.03	−0.14 ± 0.03
Palladium	46	27	1350 ± 29	0.26 ± 0.02	−0.12 ± 0.02
Antimony	51	27	2140 ± 62	0.04 ± 0.08	−0.25 ± 0.11
Lanthanum	57	27	1940 ± 70	0.12 ± 0.10	−0.52 ± 0.14
Praseodymium	59	30	1800 ± 58	0.20 ± 0.08	−0.40 ± 0.09
Platinum	78	27	2600 ± 52	0.17 ± 0.02	−0.15 ± 0.03
Lead	82	22	2274 ± 59	0.08 ± 0.08	−0.46 ± 0.09

*The yield per mole per 100 r was normalized to a yield of 2274 for the lead sample at the same energy.

REF.

R.F. Barrett, J.R. Birkelund, B.J. Thomas, K.S. Lam, and H.H. Thies
Nucl. Phys. A210, 355 (1973)

ELEM. SYM.	A	
Br		35

METHOD

REF. NO.	
73 Ba 20	egf

REACTION	RESULT	EXCITATION ENERGY	SOURCE		DETECTOR		ANGLE
			TYPE	RANGE	TYPE	RANGE	
G,N	NOX	THR- 27	C	10- 27	BF3-I		4PI

MEAN NEUT ENERGY

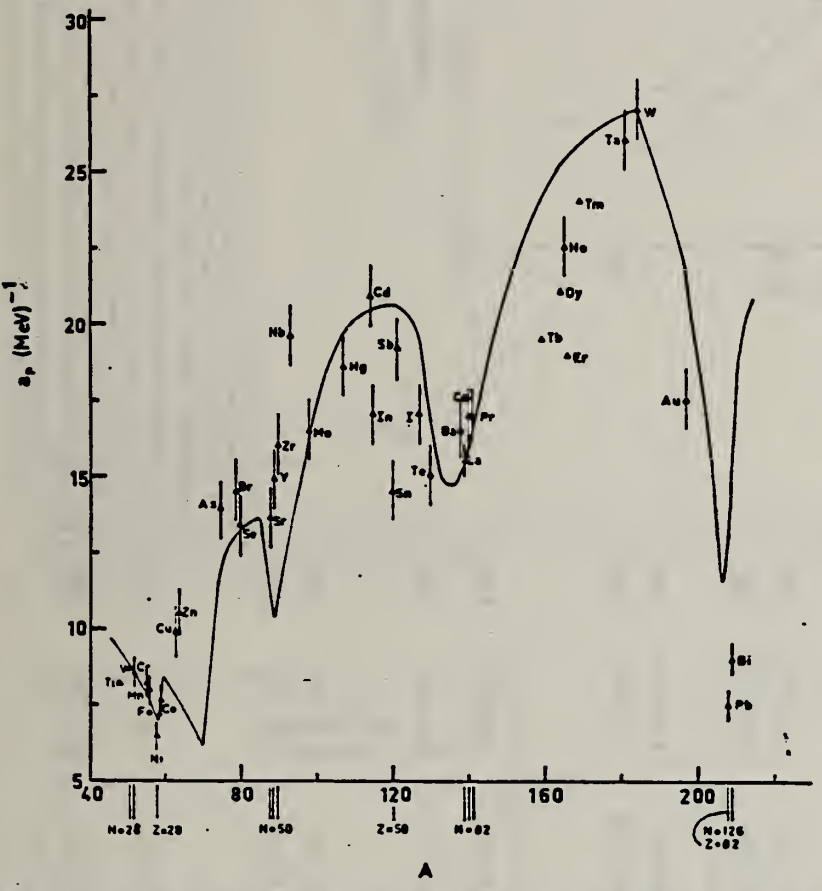

Fig. 12. Experimental values of the level density parameter a_p (Fermi gas formula plus pairing correction) versus atomic number A. The continuous curve is a least-squares fit to the data of a theoretical calculation from Newton [15].

1
H. Baba and S. Baba, Japan Atomic Energy Research Institute report JAERI-1183 (1969).
2
H. Baba, Nucl. Phys. A159, 625 (1970).
15
T.D. Newton, Can. J. Phys. 34, 804 (1956).

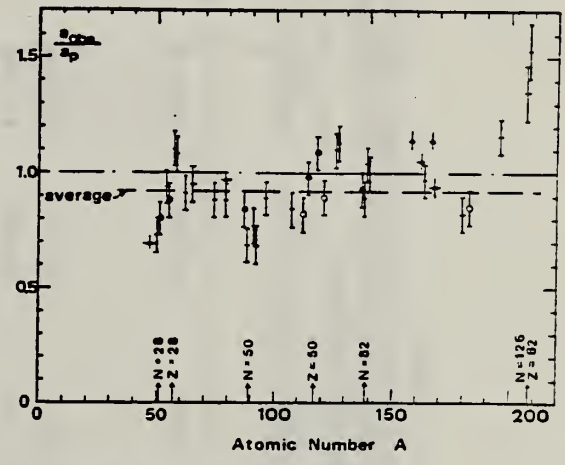

Fig. 15. Ratio a_{obs}/a_p versus atomic number A. Here a_{obs} is the level density parameter taken from the neutron resonance work of refs. [1,2]), and a_p is the level density parameter derived from the present (γ, n) work. Filled circles represent points where nuclei in the neutron resonance and in the (γ, n) experiment were the same. Open circles represent points where the respective nuclei were approximately matched. Triangles represent points which are based on measurement of neutron mean energies at two bremsstrahlung energies only.

(over)

TABLE 3

Comparison of experimental and theoretical data on nuclear level densities with Fermi gas formulae, and comparison of nuclear level density parameters from (γ, n) and n-resonance absorption experiments

Target	N (residual nucleus) [a]		Goodness of fit [b]		$\hat{E}_a(24)$ (MeV) [c]	T (MeV) [d]	a_γ (MeV^{-1}) [e]	a_{abs} (MeV^{-1}) [f]	a_{abs}/a_p
			no p.c.	with p.c.					
Ti [g]	23	8%			1.93		8.1–^{47}Ti	6.41–^{47}Ti	0.79
	24	8%							
	25	73%							
	26	5%							
	27	5%							
V [g]	27	100%			1.96		8.7–^{50}V	6.35–^{51}V	0.73
Cr	25	4%	P	G	1.89		8.6–^{51}Cr	6.9 –^{51}Cr	0.80
	27	84%							
	28	10%							
	29	2%							
Mn	29	100%	V.P.	G	2.1		8.2–^{54}Mn	7.82–^{56}Mn	0.94
Fe	27	6%	F	G	1.96		8.0–^{55}Fe	7.06–^{53}Fe	0.88
	29	92%							
	30	2%							
Co	31	100%	P	F	2.12		7.7–^{58}Co	8.35–^{60}Co	1.08
Ni	29	68%	V.P.	P	2.04	1.4	6.5–$^{57.7}$Ni	7.19–^{59}Ni	1.10
($Z = 28$)	31	26%							
	32	1%							
	33	4%							
	35	1%							
Cu	33	69%	V.P.	P	1.78	1.0	9.8–^{62}Cu	8.90–^{64}Cu	0.91
	35	31%							
Zn	33	49%	F	F	1.61		10.5–$^{64.4}$Zn	10.0–^{63}Zn	0.95
	35	28%							
	36	4%							
	37	19%							
As	41	100%	V.P.	F	1.44		14.5–^{74}As	12.81–^{76}As	0.88
Se [g]	41	9%			1.39		13.3–^{78}Se	12.8 –^{78}Se	0.97
	42	8%							
	43	24%							
	45	50%							
	47	9%							
Br	43	45%	V.P.	V.P.	1.41		14.5–^{79}Br	12.69–^{80}Br	0.88
	45	49%							
Sr	47	10%	F	G	1.31		13.6–^{87}Sr	11.4 –^{87}Sr	0.84
	48	7%							
	49	83%							

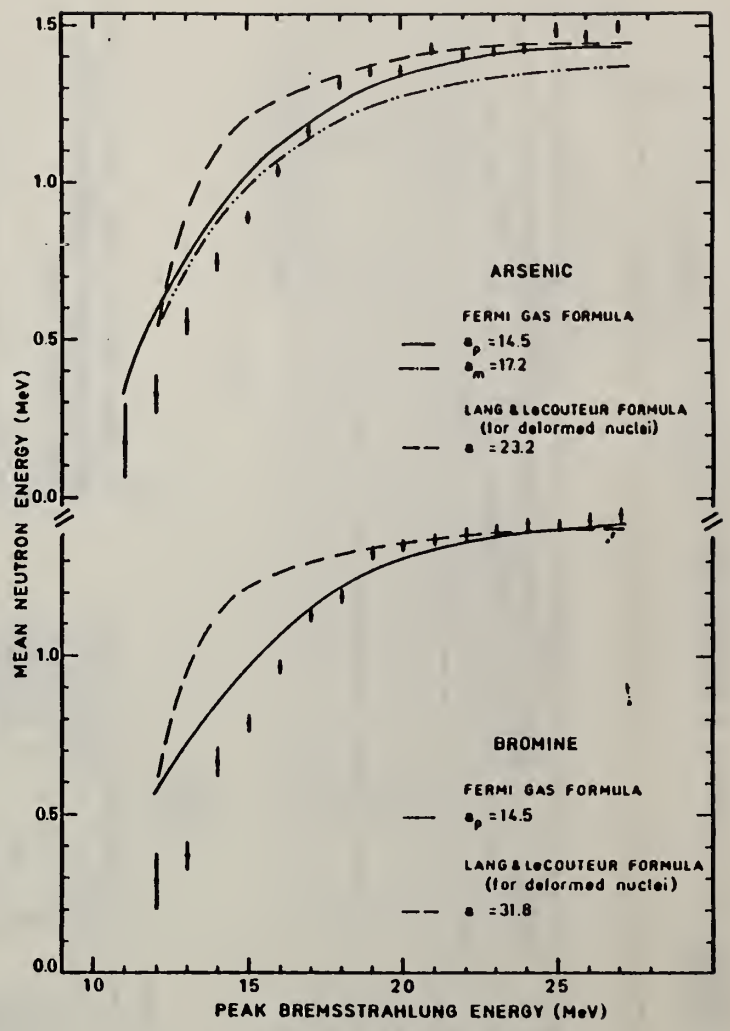

Fig. 7. Same as fig. 5, for arsenic and bromine.

[a]) Neutron numbers and abundances of respective residual nuclei in (γ, n) experiments.

[b]) These give an assessment of the goodness of fit of a calculated $\hat{E}_a$ versus E_0 curve to the observed data, using the Fermi gas level density formula both without and with pairing corrections.

[c]) Bremsstrahlung photoneutron mean energies $\hat{E}_a$ for peak bremsstrahlung energy $E_0 = 24$ MeV.

[d]) Nuclear temperature from fit with constant-temperature formula.

[e]) Level density parameter a_p derived from the present (γ, n) experiment, using a Fermi gas formula plus pairing correction, and corresponding residual nucleus (the atomic weight shown is the weighted average of atomic weights of the respective isotopes present).

[f]) As column 7, but using data on n-resonance absorption from refs. [1,2]).

[g]) Measurements of $\hat{E}_a(E_0)$ for these nuclei were made only for $E_0 = 21$, 23 and 24 MeV.

A. Järund and B. Forkman
Z. Physik A281, 39 (1977)

Br | 35

METHOD | REF. NO. 77 Ja 2 | egf

REACTION	RESULT	EXCITATION ENERGY	SOURCE TYPE	SOURCE RANGE	DETECTOR TYPE	DETECTOR RANGE	ANGLE
G,NA24	ABY	THR-999	C	400-999	ACT-I		4PI

999=1 GEV

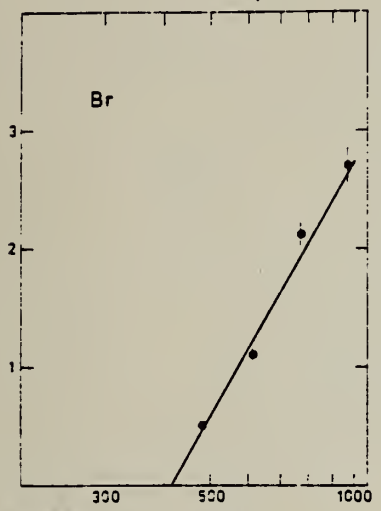

Fig. 1 b Bremsstrahlung energy (MeV)

Fig. 1 a–j. The measured yield as a function of bremsstrahlung end point energy. The error bars give the statistical errors in the numbers of γ-quanta detected. The solid lines are fitted to the yield points with the least-squares method. The yield from Cu (Fig. 1a) is measured in [1] and has been recalculated using the monitor curve of [5]

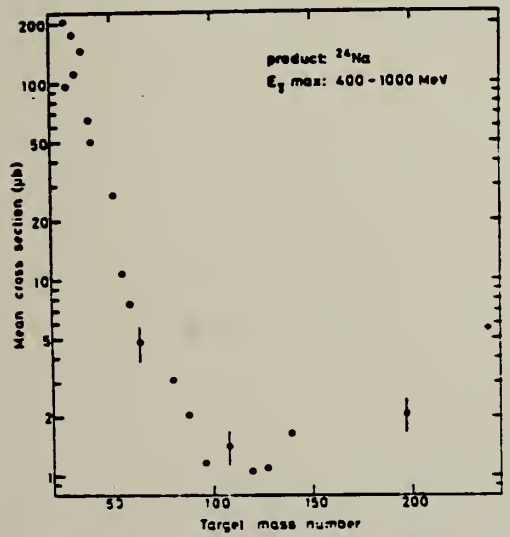

Fig. 2. The mean cross section in the energy range 400 to 1000 MeV calculated from the yields of Figure 1 in this work and of Figures 1 to [illegible]. The error is given by bars in some points

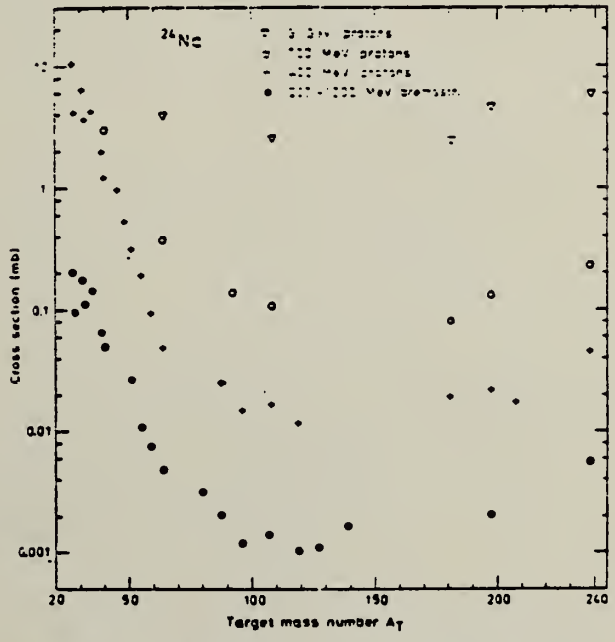

Fig. 4. Mean cross sections of the present work and of [1] (●) compared with the cross sections in proton irradiations: + 400 MeV from [4], o 700 MeV from [16] and an extrapolated value from [17]. ▽ 3 GeV from [18]

BR
A=79

BR
A=79

REF.

H. Langhoff, L. Frevert, W. Schott and A. Flammersfeld
Nucl. Phys. 79, 145 (1966)

ELEM. SYM.	A	Z
Br	79	35

METHOD

Resonance Fluorescence

[Page 1 of 2]

REF. NO. 66 La 1 JDM

REACTION	RESULT	EXCITATION ENERGY	SOURCE		DETECTOR		ANGLE
			TYPE	RANGE	TYPE	RANGE	
G,G	LFT	0 - 1	D	0 - 1	NAI-D	0 - 1	123

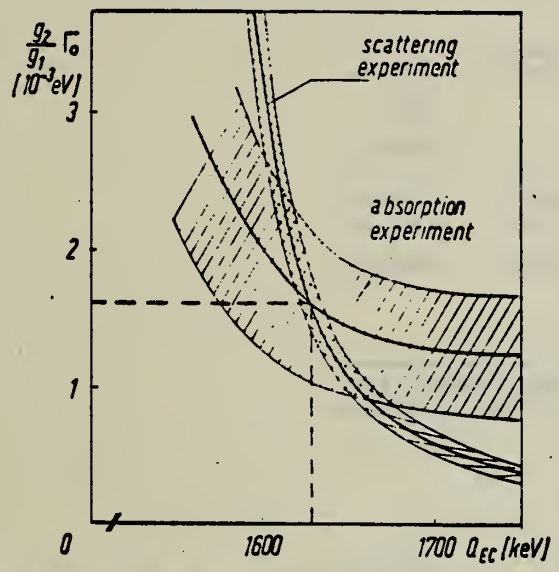

Fig. 5. $g_1\Gamma_0/g_0$ for the 834 keV transition determined by the scattering and by the absorption experiments is plotted as a function of the transition energy Q_{EC}.

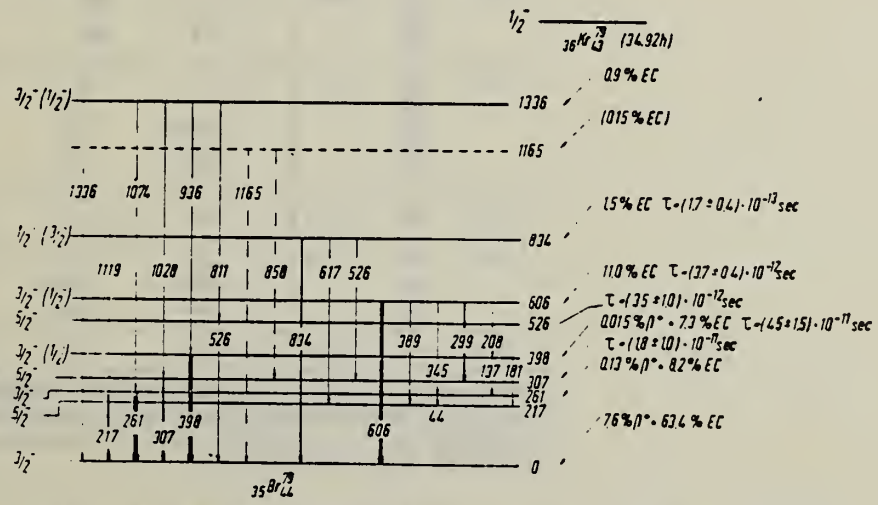

Fig. 7. Decay scheme of ^{79}Kr supplemented by the results of the present investigation.

TABLE 1

Results of resonance scattering and absorption experiments

E_γ (keV)	σ_{sc} (mb)	$\frac{g_1}{g_0}\frac{\Gamma_0^2}{\Gamma}$ (meV)	$\frac{\Gamma_0}{\Gamma}$	ε	$\frac{g_1}{g_0}\Gamma_0$ (meV)
834	70±10	1.25±0.28	0.80	(18.1±6.7) %	1.6 ±0.6
606	60±4	(0.95±0.07) · 10^{-1}	0.73	(6.0 ±1.7) %	0.15±0.04
526 a	330±90	(2.8 ±0.7) · 10^{-1}	1.00	(20.7±8.8) %	0.28±0.12
b	115±30	(1.0 ±0.3) · 10^{-1}			
398	23±4	(1.23±0.22) · 10^{-2}	0.92		
307	240±110	(5.4 ±2.5) · 10^{-2}	0.99		

The average cross sections for scattering σ_{sc} yield the values for $g_1\Gamma_0^2/g_0\Gamma$ given in column 3. ε represents the self absorption in the NaBr absorber and allows the calculation of $g_1\Gamma_0/g_0$. Γ_0/Γ have been obtained from the measurements described in sect. 3.

TABLE 4

γ-transition probabilities in ^{79}Br

E_{level} (keV)	E_γ (keV)	Spins	$\frac{\Gamma_i}{\Gamma}$	T_{M1+E2} [10^{10} sec^{-1}]	T_{E2} [10^{10} sec^{-1}]	$\lvert\delta\rvert$	$\frac{T_{M1}}{T_{sp}}$	$\frac{T_{sp}}{T_{E2}}$
834	834	$(\frac{1}{2}) \rightarrow \frac{1}{2}$	0.80	485			2	
	617	$\frac{1}{2}$	0.04	20				(90)
	526	$\frac{1}{2}$	0.16	100				(1000)
606	606	$\frac{3}{2} \rightarrow \frac{3}{2}$	0.73	20	2.1	0.32	21	10
	389	$\frac{1}{2}$	0.12	3.2			35	
	345	$\frac{3}{2}$	0.00072	0.2			400	
	299	$\frac{1}{2}$	0.077	2.1			25	
	208	$\frac{3}{2}$	0.040	1.1			15	
526	526	$\frac{1}{2} \rightarrow \frac{1}{2}$	1.00	28	3.1	0.33	10	30
398	398	$\frac{1}{2} \rightarrow \frac{1}{2}$	0.92	2.0	0.05	0.16	61	2
	181	$\frac{1}{2}$	0.008	0.018			610	
	137	$\frac{1}{2}$	0.065	0.14			34	
307	307	$\frac{1}{2} \rightarrow \frac{1}{2}$	0.99	5.6	0.05	0.10	10	7

T_{M1+E2} represents the partial transition probability determined in the resonance fluorescence investigation. The E2 transition probabilities T_{E2} obtained from Coulomb excitation experiments yield together with T_{M1+E2} the mixing ratios $|\delta|$. The results are compared with predictions of the single-particle model in column 8 and 9.

REF.

J. Schmouker, P. Erdos, P. Jordan and P. Stoll
J. Phys. Radium 16, 169 (1955)

ELEM. SYM.	A	Z
Br	81	35

METHOD

REF. NO. 55 Sc 2 EGF

REACTION	RESULT	EXCITATION ENERGY	SOURCE		DETECTOR		ANGLE
			TYPE	RANGE	TYPE	RANGE	
G,A	ABY	THR - 32	C	32	ACT-I		4PI

Betatron run at 31.5 MeV. Yields measured relative to $^{65}Cu(\gamma,n)^{64}Cu$ = 1.4 barn-MeV
$^{63}Cu(\gamma,n)^{62}Cu$ = 0.7 barn-MeV

$\bar{\sigma}$ $^{31}Br(\gamma,\alpha)^{77}As$ = 1.8±0.8 MeV-mb

Ref. P. Erdos, P. Scherrer, P. Stoll
Helva. Phys. Acta 30, 639 (1957)

Elem. Sym.	A	Z
Br	81	35

Method: Betatron; α yield; radioactivity; $Cu^{65}(\gamma,n)$ reaction

Ref. No.: 57 Er 1 | EGF

Reaction	E or ΔE	E_o	Γ	$\int \sigma dE$	$J\pi$	Notes
$Br^{81}(\gamma,\alpha)$	Bremss. 32			1.3±0.5 MeV-mb		Based on yield measurement.

Ref. A.M. King, A.F. Voigt
Phys. Rev. 105, 1310 (1957)

Elem. Sym.	A	Z
Br	81	35

Method: Iowa State 70 MeV synchrotron; neutron counter

Ref. No.: 57 Ki 1 EGF

Reaction	E or ΔE	E_o	Γ	$\int \sigma dE$	Jπ	Notes
$Br^{81}(\gamma,n)$	Bremss. 15-70					Measured relative yield of ground state to 4.4 hour Br^{80}: (17 min.) gs J = 2 (4.4 hr.) J = 5

TABLE I. Relative yields of Br^{80} and Br^{80m} from the photoneutron reaction in Br^{81}.

Experiment	Maximum bremsstrahlung energy	C_1[a]	C_2[a]	$t_{\frac{1}{2}}$ isomeric state (hr)	$t_{\frac{1}{2}}$ ground state (min)	R_2/R_1
1	15.7±1	4046±16	88190±2000	4.39±0.03	16.26±0.86	3.46±0.82
2	25 ±5	100± 4	3927± 183	4.38±0.02	17.60±0.03	2.48±0.12
3	25 ±5	124±11	4286± 18	4.36±0.12	16.65±0.81	2.38±0.21
4	27.4±1	257± 2	4206± 501	4.38±0.03	17.40±0.80	2.31±0.31
5	68.0±1	1687±18	41046± 944	4.37±0.05	16.79±0.37	2.50±0.08
6	70 ±1	1000±10	29170± 605	4.39±0.05	17.56±0.10	2.51±0.17
7	70 ±1	305± 6	9885± 300	4.36±0.07	16.72±0.17	2.36±0.07

[a] Contribution No. 490. Work performed in the Ames Laboratory of the U. S. Atomic Energy Commission.
[1] Katz, Pease, and Moody, Can. J. Phys. 30, 476 (1952).
[1a] Chien and Willard, J. Am. Chem. Soc. 77, 3441 (1955).
[2] Katz, Baker, and Montalbetti, Can. J. Phys. 31, 250 (1953).
[3] J. Goldemberg and L. Katz, Phys. Rev. 90, 308 (1953).
[4] K. Strauch, Phys. Rev. 81, 973 (1951).
[5] Koch, McElhinney, and Cunningham, Phys. Rev. 81, 318 (1951).
[6] J. L. Lawson and M. L. Perlman, Phys. Rev. 74, 1190 (1948).

K. N. Geller, J. Halpern, and E. G. Muirhead
Phys. Rev. 118, 1302-12 (1960)

ELEM. SYM.	MASS	ATOMIC NO.
Br	81	35

METHOD
Betatron; neutron threshold; ion chamber

REF. NO.
60 Ge 3 | NVB

REACTION	RESULT	EXCITATION ENERGY	SOURCE		DETECTOR		ANGLE
			TYPE	RANGE	TYPE	RANGE	
G,N	NØX	THR	C THR		BF3-I		4 PI

THRESHØLD

TABLE I. Summary and comparison of neutron separation energies inferred from present threshold measurements with values predicted from mass data and reaction energies. All energies are expressed in the center-of-mass system in Mev.

Reaction	No. runs	Present results	Other results	Method	Reference
$Br^{81}(\gamma,n)Br^{80}$	1	10.130±0.035	10.03 ±0.13	mass data	m
				$Q(\beta^-)$	n
			10.03 ±0.13	mass data	m
				$Q(\beta^+)$	o

[m] Henry E. Duckworth, *Mass Spectroscopy* (Cambridge University Press, New York, 1958), p. ....
[n] L. J. Lidofsky, Revs. Modern Phys. 29, 773 (1957).
[o] R. W. King, Revs. Modern Phys. 26, 327 (1954).

Ref. J.H. Carver, G.E. Coote, T.R. Sherwood
Nuclear Phys. 37, 449 (1962)

Elem. Sym.	A	Z
Br	81	35

Method: 30 MeV electron synchrotron; activation; NaI

Ref. No.: 62 Ca 1 JHH

Reaction	E or ΔE	E_0	Γ	$\int \sigma dE$	Jπ	Notes
$Br^{81}(\gamma,n)$	Bremss. 30					[10] L. Katz et al., Can. J. Phys. 30 (1952) 476. [11] L. Katz et al., Can. J. Phys. 31 (1953) 250. [12] R. Silva et al., An Acad. Brasil Cience 28 (1956) 275. [23] J. Goldemberg et al., Phys. Rev. 90 (1953) 308.

TABLE 1

Isomeric ratios from (γ, n) reactions

Target nucleus	J_0	Residual nucleus: Ground state		Metastable state		Intermediate state	Isomer ratio $Y_1/(Y_1+Y_2)$	σ
		Spin	Half-life	Spin	Half-life	Spin		
Co^{59}	$\frac{7}{2}^-$	Co^{58}	2^+ 71.3 d	5^+	9.2 h		0.44±0.02	3.2±0.2
Ge^{74}	0^+	Ge^{73}	$\frac{1}{2}^-$ 82 min	$\frac{7}{2}^+$	49 s		0.48±0.07	2.8±0.5
Br^{81}	$\frac{3}{2}^-$	Br^{80}	1^+ 18 min	5^-	4.4 h	2^-	0.32±0.02	6.5±1.0
Sr^{86}	0^+	Sr^{85}	$\frac{9}{2}^+$ 64 d	$\frac{1}{2}^-$	70 min	$\frac{7}{2}^+$	0.36±0.07	2.2±0.4
Zr^{90}	0^+	Zr^{89}	$\frac{9}{2}^+$ 79 h	$\frac{1}{2}^-$	4.4 min		0.33±0.10	2.8±0.7
Mo^{92}	0	Mo^{91}	$\frac{9}{2}^+$ 15.7 min	$\frac{1}{2}^-$	66 s		0.46±0.04	$6\frac{+}{-}1$
Ag^{107}	$\frac{1}{2}^-$	Ag^{106}	1^+ 24 min	6	8.3 d		0.04±0.02	2.0±0.3
In^{113}	$\frac{9}{2}^+$	In^{112}	1^+ 14.5 min	4^+	20.7 min	7^-	0.8±0.1	3.1±0.7
Cd^{116}	0^+	Cd^{115}	$\frac{1}{2}^+$ 53 h	$\frac{11}{2}^-$	43 d		≦ 0.2	≦ 3
Ce^{140}	0^+	Ce^{139}	$\frac{3}{2}^+$ 140 d	$\frac{11}{2}^-$	55 s		0.08±0.01	2.5±0.2
Hg^{198}	0^+	Hg^{197}	$\frac{1}{2}^-$ 65 h	$\frac{13}{2}^+$	24 h	$\frac{7}{2}^-$, $\frac{1}{2}^-$	0.05±0.01	3.4±0.5

	Ref.		Previous work						
Br^{81}	10)	$\frac{3}{2}^-$	Br^{80}	1^+	18 min	5^-	4.4 h	2^-	0.33	6.5
Se^{82}	12)	0^+	Se^{81}	$\frac{1}{2}^-$	18 min	$\frac{7}{2}^-$	57 min		0.5	3.0
Zr^{90}	11)	0^+	Zr^{89}	$\frac{9}{2}^+$	79 h	$\frac{1}{2}^-$	4.3 min		0.44±0.06	4.5±1
In^{115}	23)	$\frac{9}{2}^+$	In^{114}	1^+	72 s	5^-	50 d	8 ($T_{\frac{1}{2}}$ = 2.5 s)	0.85	5.0

The yields Y_1 and Y_2 are for (γ, n) reactions ending in the isomeric- or ground-state. The yield Y_1 is for the higher-spin state.

REF.

Y. Oka, T. Kato, K. Nomura, T. Saito and H. T. Tsai
Bull. Chem. Soc. Japan 41, 2660 (1968)

ELEM. SYM.	A	Z
Br	81	35

METHOD

REF. NO.	
68 Ok 1	egf

REACTION	RESULT	EXCITATION ENERGY	SOURCE		DETECTOR		ANGLE
			TYPE	RANGE	TYPE	RANGE	
G,A	ABY	THR-20	C	20	ACT-I		4PI

TABLE I. SUMMARY OF DATA ON (γ, α) REACTIONS WITH 20 MeV BREMSSTRAHLUNG

Nuclide			Observed gamma-ray			Results obtained	
Parent (Natural abundance, %)	Product (Half-life)	E_{th} ($-Q$, MeV)	Energy (MeV)	Branching ratio (%)	Type of multipole transition	μCi/mg[a]	Yield (mol^{-1}·R^{-1})
^{51}V(99.75)	^{47}Sc(3.4 d)	10.27	0.160	100	$M1+E2$	1.99×10^{-3}	2.8×10^{3}
^{63}Cu(30.9)	^{61}Co(99 min)	6.75	0.068	99	$M1+E2$	7.23×10^{-3}	9.7×10^{3}
^{71}Ga(39.6)	^{67}Cu(61 hr)	5.15	0.184	41	$M1$	2.70×10^{-3}	9.6×10^{3}
^{73}Ge(7.67)	^{69m}Zn(14 hr)	5.89	0.435	100	$M4$	1.11×10^{-3}	5.0×10^{3}
^{81}Br(49.48)	^{77}As(39 hr)	6.46	0.246	2.81	$M1+E2$	1.97×10^{-4}	4.3×10^{2}
^{109}Ag(48.65)	^{105}Rh(36 hr)	3.28	0.319+0.306	24.8	$M1+E2$	8.29×10^{-4}	3.7×10^{1}
^{115}In(95.77)	^{111}Ag(7.6 d)	3.78	0.340	6	$M1+E2$	5.70×10^{-3}	4.3×10^{1}

a) The value corrected at the end of 1 hr irradiation (9.4×10^{6} R/min).

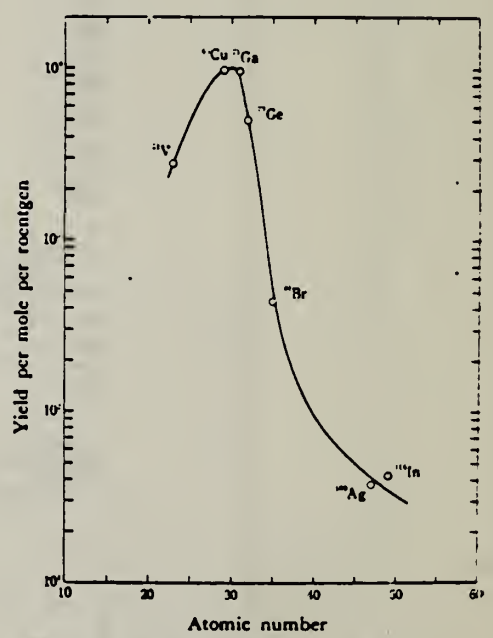

Fig. 1. The yield curve for (γ, α) reaction with 20 MeV bremsstrahlung.

# KRYPTON
Z=36

Krypton was discovered by William Ramsey and his assistant Morris Travers in 1898. They had tried in vain to find an inert gas, with an atomic weight between that of argon and helium, by heating rare minerals. Their next attempt was to diffuse argon and hopefully fractionate it into gases of different densities. They had been given a liter of liquid air which they used, not for liquefying their precious fifteen liters of argon but for obtaining sufficient skill in gas manipulation. Fortunately they were careful to save the residue of the liquid air for they found 25 cm^3 of an inert gas. This was placed in a Plücker tube and connected to an induction coil. Ramsey and Travers observed a bright yellow line with a green tint which did not coincide with any of the known lines. They named the new gas "krypton" meaning "hidden" in Greek.

REF. J. Goldemberg, Y. Torizuka, W. C. Barber, J..D. Walecka
Nuclear Phys. 43, 242 (1963)

ELEM. SYM.	A	Z
Kr		36

METHOD
Linac; electron scattering; magnetic spectrometer

REF. NO. 63 Go 4 JHH

REACTION	RESULT	EXCITATION ENERGY	SOURCE		DETECTOR		ANGLE
			TYPE	RANGE	TYPE	RANGE	
E,E/	ABX	15-21	D	41	MAG-D	17-42	180

W. Hofmann, R. Kosiek, G. Kraft and R. Mundhenke
Z. Physik 225, 303 (1969)

Kr		36

METHOD

REF. NO. 69 Ho 1 egf

REACTION	RESULT	EXCITATION ENERGY	SOURCE		DETECTOR		ANGLE
			TYPE	RANGE	TYPE	RANGE	
G,XP	ABY	THR- 33	C	24-33	SCI-D	3-14	90

Tabelle 1. *Daten zu den einzelnen Reaktionen. Die Werte für den integrierten Wirkungsquerschnitt wurden unter der Annahme ausschließlicher Grundzustandsübergänge berechnet. Für ^{23}Na und ^{39}K als Ausnahme s. Text*

Target	Anreicherungsgrad %	(γ,p)-Schwelle MeV	Druck oder Dicke	Endenergie MeV	Zahl gemess. Protonen	Ausbeute µb/MeV sr	$\int_{32.5}^{\sigma}(E)dE$ MeVmb	Figur
^{18}O	99	16,0	230 Torr	32,5	36074	58 ± 7	38 ± 6	1, 2
^{20}Ne	90,9	12,8	450 Torr	28,0	3175	7,4 ± 1	–	–
			610 Torr	32,5	6293	14,9 ± 2	61 ± 11	5, 6
^{22}Ne	99,9	15,3	240 Torr	24,0	1960	2,3 ± 0,4	–	4, 5
				28,0	4790	3,6 ± 0,6	–	4, 5
				32,5	5210	6,7 ± 0,9	45 ± 8	4, 5
^{23}Na	100	8,8	65µ	24,0	14182	6,3 ± 1,0	–	7
			60µ	32,5	11152	12,8 ± 2,0	117 ± 30	7
^{36}Ar	99	8,5	250 Torr	32,5	45173	57 ± 6	270 ± 40	8, 10
^{40}Ar	99,6	12,5	230 Torr	32,5	29559	14,2 ± 15	104 ± 15	9, 11
^{39}K	93,1	6,4	80µ	24,0	24230	17,4 ± 2,8	–	12
			90µ	32,5	24941	41,9 ± 6,7	405 ± 100	12
^{84}Kr	99	10,7	170 Torr	32,5	35515	12,7 ± 2,0	80 ± 20	14
Kr	natürl.	10	170 Torr	32,5	13570	12,5 ± 2,0	75 ± 20	13
Xe	natürl.	9	150 Torr	32,5	7553	7,6 ± 0,9	40 ± 7	15

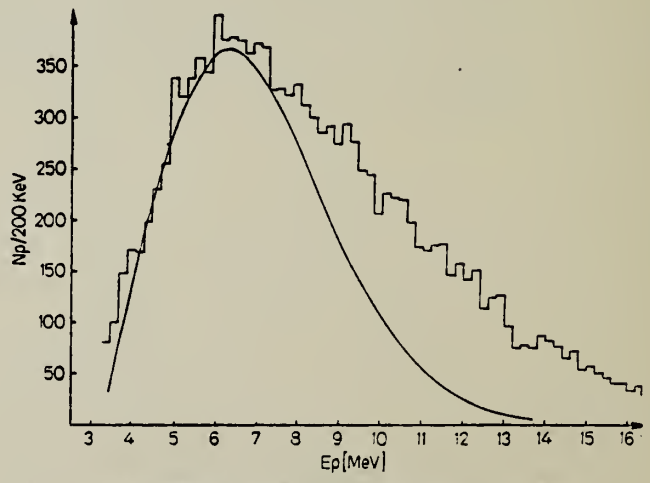

Fig. 13. Energieverteilung der Photoprotonen aus Kr für $E_0 = 32{,}5$ MeV. Kurve: Berechnetes Verdampfungsspektrum

KR
A=82

KR
A=82

REF.

G. B. Beard
Phys. Rev. 145, B862 (1966)

ELEM. SYM.	A	Z
Kr	82	36

METHOD

Resonance fluorescence; gaseous HBr source

REF. NO. 66 Be 2 JDM

REACTION	RESULT	EXCITATION ENERGY	SOURCE		DETECTOR		ANGLE
			TYPE	RANGE	TYPE	RANGE	
G,G	LFT	1(.77 - 1.47)	C	1	NAI-D	0-2	113

Used recoil energy from β-decay to give Doppler broadened spectrum.

Measured $\int \sigma ssdE$.

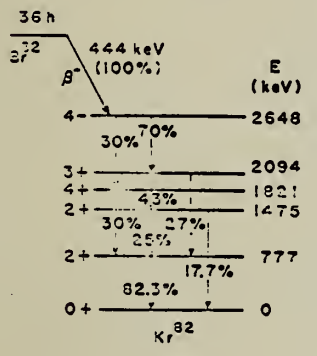

FIG. 1. Decay scheme of Br^{82}, showing only the major transitions and their percentages based on the summary (Ref. 2) of the results of recent measurements of relative gamma-ray intensities. The percentages of the gamma rays shown were then adjusted to account for the branching of the decay to the 2618-keV

TABLE II. Summary of properties of the first (2^+) excited states of even-even Kr isotopes. The values for the relative $B(E2)$ are taken from Ref. 1. Column 6 gives the ratio of the observed transition probabilities to the Weisskopf estimate (Ref. 10) for $E2$ transitions.

Isotope	$E(2^+)$ (keV)	Relative $B(E2)\uparrow$	Absolute $B(E2)\uparrow$ ($e^2\times10^{-48}$ cm^4)	τ (sec)	$\frac{B(E2)}{B(E2_W)}$
$_{36}Kr^{78}$	450	0.51	0.59	3.8×10^{-11}	54
Kr^{80}	620	0.34	0.39	1.13×10^{-11}	36
Kr^{82}	777	0.18	0.21	6.9×10^{-12}	19
Kr^{84}	880	0.15	0.17	4.7×10^{-12}	16

$^{83}_{36}$Kr
A=81

$^{84}_{36}$Kr
A=84

$^{85}_{36}$Kr
A=81

REF.

W. Hofmann, R. Kosiek, G. Kraft and R. Mundhenke
Z. Physik 225, 303 (1969)

Kr	84	36

METHOD

REF. NO. 69 Ho 1 egf

REACTION	RESULT	EXCITATION ENERGY	SOURCE		DETECTOR		ANGLE
			TYPE	RANGE	TYPE	RANGE	
G,XP	ABY	THR- 33	C	24-33	SCI-D	3-14	90

Tabelle 1. *Daten zu den einzelnen Reaktionen. Die Werte für den integrierten Wirkungsquerschnitt wurden unter der Annahme ausschließlicher Grundzustandsübergänge berechnet. Für ^{23}Na und ^{39}K als Ausnahme s. Text*

Target	Anreicherungsgrad %	(γ,p)-Schwelle MeV	Druck oder Dicke	Endenergie MeV	Zahl gemess. Protonen	Ausbeute µb/MeV sr	$\int_{32.5}^{\sigma}\sigma(E)dE$ MeVmb	Figur
^{18}O	99	16,0	230 Torr	32,5	36074	58 ± 7	38 ± 6	1, 2
^{20}Ne	90,9	12,8	450 Torr	28,0	3175	7,4 ± 1	–	–
			610 Torr	32,5	6293	14,9 ± 2	61 ± 11	5, 6
^{22}Ne	99,9	15,3	240 Torr	24,0	1960	2,3 ± 0,4	–	4, 5
				28,0	4790	3,6 ± 0,6	–	4, 5
				32,5	5210	6,7 ± 0,9	45 ± 8	4, 5
^{23}Na	100	8,8	65µ	24,0	14182	6,3 ± 1,0	–	7
			60µ	32,5	11152	12,8 ± 2,0	117 ± 30	7
^{36}Ar	99	8,5	250 Torr	32,5	45173	57 ± 6	270 ± 40	8, 10
^{40}Ar	99,6	12,5	230 Torr	32,5	29559	14,2 ± 15	104 ± 15	9, 11
^{39}K	93,1	6,4	80µ	24,0	24230	17,4 ± 2,8	–	12
			90µ	32,5	24941	41,9 ± 6,7	405 ± 100	12
^{84}Kr	99	10,7	170 Torr	32,5	35515	12,7 ± 2,0	80 ± 20	14
Kr	natürl.	10	170 Torr	32,5	13570	12,5 ± 2,0	75 ± 20	13
Xe	natürl.	9	150 Torr	32,5	7553	7,6 ± 0,9	40 ± 7	15

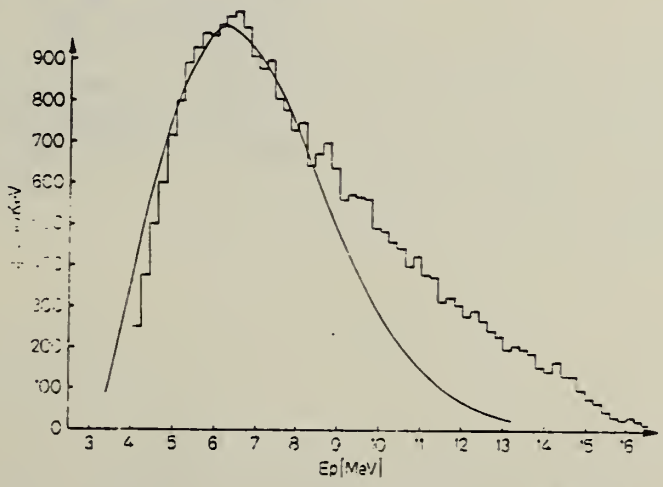

Fig. 11. Energieverteilung der Photoprotonen aus ^{84}Kr für $E_0 = 32.5$ MeV. Kurve: Berechnetes Verdampfungsspektrum

RUBIDIUM
Z=37

Rubidium was discovered by Gustav Kirchoff and Robert Bunsen who announced their discovery to the Berlin Academy of Sciences on February 23, 1861. The achievement was made possible by the spectroscope that the two investigators had developed.

Kirchoff's mind was more speculative than Bunsen's and he was thoroughly familiar with the researches of Josef Fraunhofer. Kirchoff showed Bunsen that, instead of looking through colored glass to distinguish between similarly colored flames, he should use a prism to seperate the light into its constituent rays or lines. This was the basic idea of the spectroscope which they used to examine the mineral lepidolite from Saxony. They observed two remarkable red lines just beyond the brilliant Fraunhofer lines at the extreme red end of the solar spectrum. The new lines were attributed to an unknown substance which they called rubidium from the Latin *rubidus* meaning dark red.

A. Lepretre, H. Beil, R. Bergere, P. Carlos and A. Veyssiere
Nucl. Phys. A175, 609 (1971)

CHEM. SYM.		
Rb		37

METHOD	REF. NO.	
	71 Le 1	egf

REACTION	RESULT	EXCITATION ENERGY	SOURCE		DETECTOR		ANGLE
			TYPE	RANGE	TYPE	RANGE	
G,N 375	ABX	11-24	D	11-24	MOD-I		4PI
G,2N 376+	ABX	17-24	D	11-24	MOD-I		4PI

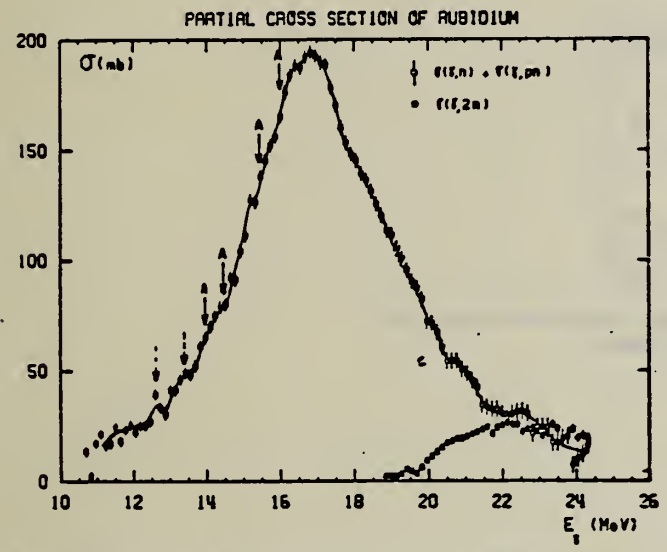

Fig. 1. Partial photoneutron cross sections $\sigma(\gamma, n)$ and $\sigma(\gamma, 2n)$ of Rb.

TABLE 1

Lorentz line parameters corresponding to fits shown in fig. 6.

	Rb	Sr	^{89}Y	^{90}Zr	^{93}Nb
σ_i (mb)	192 ±10	207 ±10	225 ±10	211 ±10	202 ±10
Γ_i (MeV)	4.1 ± 0.15	4.2± 0.1	4.1± 0.1	4.0 ± 0.1	4.7± 0.2
E_i (MeV)	16.75± 0.05	16.7± 0.05	16.7± 0.05	16.65± 0.05	16.5± 0.05

TABLE 3

Integrated cross sections (the notation used is defined in the text)

	Rb	Sr	^{89}Y	^{90}Zr	^{93}Nb
σ_0 (MeV · b)	1.14 ±0.06	1.42±0.07	1.36±0.07	1.26±0.07	1.33±0.07
$\frac{\sigma_0}{0.06\,NZ\,A^{-\frac{1}{3}}}$	0.915±0.05	1.09±0.05	1.04±0.05	0.95±0.05	0.97±0.05
σ_{-1} (mb)	67±4	80 ±5	77 ±5	71 ±5	79 ±5
σ_{-2} (mb · MeV^{-1})	4±0.2	4.6 ±0.2	4.4 ±0.2	4 ±0.2	4.8 ±0.2
E_M (MeV)	24	27	27	26	24

(over)

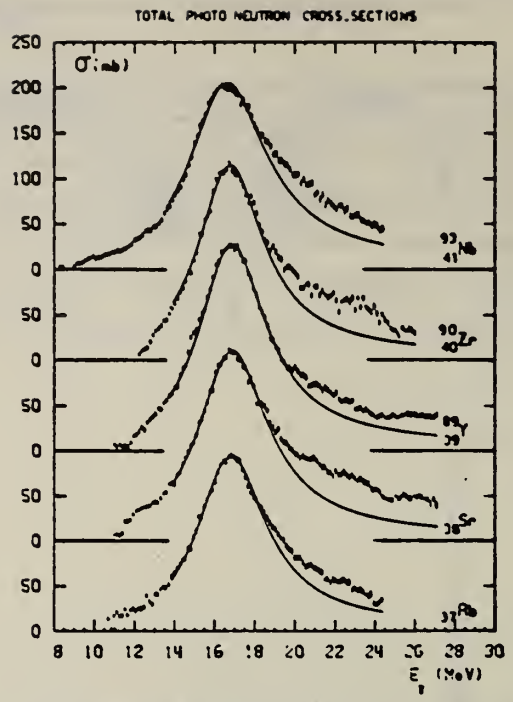

Fig. 6. Total photoneutron cross sections σ_T of Rb, Sr, ^{89}Y, ^{90}Zr and ^{93}Nb and best one Lorentz line fit corresponding to parameters given in table 1.

Rb
A=85

Rb
A=85

Ref. R. Tobin, J. McElhinney, L. Cohen
Phys. Rev. 110, 1388 (1958)

Elem. Sym.	A	Z
Rb	85	37

Method: 22 MeV Betatron

Ref. No.: 58 To 1 EH

Reaction	E or ΔE	E_o	Γ	$\int \sigma dE$	Jπ	Notes
$Rb^{85}(\gamma,n)$	Bremss 22					E_{th} = 10.50±0.08, based on counting isomers.

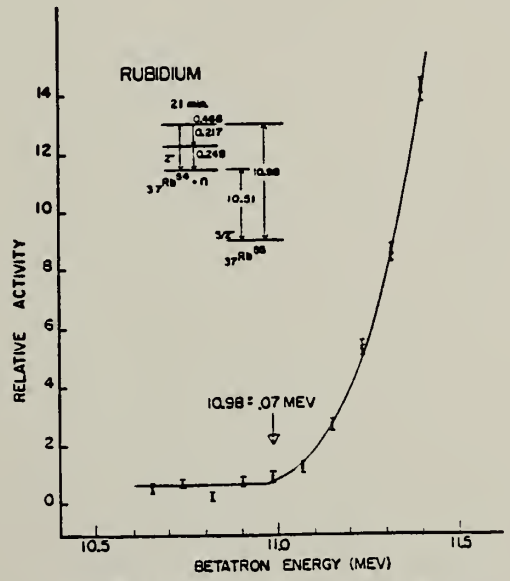

FIG. 6. Relative activity of the 21-minute isomeric state of Rb^{84} as a function of betatron energy.

K. N. Geller, J. Halpern, and E. G. Muirhead
Phys. Rev. 118, 1302-12 (1960)

ELEM.	MASS	AT. NO.
Rb	85	37

METHOD
Betatron; neutron threshold; ion chamber

REF. NO.
60 Ge 3 NVB

REACTION	RESULT	EXCITATION ENERGY	SOURCE		DETECTOR		ANGLE
			TYPE	RANGE	TYPE	RANGE	
G,N	NØX	THR	C THR		BF3-I		4 PI

THRESHØLD

TABLE I. Summary and comparison of neutron separation energies inferred from present threshold measurements with values predicted from mass data and reaction energies. All energies are expressed in the center-of-mass system in Mev.

Reaction	No. runs	Present results	Other results	Method	Reference
$Rb^{85}(\gamma,n)Rb^{84}$	1	10.65 ±0.08	10.26 ±0.16	mass data $Q(\beta^+)$	m n
			10.13 ±0.25	mass data $Q(\beta^-)$	m n

[m] Henry E. Duckworth, *Mass Spectroscopy* (Cambridge University Press, New York, 1958), p. 177.
[n] L. J. Lidofsky, Revs. Modern Phys. 29, 773 (1957).

5. Ergebnisse

Die Rechnungen für beide Reaktionen wurden mit Spin-cut-off-Parametern $\sigma = 3.5$ und $\sigma = 4$ durchgeführt und mit den gemessenen Isomerenverhältnissen verglichen. Durch Interpolation wurden Werte von σ ermittelt, für die die berechneten Isomerenverhältnisse mit den gemessenen Werten R_{exp} übereinstimmen.

Es ergaben sich folgende Resultate:

Reaktion	R_{exp}	σ
(n, 2n)	1.07±0.05	3.96±0.06
(γ, n)	0.37±0.01	3.78±0.03
		korr. 4.04±0.03

Herrn A. Heß danken wir für seine Hilfe bei der Bestrahlung am n-Generator, dem Bundesministerium für wiss. Forschung für die Bereitstellung von Sachmitteln.

Ref. P. Erdos, P. Scherrer, P. Stoll
Helva. Phys. Acta 30, 639 (1957)

Elem. Sym.	A	Z
Rb	87	37

Method: Betatron; α yield; radioactivity; $Cu^{65}(\gamma,n)$ measurement.

Ref. No.: 57 Er 1 EGF

Reaction	E or ΔE	E_o	Γ	$\int \sigma dE$	Jπ	Notes
$Rb^{87}(\gamma,\alpha)$	Bremss. 32			0.52 MeV-mb		Based on yield measurement.
$Rb^{87}(\gamma,n\alpha)$				0.05 MeV-mb		

Ref. R. Tobin, J. McElhinney, L. Cohen
Phys. Rev. 110, 1388 (1958)

Elem. Sym.	A	Z
Rb	87	37

Method 22 MeV Betatron; neutron counters

Ref. No. 58 To 1 EH

Reaction	E or ΔE	E_o	Γ	$\int \sigma dE$	Jπ	Notes
$Rb^{87}(\gamma, n)$	Bremss 22					E_{th} = 9.89±0.05

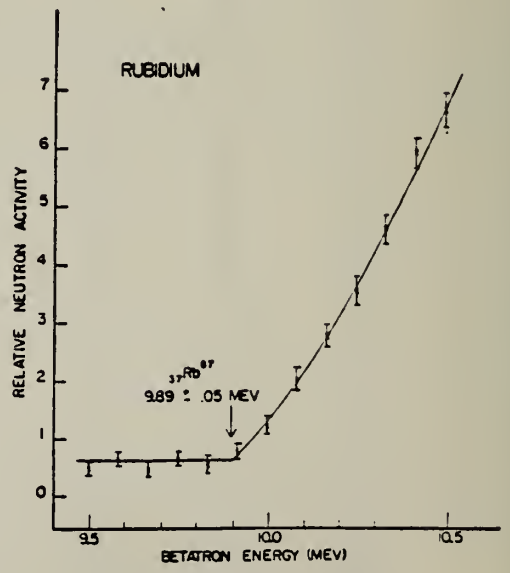

FIG. 5. Photoneutron yield from rubidium as a function of betatron energy.

REF.
K. N. Geller, J. Halpern, and E. G. Muirhead
Phys. Rev. 118, 1302-12 (1960)

ELEM. SYM.	A	
Rb	87	37

METHOD
Betatron; neutron threshold; ion chamber

REF. NO.	
60 Ge 3	NVB

REACTION	RESULT	EXCITATION ENERGY	SOURCE		DETECTOR		ANGLE
			TYPE	RANGE	TYPE	RANGE	
G,N	NØX	THR	C THR		BF3-I		4 PI

THRESHØLD

TABLE I. Summary and comparison of neutron separation energies inferred from present threshold measurements with values predicted from mass data and reaction energies. All energies are expressed in the center-of-mass system in Mev.

Reaction	No. runs	Present results	Other results	Method	Reference
$Rb^{87}(\gamma,n)Rb^{86}$	1	9.99 ±0.07	9.91 ±0.20	mass data	m
				$Q(\beta^-)$	n
			9.89 ±0.05	threshold	k

[k] See reference 2.
[l] See reference 3.
[m] Henry E. Duckworth, *Mass Spectroscopy* (Cambridge University Press, New York, 1958), p. 177.
[n] L. J. Lidofsky, Revs. Modern Phys. 29, 773 (1957).

# STRONTIUM
Z=38

Strontium was first detected in 1790 by Dr. Adair Crawford (1748-1795) of Edinburgh. He had obtained a new mineral that was found in the lead mine at Strontian, Argyleshire; most mineralogists considered the material to be an aerated barium carbonate. Crawford published a paper that showed that the salt (strontium chloride) obtained by dissolving the new mineral in hydrochloric acid differs in several respects from barium chloride. He further concluded that "the Scotch mineral is a new species of earth which has not hither to been sufficiently examined."

R.G. Baker, K.G. McNeill
Can. J. Phys. 39, 1158 (1961)

ELEM. SYM.	A	Z
Sr		38

METHOD: Betatron; fast neutron yield, angular distribution; Si threshold detector; ion chamber

REF. NO.: 61 Ba 2

REACTION	RESULT	EXCITATION ENERGY	SOURCE TYPE	SOURCE RANGE	DETECTOR TYPE	DETECTOR RANGE	ANG.
G,XN	ABY	THR-22	C	22	THR-I	5-+	DST

In Table 4:

$\bar{\sigma}$ = average cross section of detector weighted with neutron spectrum

$\bar{\Phi}$ = neutrons/100 roentgen/mole

$$W(\theta) = a_0 \sum_{n=1}^{\infty} [1 + A_n P_n (\cos \theta)]$$

TABLE IV

I Element	II a_0	III a_1	IV a_2	V $(\bar{\sigma}\bar{\Phi})\times10^{26}$	VI Φ_{fast}(22 Mev)$\times10^{9}$	VII Φ_{fast}/Φ_{total}
Vanadium	245(1±0.06)	0.01±0.08	−0.00±0.10	6.05	0.21	0.12
Chromium	104(1±0.03)	0.04±0.04	−0.05±0.05	4.05	0.17	0.10
Manganese	308(1±0.02)	0.07±0.02	−0.09±0.04	7.61	0.25	0.12
Iron	200(1±0.03)	0.05±0.04	−0.17±0.05	4.94	0.18	0.11
Cobalt	390(1±0.02)	0.08±0.03	−0.22±0.04	9.63	0.26	0.15
Nickel	145(1±0.05)	0.07±0.07	−0.23±0.09	3.58	0.12	0.12
Copper	347(1±0.02)	0.05±0.03	−0.29±0.04	8.57	0.30	0.12
Arsenic	482(1±0.03)	0.11±0.04	−0.24±0.05	11.91	0.33	0.15
Rubidium	638(1±0.05)	0.13±0.06	−0.14±0.08	15.76		
Strontium	409(1±0.05)	0.10±0.06	−0.17±0.08	10.10		
Yttrium	290(1±0.10)	0.08±0.12	−0.12±0.15	7.16		
Silver	590(1±0.04)	0.10±0.06	−0.22±0.08	14.57	0.87	0.07
Cadmium	905(1±0.02)	0.02±0.02	−0.26±0.03	22.35		
Iodine	1133(1±0.03)	0.04±0.04	−0.29±0.05	27.99	1.42	0.08
Barium	1048(1±0.04)	0.10±0.06	−0.38±0.08	25.89		
Lanthanum	1595(1±0.02)	0.02±0.03	−0.42±0.04	39.40	1.04	0.15
Cerium	1316(1±0.05)	0.05±0.06	−0.39±0.08	32.50		
Dysprosium	1652(1±0.08)	0.04±0.10	−0.34±0.13	40.80		
Tantalum	1558(1±0.02)	0.04±0.03	−0.22±0.04	38.48	2.50	0.06
Tungsten	1365(1±0.02)	−0.07±0.03	−0.24±0.04	33.71		
Mercury	1345(1±0.02)	0.04±0.03	−0.31±0.04	33.22		
Lead	2274(1±0.01)	0.02±0.02	−0.42±0.03	56.17	2.72	0.08
Bismuth	2162(1±0.02)	0.05±0.03	−0.45±0.04	53.40	3.36	0.06
Thorium	3031(1±0.04)	0.06±0.05	−0.32±0.07	74.87		
Uranium	4630(1±0.02)	0.05±0.03	−0.17±0.04	114.36		

*$(\bar{\sigma}\bar{\Phi})$ = 2.47×10⁹ a_0 millibarn-neutron. Errors are standard errors due to counting statistics only.

T. Kaminishi, C. Kojima
Jap. J. Appl. Phys. 2, 399 (1963)

Sr		38

METHOD: Linac; isomer yield; activity

REF. NO.: 63 Ka 2 | NVB

REACTION	RESULT	EXCITATION ENERGY	SOURCE TYPE	SOURCE RANGE	DETECTOR TYPE	DETECTOR RANGE	ANGLE
G,G/	RLY	1	C6		ACT-I		4PI
		(0.39)					

Table II. The isomers observed

Isomer	Observed value		Referenced value[11][13]	
	Half-life	Energy (MeV)	Half-life	Energy (MeV)
Se-77m	17.5 sec	0.160	17.5 sec	0.161
Br-79m	4.80 sec	0.209	4.8 sec	0.208
Sr-87m	2.3 hr	0.390	2.8 hr	0.388
Y-89m	15.0 sec	0.920	14 sec	0.915
Rh-103m	58 min	*	57 min	0.040
Ag-107m	42 sec	0.95	44 sec	0.094
Ag-109m			40 sec	0.088
Cd-111m	47 min	0.150,0.255	49 min	0.150,0.247
In-115m	4.5 hr	0.335	4.5 hr	0.335
Sn-117m	17 day	0.160	14 day	0.159,0.161
Ba-137m	2.6 min	0.660	2.6 min	0.662
Er-167m	2.10 sec	0.209	2.5 sec	0.208
Hf-179m	18.5 sec	0.157,0.215	19 sec	0.161,0.217
W-183m	5.4 sec	0.200,0.170,0.115	5.5 sec	0.1025,0.2915 others
Ir-191m	4.90 sac	0.129, <0.07	4.9 sec	0.042-0.129
Pt-195m	4.5 day	0.065**	4.1 day	0.031-0.130
Au-197m	7.0 sec	0.10,0.27,0.40	7.2 sec	0.130,0.270,0.407
Hg-199m	43 min	0.160,0.370	42 min	0.158,0.368

* This isomer was measured with a G-M flow counter.
** This value corresponds to Pt-K X-ray energy.

Table III. Induced activation rate

Element	Beam energy (MeV)	Counting rate (×10000 cpm)	Sample form
Se	5	1300	metallic pellet
Br	4	1600	NaBr grain
Sr	6	0.3	$SrCO_3$ powder
Y	5	90	metallic grain
Rh	5	(0.2)*	$RhCl_3$ grain
Ag	5	180	metallic plate
Cd	6	0.5	$CdCl_2$ grain
In	6	8	metallic plate
Sn	6	0.0005	metallic plate
Ba	5	0.6	BaS powder
Er	4	4900	Er_2O_3 powder
Hf	5	1600	metallic plate
W	5	120	metallic powder
Ir	5	2100	metallic powder
Pt	5	0.3	metallic plate
Au	4	4300	metallic plate
Hg	6	0.09	metallic liquid

* The value measured with a G-M flow counter.

REF.

A. Veres
Acta Phys. Acad. Sci. Hung. 16, 261-73 (1963)

ELEM. SYM.	A	-
Sr		38

METHOD

Radioactive source

REF. NO.

63 Ve 2 NVB

REACTION	RESULT	EXCITATION ENERGY	SOURCE		DETECTOR		ANGLE
			TYPE	RANGE	TYPE	RANGE	
G,G/	ABX	0-1	D	0-1	NAI-D		

ISOMERS

Таблица II

Измеренные значения после облучения, сравниваемые с другими литературными данными

Элемент	Активность облучения после первого измерения (имп/мин.)	Активн. экстрп. в конце облуч. (имп/мин.)	Лутературные данные		Данные измерений		σ_{m} (10^{-28}см^2)	Γ_{ym} (10^{-3}эв)
			$T_{1/2}$	E (кэв)	$T_{1/2}$	E (кэв)		
Se-77m	3842±96	5400	17,5 сек.	160	18,1±1 сек.	160±10	9,5	1,75
Sr-87m	191±5	200	2,8 ч.	390	2,9±0,1 ч.	365±25	0,85	0,2
Y-89m	96±20	170	16 сек.	910	16,7±5 сек.		0,08	0,02
Rh-103m	28±5	31	57 мин.	40	58±2 мин.	20,5±0,5	0,08	0,01
Ag-107m	220±14	250	44 сек.	93	43,8±0,6 сек	91±10	0,8	0,2
Ag-109m			39 сек.	88				
Hf-179m	80±18	155	19 сек.	160; 215	19±2 сек.		1	0,2
Ir-191m	90±20	250	4,9 сек.	42; 130	5±2 сек.		5,6	1
Pt-195m	90±9	100	3,5 д.	31; 100; 130;	3,5±0,2 д.	32±3 67,5±5 96±5 130±10	0,2	0,04
Au-197m	240±16	520	7,2 сек.	130; 277; 407	7,2±1 сек.	68:130: 280±20 390±20	0,07	0,01
Hg-199m	9,6±3,2		42 мин.	160; 370			0,005	0,001

REF. R. S. Hicks and B. M. Spicer
Nucl. Phys. A159, 265 (1970)

ELEM. SYM.	A	Z
Sr		38

METHOD

REF. NO.	
70 Hi 1	egf

REACTION	RESULT	EXCITATION ENERGY	SOURCE		DETECTOR		ANGLE
			TYPE	RANGE	TYPE	RANGE	
G,XN	ABX	10-27	C	10-27	BF3-I		4PI

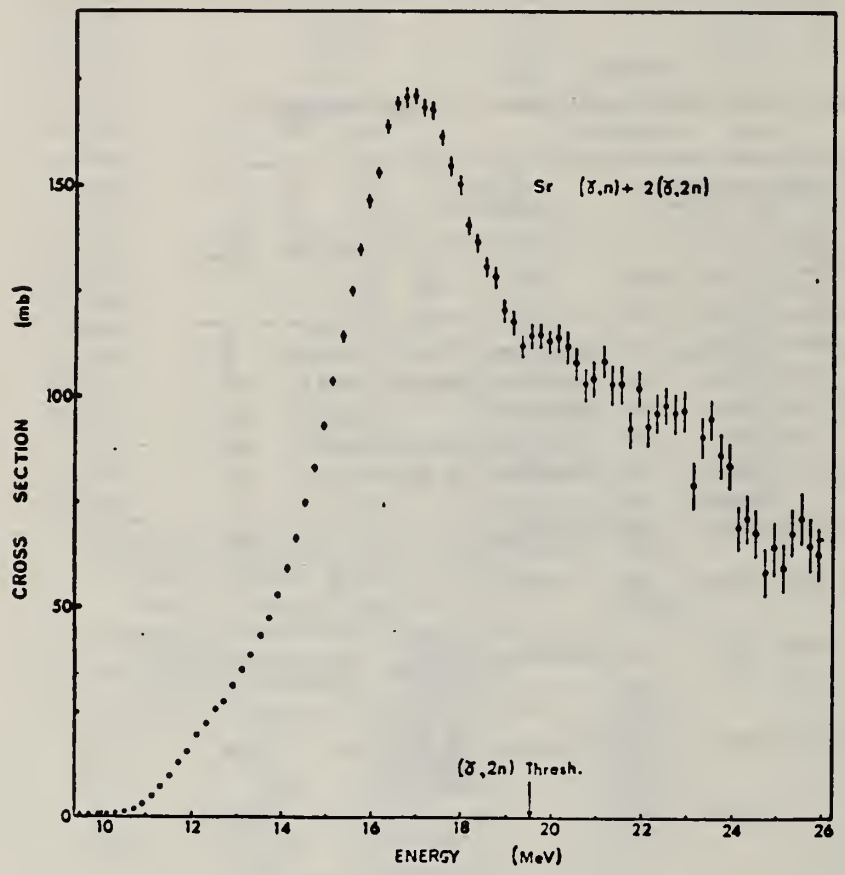

Fig. 1. The [Sr(γ, n) + 2Sr(γ, 2n)] cross section obtained by analysis of the yield curve using three interlacing second difference calculations. The resolution applied is 1.08 MeV.

[over]

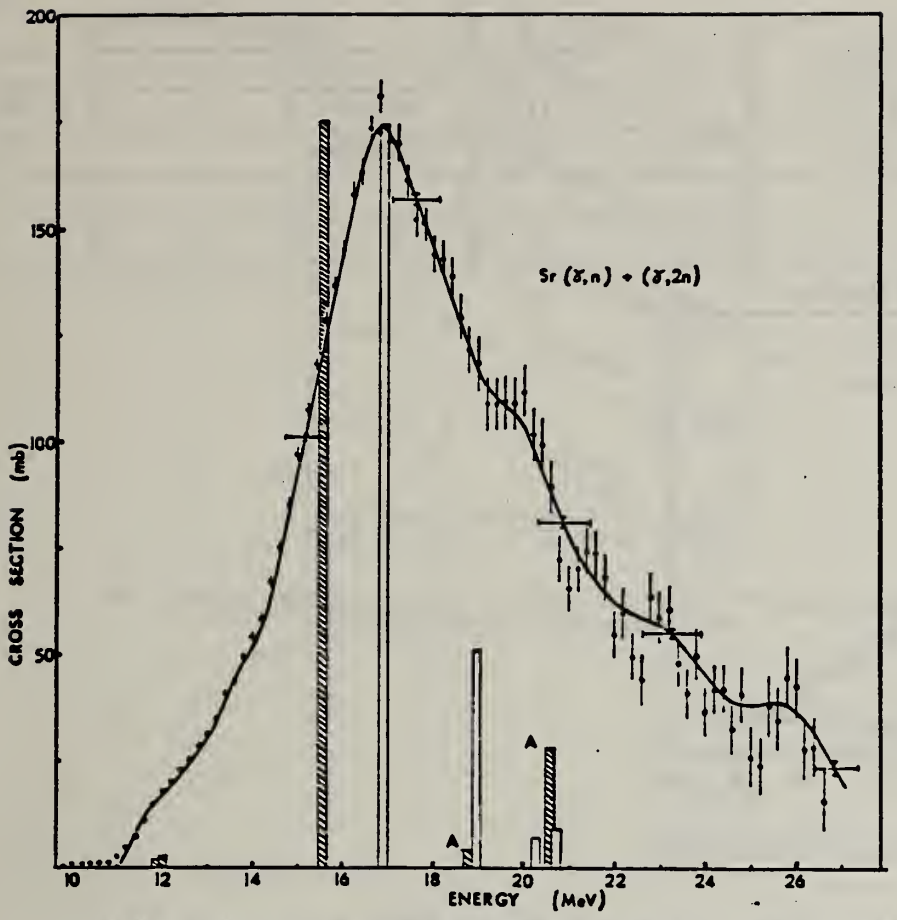

Fig. 2. The [Sr(γ, n)+Sr(γ, 2n)] cross section and calculated dipole spectra. The points portray the result obtained by 0.72 MeV second difference analysis and the continuous curve is obtained by Cook least-structure analysis, for which the resolution, implicit within the method, is indicated by the horizontal bars. Plain vertical bars represent the predictions of the dynamic collective model, whilst the hatched bars show the results of the particle-hole calculation of ref. [1]). Analogue $\Gamma_>$ states arising from the latter calculation are designated A.

1)B. Goulard, T.A. Hughes, S. Fallieros,
Phys. Rev. 176 (1968)1345.

REF.

A. Lepretre, H. Beil, R. Bergere, P. Carlos and A. Veyssiere
Nucl. Phys. A175, 609 (1971)

ELEM. SYM.	A	Z
Sr		38

METHOD

REF. NO.	
71 Le 1	egf

REACTION	RESULT	EXCITATION ENERGY	SOURCE		DETECTOR		ANGLE
			TYPE	RANGE	TYPE	RANGE	
G,N 378	ABX	11-27	D	11-27	MOD-I		4PI
G,2N 379+	ABX	19-27	D	11-27	MOD-I		4PI

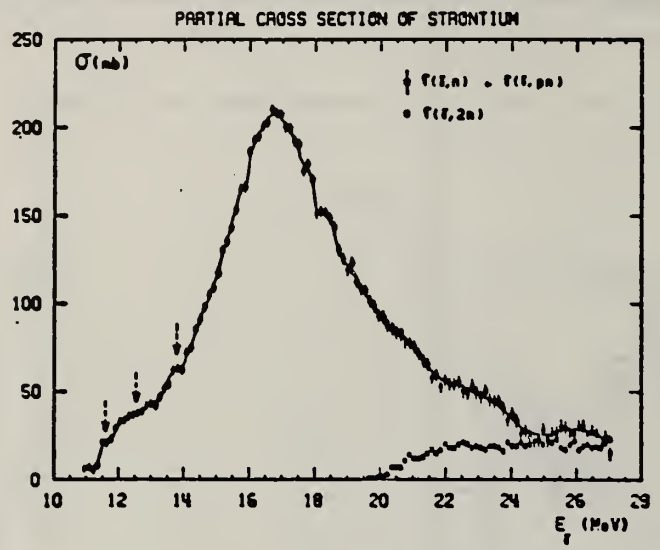

Fig. 2. Partial photoneutron cross sections $\sigma(\gamma, n)$ and $\sigma(\gamma, 2n)$ of Sr.

TABLE 1

Lorentz line parameters corresponding to fits shown in fig. 6.

	Rb	Sr	^{89}Y	^{90}Zr	^{93}Nb
σ_1 (mb)	192 ±10	207 ±10	225 ±10	211 ±10	202 ±10
Γ_1 (MeV)	4.1 ± 0.15	4.2± 0.1	4.1± 0.1	4.0 ± 0.1	4.7± 0.2
E_1 (MeV)	16.75± 0.05	16.7± 0.05	16.7± 0.05	16.65± 0.05	16.5± 0.05

TABLE 3

Integrated cross sections (the notation used is defined in the text)

	Rb	Sr	^{89}Y	^{90}Zr	^{93}Nb
σ_0 (MeV · b)	1.14 ±0.06	1.42±0.07	1.36±0.07	1.26±0.07	1.33±0.07
$\frac{\sigma_0}{0.06\,NZA^{-\frac{1}{3}}}$	0.915±0.05	1.09±0.05	1.04±0.05	0.95±0.05	0.97±0.05
σ_{-1} (mb)	67±4	80 ±5	77 ±5	71 ±5	[illegible] ±5
σ_{-2} (mb · MeV^{-1})	4±0.2	4.6 ±0.2	4.4 ±0.2	4 ±0.2	[illegible] ±0.2
E_M (MeV)	24	27	27	26	24

(over)

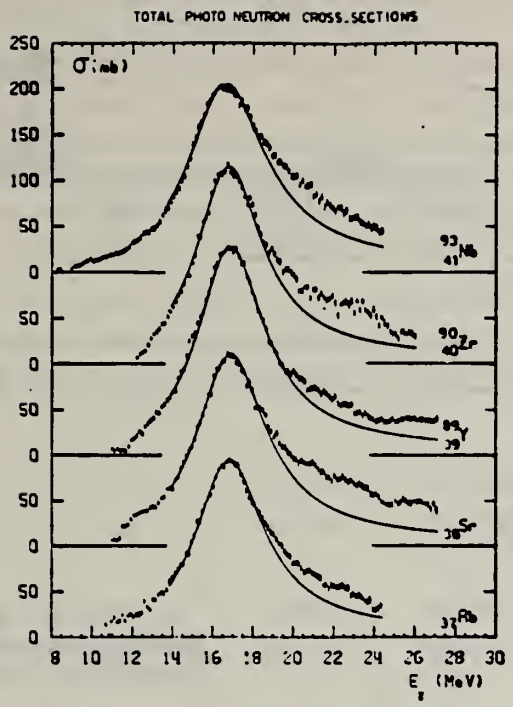

Fig. 6. Total photoneutron cross sections σ_T of Rb, Sr, ^{89}Y, ^{90}Zr and ^{93}Nb and best one Lorentz line fit corresponding to parameters given in table 1.

REF.

R.F. Barrett, J.R. Birkelund, B.J. Thomas, K.S. Lam, and H.H. Thies
Nucl. Phys. A210, 355 (1973)

ELEM. SYM.	A	Z
Sr		38

METHOD

REF. NO. 73 Ba 20 egf

REACTION	RESULT	EXCITATION ENERGY	SOURCE		DETECTOR		ANGLE
			TYPE	RANGE	TYPE	RANGE	
G,N	NOX	THR- 27	C	10- 27	BF3-I		4PI

MEAN NEUT ENERGY

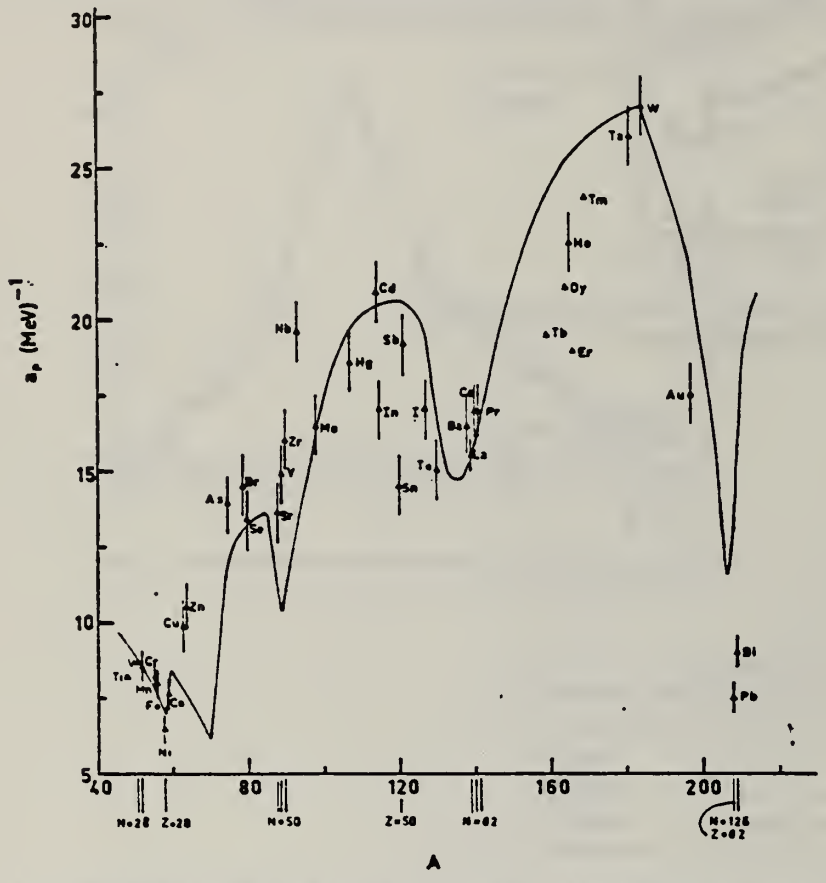

Fig. 12. Experimental values of the level density parameter a_p (Fermi gas formula plus pairing correction) versus atomic number A. The continuous curve is a least-squares fit to the data of a theoretical calculation from Newton [15].

1
H. Baba and S. Baba, Japan Atomic Energy Research Institute report JAERI-1183 (1969).
2
H. Baba, Nucl. Phys. A159, 625 (1970).
15
T.D. Newton, Can. J. Phys. 34, 804 (1956).

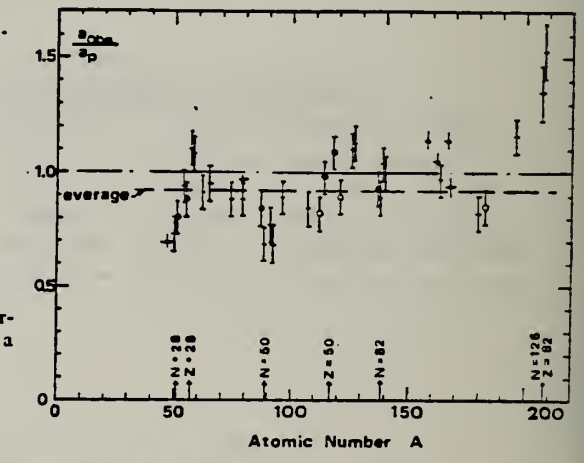

Fig. 15. Ratio a_{obs}/a_p versus atomic number A. Here a_{obs} is the level density parameter taken from the neutron resonance work of refs. [1,2]), and a_p is the level density parameter derived from the present (γ, n) work. Filled circles represent points where nuclei in the neutron resonance and in the (γ, n) experiment were the same. Open circles represent points where the respective nuclei were approximately matched. Triangles represent points which are based on measurement of neutron mean energies at two bremsstrahlung energies only.

(over)

TABLE 3

Comparison of experimental and theoretical data on nuclear level densities with Fermi gas formulae, and comparison of nuclear level density parameters from (γ, n) and n-resonance absorption experiments

Target	N (residual nucleus) [a]		Goodness of fit [b]		$\hat{E}_n(24)$ (MeV) [c]	T (MeV) [d]	a_p (MeV^{-1}) [e]	a_{obs} (MeV^{-1}) [f]	a_{obs}/a_p
			no p.c.	with p.c.					
Ti [g]	23	8%			1.93		8.1–^{47}Ti	6.41–^{47}Ti	0.79
	24	8%							
	25	73%							
	26	5%							
	27	5%							
V [g]	27	100%			1.96		8.7–^{50}V	6.35–^{51}V	0.73
Cr	25	4%	P	G	1.89		8.6–^{51}Cr	6.9 –^{51}Cr	0.80
	27	84%							
	28	10%							
	29	2%							
Mn	29	100%	V.P.	G	2.1		8.2–^{54}Mn	7.82–^{56}Mn	0.94
Fe	27	6%	F	G	1.96		8.0–^{55}Fe	7.06–^{55}Fe	0.88
	29	92%							
	30	2%							
Co	31	100%	P	F	2.12		7.7–^{58}Co	8.35–^{60}Co	1.08
Ni	29	68%	V.P.	P	2.04	1.4	6.5–$^{57.7}$Ni	7.19–^{59}Ni	1.10
($Z = 28$)	31	26%							
	32	1%							
	33	4%							
	35	1%							
Cu	33	69%	V.P.	P	1.78	1.0	9.8–^{62}Cu	8.90–^{64}Cu	0.91
	35	31%							
Zn	33	49%	F	F	1.61		10.5–$^{64.4}$Zn	10.0–^{65}Zn	0.95
	35	28%							
	36	4%							
	37	19%							
As	41	100%	V.P.	F	1.44		14.5–^{74}As	12.81–^{76}As	0.88
Se [g]	41	9%			1.39		13.3–^{78}Se	12.8 –^{78}Se	0.97
	42	8%							
	43	24%							
	45	50%							
	47	9%							
Br	43	45%	V.P.	V.P.	1.41		14.5–^{79}Br	12.69–^{80}Br	0.88
	45	49%							
Sr	47	10%	F	G	1.31		13.6–^{87}Sr	11.4 –^{87}Sr	0.84
	48	7%							
	49	83%							

[a]) Neutron numbers and abundances of respective residual nuclei in (γ, n) experiments.

[b]) These give an assessment of the goodness of fit of a calculated $\hat{E}_n$ versus E_0 curve to the observed data, using the Fermi gas level density formula both without and with pairing corrections.

[c]) Bremsstrahlung photoneutron mean energies $\hat{E}_n$ for peak bremsstrahlung energy $E_0 = 24$ MeV.

[d]) Nuclear temperature from fit with constant-temperature formula.

[e]) Level density parameter a_p derived from the present (γ, n) experiment, using a Fermi gas formula plus pairing correction, and corresponding residual nucleus (the atomic weight shown is the weighted average of atomic weights of the respective isotopes present).

[f]) As column 7, but using data on n-resonance absorption from refs. [1,2]).

[g]) Measurements of $\hat{E}_n(E_0)$ for these nuclei were made only for $E_0 = 21$, 23 and 24 MeV.

A. Järund and B. Forkman
Z. Physik A281, 39 (1977)

						Sr		38
						REF. NO.		
						77 Ja 2		egf
REACTION	PRODUCT	EXCITATION ENERGY	SOURCE		DETECTOR			ANGLE
			TYPE	RANGE	TYPE	RANGE		
G,NA24	ABY	THR-999	C	400-999	ACT-I			4PI
								999=1 GEV

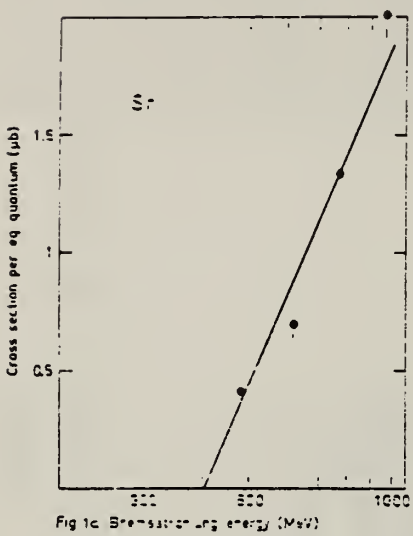

Fig 1c. Bremsstrahlung energy (MeV)

Fig. 1a-j. The measured yield as a function of bremsstrahlung end point energy. The error bars give the statistical errors in the numbers of γ-quanta detected. The yield curves are fitted to the yield points with the least-squares method. The yield from Cu (Fig. 1a) is measured in [1] and has been recalculated using the monitor curve of [5]

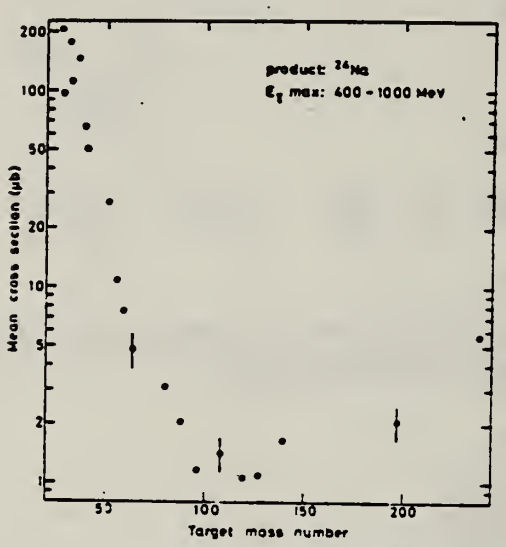

Fig. 2. The mean cross section in the energy range 400 to 1000 MeV calculated from the yields of Figure 1 in this work and of Figures 1 to [illegible]. The error is given by bars in some points

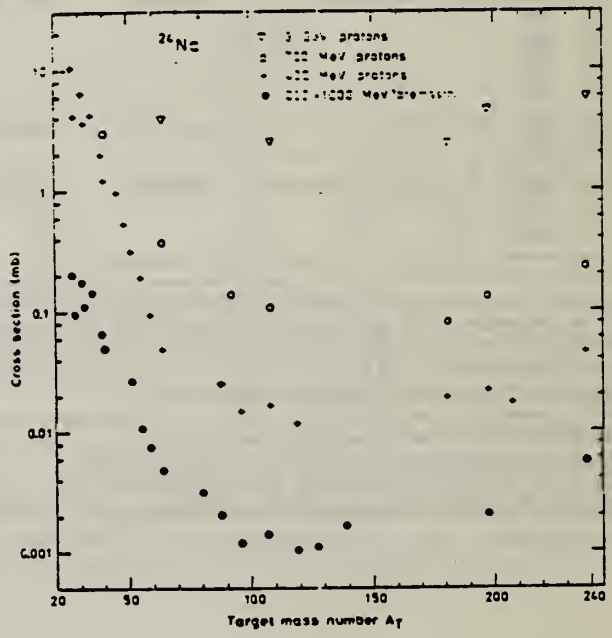

Fig. 4. Mean cross sections of the present work and of [1] (●) compared with the cross sections in proton irradiations: + 400 MeV from [4], o 700 MeV from [16] and an extrapolated value from [17]. ▽ 3 GeV from [18]

Ref. P. F. Yergin, B. P. Fabricand
Phys. Rev. 104, 1334 (1956)

Elem. Sym.	A	Z
Sr	86	38

Method 24 MeV Betatron; 250r Victoreen in 3.75 Lucite; neutron detector

Ref. No. 56 Ye 2 EGF

Reaction	E or ΔE	E_o	Γ	$\int \sigma dE$	Jπ	Notes
$Sr^{86}(\gamma,xn)$	Bremss. 24	15.9	5.0MeV	$\int_0^{23} = 0.92$ MeV-b		

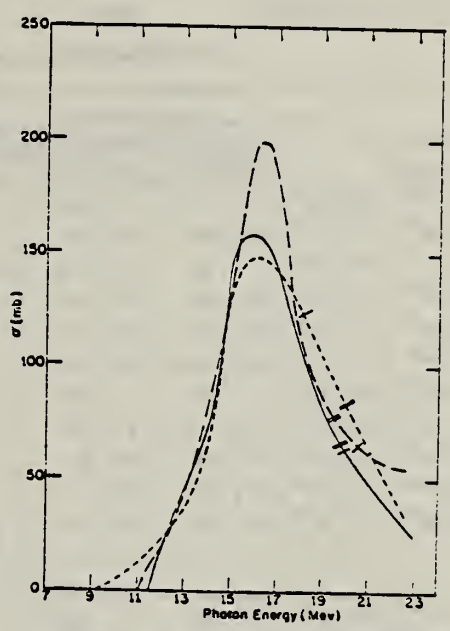

FIG. 2. Cross sections for the (γ,n) reactions in strontium isotopes. Full curve Sr^{88}, short dashes Sr^{87}, long dashes Sr^{86}. The single and double slash marks on each curve represent the locations of the (γ,pn) and $(\gamma,2n)$ thresholds, respectively. The units of the ordinate are 10^{-27} cm².

TABLE III. Parameters of giant-resonance cross-section curves for (γ,n) reactions in nuclei near 50 neutrons. Nuclides $_{33}As^{75}$, $_{41}Nb^{93}$, and $_{45}Rh^{103}$ from reference 4, $_{40}Zr^{90}$ and $_{40}Zr^{91}$ from reference 5 recomputed in present work. Neutron number is shown in column 2, location of peak cross-section value in column 3, peak cross-section value in column 4, half-height width of curve in column 5, and area under curve from threshold to 23 Mev in column 6.

Nuclide	N	E_m (Mev)	σ_m (millibarns)	Γ (Mev)	$\int_0^{23}\sigma dE$ (Mev-barns)
$_{33}As^{75}$	42	17.3	90.3	9.0	0.80
$_{38}Sr^{86}$	48	15.9	160	5.0	0.92
$_{38}Sr^{87}$	49	15.8	146	5.3	1.00
$_{38}Sr^{88}$	50	16.3	201	4.0	1.05
$_{39}Y^{89}$	50	16.3	191	3.8	0.87
$_{40}Zr^{90}$	50	15.8	199	4.3	0.98
$_{40}Zr^{91}$	51	16.5	200	5.0	1.22
$_{40}Zr^{92}$	52	16.9	193	5.5	1.24
$_{41}Nb^{93}$	52	17.0	195	6.8	1.46
$_{45}Rh^{103}$	58	16.5	205	8.9	1.94

Ref. J.H. Carver, G.E. Coote, T.R. Sherwood
Nuclear Phys. 37, 449 (1962)

Elem. Sym.	A	Z
Sr	86	38

Method: 30 MeV electron synchrotron; activation; NaI

Ref. No.: 62 Ca 1 JHH

Reaction	E or ΔE	E_0	Γ	$\int \sigma dE$	Jπ	Notes
$Sr^{86}(\gamma,n)$	Bremss. 30					

TABLE 1

Isomeric Ratios from (γ,n) reactions

Target Nucleus	J_g	Residual Nucleus: Ground state	Spin	Half-life	Metastable state: Spin	Half-life	Lower state: Spin	Isomer ratio $Y_1/(Y_1+Y_2)$	σ
Co^{59}	$7/2^-$	Co^{58}	2^+	71.3d	5^+	9.2h		0.44 ± 0.02	3.2 ± 0.2
Ge^{76}	0^+	Ge^{75}	$1/2^-$	82m	$7/2^+$	49s		0.48 ± 0.07	2.8 ± 0.5
Br^{81}	$3/2^-$	Br^{80}	1^+	18m	5^-	4.4h	2^-	0.32 ± 0.02	6.5 ± 1.0
Sr^{86}	0^+	Sr^{85}	$9/2^+$	64d	$1/2^-$	70m	$7/2^+$	0.36 ± 0.07	2.2 ± 0.4
Zr^{90}	0^+	Zr^{89}	$9/2^+$	79h	$1/2^-$	4.4m		0.33 ± 0.10	2.8 ± 0.7
Mo^{92}	0	Mo^{91}	$9/2^+$	15.7m	$1/2^-$	66s		0.46 ± 0.04	6^{+4}_{-2}
Ag^{107}	$1/2^-$	Ag^{106}	1^+	24m	6	8.3d		0.04 ± 0.02	2.0 ± 0.3
In^{113}	$9/2^+$	In^{112}	1^+	14.5m	4^+	20.7m	7^-	0.8 ± 0.1	3.1 ± 0.7
Cd^{116}	0^+	Cd^{115}	$1/2^+$	55h	$11/2^-$	43d		≤ 0.2	≤ 3
Ce^{140}	0^+	Ce^{139}	$3/2^+$	140d	$11/2^-$	55s		0.08 ± 0.01	2.5 ± 0.2
Hg^{198}	0^+	Hg^{197}	$1/2^-$	65h	$13/2^+$	24h	$3/2^-$ $5/2^-$	0.05 ± 0.01	3.4 ± 0.5
Previous work									
Br^{81} [10]	$3/2^-$	Br^{80}	1^+	18m	5^-	4.4h	2^-	0.33	6.5
Se^{82} [12]	0^+	Se^{81}	$1/2^-$	18m	$7/2^+$	57m		0.5	3.0
Zr^{90} [11]	0^+	Zr^{89}	$9/2^+$	79h	$1/2^-$	4.3h		0.44 ± 0.06	4.5 ± 1
In^{115} [23]	$9/2^+$	In^{114}	1^-	72s	5^+	50d	θ (T_γ = 2.5s)	0.85	5.0

REFERENCES

1) J. R. Huizenga and R. Vandenbosch, Phys. Rev. 120 (1960) 1305
2) T. Ericson, Advances in Physics, 9 (1960) 425
3) D. L. Allan, Nuclear Physics 24 (1961) 274
4) C. T. Hibdon, Phys. Rev. 114 (1959) 179
5) C. T. Hibdon, Phys. Rev. 122 (1961) 1235
6) T. Ericson, Nuclear Physics 11 (1959) 481
7) J. H. Carver and G. A. Jones, Nuclear Physics 19 (1960) 184
8) A. C. Douglas and N. Macdonald, Nuclear Physics 13 (1959) 382
9) T. Ericson and V. M. Scrutinski, Nuclear Physics 8 (1958) 284
10) L. Katz, L. Pease and H. Moody, Can. J. Phys. 30 (1952) 476
11) L. Katz, R. G. Baker and R. Montalbetti, Can. J. Phys. 31 (1953) 250
12) E. Silva and J. Goldemberg, An. Acad. Brasil Ciense 28 (1956) 275
13) J. H. Carver and D. C. Peaslee, Phys. Rev. 120 (1960) 2155
14) J. M. Blatt and V. F. Weisskopf "Theoretical Nuclear Physics" New York: Wiley (1952)
15) S. H. Vegors, L. L. Marsden and R. L. Heath, U.S. Atomic Energy Commission Report IDO-16370 (1958)
16) Nuclear Data Sheets, National Research Council, Washington (1960, up to and including Set 5)
17) R. Vandenbosch and J. R. Huizenga, Phys. Rev. 120 (1960) 1313
18) E. Weigold and R. Glover, Nuclear Physics (in press)
19) K. J. Le Couteur and D. W. Lang, Nuclear Physics 13 (1959) 32
20) T. D. Newton, Can. J. Phys. 34 (1956) 804
21) D. W. Lang, Nuclear Physics 26 (1961) 434
22) M. E. Rose, "Internal Conversion Coefficients", Amsterdam: North Holland Publishing Co. (1958)
23) J. Goldemberg and L. Katz, Phys. Rev. 90 (1953) 308

REF. F.Z. Khien, N.K. Zui, N.T. An
Yad. Fiz. 35, 257 (1982)
Sov. J. Nucl. Phys. 35, 145 (1982)

ELEM. SYM.	A	Z
Sr	86	38

METHOD

REF. NO. 82 Kh 2 egf

REACTION	RESULT	EXCITATION ENERGY	SOURCE		DETECTOR		ANGLE
			TYPE	RANGE	TYPE	RANGE	
G,N	NOX	12-14	C	14	ACT-I		4PI

ISOMERIC RATIO

The method is developed for calculation of the isomeric ratio for the case of low excitation energy of the residual nucleus, and the isomeric ratio is measured in the $(n, 2n)$ and (γ, n) reactions in the neutron-deficient nuclei ^{92}Mo, ^{90}Zr, ^{86}Sr, and ^{74}Se. The good agreement between the experimental and theoretical results on the (γ, n) reaction has confirmed the reliability of the characteristics of the residual nuclei, the transmission coefficients of the emitted neutrons, etc., used in the calculations. From study of the $(n, 2n)$ reaction we have obtained values of the parameters of the spin dependence of the level density of the nucleus in the excitation-energy region ~ 14 MeV.

PACS numbers: 25.20. + y, 25.40.Gr, 27.50. + e, 27.60. + j

TABLE III. Isomeric ratio in the (γ, n) reaction.

Target nucleus	σ_{exp}	σ_{theor}	Published data[1]
^{92}Mo	1.54±0.15	1.36	1.82±0.15 (70) [9] 1.03±0.21 (10) 0.85±0.07 (30) [15]
^{90}Zr	1.52±0.04	1.49	0.50±0.15 (30) [15]
^{86}Sr	0.70±0.07	0.86	0.68±0.14 (30) [15]
^{74}Se	7.5±1.0	10.5[2] 8.8[3]	

[1] In parentheses we have given the values of the bremsstrahlung maximum energy.
[2] In the calculations we used the ^{73}Se level scheme of Ref. 2, $I_g = 7/2^+$ and $I_m = 1/2^-$.
[3] In the calculations we used the level scheme of ^{73}Se in Ref. 3, $I_g = 9/2^+$ and $I_m = 3/2^-$.

SR
A=87

SR
A=87

Ref. P.F. Yergin, B.P. Fabricand
Phys. Rev. 104, 1334 (1956)

Elem. Sym.	A	Z
Sr	87	38

Method 24 MeV Betatron; 250 r Victoreen in 3.75 cm Lucite; neutron detector

Ref. No. 56 Ye 2 | EGF

Reaction	E or ΔE	E_0	Γ	$\int \sigma dE$	Jπ	Notes
$Sr^{87}(\gamma,xn)$	Bremss. 24	15.8	5.3 MeV	$\int_0^{23}$ = 1.00 MeV-b		

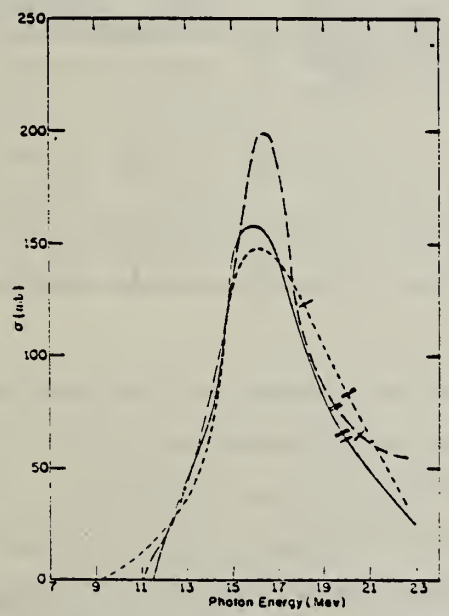

FIG. 2. Cross sections for the (γ,n) reactions in strontium isotopes. Full curve Sr^{88}, short dashes Sr^{87}, long dashes Sr^{86}. The single and double slash marks on each curve represent the locations of the (γ,pn) and $(\gamma,2n)$ thresholds, respectively. The units of the ordinate are 10^{-27} cm².

TABLE III. Parameters of giant-resonance cross-section curves for (γ,n) reactions in nuclei near 50 neutrons. Nuclides $_{33}As^{75}$, $_{41}Nb^{93}$, and $_{45}Rh^{103}$ from reference 4, $_{40}Zr^{90}$ and $_{40}Zr^{91}$ from reference 5 recomputed in present work. Neutron number is shown in column 2, location of peak cross-section value in column 3, peak cross-section value in column 4, half-height width of curve in column 5, and area under curve from threshold to 23 Mev in column 6.

Nuclide	N	E_m (Mev)	σ_m (millibarns)	Γ (Mev)	$\int_{th}^{23}\sigma dE$ (Mev-barns)
$_{33}As^{75}$	42	17.3	90.3	9.0	0.80
$_{38}Sr^{86}$	48	15.9	160	5.0	0.92
$_{38}Sr^{87}$	49	15.8	146	5.3	1.00
$_{38}Sr^{88}$	50	16.3	201	4.0	1.05
$_{39}Y^{89}$	50	16.3	191	3.8	0.87
$_{40}Zr^{90}$	50	15.8	199	4.3	0.98
$_{40}Zr^{91}$	51	16.5	200	5.0	1.22
$_{40}Zr^{92}$	52	16.9	193	5.5	1.24
$_{41}Nb^{93}$	52	17.0	195	6.8	1.46
$_{45}Rh^{103}$	58	16.5	205	8.9	1.94

REF. Y. Oka, T. Kato, K. Nomura, T. Saito, Hui-Tuh Tsai
Bull. Chem. Soc. Japan 41, 380 (1968)

ELEM. SYM.	A	Z
Sr	87	38

METHOD

REF. NO. 68 Ok 3 egf

REACTION	RESULT	EXCITATION ENERGY	SOURCE		DETECTOR		ANGLE
			TYPE	RANGE	TYPE	RANGE	
G,P	ABY	THR-20	C	20	ACT-I		/PI

TABLE 1. SUMMARY OF DATA ON (γ, p) REACTIONS WITH 20 MeV BREMSSTRAHLUNG

Nuclide: Parent (Natural abundance, %)	Nuclide: Residual (Half-life)	S_p (MeV)	Observed γ-ray: Energy (MeV)	Observed γ-ray: Branching ratio (%)	Observed γ-ray: Type of multipole transition	Yield determined: μCi/mg[a]	Yield determined: Yield/mol·R
^{25}Mg (10.11)	^{24}Na (15 hr)	12.06	1.37	100	$E2$	1.48×10^{-1}	1.7×10^{5}
^{29}Si (4.71)	^{28}Al (2.27 min)	12.33	1.78	100	$E2$	1.91	2.8×10^{5}
^{30}Si (3.12)	^{29}Al (6.56 min)	13.59	1.28	93.8	$E2+M1$	6.51×10^{-1}	1.5×10^{5}
^{44}Ca (2.06)	^{43}K (22.4 hr)	12.17	0.374	85	$E2+M1$	7.86×10^{-3}	1.3×10^{5}
^{47}Ti (7.32)	^{46}Sc (84.1 d)	10.47	0.887	100	$E2$	7.11×10^{-4}	3.1×10^{5}
^{48}Ti (73.99)	^{47}Sc (3.4 d)	11.44	0.160	100	$E2+M1$	6.83×10^{-2}	1.2×10^{5}
^{49}Ti (5.46)	^{48}Sc (1.8 d)	11.35	1.31	100	$E2$	4.40×10^{-3}	5.8×10^{4}
^{53}Cr (9.55)	^{52}V (3.8 min)	11.15	1.43	100	$E2$	5.01×10^{-1}	6.6×10^{4}
^{57}Fe (2.17)	^{56}Mn (2.58 hr)	10.57	1.81	23.5	$E2+M1$	8.10×10^{-2}	2.1×10^{5}
^{74}Ge (36.74)	^{73}Ga (4.8 hr)	10.92	0.295	97	$(E2)$	3.70×10^{-1}	1.3×10^{5}
^{77}Se (7.58)	^{76}As (26.5 hr)	9.61	0.559	41	$E2$	1.48×10^{-2}	1.3×10^{5}
^{87}Sr (7.02)	^{86}Rb (19 d)	9.41	1.08	9	$E2$	5.15×10^{-4}	9.9×10^{4}
^{113}Cd (12.26)	^{112}Ag (3.2 hr)	9.74	1.39	35	$E2$	1.91×10^{-2}	2.1×10^{4}
^{117}Sn (7.57)	^{116m}In (54 min)	9.58	1.27	84	$E2$	9.80×10^{-3}	6.9×10^{3}
^{137}Ba (11.32)	^{136}Cs (13 d)	8.67	0.830	100	$E2$	1.68×10^{-4}	2.2×10^{4}
^{199}Hg (16.84)	^{198}Au (2.7 d)	7.27	0.412	100	$E2$	8.43×10^{-4}	2.2×10^{4}

a) The value corrected at the end of 1 hr irradiation (9.4×10^{6} R/min).

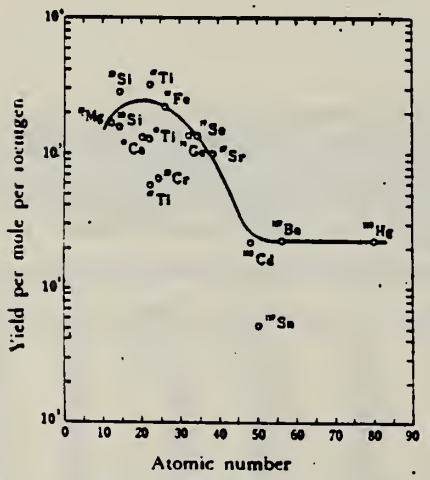

Fig. 2. The yield curve for the (γ, p) reaction with 20 MeV bremsstrahlung.

REF. E. J. Winhold, B. H. Patrick, E. M. Bowey, and D. B. Gayther
PICNS-73, Vol. I, p. 701 Asilomar

ELEM. SYM.	A	Z
Sr	87	38

METHOD

REF. NO. 73 Wi 6 hmg

REACTION	RESULT	EXCITATION ENERGY	SOURCE		DETECTOR		ANGLE
			TYPE	RANGE	TYPE	RANGE	
G,N	ABX	8- 11	C	9- 12	TOF-D		130

NO PEAK OBSERVED

Table I

Reaction	Thres-hold (MeV)	Energy Range of Expcriment (MeV)	Observed Peaks		
			Peak Energy (MeV)	$\frac{d\sigma}{d\omega}$ at peak (mb/ster.)	$4\pi \int_{\text{peak}} \left(\frac{d\sigma}{d\omega}\right)_{130^\circ} dE_\gamma$
$^{87}Sr(\gamma,n_o)$	8.44	9.4-11.1			(MeV-mb)
$^{87}Sr(\gamma,n_1)$	9.52	10.5-11.1			
$^{91}Zr(\gamma,n_o)$	7.19	7.8-10.3	9.1	1.2	20
$^{97}No(\gamma,n_o)$	6.82	7.8-9.2	8.1	0.3	3
$^{113}Cd(\gamma,n_o)$	6.54	7.4-9.3	7.7	0.9	7
$^{117}Sn(\gamma,n_o)$	6.94	7.6-8.8	7.8	2.5	20
$^{119}Sn(\gamma,n_o)$	6.48	7.1-9.0	7.8	1.6	18

The ^{87}Sr cross sections display no peaking. The ground state (γ,n_o) cross section is small and by 11 MeV is overwhelmed by the (γ,n_1) cross section to the first excited state of ^{86}Sr. At 11 MeV the (γ,n_1) cross section is roughly 0.8 millibarns per steradian, and is order-of-magnitude larger than the (γ,n_o) cross section, and comparable to the extrapolated giant resonance cross section. This general behavior is not unexpected since ^{87}Sr has $J^\pi = 9/2^+$ so that for dipole absorption the emitted ground state neutrons must have $\ell \geq 3$.

REF. Yoshihisa Watanabe, Takeshi Mukoyama
Nucl. Sci. Eng. 80, 92 (1982)

EL EM. SYM.	A	Z
Sr	87	38

METHOD

REF. NO. 82 Wa4 egf

REACTION	RESULT	EXCITATION ENERGY	SOURCE		DETECTOR		ANGLE
			TYPE	RANGE	TYPE	RANGE	
G,G/	ABY	1	C	1.3*	ACT-I		4PI

1=1.23 MEV, *CO-60

A photoexcitation process by gamma rays from a ^{60}Co source has been studied for the nuclei of ^{87}Sr, ^{111}Cd, ^{115}In, and ^{176}Lu. The induced isomeric activity was measured with a Ge(Li) detector. The flux of photons scattered into the target has been estimated with the Monte Carlo method using the single-scattering approximation. From the observed induced activities and the calculated photon flux, the integral cross sections for isomer production by photoexcitation were obtained and compared with other experimental data.

TABLE II

Integral Cross Sections for the Isomer Production by Photoexcitation ($\times 10^{-25}$ cm^2·eV)

	^{87}Sr	^{111}Cd	^{115}In	^{176}Lu	Photon Source	Reference
Chertok and Booth		0.6 ± 0.2	0.71 ± 0.23		Bremsstrahlung	5
Booth and Brownson	$0.85^{+0.4}_{-0.3}$		1.15 ± 0.4		Bremsstrahlung	6
Boivin et al.		$0.8^{+0.4}_{-0.05}$	3^{+4}_{-2}		Bremsstrahlung	7
Lakosi et al.		1.02 ± 0.26	1.05 ± 0.27		^{60}Co	11
Yoshihara	3.0 ± 0.8[a]	1.5 ± 0.3	2.3 ± 0.4	69 ± 12[a] 140 ± 30[a]	^{60}Co	3
Veres	0.5 to 0.62	0.8 to 1.5	0.9 to 5		^{60}Co	23
Present work	4.2 ± 0.6[b] 5.6 ± 0.8[c]	1.1 ± 0.2	3.5 ± 0.2	39 ± 27[b] 48 ± 34[c]	^{60}Co	

[a]Obtained as the relative value to ^{115}In.
[b]Provided that the partial level width $g\Gamma_0 = 1 \times 10^{-3}$ eV.
[c]Provided that the partial level width $g\Gamma_0 = 1 \times 10^{-4}$ eV.

Sr
A=88

Sr
A=88

REF.

R. H. Helm
Phys. Rev. 104, 1466 (1956)

ELEM. SYM.	A	Z
Sr	88	38

METHOD

REF. NO. 56 He 3 hmg

REACTION	RESULT	EXCITATION ENERGY	SOURCE		DETECTOR		ANGLE
			TYPE	RANGE	TYPE	RANGE	
E,E/	FMF	1-7	D	187	MAG-D		DST

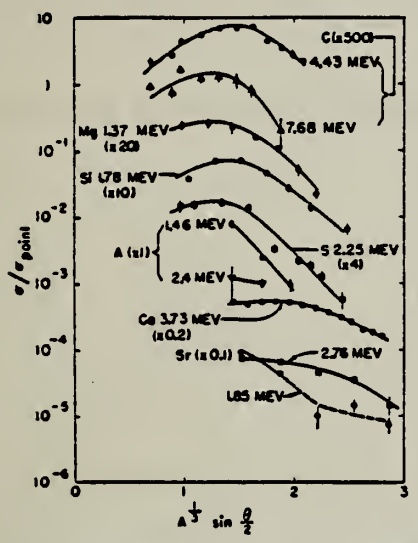

FIG. 3. Inelastic angular distributions (observed cross section divided by Feshback point-charge cross sections). The results of Hahn *et al.* (reference 8) for Ca and of Fregeau and Hofstadter (reference 11) are included for comparison.

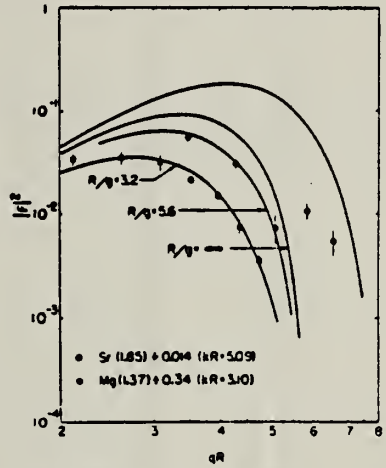

FIG. 6. Comparison of typical experimental and calculated squared inelastic form factors. Both the Sr (1.85 Mev) and Mg (1.37 Mev) are known to be 2+ levels. The calculated curves are for a "smeared δ-function" transition charge density (see Sec. V) with values of R/g taken from the elastic results. The abscissae for the experimental data are scaled by values of R taken from the elastic results [Table III (a)]. Shown for comparison (upper curve) is a squared form factor calculated from a quadrupole transition charge density whose radial dependence is constant for $r<R$, zero for $r>R$. This would give a poorer fit to the data than the δ-function distribution, indicating that the quadrupole vibrational mode is approximated better by a transverse wave in an incompressible nuclear fluid than by some sort of a compressional body wave.

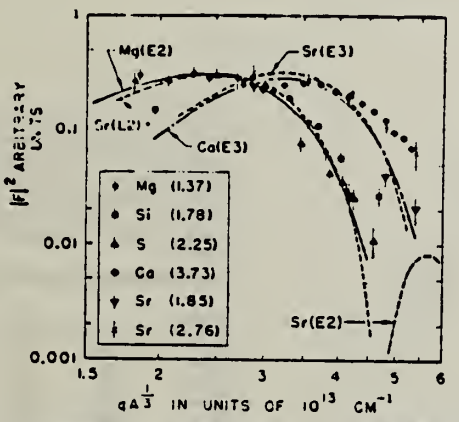

FIG. 7. Inelastic "universal curves." A composite plot of inelastic data from Mg, Si, S, Ca, and Sr against $qA^{\frac{1}{3}}$. The various form factors are arbitrarily normalized to minimize the spread of points. The point from sulfur and the point from silicon which seem to deviate from the "universal curve" are assumed to contain undetected experimental errors. The curves labeled Mg($E2$), Sr($E2$), Ca($E3$), and Sr($E3$) are calculated for electric-quadrupole and-octupole transitions using the "smeared δ-function" transition charge densities of Sec. V, and are arbitrarily normalized.

Ref. P.F. Yergin, B.P. Fabricand
Phys. Rev. 104, 1334 (1956)

Elem. Sym.	A	Z
Sr	88	38

Method: 24 MeV Betatron; 250 r Victoreen in 3.75 cm Lucite; neutron detector

Ref. No.: 56 Ye 2 | EGF

Reaction	E or ΔE	E_o	Γ	$\int \sigma dE$	Jπ	Notes
$Sr^{88}(\gamma,xn)$	Bremss. 24	16.3	4.0 MeV	$\int_0^{23}$ = 1.05 MeV-b		

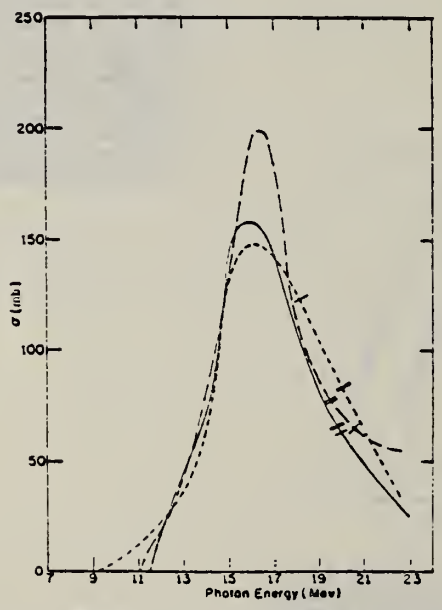

FIG. 2. Cross sections for the (γ,n) reactions in strontium isotopes. Full curve Sr^{86}, short dashes Sr^{87}, long dashes Sr^{88}. The single and double slash marks on each curve represent the locations of the (γ,pn) and $(\gamma,2n)$ thresholds, respectively. The units of the ordinate are 10^{-27} cm².

TABLE III. Parameters of giant-resonance cross-section curves for (γ,n) reactions in nuclei near 50 neutrons. Nuclides $_{33}As^{75}$, $_{41}Nb^{93}$, and $_{45}Rh^{103}$ from reference 4. $_{40}Zr^{90}$ and $_{40}Zr^{91}$ from reference 5 recomputed in present work. Neutron number is shown in column 2, location of peak cross-section value in column 3, peak cross-section value in column 4, half-height width of curve in column 5, and area under curve from threshold to 23 Mev in column 6.

Nuclide	N	E_m (Mev)	σ_m (millibarns)	Γ (Mev)	$\int_{th}^{23}\sigma dE$ (Mev-barns)
$_{33}As^{75}$	42	17.3	90.3	9.0	0.80
$_{38}Sr^{86}$	48	15.9	160	5.0	0.92
$_{38}Sr^{87}$	49	15.8	146	5.3	1.00
$_{38}Sr^{88}$	50	16.3	201	4.0	1.05
$_{39}Y^{89}$	50	16.3	191	3.8	0.87
$_{40}Zr^{90}$	50	15.8	199	4.3	0.98
$_{40}Zr^{91}$	51	16.5	200	5.0	1.22
$_{40}Zr^{92}$	52	16.9	193	5.5	1.24
$_{41}Nb^{93}$	52	17.0	195	6.8	1.46
$_{45}Rh^{103}$	58	16.5	205	8.9	1.94

REF.

R.B. Begzhanov and A. A. Islamov
J. Exptl. Theoret. Phys. (USSR) 47, 768 (1964)
Soviet Phys. JETP 20, 513 (1965)

ELEM. SYM.	A	Z
Sr	88	38

METHOD

Resonance scattering, self-absorption

REF. NO.	
64 Be 7	J0C

REACTION	RESULT	EXCITATION ENERGY	SOURCE		DETECTOR		ANGLE
			TYPE	RANGE	TYPE	RANGE	
G,G	LFT	2	D	2	D		
		(1.85)		(1.85)			

$\Gamma_\gamma = (6.0 \pm 1.2) \times 10^{-3}$ eV or

$\tau_\gamma = (1.10 \pm 0.22) \times 10^{-13}$ sec, for the 1.85 MeV level.

REF. G. A. Peterson and J. Alster
Phys. Rev. 166, 1136 (1968)

ELEM. SYM.	A	Z
Sr	88	38

METHOD

REF. NO. 68 Pe 1 HMG

REACTION	RESULT	EXCITATION ENERGY	SOURCE		DETECTOR		ANGLE
			TYPE	RANGE	TYPE	RANGE	
E,E/	RLX	1-7	D	65,70	MAG-D	58-70	DST

B(EL); SEP ISOTPS

TABLE I. Experimentally determined values of the reduced nuclear radiative transition probabilities $B(EL)$ for the excitation of a nucleus to a level at energy E^* above its ground state by a transition of electric character and multipolarity L, in units of e^2F^{2L}, where $1\ F = 10^{-13}$ cm. The last column gives $B(EL)$ in single-particle Weisskopf units according to Eq. (4).

E^*	L	$B(E0 \rightarrow L)$ (e^2F^{2L})	G (W.u.)
		Sr^{88}	
1.84	2	990±50	8.5
2.74	3	80 600±3000	25.0
4.0	2	190±40	1.6
6.5	(2)	130±30	1.1
	(3)	13 000±3000	4.0
		Y^{89}	
1.50	2	120±50	1.0
1.73	2	140±40	1.2
2.21	3	33 700±3000	10.2
2.52	3	37 800±3000	11.4
2.86	3	32 300±3000	9.8

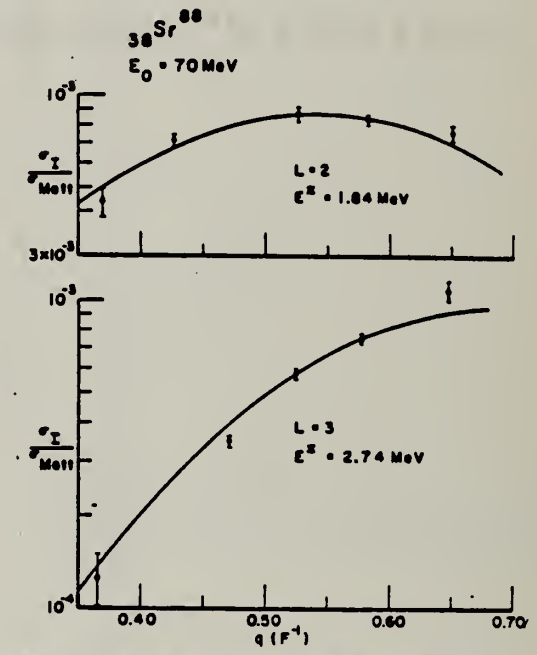

FIG. 5. Distorted-wave inelastic cross section in units of the Mott cross section versus momentum transferred to the Sr^{88} nucleus for the electric quadrupole excitation at 1.84 MeV and for the electric octupole excitation at 2.74 MeV. An incompressible and irrotational hydrodynamical model was assumed.

REF.

M. Hasinoff, G. A. Fisher, H. M. Kuan and S. S. Hanna
Phys. Letters 30B, 337 (1969)

Sr	88	38

METHOD

REF. NO. 69 Ha 1 egf

REACTION	RESULT	EXCITATION ENERGY	SOURCE		DETECTOR		ANGLE
			TYPE	RANGE	TYPE	RANGE	
P,G	RLX	15-22	D	4-12	NAI-D	10-22	90

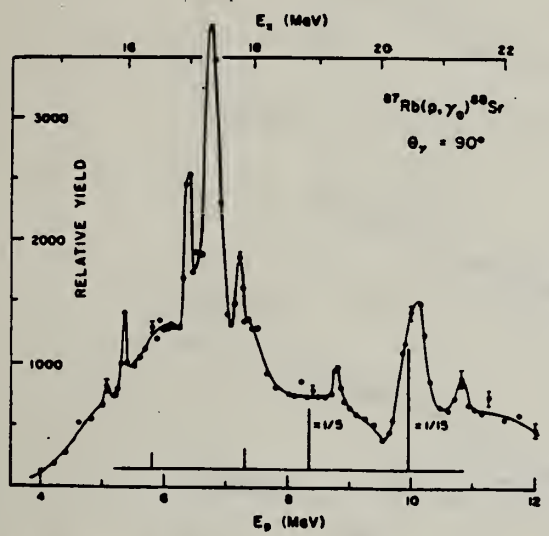

Fig. 3. Yield curve of $^{87}Rb(p,\gamma_0)^{88}Sr$ at 90°. The predicted resonances [1] are shown as vertical lines whose heights are proportional to Γ_{γ_0}. The two highest lines have been suppressed by factors of 5 and 15, as indicated.

REF.

K. Shoda, M. Sugawara, T. Saito, and H. Miyase
Phys. Rev. Letters 23, 800 (1969)

ELEM. SYM.	A	Z
Sr	88	38

METHOD

REF. NO.
69 Sh 5
hmg

REACTION	RESULT	EXCITATION ENERGY	SOURCE		DETECTOR		ANGLE
			TYPE	RANGE	TYPE	RANGE	
E,P	ABX	14-25	D	16-30	MAG-D		

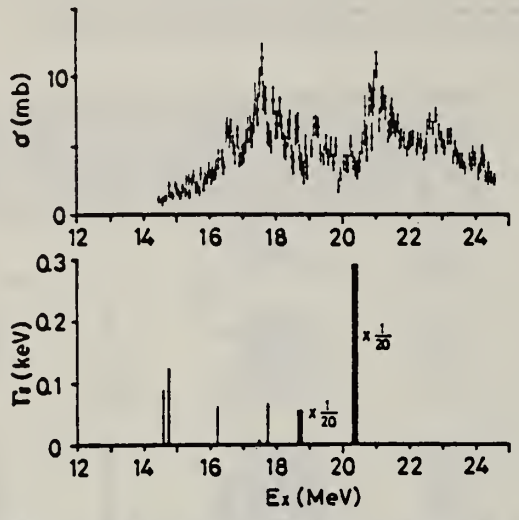

FIG. 1. Cross section of $^{88}Sr(\gamma,p_0)$. The vertical lines show the theoretical radiative widths of IAS from Ref. 5.

Assumption is made that photoproton emission leaves the residual nucleus in the ground state.

[5]B. Goulard, T. A. Hughes, and S. Fallieros, Phys. Rev. 176, 1345 (1968).

REF. K. Shoda, M. Sugawara, T. Saito & H. Miyase
PICNS-69 Proceedings of the Conference on Nuclear Isospin. Asilomar-Pacific Grove, California, 1969 (Academic Press, New York & London 1969) p.125.

ELEM. SYM.	A	Z
Sr	88	38

METHOD

REF. NO. 69 Sh 6 egf

REACTION	RESULT	EXCITATION ENERGY	SOURCE		DETECTOR		ANGLE
			TYPE	RANGE	TYPE	RANGE	
E,P	SPC	14-30	D	30	MAG-D		UKN

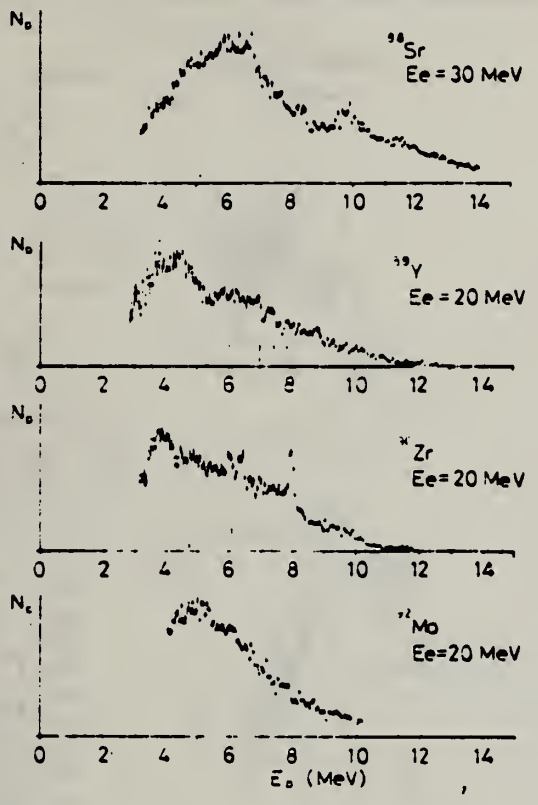

Fig. 1. Energy distributions of photoprotons. Vertical broken lines and solid lines indicate the position of p_o corresponding to the ground IAS and electric dipole IAS ($\underline{2}$-$\underline{4}$) respectively.

REF. I. Blomqvist, G. Nydahl and B. Forkman
Nucl. Phys. A162, 193 (1971)

ELEM. SYM.	A	Z
Sr	88	38

METHOD

REF. NO. 71 B1 1 egf

REACTION	RESULT	EXCITATION ENERGY	SOURCE		DETECTOR		ANGLE
			TYPE	RANGE	TYPE	RANGE	
G,PI+	ABY	150-700	C	150-700	ACT-I		4PI

SEE 68 NY 1

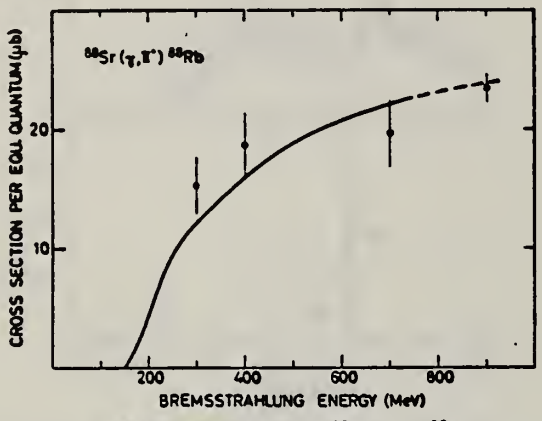

Fig. 4. Absolute yield for $^{88}Sr(\gamma,\pi^+)^{88}Rb$.

REF.

K. Shoda, M. Sugawara, T. Saito, H. Miyase, A. Suzuki, S. Oikawa, and J. Uegaki
PICNS-72, 321 Sendai

ELEM. SYM.	A	Z
Sr	88	38

METHOD

REF. NO. 72 Sh 10 hvm

REACTION	RESULT	EXCITATION ENERGY	SOURCE TYPE	SOURCE RANGE	DETECTOR TYPE	DETECTOR RANGE	ANGLE
E,P	SPC	17	C	16- 18	MAG-D		UKN
		(17.2)					

I A STATES

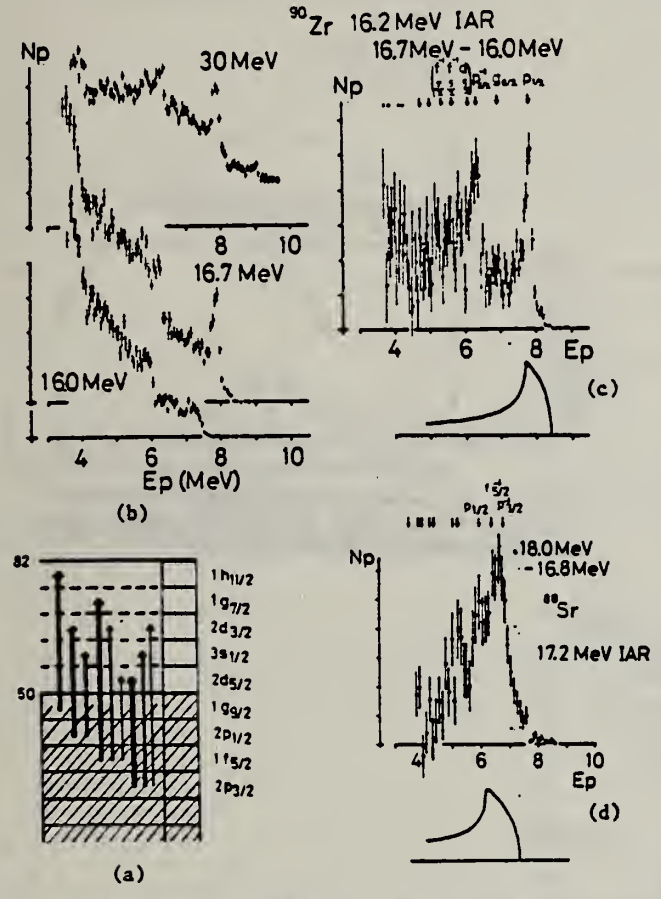

Fig. 7 (a): Shell model diagram of ^{90}Zr and ^{88}Sr.
(b): Energy distributions of $^{90}Zr(e,e'p)$.
(c): Energy distributions obtained from difference method. Residual states for 16.2 MeV IAR are shown by arrows.
(d): Energy distributions obtained from difference method for ^{88}Sr. Residual states for 17.2 MeV IAR are shown by arrows.

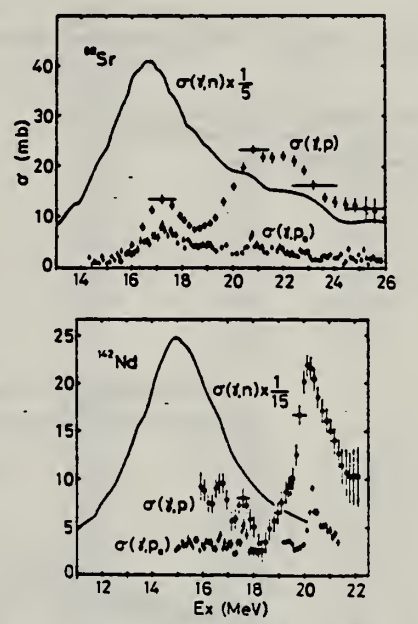

Fig. 11 The (γ,p) cross sections of ^{88}Sr and ^{142}Nd. The (γ,p_0) and (γ,n) cross sections are also shown.

REF.

S. Datta and J.S. Allen
Phys. Rev. C8, 1421 (1973)

Sr	88	38

METHOD

REF. NO.

73 Da 10 hmg

REACTION	RESULT	EXCITATION ENERGY	SOURCE		DETECTOR		ANGLE
			TYPE	RANGE	TYPE	RANGE	
G,G	ABX	8- 12	D	8- 12	NAI-D		131

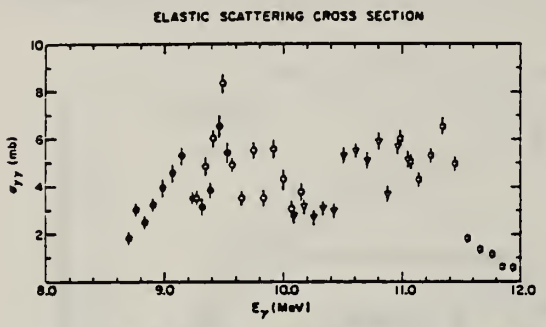

FIG. 1. The elastic scattering cross section of monochromatic photons on ^{88}Sr. The different symbols represent four sets of experimental data.

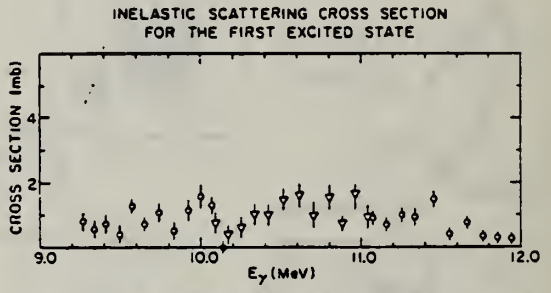

FIG. 2. The inelastic scattering cross section for the first excited state of ^{88}Sr. The different symbols represent three sets of our experimental data.

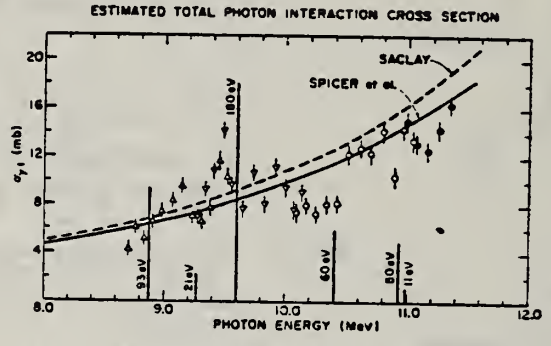

FIG. 3. The total photon-interaction cross section estimated from four sets of elastic scattering data. The dashed curve is an extrapolation of the (γ,n) cross section of ^{88}Sr measured by Lepetre *et al.* (Ref. 2). The solis curve is an extrapolation of the ^{88}Sr(γ,n) cross section of Spicer *et al.* (Ref. 1). Both of these curves were drawn with the assumption that the giant dipole resonance can be represented by a Lorentz resonance function. The levels predicted by Goulard, Hughes, and Fallieros (Ref. 4) are shown by vertical bars with values of the predicted ground-state radiative widths in eV.

REF.

S. P. Fivozinsky, S. Penner, J.W. Lightbody,Jr., and D. Blum
Phys. Rev. C9, 1533 (1974)

ELEM. SYM.	A	Z
Sr	88	38

METHOD

REF. NO. 74 Fi 1 hmg

REACTION	RESULT	EXCITATION ENERGY	SOURCE TYPE	SOURCE RANGE	DETECTOR TYPE	DETECTOR RANGE	ANGLE
E,E/	FMF	1, 3	C	45-121	MAG-D		DST
		(1.84,2.74)					

LEVELS 1.84,2.74 MEV

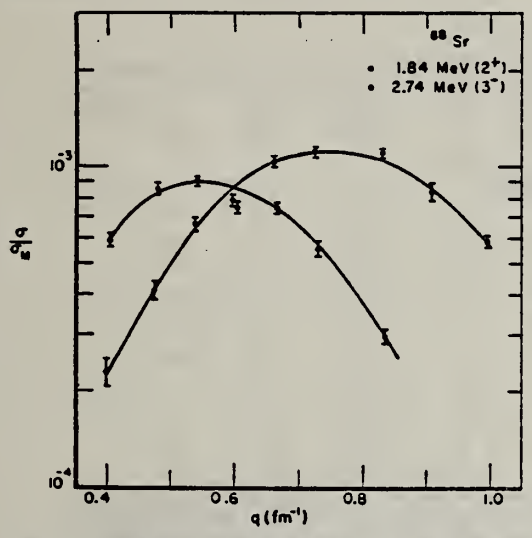

FIG. 5. Tassie-model fits to ^{88}Sr 2^+ and 3^- form factors.

Elastic scattering data for ^{88}Sr and ^{89}Y.

TABLE III. Electron scattering form factors for ^{88}Sr.

Level	Incident energy (MeV)	Lab scattering angle (deg)	q (fm^{-1})	$\|F\|^2$	Standard deviation (%)
Ground state 0^+	120.85	110.5	1.005	0.6695×10^{-2}	1.2
	100.87	128.2	0.919	0.8558×10^{-2}	1.6
	101.17	110.5	0.842	0.6633×10^{-2}	1.2
	80.86	128.2	0.737	0.1004×10^{-1}	1.7
	80.95	110.5	0.674	0.1984×10^{-1}	0.7
	67.07	128.2	0.611	0.4660×10^{-1}	0.6
	60.48	128.3	0.551	0.9065×10^{-1}	0.7
	53.46	128.3	0.487	0.1790	0.6
	45.42	128.3	0.414	0.3351	0.5
1.84 MeV 2^+	120.85	110.5	...	...	...
	100.87	128.2	...	...	...
	101.17	110.5	0.834	0.2953×10^{-3}	4.7
	80.86	128.2	0.728	0.5591×10^{-3}	5.8
	80.95	110.5	0.666	0.7535×10^{-3}	3.6
	67.07	128.2	0.603	0.7610×10^{-3}	4.1
	60.48	128.3	0.543	0.9175×10^{-3}	3.1
	53.46	128.3	0.479	0.8745×10^{-3}	4.1
	45.42	128.3	0.406	0.6099×10^{-3}	4.6
2.74 MeV 3^-	120.85	110.5	0.994	0.5636×10^{-3}	4.1
	100.87	128.2	0.906	0.8164×10^{-3}	5.9
	101.17	110.5	0.830	0.1086×10^{-2}	2.2
	80.86	128.2	0.724	0.1139×10^{-2}	3.2
	80.95	110.5	0.662	0.1048×10^{-2}	2.9
	67.07	128.2	0.499	0.7969×10^{-3}	3.8
	60.48	128.3	0.539	0.6788×10^{-3}	4.7
	53.46	128.3	0.475	0.4209×10^{-3}	5.9
	45.42	128.3	0.401	0.2373×10^{-3}	9.1

(over)

TABLE V. Reduced transition probabilities [$B(EL)\uparrow$].

Nucleus	Level	$B(EL)\uparrow$ (Tassie model) (e^2 fm^{2L})	Weisskopf units	Prediction of mixed model $B(EL)\uparrow$ for ^{89}Y 3^- transitions (e^2 fm^6)	Weisskopf units
^{88}Sr	2^+, 1.84 MeV	822.4 ± 23.8	7.0 ± 0.2		
	3^-, 2.74 MeV	62 034 ± 4015	19.3 ± 1.2		
^{89}Y	$\frac{1}{2}^-$, $L=2$ 1.51 MeV	130.7 ± 17.57	1.1 ± 0.1		
	$\frac{5}{2}^-$, $L=2$ 1.74 MeV	196.8 ± 13.89	1.7 ± 0.1		
	$\frac{5}{2}^+$, $L=3$ 2.21 MeV	25 777 ± 2251	7.8 ± 0.7	24 836	7.5
	$\frac{7}{2}^+$, $L=3$ 2.52 MeV	36 603 ± 2818	11.1 ± 0.9	25 764	7.8
	$(\frac{5}{2}^+, \frac{7}{2}^+)$, $L=3$ 2.86 MeV	50 536 ± 5000	15.3 ± 1.5	30 160	9.2
	$(\frac{3}{2}^-, \frac{5}{2}^-)$, $L=2$ 3.1 MeV	144.6 ± 11.66	1.2 ± 0.1		

REF.

K. Shoda, M. Sugawara, T. Saito, and H. Miyase
Nucl. Phys. A221, 125 (1974)

ELEM. SYM.	A	Z
Sr	88	38

METHOD

REF. NO.: 74 Sh 6 egf

REACTION	RESULT	EXCITATION ENERGY	SOURCE TYPE	SOURCE RANGE	DETECTOR TYPE	DETECTOR RANGE	ANGLE
E,P	ABX	14- 26	D	14- 30	MAG-D		DST

TABLE 5

The radiative width of the narrow E1 IAR obtained from the proton group in the proton spectra

Nucleus	E_x (MeV)	E_p (MeV)	$E_{Rf}(J^\pi)$ (MeV)	Γ_γ (eV)	Γ_{p1}/Γ [a]	Γ_γ [a] (eV)	$2(T+1)\frac{\Gamma_\gamma}{\Gamma_w}$ [a]	$2(T+1)\frac{\Gamma_\gamma}{\Gamma_{s.p.}}$ [a]	(p,γ₀) data Γ_γ (eV)
^{90}Zr	14.5	6.0	0 ($\frac{1}{2}^-$)	26	26 [b]	0.076			> 30 [g]
	16.3	7.9	0 ($\frac{1}{2}^-$)	74	126 [c]	0.26			> 60 [g]
	16.3	6.3	1.51 ($\frac{3}{2}^-$)	52					
^{89}Y	13.0 [d]	5.9	0 (0^+)	13	13 [b]			0.13 [f]	18±3 [h]
	14.5 [e]	7.3	0 (0^+)	16	16 [b]			0.14 [f]	11±2 [h]
	15.9 [d]	8.7	0 (0^+)	42	42 [b]			0.68 [f]	40±8 [h]
^{88}Sr	17.1	6.5	0 ($\frac{3}{2}^-$)	9.5	14 [c]	0.029			
	17.1	5.6	0.85 (($\frac{1}{2}^-$))	4.9					
	17.3	6.7	0 ($\frac{3}{2}^-$)	30	48 [c]	0.094			
	17.3	5.9	0.85 (($\frac{1}{2}^-$))	18					

The available data with the (p, γ₀) experiment are shown in the last column.

[a]) The errors may be ≈ 30% (for ^{90}Zr, ^{88}Sr) and ≈ 50% (for ^{89}Y) including the uncertainty of the process to separate the proton group.

[b]) $\Gamma_{p_0}/\Gamma = 1$ was assumed.

[c]) $(\Gamma_{p_0}+\Gamma_{p_2})/\Gamma = 1$ was assumed.

[d]) $J^\pi = \frac{1}{2}^+$ was assigned as shown in table 3.

[e]) $J^\pi = \frac{1}{2}^+$ was assigned as shown in table 3.

[f]) Correction was made for the spectroscopic factors on the ground state and the excited state with the data of the (He^3, d) and (d, p) reactions respectively.

[g]) Ref. [27]).

[h]) Ref. [6]).

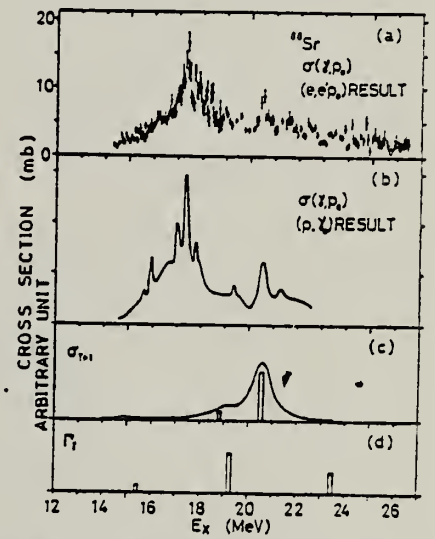

Fig. 13. Comparison of photoproton cross sections of ^{88}Sr. (a) Present result. (b) Ref. [5]). (c), (d) Theoretical estimates, refs. [11, 15]) respectively.

[5] M. Hasinoff et al., Phys. Lett. 30B (1969) 337.

[6] P. Paul, Proc. nuclear structure studies using electron scattering and photoreaction, ed. K. Shoda and H. Ui (Research report of Lab. Nucl. Sci. Tohoku Univ., vol. 5, 1972) p. 343.

[11] B. Goulard et al., Phys. Rev. 176 (1968) 1345.

[15] J.D. Vergados et al., Phys. Lett. 35B (1971) 93.

[27] J.L. Black et al., Nucl. Phys. A92 (1967) 365.

(over)

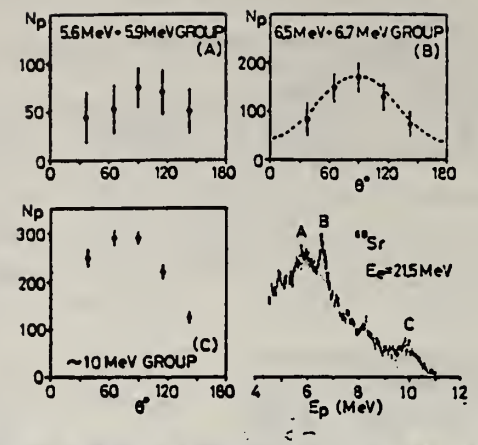

Fig. 16. Angular distributions of proton groups indicated by hatching in the proton spectrum which is summed over various angles. The result for group B is compared with that of the $E_p = 7.9$ MeV group of ^{90}Zr (dashed line).

REF. F. R. Metzger
Phys. Rev. C11, 2085 (1975)

ELEM. SYM.	A	Z
Sr	88	38

METHOD

REF. NO. 75 Me 5 hmg

REACTION	RESULT	EXCITATION ENERGY	SOURCE		DETECTOR		ANGLE
			TYPE	RANGE	TYPE	RANGE	
G,G	LFT	4	C	4	SCD-D		DST
		(4.744)		(4.944)			

Γ_0^2/Γ = 95±20 meV

4=4.744 MEV

TABLE I. Comparison of the angular distribution results with theoretical predictions.

		$\frac{N_{sc}(98°)}{N_{sc}(127°)}$
EXPERIMENT	3487 1⁻	0.70± 0.05
	4743	0.75± 0.20
THEORY	Spin 1 (0-1-0)	0.75
	Spin 2 (0-2-0)	2.08

REF. K. Shoda, H. Miyase, M. Sugawara, T. Saito, S. Oikawa, A. Suzuki, J. Uegaki
Nucl. Phys. A239, 397 (1975)

ELEM. SYM.	A	Z
Sr	88	38

METHOD

REF. NO. 75 Sh 4 egf

REACTION	RESULT	EXCITATION ENERGY	SOURCE TYPE	SOURCE RANGE	DETECTOR TYPE	DETECTOR RANGE	ANGLE
E,P	ABX	16- 26	D	14- 25	MAG-D		90

El virtual photon spectrum used to obtain (γ,p) cross sections.

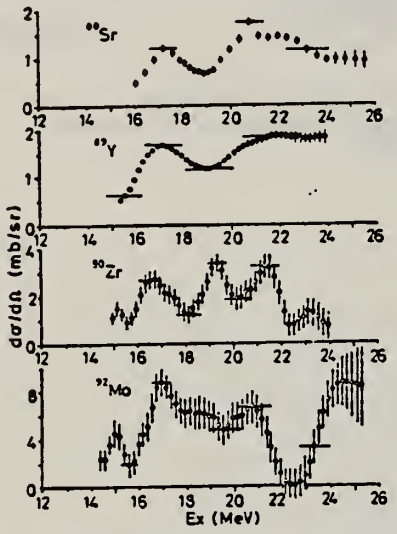

Fig. 3. Differential (γ, p) cross sections at $\theta = 90°$ analysed from (e, e'p) cross sections by the least structure method.

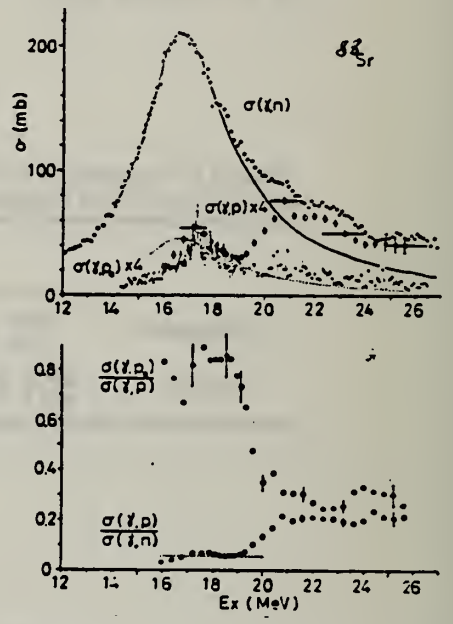

Fig. 5. Upper figure: open circles, $\sigma(\gamma, p)$; closed circles, $\sigma(\gamma, n)$ [ref. [18]]; closed points, $\sigma(\gamma, p_0)$ [ref. [15]]; solid line, Lorentz line fit to the $T_<$ region of $\sigma(\gamma, n)$ [ref. [18]]; dotted line, Lorentz line fit to the $T_<$ region of $\sigma(\gamma, p)$ with Γ_i and E_R equal to those of $\sigma(\gamma, n)$. Lower figure: ratio between cross sections. Dotted line: constant for $\sigma(\gamma, p)/\sigma(\gamma, n)$ determined around $T_<$ GDR.

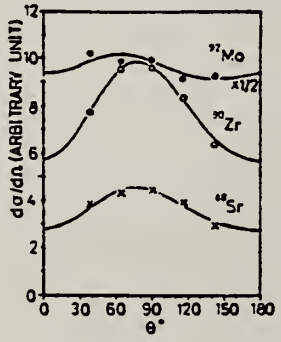

Fig. 4. Angular distributions of protons from the (e, e'p) reaction. The bombarding energies are 21.5, 22 and 20 MeV for ^{88}Sr, ^{90}Zr and ^{92}Mo respectively. The best fit curves obtained with eq. (7) are also shown.

15
K. Shoda et al., Nucl. Phys. A221 (1974) 125
18
A. Lepretre et al., Nucl. Phys. A175 (1971) 609

(over)

TABLE 2

The parameters of the angular distributions determined by the least-squares fits with $d\sigma/d\Omega = A[1 + B\sin^2\theta(1 - p\cos\vartheta)]$

	^{88}Sr	^{90}Zr	^{92}Mo
E_n (MeV)	21.5	22	20
A [a])	1	2.04	6.67
B	0.59	0.69	0.057
p	0.59	0.47	2.3

[a]) Relative value.

REF. F.R. Metzger
Phys. Rev. C 15, 2253 (1977)

ELEM. SYM.	A	Z
Sr	88	38

METHOD

REF. NO. 77 Me 5 hmg

REACTION	RESULT	EXCITATION ENERGY	SOURCE TYPE	SOURCE RANGE	DETECTOR TYPE	DETECTOR RANGE	ANGLE
G,G	LFT	1	C	2-3	SCD-D		DST
				(2-2.31)			

[NUCLEAR REACTIONS ^{88}Sr(γ,γ), bremsstrahlung $2.0 \leq E_\gamma \leq 2.31$ MeV; measured σ (96°) and σ (126°), deduced Γ (1.836). Natural target.]

1=1.836 MeV

TABLE II. Summary of experimental values for the width of the 1.836-MeV 2$^+$ level in ^{88}Sr.

Method	Ref.	1.836 (meV)
(γ,γ), ^{88}Rb source	6	4.2±1.0
Coulomb excitation	7	6.7±3.0
Coulomb excitation	9	3.8±0.5
(e,e')	5	4.7±0.3
(e,e')	8	3.33±0.17
(e,e')	10	2.76±0.08
(γ,γ), bremsstrahlung	This paper	2.94±0.15

REF. G. Isoyama, T. Ishimatsu, E. Tanaka, K. Kageyama, N. Kumagai
Nucl. Phys. A342, 124 (1980)

ELEM. SYM.	A	Z
Sr	88	38

METHOD

REF. NO. 80 Is 1 hg

REACTION	RESULT	EXCITATION ENERGY	SOURCE		DETECTOR		ANGLE
			TYPE	RANGE	TYPE	RANGE	
G,G	LFT	6-8	C	14	SCD-D		DST

Abstract: The resonant scattering of bremsstrahlung γ-rays by a $SrCO_3$ target has been studied for γ-ray energies of 5–11 MeV. Six γ-transitions of energies between 6–8 MeV, which indicate six resonant states in ^{88}Sr, were observed. The relative intensities of the resonantly scattered γ-rays at 125 and 150° were found to be compatible only with the assignment of spin 1 to the six states. Radiative widths of the resonant states were deduced. The possibility that these states are components of the giant M1 resonance in ^{88}Sr is discussed.

BML, SIX SPIN 1 STATES

E NUCLEAR REACTIONS ^{88}Sr(γ, γ), E = 14 MeV bremsstrahlung; measured E_γ, $I_\gamma(\theta)$. ^{88}Sr deduced levels, J, Γ_γ. Natural targets.

TABLE 2

Summary of the experimental results

Level energy (MeV)	R	J	Γ [a] (eV)	B(M1; $1^+ \rightarrow 0^+$) [b] (μ_N^2)	Γ_0 [c] (eV)
6.215	1.45±0.29	1	1.81±0.22	0.65	3.0±0.4
6.335	1.37±0.20	1	2.83±0.29	0.96	4.5±0.6
7.091	1.39±0.19	1	4.14±0.45	1.00	
7.537	1.18±0.42	1	1.31±0.27	0.26	
7.841	1.50±0.41	1	2.53±0.45	0.45	
8.047	1.34±0.47	1	3.76±0.77	0.62	

[a]) Deduced on the assumption of 100 % ground-state decay.
[b]) Deduced on the assumption of positive parity.
[c]) Ref. [1]).

REF. K. Wienhard, C. Bläsing, K. Ackermann, K. Bangert, U.E.P. Berg, K. Kobras, W. Naatz, D. Rück, R.K.M. Schneider, R. Stock
Z. Phys. A302, 185 (1981)

ELEM. SYM.	A	Z
Sr	88	38

METHOD

REF. NO.	
81 Wi 1	hg

REACTION	RESULT	EXCITATION ENERGY	SOURCE		DETECTOR		ANGLE
			TYPE	RANGE	TYPE	RANGE	
$ G,G	NOX	6-8	C	UKN	SCD-D		90

POL INCOMING PHOTONS

Abstract. The unknown parities of five strong dipole states between 6 and 8 MeV in ^{88}Sr are shown to be negative.

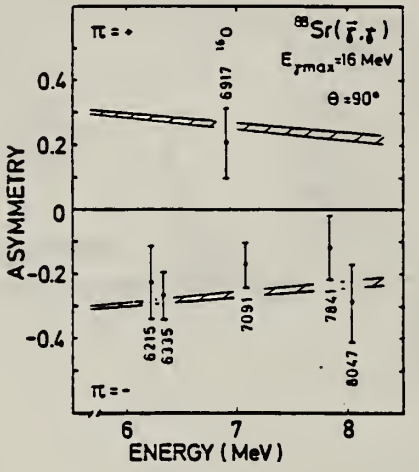

Fig. 1. Observed asymmetries for five ground state dipole transitions in ^{88}Sr and for the 2^+ transition at 6917 keV in ^{16}O. The energies for the ^{88}Sr states were taken from /2/. The hatched band represents the expected asymmetry for states with positive parity (upper part) and negative parity (lower part)

Sr
A=89

Sr
A=89

REF. A. Likar, A. Lindholm, L. Nilsson, I. Bergqvist and B. Palsson
Nucl. Phys. A298, 217 (1978)

ELEM. SYM.	A	Z
Sr	89	38

METHOD

REF. NO. 78 Li 2 rs

REACTION	RESULT	EXCITATION ENERGY	SOURCE		DETECTOR		ANGLE
			TYPE	RANGE	TYPE	RANGE	
N,G	RLX	13- 17	D	7- 11	NAI-D		DST

Abstract: Gamma-ray spectra from neutron capture in natural samples of strontium and yttrium have been recorded at various angles with respect to the direction of the incident neutron flux. Angular yields have been observed at six neutron energies in the range 7 to 11 MeV using time-of-flight techniques to improve the signal-to-background ratio. The γ-radiation was detected by a large NaI(Tl) crystal placed in a heavy radiation shield. Certain combinations of Legendre polynomial coefficients were extracted for transitions to low-lying single-particle states ($2d_{5/2}$ and $3s_{1/2}$) in the final nuclei. The energy dependence of the angular distribution coefficients indicates interference between the electric dipole amplitude and amplitudes of opposite parity. The results are compared with theoretical calculations based on the direct-semidirect model.

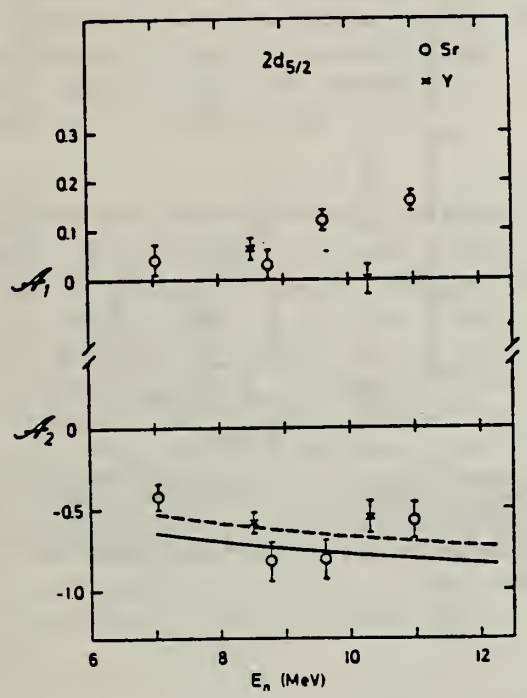

Fig. 2. Angular distribution coefficients A_1 and A_2 versus neutron energy for the reactions $^{88}Sr(n,\gamma_0)^{89}Sr$ (open circles) and $^{89}Y(n,\gamma_0+\gamma_1)^{90}Y$ (crosses). The curves for the A_2 coefficient represent the results of theoretical calculations for E1 transitions to the $2d_{5/2}$ state in ^{89}Sr from the direct (solid line) and DSD (dashed line) capture models.

over

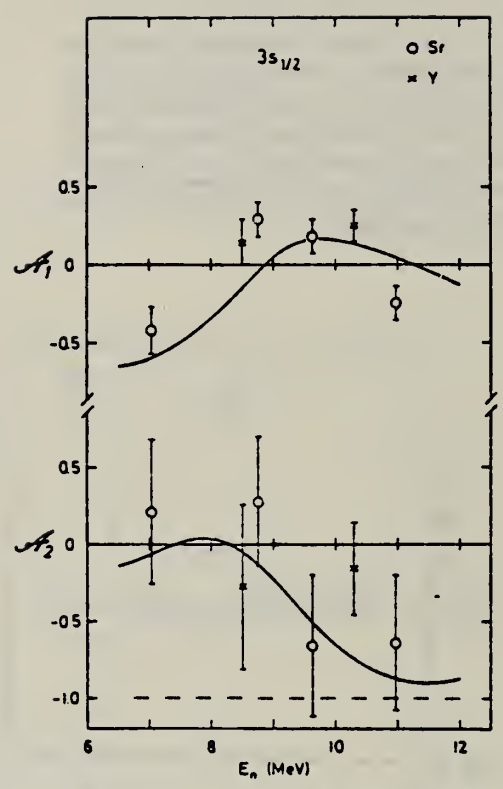

Fig. 3. Angular distribution coefficients A_1 and A_2 versus neutron energy for γ-rays to the $3s_{1/2}$ states from the reactions $^{88}Sr(n,\gamma)^{89}Sr$ (open circles) and $^{89}Y(n,\gamma)^{90}Y$ (crosses). The theoretical result for DSD model calculations are shown as dashed curve for pure E1 transitions and as solid curves assuming E1 and E2 transitions associated with collective excitation of the GDR and the isoscalar GQR.

# YTTRIUM
Z=39

"The rare earths perplex us in our researches, baffle us in our speculations, and haunt us in our very dreams. They stretch like an unknown sea before us, mocking, mystifying, and murmuring strange revelations and possibilities."(1)

Y
A=89

Yttrium was discovered in 1794 by the Scandinavian chemist Johan Gadolin (1760-1852) and was named after the small town of Ytterby, Sweden where the ore was found. It always occurs with the other rare earth elements and is very similiar to them in both chemical and metalurgical respects. In 1848 Carl Gustav Mosander (1797-1858) showed that yttria from which all the ceria, lanthana, and didymia had been removed contains at least three other rare earths. These are: a colorless oxide, for which he kept the name yttria; a yellow earth erbia, and a rose colored ore, terbia. These were all seperated by fractional precipitation with ammonium hydroxide.

(1) Quotation from Sir William Crookes.

Y
A=89

Ref. P.F. Yergin, B.P. Fabricand
Phys. Rev. 104, 1334 (1956)

Elem. Sym.	A	Z
Y	89	39

Method: 24 MeV betatron; 250 r Victoreen in 3.75 cm Lucite; neutron detector

Ref. No.: 56 Ye 2 | EGF

Reaction	E or ΔE	E_0	Γ	$\int \sigma dE$	Jπ	Notes
$Y^{89}(\gamma,xn)$	Bremss 24	16.3	3.8 MeV	$\int_0^{23}$ = 0.87 MeV-b		

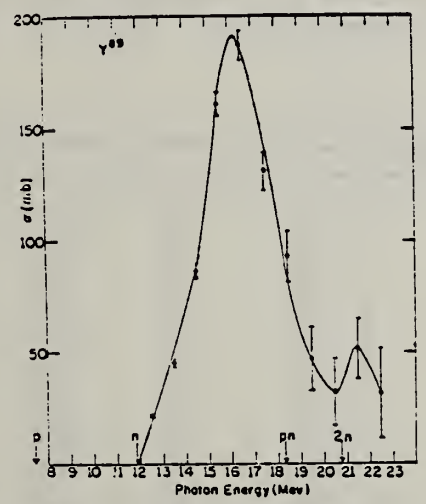

FIG. 1. Cross section for the (γ,n) reaction in Y^{89}, calculated from the yield data, at an intermediate stage of the smoothing process (see text). The vertical lines through the calculated points show the rms uncertainty in the cross-section values, produced by the statistical uncertainty of the recorded counts of the raw yield data. Other sources of errors, and the partial smoothing already done have been ignored in calculating these uncertainties. The arrows along the abscissa indicate the thresholds for emission of the particles indicated by the labels therewith. The units of the ordinate are 10^{-27} cm².

TABLE III. Parameters of giant-resonance cross-section curves for (γ,n) reactions in nuclei near 50 neutrons. Nuclides $_{33}As^{75}$, $_{41}Nb^{93}$, and $_{45}Rh^{103}$ from reference 4, $_{40}Zr^{90}$ and $_{40}Zr^{91}$ from reference 5 recomputed in present work. Neutron number is shown in column 2, location of peak cross-section value in column 3, peak cross-section value in column 4, half-height width of curve in column 5, and area under curve from threshold to 23 Mev in column 6.

Nuclide	N	E_m (Mev)	σ_m (millibarns)	Γ (Mev)	$\int_{th}^{23}\sigma dE$ (Mev-barns)
$_{33}As^{75}$	42	17.3	90.3	9.0	0.80
$_{38}Sr^{86}$	48	15.9	160	5.0	0.92
$_{38}Sr^{87}$	49	15.8	146	5.3	1.00
$_{38}Sr^{88}$	50	16.3	201	4.0	1.05
$_{39}Y^{89}$	50	16.3	191	3.8	0.87
$_{40}Zr^{90}$	50	15.8	199	4.3	0.98
$_{40}Zr^{91}$	51	16.5	200	5.0	1.22
$_{40}Zr^{92}$	52	16.9	193	5.5	1.24
$_{41}Nb^{93}$	52	17.0	195	6.8	1.46
$_{45}Rh^{103}$	58	16.5	205	8.9	1.94

..G. Chidley, L. Katz, S. Kowalski
Can. J. Phys. 36, 407 (1958)

ELEM. SYM.	A	Z
Y	89	39

CD

Betatron

REF. NO.	
58 Ch 2	NVB

REACTION	RESULT	EXCITATION ENERGY	SOURCE		DETECTOR		ANGLE
			TYPE	RANGE	TYPE	RANGE	
G,N	RLY	THR	C	THR	BF3-I		4PI

See 58 Ka 1 for cross sections;

THRESHOLD

TABLE I

MEASURED PHOTONEUTRON THRESHOLDS

Reaction	Measured Q value, Mev.	Other Q values, Mev.	Method	Reference
$Y^{89}(\gamma, n)Y^{88}$	11.82±0.05			
		11.76 ±0.15	Mass data	Duckworth (unpublished)
			Q^+ value	Way *et al.* (1955)
		11.80 ±0.33	Mass data	Wapstra (1955)

L. Katz, G.B. Chidley
Nuclear Reactions at Low and Medium Energies (Academy of Science, USSR: 1958) 371

Y	89	39

METHOD: Betatron; neutron cross section; BF_3 counters; ion chamber monitor

REF. NO.: 58 Ka 1 | NVB

REACTION	RESULT	EXCITATION ENERGY	SOURCE		DETECTOR		ANGLE
			TYPE	RANGE	TYPE	RANGE	
G,XN	ABX	12-22	C	12-22	BF3-I		4PI

Таблица 2

Пороги испускания фотонейтронов

Изотоп	B_n, *Мэв*	B_{2n}, *Мэв*	Изотоп	B_n, *Мэв*	B_{2n}, *Мэв*
V^{51}	11,16	20,5	La^{139}	8,81	16,1
Mn^{55}	10,14	19,2	Pr^{141}	9,46	17,6
Co^{59}	10,44	18,6	Tb^{159}	8,16	14,8
As^{75}	10,24	18,1	Ho^{165}	8,10	14,6
Y^{89}	11,82	20,7	Tm^{169}	8,00	14,7
Nb^{93}	8,86	17,1	Lu^{175}	7,77	14,2
Rh^{103}	9,46	16,8	Ta^{181}	7,66	13,8
J^{127}	9,14	16,2	Au^{197}	7,96	13,3
Cs^{133}	9,11	16,5	Bi^{209}	7,43	14,5

THRESHOLDS

не приведены, поскольку они превышают 22 *Мэв* во всех случаях, кроме золота, для которого B_{2n}=21 *Мэв*. Свойства сечений $\sigma_G(\gamma)$ сведены в табл. 3.

Таблица 1

Изотоп	$E_{макс}$, *Мэв*	$\sigma_n(E_\gamma)$, барн	Γ, *Мэв*	$\int\sigma d\gamma$, *Мэв·барн*	$Y(22)$, 10^6 нейтрон/100 р·моль
V^{51}	18,4	0,062	5,2	0,33	1,62
Mn^{55}	20,2	0,060	7,0	0,39	2,01
Co^{59}	18,3	0,068	6,3	0,44	2,30
As^{75}	16,4	0,090	9,5	0,74	4,25
Y^{89}	17,1	0,172	5,2	0,93	5,33
Nb^{93}	18,0	0,156	7,5	1,17	6,80
Rh^{103}	17,5	0,160	9,4	1,40	8,28
J^{127}	15,2	0,273	6,8	1,76	11,9
Cs^{133}	16,5	0,238	7,7	1,59	10,7
La^{139}	15,5	0,325	3,8	1,55	11,2
Pr^{141}	15,0	0,320	4,9	1,93	13,1
Tb^{159}	15,6	0,274	9,8	2,49	18,1
Ho^{165}	13,5	0,305	8,9	2,52	18,7
Tm^{169}	16,4	0,250	8,4	1,91	14,9
Lu^{175}	16,0	0,225	8,4	1,90	23,0
Ta^{181}	14,5	0,380	8,5	3,15	22,0
Au^{197}	13,8	0,475	4,7	3,04	22,6
Bi^{209}	13,2	0,455	5,9	2,89	23,2

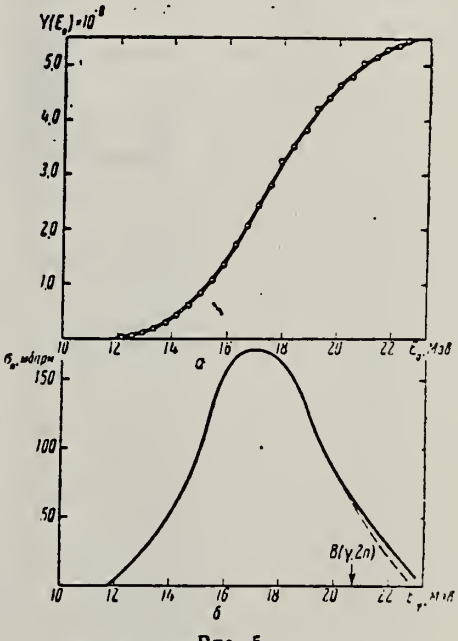

Рис. 5.

а — Выход фотонейтронов для Y; *б* — $\sigma_n(E_\gamma)$ и $\sigma_G(\gamma)$ для Y

Ref. E. Silva, J. Goldemberg
Phys. Rev. 110, 1102 (1958)

Elem. Sym.	A	Z
Y	89	39

Method
Betatron; photon difference analysis

Ref. No. 58 Si 1 EH

Reaction	E or ΔE	E_o	Γ	$\int \sigma dE$	Jπ	Notes
(γ,γ')	4-22	10.5 16				

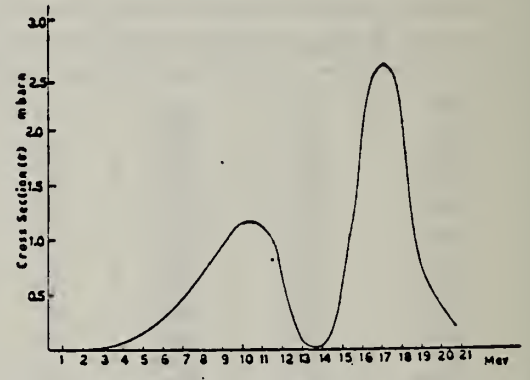

FIG. 2. Cross section as a function of energy for formation of the isomeric state of Y^{89}.

... Geller, J. Halpern, and E. G. Muirhead
Phys. Rev. 118, 1302-12 (1960)

Y	89	39

METHOD	REF. NO.	
Betatron; neutron threshold; ion chamber	60 Ge 3	NVB

REACTION	RESULT	EXCITATION ENERGY	SOURCE		DETECTOR		ANGLE
			TYPE	RANGE	TYPE	RANGE	
G,N	NØX	THR	C THR		BF3-I		4 PI

THRESHØLD

TABLE I. Summary and comparison of neutron separation energies inferred from present threshold measurements with values predicted from mass data and reaction energies. All energies are expressed in the center-of-mass system in Mev.

Reaction	No. runs	Present results	Other results	Method	Reference
$Y^{89}(\gamma,n)Y^{88}$	3	$\leqslant 11.59 \pm 0.08$	11.53 ± 0.40	mass data	m
				$Q(\beta^+)$	n
			11.82 ± 0.05	threshold	f

[m] Henry E. Duckworth, *Mass Spectroscopy* (Cambridge University Press, New York, 1958), p. 177.
[n] L. J. Lidofsky, Revs. Modern Phys. 29, 773 (1957).

TABLE II. Comparison of measured threshold energies with neutron binding energies predicted by mass data for transitions with $\Delta I \geq 7/2$. All energies in Mev.

Reaction	ΔI[a]	Observed threshold	Mass data Q value	$E_{th}-Q$	Excited state energy
$Cr^{52}(\gamma,n)Cr^{51}$	7/2	12.18±0.14	12.053±0.004[b]	0.13±0.14	...
$Y^{89}(\gamma,n)Y^{88}$	7/2	11.59±0.08	11.53 ±0.40[a]	0.06±0.41	0.387[d]
$In^{115}(\gamma,n)In^{114}$	7/2	9.22±0.03	9.35 ±0.43[e]	−0.13±0.43	0.191[a]
$Ce^{142}(\gamma,n)Ce^{141}$	(7/2)[e]	7.24±0.07	6.97 ±0.07[f]	0.27±0.10	...
$Nd^{143}(\gamma,n)Nd^{142}$	7/2	6.38±0.16	5.97 ±0.19[f]	0.41±0.25	0.690[a]
$Sm^{149}(\gamma,n)Sm^{148}$	7/2	6.45±0.16	5.87 ±0.28[f]	0.58±0.33	0.562[a]
$Er^{167}(\gamma,n)Er^{166}$	7/2	6.65±0.08	6.45 ±0.06[g]	0.20±0.10	0.081[a]
$Hf^{177}(\gamma,n)Hf^{176}$	7/2	6.69±0.03	6.28 ±0.06[g]	0.64±0.07	0.088[a]
$Hf^{179}(\gamma,n)Hf^{178}$	9/2	6.31±0.07	6.17 ±0.06[g]	0.14±0.09	0.093[a]
$Hf^{180}(\gamma,n)Hf^{179}$	9/2	7.85±0.11	7.32 ±0.06[g]	0.53±0.13	0.375[a]

[a] D. Strominger, J. M. Hollander, and G. T. Seaborg, Revs. Modern Phys. 30, 585 (1958).
[b] C. F. Giese and J. L. Benson, Phys. Rev. 110, 712 (1958).
[c] Henry E. Duckworth, *Mass Spectroscopy* (Cambridge University Press, New York, 1958), p. 177.
[d] Dzelepov and L. K. Peker, Atomic Energy of Canada Limited Report Tr. AECL-457 (unpublished).
[e] The discrepancy in the case of Ce^{142} predicts a ground-state spin for Ce^{141} of 0, since the spin of Ce^{141} is known to be 7/2.
[f] W. H. Johnson, Jr., and A. O. Nier, Phys. Rev. 105, 1014 (1957).
[g] W. H. Johnson, Jr., and V. B. Bhanot, Phys. Rev. 107, 6 (1957).

R.G. Baker, K.G. McNeill
Can. J. Phys. 39, 1158 (1961)

ITEM		
Y	89	39

METHOD: Betatron; fast neutron yield, angular distribution; Si threshold detector; ion chamber

REF. NO.: 61 Ba 2 | NVB

REACTION	RESULT	EXCITATION ENERGY	SOURCE		DETECTOR		ANGLE
			TYPE	RANGE	TYPE	RANGE	
G,XN	ABY	THR-22	C	22	THR-I	5-+	DST

In Table 4:

$\bar{\sigma}$ = average cross section of detector weighted with neutron spectrum

$\bar{\Phi}$ = neutrons/100 roentgen/mole

$$W(\theta) = a_o \sum_{n=1}^{\infty} [1 + A_n P_n (\cos\theta)]$$

=

TABLE IV

I Element	II a_0	III a_1	IV a_2	V $(\bar{\sigma}\bar{\Phi})\times10^{26}$	VI Φ_{total} (22 Mev)$\times10^{9}$	VII $\Phi_{>11}/\Phi_{total}$
Vanadium	245 (1±0.03)	0.01±0.08	−0.90±0.10	8.05	0.21	0.12
Chromium	164 (1±0.03)	0.04±0.04	−0.05±0.05	4.05	0.17	0.16
Manganese	308 (1±0.02)	0.07±0.03	−0.09±0.04	7.61	0.25	0.12
Iron	200 (1±0.03)	0.05±0.04	−0.17±0.05	4.94	0.18	0.11
Cobalt	390 (1±0.02)	0.08±0.03	−0.22±0.04	9.63	0.26	0.15
Nickel	145 (1±0.05)	0.07±0.07	−0.23±0.09	3.58	0.12	0.12
Copper	347 (1±0.02)	0.05±0.03	−0.29±0.04	8.57	0.30	0.12
Arsenic	482 (1±0.03)	0.11±0.04	−0.24±0.05	11.91	0.33	0.15
Rubidium	638 (1±0.05)	0.13±0.06	−0.14±0.08	15.76		
Strontium	409 (1±0.05)	0.16±0.06	−0.17±0.08	10.10		
Yttrium	290 (1±0.10)	0.08±0.12	−0.12±0.15	7.16		
Silver	590 (1±0.04)	0.10±0.06	−0.22±0.08	14.57	0.87	0.07
Cadmium	905 (1±0.02)	0.02±0.02	−0.26±0.03	22.35		
Iodine	1133 (1±0.03)	0.04±0.04	−0.29±0.05	27.99	1.42	0.08
Barium	1048 (1±0.04)	0.10±0.06	−0.38±0.08	25.89		
Lanthanum	1595 (1±0.02)	0.02±0.03	−0.32±0.04	39.40	1.04	0.15
Cerium	1316 (1±0.05)	0.05±0.06	−0.39±0.08	32.50		
Dysprosium	1652 (1±0.08)	0.04±0.10	−0.33±0.13	40.80		
Tantalum	1558 (1±0.02)	0.04±0.03	−0.22±0.04	38.48	2.50	0.06
Tungsten	1365 (1±0.02)	0.07±0.03	−0.24±0.04	33.71		
Mercury	1345 (1±0.02)	0.04±0.03	−0.31±0.04	33.22		
Lead	2274 (1±0.01)	0.02±0.02	−0.42±0.03	56.17	2.72	0.03
Bismuth	2162 (1±0.02)	0.05±0.03	−0.45±0.04	53.40	3.36	0.06
Thorium	3031 (1±0.04)	0.00±0.05	−0.32±0.07	74.87		
Uranium	4630 (1±0.02)	0.05±0.03	−0.17±0.04	114.36		

*$(\bar{\sigma}\Phi) = 2.47\times10^{9}$ σ millibarn-neutron. Errors are standard errors due to counting statistics only.

Ref. G.C. Reinhardt, W.D. Whitehead
Nuclear Phys. 30, 201 (1962)

Elem. Sym.	A	Z
Y	89	39

Method 55 MeV betatron; synchrotron; $Si^{28}(n,p)Al^{28}$ activity; $Cu^{63}(\gamma,n)Cu^{62}$ monitor.

Ref. No. 62 Re 1 | EGF

Reaction	E or ΔE	E_o	Γ	$\int \sigma dE$	Jπ	Notes
$Y^{89}(\gamma,n)$	Bremss. 55					Figure 11: Dotted curve is of form $a_o + a_1\cos\theta + a_2\cos^2\theta + a_2\cos^2\theta - a_1\cos^2\theta$; solid curve is of form $a_o + a_1\cos\theta + a_2\cos^2\theta$; errors on points are statistical errors in counting only.

TABLE 2

Parameters of the fit (1) for the expressions $a_0+a_1\cos\theta+a_2\cos^2\theta$, $a+b\sin^2\theta+c\cos\theta$ and $A_0+A_1P_1+A_2P_2$

	Bi(1)	Bi(2)	Pr	Au	Y	Ho	La
a_0	1.00±0.02	1.00±0.02	1.00±0.02	1.00±0.02	1.00±0.03	1.00±0.02	1.00±0.01
a_1	0.15±0.03	0.18±0.04	0.17±0.04	0.14±0.03	0.17±0.06	0.12±0.03	0.14±0.03
$-a_2$	0.47±0.06	0.40±0.08	0.41±0.09	0.21±0.07	0.15±0.11	0.34±0.06	0.39±0.06
A_1 a)	0.18±0.04	0.21±0.05	0.20±0.05	0.15±0.04	0.18±0.06	0.14±0.04	0.16±0.03
$-A_2$ a)	0.37±0.05	0.31±0.06	0.32±0.07	0.15±0.05	0.11±0.08	0.26±0.05	0.30±0.04
a	0.53±0.06	0.60±0.08	0.59±0.09	0.79±0.07	0.85±0.11	0.66±0.06	0.61±0.06
b	0.47±0.06	0.40±0.08	0.41±0.09	0.21±0.07	0.15±0.11	0.34±0.06	0.39±0.06
c	0.15±0.03	0.18±0.04	0.17±0.04	0.14±0.03	0.17±0.06	0.12±0.03	0.14±0.03

a) Renormalized so that $A_0 = 1$

TABLE 4

Parameters of the fit (3) for the expressions $a_0+a_1\cos\theta+a_2\cos^2\theta+a_3\cos^3\theta$, $1+A_1P_1+A_2P_2+A_3P_3$

	Bi(1)	Bi(2)	Pr	Au	Y	Ho	La
a_0	1.01±0.02	1.00±0.02	1.01±0.03	0.98±0.02	1.00±0.03	1.00±0.02	1.01±0.02
a_1	0.19±0.05	0.17±0.07	0.21±0.07	0.07±0.06	0.16±0.09	0.12±0.05	0.17±0.05
$-a_2$	0.56±0.11	0.37±0.15	0.50±0.16	0.05±0.12	0.13±0.20	0.33±0.12	0.47±0.11
a_3	−0.17±0.18	0.05±0.24	−0.17±0.25	0.31±0.19	0.05±0.32	0.03±0.19	−0.17±0.17
A_1 a)	0.11±0.15	0.23±0.18	0.13±0.20	0.27±0.13	0.20±0.22	0.15±0.14	0.09±0.13
$-A_2$ a)	0.45±0.09	0.28±0.11	0.39±0.12	0.03±0.08	0.09±0.14	0.24±0.09	0.37±0.09
A_3 a)	−0.08±0.09	0.02±0.11	−0.08±0.12	0.13±0.08	0.02±0.13	0.01±0.08	−0.08±0.08

a) Renormalized so that $A_0 = 1$

Ref. K.N. Geller
Nuclear Phys. 40, 177 (1963)

Elem. Sym.	A	Z
Y	89	39

Method: Betatron; neutron yield; 4π neutron

Ref. No.: 63 Ge 1 JHH

Reaction	E or ΔE	E_o	Γ	$\int \sigma dE$	Jπ	Notes
$Y^{89}(\gamma,n)$	Bremss. ~11–~12					$E_{(\gamma,n)th}$ to ground state of Y^{88} = 11.54±0.04 MeV

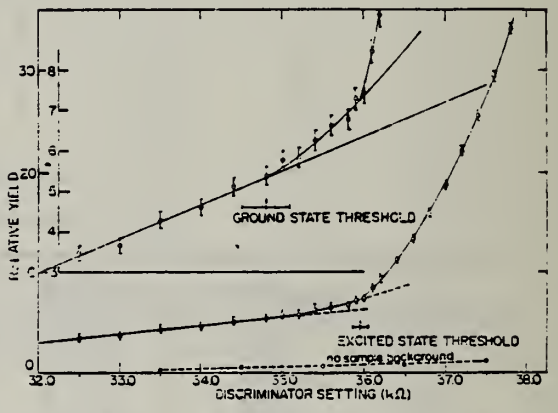

Fig. 1. The $Y^{89}(\gamma, n)$ yield curve in the vicinity of threshold.

TABLE 1

Summary of experimental threshold observation for $Y^{89}(\gamma, n)$

Threshold observed	Threshold energy (MeV)
Ground state	11.55 ±0.10
Excited state	11.947±0.039
Ground state (computed)[a]	11.554±0.039
Ground state, corrected for extrapolation error[b]	11.539±0.039

a) Ground state threshold obtained by combining energy of excited state (393 keV) with observed excited state threshold.
b) An extrapolation error of 15 keV exists in the (γ, n) threshold determination when the energy calibration is based on a resonance observation (see text).

T. Kaminishi, C. Kojima
Jap. J. Appl. Phys. 2, 399 (1963)

Y	89	39

METHOD: Linac; isomer yield; activity

REF. NO.: 63 Ka 2 | NVB

REACTION	RESULT	EXCITATION ENERGY	SOURCE TYPE	SOURCE RANGE	DETECTOR TYPE	DETECTOR RANGE	ANGLE
G,G/	RLY	1	C5		ACT-I		4PI
		(0.92)					

Table II. The isomers observed

Isomer	Observed value		Referenced value[11][13]	
	Half-life	Energy (MeV)	Half-life	Energy (MeV)
Se-77m	17.5 sec	0.160	17.5 sec	0.161
Br-79m	4.80 sec	0.209	4.8 sec	0.208
Sr-87m	2.3 hr	0.390	2.8 hr	0.388
Y-89m	15.0 sec	0.920	14 sec	0.915
Rh-103m	58 min	*	57 min	0.040
Ag-107m	42 sec	0.95	44 sec	0.094
Ag-109m			40 sec	0.088
Cd-111m	47 min	0.150,0.255	49 min	0.150,0.247
In-115m	4.5 hr	0.335	4.5 hr	0.335
Sn-117m	17 day	0.160	14 day	0.159,0.161
Ba-137m	2.6 min	0.660	2.6 min	0.662
Er-167m	2.10 sec	0.209	2.5 sec	0.208
Hf-179m	18.5 sec	0.157,0.215	19 sec	0.161,0.217
W-183m	5.4 sec	0.200,0.170,0.115	5.5 sec	0.1025,0.2315 others
Ir-191m	4.90 sac	0.129, <0.07	4.9 sec	0.042-0.129
Pt-195m	4.5 day	0.065**	4.1 day	0.031-0.130
Au-197m	7.0 sec	0.10,0.27,0.40	7.2 sec	0.130,0.270,0.407
Hg-199m	43 min	0.160,0.370	42 min	0.158,0.368

* This isomer was measured with a G-M flow counter.
** This value corresponds to Pt-K X-ray energy.

Table III. Induced activation rate

Element	Beam energy (MeV)	Counting rate (×10000 cpm)	Sample form
Se	5	1300	metallic pellet
Br	4	1600	NaBr grain
Sr	6	0.3	$SrCO_3$ powder
Y	5	90	metallic grain
Rh	5	(0.2)*	$RhCl_3$ grain
Ag	5	180	metallic plate
Cd	6	0.5	$CdCl_2$ grain
In	6	8	metallic plate
Sn	6	0.0005	metallic plate
Ba	5	0.6	BaS powder
Er	4	4900	Er_2O_3 powder
Hf	5	1600	metallic plate
W	5	120	metallic powder
Ir	5	2100	metallic powder
Pt	5	0.3	metallic plate
Au	4	4300	metallic plate
Hg	6	0.09	metallic liquid

* The value measured with a G-M flow counter.

REF.

A. Veres
Acta Phys. Acad. Sci.Hung. 16, 261-73 (1963)

ELEM. SYM.	A	Z
Y	89	39

METHOD

Radioactive source

REF. NO. 63 Ve 2 NVB

REACTION	RESULT	EXCITATION ENERGY	SOURCE		DETECTOR		ANGLE
			TYPE	RANGE	TYPE	RANGE	
G,G/	ABX	0-1	D	0-1	NAI-D		

ISØMERS

Таблица II

Измеренные значения после облучения, сравниваемые с другими литературными данными

Элемент	Активность облучения после первого измерения (имп/мин.)	Активн. экстрп. в конце облуч. (имп/мин.)	Литературные данные		Данные измерений		σ_{ma} (10^{-28}см^2)	Γ_{ym} (10^{-3}эв)
			$T_{1/2}$	E (кэв)	$T_{1/2}$	E (кэв)		
Se-77m	3842±96	5400	17,5 сек.	160	18,1±1 сек.	160±10	9,5	1,75
Sr-87m	191±5	200	2,8 ч.	390	2,9±0,1 ч.	365±25	0,85	0,2
У-89m	96±20	170	16 сек.	910	16,7±5 сек.		0,08	0,02
Rh-103m	28±5	31	57 мин.	40	58±2 мин.	20,5±0,5	0,08	0,01
Ag-107m	220±14	250	44 сек.	93	43,8±0,6 сек	91±10	0,8	0,2
Ag-109m			39 сек.	88				
Hf-179m	80±18	155	19 сек.	160; 215	19±2 сек.		1	0,2
Ir-191m	90±20	250	4,9 сек.	42; 130	5±2 сек.		5,6	1
Pt-195m	90±9	100	3,5 д.	31; 100; 130;	3,5±0,2 д.	32±3 67,5±5 96±5 130±10	0,2	0,04
Au-197m	240±16	520	7,2 сек.	130; 277; 407	7,2±1 сек.	68:130: 280±20 390±20	0,07	0,01
Hg-199m	9,6±3,2		42 мин.	160; 370			0,005	0,001

Acta Phys. Hung. Tom. XVI. Fasc. 3.

REF. S. C. Fultz, R. L. Bramblett, B. L. Berman, J. T. Caldwell, and M. A. Kelly
Proc. Gatlinburg Conference 397 (1966)

ELEM. SYM.	A	Z
Y	89	39

METHOD

REF. NO. 66 Fu 2 hmg

REACTION	RESULT	EXCITATION ENERGY	SOURCE		DETECTOR		ANGLE
			TYPE	RANGE	TYPE	RANGE	
G,XN	ABI	THR-28	D	THR-28	BF3-I		4PI
G,2N	ABI	THR-28	D	THR-28	BF3-I		4PI

TABLE 1

Integrated Cross Sections for Zirconium and Yttrium

Isotope	E_{max} $a = \int \sigma_{tot} dE$ (MeV - barns)	E_{max} $b = \int \sigma_{Y,2n} dE$ (MeV - barns)	b/a	E_{max} (MeV)
^{90}Zr	0.980	0.108	0.110	28
^{91}Zr	1.078	0.202	0.187	30
^{92}Zr	1.096	0.447	0.408	28
^{94}Zr	1.041	0.577	0.554	30
^{89}Y	0.991	0.095	0.096	28

REF.

W. B. Walters and J. P. Hummel
Phys. Rev. 150, 867 (1966)

ELEM. SYM.	A	Z
Y	89	39

METHOD

Betatron

REF. NO.

66 Wa 1

JDM

REACTION	RESULT	EXCITATION ENERGY	SOURCE		DETECTOR		ANGLE
			TYPE	RANGE	TYPE	RANGE	
G,2N	RLY	THR-280	C	150,280	ACT-I		4PI

Measured isomeric yield ratios.

TABLE IV. Summary of the results for the photoproduction of the Y^{87} isomers (spins $\frac{1}{2}$ and $\frac{9}{2}$).

Target isotope and spin	Bremsstrahlung energy (MeV)	Fraction of yield to high-spin isomer
Y^{89} ($I=\frac{1}{2}$)	150	0.42±0.03
	280	0.42±0.03
Nb^{93} ($I=\frac{9}{2}$)	150	0.71±0.13
	280	0.69±0.13

REF. B.L. Berman, J.T. Caldwell, R.R. Harvey, M.A. Kelly, R.L. Bramblett, and S.C. Fultz
Phys. Rev. 162, 1098 (1967)

EL EM. SYM.	A	Z
Y	89	39

METHOD

REF. NO. 67 Be 2 hmg

REACTION	RESULT	EXCITATION ENERGY	SOURCE TYPE	SOURCE RANGE	DETECTOR TYPE	DETECTOR RANGE	ANGLE
G,N 1	ABX	THR-28	D	THR-28	BF3-I		4PI
G,2N 2+	ABX	THR-28	D	THR-28	BF3-I		4PI

TABLE IV. Integrated cross sections.

Nucleus	$\sigma_{int}[(\gamma,n)+(\gamma,pn)]$ (MeV-b)[a]	$\sigma_{int}(\gamma,2n)$ (MeV-b)[a]	$E_{\gamma max}$ (MeV)	$\frac{\sigma_{int}(\gamma,2n)}{\sigma_{int}(\gamma,\text{total})}$[b]	$(\frac{1}{2}\pi)\sigma_m\Gamma$ (MeV-b)	$0.06NZ/A$ (MeV-b)
Y^{89}	0.94	0.10	28	0.10	1.14	1.31
Zr^{90}	0.96	0.10	28	0.09	1.16	1.33
Zr^{91}	0.88	0.20	30	0.19	1.22	1.35
Zr^{92}	0.65	0.45	28	0.41	1.23	1.36
Zr^{94}	0.43	0.58	30	0.56[c]	1.32	1.38

1 +

[a] All measured integrated cross-section values are given for an energy region from threshold to $E_{\gamma max}$. For the Zr^{91} and Zr^{92} cases, it was necessary to extrapolate the low-energy part of the total photoneutron cross section down to threshold; the error introduced in this process, however, is less than 0.5%.
[b] The word "total" in this table refers to the total photoneutron cross section $\sigma([\gamma,n)+(\gamma,pn)+(\gamma,2n)+(\gamma,3n)]$, and excludes the (γ,γ) and (γ,p) cross sections.
[c] This value includes the contribution of $\sigma_{int}(\gamma,3n)$, which equals 0.03 MeV-b from threshold to 30 MeV.

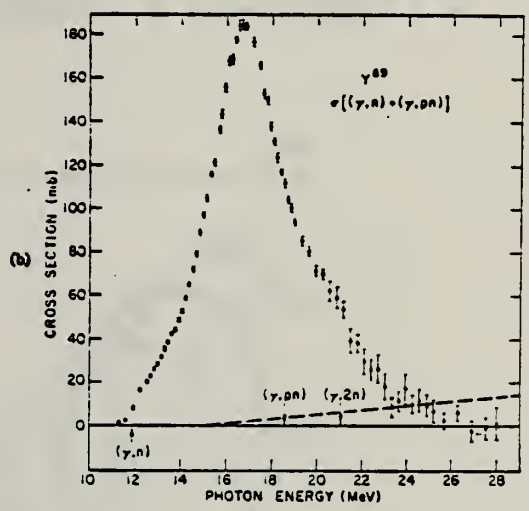

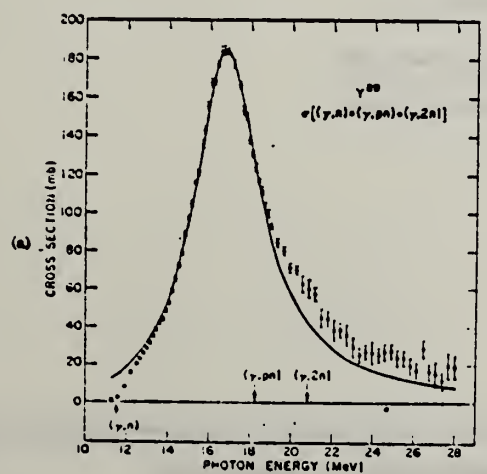

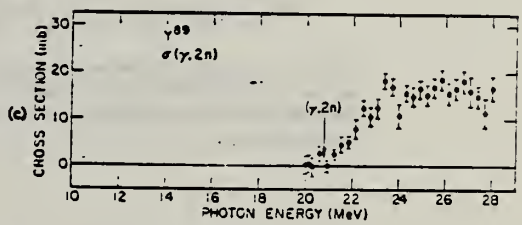

FIG. 8 (a) Total photoneutron cross section $\sigma[(\gamma,n)+(\gamma,np)+(\gamma,2n)]$ for Y^{89}. The solid curve is a Lorentz-line fit to the giant-resonance data (14 to 19 MeV). The thresholds (arrows), except when otherwise noted, are from Ref. 10. In this case, the $(\gamma,2n)$ threshold is taken from the data. (b) Single photoneutron cross section $\sigma[(\gamma,n)+(\gamma,pn)]$ for Y^{89}. The dashed line represents the maximum possible systematic error owing to the uncertainty in the normalization constant for the bremsstrahlung subtraction (see text). (c) The $(\gamma,2n)$ cross section for Y^{89}. The threshold determination of 20.8±0.1 MeV determines the mass of Y^{87} (see text). The threshold value is taken from the data. The cross-section scale has been doubled for clarity.

FORM NBS-418
(REV. 7-14-64)
USCOMM-OC 26010-P64

REF. N. G. Shevchenko, N. G. Afanas'ev, G. A. Savitskii, V. M. Khvastunov, V. D. Kovalev, A. S. Omelaenko, and I. S. Gul'karov
J. Nucl. Phys. (USSR) 5, 948 (1967)
Sov. J. Nucl. Phys. 5, 676 (1967)

ELEM. SYM.	A	Z
Y	89	39

METHOD

REF. NO. 67 Sh 1 HMG

REACTION	RESULT	EXCITATION ENERGY	SOURCE TYPE	SOURCE RANGE	DETECTOR TYPE	DETECTOR RANGE	ANGLE
E,E/	FMF	2-3	D	225	MAG-D		DST
		(2.2)					

G-WIDTH, J-PI

Table II

Absolute differential cross section for inelastic scattering of electrons with energy 225 ± 1 MeV by Y^{89} with excitation of levels at 2.5 ± 0.2 MeV

θ, deg	Cross section, cm²/sr	θ, deg	Cross section, cm²/sr	θ, deg	Cross section, cm²/sr
35	$(3.15\pm0.33)\cdot10^{-29}$	50	$(2.44\pm0.09)\cdot10^{-30}$	80	$(3.34\pm0.21)\cdot10^{-32}$
35	$(3.77\pm0.28)\cdot10^{-29}$	50	$(2.28\pm0.23)\cdot10^{-30}$	82	$(3.40\pm0.23)\cdot10^{-32}$
40	$(1.26\pm0.06)\cdot10^{-29}$	52	$(2.45\pm0.14)\cdot10^{-30}$	84	$(2.97\pm0.22)\cdot10^{-32}$
44	$(7.72\pm0.31)\cdot10^{-30}$	55	$(9.13\pm0.28)\cdot10^{-31}$	86	$(2.42\pm0.18)\cdot10^{-32}$
46	$(5.05\pm0.18)\cdot10^{-30}$	60	$(4.48\pm0.55)\cdot10^{-31}$	88	$(1.94\pm0.15)\cdot10^{-32}$
48	$(4.74\pm0.18)\cdot10^{-30}$	65	$(2.12\pm0.19)\cdot10^{-31}$	90	$(1.68\pm0.15)\cdot10^{-32}$
48	$(2.59\pm0.12)\cdot10^{-30}$	78	$(4.32\pm0.32)\cdot10^{-32}$	95	$(1.46\pm0.18)\cdot10^{-32}$

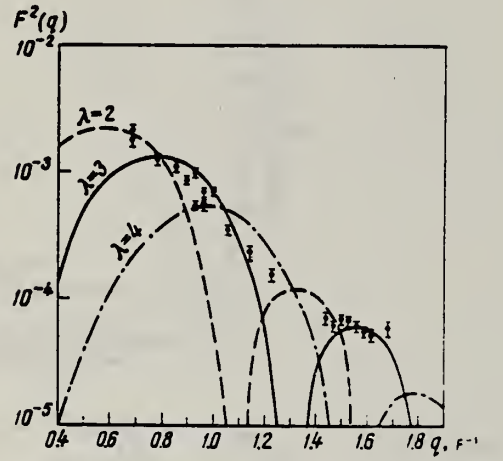

Fig. 4. Squared form factor as a function of momentum transfer for the 2.5 ± 0.2 MeV inelastic peak of Y^{89}. The curves are calculated in the Born approximation for different values of transition multipolarity λ.

REF. H. Taneichi and K. Shoda
J. Phys. Soc. Japan 22, 664 (1967)

ELEM. SYM.	A	Z
Y	89	39

METHOD

REF. NO. 67 Ta 2 egf

REACTION	RESULT	EXCITATION ENERGY	SOURCE		DETECTOR		ANGLE
			TYPE	RANGE	TYPE	RANGE	
G,XP	SPC	THR-24	C	17,24	EMU-D	2-16	4PI

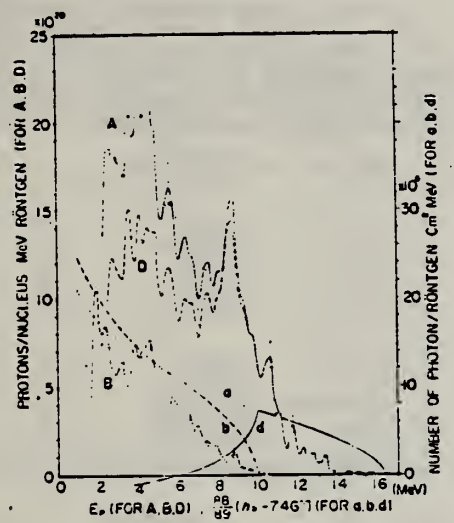

Fig. 1. Energy distributions of photoprotons. Plots and curves A and B—The observed results for 24.0 and 17.5 MeV of the bremsstrahlung maximum energy respectively. Curve a and b—The corresponding spectra of the bremsstrahlung. Curve D and d—The difference between A and B and between a and b.

†7.46 is the threshold energy of $Y^{89}(\gamma, p)$ in MeV.

REF. W. J. Alston III, H. H. Wilson and E. C. Booth
Nucl. Phys. A116, 281 (1968)

ELEM. SYM.	A	Z
Y	89	39

METHOD

REF. NO. 68 Al 1 egf

REACTION	RESULT	EXCITATION ENERGY	SOURCE TYPE	SOURCE RANGE	DETECTOR TYPE	DETECTOR RANGE	ANGLE
G,G	LFT	0-2	C	4	SCD-D	0-3	130
		(1.51)					

Angle greater than 90° for all measurements.

SELF-ABSORPTION

TABLE 1
Direct and absorption measurements of resonance fluorescence

Nucleus	E_r (MeV)	J_r	Γ_0/Γ	$gW\Gamma_0\Gamma_0/\Gamma$ (meV)	Error (%)	This work Γ_0 (meV)	Other work Γ_0
^{55}Mn	0.000	$\frac{5}{2}^-$					
	1.527	$(\frac{3}{2}^-)$	0.9	5.2	25	8–12	
				abs [a]	40	8.0	
	1.884	?	0.82 [b]	41	25	$50/gW$	
				abs [a]	10	$55/g$	
	2.197	?	(0.8) [c]	17	25	$21/gW$	
				abs	20	$17/g$	
	2.252	?	(0.9) [c]	17	25	$19/gW$	
				abs	20	$13/g$	
	2.365	?	?	3.5	36	$(2–6)\Gamma/\Gamma_0$	
	2.564	?	(1.0)	50	25	$50/gW$	
				abs [a]	20	$61/g$	
	2.751	?	?	6.7	42	$6.7(\Gamma/\Gamma_0)/gW$	
^{59}Co	0.000	$\frac{7}{2}^-$					
	1.187	$(\frac{7}{2}^-)$	(1.0)	6.8	25	7.5	0.33(E2) [d]
				abs	25 [a]	12	
		$(\frac{9}{2}^-)$	(1.0)	6.8	25	(5.4–6.5)	0.27(E2)
				abs	25 [a]	9.6	
^{63}Cu	0.000	$\frac{3}{2}^-$					
	1.414	$\frac{1}{2}^-$	?	1.6	30	$(1.1–1.7)\Gamma/\Gamma_0$	
	1.551	$\frac{3}{2}^-$	?	1.7	37	$(1.7–2.5)\Gamma/\Gamma_0$	0.1(E2) [e]
^{69}Ga	0.000	$\frac{3}{2}^-$					
	0.872	$(\frac{1}{2}^-)$	0.95	1.1	35	$0.8/W$	
	1.107	$(\frac{1}{2}^-)$	0.95	8.0	20	$8.4/W$	
^{75}As	0.000	$\frac{3}{2}^-$					
	0.86	?	?	1.7	20	$1.7\,\Gamma/gW\Gamma_0$	
	1.07	?	?	2.6	30	$2.6\,\Gamma/gW\Gamma_0$	
	1.35	?	?	3.6	20	$3.6\,\Gamma/gW\Gamma_0$	
^{89}Y	0.000	$\frac{1}{2}^-$					
	1.51	$\frac{3}{2}^-$	(1.0)	52 [a]	30	28	0.37(E2) [f]
				abs [a]	15	22	

[a] Measured with NaI.
[b] Ref. [24]).
[c] Measured with a Ge(Li) detector to ±10 %.
[d] Ref. [13]). [e] Ref. [14]). [f] Ref. [23]).

[13] D.G. Alkhazov, K.I. Erokhina and I.K. Lemberg, Izv.Akad.Nauk.SSSR(ser.fiz.) 28 (1964) 1667.
[14] B.G. Harvey, J.R. Meriwether and A.Bussière, Nucl. Phys. 70 (1965) 305.
[23] G.A. Peterson and J. Alster, Phys. Rev. 166 (1968) 136.
[24] N. Nath, M.A. Rothman, D.M. Van Patter and C.E. Mandeville, Nucl. Phys. 13 (1959) 74.

REF. G. A. Peterson and J. Alster
Phys. Rev. 166, 1136 (1968)

ELEM. SYM.	A	Z
Y	89	39

METHOD

REF. NO. 68 Pe 1 HMG

REACTION	RESULT	EXCITATION ENERGY	SOURCE		DETECTOR		ANGLE
			TYPE	RANGE	TYPE	RANGE	
E,E/	RLX	1-3	D	65,70	MAG-D	60-70	DST

SEP ISOTPS

TABLE I. Experimentally determined values of the reduced nuclear radiative transition probabilities $B(EL)$ for the excitation of a nucleus to a level at energy E^* above its ground state by a transition of electric character and multipolarity L, in units of e^2F^{2L}, where $1\ F=10^{-13}$ cm. The last column gives $B(EL)$ in single-particle Weisskopf units according to Eq. (4).

E^*	L	$B(E0\rightarrow L)$ (e^2F^{2L})	G (W.u.)
		Sr^{88}	
1.84	2	990±50	8.5
2.74	3	80 600±3000	25.0
4.0	2	190±40	1.6
6.5	(2)	130±30	1.1
	(3)	13 000±3000	4.0
		Y^{89}	
1.50	2	120±50	1.0
1.73	2	140±40	1.2
2.21	3	33 700±3000	10.2
2.52	3	37 800±3000	11.4
2.86	3	32 300±3000	9.8

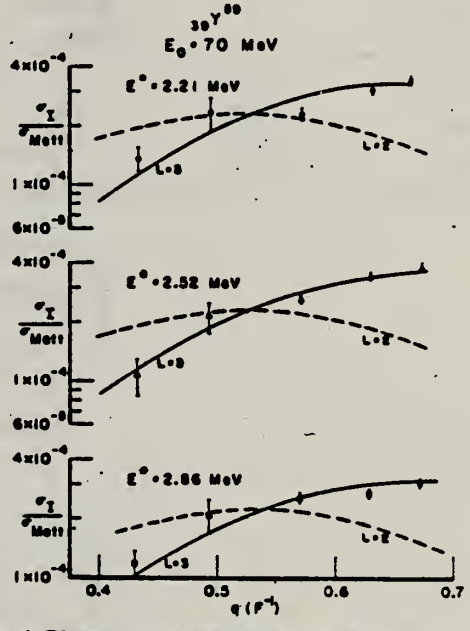

FIG. 6. Distorted-wave inelastic cross section in units of the Mott cross section versus momentum transferred to the Y^{89} nucleus for electric octupole (solid lines) excitations at 2.21, 2.52, and 2.86 MeV. An incompressible and irrotational hydrodynamical model was assumed. For comparison, curves are shown for electric quadrupole excitations.

REF.	ELEM. SYM.	A	Z
S. M. Shafroth and G. J. F. Legge Nucl. Phys. A107, 181 (1968)	Y	89	39

METHOD	REF. NO.
[Page 1 of 2]	68 Sh 1 EGF

REACTION	RESULT	EXCITATION ENERGY	SOURCE		DETECTOR		ANGLE
			TYPE	RANGE	TYPE	RANGE	
P,G	ABX	13-15	D	5-9	NAI-D	0-15	DST

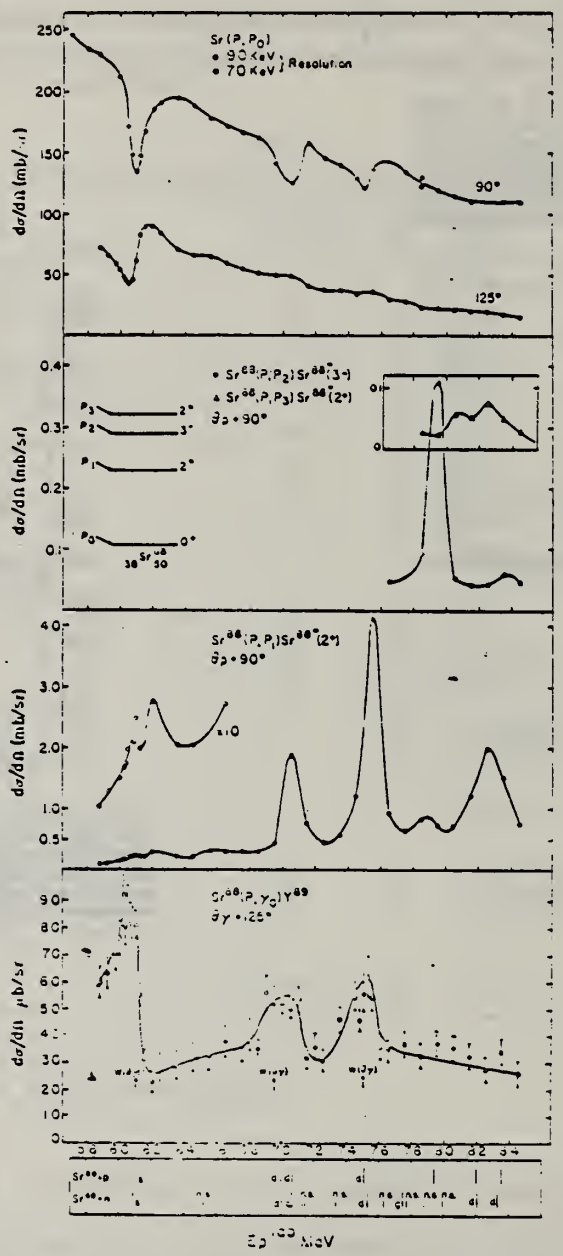

Fig. 3. Excitation curves for several exit channels taken simultaneously. Upper two curves elastic proton scattering from Sr at 90° and 125°. Inset at far right excitation curve for the reaction ^{88}Sr (p, p_3) at 90°. Curve labeled p_2 excitation curve for the ^{86}Sr(p, p_2) reaction at 90°. Note the striking resonance at 7.92 MeV. Curves labeled p_1 excitation curve for the ^{86}Sr(p, p_1) reaction at 90°. Bottom curve excitation curve for the ^{88}Sr(p, γ_0) reaction at 125°. Underlying box upper set of levels: resonance energies (lab) in ^{88}Sr—p reaction. The energy scale was set to agree with that of ref. [18]). Lower set of levels from ref. [2]) arbitrarily matched at 7.0 MeV and with energy intervals stretched by 89/88 to convert to "equivalent" lab energy. Levels shown with half the usual length are non-stripping levels.

REACTION	RESULT	EXCITATION ENERGY	SOURCE		DETECTOR		ANGLE
			TYPE	RANGE	TYPE	RANGE	

TABLE 1

Radiative widths of analogue resonances in ^{89}Y (present work)

Resonance energy E_p lab (MeV)	Single-particle component of resonance	J^π	$(2J+1)\Gamma_p\Gamma_{\gamma_0}/\Gamma$ (eV)
6.10	$s_{\frac{1}{2}}$	$\frac{1}{2}^+$	14±5
7.00 [a]	$(d_{\frac{3}{2}})$	$(\frac{3}{2}^+)$	(13±5) [d]
7.07 [a]	$d_{\frac{3}{2}}$	$\frac{3}{2}^+$ [b]	
7.51	$d_{\frac{3}{2}}$	$\frac{3}{2}^+$ [c]	17±6

[a] Ref. [2]).
[b] Ref. [7]).
[c] Present work.
[d] Unresolved (assuming a single $\frac{3}{2}^+$ level).

TABLE 1a

Partial widths of analogue resonances in ^{89}Y

Parent level in ^{89}Sr	E_p lab resonance	l_j	$(2T_0+1)/A_p^2=\theta_n^2$	Γ (keV)	Γ_p (keV)	Γ_{γ_0} (eV)	$\Gamma_{s.p.}$ [c] (keV)	$(2T_0+1)\Gamma_{\gamma_0}/\Gamma_{s.p.}$
1.031	6.10	$s_{\frac{1}{2}}$	0.96 [a]	70 [a]	46 [a]	11±4	1.66	0.08
1.931	7.00	$d_{(\frac{3}{2})}$	0.30 [a]	50 [a]	11 [a]			
2.000	7.07	$d_{\frac{3}{2}}$	0.60 [a]	50 [a]	23 [a]	7±3	3.32	0.03
2.455	7.51	$d_{\frac{3}{2}}$	0.3 [b]	60 [b]	13 [b]	14±5	3.86	0.05

[a] Ref. [2]). [b] Ref. [10]). [c] Calculated using shell-model wave functions. See text.

TABLE 2

Gamma-ray angular distribution results

lab E_p (MeV)	l_j	$W(\theta)$
6.10	$s_{\frac{1}{2}}$	$1-(0.1\ \pm 0.1\ )P_2(\cos^2\theta)$
7.51	$d_{\frac{3}{2}}$	$1-(0.53\pm 0.12)P_2(\cos^2\theta)$

REF.

R. Bergere, P. Carlos, A. Veyssiere, H. Beil
Contributions Montreal Conference 352 (1969)

ELEM. SYM.	A	Z
Y	89	39

METHOD

REF. NO.: 69 Be 4 egf

REACTION	RESULT	EXCITATION ENERGY	SOURCE TYPE	SOURCE RANGE	DETECTOR TYPE	DETECTOR RANGE	ANGLE
G,N 188	ABX	11-25	D	11-26	MOD-I		4PI
G,2N 189	ABX	21-27	D	19-28	MOD-I		4PI

RECHERCHE d'ETATS QUASI-LIES ANALOGUES 2p-2h dans la RESONANCE GEANTE de Y^{89}

R. BERGERE, P. CARLOS, A. VEYSSIERE, H. BEIL - CEN/Saclay - FRANCE - (91)

Nous avons étudié avec des γ monochromatiques les réactions $Y^{89}(\gamma,n)$ et $Y^{89}(\gamma,2n)$. Les résultats $\sigma_{\gamma,n}$ et à fortiori $\sigma_{\gamma,n}+\sigma_{\gamma,2n}$ montrent sans ambiguité le dédoublement de la résonance géante déjà signalé par B.L. Berman dans cette même région de masse (Phys. Rev. 169, 1967, 1098). On peut représenter entre 13 Mev et 22 Mev la section efficace photoneutronique totale $\sigma_{\gamma,n}$ par une somme de deux raies de Lorentz ayant respectivement les paramètres : $E_1 = 16,57$ Mev ; $\Gamma_1 = 4,25$ Mev ; $\sigma_1 = 215$ mbarns ; $E_2 = 20,87$ Mev ; $\Gamma_2 = 2,87$ Mev ; $\sigma_2 = 45$ mbarns. Les sections efficaces intégrées sous chacune de ces deux raies sont respectivement $\Sigma_1 = \frac{\pi}{2}\sigma_1\Gamma_1 = 1,435$ Mev barns et $\Sigma_2 = 0,203$ Mev barns et sont donc dans le rapport $\frac{\Sigma_2}{\Sigma_1} = 0,14$. Un essai de détermination de la section efficace nucléaire totale $\sigma_{\gamma,n}+\sigma_{\gamma,p}$ a été fait par une mesure de transmission de γ monochromatiques à travers Y^{89}. Les incertitudes sur les données actuelles de l'absorption électronique des γ (rapport UCRL 50 400 et NBS 583) permettent simplement de conclure que de 16 à 21 Mev on a $\sigma_{\gamma,p} \simeq 15 \pm 30$ mbarns.

Ce dédoublement est à rapprocher de la prédiction de S. Fallieros sur le dédoublement isobarique des états dipolaires (Phys. Lett. 19, 1965, 398) caractérisé par $\Delta E \simeq U\frac{T_>}{T} \simeq 5$ Mev pour Y^{89} (U = énergie de symétrie et $T = \frac{11}{2}$) en bon accord avec notre valeur expérimentale 4,3 Mev. Fallieros prévoit un rapport des intensités dipolaires des transitions $\frac{T_>}{T_<} = \frac{4}{T} = 0,48$. Cette valeur n'est pas incompatible avec nos mesures si on suppose que $\sigma_{\gamma,p} \simeq 0,25\,\sigma_{\gamma,n}(T_>)$. Goulard et al (Can. Journ. Phys. 45, 1967, 3221 et 46, 1968, 2771 - Phys. Rev. 176, 1968, 1345) tenant compte de tous les états 1p-1h concluent à un dédoublement ΔE trop faible et à un rapport d'intensité $\frac{T_>}{T_<} \simeq 0,11$ ce qui est insuffisant même en ne tenant compte que de la valeur $\sigma_{\gamma,n}(T_>)$. Il est probable que la considération du couplage d'états du continu aux états quasi-liés 2p-2h permettrait de mieux préciser les caractéristiques de ce dédoublement (V. Gillet et al - Nucl. Phys. A 97, 1967, 631). Notons enfin que notre valeur expérimentale $\sigma_{\gamma,n}(T_>)$ plus grande que $\sigma_{\gamma,p}$ pourrait provenir, comme indiqué par Gellie (Aust. J. Phys. 1968, 765) d'une désexcitation de $Y^{89*}(T_>)$ par émission d'un neutron vers les états $T_>$ de Y^{88} dès que cette voie est ouverte.

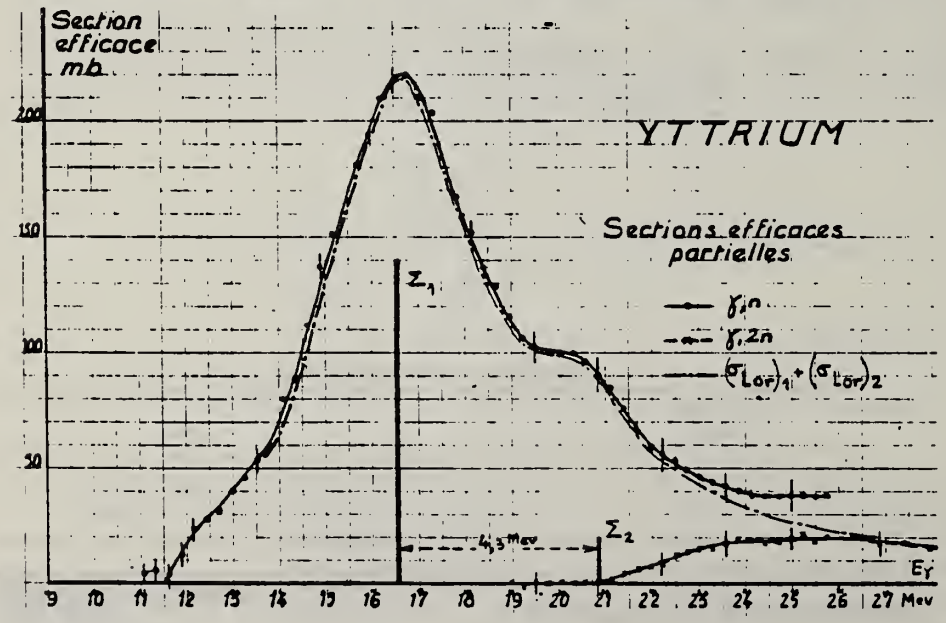

P. Richard, F. Gabbard, A. C. Porter and F. F. Hopkins
Phys. Letters 29B, 646 (1969)

ELEM. SYM.	A	Z
Y	89	39

METHOD

REF. NO. 69 Ri 1 egf

REACTION	RESULT	EXCITATION ENERGY	SOURCE		DETECTOR		ANGLE
			TYPE	RANGE	TYPE	RANGE	
P,G	ABX	12	D	5	SCD_D	9-12	90
				(4.97-5.15)			

5=4.97-5.15 MEV

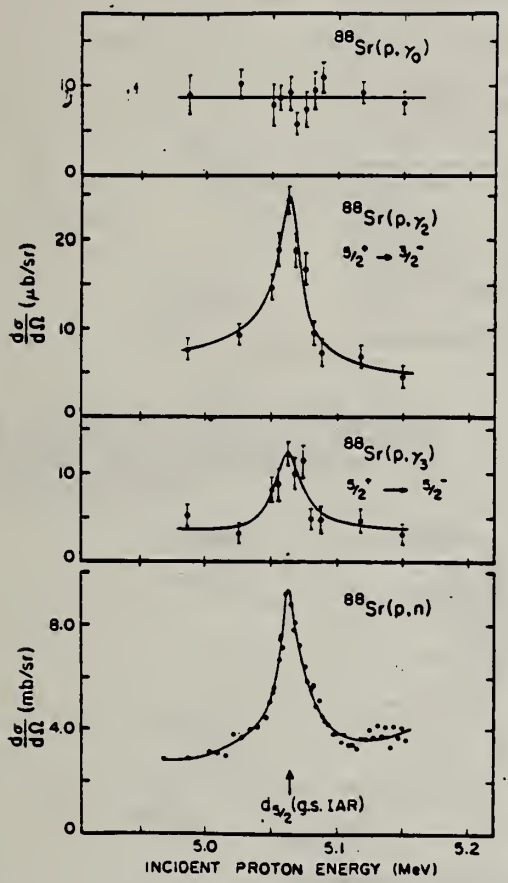

Fig. 2. The excitation functions for the indicated reactions in a proton energy range covering the $d_{\frac{5}{2}}$ ground-state isobaric analogue resonance.

Table 1
Results for the $^{88}Sr(p,\ )^{89}Y$ reaction.

		γ_0	γ_2	γ_3
$\frac{d\bar{\sigma}}{d\Omega}(90^o)(\mu b/sr)$	off resonance	8.7	6	4
	on resonance	8.7	25	12
Γ_γ^{exp} (eV)		-	7 ± 2	4 ± 3
Γ_γ^{sp} (eV)		-	1840	27
Γ_γ^{Tll} (eV)		-	49	0.8
σ_n/σ_γ		-	360	560

K. Shoda and H. Taneichi
J. Phys. Soc. Japan 26, 217 (1969)

ELEM. SYM.	A	Z
Y	89	39

METHOD

REF. NO. 69 Sh 4 hmg

REACTION	RESULT	EXCITATION ENERGY	SOURCE		DETECTOR		ANGLE
			TYPE	RANGE	TYPE	RANGE	
G,P	ABX	7-24	C	17-24	EMU-D	2-16	DST
				(17.5)			

Table II. Anisotropic factor B/A and asymmetry factor p of angular distributions determined by least-square fits with $A+B(1+p\cos\theta)\sin^2\theta$.

^{89}Y

E_γ(MeV)	($E_{\gamma max}$=17.5 MeV)		($E_{\gamma max}$=19.0 MeV)		($E_{\gamma max}$=24.0 MeV)	
	B/A	p	B/A	p	B/A	p
3.5– 5.1	0.3±0.2	0.6±0.7	1.1±0.4	0.3±0.3	0.5±0.2	−0.4±0.5
5.1– 7.2	1.1±0.4	0.0±0.3	2.2±0.4	0.1±0.1	0.9±0.3	0.2±0.2
7.2– 10.0	∞[a]	0.2±0.2	3.2±2.0	−0.2±0.2	1.6±0.6	0.0±0.2
10.0≧					4.5±3.0	−0.2±0.2

a) The notation ∞ indicates that the distribution is almost $(1+p\cos\theta)\sin^2\theta$. It is used when the result has stronger maximum than that of $1+10(1+p\cos\theta)\sin^2\theta$.

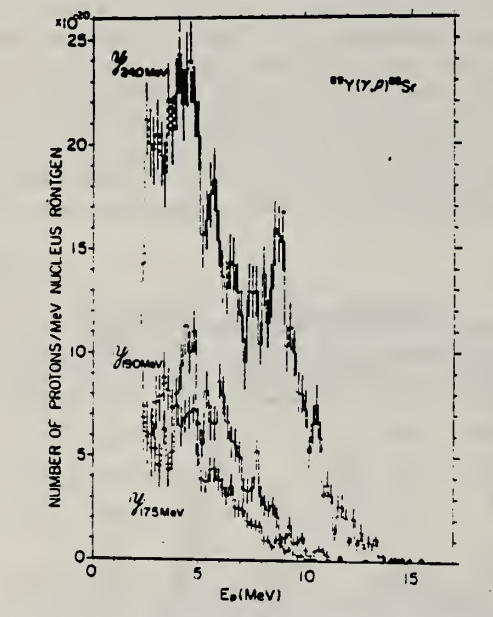

Fig. 1. Energy distributions of photoprotons from ^{89}Y irradiated with the bremsstrahlung at maximum energies of 24.0, 19.0 and 17.5 MeV.

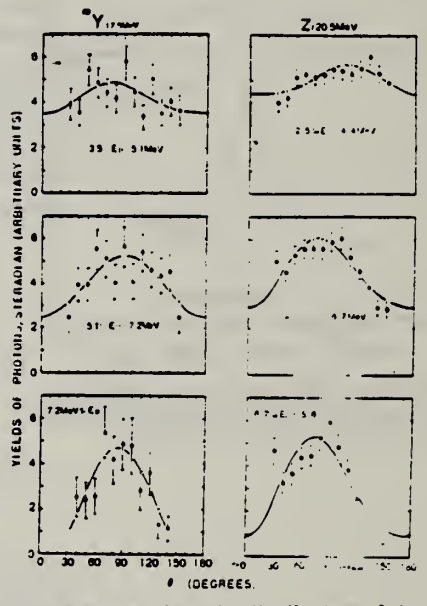

Fig. 3. Examples of angular distributions of photoprotons from ^{89}Y and Zr.

REACTION	RESULT	EXCITATION ENERGY	SOURCE TYPE	SOURCE RANGE	DETECTOR TYPE	DETECTOR RANGE	ANGLE

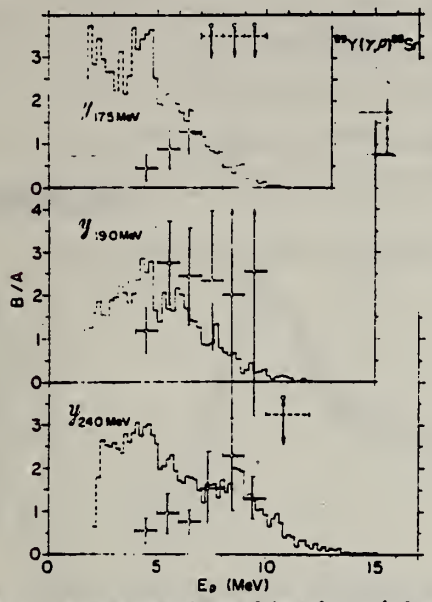

Fig. 4. Energy dependence of the anisotropic factor B/A of the angular distributions for photoprotons from ^{89}Y. A sign $\frac{3}{4}$ indicates that B/A is too large to plot the figure.

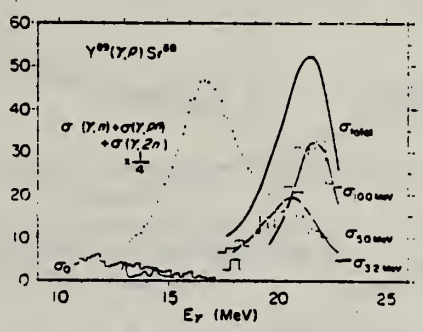

Fig. 10. Cross sections for strong photoproton transitions on ^{89}Y. The neutron emission cross section[89] and the result of the ^{88}Sr$(p,\gamma_0)^{89}$Y reaction[6] are also shown.

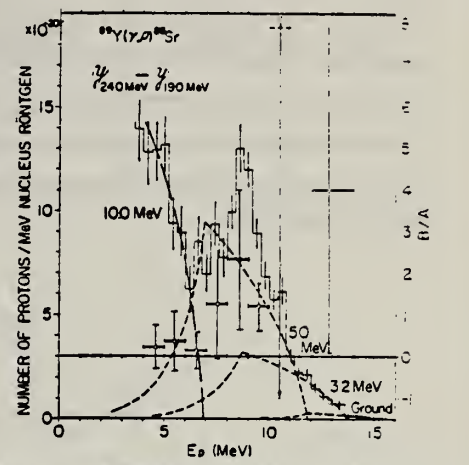

Fig. 6. The energy distribution and the anisotropic factor B/A for photoprotons from ^{89}Y obtained by subtraction of $Y_{19.9MeV}$ from $Y_{24.0MeV}$. The broken curves show transition groups to the selected residual states.

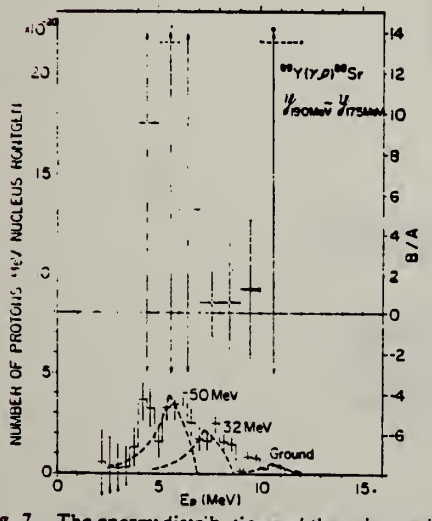

Fig. 7. The energy distribution and the anisotropic factor B/A for photoprotons from ^{89}Y obtained by subtraction of $Y_{17.5MeV}$ from $Y_{19.9MeV}$. See also the caption for Fig. 6.

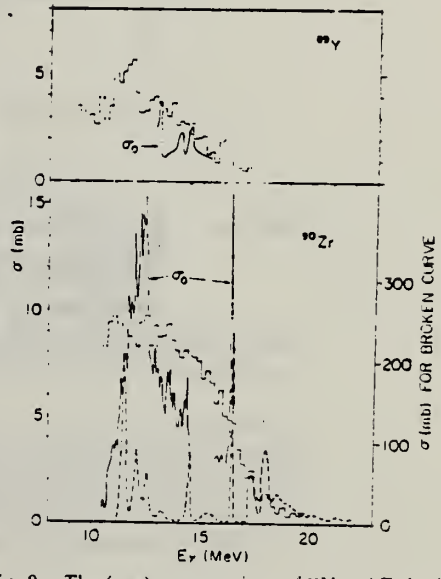

Fig. 9. The (γ, p) cross sections of ^{89}Y and Zr in the photon energy region lower than 20 MeV. The (γ, p_0) cross sections deduced from the inverse reaction cross sections are shown by solid lines indicated by σ_0. Theoretical ^{90}Zr$(\gamma, p_0)^{89}$Y cross section[19] is shown by broken line.

REF.

K. Shoda, M. Sugawara, T. Saito & H. Miyase
PICNS-69 Proceedings of the Conference on Nuclear Isospin. Asilomar-Pacific Grove, California 1969 (Academic Press, New York & London 1969) p.125.

ELEM. SYM.	A	Z
Y	89	39

METHOD

REF. NO. 69 Sh 6 egf

REACTION	RESULT	EXCITATION ENERGY	SOURCE		DETECTOR		ANGLE
			TYPE	RANGE	TYPE	RANGE	
E,P	SPC	10-26	D	20	MAG-D		UKN

UKN= UNKNOWN

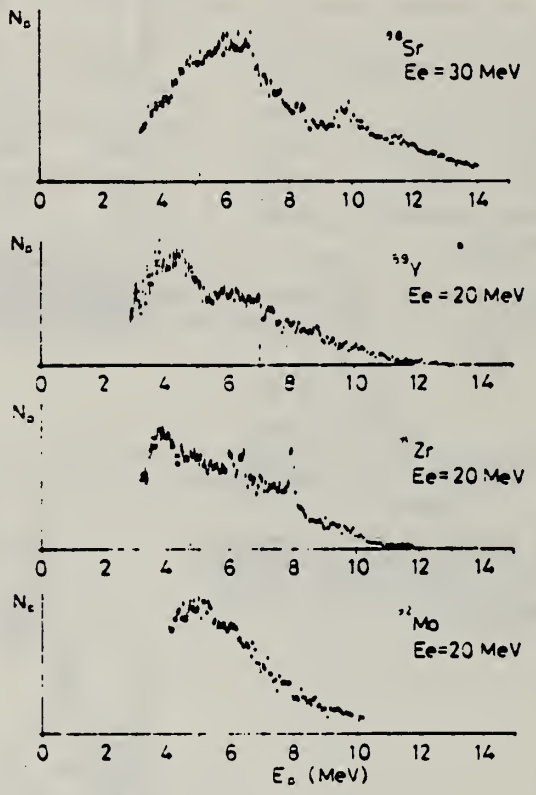

Fig. 1. Energy distributions of photoprotons. Vertical broken lines and solid lines indicate the position of p_o corresponding to the ground IAS and electric dipole IAS (2-4) respectively.

REF. H. Arenhovel, J. M. Maison
Nucl. Phys. A147, 305 (1970)

ELEM. SYM.	A	Z
Y	89	39

METHOD

REF. NO.: 70 Ar 1 egf

REACTION	RESULT	EXCITATION ENERGY	SOURCE		DETECTOR		ANGLE
			TYPE	RANGE	TYPE	RANGE	
G,G	ABX	12-30	C	32	NAI	12-30	DST

GETS G,G/ TO 2+

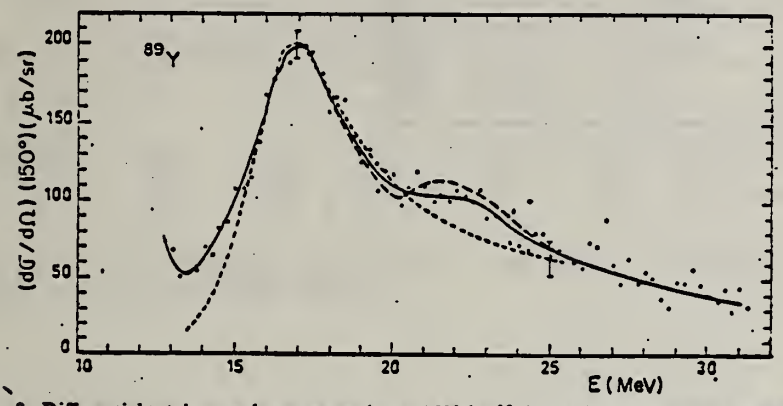

Fig. 9. Differential total scattering cross section at 150° for ^{89}Y. The dashed curves are the scattering cross section calculated with one Lorentz line at $E_1 = 16.4$ MeV and with two Lorentz lines at $E_1 = 16.4$ MeV and $E_1 = 21.5$ MeV.

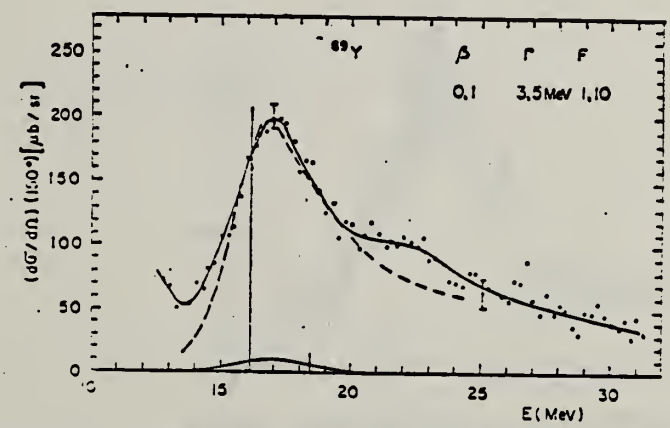

Fig. 10. Differential total scattering cross section at 150° for ^{89}Y and theoretical scattering cross section (dashed curve) given by the D.C.M. calculations. See caption for fig. 4. Here E_1 is given by table 3.

Fig. 4. Differential total scattering cross section at 150° for natural Ti. The full curve through experimental points is only a guide for the eyes. The vertical bars represent the relative strength of dipole levels calculated by the D.C.M. with parameters of table 1. Theoretical elastic plus inelastic scattering is computed from these levels with a common width Γ (dashed curve). Experimental inelastic scattering (histogram) and theoretical inelastic scattering to the first 2^+ (full curve) are shown in the lower part of the figure. Open circles give the cross section after background subtraction.

over

TABLE 4

Integrated inelastic scattering cross section

Nucleus	Limits of integration (in MeV)	Experimental [a]) $\int \sigma_i(E)dE$ (MeV · μb)	Theoretical [a]) 2^+	$2^{+\prime}$ (MeV · μb)	Total
Ti(^{48}Ti)	16 −24	250 ± 50	425	109	534
^{51}V(^{52}Cr)	16.4−24.9	492 ± 50	509	116	579
Cr	16.4−23.4	431 ± 60	509	116	579
^{75}As(^{76}Se)	14.1−23.6	1254 ± 120	1373	414	1787
Se(^{80}Se)	14.1−24.6	1035 ± 100	1066	353	1419
^{89}Y					364
Cd(^{112}Cd)	13.6−23.3	3264 ± 240	1894	370	2264
In(^{114}Cd)	13.6−23.6	2840 ± 220	2173	388	2561
Sn(^{110}Sn)	14.2−24.2	2363 ± 220			643

[a]) We assume an angular distribution of the form $1 + \frac{1}{13}\cos^2\theta$.

REF. B. S. Ishkhanov, I. M. Kapitonov, E. V. Lazutin, I. M. Piskarev, and O. P. Shevchenko
Izv. Akad. Nauk Fiz. 34, 2232 (1970)
Bull. Acad. Sci. USSR Phys. 34, 1991 (1970)

ELEM. SYM.	A	Z
Y	89	39

METHOD

REF. NO.: 70 Is 8 hmg

REACTION	RESULT	EXCITATION ENERGY	SOURCE TYPE	SOURCE RANGE	DETECTOR TYPE	DETECTOR RANGE	ANGLE
G,XN	ABX	11- 29	C	11- 29	BF3-I		4PI

Reaction	Position of peak MeV	Cross section at peak mb	Width of peak MeV	Integral cross section mb·MeV	Integration limit MeV	Reference
$\sigma(\gamma, Tn)$	16,0	270	3,7	1,57	29	The present work
$\sigma(\gamma, Tn)$	16,6	184	3,7	1,14	28	Ref.5
σ_n	16,0	270	3,7	1,36	29	The present work
σ_n	16,6	184	3,7	1,04	28	Ref.5

5. B.L.Berman, J.T.Caldwell, R.R.Harvey, M.A.Kelly, R.L.Bramblett & S.C.Fultz, Phys. Rev. 162, 1098 (1967).

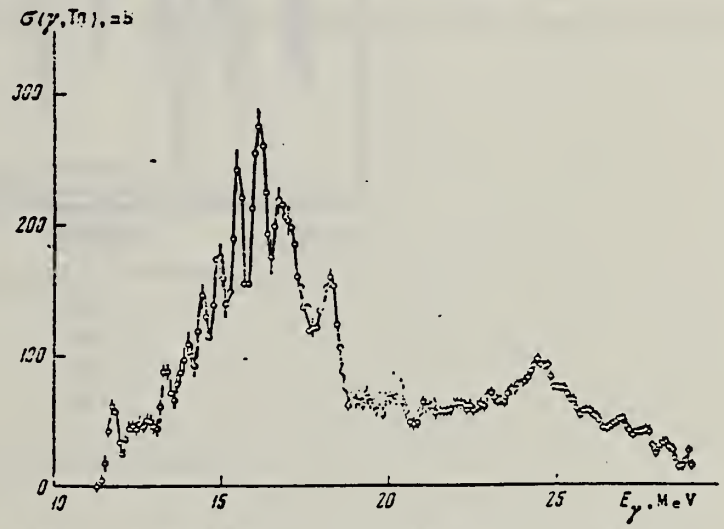

Fig.1. Cross section for the $^{89}Y(\gamma,Tn)$ reaction.

REF. W. B. Walters, J. R. Van Hise, W. L. Switzer, J. P. Hummel
Nucl. Phys. A157, 73 (1970)

ELEM. SYM.	A	Z
Y	89	39

METHOD

REF. NO. 70 Wa 3 egf

REACTION	RESULT	EXCITATION ENERGY	SOURCE		DETECTOR		ANGLE
			TYPE	RANGE	TYPE	RANGE	
G,2N	RLY	THR-305	C	150-305	ACT-I		4PI
G,PN	RLY	THR-305	C	150-305	ACT-I		4PI

TABLE 1
Summary of measured yield ratios

Target	Bremsstrahlung energy (MeV)	Measured yield ratio
natural Cr	150	$^{48}Cr/^{48}V = 0.043 \pm 0.002$
	250	0.047 ± 0.009
	305	0.042 ± 0.002
enriched ^{52}Cr	250	0.025 ± 0.005
natural Fe	250	$^{52}Fe/^{52}Mn = 0.037 \pm 0.003$
enriched ^{56}Fe	250	0.024 ± 0.005
		$^{52g}Mn/(^{52m}Mn + ^{52g}Mn) = 0.47 \pm 0.02$
natural Y	150	$^{87}Y/^{87m}Sr = 12.9 \pm 1.6$
natural Mo	150	$^{90}Mo/^{90}Nb = 0.41 \pm 0.05$
	280	0.49 ± 0.05

TABLE 2
Summary of experimental and theoretical ratios of $(\gamma, 2n)$ to (γ, pn) yields

Target isotope	Bremsstrahlung energy (MeV)	Experimental $(\gamma, 2n)/(\gamma, pn)$ yield ratio	Calculated $(\gamma, 2n)/(\gamma, pn)$ yield ratio
^{50}Cr	250	0.095 ± 0.025	0.14
^{54}Fe	250	0.10 ± 0.03	0.07
^{89}Y	150	7.4 ± 1.0	6.7
^{92}Mo	150	0.41 ± 0.05	0.15
	280	0.49 ± 0.05	0.16

REF. B.I. Goryachev, B.S. Ishkhanov, and V.G. Shevchenko
Proceedings of the Second Symposium on the Problems of Nuclear Physics, Novosibirsk, USSR, June 1970 (Kolybasov, V.M., Ed., Izdatel'stvo Nauka, Moscow 1971), pp. 362-78

ELEM. SYM.	A	Z
Y	89	39

METHOD

REF. NO. 71 Go 3 egf

REACTION	RESULT	EXCITATION ENERGY	SOURCE		DETECTOR		ANGLE
			TYPE	RANGE	TYPE	RANGE	
G,P	ABX	10- 29	C	10- 29	UKN		4PI

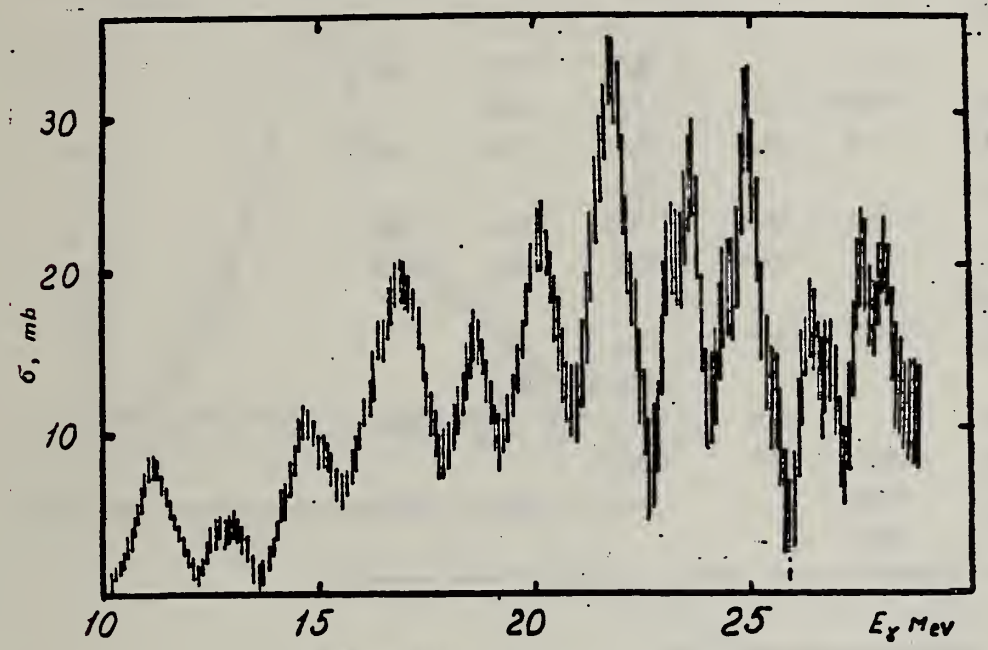

Фиг. 6. Сечение реакции $Y^{89}(\gamma,n)$.

(over)

Таблица 3

Cr^{52} E_m Мэв	Ni^{58} E_m Мэв	Ni^{60} E_m Мэв	Y^{89} E_m Мэв	Nb^{93} E_m Мэв	Ag^{107} E_m Мэв	Cd^{110} E_m Мэв
			11,2	12,0	11,3	
			12,7		12,7	
	13,9				13,9	14,2
			14,7	14,5	14,6	
	15,1					
16,0						
		16,4		16,2		16,5
	16,8	(17,0)	16,8	17,0	17,0	
18,7	18,4	18,6	18,6	18,4	18,4	18,7
	19,1			19,3		
20,4		20,4	20,1	(19,7)	20,3	20,8
	21,1		21,8	21,5	21,7	22,4
22,2	(22,1)					
22,9	23,4	23,3	23,7	23,3	23,7	
23,8					24,2	
24,8	25,2		25,0			25,0
26,2	26,5	25,8	26,4	26,5		
	28,2	(27,5)			27,0	27,0
	29,7	29,4				

A. Lepretre, H. Beil, R. Bergere, P. Carlos , &A. Veyssiere
Nucl. Phys. A175, 609 (1971)

Y	89	39

METHOD

REF. NO. 71 Le 1 egf

REACTION	RESULT	EXCITATION ENERGY	SOURCE		DETECTOR		ANGLE
			TYPE	RANGE	TYPE	RANGE	
G,N 381	ABX	11-27	D	11-27	MOD-I		4PI
G,2N 382+	ABX	21-27	D	11-27	MOD-I		4PI

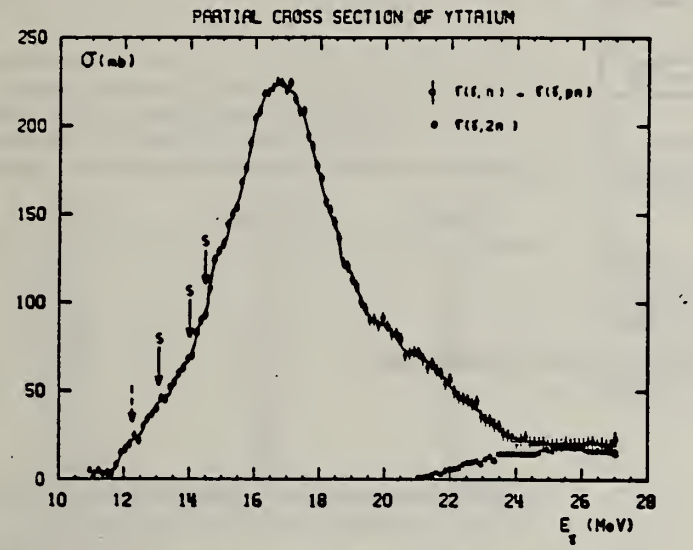

Fig. 3. Partial photoneutron cross sections $\sigma(\gamma, n)$ and $\sigma(\gamma, 2n)$ of ^{89}Y.

TABLE 1

Lorentz line parameters corresponding to fits shown in fig. 6.

	Rb	Sr	^{89}Y	^{90}Zr	^{93}Nb
σ_1 (mb)	192 ±10	207 ±10	225 ±10	211 ±10	202 ±10
Γ_1 (MeV)	4.1 ± 0.15	4.2± 0.1	4.1± 0.1	4.0 ± 0.1	4.7± 0.2
E_1 (MeV)	16.75± 0.05	16.7± 0.05	16.7± 0.05	16.65± 0.05	16.5± 0.05

TABLE 3

Integrated cross sections (the notation used is defined in the text)

	Rb	Sr	^{89}Y	^{90}Zr	^{93}Nb
σ_0 (MeV · b)	1.14 ±0.06	1.42±0.07	1.36±0.07	1.26±0.07	1.33±0.07
$\frac{\sigma_0}{0.06\,NZ\,A^{-1}}$	0.915±0.05	1.09±0.05	1.04±0.05	0.95±0.05	0.97±0.05
σ_{-1} (mb)	67±4	80 ±5	77 ±5	71 ±5	79 ±5
σ_{-2} (mb · MeV^{-1})	4±0.2	4.6 ±0.2	4.4 ±0.2	4 ±0.2	4.8 ±0.2
E_M (MeV)	24	27	27	26	24

(over)

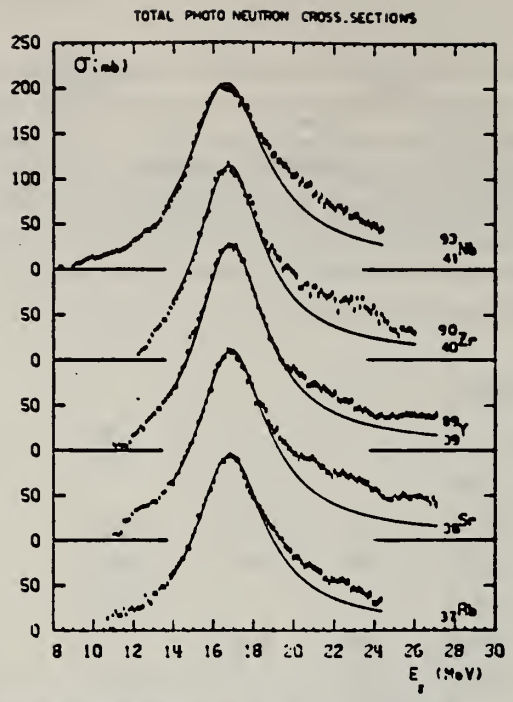

Fig. 6. Total photoneutron cross sections σ_T of Rb, Sr, ^{89}Y, ^{90}Zr and ^{93}Nb and best one Lorentz line fit corresponding to parameters given in table I.

REF.

E. J. Moniz, I. Sick, R. R. Whitney, J. R. Ficenec, R. G. Kephart and W. P. Trower
Phys. Rev. Letters 26, 445 (1971)

ELEM. SYM.	A	Z
Y	89	39

METHOD

REF. NO. 71 Mo 3 hmg

REACTION	RESULT	EXCITATION ENERGY	SOURCE		DETECTOR		ANGLE
			TYPE	RANGE	TYPE	RANGE	
E,E/	ABX	0-240	D	500	MAG-D		60

Table I. Nuclear Fermi momentum k_F and average nucleon interaction energy $\bar{\epsilon}$ determined by least-squares fit of theory to quasielastic peak.

Nucleus	k_F (MeV/c)[a]	$\bar{\epsilon}$ (MeV)[b]
$_3Li^6$	169	17
$_6C^{12}$	221	25
$_{12}Mg^{24}$	235	32
$_{20}Ca^{40}$	251	28
$_{28}Ni^{58.7}$	260	36
$_{39}Y^{89}$	254	39
$_{50}Sn^{118.7}$	260	42
$_{73}Ta^{181}$	265	42
$_{82}Pb^{208}$	265	44

[a]The fitting uncertainty in these numbers is approximately ±5 MeV/c.

[b]The fitting uncertainty in these numbers is approximately ±3 MeV. Simple estimates for $\bar{\epsilon}$ give numbers in reasonable agreement with those in the table.

REF.

Tatsuya Saito
Nippon Kagaku Zasshi 92, 164 (1971)

ELEM. SYM.	A	Z
Y	89	39

METHOD

REF. NO. 71 Sa 1 egf

REACTION	RESULT	EXCITATION ENERGY	SOURCE		DETECTOR		ANGLE
			TYPE	RANGE	TYPE	RANGE	
G,N	ABY	11-68	C	10-68	ACT-I		4PI

Nippon Kagaku Zasshi, 92, 164~168(1971)

The Yields of Radioactivities Induced by (γ, n) Reactions with Bremsstrahlung up to 68 MeV

by Tatsuya SAITO

The (γ, n) yields of 12 target nuclides have been measured at 10, 13, 16, 30, 45 and 68 MeV bremsstrahlung by observing the induced activities.

The energy dependence of the yields has been investigated extensively in the same way as in the previous work at 20 MeV bremsstrahlung.

In the case of heavy nuclides, the yields rise greatly as a function of maximum bombarding energy up to 20 MeV, and rise gradually from 20 MeV up to 68 MeV. However, in the case of light nuclides, the yields rise greatly up to 30 MeV, because the neutron separation energies of light ones are larger than those of heavy ones, and the bremsstrahlung spectrum covers the giant resonance and so the yields rise gradually from 30 MeV up to 68 MeV.

The yields have approximately been estimated from the parameter of the giant resonance, that is the peak cross section and the half width, in order to compare with the experimental data. As a result, the experimental data of light nuclides and heavy ones are nearly in agreement with the estimated data of Nathans et al., Johns et al. and Montalbetti et al., but those of medium weight ones are relatively lower values.

Department of Chemistry, Faculty of Science, Tohoku University; Katahira-cho, Sendai-shi, Japan

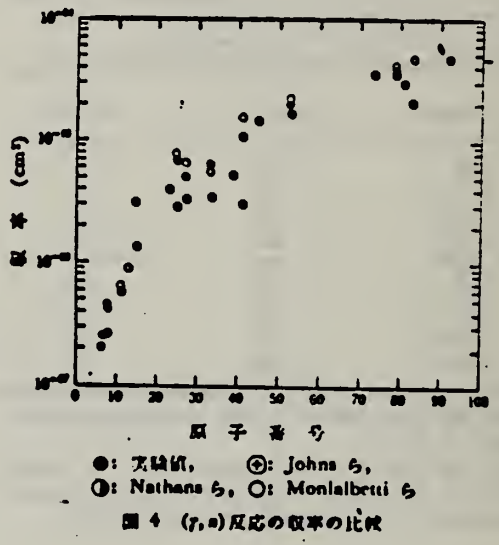

図 4 (γ, n)反応の収率の比較

REF. C.J. Umbarger, D.A. Close, W.L. Sievers, and R.C. Bearse
Phys. Rev. C3, 199 (1971)

ELEM. SYM.	A	Z
Y	89	39

METHOD

REF. NO. 71 Um 1 hmg

REACTION	RESULT	EXCITATION ENERGY	SOURCE		DETECTOR		ANGLE
			TYPE	RANGE	TYPE	RANGE	
P,G	ABX	10-11	D	2-3	NAI-D		0
				(2.3-3.0)			

The $^{88}Sr(p,\gamma)^{89}Y$ and $^{89}Y(p,\gamma)^{90}Zr$ reactions have been investigated in the energy range E_p = 2.3 to 3.0 MeV. Excitation functions for the transition to the ground state, with a total resolution of 2 keV, were determined for each reaction over this energy region. Using thick targets and both a single Ge(Li) detector and a Ge(Li) detector incorporated into a pair spectrometer, total summed spectra for the 700-keV region were obtained. The average total cross section of $^{88}Sr(p,\gamma_0)^{89}Y$ and $^{89}Y(p,\gamma_0)^{90}Zr$ was 12 ± 5 μb and 17 ± 7 μb, respectively. These total summed spectra, which represent the total γ-ray yield in this region, have been examined for a possible dependence of the intensity on the J^π of the final state. The data suggest such a J-dependence hypothesis, but detailed theoretical analysis of the $^{88}Sr(p,\gamma)^{89}Y$ reaction does not completely agree with experiment. A spectrum from a Ge(Li) detector in coincidence with a NaI(Tl) detector was accumulated for the $^{88}Sr(p,\gamma)^{89}Y$ reaction. The decay scheme of the states of ^{89}Y up to an excitation energy of 3.621 MeV was determined and the implications about spins and parities are consistent with accepted assignments.

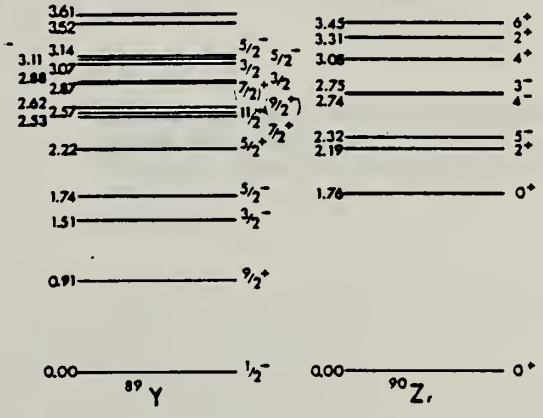

FIG. 1. Presently accepted level schemes for ^{89}Y and ^{90}Zr taken from the data of Van Patter (Ref. 8) and Ball (Ref. 9), respectively.

[8] D. M. Van Patter, Bull. Am. Phys. Soc. 15, 573 (1970).
[9] J. B. Ball, Bull. Am. Phys. Soc. 15, 574 (1970).

[over]

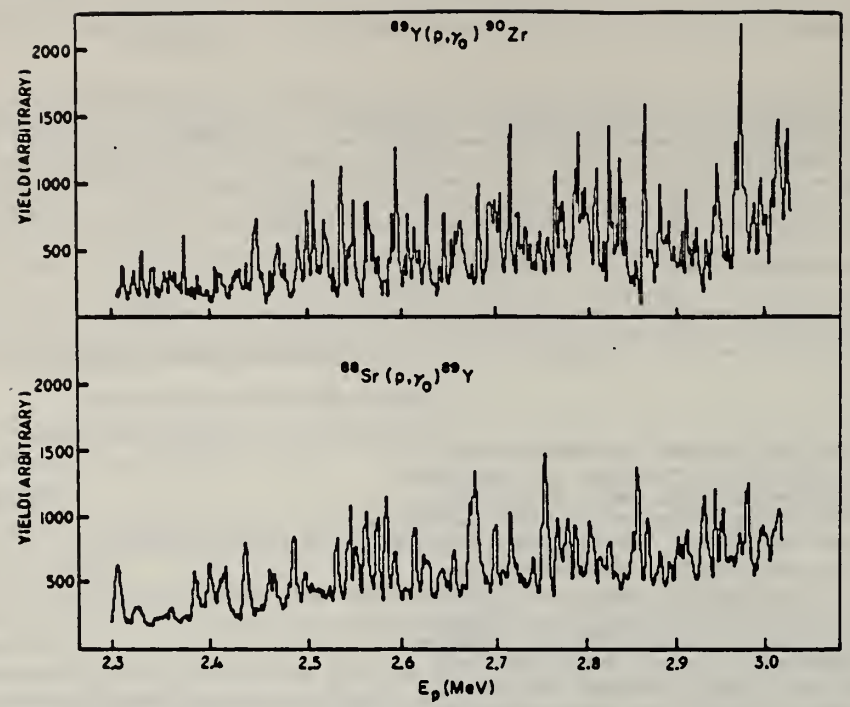

FIG. 2. Excitation functions for $^{88}Sr(p,\gamma_0)^{89}Y$ and $^{89}Y(p,\gamma_0)^{90}Zr$ over the energy region $E_p = 2.3$ to 3.0 MeV.

REF.		ELEM. SYM.	A	Z
	P. Paul PICNS-72, p. 343 Sendai	Y	89	39
METHOD		REF. NO.		
		72 Pa 4		hvm

REACTION	RESULT	EXCITATION ENERGY	SOURCE		DETECTOR		ANGLE
			TYPE	RANGE	TYPE	RANGE	
P,G	LFT	13- 15	D	5- 9	NAI-D		DST

Table III. E1 transition strengths from the $2d_{5/2}$, $3s_{1/2}$ and $2d_{3/2}$ IAR in $Y^{87,89}$ and Nb^{91}.

	Transition	E_p (MeV)	Γ_γ(ex) (eV)	S(d,p)	S(He^3,d)	Γ_γ(ex)/Γ_γ(th)
	$5/2^+ \to 5/2^-$	4.80	7 ± 2	0.46	0.19	28*
Y^{87}	$5/2^+ \to 3/2^-$	"	13 ± 3	"	0.14	1.5*
	$5/2^+ \to 5/2^-$	"	7 ± 2	"	0.19	28*
	$5/2^+ \to 3/2^-$	5.08	8 ± 2	0.8	0.11	0.6*
	$5/2^+ \to 5/2^-$	"	3.5 ± 1	"	0.09	17*
Y^{89}	$1/2^+ \to 1/2^-$	6.08	18 ± 3	"	0.9	0.18
	$3/2^+ \to 1/2^-$	7.51	11 ± 2	0.34	"	0.10
	$1/2^+ \to 1/2^-$	8.86	40 ± 8	0.11	"	0.65
Nb^{91}	$3/2^+ \to 1/2^-$	6.82	26 ± 6	0.63	0.36	0.52*

*Below effective neutron threshold

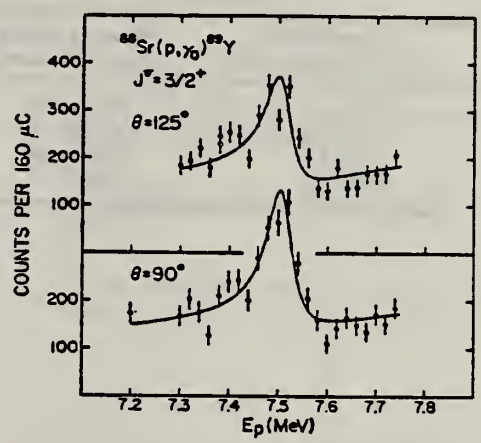

Fig.7. Observation of the transition to the ground state($2p_{1/2}$) of Y^{89} near a $2d_{3/2}$ IAR. The solid curves are theoretical fits (see text).

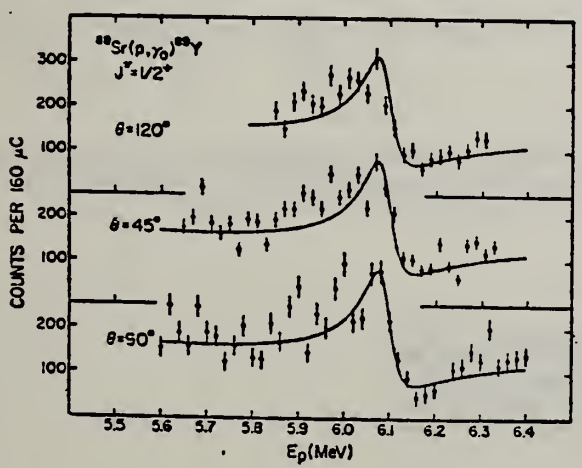

Fig. 6. Excitation functions of the ground-state transition in Y^{89} near the $3s_{1/2}$ IAR observed in radiative proton capture. The solid curves are theoretical fits described in the text.

REF. J. W. Watson, H. A. Medicus, and R. E. Turner
Phys. Rev. C6, 497 (1972)
See Erratum: Phys. Rev. C7, 1273 (1973)

ELEM. SYM.	A	Z
Y	89	39

METHOD

REF. NO. 72 Wa 3 egf

REACTION	RESULT	EXCITATION ENERGY	SOURCE		DETECTOR		ANGLE
			TYPE	RANGE	TYPE	RANGE	
G,2N	NOX	20- 50	D	23- 50	ACT-I		4PI

ISOMERS

TABLE I. Experimental isomer ratios: $Y^{89}(\gamma,2n)Y^{87m},Y^{87g}$.

Bremsstrahlung end-point energy (MeV)	Measured isomer ratio Metastable state/total
23.0±1.5	0.2 ±0.02
25.6±1.5	0.26±0.025
28.6±1.6	0.30±0.03
50.0±2.3	0.35±0.03

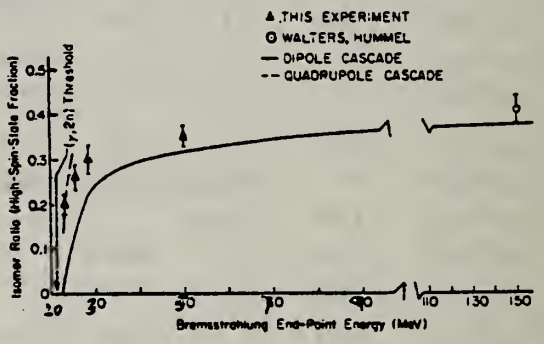

FIG. 4. Isomer ratio in Y^{87} from the reaction $Y^{89}(\gamma,2n)Y^{87}$ vs end-point energy of thin-target bremsstrahlung.

Isomer Ratios from Low Primary Excitation of Residual Nuclei. J. W. Watson, H. A. Medicus, and R. E. Turner [Phys. Rev. C 6, 497 (1972)]. In Figs. 3 and 4 the abcissas are incorrectly labeled. In Fig. 3 all energy values should be increased by 2 MeV, and in Fig. 4 they should be increased by 10 MeV in the range up to 90 MeV. Furthermore, on p. 505, right column, second line from top, Refs. 11 and 22 should read Refs. 12 and 23.

REF.

R.F. Barrett, J.R. Birkelund, B.J. Thomas, K.S. Lam, and H.H. Thies
Nucl. Phys. A210, 355 (1973)

ELEM. SYM.	A	Z
Y	89	39

METHOD

REF. NO. 73 Ba 20 egf

REACTION	RESULT	EXCITATION ENERGY	SOURCE		DETECTOR		ANGLE
			TYPE	RANGE	TYPE	RANGE	
G,N	NOX	THR- 27	C	10- 27	BF3-I		4PI

MEAN NEUT ENERGY

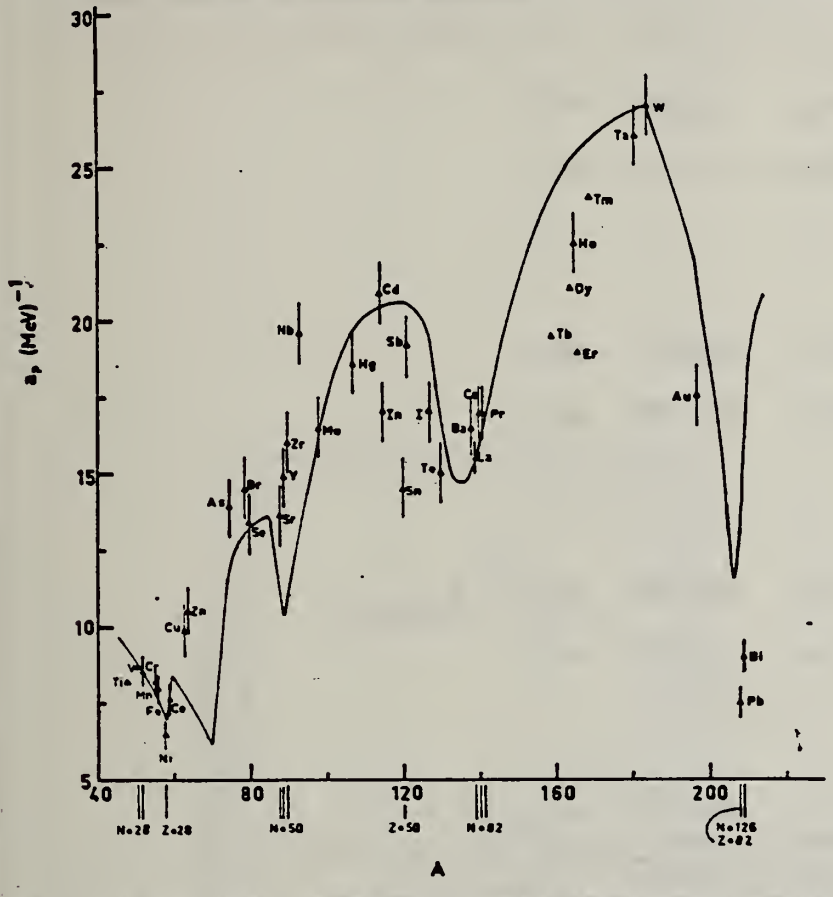

Fig. 12. Experimental values of the level density parameter a_p (Fermi gas formula plus pairing correction) versus atomic number A. The continuous curve is a least-squares fit to the data of a theoretical calculation from Newton [15]).

1
H. Baba and S. Baba, Japan Atomic Energy Research Institute report JAERI-1183 (1969).
2
H. Baba, Nucl. Phys. A159, 625 (1970).
15
T.D. Newton, Can. J. Phys. 34, 804 (1956).

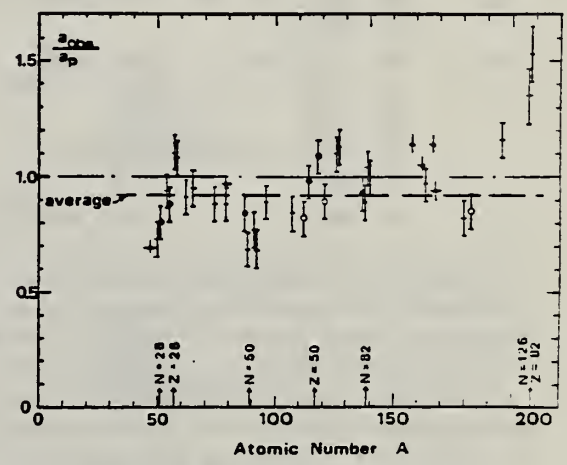

Fig. 15. Ratio a_{obs}/a_p versus atomic number A. Here a_{obs} is the level density parameter taken from the neutron resonance work of refs. [1,2]), and a_p is the level density parameter derived from the present (γ, n) work. Filled circles represent points where nuclei in the neutron resonance and in the (γ, n) experiment were the same. Open circles represent points where the respective nuclei were approximately matched. Triangles represent points which are based on measurement of neutron mean energies at two bremsstrahlung energies only.

(over)

TABLE 3 (continued)

Target	N (residual nucleus) [a]		Goodness of fit [b]		$\hat{E}_n(24)$ (MeV) [c]	T (MeV) [d]	a_p (MeV^{-1}) [e]	a_{obs} (MeV^{-1}) [f]	a_{obs}/a_p
			no p.c.	with p.c.					
Y	49	100%	G	G	1.30		14.9–^{88}Y	10.17–^{90}Y	0.68
Zr	49	52%	F	F	1.28		16.0–^{90}Zr	12.2 –^{91}Zr	0.77
	50	11%							
	51	17%							
	53	17%							
	55	3%							
Nb	51	100%	F	F	1.28		19.6–^{92}Nb	13.15–^{94}Nb	0.68
Mo	49	16%	G	G	1.27		16.5–^{95}Mo	14.7 –^{97}Mo	0.89
	51	9%							
	52	16%							
	53	17%							
	54	10%							
	55	24%							
	57	8%							
Ag	59	51%	V.P.	F	1.27	0.55	18.6–^{107}Ag	15.61–^{109}Ag	0.84
	61	49%							
Cd	57	1%	V.P.	F	1.24	0.54	20.9–^{111,4}Cd	17.0 –^{112}Cd	0.82
	61	12%							
	62	13%							
	63	24%							
	64	12%							
	65	29%							
	67	8%							
In	63	4%	V.P.	F	1.26	0.57	17.0–^{114}In	16.66–^{114}In	0.98
	65	96%							
Sn ($Z = 50$)	65	14%	V.P.	V.P.	1.38	0.73	14.5–^{118}Sn	15.9 –^{118}Sn	1.09
	66	8%							
	67	24%							
	68	9%							
	69	33%							
	71	5%							
	73	6%							
Sb	69	57%	V.P.	P	1.2	0.68	19.2–^{121}Sb	17.0 –^{121}Sb	0.89
	71	43%							
Te	69	2%	V.P.	F	1.36	0.83	15.0–^{127}Te	17.0 –^{127}Te	1.13
	71	5%							
	72	7%							
	73	19%							
	75	32%							
	77	34%							
I	73	100%	F	G	1.23	0.70	17.0–^{126}I	17.02–^{128}I	1.00

[a]) Neutron numbers and abundances of respective residual nuclei in (γ, n) experiments.

[b]) These give an assessment of the goodness of fit of a calculated $\hat{E}_n$ versus E_0 curve to the observed data, using the Fermi gas level density formula both without and with pairing corrections.

[c]) Bremsstrahlung photoneutron mean energies $\hat{E}_n$ for peak bremsstrahlung energy $E_0 = 24$ MeV.

[d]) Nuclear temperature from fit with constant-temperature formula.

[e]) Level density parameter a_p derived from the present (γ, n) experiment, using a Fermi gas formula plus pairing correction, and corresponding residual nucleus (the atomic weight shown is the weighted average of atomic weights of the respective isotopes present).

[f]) As column 7, but using data on n-resonance absorption from refs. [1,2]).

[g]) Measurements of $\hat{E}_n(E_0)$ for these nuclei were made only for E_0 21, 23 and 24 MeV.

REF. K. Lindgren, G. G. Jonsson and B. Forkman
PICNS-73, Vol.II, p.991 (1973) Asilomar

ELEM. SYM.	A	Z
Y	89	39

METHOD

REF. NO. 73 Li 3 egf

REACTION	RESULT	EXCITATION ENERGY	SOURCE		DETECTOR		ANGLE
			TYPE	RANGE	TYPE	RANGE	
G,G/	ABX	0-800	C	100-800	ACT-I		4PI

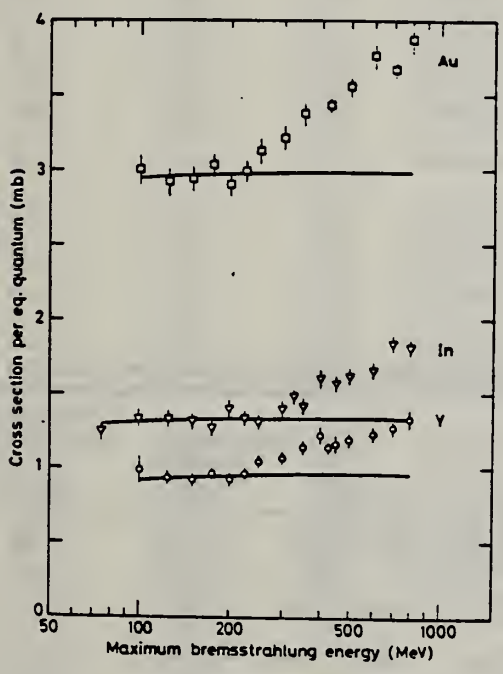

Fig. 1

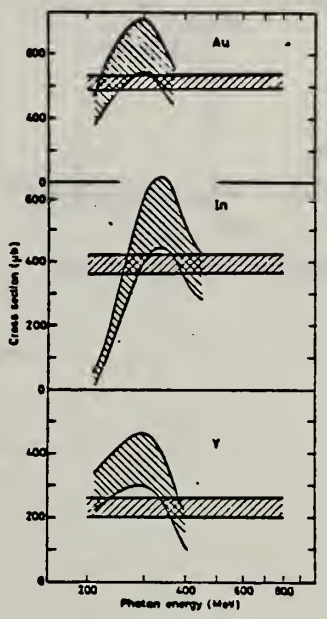

Fig. 2

REF.

S. P. Fivozinsky, S. Penner, J.W. Lightbody,Jr., and D. Blum
Phys. Rev. C9, 1533 (1974)

ELEM. SYM.	A	Z
Y	89	39

METHOD

REF. NO. 74F1 1 hmg

REACTION	RESULT	EXCITATION ENERGY	SOURCE TYPE	SOURCE RANGE	DETECTOR TYPE	DETECTOR RANGE	ANGLE
E,E/	FMF	1- 4	C	45-121	MAG-D		DST

6 LEVELS

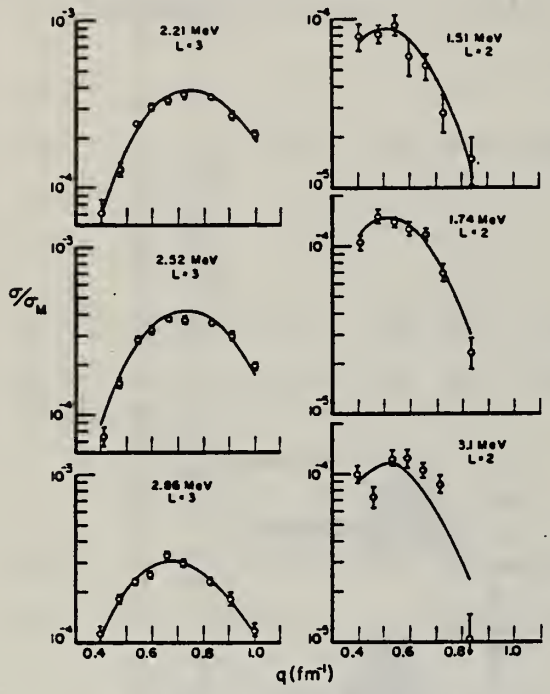

FIG. 6. Tassie-model fits to ^{89}Y form factors.

Elastic scattering data for ^{88}Sr and ^{89}Y.

TABLE V. Reduced transition probabilities [$B(EL)\uparrow$].

Nucleus	Level	$B(EL)\uparrow$ (Tassie model) (e^2 fm^{2L})	$B(EL)\uparrow$ (Tassie model) Weisskopf units	Prediction of mixed model $B(EL)\uparrow$ for ^{89}Y 3$^-$ transitions (e^2 fm^6)	Prediction of mixed model $B(EL)\uparrow$ for ^{89}Y 3$^-$ transitions Weisskopf units
^{88}Sr	2^+, 1.84 MeV	822.4± 23.8	7.0±0.2		
	3^-, 2.74 MeV	62 034 ±4015	19.3±1.2		
^{89}Y	$\frac{1}{2}^-$, $L=2$ 1.51 MeV	130.7± 17.57	1.1±0.1		
	$\frac{5}{2}^-$, $L=2$ 1.74 MeV	196.8± 13.89	1.7±0.1		
	$\frac{5}{2}^+$, $L=3$ 2.21 MeV	25 777 ±2251	7.8±0.7	24 836	7.5
	$\frac{1}{2}^+$, $L=3$ 2.52 MeV	36 603 ±2818	11.1±0.9	25 764	7.8
	$(\frac{5}{2}^+, \frac{1}{2}^+)$, $L=3$ 2.86 MeV	50 536 ±5000	15.3±1.5	30 160	9.2
	$(\frac{1}{2}^-, \frac{5}{2}^-)$, $L=2$ 3.1 MeV	144.6± 11.66	1.2±0.1		

[over]

TABLE IV. Electron scattering form factors for ^{89}Y.

Level	Incident energy (MeV)	Lab scattering angle (deg)	q (fm^{-1})	$\|F\|^2$	Standard deviation (%)
Ground state $\frac{1}{2}^-$	120.85	110.5	1.005	0.6027×10^{-2}	0.9
	100.87	128.2	0.919	0.8147×10^{-2}	1.0
	101.17	110.5	0.842	0.6544×10^{-2}	0.8
	80.86	128.2	0.737	0.9522×10^{-2}	1.1
	80.95	110.5	0.674	0.1802×10^{-1}	0.4
	67.07	128.2	0.611	0.3496×10^{-1}	0.5
	60.48	128.3	0.551	0.8321×10^{-1}	0.5
	53.46	128.3	0.487	0.1641	0.4
	45.42	128.3	0.414	0.3258	0.3
1.51 MeV	120.85	110.5	...	...	...
$L=2$	100.87	128.2	...	...	...
$\frac{3}{2}^-$	101.17	110.5	0.836	0.1463×10^{-4}	37.5
	80.86	128.2	0.730	0.2769×10^{-4}	39.0
	80.95	110.5	0.667	0.5404×10^{-4}	18.6
	67.07	128.2	0.604	0.6197×10^{-4}	24.1
	60.48	128.3	0.544	0.9577×10^{-4}	13.5
	53.46	128.3	0.480	0.8497×10^{-4}	12.4
	45.42	128.3	0.407	0.8282×10^{-4}	17.4
1.74 MeV	120.85	110.5	...	...	...
$L=2$	100.87	128.2	...	...	...
$\frac{5}{2}^-$	101.17	110.5	0.835	0.2266×10^{-4}	20.8
	80.86	128.2	0.729	0.6865×10^{-4}	18.3
	80.95	110.5	0.666	0.1193×10^{-3}	8.5
	67.07	128.2	0.603	0.1301×10^{-3}	10.5
	60.48	128.3	0.543	0.1427×10^{-3}	7.2
	53.46	128.3	0.479	0.1548×10^{-3}	8.0
	45.42	128.3	0.406	0.1105×10^{-3}	11.6
2.21 MeV	120.85	110.5	0.996	0.1969×10^{-3}	4.5
$L=3$	100.87	128.2	0.909	0.2645×10^{-3}	7.8
$\frac{5}{2}^+$	101.17	110.5	0.833	0.3397×10^{-3}	2.9
	80.86	128.2	0.727	0.3584×10^{-3}	5.1
	80.95	110.5	0.664	0.3334×10^{-3}	3.4
	67.07	128.2	0.601	0.3048×10^{-3}	5.7
	60.48	128.3	0.541	0.2478×10^{-3}	5.0
	53.46	128.3	0.477	0.1328×10^{-3}	6.5
	45.42	128.3	0.404	0.7320×10^{-4}	15.5
2.52 MeV	120.85	110.5	0.995	0.1883×10^{-3}	4.8
$L=3$	100.87	128.2	0.907	0.2926×10^{-3}	7.3
$\frac{7}{2}^+$	101.17	110.5	0.831	0.3498×10^{-3}	2.8
	80.86	128.2	0.725	0.3711×10^{-3}	4.5
	80.95	110.5	0.663	0.3793×10^{-3}	3.0
	67.07	128.2	0.600	0.3286×10^{-3}	5.1
	60.48	128.3	0.540	0.2918×10^{-3}	2.9
	53.46	128.3	0.476	0.1593×10^{-3}	7.2
	45.42	129.3	0.402	0.7639×10^{-4}	12.9
2.86 MeV	120.85	110.5	0.994	0.1158×10^{-3}	7.7
$L=3$	100.87	129.2	0.906	0.1772×10^{-3}	9.6
$(\frac{5}{2}^+, \frac{7}{2}^+)$	101.17	110.5	0.830	0.2310×10^{-3}	4.1
	80.86	128.2	0.724	0.2997×10^{-3}	5.4
	80.95	110.5	0.662	0.3339×10^{-3}	3.6
	67.07	128.2	0.598	0.2550×10^{-3}	5.0
	60.48	128.3	0.538	0.2357×10^{-3}	4.5
	53.46	128.3	0.474	0.1861×10^{-3}	5.2
	45.42	128.3	0.401	0.1158×10^{-3}	8.9
3.1 MeV	120.85	110.5	...	...	...
$L=2$	100.87	128.2	...	...	...
$(\frac{3}{2}^-, \frac{5}{2}^-)$	101.17	110.5	0.829	0.1007×10^{-4}	38.1
	80.86	128.2	0.722	0.8593×10^{-4}	12.8
	80.95	110.5	0.661	0.1056×10^{-3}	9.0
	67.07	128.2	0.597	0.1260×10^{-3}	11.2
	60.48	128.3	0.537	0.1256×10^{-3}	8.9
	53.46	128.3	0.473	0.6261×10^{-4}	15.2
	45.42	128.3	0.400	0.1038×10^{-3}	11.1

REF.

K. Shoda, M. Sugawara, T. Saito, and H. Miyase
Nucl. Phys. A221, 125 (1974)

ELEM. SYM.	A	Z
Y	89	39

METHOD

REF. NO.	
74 Sh 6	egf

REACTION	RESULT	EXCITATION ENERGY	SOURCE		DETECTOR		ANGLE
			TYPE	RANGE	TYPE	RANGE	
E,P	ABX	10- 24	D	10- 30	MAG-D		90

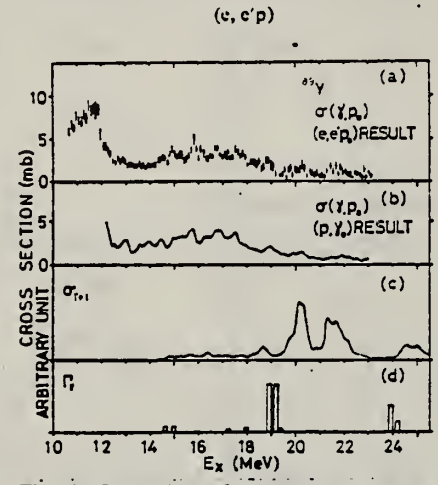

Fig. 12. Comparison of photoproton cross sections of ^{89}Y. (a) Present result. (b) Ref. [7]). (c), (d) Theoretical estimates, refs. [13,16]) respectively.

TABLE 5

The radiative width of the narrow E1 IAR obtained from the proton group in the proton spectra

Nucleus	E_x (MeV)	E_p (MeV)	$E_{R_i}(J^\pi)$ (MeV)	$\Gamma_\gamma \frac{\Gamma_{p_i}}{\Gamma}$ [a] (eV)	Γ_γ [a] (eV)	$2(T+1)\frac{\Gamma_\gamma}{\Gamma_w}$ [a]	$2(T+1)\frac{\Gamma_\gamma}{\Gamma_{s.p.}}$ [a]	(p,γ_0) data Γ_γ (eV)
^{90}Zr	14.5	6.0	0 ($\frac{1}{2}^-$)	26	26 [b]	0.076		> 30 [g]
	16.3	7.9	0 ($\frac{1}{2}^-$)	74	126 [c]	0.26		> 60 [g]
	16.3	6.3	1.51 ($\frac{3}{2}^-$)	52				
^{89}Y	13.0 [d]	5.9	0 (0^+)	13	13 [b]		0.13 [f]	18±3 [h]
	14.5 [e]	7.3	0 (0^+)	16	16 [b]		0.14 [f]	11±2 [h]
	15.9 [d]	8.7	0 (0^+)	42	42 [b]		0.68 [f]	40±8 [h]
^{88}Sr	17.1	6.5	0 ($\frac{1}{2}^-$)	9.5	14 [c]	0.029	-	
	17.1	5.6	0.85 (($\frac{1}{2}^-$))	4.9				
	17.3	6.7	0 ($\frac{3}{2}^-$)	30	48 [c]	0.094		
	17.3	5.9	0.85 (($\frac{1}{2}^-$))	18				

The available data with the (p,γ_0) experiment are shown in the last column.

[a]) The errors may be ≈ 30% (for ^{90}Zr, ^{88}Sr) and ≈ 50% (for ^{89}Y) including the uncertainty of the process to separate the proton group.

[b]) $\Gamma_{p_0}/\Gamma = 1$ was assumed.

[c]) $(\Gamma_{p_0}+\Gamma_{p_2})/\Gamma = 1$ was assumed.

[d]) $J^\pi = \frac{1}{2}^+$ was assigned as shown in table 3.

[e]) $J^\pi = \frac{3}{2}^+$ was assigned as shown in table 3.

[f]) Correction was made for the spectroscopic factors on the ground state and the excited state with the data of the (He^3, d) and (d, p) reactions respectively.

[g]) Ref. [27]).

[h]) Ref. [6]).

(over)

[6]P. Paul, Proc. nuclear structure studies using electron scattering and photoreaction, ed. K. Shoda and H. Ui (Research report of Lab. Nucl. Sci. Tohoku Univ. 5, 1972) p.343.

[7]P. Paul, Proc. Int. Conf. on photonuclear reactions and applications, ed. B.L. Berman (Lawrence Livermore Laboratory Univ. of California, 1973)p.407.

[13]T.A. Hughes et al., Phys. Rev. C3 (1971) 1950.

[16]J.D. Vergados et al., Nucl. Phys. A168 (1971) 225.

[27]J.L. Black et al., Nucl. Phys. A92 (1967) 365.

REF. R.R. Whitney, I. Sick, J.R. Ficenec, R.D. Kephart, and W.P. Trower
Phys. Rev. C9, 2230 (1974)

ELEM. SYM.	A	Z
Y	89	39

METHOD

REF. NO. 74 Wh 3 hmg

REACTION	RESULT	EXCITATION ENERGY	SOURCE		DETECTOR		ANGLE
			TYPE	RANGE	TYPE	RANGE	
E,E/	ABX	0-300	D	500	MAG-D		60

QUASIELASTIC SCAT

See further analysis of this data in reference 79Zi1

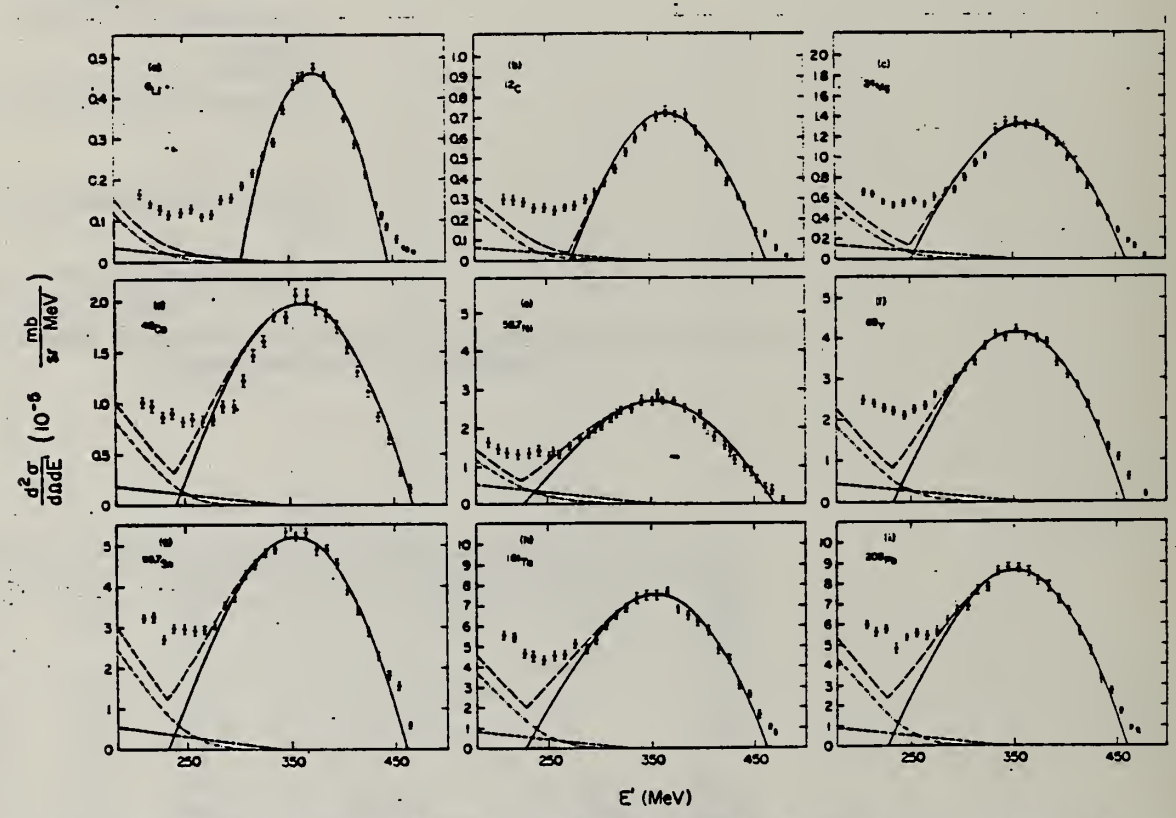

FIG. 1. The measured quasielastic peaks; the errors on the data points do not include an over-all 3% normalization uncertainty. The solid curve is a fit by the Fermi-gas model which yielded k_F (in MeV/c) and $\bar{\epsilon}$ (in MeV) as follows: (a) ^{6}Li (169, 17); (b) ^{12}C (221, 25); (c) ^{24}Mg (235, 32); (d) ^{40}Ca (249, 33); (e) $^{58.7}$Ni (260, 36); (f) ^{89}Y (254, 39); (g) $^{118.7}$Sm (260, 42); (h) ^{181}Ta (265, 42); (i) ^{208}Pb (265, 44). The fitting uncertainty in k_F is ±5 MeV/c and in $\bar{\epsilon}$ it is ±3 MeV. The small-amplitude dashed curve is the s-wave π-production contribution, the dot-dashed curve is the isobar excitation, and the large-amplitude dashed curve is the total result.

(over)

TABLE 1. Proton-normalized and radiative-corrected cross sections $d^2\sigma/d\Omega dE' = (N \pm \Delta N) \times 10^{-3}$ in mb/sr MeV, for $E = 500$ MeV and $\theta = 60°$.

E'	^{6}Li			^{12}C			^{24}Mg			^{40}Ca			^{58,7}Ni			^{89}Y			^{118,7}Sn			^{180,95}Ta			^{208}Pb		
(MeV)	N	ΔN	n	N	ΔN	n	N	ΔN	n	N	ΔN	n	N	ΔN	n	N	ΔN	n	N	ΔN	n	N	ΔN	n	N	ΔN	n
480.0	···			1.79	0.19	7	3.83	0.42	7	···			1.22	0.17	6	1.71	0.19	6	···			···			···		
474.0	···			1.02	0.13	7	···			···			···			···			···			···			···		
470.0	1.72	0.18	7	5.75	0.52	7	1.55	0.15	6	···			3.90	0.29	6	5.85	0.41	6	···			7.09	0.67	6	7.00	0.68	5
464.0	2.49	0.29	7	1.38	0.11	6	1.91	0.17	6	2.72	0.15	6	4.48	0.33	5	5.68	0.37	6	8.32	0.71	5	1.15	0.08	5	9.82	0.79	6
460.0	2.96	0.30	7	1.20	0.09	6	2.58	0.19	6	···			···			···			···			1.54	0.10	5	1.81	0.10	5
454.1	5.02	0.47	7	9.21	0.71	7	2.96	0.20	6	4.20	0.17	6	7.00	0.41	6	1.07	0.05	5	1.85	0.09	5	1.70	0.11	5	2.31	0.11	5
450.0	···			···			···			···			8.92	0.47	6	1.03	0.05	5	1.83	0.09	5	···			···		
444.3	8.68	0.58	7	1.26	0.07	6	4.11	0.25	6	6.67	0.27	6	1.02	0.05	5	1.33	0.05	5	···			2.77	0.14	5	2.74	0.13	5
440.0	1.11	0.06	6	2.59	0.13	6	5.23	0.26	6	···			···			···			···			3.43	0.16	5	3.24	0.13	5
434.2	1.32	0.08	6	2.99	0.14	6	5.50	0.28	6	8.74	0.35	5	1.19	0.05	5	1.90	0.07	5	2.27	0.09	5	3.14	0.15	5	3.34	0.14	5
430.0	···			···			···			···			1.40	0.07	5	2.11	0.08	5	2.77	0.11	5	···			···		
424.3	2.12	0.08	6	3.75	0.15	6	7.31	0.29	6	1.12	0.04	5	1.54	0.08	5	2.31	0.09	5	2.88	0.12	5	4.43	0.18	5	4.74	0.19	5
414.4	2.88	0.12	8	4.75	0.19	6	8.78	0.35	6	1.32	0.05	5	1.78	0.10	5	2.88	0.11	5	3.40	0.14	5	4.98	0.20	5	5.64	0.23	5
404.5	3.51	0.14	6	5.46	0.22	6	1.02	0.04	5	1.56	0.06	5	2.09	0.08	5	3.09	0.12	5	3.90	0.16	5	5.89	0.24	5	5.57	0.26	5
400.0	···			6.25	0.25	6	1.09	0.04	5	···			2.35	0.09	5	3.34	0.13	5	4.29	0.17	5	5.58	0.27	5	7.00	0.28	5
394.7	4.16	0.17	6	6.32	0.26	6	1.15	0.05	5	1.75	0.07	5	2.22	0.09	5	3.41	0.14	5	4.56	0.18	5	6.29	0.25	5	7.25	0.29	5
385.7	4.55	0.18	6	7.09	0.28	6	1.21	0.05	5	1.86	0.07	5	2.51	0.10	5	3.91	0.16	5	4.88	0.19	5	6.36	0.26	5	7.88	0.32	5
374.9	4.76	0.19	6	6.97	0.28	8	1.33	0.05	5	1.94	0.08	5	2.72	0.11	5	4.02	0.16	5	4.88	0.19	5	5.87	0.28	5	8.19	0.33	5
365.0	4.58	0.18	6	7.28	0.29	6	1.32	0.05	5	2.08	0.08	5	2.69	0.10	5	4.04	0.16	5	5.34	0.21	5	7.77	0.31	5	8.61	0.34	5
360.0	4.50	0.18	8	8.61	0.28	8	1.32	0.05	5	···			2.88	0.11	5	4.11	0.16	5	5.69	0.23	5	7.92	0.33	5	8.42	0.34	5
355.2	4.35	0.17	6	8.97	0.28	6	1.36	0.05	5	2.08	0.08	5	2.69	0.11	5	4.23	0.17	5	5.22	0.21	5	7.51	0.30	5	···		
345.3	3.68	0.15	6	6.54	0.26	6	1.35	0.05	5	1.85	0.07	5	2.72	0.11	5	4.02	0.18	5	5.37	0.21	5	7.59	0.30	5	8.83	0.35	5
335.4	2.90	0.12	6	5.91	0.24	6	1.29	0.05	5	1.87	0.08	5	2.48	0.10	5	4.08	0.18	5	4.92	0.19	5	7.44	0.29	5	8.68	0.35	5
325.5	2.59	0.10	8	5.23	0.21	6	1.05	0.04	5	1.61	0.07	5	2.48	0.11	5	3.78	0.15	5	4.83	0.19	5	6.93	0.28	5	7.81	0.31	5
320.0	···			···			···			···			2.35	0.09	5	3.34	0.14	5	4.53	0.18	5	···			···		
315.7	2.18	0.10	6	4.43	0.18	6	9.41	0.38	6	1.47	0.06	5	2.26	0.09	5	3.43	0.14	5	4.34	0.17	5	6.61	0.25	5	7.76	0.31	5
305.8	1.84	0.09	8	3.79	0.15	6	8.81	0.32	6	1.23	0.05	5	2.03	0.08	5	3.27	0.13	5	4.32	0.17	5	6.11	0.24	5	6.92	0.28	5
300.0	···			···			···			···			1.97	0.08	5	3.11	0.12	5	4.03	0.16	5	···			···		
295.9	1.55	0.09	6	3.38	0.14	8	6.77	0.29	5	9.97	0.40	6	1.80	0.07	5	3.02	0.12	5	3.74	0.15	5	5.38	0.22	5	6.73	0.27	5
285.9	1.50	0.09	6	2.98	0.14	6	6.64	0.31	6	9.73	0.39	6	1.72	0.07	5	2.80	0.13	5	3.55	0.15	5	4.92	0.23	5	5.30	0.29	5
276.2	1.14	0.08	6	2.64	0.13	6	6.03	0.32	6	8.35	0.41	5	1.50	0.07	5	2.64	0.13	5	3.10	0.15	5	5.22	0.24	5	5.73	0.30	5
266.3	1.08	0.08	6	2.61	0.14	6	5.32	0.33	5	8.57	0.43	6	1.31	0.08	5	2.37	0.14	5	2.72	0.16	5	4.62	0.26	5	5.51	0.31	5
260.0	···			···			···			···			1.39	0.08	5	1.95	0.13	5	2.94	0.18	5	···			···		
256.4	1.28	0.09	6	2.43	0.15	6	5.71	0.35	6	8.33	0.45	6	1.27	0.08	5	2.27	0.14	5	2.87	0.18	5	4.57	0.28	5	5.63	0.33	5
248.8	1.20	0.09	6	2.55	0.18	6	5.47	0.38	5	8.55	0.48	6	1.30	0.09	5	2.14	0.14	5	2.95	0.19	5	4.33	0.28	5	5.40	0.35	5
236.7	1.15	0.10	6	2.54	0.16	8	5.18	0.38	6	8.71	0.51	6	1.34	0.09	5	2.24	0.15	5	3.02	0.20	5	4.35	0.30	5	4.90	0.34	5
228.8	1.27	0.11	6	2.88	0.19	6	5.62	0.42	6	8.72	0.51	6	1.29	0.10	5	2.29	0.16	5	2.73	0.20	5	4.57	0.30	5	5.88	0.37	5
216.9	1.43	0.14	8	2.94	0.21	8	8.35	0.49	6	9.81	0.55	6	1.34	0.10	5	2.38	0.17	5	3.25	0.22	5	5.42	0.35	5	5.76	0.38	5
207.0	1.66	0.16	6	2.94	0.21	6	6.59	0.52	6	1.02	0.08	5	1.43	0.11	5	2.51	0.18	5	3.24	0.22	5	5.58	0.37	5	6.11	0.40	5
197.2	1.78	0.17	6	3.42	0.24	6	7.01	0.59	6	···			1.59	0.12	5	2.77	0.20	5	3.43	0.24	5	5.57	0.38	5	5.99	0.41	5

REF. K. Shoda, H. Miyase, M. Sugawara, T. Saito, S. Oikawa, A. Suzuki, J. Uegaki
Nucl. Phys. A239, 397 (1975)

ELEM. SYM.	A	Z
Y	89	39

METHOD

REF. NO. 75 Sh 4 egf

REACTION	RESULT	EXCITATION ENERGY	SOURCE TYPE	SOURCE RANGE	DETECTOR TYPE	DETECTOR RANGE	ANGLE
E,P	ABX	15- 24	D	14- 25	MAG-D		90

El virtual photon spectrum used to obtain (γ,p) cross sections.

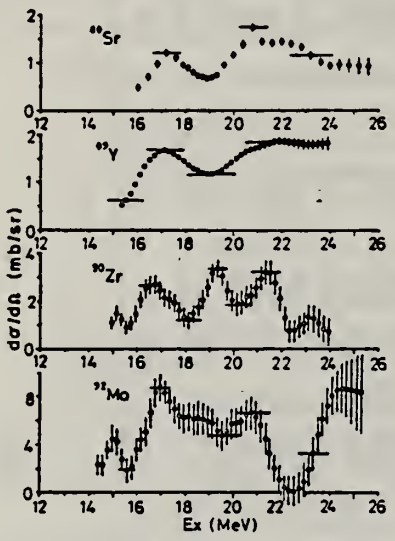

Fig. 3. Differential (γ, p) cross sections at θ = 90° analysed from (e, e'p) cross sections by the least-structure method.

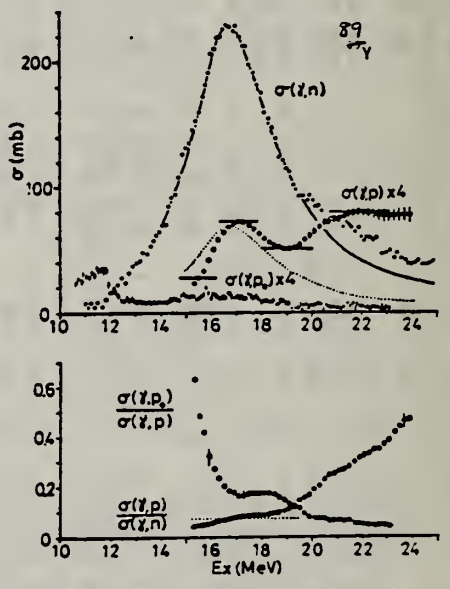

Fig. 6. The caption is the same as in fig. 5.

15
K. Shoda et al., Nucl. Phys. A221 (1974) 125
18
A. Lepretre et al., Nucl. Phys. A175 (1971) 609

Fig. 5. Upper figure: open circles, σ(γ, p); closed circles, σ(γ, n) [ref. [18])]; closed points, σ(γ, p0) [ref. [15])]; solid line, Lorentz line fit to the $T_<$ region of σ(γ, n) [ref. [18])]; dotted line, Lorentz line fit to the $T_<$ region of σ(γ, p) with Γ_i and E_R equal to those of σ(γ, n). Lower figure: ratio between cross sections. Dotted line: constant for σ(γ, p)/σ(γ, n) determined around $T_<$ GDR.

REF. H. Bartsch, K. Huber, U. Kneissl, H. Krieger
Nucl. Phys. A256, 243 (1976)

ELEM. SYM.	A	Z
Y	89	39

METHOD

REF. NO. 76 Ba 1 egf

REACTION	RESULT	EXCITATION ENERGY	SOURCE TYPE	SOURCE RANGE	DETECTOR TYPE	DETECTOR RANGE	ANGLE
G,N	RLY	THR-UKN	C	UKN	SCD-D		4PI

ISOMER RATIO

TABLE 1
Experimental and theoretical results

Process	Target-spin	E_γ (keV)	$T_{\frac{1}{2}}$	Spin high	Spin low	$R_{exp} = \frac{\sigma_{high}}{\sigma_{low}}$	SCOP ($\hbar$)
^{181}Ta(γ, 3n)	$\frac{7}{2}^+$	93	2.2 h 9.31 min 8.15 h	7^-	1^+	0.51 ±0.09	3.6 ±0.2
^{142}Nd(γ, n)	0^+	755 1100–1300, 145	63 s 2.5 h	$\frac{11}{2}^-$	$\frac{3}{2}^+$	0.055±0.006 0.19 ±0.01 [a]	2.20±0.06
^{92}Mo(γ, n)	0^+	652.9 1208, 1508, 1581, 1637	66 s 15.49 min	$\frac{9}{2}^+$	$\frac{1}{2}^-$	1.03 ±0.21 0.85 ±0.07 [b] 1.92 ±0.15 [a]	5.03±0.75 4^{+6}_{-3}
^{100}Mo(γ, n)	0^+	97.3 140.5	16.8 μs 66.02 h	$\frac{1}{2}^+$	$\frac{1}{2}^+$	0.85 ±0.24	1.72±0.25
^{108}Pd(γ, n)	0^+	214.5 115	22 s 850 ns	$\frac{11}{2}^-$	$\frac{1}{2}^+$	0.5 ±0.2	3.4 ±0.5
^{110}Pd(γ, n)	0^+	188 113 87.7	4.7 min 390 ns 13.47 h	$\frac{11}{2}^-$ $\frac{11}{2}^-$ $\frac{9}{2}^+$	$\frac{3}{2}^+$ $\frac{1}{2}^+$ $\frac{1}{2}^+$	0.11 ±0.02 0.41 ±0.09 3.2 ±0.7	3.14±0.15 3.0 ±0.25 3.3 ±0.4
^{89}Y(γ, n)	$\frac{1}{2}^-$	231.7 442.3 392.5	14.2 ms 300 μs	8^+	1^+	0.056±0.008	

[a]) Ref. [14]). [b]) Ref. [15]).

[14] P.E. Haustein et al., J. Inorg. Nucl. Chem. 33, 289 (1971)
[15] J. H. Carver et al., Nucl. Phys. 37, 449 (1962)

REF. R. Pitthan, F.R. Buskirk, E.B. Dally, J.O. Shannon, and W.H. Smith
Phys. Rev. C 16, 970 (1977)

ELEM. SYM.	A	Z
Y	89	39

METHOD

REF. NO. 77 Pi 1 hmg

REACTION	RESULT	EXCITATION ENERGY	SOURCE TYPE	SOURCE RANGE	DETECTOR TYPE	DETECTOR RANGE	ANGLE
E,E/	ABX	2- 55	C	93	MAG-D		DST
				(92.5)			

NUCLEAR REACTIONS $^{89}Y(e,e')$, E_0=92.5 MeV. Measured $d^2\sigma/d\Omega dE_x$, bound and continuum states. Deduced multipolarity λ, reduced matrix element $B(E\lambda)$, radiative width Γ_γ^0, sum rule exhaustion, single particle strength, and total width of the continuum and clustered states.

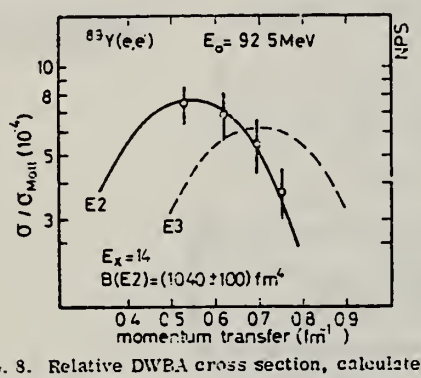

FIG. 8. Relative DWBA cross section, calculated using the Goldhaber-Teller model, as fitted to the experimental cross sections for the resonance at 14 MeV with a width of Γ=4.5 MeV. The comparison rules out any assignment other than *E*2.

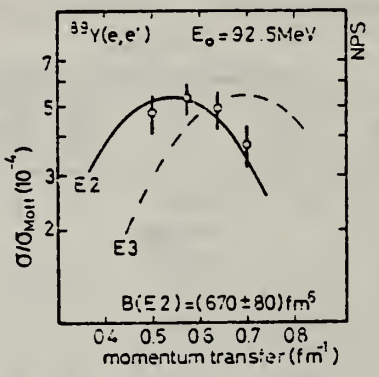

FIG. 9. Relative DWBA cross section using the Goldhaber-Teller model as compared with the resonance at 28 MeV assuming a width of Γ = 8 MeV. The comparison shows that the cross section in this region is predominantly *E*2 with the possibility of some *E*3 contribution.

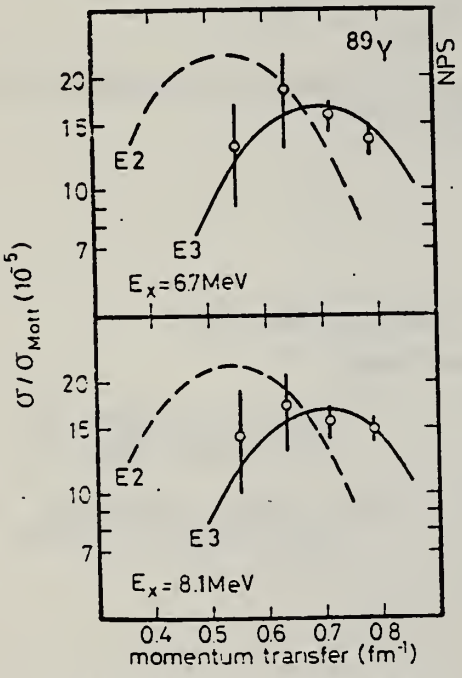

FIG. 10. Relative DWBA cross section using the Goldhaber-Teller model as compared with the cluster of states concentrated around 7 and 8 MeV. The comparison favors an *E*3 assignment for these states. The large error at the lower momentum transfer is due to the subtraction of the ghost peak.

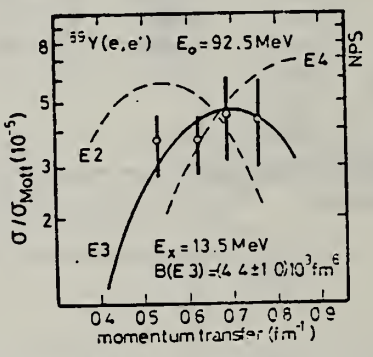

FIG. 11. Relative DWBA cross section calculated with the Goldhaber-Teller model for the structure at 13.5 MeV with a width of 1.2 MeV. Comparison with experiment favors an *E*3 assignment. *M*2 assignment would be possible, too, but was not considered seriously possible, due to the great *M*2 strength necessary to explain the data.

[over]

TABLE I. Comparison of some results for the $E1$ (GDR) resonance in $N=50$ nuclei.

Ref.	E_0 (MeV)	Γ (MeV)	R (%)[a]	Method	Nucleus
22	16.79	3.95 ± 0.06	87 ± 6	(γ,n)	^{89}Y
23	16.74	4.1 ± 0.1	111 ± 5	(γ,n)	^{89}Y
5	16.65	4.0	107 ± 32	(e,e')	^{90}Zr
8	...[b]	4.0	113 ± 25	(e,e')	^{90}Zr
This work	16.6	3.9 ± 0.2	104 ± 10	(e,e')	^{89}Y

[a] $R = E_x B(E1)/\mathrm{EWSR}(E1, \Delta T=1) \times 100$.

[b] The authors used the (γ,n) value.

[5] S. Fukuda and Y. Torizuka, Phys. Rev. Lett. 29, 1109 (1972).
[8] S. Fukuda and Y. Torizuka, Phys. Lett. 62B, 146 (1976).
[22] B. L. Berman, J. T. Caldwell, R. R. Harvey, M. A. Kelly, R. L. Bramblett, and S. C. Fultz, Phys. Rev. 162, 1099 (1967).
[23] A. Leprêtre, H. Beil, R. Bergère, P. Carlos, A. Veyssière, and M. Sugawara, Nucl. Phys. A175, 609 (1971).

TABLE II. Compilation of some results for the $E2$ ($\Delta T=0$) resonance in $N=50$ nuclei.

Ref.	E_0 (MeV)	Γ (MeV)	R (%)[a]	Method	Nucleus
5	14	4.8 ± 0.6	56 ± 17	(e,e')	^{90}Zr
6	14.5 ± 0.3	4.0 ± 0.2	54 ± 15	(α,α')	^{90}Zr
8	14[b]	4.5[b]	84	(e,e')	^{90}Zr
40	13.8 ± 0.2	3.2	24 ± 5	(p,p')	^{89}Y
This work	14.0 ± 0.2	4.5 ± 0.4	56 ± 6[c]	(e,e')	^{89}Y

[a] $R = E_x B(E2)/\mathrm{EWSR}(\Delta T=0, E2) \times 100$.

[b] Values were taken from Ref. 41.

[c] The rms radius $R = 4.27$ fm of Ref. 13 was used for calculating the sum rule yielding an EWSR ($E2$, $\Delta T=0$) of 25800 MeV fm^4.

[5] S. Fukuda and Y. Torizuka, Phys. Rev. Lett. 29, 1109 (1972).
[6] D. H. Youngblood, J. M. Moss, C. M. Rozsa, J. D. Bronson, A. D. Bacher, and D. R. Brown, Phys. Rev. C 13, 994 (1976).
[8] S. Fukuda and Y. Torizuka, Phys. Lett. 62B, 146 (1976).
[41] N. Marty, M. Morlet, A. Willis, V. Comparat, and R. Frascaria, Nucl. Phys. A238, 93 (1975).

TABLE III. Compilation of results for the $E2$ ($\Delta T=1$) resonance in some $N=50$ nuclei.

Ref.	E_0 (MeV)	Γ (MeV)	R (%)[a]	Method	Nucleus
5	27	...	23	(e,e')	^{90}Zr
8	26	7	73	(e,e')	^{90}Zr
43		...	≈40[b]	(p,γ)	^{90}Zr
This work	28.0 ± 0.5	10	82 ± 10	(e,e')	^{89}Y
		8	57 ± 6		
		7	48 ± 5		

[a] $R = E_x B(E2)/\mathrm{EWSR}(\Delta T=1, E2) \times 100$. The $\Delta T=1$ sum rule is connected with that of Table II by a factor of N/Z.

[b] The value for the sum rule percentage depends on the coupling used for the model.

[5] S. Fukuda and Y. Torizuka, Phys. Rev. Lett. 29, 1109 (1972).
[8] S. Fukuda and Y. Torizuka, Phys. Lett. 62B, 146 (1976).
[43] F. S. Dietrich, D. W Heikkinen, K. A. Snover, and K. Ebisawa, Phys. Rev. Lett. 39, 156 (1977).

TABLE VI. Compilation of all the results from this experiment.

E_x (MeV)	E_x ($A^{-1/3}$ MeV)	Γ (MeV)[a]	B (fm$^{2\lambda}$)	R (%)[b]	Γ_γ^0 (eV)	spu	λ	ΔT
2.6	...	1.0 ± 0.2	(1.12 ± 0.15) × 10^5	15 ± 3	5.3 × 10^{-6}	34	3	0
4.0	...	1.0 ± 0.2	700 ± 140	11 ± 3	1.2 × 10^{-1}	6	2	0
6.75	30	1.0 ± 0.2	(16.5 ± 3.0) × 10^3	6 ± 1	6.2 × 10^{-4}	5	3	0
8.05	36	1.2 ± 0.2	(16.5 ± 2.5) × 10^3	7 ± 1	2.1 × 10^{-3}	5	3	0
13.5	60	1.2 ± 0.2	(4.4 ± 1.0) × 10^3	2.5 ± 0.6	2.1 × 10^{-2}	1.4	3	1
14.0	63	4.5 ± 0.4	1040 ± 100	56 ± 6	9.0 × 10^1	8.8	2	0
16.6	74	3.9 ± 0.2	20.5 ± 2.0	104 ± 10	3.3 × 10^4	5.3	1	1
28.0	125	Γ = 7	565 ± 65	48 ± 5	1.57 × 10^3	4.8		
		Γ = 8	670 ± 80	57 ± 6	1.86 × 10^3	5.6	2	1
		Γ = 10	960 ± 130	82 ± 10	2.67 × 10^3	8.1		

[a] The width may be either the width of the enveloping curve of unresolved discrete states or the width of a coherent resonant state.

[b] $R = E_x B(E\lambda)/\mathrm{EWSR}(E\lambda, \Delta T) \times 100$.

REF. K. Masumoto, T. Kato, N. Suzuki
Nucl. Inst. Meth. 157, 567 (1978)

ELEM. SYM.	A	Z
Y	89	39

METHOD

REF. NO. 78 Ma 10 hg

REACTION	RESULT	EXCITATION ENERGY	SOURCE		DETECTOR		ANGLE
			TYPE	RANGE	TYPE	RANGE	
G,N	ABY	12-68	C	30-68	ACT		4PI

Analysis is made of reactions interfering with photon activation analysis procedures.

The activation yield curves have been presented for a number of photonuclear reactions in the energy range from 30 to 68 MeV, in order to evaluate quantitatively the interferences due to competing reactions in multielement photon activation analysis. The general features of the yields as functions of both target mass number and excitation energy were elucidated from the data obtained, discussion being given on the results in terms of the reaction mechanism.

Simultaneous neutron activation due to appreciable neutron production from the converter and surrounding materials has also been studied, and, finally, the magnitudes of interferences in real multielement analysis were given in the form of their energy dependences.

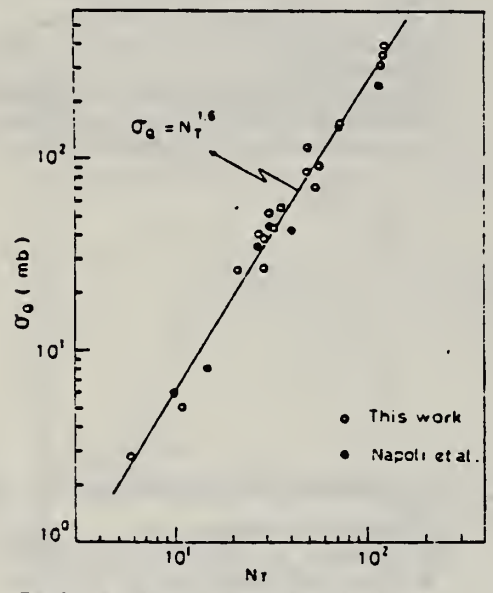

Fig. 2. Yield per equivalent quanta versus target neutron number.

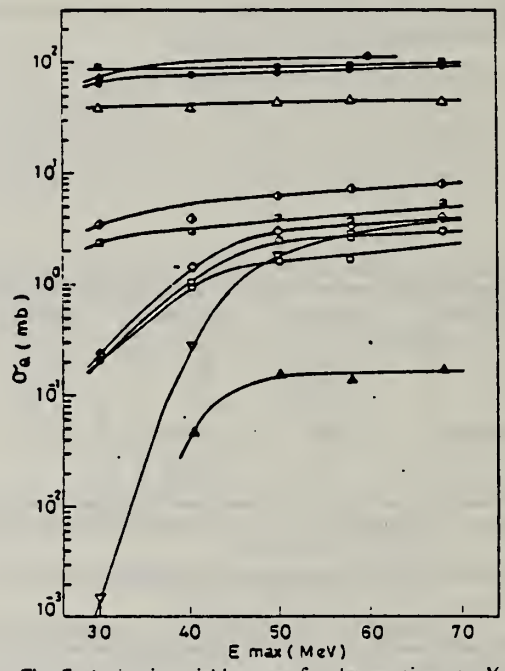

Fig. 7. Activation yield curves for the reactions on Y, Zr, Nb and Mo.
◆ $^{89}Y(\gamma, n)^{88}Y$, ● $^{90}Zr(\gamma, n)^{89}Zr$, ○ $^{90}Zr(\gamma, pn)^{88}Y$,
△ $^{93}Nb(\gamma, n)^{92m}Nb$, ▲ $^{93}Nb(\gamma, 2n)^{88}Y$, ■ $^{100}Mo(\gamma, n)^{99}Mo$,
◈ $^{97}Mo(\gamma, p)^{96}Nb$, ◪ $^{96}Mo(\gamma, p)^{95m}Nb$, ◇ $^{94}Mo(\gamma, pn)^{92m}Nb$,
□ $^{92}Mo(\gamma, 2n)^{90}Mo$, ▽ $^{94}Mo(\gamma, 2n)^{89}Zr$.

(over)

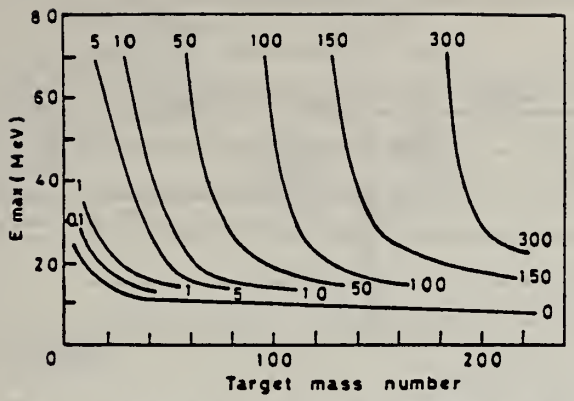

Fig. 9. Yields of the (γ, n) reactions as a function of bremsstrahlung maximum energy and target mass number. The numerical values in the figure are yields per equivalent quanta in mb.

REF. H.R. Weller, N.R. Roberson & S.R. Cotanch
Phys. Rev. C18, 65 (1978)

ELEM. SYM.	A	Z
Y	89	39

METHOD

REF. NO. 78 We 4 hmg

REACTION	RESULT	EXCITATION ENERGY	SOURCE		DETECTOR		ANGLE
			TYPE	RANGE	TYPE	RANGE	
$ P,G	RLX	14-24	D	6-16	UKN-D		DST

Analysis of data in reference 5.

POLARIZED PROTONS

Measurements of cross sections and analyzing powers are examined for polarized proton capture on ^{14}C, ^{30}Si, ^{54}Fe, ^{56}Fe, ^{58}Fe, ^{59}Co, and ^{88}Sr at energies which cover the giant dipole resonance region. These data are used to extract the relative amplitudes and phases of the contributing $E1$ T-matrix elements. A typical result exhibits two solutions. Calculations using the direct (or a direct-semidirect) capture model appear to provide a means for choosing the physical solution.

[NUCLEAR REACTIONS: $^{14}C(\vec{p},\gamma_0)$, $^{30}Si(\vec{p},\gamma_0)$, $^{54}Fe(\vec{p},\gamma_0)$, $^{56}Fe(\vec{p},\gamma_0)$, $^{58}Fe(\vec{p},\gamma_0)$, $^{59}Co(\vec{p},\gamma_0)$, $^{88}Sr(\vec{p},\gamma_0)$; measured $\sigma(\theta)$ and $A(\theta)$ over energy region of the giant dipole resonance. Deduced T-matrix amplitudes and phases. Compare results to direct-semidirect model calculations.]

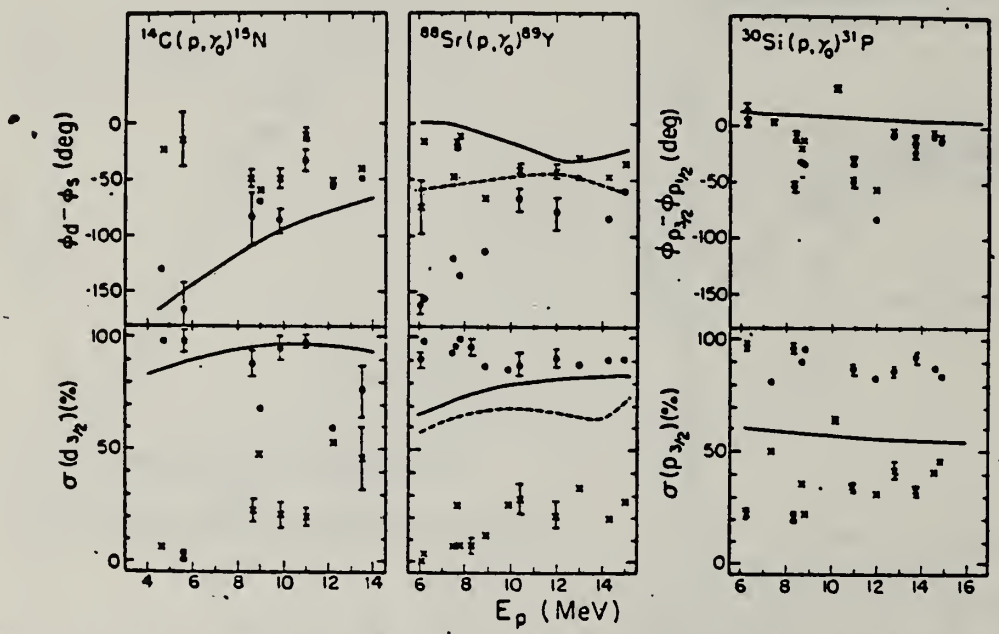

FIG. 1. The two solutions (dots and x's) resulting from a pure $E1$ analysis of the data are shown along with the results of the calculation for target nuclei of ^{14}C, ^{88}Sr, and ^{30}Si. The remaining cross section in the case of ^{14}C and ^{88}Sr is due to the $s_{1/2}$ matrix element. In the case of ^{30}Si it arises from the $p_{1/2}$ matrix element. The error bars represent typical statistical errors associated with the data points. The amplitudes are presented in terms of the percentage of the total cross section for which they are responsible. The curves represent DSD calculations as described in the text. The dashed curves in the case of ^{88}Sr were obtained using the optical model parameters of Ref. 16 while the solid lines were obtained from the parameters of Ref. 18.

[over]

[2]H. R. Weller, R. A. Blue, N. R. Roberson, D. G. Rickel, S. Maripuu, C. P. Cameron, R. D. Ledford, and D. R. Tilley, Phys. Rev. C 13, 922 (1976). (Note: an error exists in the sign of the phase in this paper. The quantity $\phi_s-\phi_d$ should be $\phi_d-\phi_s$ wherever it appears.)
[3]C. P. Cameron, N. R. Roberson, D. G. Rickel, R. D. Ledford, H. R. Weller, R. A. Blue, and D. R. Tilley, Phys. Rev. C 14, 553 (1976).
[4]C. P. Cameron, Ph.D. thesis, Duke University, 1976 (unpublished).
[5]R. D. Ledford, Ph.D. thesis, Duke University, 1976 (unpublished).
[6]J. D. Turner, C. P. Cameron, N. R. Roberson, H. R. Weller, and D. R. Tilley, Phys. Rev. C 17, 1853 (1978).

REF. E. Van Camp, R. Van de Vyver, H. Ferdinande, E. Kerkhove, R. Carchon, J. Devos
Phys. Rev. C22, 2396 (1980)

ELEM. SYM.	A	Z
Y	89	39

METHOD

REF. NO. 80 Va 1 hg

REACTION	RESULT	EXCITATION ENERGY	SOURCE		DETECTOR		ANGLE
			TYPE	RANGE	TYPE	RANGE	
G,PØ	ABX	13-25	C	13-25	SCD-D		DST
G,P1	ABX	15-25	C	13-25	SCD-D		DST

Absolute (γ,p_0) and (γ,p_1) differential cross sections for ^{89}Y were measured at seven angles in the energy interval between 13 and 24.6 MeV, from which the angular distribution coefficients were deduced by fitting a sum of Legendre polynomials. In these cross sections we observe a number of isolated resonances which can be identified as the isobaric analogs of known $1/2^+$ and $3/2^+$ excited states in the ^{89}Sr parent nucleus. The appearance of a maximum around 21 MeV excitation energy in both total cross sections may indicate the existence of the $T_<$ coherent dipole state. From the angular distribution coefficients in the (γ,p_0) channel, an upper and lower limit for the $E2$ photon absorption were estimated as being equal to 22% and 6%, respectively, of the total $E2$ energy-weighted sum rule.

[NUCLEAR REACTIONS ^{89}Y(γ,p_0), (γ,p_1), $E=13.0$–24.6 MeV, $\theta=37$–$143°$; measured $\sigma(E;\theta)$ absolutely. Deduced $\sigma(E;p_0)$, $\sigma(E;p_1)$; $E1$, $E2$ strengths, isobaric analog states, isospin splitting. Natural target.]

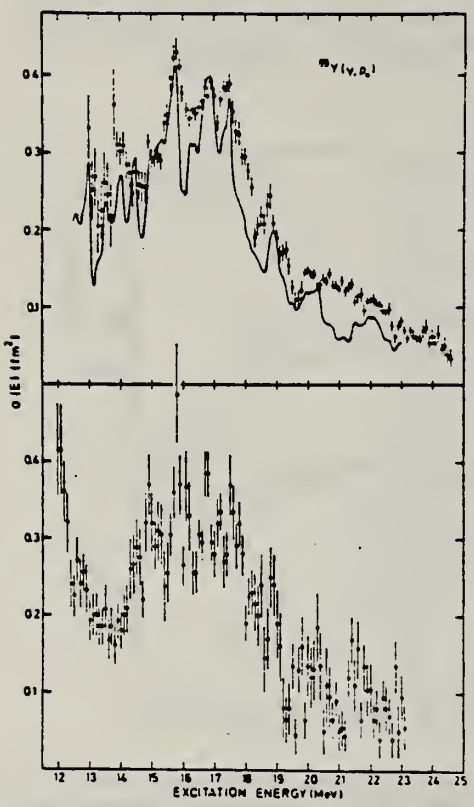

FIG. 5. The points with error bars in the upper half of the figure show our experimentally determined total ^{89}Y(γ,p_0) cross section, while the full line represents the results deduced from the ^{88}Sr(p,γ_0) data of Paul *et al.* (Ref. 8); the bottom half of the figure shows the (γ,p_0) cross section resulting from the $(e,e'p)$ experiment of Shoda *et al.* (Ref. 9).

Only statistical shown, systematic uncertainty is of the order of 5%.

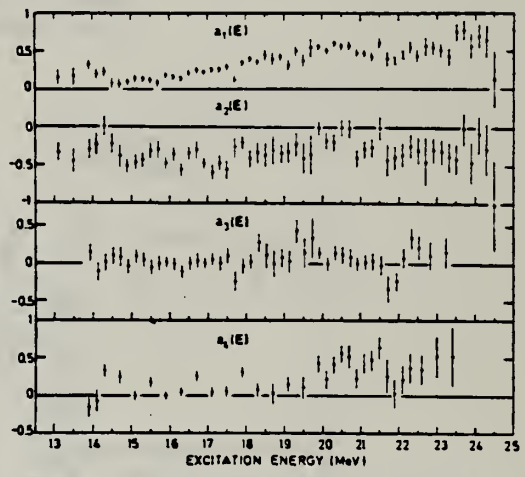

FIG. 6. The angular distribution coefficients $a_l(E)$, $l=1,\ldots,4$, as a function of excitation energy for the ^{89}Y(γ,p_0) reaction.

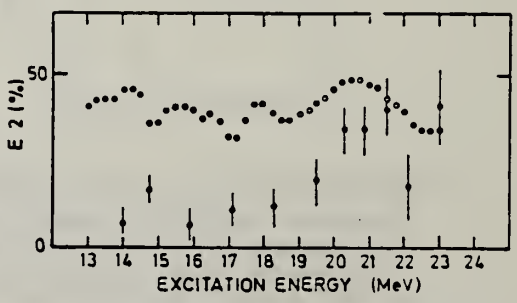

FIG. 7. Upper (open circles) and lower (dotted points) limits of the $E2$ contribution to the ^{89}Y(γ,p_0) photoabsorption.

(OVER)

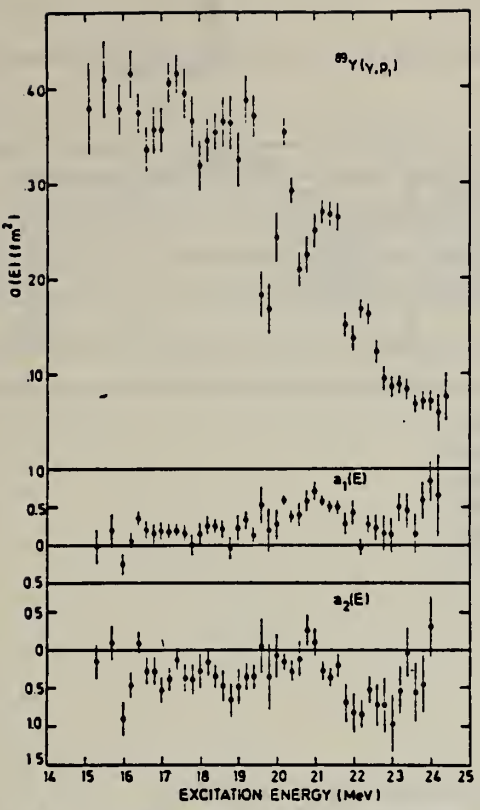

FIG. 8. The upper half of the figure shows the total $^{89}Y(\gamma,p_1)$ cross section, while in the lower half the angular distribution coefficients $a_1(E)$ and $a_2(E)$ are represented.

REF.	ELEM. SYM.	A	Z
E. Van Camp, R. Van de Vyver, E. Kerkhove, D. Ryckbosch, H. Ferdinande, P. Van Otten, P. Berkvens Phys. Rev. C24, 2499 (1981)	Y	89	39

METHOD	REF. NO.
	81 Va 1 hg

REACTION	RESULT	EXCITATION ENERGY	SOURCE		DETECTOR		ANGLE
			TYPE	RANGE	TYPE	RANGE	
G,PØ	ABX	7-25	C	14-25	SCD-D		DST
G,PL	ABX	7-25	C	14-25	SCD-D		DST

The $^{89}Y(\gamma,p)^{88}Sr$ reaction was studied at various bremsstrahlung end point energies in the giant dipole resonance region. Using an artificially constructed pseudomonoenergetic photon spectrum, it was possible to determine the absolute cross sections for various photoproton reaction channels. From the direct decay cross sections the proton escape width $\Gamma_p^{\downarrow}$ of the $T_<$ giant dipole resonance was derived; its value amounts to 0.30—0.35 MeV. The nondirect contribution equals about 25% of the total energy-integrated photoproton cross section.

[NUCLEAR REACTIONS $^{89}Y(\gamma,p)$, E = 14—24 MeV; measured $\sigma(E)$ absolutely. Deduced $\Gamma_p^{\downarrow}$. Natural target.]

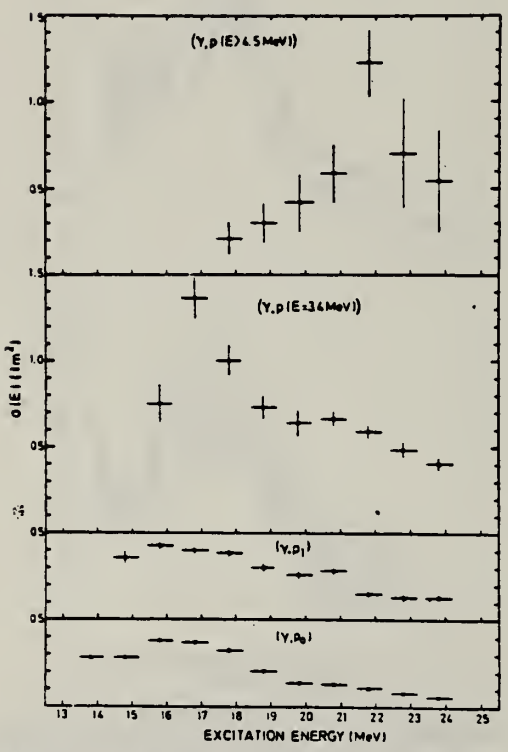

FIG. 6. The absolute $^{89}Y(\gamma,p)$ cross sections for the various proton channels which could be identified.

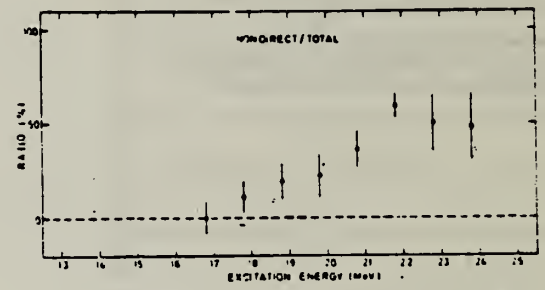

FIG. 7. The ratio of the nondirect to the total cross section for the ^{89}Y (γ,p) reaction, as a function of excitation energy.

TABLE II. Integrated cross sections for the various photoproton channels observed in the $^{89}Y(\gamma,p)$ reactions.

Channel	Integration limits E_1 (MeV)—E_2 (MeV)	$\int_{E_1}^{E_2}\sigma(E)dE$ (MeV fm²)	$\frac{\int\sigma(p_i,E)dE}{\int\sigma(p,E)dE}\times 100$
(γ,p_0)	13.8—24.6	2.45±0.02	15.6
(γ,p_1)	15.1—24.4	2.77±0.03	17.7
$[\gamma,p(E=3.4$ MeV)]	15.8—23.8	6.59±0.18	42.1
$[\gamma,p(E>4.5$ MeV)]	17.8—23.8	3.86±0.57	24.6
$(\gamma,p)_{total}$	13.8—24.6	15.67±0.60	100.0

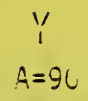
Y
A=90

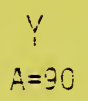
Y
A=90

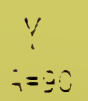
Y
A=90

REF. L. Nilsson, A. Lindholm, I. Bergqvist, B. Palsson, and J. Eriksson
PICNS-73, Vol.II, p.949 (1973) Asilomar

ELEM. SYM.	A	Z
Y	90	39

METHOD

REF. NO. 73 Ni 2 egf

REACTION	RESULT	EXCITATION ENERGY	SOURCE		DETECTOR		ANGLE
			TYPE	RANGE	TYPE	RANGE	
N,G	RLY	14- 16	D	6- 9	NAI-D		-

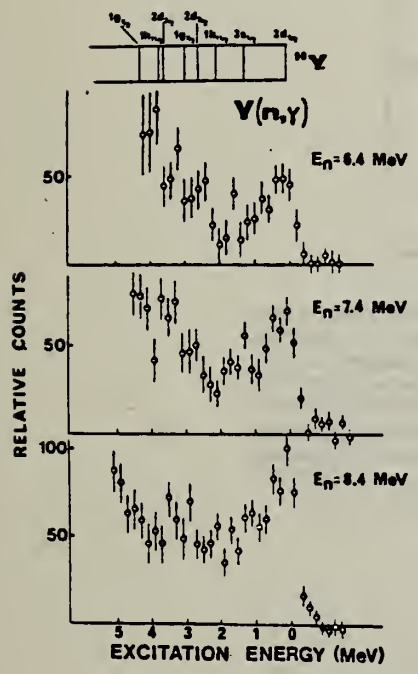

Fig 1. Gamma-ray spectra from $^{89}Y(n,\gamma)^{90}Y$ at various neutron energies plotted versus residual excitation energy. The spectra are normalized to the same neutron flux. The single-particle structure of ^{90}Y is given on top of the figure.

REF.

I. Bergqvist, B. Palsson, L. Nilsson, A. Lindholm, D.M. Drake, E. Arthur, D.K. McDaniels and P. Varghese
Nucl. Phys. A295, 256 (1978)

ELEM. SYM.	A	Z
Y	90	39

METHOD

REF. NO. 78 Be 1 rs

REACTION	RESULT	EXCITATION ENERGY	SOURCE		DETECTOR		ANGLE
			TYPE	RANGE	TYPE	RANGE	
N,G	ABX	13- 23	D	6- 16	NAI-D		90

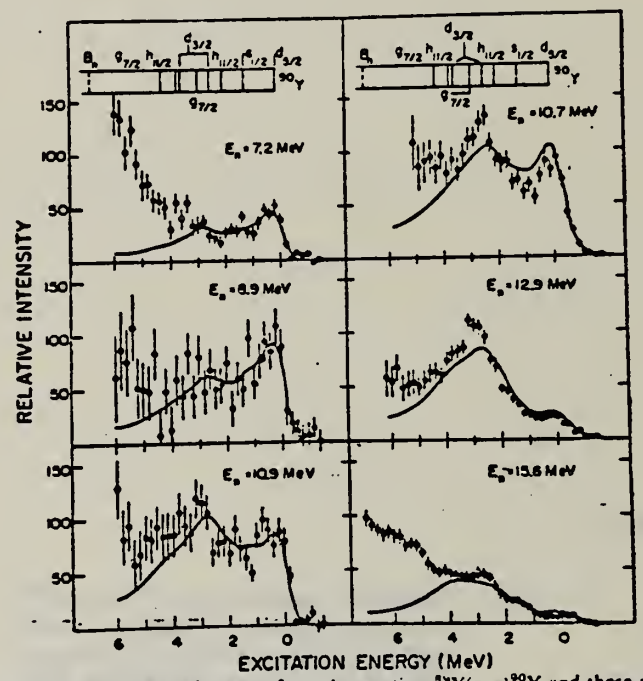

Fig. 1. Comparison of the measured spectra from the reaction $^{89}Y(n,\gamma)^{90}Y$ and those predicted from the direct-semidirect (DSD) capture theory at neutron energies from 7.2 to 15.6 MeV. The theoretical spectra were computed using the DSD cross section predictions with a complex interaction for γ-ray transitions to the single-particle states of ^{90}Y shown on top of the figure. The cross sections were multiplied by the NaI(Tl) detector response function and corrected for γ-ray attenuation and detector efficiency. The observed and theoretical spectra were normalized to each other in the region corresponding to excitation energies below 3.2 MeV. The GDR parameters used are given in the text while the interaction parameters chosen were r_1 = 75 MeV, and w_1 = 110 MeV. The data at neutron energies of 7.2, 8.9 and 10.9 MeV were taken with the TLU system while the higher energy data were taken at LASL.

over

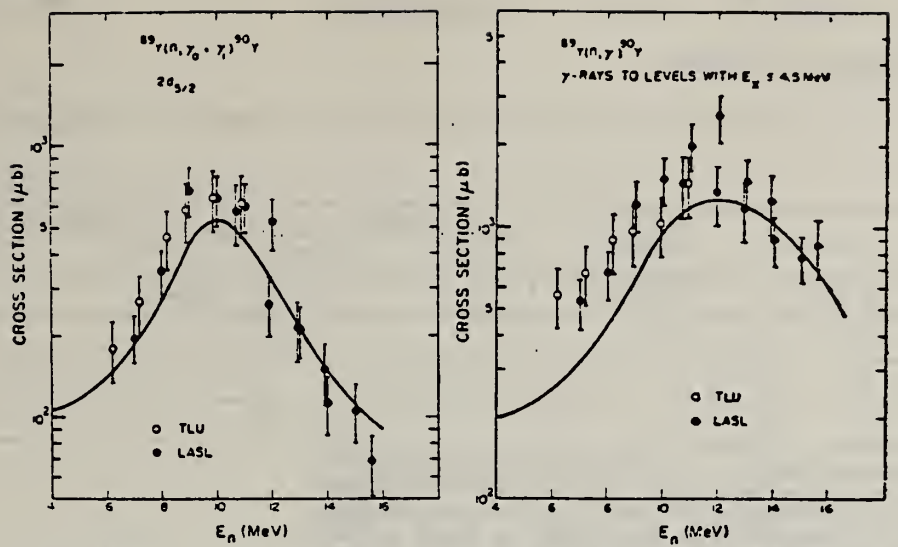

Fig. 3. Experimental (n, γ) cross sections for γ-ray transitions to the two $2d_{5/2}$ states at 0 and 203 keV in ^{90}Y and the integrated cross section for γ-rays to levels below E_x = 4.5 MeV. The differential cross sections at 90° were multiplied by 4π. The results from the TLU experiment are indicated by open circles and the LASL data are shown by solid circles. The solid lines represent the cross section predicted from the DSD theory using a complex coupling function for the particle-vibration interaction.

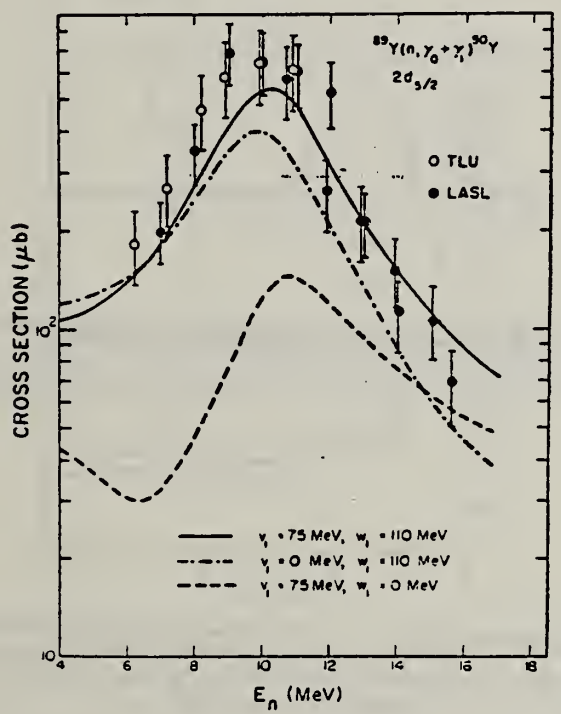

Fig. 5. Detailed comparison of the experimental (n, γ) cross sections for γ-ray transitions to the ground-state doublet of ^{90}Y. The data are compared to the predictions of the DSD model using various particle-vibration interaction functions.

REF. A. Likar, A. Lindholm, L. Nilsson, I. Bergqvist and B. Palsson
Nucl. Phys. A298, 217 (1978)

ELEM. SYM.	A	Z
Y	90	39

METHOD

REF. NO. 78 Li 2 rs

REACTION	RESULT	EXCITATION ENERGY	SOURCE		DETECTOR		ANGLE
			TYPE	RANGE	TYPE	RANGE	
N,G	RLX	14- 18	D	7- 11	NAI-D		DST

Abstract: Gamma-ray spectra from neutron capture in natural samples of strontium and yttrium have been recorded at various angles with respect to the direction of the incident neutron flux. Angular yields have been observed at six neutron energies in the range 7 to 11 MeV using time-of-flight techniques to improve the signal-to-background ratio. The γ-radiation was detected by a large NaI(Tl) crystal placed in a heavy radiation shield. Certain combinations of Legendre polynomial coefficients were extracted for transitions to low-lying single-particle states ($2d_{5/2}$ and $3s_{1/2}$) in the final nuclei. The energy dependence of the angular distribution coefficients indicates interference between the electric dipole amplitude and amplitudes of opposite parity. The results are compared with theoretical calculations based on the direct-semidirect model.

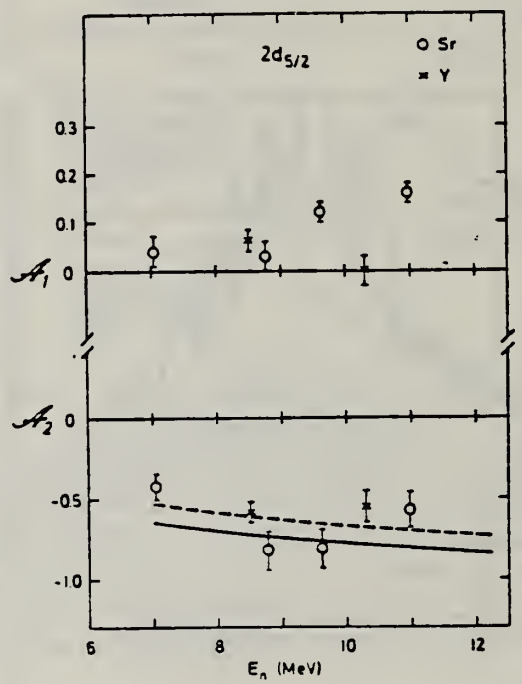

Fig. 2. Angular distribution coefficients A_1 and A_2 versus neutron energy for the reactions $^{88}Sr(n, \gamma_0)^{89}Sr$ (open circles) and $^{89}Y(n, \gamma_0 + \gamma_1)^{90}Y$ (crosses). The curves for the A_2 coefficient represent the results of theoretical calculations for E1 transitions to the $2d_{5/2}$ state in ^{89}Sr from the direct (solid line) and DSD (dashed line) capture models.

over

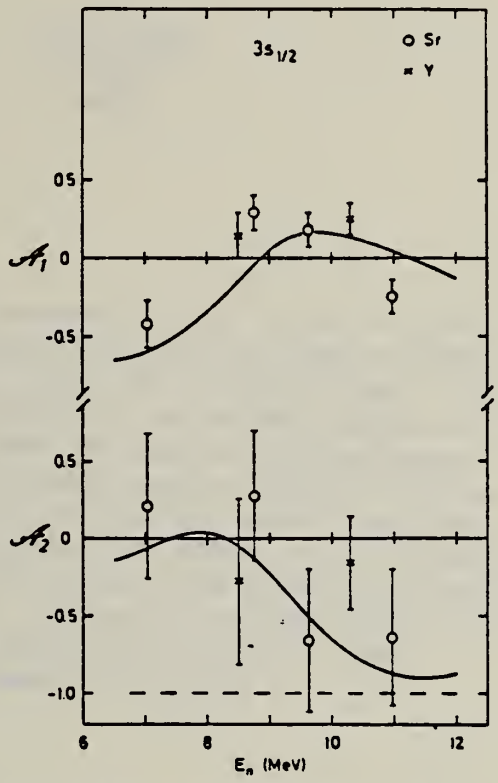

Fig. 3. Angular distribution coefficients $\mathscr{A}_1$ and $\mathscr{A}_2$ versus neutron energy for γ-rays to the $3s_{1/2}$ states from the reactions $^{88}Sr(n, \gamma)^{89}Sr$ (open circles) and $^{89}Y(n, \gamma)^{90}Y$ (crosses). The theoretical result for DSD model calculations are shown as dashed curve for pure E1 transitions and as solid curves assuming E1 and E2 transitions associated with collective excitation of the GDR and the isoscIar GQR.

ZIRCONIUM
Z=40

Although zircon was frequently used by the ancients for intagli and although hyacinth and jargon (semi-precious stones) were known in the middle ages, the presence in these minerals of an unknown metal was not suspected until near the end of the eighteenth century. The earth zirconia was overlooked because of its great similarity to alumin, and it took the analytical skill of Klaproth to detect it. He worked with zirconium silicate in the form of semiprecious gemstones from Ceylon. These zircon gems derive their name from the Arabic *zargun* (gold color), and Klaproth named the element zirconium.

ZR

Ref.	Elem. Sym.	A	Z
K. Reibel; A.K. Mann Phys. Rev. 118, 701 (1960)	Zr		40

Method	Ref. No.	
γ's from $F^{19}(p,\alpha\gamma)$ reaction; protons from Vande Graaff; Ne I.	60 Re 1	JHH

Reaction	E or ΔE	E_o	Γ	$\int \sigma dE$	Jπ	Notes
(γ,γ)	E_γ = ~ 7					$\langle\sigma\rangle$ (E_p = 2.03 MeV) = 1.0 ± 0.1 mb

Ref. O.M.M. Mitchell, K.G. McNeill
Can. J. Phys. 41, 871 (1963)

Elem. Sym.	A	Z
Zr		40

Method: Betatron; proton yield; angular distribution; sctintillator; ion chamber.

Ref. No.: 63 Mi 5 | NVB

Reaction	E or ΔE	E_o	Γ	$\int \sigma dE$	Jπ	Notes
Zr(γ,xp)	Bremss. 22					Angular distribution: $Y(\theta) = a + b \sin^2\theta (1 + p \cos\theta)^2$ where a = 24±8; b = 74±14; p = 0.2 ±0.1 and b/a = 3.1±1.2. Yield (E_p > 8 MeV): (2.6±0.6) 10^5 protons/mole-r. Yield (3.7 < E_p < 14): (29±3) 10^5

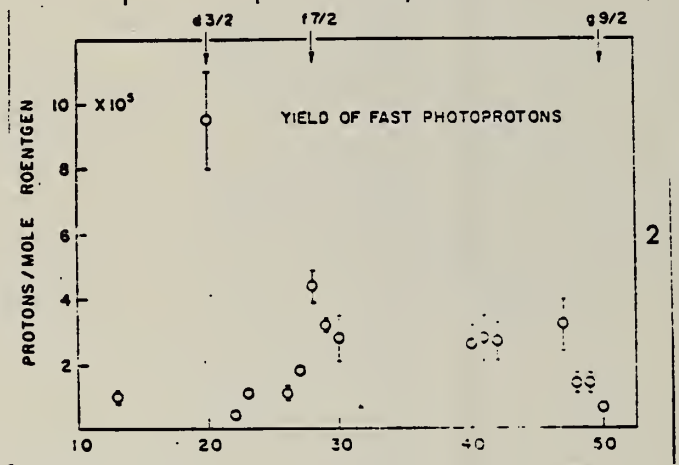

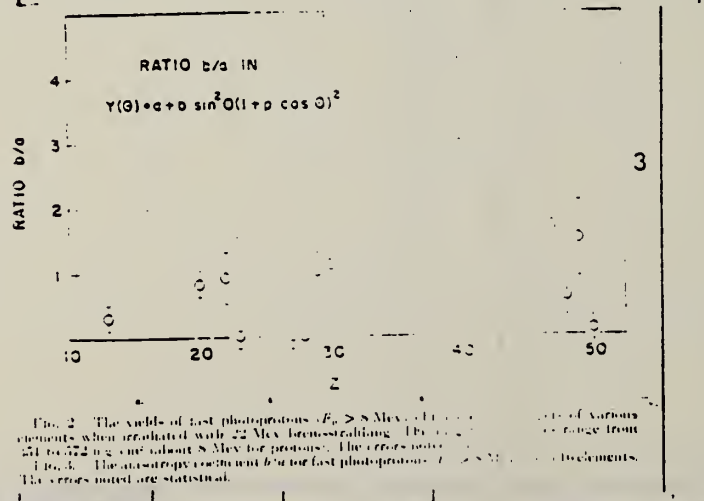

Fig. 2. The yields of fast photoprotons (E_p > 8 Mev) [illegible] of various elements when irradiated with 22 Mev bremsstrahlung. The [illegible] range from 251 to 272 mg/cm² (about 8 Mev for protons). The errors noted [illegible] Fig. 3. The anisotropy constant b/a for fast photoprotons [illegible] elements. The errors noted are statistical.

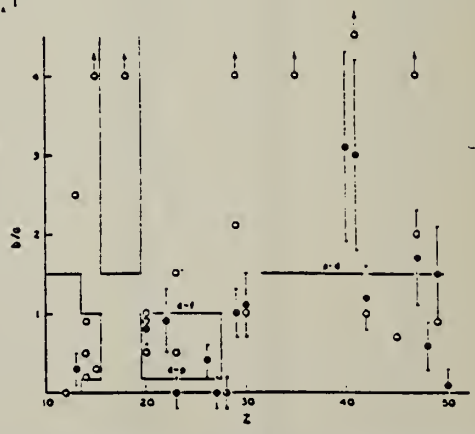

Fig. 4. The values of the fast photoproton anisotropy coefficient b/a found by the present authors (●) and other workers (○) in the region of the periodic table 10 ≤ Z ≤ 50. Arrows indicate off-scale points. The references to the results of other workers are given in Table II. The demarcations are explained in the text.

REF.

I.I. Dushkov, B.S. Ishkhanov, I.M. Kapitonov, B.A. Yur'ev, V.G. Shevchenko
Phys. Letters 10, 310 (1964)

ELEM. SYM.	A	Z
Zr		40

METHOD: Betatron

[Page 1 of 2]

REF. NO.: 64 Du 1 | JOC

REACTION	RESULT	EXCITATION ENERGY	SOURCE		DETECTOR		ANGLE
			TYPE	RANGE	TYPE	RANGE	
G,P	ABX	THR-34	C	22-34	MAG-D	2-16	DST

ABX

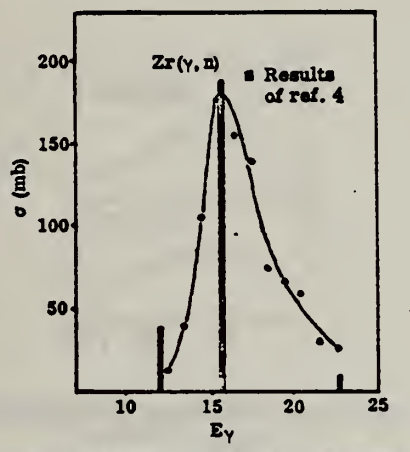

Fig. 1. Comparison of theoretical and experimental data for the (γ,n) reaction.

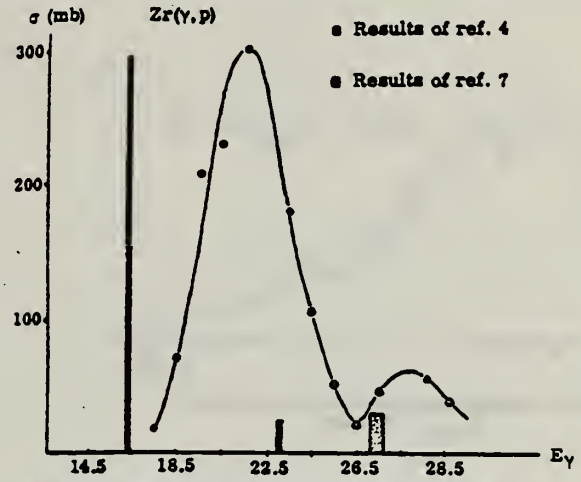

Fig. 2. Comparison of theoretical and experimental data for the (γ,p) reaction.

Fig. 3a. Energy distribution of photoprotons at $E_{\gamma max}$ = 22 MeV.

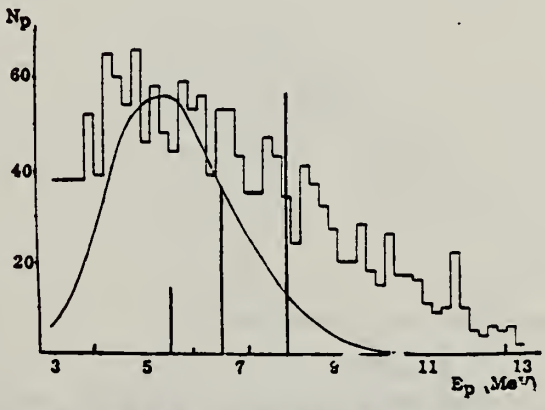

Fig. 3b. Energy distribution of photoprotons at $E_{\gamma max}$ = 25 MeV.

REACTION	RESULT	EXCITATION ENERGY	SOURCE TYPE	SOURCE RANGE	DETECTOR TYPE	DETECTOR RANGE	ANGLE

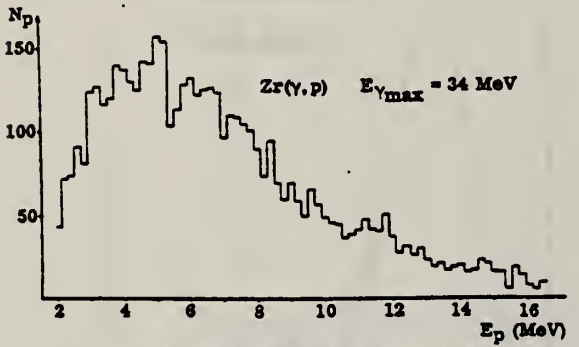

Fig. 3c. Energy distribution of photoprotons at $E_{\gamma max}$ = 34 MeV.

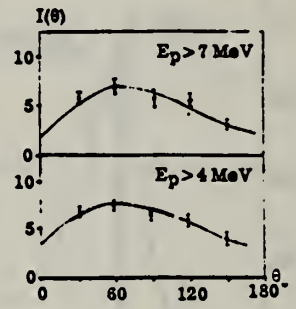

Fig. 4. Angular distributions of photoprotons at $E_{\gamma max}$ = 25 MeV.

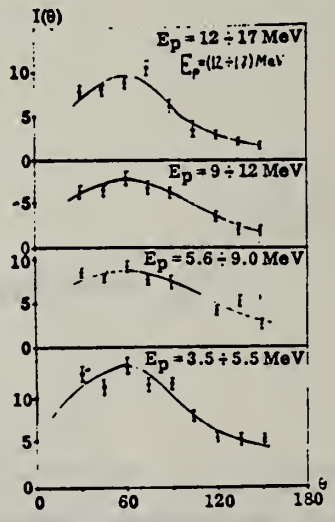

Fig. 5. Angular distributions of photoproton at $E_{\gamma max}$ = 34 MeV.

REF. I. I. Dushkov, B. S. Ishkhanov, I. M. Kapitonov, V. G. Shevchenko, and B. A. Yur'ev
Izv. Akad. Nauk Fiz. 29, 213 (1965)
Bull. Acad. Sci. USSR- Phys. 29, 213 (1965)

ELEM. SYM.	A	Z
Zr		40

METHOD

REF. NO. 65 Du 1

EGF

REACTION	RESULT	EXCITATION ENERGY	SOURCE		DETECTOR		ANGLE
			TYPE	RANGE	TYPE	RANGE	
G,P	ABX	18-26	D	17-24	EMU-D	3-13	DST

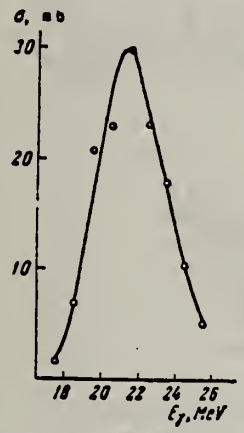

Fig.1. Variation of the Zr(γ,p) reaction cross section with E_γ.

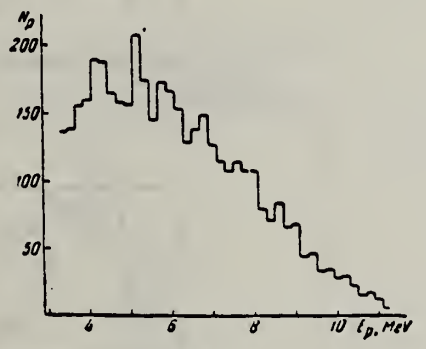

Fig. 2

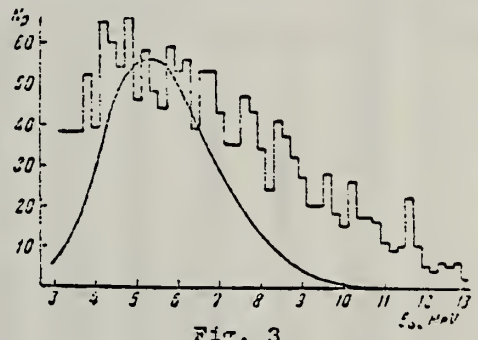

Fig. 3

Fig.2. Spectrum of photoprotons from zirconium with irradiation of the target by γ rays with $E_{\gamma\ max}$ = 22 MeV.

Fig.3. Spectrum of photoprotons from zirconium with $E_{\gamma\ max}$ = 25 MeV. The smooth curve represents the spectrum calculated on the basis of the statistical model.

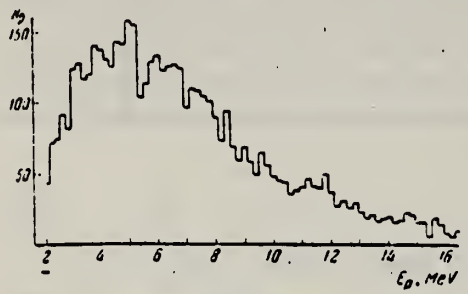

Fig. 4

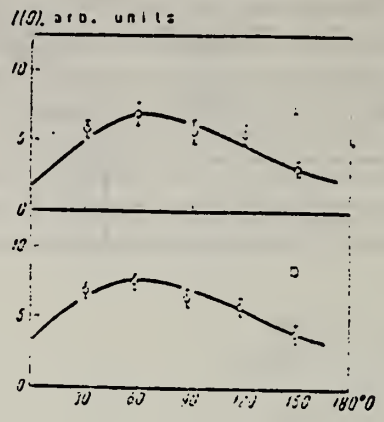

Fig. 5

Fig.4. Spectrum of photoprotons from zirconium with $E_{\gamma\ max}$ = 34 MeV.

Fig.5. Angular distributions of different groups of protons (Zr target irradiated with $E_{\gamma\ max}$ = 25 MeV bremsstrahlung): a - E_p > 7 MeV, b - E_p > 4 MeV.

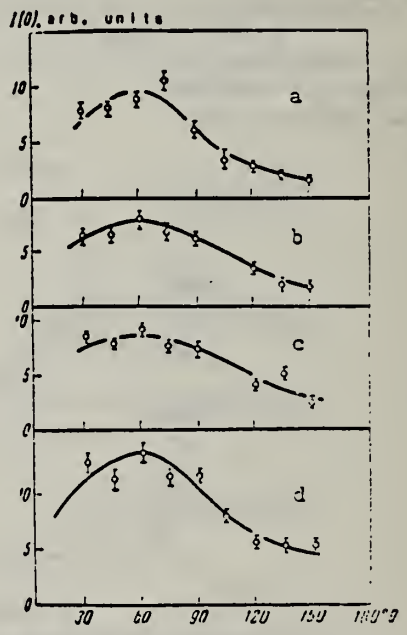

Fig.6. Angular distributions of different proton groups (target irradiated with $E_{\gamma\ max}$ = 34 MeV bremsstrahlung): a - E_p = 12-17 MeV, b - E_p = 9-12 MeV, c - E_p = 5.6-9.0 MeV, d - E_p = 3.5-5.5 MeV.

REF. G. Ben-David, B. Arad, J. Balderman, and Y. Schlesinger
Phys. Rev. 146, B852 (1966)

ELEM. SYM.	A	Z
Zr		40

METHOD

Nuclear Resonance Scattering using N,G reactions.

REF. NO. 66 Be 3 JDM

REACTION	RESULT	EXCITATION ENERGY	SOURCE TYPE	SOURCE RANGE	DETECTOR TYPE	DETECTOR RANGE	ANGLE
G,G	RLX	5 - 10	D	5 - 10	NAI-D	5 - 10	135

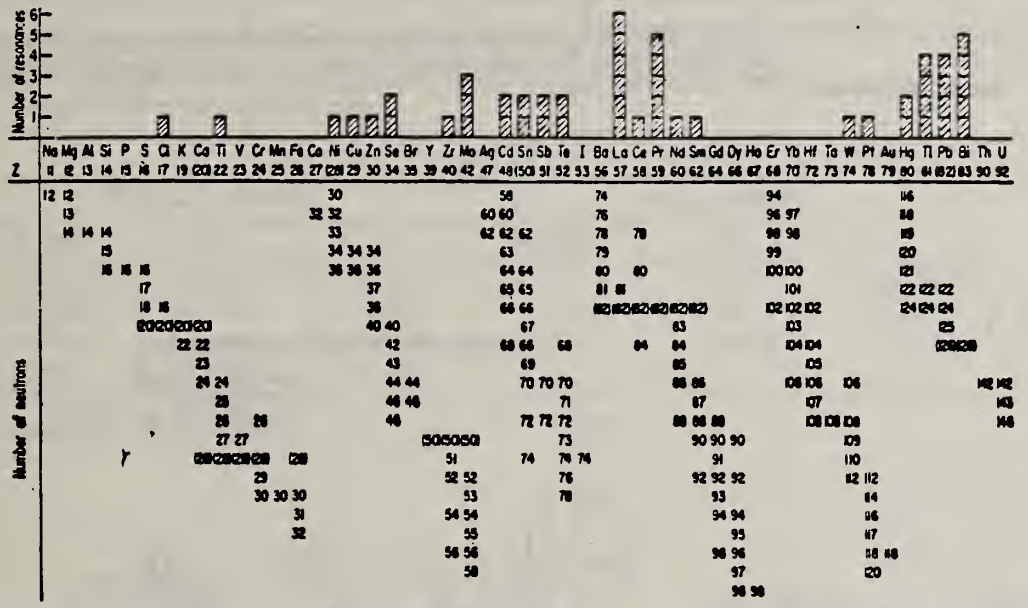

FIG. 3. Histogram of distribution of observed resonances among the different targets. The atomic number is given directly beneath the chemical symbol followed by the neutron numbers of the naturally occurring isotopes. Magic numbers are shown in brackets.

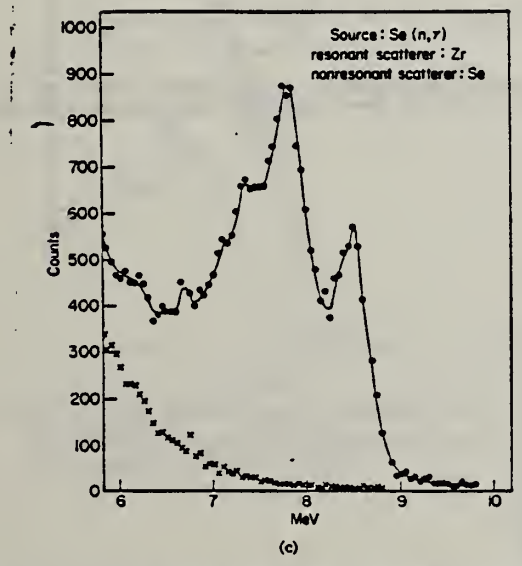

Fig. 1.(c)Complex scattered spectrum from Zr excited by Se capture gamma rays (with Se background).

TABLE III. List of effective cross sections.

Scatterer	Energy (MeV)	Gamma source	δ (mb)	Scatterer	Energy (MeV)	Gamma source	δ (mb)
Sm^{146}	8.997	Ni	100	Sn	7.01	Cu	110
Pr^{141}	8.881	Cr	9	Nd	6.867	Co	30
La	8.532	Ni	6	Pr^{141}	6.867	Co	3
Te	8.532	Ni	3[a]	Te	6.7	Ni	...
Cu	8.499	Cr	24	La	6.54	Ag	12
Zr	8.496	Se	3050	Cd	6.474	Co	110
Zn	8.119	Ni	13	Mo	6.44	Hg	25[g]
Se	7.817	Ni	50	La	6.413	Ti	72
Se	7.76	K	90	Mo	6.413	Ti	10
Sb	7.67	V	...[b]	Tl	6.413	Ti	25
Cd	7.64	Fe	40[a]	W	~6.3	Ti	...[b]
Ni	7.64	Fe	7[a]	Sb	6.31	Hg	6[a]
Pr^{141}	7.64	Fe	12[a]	Ti	6.31	Hg	2[a]
Tl	7.64	Fe	370[a]	Sn	6.27	Ag	75
La	7.634	Cu	7	Pb^{206}	6.15	Gd	...[g]
Mo	7.634	Cu	11	Te	5.8	Ni	...[f]
Bi^{209}	7.634	Cu	4	La	6.12	Cl	35
Te	7.528	Ni	66[d]	Pr^{141}	6.12	Cl	110
Bi^{209}	7.416	Se	100	Pt	5.99	Hg	40[a,g]
Bi^{209}	7.300	As	80[a]	Tl	5.99	Hg	5[g]
Pb^{206}	7.285	Fe	4100	Pb^{206}	5.9	Sr	...[h]
Cl	7.285	Fe	34	Ce	5.646	Co	17
Pr^{141}	7.185	Se	80	Bi^{209}	5.646	Co	55
Tl	7.16	Cu	120	Pb^{206}	5.53	Ag	70
La	7.15	Mn	50	Hg	5.44	Hg	75[g]
Bi^{209}	7.149	Ti	2000	Hg	4.903	Co	385

[a] High-energy component of a complex spectrum.
[b] A broad scattered spectrum with no observable peak structure.
[c] There are actually two lines of energies 7.647 and 7.633 MeV having equal intensities in the iron capture gamma spectrum. The cross section has therefore been corrected, although there is no possibility at present of deciding which line is responsible for each resonance.
[d] Is probably an independent level in the complex spectrum of Ni γ rays on Te.
[e] Rough estimate.
[f] May be inelastic component from 7.528 level in Te.
[g] The relative line intensities in this case are due to Groshev and co-workers.
[h] No line is known for the source at this energy.
[i] Difficult to resolve among the many source lines present at this energy.

REF. S. M. Hussain and K. G. McNeill
Can. J. Phys. 45, 2851 (1967)

ELEM. SYM.	A	Z
Zr		40

METHOD

REF. NO. 67 Hu 2 — EGF

REACTION	RESULT	EXCITATION ENERGY	SOURCE		DETECTOR		ANGLE
			TYPE	RANGE	TYPE	RANGE	
G,N	ABY	THR-22	C	22	THR	4-	DST

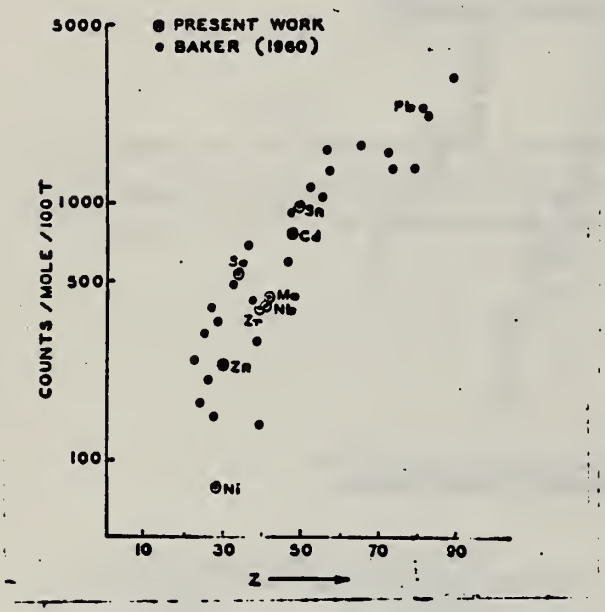

FIG. 3. The yields of fast photoneutrons from various elements as measured in the present work and by Baker. The present results have been normalized to Baker's measurements for lead.

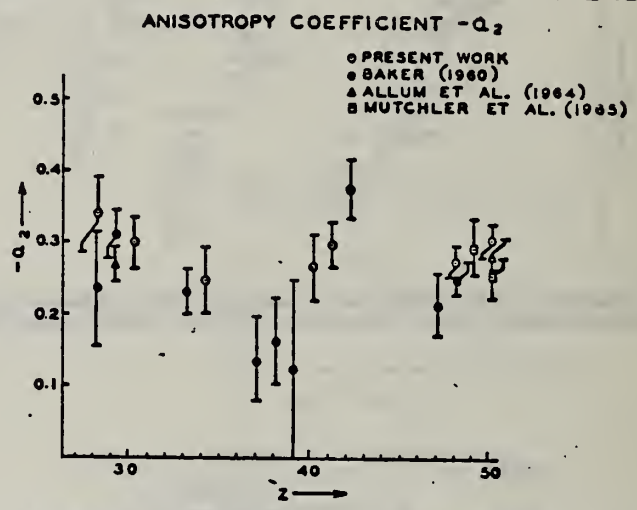

FIG. 2. The anisotropy coefficients a_2, in the formula $W(\theta) = a_0(1 + a_1P_1 + a_2P_2)$, obtained in the present work, and those obtained by other workers in the same part of the Periodic Table.

TABLE I

Element	a_0*	a_1	a_2
Nickel	77 (1.0±0.05)	0.14±0.04	−0.34±0.06
Zinc	236 (1.0±0.04)	0.06±0.03	−0.30±0.04
Selenium	525 (1.0±0.05)	0.10±0.04	−0.25±0.05
Zirconium	380 (1.0±0.05)	0.03±0.04	−0.27±0.05
Niobium	392 (1.0±0.03)	0.01±0.02	−0.30±0.03
Molybdenum	410 (1.0±0.03)	0.05±0.03	−0.41±0.04
Cadmium	755 (1.0±0.02)	0.05±0.01	−0.28±0.02
Tin	955 (1.0±0.02)	0.08±0.02	−0.30±0.02
Lead	2274 (1.0±0.02)	0.06±0.02	−0.48±0.02

*For comparison purposes the experimental value of a_0 for Pb has been normalized to coincide with that obtained by Baker and McNeill (1961) and is the yield per mole per 100 roentgen. All other values of a_0 have also been quoted with the same normalization.

REACTION	RESULT	EXCITATION ENERGY	SOURCE		DETECTOR		ANGLE
			TYPE	RANGE	TYPE	RANGE	
G,P	ABX	8-24	C	20,24	EMU-D	2-14	DST
				(20.5)			

Table II. Anisotropic factor B/A and asymmetry factor p of angular distributions determined by least-square fits with $A+B(1+p\cos\theta)\sin^2\theta$.

Zr					
($E_{\gamma max}$=20.5 MeV)			($E_{\gamma max}$=24.0 MeV)		
E_p(MeV)	B/A	p	E_p(MeV)	B/A	p
2.5–4.4	6.26±0.09	−0.9±0.4	3.5– 7.3	−0.1±0.1	−2.4±2.6
4.4–6.7	1.0 ±0.2	0.6±0.2	7.3–11.5	0.7±0.4	1.0±0.7
6.7–8.6	4.3 ±3.4	0.7±0.3	11.5≦	1.3±1.9	1.2±1.6
8.6≦	7.1 ±9.5	1.3±0.4			

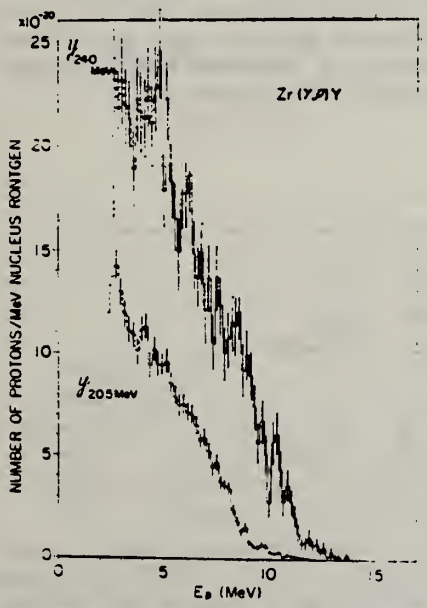

Fig. 2. Energy distributions of photoprotons from Zr irradiated with the bremsstrahlung at maximum energy of 24.0 and 20.5 MeV.

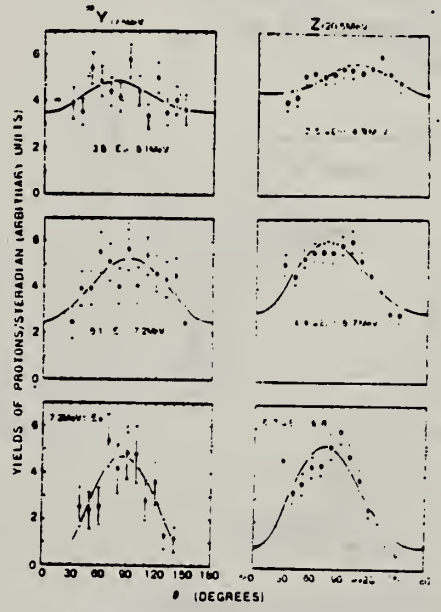

Fig. 3. Examples of angular distributions of photoprotons from ^{89}Y and Zr.

REACTION	RESULT	EXCITATION ENERGY	SOURCE TYPE	SOURCE RANGE	DETECTOR TYPE	DETECTOR RANGE	ANGLE

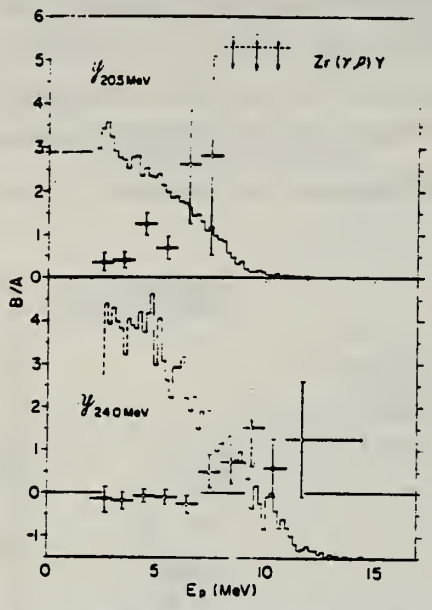

Fig. 5. Energy dependence of the anisotropic factor B/A of the angular distributions for photoprotons from Zr. See also the caption for Fig. 4.

A sign ⊣ indicates that B/A is too large to plot the figure.

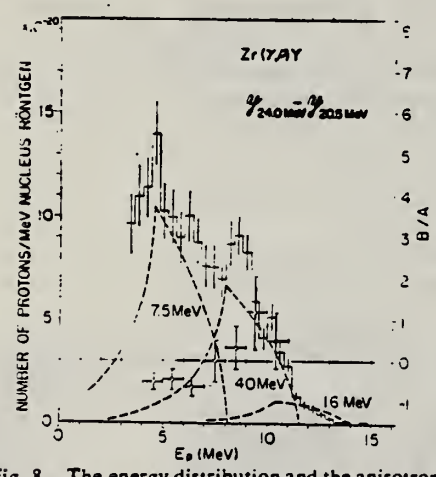

Fig. 8. The energy distribution and the anisotropic factor B/A for photoprotons from Zr obtained by subtraction of $\gamma_{20.5\,MeV}$ from $\gamma_{24.0\,MeV}$. See also the caption for Fig. 6.

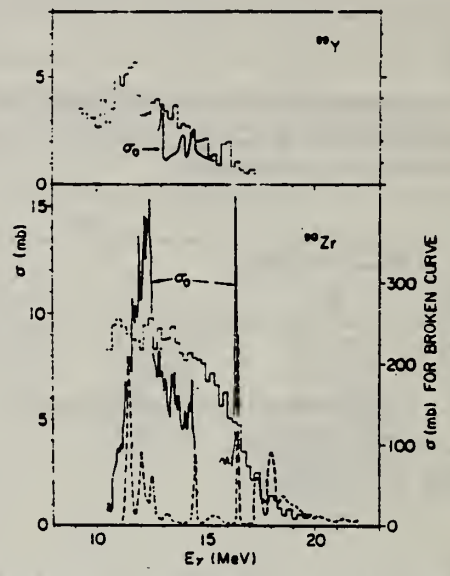

Fig. 9. The (γ, p) cross sections of ^{89}Y and Zr in the photon energy region lower than 20 MeV. The (γ, p_0) cross sections deduced from the inverse reaction cross sections are shown by solid lines indicated by σ_0. Theoretical $^{90}Zr(\gamma, p_0)^{89}Y$ cross section[19] is shown by broken line.

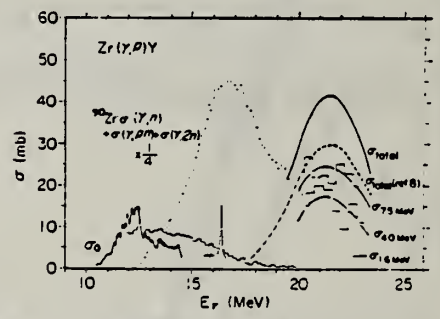

Fig. 11. Cross sections for strong photoproton transitions on Zr. Photoproton cross section obtained from the yield curve,[9] neutron emission cross section[20] and the results of the $^{89}Y(p, \gamma_0)^{90}Zr$ reaction[4,5,11,12] are also shown.

REF. P. Axel, K. K. Min, and D. C. Sutton
Phys. Rev. C2, 689 (1970)

EL EM. SYM.	A	Z
Zr		40

METHOD

REF. NO.	
70 Ax 1	hmg

REACTION	RESULT	EXCITATION ENERGY	SOURCE		DETECTOR		ANGLE
			TYPE	RANGE	TYPE	RANGE	
G,G	ABX	8-13	D	8-13	NAI-D		22

Total photon interaction cross section inferred.

[13]B.L. Berman, J.T. Caldwell, R.R. Harvey, M.A. Kelly, R.L. Bramblett, and S.C. Fultz, Phys. Rev. 162, 1098 (1967).

[19]E. Obst, F. Rauch, and E. Rossle, Phys. Letters 21, 50 (1966).

[20]E. Obst, F. Rauch, and H. G. Wahsweiler, Nucl. Phys. A103, 17 (1967).

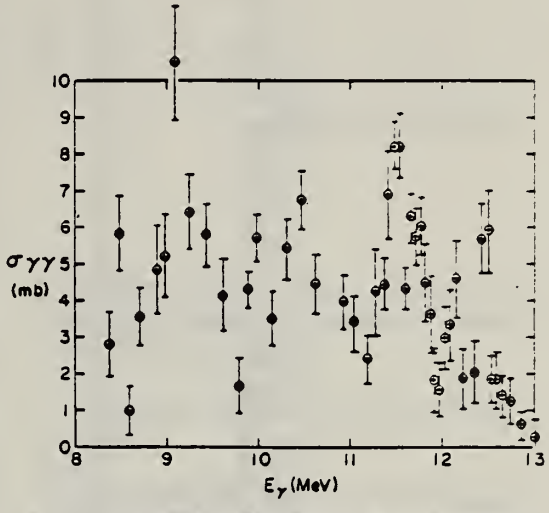

FIG. 1. The photon elastic-scattering cross section of Zr. The values assume that only ^{90}Zr contributes above 8.68 MeV. Numerical values are given in Table II.

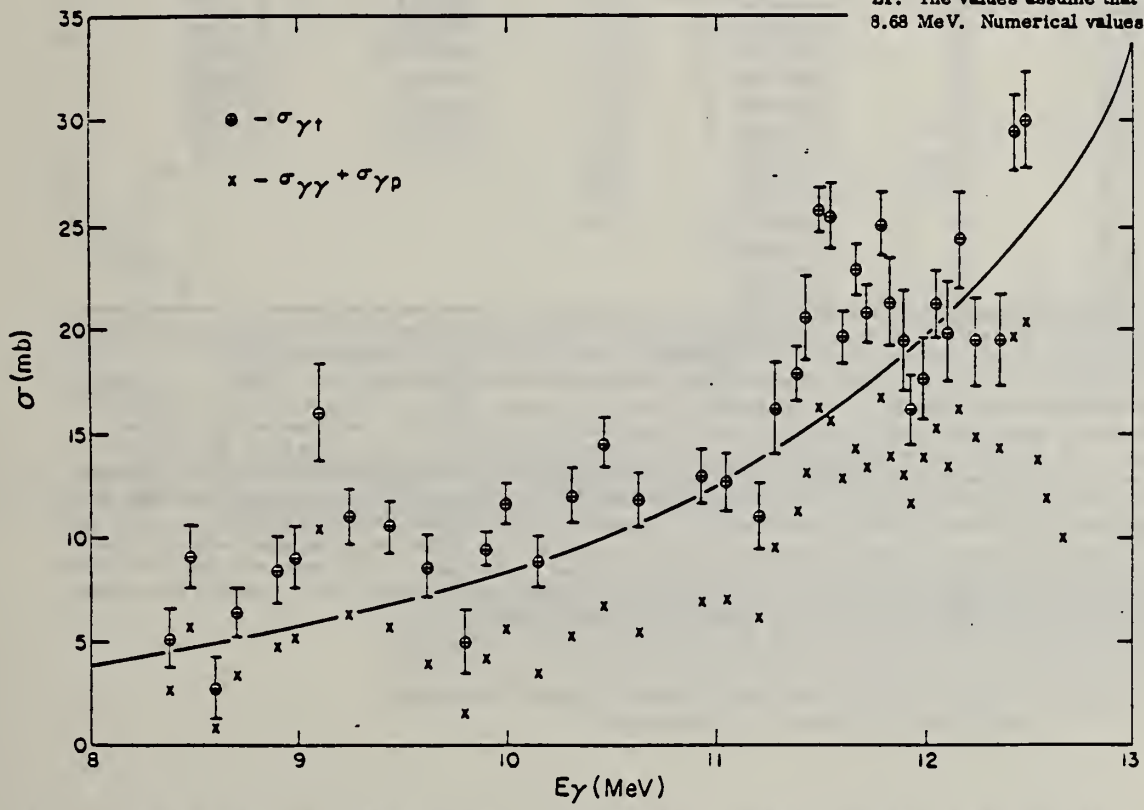

FIG. 4. The photon interaction cross section of ^{90}Zr. It was assumed that the elastic photon scattering above 8.68 MeV was due to ^{90}Zr. The inferred cross sections are shown by the circled crosses with experimental errors corresponding to the statistical uncertainty in only the elastic-scattering cross section. Below 10.62 MeV, the measured photon scattering cross section is shown by the diagonal crosses; at and above the 10.62 MeV the diagonal crosses represent the sum of the elastic scattering and photoproton cross sections inferred from the data in Refs. 19 and 20. The line is the low-energy extrapolation of the Lorentz line which matches the photoneutron cross section of ^{90}Zr in the giant resonance region according to Ref. 19.

over

TABLE II. Photon cross sections for ^{90}Zr. See Sec. IX for an explanation of the headings and entries in this table.

E_γ (MeV)	ΔE_γ (keV)	$\sigma_{\gamma\gamma}$[a] (mb)	$\sigma_{\gamma p_0}$[b] (mb)	$\sigma_{\gamma t}$[a] (mb)	Single-particle units per MeV
8.38	60	2.79 ± 0.90		5.2 ± 1.4	0.047
8.49	60	5.84 ± 1.03		9.2 ± 1.5	0.082
8.60	60	1.00 ± 0.69		2.8 ± 1.5	0.024
8.70	110	3.55 ± 0.80		6.5 ± 1.2	0.055
8.89	60	4.84 ± 1.22		8.5 ± 1.6	0.068
8.98	60	5.21 ± 1.15		9.1 ± 1.5	0.072
9.09	60	10.51 ± 1.61		15.8 ± 2.3	0.125
9.24	60	6.38 ± 0.95		11.1 ± 1.3	0.083
9.43	120	5.78 ± 0.87		10.6 ± 1.2	0.076
9.61	60	4.14 ± 0.99		8.7 ± 1.5	0.061
9.79	60	1.68 ± 0.76		5.0 ± 1.5	0.033
9.88	70	4.31 ± 0.49		9.5 ± 0.8	0.063
9.98	70	5.70 ± 0.63		11.7 ± 1.0	0.075
10.14	110	3.48 ± 0.74		8.9 ± 1.3	0.055
10.31	70	5.40 ± 0.85		12.1 ± 1.3	0.073
10.46	80	6.75 ± 0.08		14.6 ± 1.2	0.085
10.62	120	4.45 ± 0.78	1.1	11.9 ± 1.3	0.056
10.92	70	3.95 ± 0.73	3.1	13.0 ± 1.3	0.069
11.04	70	3.39 ± 0.76	3.7	12.7 ± 1.4	0.067
11.20	70	2.41 ± 0.66	3.8	11.1 ± 1.6	0.057
11.28	70	4.28 ± 1.15	5.3	16.3 ± 2.2	0.082
11.38	70	4.48 ± 0.73	6.8	17.9 ± 1.3	0.088
11.42	70	6.88 ± 1.19	6.3	20.6 ± 2.0	0.100
11.49	70	8.20 ± 0.66	8.0	25.7 ± 1.1	0.124
11.54	70	8.20 ± 0.88	7.5	25.4 ± 1.6	0.122
11.60	70	4.33 ± 0.57	8.6	19.6 ± 1.2	0.095
11.66	70	6.28 ± 0.67	8.1	22.9 ± 1.2	0.109
11.71	70	5.75 ± 0.80	7.7	21.8 ± 1.4	0.101
11.78	70	6.05 ± 0.80	10.7	25.0 ± 1.5	0.116
11.82	70	4.50 ± 1.04	9.6	21.3 ± 2.1	0.098
11.88	70	3.63 ± 1.08	9.5	19.5 ± 2.4	0.089
11.92	70	1.85 ± 0.87	9.9	16.2 ± 1.7	0.073
11.98	70	1.55 ± 0.74	12.4	17.7 ± 2.0	0.079
12.04	70	2.99 ± 0.87	12.3	21.2 ± 1.6	0.093
12.09	70	3.33 ± 0.97	10.2	19.9 ± 2.4	0.088
12.16	70	4.60 ± 1.08	11.6	24.3 ± 2.3	0.105
12.23	70	1.88 ± 0.81	13.0	19.4 ± 2.1	0.083
12.35	70	2.05 ± 0.84	12.3	19.5 ± 2.2	0.082
12.42	70	5.71 ± 0.94	14.0	29.4 ± 1.8	0.122
12.47	70	5.91 ± 1.14	14.4	30.0 ± 2.3	0.124
12.54	80	1.85 ± 0.64	12.0		
12.58	80	1.85 ± 0.81	10.2		
12.66	80	1.38 ± 0.57	8.6		
12.74	80	1.28 ± 0.64			
12.86	80	0.60 ± 0.40			
13.01	80	0.27 ± 0.50			

[a] Assuming that ^{90}Zr and ^{92}Zr have equal cross sections below 8.68 MeV and that only ^{90}Zr contributes above 8.68 MeV. The listed errors include only the effects of the statistical uncertainty in the number of scattered γ rays.

[b] The photoproton cross sections were calculated from the graphs of the p,γ_0 reaction in Refs. 19 and 20. An isotropic angular distribution was assumed. The cross section in Ref. 20 was used to obtain an absolute scale for the data of Ref. 19 near 12-MeV excitation. In accordance with a private communication from Rauch, it was assumed that the detector used in Ref. 19 decreased in efficiency with increasing energy by 5% per MeV. Above 11.95 MeV, the photoproton cross sections are averages of the precise, very good resolution data of Ref. 20 over 100-keV intervals; the relative cross sections in this energy region should have negligible error. The reliability of the relative cross sections at lower energy appears to be of the order of or less than 10%. For example, there are local maxima at about 11.36, 11.45, and 11.63 MeV which are about 10% and which appeared in both the 0 and 90° data of Ref. 19; on the other hand, the 0 and 90° data differ from each other by about 10% in the energy range covered. The absolute cross section was estimated to have an uncertainty of 20% in Ref. 20. However, near 12.4 MeV, the absolute cross section of Ref. 21 (which is also estimated as being correct to within 20%) is about 1.5 times the value given in Ref. 20.

REF.

R.F. Barrett, J.R. Birkelund, B.J. Thomas, K.S. Lam, and H.H. Thies
Nucl. Phys. A210 , 355 (1973)

ELEM. SYM.	A	Z
Zr		40

METHOD

REF. NO.	
73 Ba 20	egf

REACTION	RESULT	EXCITATION ENERGY	SOURCE		DETECTOR		ANGLE
			TYPE	RANGE	TYPE	RANGE	
G,N	NOX	THR- 27	C	10- 27	BF3-I		4PI

MEAN NEUT ENERGY

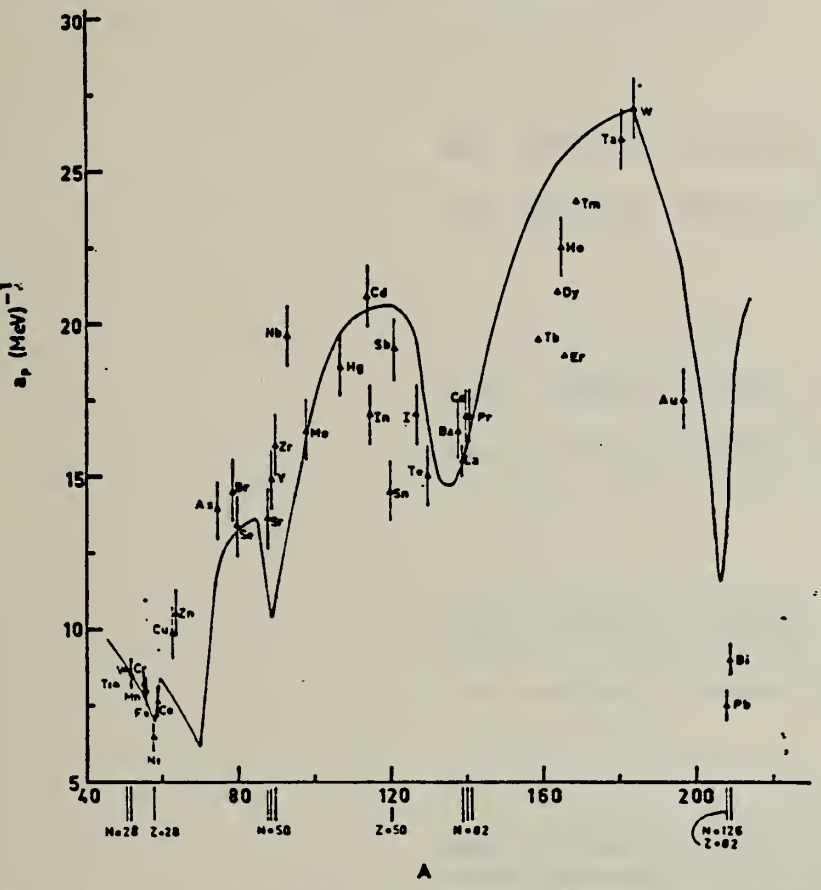

Fig. 12. Experimental values of the level density parameter a_p (Fermi gas formula plus pairing correction) versus atomic number A. The continuous curve is a least-squares fit to the data of a theoretical calculation from Newton [15].

1
H. Baba and S. Baba, Japan Atomic Energy Research Institute report JAERI-1183 (1969).

2
H. Baba, Nucl. Phys. A159, 625 (1970).

15
T.D. Newton, Can. J. Phys. 34, 804 (1956).

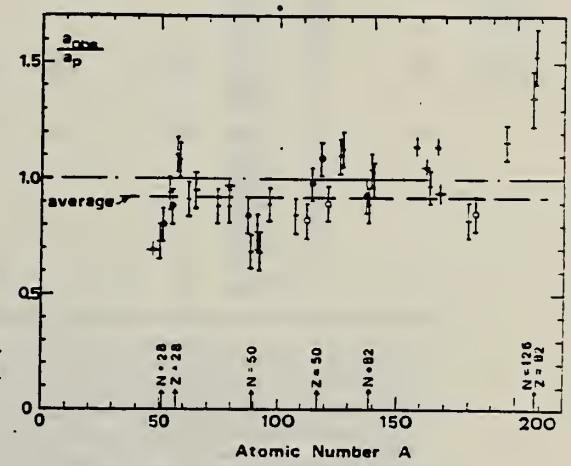

Fig. 15. Ratio a_{obs}/a_p versus atomic number A. Here a_{obs} is the level density parameter taken from the neutron resonance work of refs. [1,2]), and a_p is the level density parameter derived from the present (γ, n) work. Filled circles represent points where nuclei in the neutron resonance and in the (γ, n) experiment were the same. Open circles represent points where the respective nuclei were approximately matched. Triangles represent points which are based on measurement of neutron mean energies at two bremsstrahlung energies only.

(over)

TABLE 3 (continued)

Target	N (residual nucleus) [a]		Goodness of fit [b]		$\hat{E}_0(24)$ (MeV) [c]	T (MeV) [d]	a_p (MeV^{-1}) [e]	a_{obs} (MeV^{-1}) [f]	a_{obs}/a_p
			no p.c.	with p.c.					
Y	49	100%	G	G	1.30		14.9–^{88}Y	10.17–^{90}Y	0.68
Zr	49	52%	F	F	1.28		16.0–^{90}Zr	12.2 –^{91}Zr	0.77
	50	11%							
	51	17%							
	53	17%							
	55	3%							
Nb	51	100%	F	F	1.28		19.6–^{92}Nb	13.15–^{94}Nb	0.68
Mo	49	16%	G	G	1.27		16.5–^{93}Mo	14.7 –^{97}Mo	0.89
	51	9%							
	52	16%							
	53	17%							
	54	10%							
	55	24%							
	57	8%							
Ag	59	51%	V.P.	F	1.27	0.55	18.6–^{107}Ag	15.61–^{108}Ag	0.84
	61	49%							
Cd	57	1%	V.P.	F	1.24	0.54	20.9–$^{111.4}$Cd	17.0 –^{112}Cd	0.82
	61	12%							
	62	13%							
	63	24%							
	64	12%							
	65	29%							
	67	8%							
In	63	4%	V.P.	F	1.26	0.57	17.0–^{114}In	16.66–^{114}In	0.98
	65	96%							
Sn ($Z = 50$)	65	14%	V.P.	V.P.	1.38	0.73	14.5–^{118}Sn	15.9 –^{118}Sn	1.09
	66	8%							
	67	24%							
	68	9%							
	69	33%							
	71	5%							
	73	6%							
Sb	69	57%	V.P.	P	1.2	0.68	19.2–^{121}Sb	17.0 –^{121}Sb	0.89
	71	43%							
Te	69	2%	V.P.	F	1.36	0.83	15.0–^{127}Te	17.0 –^{127}Te	1.13
	71	5%							
	72	7%							
	73	19%							
	75	32%							
	77	34%							
I	73	100%	F	G	1.23	0.70	17.0–^{126}I	17.02–^{128}I	1.00

[a]) Neutron numbers and abundances of respective residual nuclei in (γ, n) experiments.

[b]) These give an assessment of the goodness of fit of a calculated $\hat{E}_n$ versus E_0 curve to the observed data, using the Fermi gas level density formula both without and with pairing corrections.

[c]) Bremsstrahlung photoneutron mean energies $\hat{E}_n$ for peak bremsstrahlung energy $E_0 = 24$ MeV.

[d]) Nuclear temperature from fit with constant-temperature formula.

[e]) Level density parameter a_p derived from the present (γ, n) experiment, using a Fermi gas formula plus pairing correction, and corresponding residual nucleus (the atomic weight shown is the weighted average of atomic weights of the respective isotopes present).

[f]) As column 7, but using data on n-resonance absorption from refs. [1,2]).

[g]) Measurements of $\hat{E}_n(E_0)$ for these nuclei were made only for $E_0 = 21$, 23 and 24 MeV.

Zr
A=89

Zr
A=89

Zr
A=89

REF.

S. Costa, F. Ferrero, S. Ferroni, L. Pasqualini and E. Silva - also Istituto Nazionale di Fisica Nucleare - Sezione di Torino
Nuclear Phys. 72, 158 (1965)

ELEM. SYM.	A	Z
Zr	89	40

METHOD

REF. NO.	
65 Co 1	EGF

REACTION	RESULT	EXCITATION ENERGY	SOURCE		DETECTOR		ANGLE
			TYPE	RANGE	TYPE	RANGE	
G,N	ABX	THR - 70	C	12 - 70	ACT-I		4PI

Measured isomer production ratio.
Spin cut off < 1.5

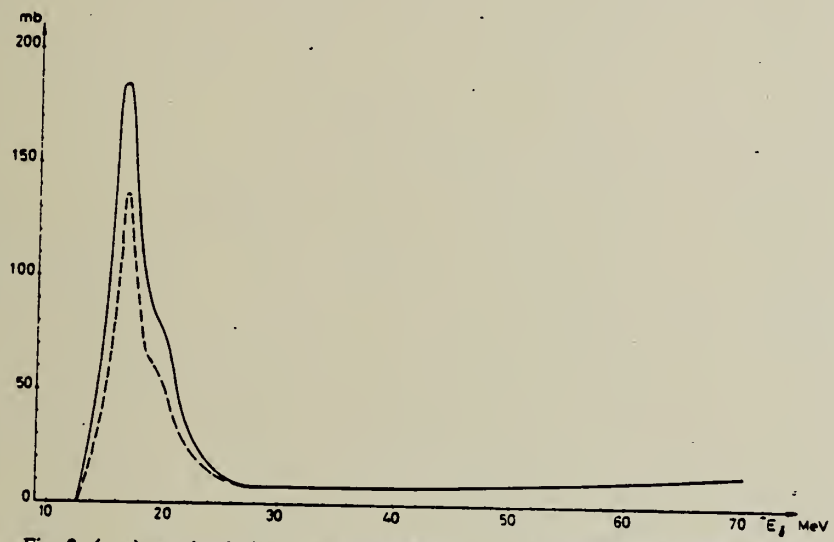

Fig. 2. (γ, n) reaction in ^{90}Zr, total (solid line) and $\frac{1}{2}^-$ state (dashed line) cross sections.

TABLE 1
Spins and half-lives of isomeric states

Target nucleus	Spin of isomeric states	Half-life	Modes of decay (used for detection)	Detection method
^{39}K	0^+	0.95 sec	β^+ (100 %)	γ–γ fast-slow coincidence (resolving time 0.2 and 2 μsec)
$J = \frac{3}{2}$	3^+	7.7 min	β^+ (> 99 %)	γ–γ coincidence
^{90}Zr	$\frac{1}{2}^-$	4.3 min	γ (93 %)	NaI (well type) spectrometer centered on the 0.588 MeV γ ray line
			β^+ (1.7 %)	γ–γ coincidence
$J = 0$	$\frac{1}{2}^+$	79 h	β^+ (30 %)	γ–γ coincidence
^{93}Mo	$\frac{1}{2}^-$	66 sec	γ (57 %)	NaI (well type) spectrometer centered on the 0.658 MeV γ ray line
			β^+ (38 %)	γ–γ coincidence
$J = 0$	$\frac{1}{2}^+$	16 min	β^+ (94 %)	γ–γ coincidence

Zr
A=90

Zr
A=90

Zr
A=90

Ref. P. Axel, J.D. Fox
Phys. Rev. 102, 400 (1956)

Elem. Sym.	A	Z
Zr	90	40

Method: Betatron; Victoreen ionization in 8 cm Lucite; radioactivity

Ref. No.: 56 Ax 1 EGF

Reaction	E or ΔE	E_o	Γ	$\int \sigma dE$	Jπ	Notes
(γ,n)	Bremss. 11.8-22.5					79 hour (ground state) E_{th}=11.78±0.09 MeV. 4.4 min (m.s.), E_{th}= 12.37±0.09 MeV. Figure 7: Work based on separation of 913 keV γ (79 hour) from 588 keV (4.4 min). Rise in "c" above 18.5 MeV probably comes from $Zr^{91}(\gamma,2n)Zr^{89}$ ground state. Zr^{90} - 51.5% Zr^{91} - 11.2% Zr^{92} - 17.1% Zr^{94} - 17.4% Zr^{96} - 2.8%

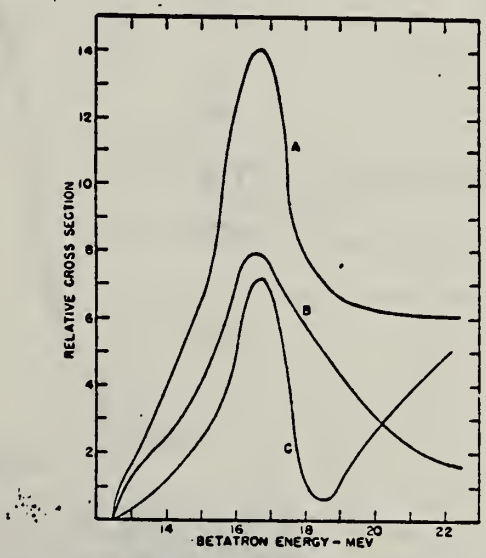

FIG. 7. Relative cross sections. Curve *A* is the cross section for the formation of the 79-hour activity, Curve *B* the formation cross section of the 4.4-minute activity, and Curve *C* the direct production cross section of the 79-hour activity.

Ref. P.F. Yergin, B.P. Fabricand
Phys. Rev. 104, 1334 (1956)

Elem. Sym.	A	Z
Zr	90	40

Method: 24 MeV betatron; 250r Victoreen in 3.75 cm Lucite; neutron detector

Ref. No.: 56 Ye 2 | EGF

Reaction	E or ΔE	E_o	Γ	$\int \sigma dE$	Jπ	Notes
Zr^{90} (γ,xn)	Bremss. 24	15.8	4.3 MeV	$\int_0^{23}$ =0.98 MeV-b		

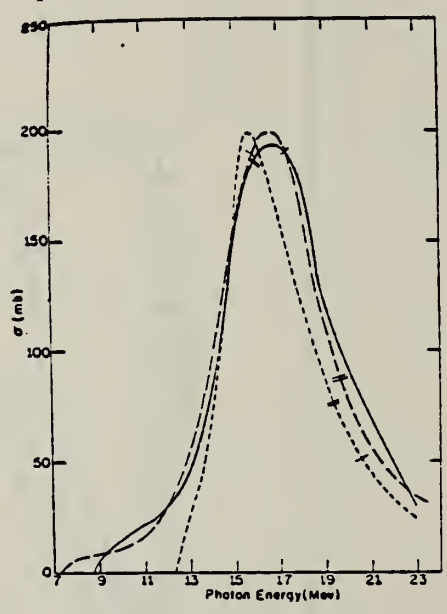

FIG. 5. Cross sections for the (γ,n) reactions in zirconium isotopes. Short dashes Zr^{90}, long dashes Zr^{91}, full curve Zr^{92}. The previously published Zr^{90} and Zr^{91} results have been recomputed, taking into account the present Zr^{92} measurements. The single and double slash marks on each curve represent the locations of the (γ,pn) and (γ,2n) thresholds respectively. The units of the ordinate are 10^{-27} cm².

TABLE III. Parameters of giant-resonance cross-section curves for (γ,n) reactions in nuclei near 50 neutrons. Nuclides $_{33}As^{75}$, $_{41}Nb^{93}$, and $_{45}Rh^{103}$ from reference 4, $_{40}Zr^{90}$ and $_{40}Zr^{91}$ from reference 5 recomputed in present work. Neutron number is shown in column 2, location of peak cross-section value in column 3, peak cross-section value in column 4, half-height width of curve in column 5, and area under curve from threshold to 23 Mev in column 6.

Nuclide	N	E_m (Mev)	σ_m (millibarns)	Γ (Mev)	$\int_0^{23}\sigma dE$ (Mev-barns)
$_{33}As^{75}$	42	17.3	90.3	9.0	0.80
$_{38}Sr^{86}$	48	15.9	160	5.0	0.92
$_{38}Sr^{87}$	49	15.8	146	5.3	1.00
$_{38}Sr^{88}$	50	16.3	201	4.0	1.05
$_{39}Y^{89}$	50	16.3	191	3.8	0.87
$_{40}Zr^{90}$	50	15.8	199	4.3	0.98
$_{40}Zr^{91}$	51	16.5	200	5.0	1.22
$_{40}Zr^{92}$	52	16.9	193	5.5	1.24
$_{41}Nb^{93}$	52	17.0	195	6.8	1.46
$_{45}Rh^{103}$	58	16.5	205	8.9	1.94

Ref. N. Mutsuro, Y. Ohnuki, K. Sato, M. Kimura
J. Phys. Soc. Japan 14, 1649 (1959)

Elem. Sym.	A	Z
Zr	90	40

Method Betatron; neutron yield; radioactivity; r- chamber

Ref. No. 59 Mu 2 | NVB

Reaction	E or ΔE	E_o	Γ	$\int \sigma dE$	Jπ	Notes
$Zr^{90}(\gamma,n)$	Bremss. 12-25	16.8	2.9 MeV			

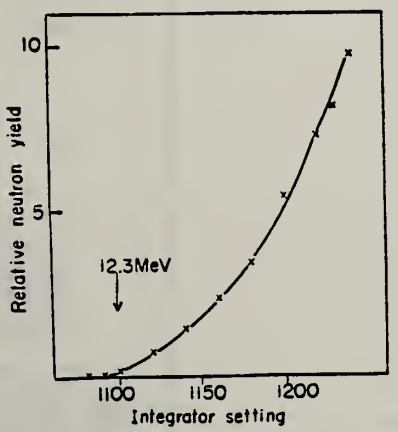

Fig. 3-1. Activation curve near threshold for $Zr^{90}(\gamma, n)Zr^{89m}$.

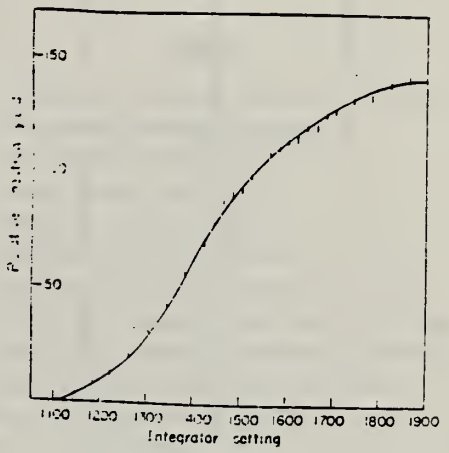

Fig. 4-1. Activation curve for $Zr^{90}(\gamma, n)Zr^{89m}$.

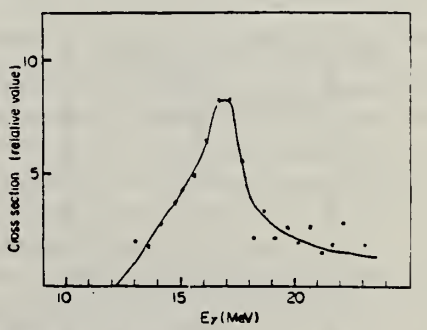

Fig. 5-1. Cross section curve for $Zr^{90}(\gamma, n)Zr^{89m}$.

Ref. R. Nathans, P.F. Yergin
Phys. Rev. 98, 1296 (1955)

Elem. Sym.	A	Z
Zr	90	40

Method BF_3 counters; 24 MeV Bremss.; Betatron

Ref. No. 59 Na 1 EGF

Reaction	E or ΔE	E_o	Γ	$\int \sigma dE$	Jπ	Notes
(γ,xn)	5.0-24	16.0	4.1	0.89 MeV-mb		E_{th} = 12.2 MeV; σ_{max} = 18.5 mb. No Corrections. [NOTE: Figure 3: Ref 8: Katz, Baker, Montalbetti, Can j. Phys. 31, 250 (1953).]

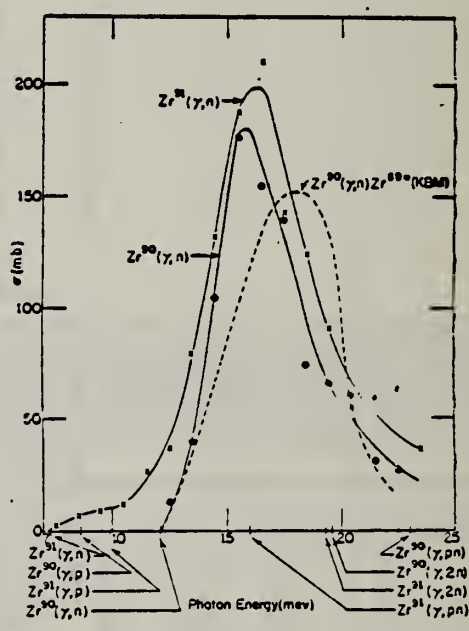

FIG. 3. (γ,n) cross sections for Zr^{90} and Zr^{91}. The ordinate scale is in millibarns (10^{-27} cm^2). The points shown are those calculated from the yield data. The solid curves are drawn to fit the points. The dashed curve is the cross section reported (see reference 8) for the production of the isomeric state of Zr^{89} by photon bombardment of natural Zr. The locations of the thresholds for various reactions in the two isotopes are indicated by the arrows.

Ref. J.H. Carver, G.E. Coote, T.R. Sherwood
Nuclear Phys. 37, 449 (1962)

Elem. Sym.	A	Z
Zr	90	40

Method: 30 MeV electron synchrotron; activation; NaI

Ref. No.: 62 Ca 1 JHH

Reaction	E or ΔE	E_0	Γ	$\int \sigma dE$	Jπ	Notes
$Zr^{90}(\gamma,n)$	Bremss. 30					

TABLE 1

Isomeric Ratios from (γ,n) reactions

Target Nucleus	J_0	Residual Nucleus	Ground state Spin	Ground state Half-life	Metastable state Spin	Metastable state Half-life	Isomer state Spin	Isomer ratio $Y_1/(Y_1+Y_2)$	*
Co^{59}	$7/2^-$	Co^{58}	2^+	71.3d	5^+	9.2h		0.44 ± 0.02	3.2 ± 0..
Ge^{76}	0^+	Ge^{75}	$1/2^-$	82m	$7/2^+$	49s		0.48 ± 0.07	2.8 ± 0..
Br^{81}	$3/2^-$	Br^{80}	1^+	18m	5^-	4.4h	2^-	0.32 ± 0.02	6.5 ± 1..
Sr^{86}	0^+	Sr^{85}	$9/2^+$	64d	$1/2^-$	70m	$7/2^+$	0.36 ± 0.07	2.2 ± 0..
Zr^{90}	0^+	Zr^{89}	$9/2^+$	79h	$1/2^-$	4.4m		0.33 ± 0.10	2.8 ± 0.7
Mo^{92}	0	Mo^{91}	$9/2^+$	15.7m	$1/2^-$	66s		0.46 ± 0.04	6^{+4}_{-2}
Ag^{107}	$1/2^-$	Ag^{106}	1^+	24m	6	9.3d		0.04 ± 0.02	2.0 ± 0.5
In^{115}	$9/2^+$	In^{112}	1^+	14.5m	4^+	20.7m	7^-	0.6 ± 0.1	3.1 ± 0.7
Cd^{116}	0^+	Cd^{115}	$1/2^+$	53h	$11/2^-$	45d		≤ 0.2	≤ 5
Ce^{140}	0^+	Ce^{139}	$3/2^+$	140d	$11/2^-$	55s		0.38 ± 0.01	2.5 ± 0.2
Hg^{198}	0^+	Hg^{197}	$1/2^-$	65h	$13/2^+$	24h	$3/2^-$ $5/2^-$	0.05 ± 0.01	3.4 ± 0.5
Previous work									
Br^{81} [10]	$3/2^-$	Br^{80}	1^+	18m	5^-	4.4h	2^-	0.33	6.5
Se^{82} [12]	0^+	Se^{81}	$1/2^-$	18m	$7/2^+$	57m		0.5	3.0
Zr^{90} [11]	0^+	Zr^{89}	$9/2^+$	79h	$1/2^-$	4.5h		0.44 ± 0.06	4.3 ± 1
In^{115} [23]	$9/2^+$	In^{114}	1⁻	72s	5^+	50d	a ($T_{1/2}$ = 2.5s)	0.85	5.0

The yields, Y_1 and Y_2, are for (γ,n) reactions ending in the isomeric - or ground - state. The yield Y_1 is for the higher-spin state

REFERENCES

1) J. R. Huizenga and R. Vandenbosch, Phys. Rev. 120 (1960) 1305
2) T. Ericson, Advances in Physics, 9 (1960) 425
3) D. L. Allan, Nuclear Physics 24 (1961) 274
4) C. T. Hibdon, Phys. Rev. 114 (1959) 179
5) C. T. Hibdon, Phys. Rev. 122 (1961) 1235
6) T. Ericson, Nuclear Physics 11 (1959) 481
7) J. H. Carver and G. A. Jones, Nuclear Physics 19 (1960) 184
8) A. C. Douglas and N. Macdonald, Nuclear Physics 13 (1959) 382
9) T. Ericson and V. M. Scrutinski, Nuclear Physics 8 (1958) 284
10) L. Katz, L. Pease and H. Moody, Can. J. Phys. 30 (1952) 476
11) L. Katz, R. G. Baker and R. Montalbetti, Can. J. Phys. 31 (1953) 250
12) E. Silva and J. Goldemberg, An. Acad. Brasil Ciencs 28 (1956) 275
13) J. H. Carver and D. C. Peaslee, Phys. Rev. 122 (1960) 2155
14) J. M. Blatt and V. F. Weisskopf "Theoretical Nuclear Physics" New York: Wiley (1952)
15) S. E. Vegors, L. L. Marsden and R. L. Heath, U.S. Atomic Energy Commission Report IDO-16370 (1958)
16) Nuclear Data Sheets, National Research Council, Washington (1960, up to and including Set 5)
17) R. Vandenbosch and J. R. Huizenga, Phys. Rev. 120 (1960) 1313
18) E. Weigold and R. Glover, Nuclear Physics (in press)
19) K. J. Le Couteur and D. W. Lang, Nuclear Physics 13 (1959) 32
20) T. D. Newton, Can. J. Phys. 34 (1956) 804
21) D. W. Lang, Nuclear Physics 26 (1961) 434
22) M. E. Rose, "Internal Conversion Coefficients", Amsterdam: North Holland Publishing Co. (1958)
23) J. Goldemberg and L. Katz, Phys. Rev. 90 (1953) 308

Ref. P. Axel, K. Min, N. Stein, D.C. Sutton

Phys. Rev. Letters 10, 299 (1963)

Elem. Sym.	A	Z
Zr	90	40

Method: Betatron; bremsstrahlung monochromator; photon scattering; NaI spectrometer

Ref. No.: 63Ax1

Reaction	E or ΔE	E_o	Γ	$\int \sigma dE$	Jπ	Notes
$Zr^{90}(\gamma,\gamma)$		9.1 10.4 11.5	(500 KeV)			Quasi-elastic scattering - poor resolution of photon detector did not separate high-energy inelastic scattering from elastic scattering. Fig.: 135°-quasi elastic cross section. Optical model considered. Natural target - assumes all scattering from Zr^{90}.

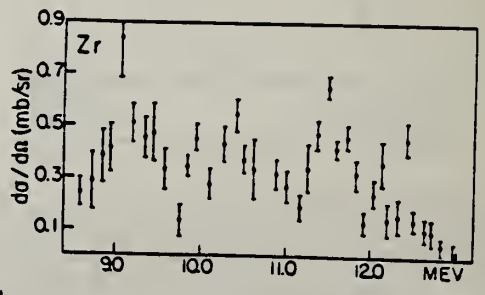

REF.

J. L. Black and N. W. Tanner
Phys. Letters 11, 135 (1964)

ELEM. SYM.	A	Z
Zr	90	40

METHOD

Tandem; $Y^{89}(p,\gamma_0)Zr^{90}$

REF. NO. 64 B1 2 JOC

REACTION	RESULT	EXCITATION ENERGY	SOURCE TYPE	SOURCE RANGE	DETECTOR TYPE	DETECTOR RANGE	ANGLE
P,G	RLX	13-17	D	5-9	NAI-D		DST
				(5.5 - 8.5)			

ANALØGUE T =

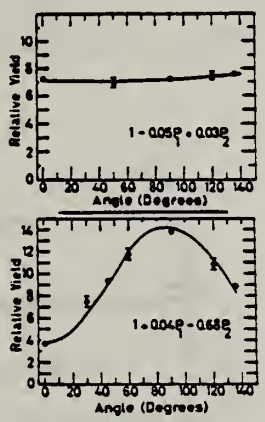

Fig. 2. Angular distributions of $Y^{89}(p,\gamma)Zr^{90}$. Upper: Measured at the peak of the 6.15 MeV resonance. Lower: Measured at the peak of the 8.04 MeV resonance. The full curves are plots of the Legendre polynomial fits given on the figure.

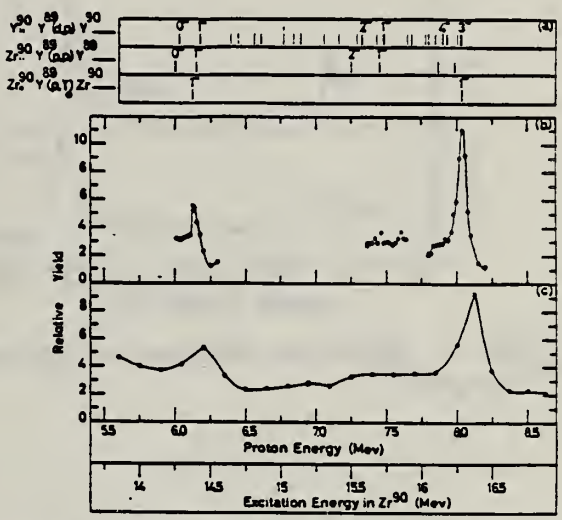

Fig. 1a. Upper: Energy levels of Y^{90} from $Y^{89}(d,p)Y^{90}$. The energy scale has been adjusted so that the ground state corresponds to the 4.82 MeV bombarding energy resonance seen in $Y^{89}(p,n)Zr^{89}$. Middle: Sharp resonances observed in $Y^{89}(p,p)Y^{89}$ and $Y^{89}(p,n)Zr^{89}$. Lower: Sharp resonances observed in $Y^{89}(p,\gamma_0)Zr^{90}$. The energy scale for the three sections is the same as the energy scale for the main diagram. 1b. Excitation function measured at 90° for the $Y^{89}(p,\gamma_0)Zr^{90}$ reaction. Resolution 20 keV. 1c. Excitation function measured at 90° with 150 keV resolution.

E_p = 6.15 MeV $\quad W(\theta) = 1 - (0.05 \pm .03)\ P_1(\cos\theta)$

E_p = 8.04 MeV $\quad W(\theta) = 1 + (0.04 \pm 0.04)\ P_1(\cos\theta) - (0.68 + .04)\ P_2(\cos\theta)$

REF. J. Black, M. M. Islam, G. A. Jones, G. C. Morrison and R. B. Taylor
Conference on Isobaric Spin (1966)

ELEM. SYM.	A	Z
Zr	90	40

METHOD

REF. NO. 66 B1 1 JOC

REACTION	RESULT	EXCITATION ENERGY	SOURCE TYPE	SOURCE RANGE	DETECTOR TYPE	DETECTOR RANGE	ANGLE
P,G	RLY	14-17	D	5-9	NAI-D		DST

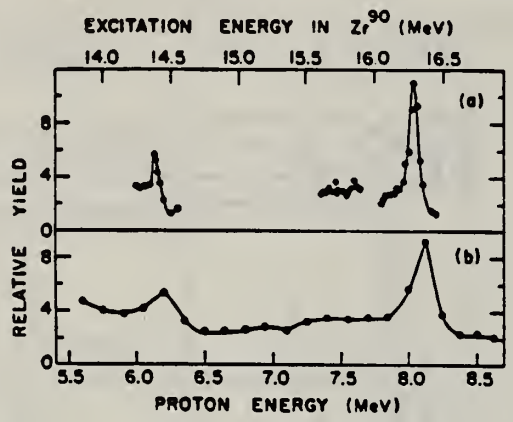

Fig. 1. Excitation function for the reaction $Y^{89}(p,\gamma_0)Zr^{90}$.

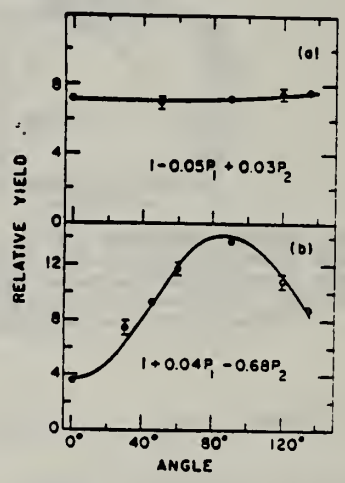

Fig. 2. Upper: Angular distribution of resonance at 6.15 MeV in $Y^{89}(p,\gamma_0)$; Lower: Angular distribution of resonance at 8.04 MeV in $Y^{89}(p,\gamma_0)$.

$W(\theta) = 1 - (0.05 \pm 0.03)P_1 + (0.03 \pm 0.04)P_2$ for the 6.15 MeV resonance and

$W(\theta) = 1 + (0.04 \pm 0.04)P_1 - (0.68 \pm 0.04)P_2$ for the 8.04 MeV resonance.

REF. S. C. Fultz, R. L. Bramblett, B. L. Berman, J. T. Caldwell and M. A. Kelly
Proc. Gatlinburg Conference 397 (1966)

ELEM. SYM.	A	Z
Zr	90	40

METHOD

REF. NO. 66 Fu 2 hmg

REACTION	RESULT	EXCITATION ENERGY	SOURCE		DETECTOR		ANGLE
			TYPE	RANGE	TYPE	RANGE	
G,XN	ABI	THR-28	D	THR-28	BF3-I		4PI
G,2N	ABI	THR-28	D	THR-28	BF3-I		4PI

TABLE 1

Integrated Cross Sections for Zirconium and Yttrium

Isotope	E_{max} $a = \int \sigma_{tot}\, dE$ (MeV - barns)	E_{max} $b = \int \sigma_{\gamma,2n} dE$ (MeV - barns)	b/a	E_{max} (MeV)
^{90}Zr	0.980	0.108	0.110	28
^{91}Zr	1.078	0.202	0.187	30
^{92}Zr	1.096	0.447	0.408	28
^{94}Zr	1.041	0.577	0.554	30
^{89}Y	0.991	0.095	0.096	28

REF.

E. Obst, F. Rauch and E. Rossle
Phys. Letters 21, 50 (1966)

EL EM. SYM.	A	Z
Zr	90	40

METHOD

REF. NO.	
66 Ob 1	EGF

REACTION	RESULT	EXCITATION ENERGY	SOURCE		DETECTOR		ANGLE
			TYPE	RANGE	TYPE	RANGE	
P,G	RLX	11 - 14	D	2 - 6	NAI-D	0 - 14	0,90

E_o 3.5-6.5

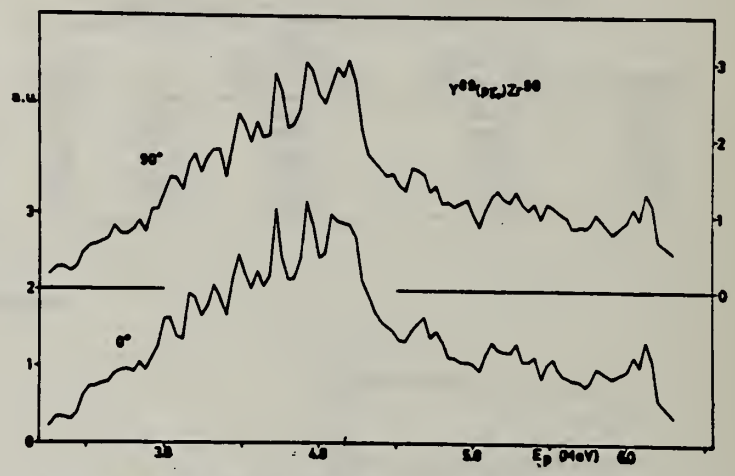

Fig. 1. Excitation curves of the reaction $^{89}Y(p,\gamma_0)^{90}Zr$ at 0^o and 90^o in relative units.

REF. P. Axel, D. M. Drake, S. Whetstone and S. S. Hanna
Phys. Rev. Letters 19, 1343 (1967)

ELEM. SYM.	A	Z
Zr	90	40

METHOD

REF. NO. 67 Ax 1 EGF

REACTION	RESULT	EXCITATION ENERGY	SOURCE		DETECTOR		ANGLE
			TYPE	RANGE	TYPE	RANGE	
P,G	ABX	14-25	D	5-17	NAI-D	10-24	90

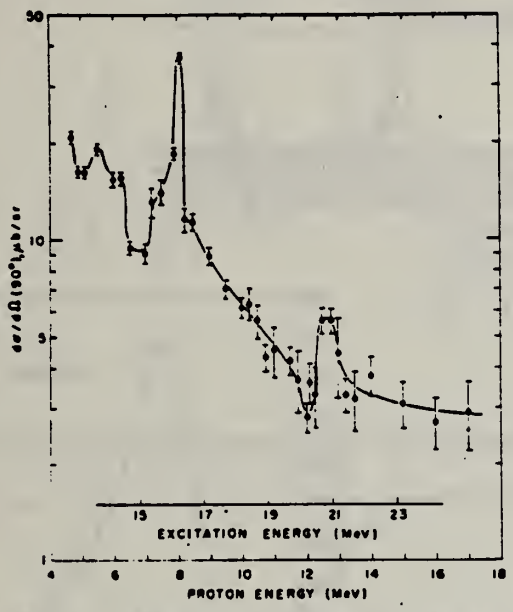

FIG. 1. Differential cross section of process $^{89}Y(p, \gamma_0)^{90}Zr$ at 90°. The errors shown are statistical. Because of some uncertainty in the gamma-detector efficiency, absolute values are good probably to within 35%.

REF. B.L. Berman, J.T. Caldwell, R.R. Harvey, M.A. Kelly, R.L. Bramblett, and S.C. Fultz
Phys. Rev. 162, 1098 (1967)

ELEM. SYM.	A	Z
Zr	90	40

METHOD

REF. NO. 67 Be 2 hmg

REACTION	RESULT	EXCITATION ENERGY	SOURCE TYPE	SOURCE RANGE	DETECTOR TYPE	DETECTOR RANGE	ANGLE
G,N 6+	ABX	THR-28	D	THR-28	BF3-I		4PI
G,2N 5	ABX	THR-28	D	THR-28	BF3-I		4PI

TABLE IV. Integrated cross sections.

Nucleus	$\sigma_{int}[(\gamma,n)+(\gamma,pn)]$ (MeV-b)[a]	$\sigma_{int}(\gamma,2n)$ (MeV-b)[a]	$E_{\gamma max}$ (MeV)	$\frac{\sigma_{int}(\gamma,2n)}{\sigma_{int}(\gamma,\text{total})}$[b]	$(\frac{1}{2}\pi)\sigma_m\Gamma$ (MeV-b)	$0.06NZ/A$ (MeV-b)
Y^{89}	0.94	0.10	28	0.10	1.14	1.31
Zr^{90}	0.96	0.10	28	0.09	1.16	1.33
Zr^{91}	0.88	0.20	30	0.19	1.22	1.35
Zr^{92}	0.65	0.45	28	0.41	1.23	1.36
Zr^{94}	0.43	0.58	30	0.56[c]	1.32	1.38

[a] All measured integrated cross-section values are given for an energy region from threshold to $E_{\gamma max}$. For the Zr^{91} and Zr^{92} cases, it was necessary to extrapolate the low-energy part of the total photoneutron cross section down to threshold; the error introduced in this process, however, is less than 0.5%.
[b] The word "total" in this table refers to the total photoneutron cross section $\sigma([\gamma,n)+(\gamma,pn)+(\gamma,2n)+(\gamma,3n)]$, and excludes the (γ,γ) and (γ,p) cross sections.
[c] This value includes the contribution of $\sigma_{int}(\gamma,3n)$, which equals 0.03 MeV-b from threshold to 30 MeV.

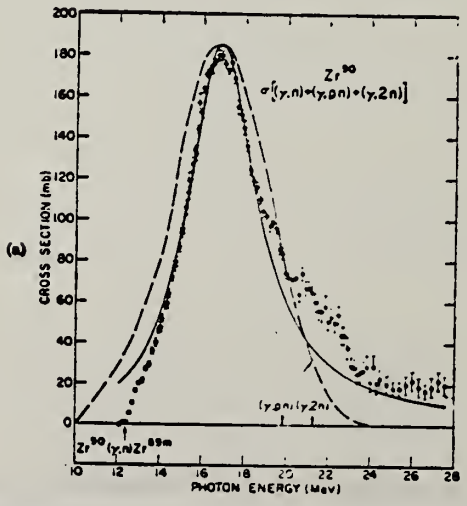

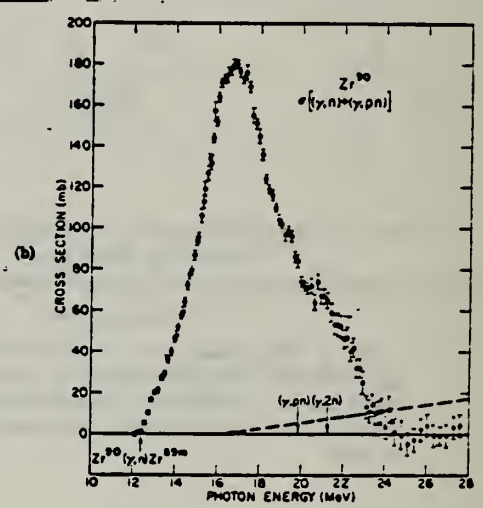

FIG. 9 (a) Total photoneutron cross section for Zr^{90}. The dashed curve is the theoretical prediction of a shell-model calculation by Shitikova and co-workers, (Refs. 13 and 14) normalized both in energy and in cross section to the present data. The predicted giant resonance is too broad, and falls off too rapidly at high energies. Balashov and Yadrovsky (Ref. 15) also have done a particle-hole calculation for Zr^{90}, but here the giant resonance occurs at too low an energy ($\simeq$15 MeV). The (γ,n) and $(\gamma,2n)$ thresholds are taken from the data. (b) Single photoneutron cross section for Zr^{90}. (c) The $(\gamma,2n)$ cross section for Zr^{90}. The threshold determination of 21.3±0.1 MeV determines the mass of Zr^{88} (see text).

REF. E. Obst, F. Rauch and H. G. Wahsweiler
Nucl. Phys. A103, 17 (1967)

ELEM. SYM.	A	Z
Zr	90	40

METHOD

REF. NO.	
67 Ob 1	EGF

REACTION	RESULT	EXCITATION ENERGY	SOURCE		DETECTOR		ANGLE
			TYPE	RANGE	TYPE	RANGE	
P,G	ABX	12-13	D	4-5	NAI-D	9-13	0

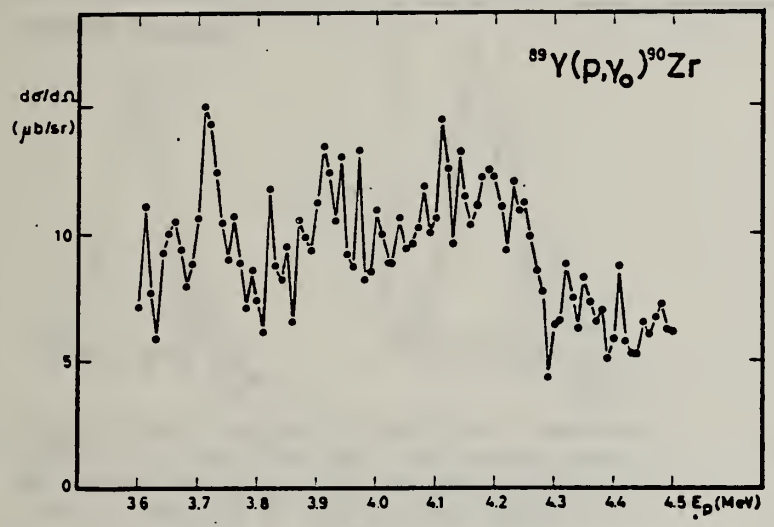

Fig. 4. Excitation curve of the transition γ_0 measured in steps of 10 keV.

TABLE 1
Cross-section values

	$\frac{\sigma_i}{\sigma_0}$	$\frac{B_i\,(E1)}{B_0\,(E1)}$
γ_0	1	1
γ_1	0.3±0.1	0.45±0.15
γ_2	1.0±0.2	1.75±0.35

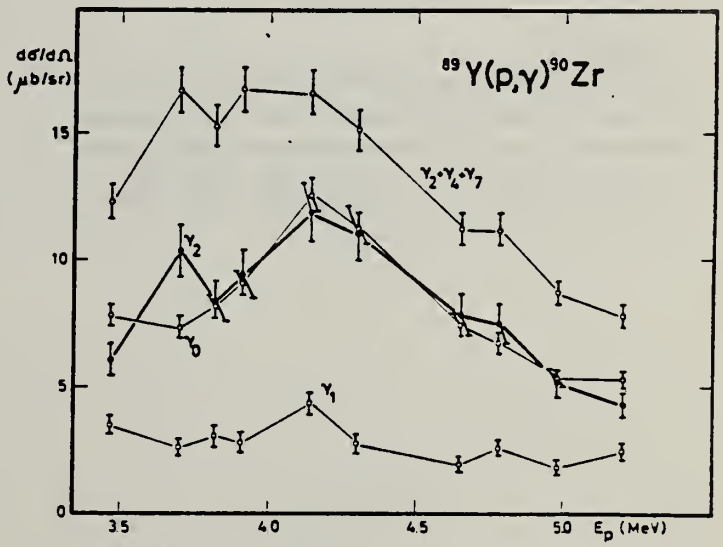

Fig. 5. Excitation curves of the transitions γ_0, γ_1, γ_2, and $\gamma_2+\gamma_4+\gamma_7$.

REF. K. Shoda, M. Sugawara, T. Saito, and H. Miyase
Phys. Letters 23B, 30 (1968).

ELEM. SYM.	A	Z
Zr	90	40

METHOD

REF. NO. 68 Sh 4 egf

REACTION	RESULT	EXCITATION ENERGY	SOURCE		DETECTOR		ANGLE
			TYPE	RANGE	TYPE	RANGE	
E,P	SPC	11-20	D	20	MAG-D	3-12	90

ANALOGUE STATES

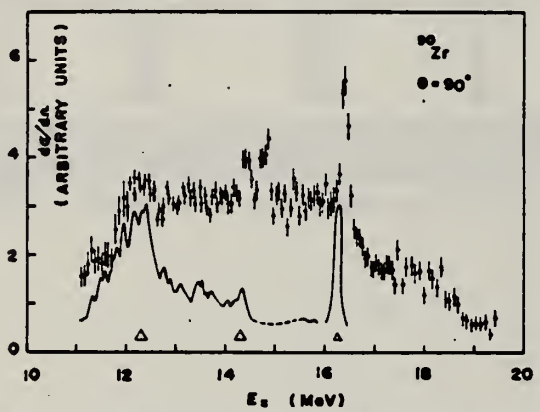

Fig. 1. Photoproton cross section for ^{90}Zr calculated from the energy distribution of the E_e = 20.0 MeV bombardment. The scale was constructed under the assumption that observed protons correspond to ground-state transitions. The triangles show the energy resolution. The solid curve is the (γ, p_0) cross section calculated from the (p,γ_0) data.

REF. G. P. Antropov, I. E. Mitrofanov, A. I. Prokof'ev and V. S. Russkikh
Izv. Akad. Nauk Fiz. 33, 700 (1969)
Bull. Acad. Sci. USSR-Phys. 33, 645 (1969)

ELEM. SYM.	A	Z
Zr	90	40

METHOD

REF. NO.	
69 An 7	egf

REACTION	RESULT	EXCITATION ENERGY	SOURCE		DETECTOR		ANGLE
			TYPE	RANGE	TYPE	RANGE	
G,XN	ABX	12-23	C	12-23	BF3-I		4PI

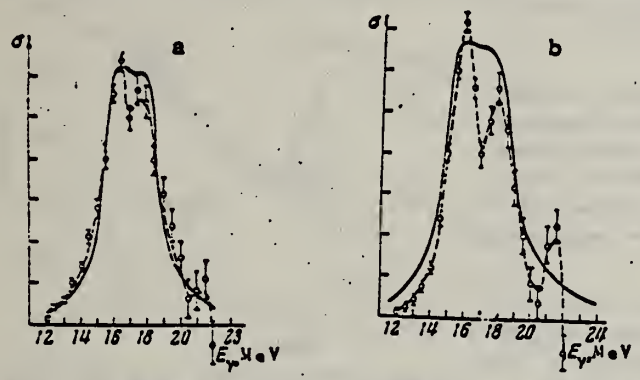

Fig.1. Cross section for the (γ,n) reaction in ^{90}Zr (a) and ^{91}Zr (b). The points and the dashed curve are experimental; the full curve is the sum of two Lorentz curves.

Table 1

Nucleus	0,06 NZ/A	22,5 MeV, $\int \sigma(E)\,dE$,	Γ_{exp}, MeV	$\sigma_{-}/0,00225A^{1/3}$
^{90}Zr	1,33	1,27	4,0	0,91
^{91}Zr	1,35	1,42	4,2	1,02

Table 2

Nucleus	σ_M	σ_0	Γ_1, MeV	Γ_2, MeV	E_1, MeV	E_2, MeV
^{90}Zr	175	120	2,3	1,7	16,5	17,7
^{91}Zr	200	135	2,75	2	16,0	18

REF.

C. K. Bockelman, T. H. Curtiss, R. A. Eisenstein, D. W. Madsen
Contributions Montreal Conference 132 (1969)

EL.SM. SYM.	A	Z
Zr	90	40

METHOD

REF. NO.	
69 Bo 2	egf

REACTION	RESULT	EXCITATION ENERGY	SOURCE		DETECTOR		ANGLE
			TYPE	RANGE	TYPE	RANGE	
E,E/	FMF	2-4	D	58	MAG-D	50-58	DST
		(2.18,2.74,3.84)					

INELASTIC ELECTRON SCATTERING FROM ^{90}Zr

2.18 - 3.84 MEV

C.K. Bockelman, T.H. Curtiss, R.A. Eisenstein and D.W. Madsen, Electron Accelerator Laboratory, Yale University, New Haven, Connecticut, U.S.A. and J.B. Bellicerd and P. Leconte, Service de Physique Nucléaire à Haute Energie, Centre d'Etudes Nucléaires de Sacley, France.

We have studied the collective states of zirconium-90 with the 70 MeV Lineac of the Yale University. At low energy such measurements determine by an unique way the reduced transition probabilities. For ^{90}Zr these B(EL) values may be compared with those given by the R.P.A. description of vibration for even isotones (Gillet et el., Phys. Letters 27B (1968) 483). We have carried out measurements on an enriched target of ^{90}Zr using 58 MeV electrons. The momentum transfer varied from 0.3 to 0.6 fm. The total energy resolution was 120 keV. The prominent peaks at 2.18, 2.74 and 3.84 MeV are known to be 2^+, 3^- and 2^+ respectively.

At high Z, we must use a distorted wave calculation to analyse our inelastic data, we have chosen the GEROW code (D.S. Onley, Phys. Rev. 134B (1964) 945). This code assumes an hydrodynamical model for the nucleus. For an EL transition, the transition charge density $\rho_L \propto r^{L-1} \rho(r)$ contains the derivative of the static charge density described by the Fermi model. At low energy absolute Zr elastic static measurements have given us the value of the r.m.s. radius of $\rho(r)$. Starting from this r.m.s. value $\langle r^2 \rangle^{1/2}$ = (4.12 ± 0.05)fm, we may choose the values c = 4.66 fm and t = 2.34 fm to compute the inelastic cross-sections.

J_π	E (MeV)	B(EL) s.p. units		
		2 Q.P.	2 Q.P. + core	Experiment
2^+	2.18	1.35	1.71	6.8 ± 1
3^-	2.74	4.35	16.9	32 ± 4

The comparison with the R.P.A. description given by Gillet is shown on the table. For the 3^- state the inclusion of the particle hole core polarization has increased the B(EL) by an order of magnitude. This help to account for the experiment although there is still a discrepancy by a factor two which may not be serious because the B(EL) depend strongly on the detail shape of the transition charge density. However, for the 2^+, the discrepancy is much more important. Thus it is seen that the particle hole core excitation model may account for the odd parity state collectivity ; however it seems to fail for the even parity states.

Figure 2 is a plot of σ/σ_{Mott} vs q_I for 2^+ levels at 2.18 and 3.84 MeV. The solid curves are a theoretical calculation using the GEROW code with the indicated parameters. These states are not very collective as may be shown from their B(E2) values. Figure 3 shows the fit for the 3^- state at 2.74 MeV. The collective character of this level is emphasized by the B(E3) value (32 ± 4) s.p. units.

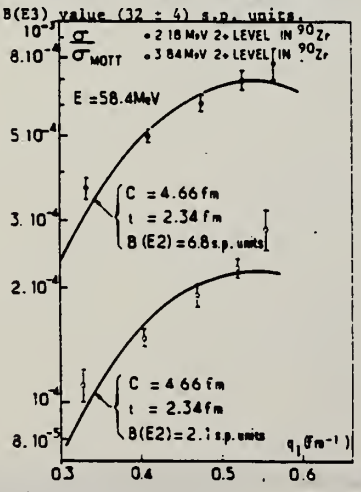

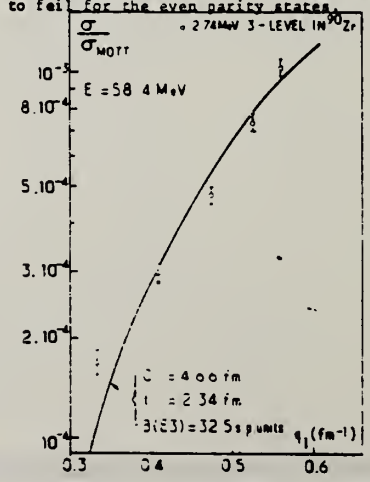

REF.

M. Hasinoff, G. A. Fisher, H. M. Kuan and S. S. Hanna
Phys. Letters 30B, 337 (1969)

ELEM. SYM.	A	Z
Zr	90	40

METHOD

REF. NO.	
69 Ha 1	egf

REACTION	RESULT	EXCITATION ENERGY	SOURCE		DETECTOR		ANGLE
			TYPE	RANGE	TYPE	RANGE	
P,G	RLX	16-22	D	7-14	NAI-D	10-22	DST

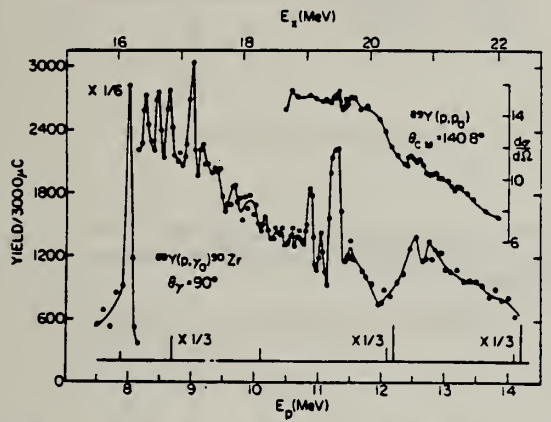

Fig. 1. Yield curves of $^{89}Y(p,\gamma_0)^{90}Zr$ at 90° and $^{89}Y(p,p_0)^{89}Y$ at 140.8°. The predicted resonances [2] are shown as vertical lines whose heights are proportional to Γ_{γ_0}. The 2nd, 4th, 5th, 6th, and 7th lines have been suppressed by a factor of 3.

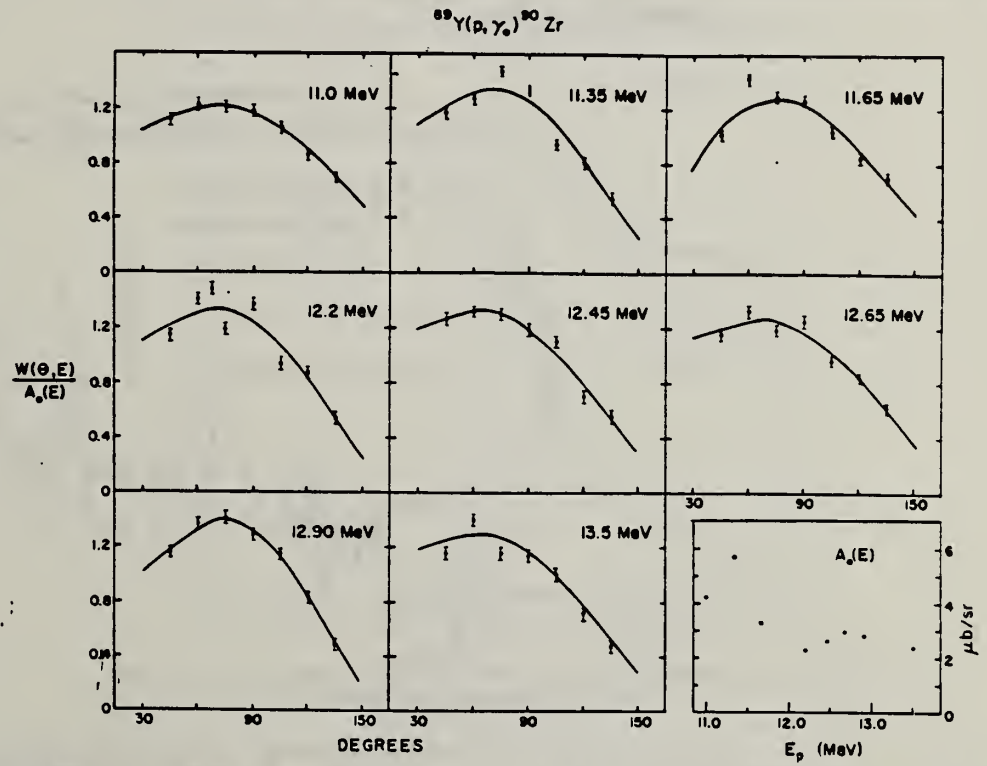

Fig. 2. Angular distributions in $^{89}Y(p,\gamma_0)^{90}Zr$ at several energies on and off the resonances of fig. 1. The listed energies are values of E_p.

REACTION	RESULT	EXCITATION ENERGY	SOURCE		DETECTOR		ANGLE
			TYPE	RANGE	TYPE	RANGE	
P,G	ABX	10-27	D	2-19	NAI-D	10-27	DST

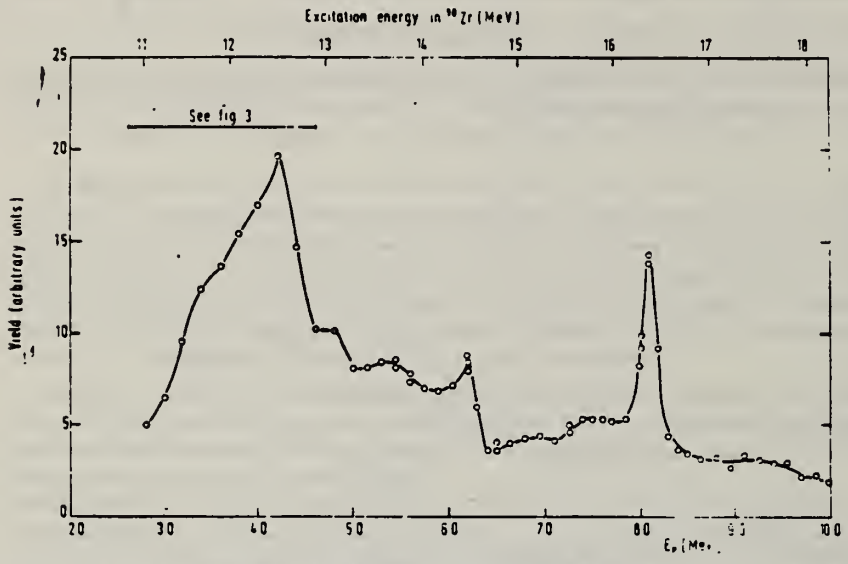

Fig. 2. The excitation function for the reaction $^{89}Y(p,\gamma_0)^{90}Zr$ measured at $\vartheta = 90°$ with an energy resolution of 150 to 200 keV.

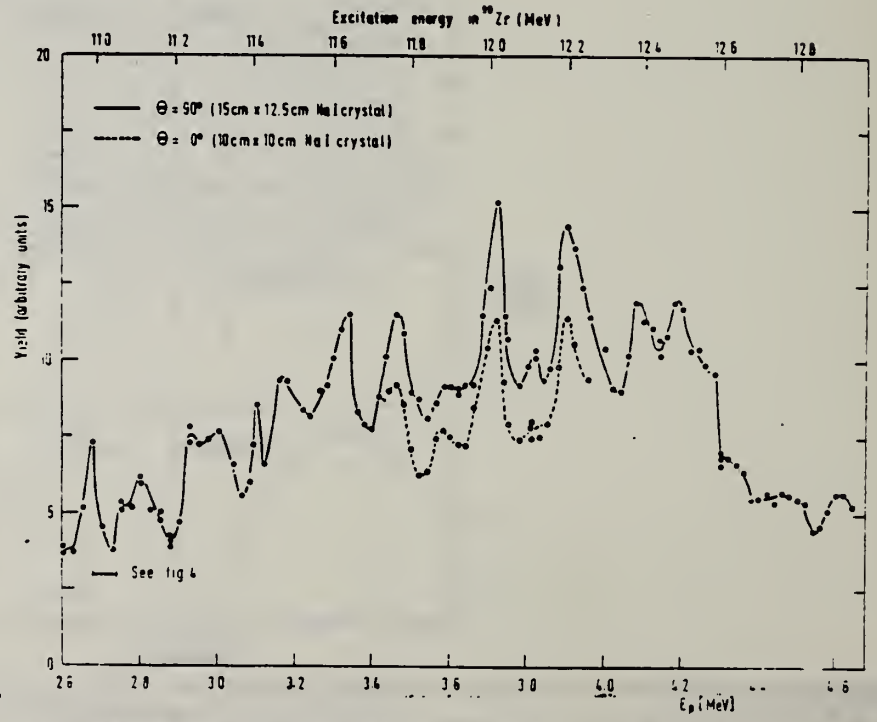

Fig. 3. The excitation functions for the reaction $^{89}Y(p,\gamma_0)^{90}Zr$ measured at $\vartheta = 90°$ and $\vartheta = 0°$ with an energy resolution of 25 keV. The curves are not normalized to one another.

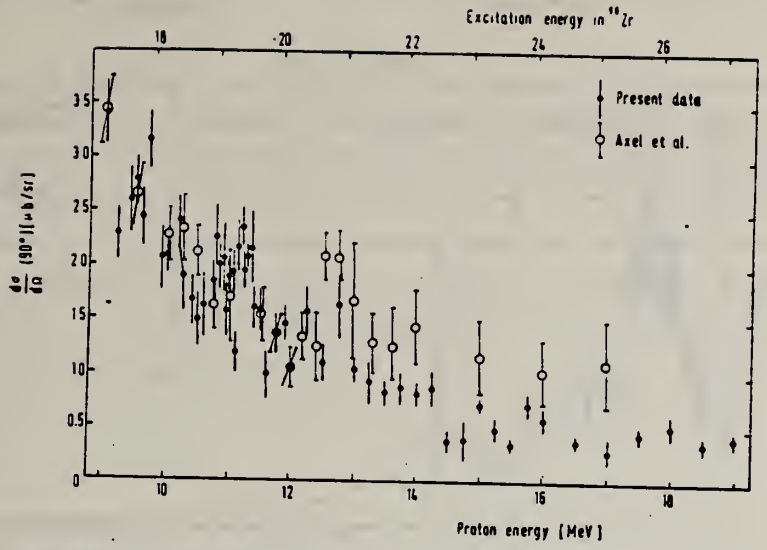

Fig. 6. The excitation function for the reaction $^{89}Y(p,\gamma_0)^{90}Zr$ measured at $\vartheta = 90°$ with the 24 cm × 30 cm NaI(Tl) crystal. Points measured by Axel *et al.* [9]) have been included but scaled by a factor 5.3/14.

[9] P. Axel, D. M. Drake, S. Whetstone and S. S. Hanna, Phys. Rev. Lett. 19 (1967) 1343

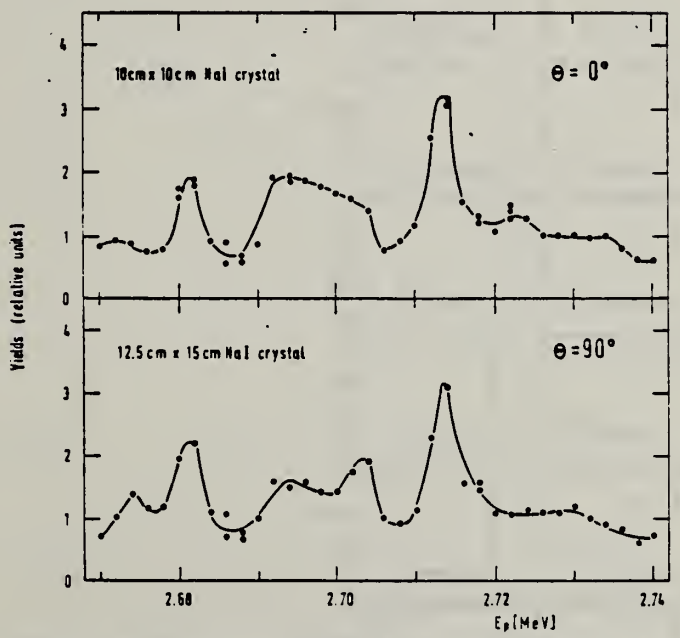

The excitation functions for the reaction $^{89}Y(p,\gamma_0)^{90}Zr$ measured at $\vartheta = 0°$ and $\vartheta = 90°$ with an energy resolution of 2 keV.

REACTION	RESULT	EX E

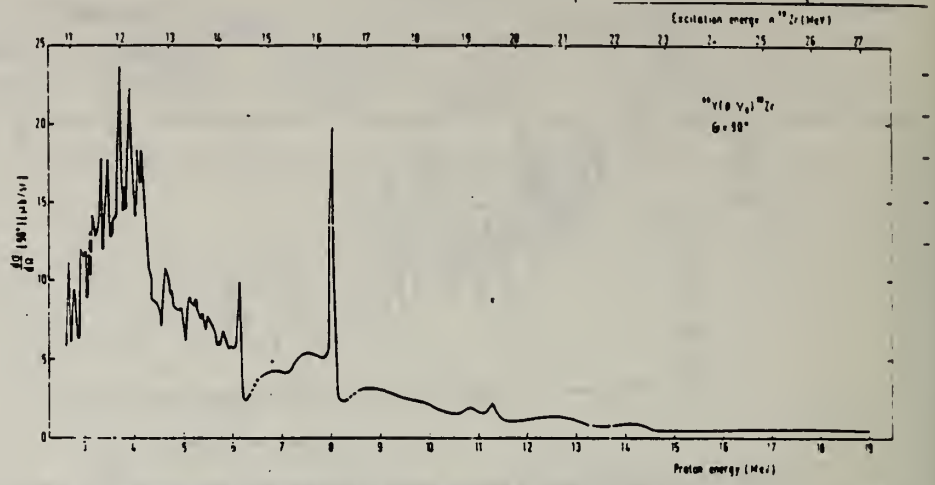

Fig. 9. Combined lower and higher energy excitation functions at $\vartheta = 90°$ with inclusion of some data from refs. [6,10]). The cross section is normalized to the values given in the text. For the energy regions $E_p = 6.5$-7.8 MeV and $E_p = 8.6$-9 MeV, the data from the 150 keV excitation function (fig. 2) were used.

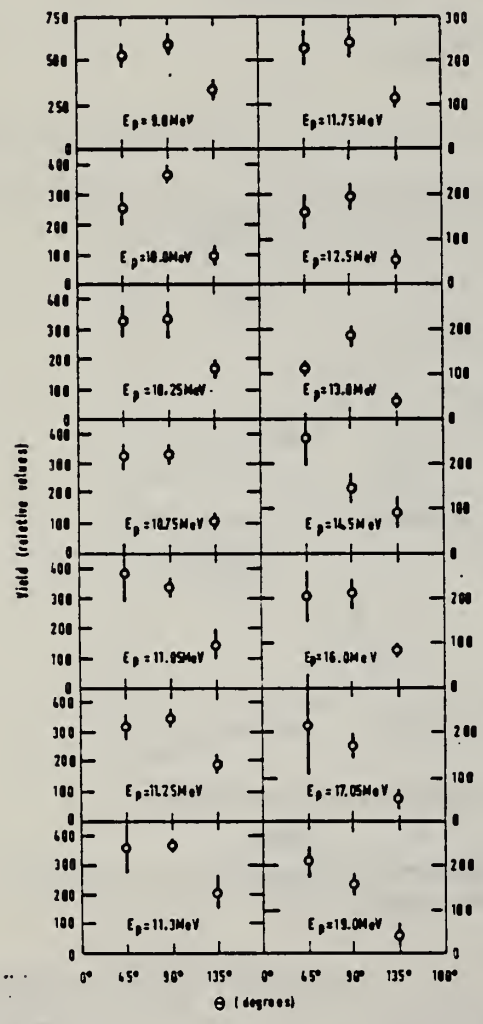

Fig. 7. Three point "angular distributions" for the energy region $E_p = 9$-19 MeV.

[6] J. L. Black and N. W. Tanner, Phys. Lett. 11 (1964) 135
[10] E. Obst, F. Rauch and E. Rössle, Phys. Lett. 21 (1966) 50;
E. Obst, F. Rauch and H. G. Wahsweiler, Nucl. Phys. A103 (1967) 17

REF.

S. Ramchandran and J. A. McIntyre
Phys. Rev. 179, 1153 (1969)

Zr	90	40

METHOD

REF. NO. 69 Ra 1

hmg

REACTION	RESULT	EXCITATION ENERGY	SOURCE		DETECTOR		ANGLE
			TYPE	RANGE	TYPE	RANGE	
G,G	LFT	9	D	9	NAI		DST

9 = 8.496 MEV

$W(\theta) \sim [1 + a\ P_2(\cos\theta)]$

over

TABLE II. Experiment compared to theory assuming a pure dipole transition.

$\alpha \pm \Delta\alpha$ (Experimental)										
^{90}Zr	Cd	Sn	Hg	^{205}Tl	^{208}Pb	^{209}Bi (7.416 MeV)	^{209}Bi (7.149 MeV)	$A_2^3(J_0, J_1, L=1)$ (Theoretical)	J_0	J_1
0.489±0.027	0.488±0.034	0.490±0.095	0.48±0.11		0.485±0.026			0.500	0	1
	0.488±0.034	0.490±0.095	0.48±0.11	0.0017±0.0110				0.000	1/2	1/2
	0.488±0.034	0.490±0.095	0.48±0.11	0.0017±0.0110				0.250	1/2	3/2
			0.48±0.11					0.000	3/2	1/2
			0.48±0.11					0.160	3/2	3/2
			0.48±0.11					0.140	3/2	5/2
						0.195±0.033	0.184±0.074	0.024	9/2	7/2
						0.195±0.033	0.184±0.074	0.194	9/2	9/2
						0.195±0.033	0.184±0.074	0.083	9/2	11/2

TABLE V. Summary of energy-level parameters.

Element	^{90}Zr	Cd	Sn	Hg	^{205}Tl	^{208}Pb	^{209}Bi	^{209}Bi
Level energy (MeV)	8.496[a]	6.485[b]	6.988[c]	4.906[b]	7.647[d]	7.277[e]	7.416[e]	7.149[e]
γ ray source	Se	Co	Cu	Co	Fe	Fe	Se	Ti
$J_0 \rightarrow J_1$	0→1	0→1	0→1	0→1	1/2→1/2	0→1	9/2→7/2	9/2→7/2
		(1/2→3/2)	(1/2→3/2)	3/2→5/2	(1/2→3/2)		9/2→9/2	9/2→9/2
				(1/2→3/2)			9/2→11/2	9/2→11/2
				(3/2→3/2)				
Γ_0/Γ	0.8±0.2				0.85±0.17[f]	$0.95_{-0.17}^{+0.05}$	0.6±0.2	
Γ_0 (eV)	1.68±0.02				1.0[f]	0.68±0.03	0.14±0.09	
ϵ (eV)	5.60±0.15				11.5±0.2[f]	8.00±0.14	3.4±1.6	

[a] L. V. Groshev, V. N. Lutsenko, A. M. Demidov, and V. I. Polekov, *Atlas of Gamma Spectra from Radiative Capture of Thermal Neutrons* (Pergamon Press, Inc., New York, 1959).
[b] E. B. Shera and D. W. Hafemeister, Phys. Rev. 150, 894 (1966).
[c] H. H. Bolotin (private communication from L. M. Bollinger).
[d] R. Moreh and G. Ben-Yaacov, Nuclear Research Center—Negev Report, NRCN-180, 1967, (unpublished).
[e] L. V. Groshev, A. M. Demidov, G. A. Kotelnikov, and V. N. Lutsenko, Nucl. Phys. 58, 465 (1964); G. T. Ewan and A. J. Tavendale, Nucl. Instr. Methods 26, 183 (1964).
[f] See Ref. 24a.

K. Shoda, M. Sugawara, T. Saito, and H. Miyase
Phys. Rev. Letters 23, 800 (1969)

Zr	90	40

METHOD

REF. NO.: 69 Sh 5 | hmg

REACTION	RESULT	EXCITATION ENERGY	SOURCE TYPE	SOURCE RANGE	DETECTOR TYPE	DETECTOR RANGE	ANGLE
E,P	ABX	12-23	D	16-24	MAG-D		

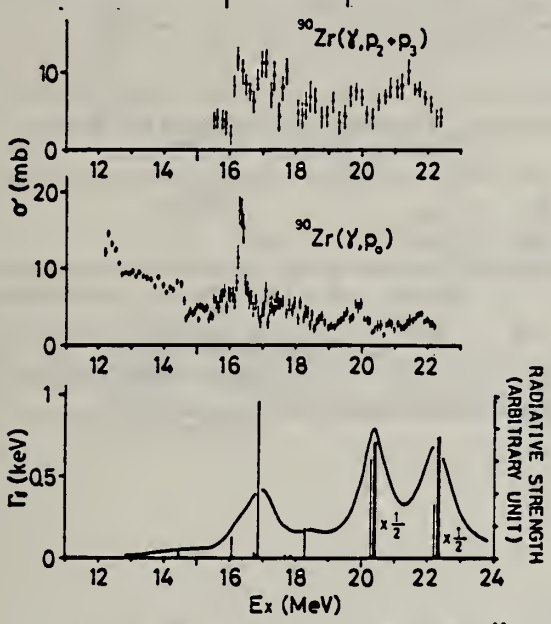

FIG. 2. (γ,p_0) and (γ,p_2+p_3) cross sections of ^{90}Zr. The vertical lines show the theoretical radiative widths of the IAS from Ref. 6. The smooth curve is an averaging of them (see Ref. 6).

Assumption is made that photoproton emission leaves the residual nucleus in the ground state.

[6]T. A. Hughes and S. Fallieros, private communication.

REF.

K. Shoda, M. Sugawara, T. Saito & H. Miyase
PICNS-69 Proceedings of the Conference on Nuclear Isospin. Asilomar-Pacific Grove, California 1969 (Academic Press, New York & London 1969) p.125.

ELEM. SYM.	A	Z
Zr	90	40

METHOD

REF. NO. 69 Sh 6 egf

REACTION	RESULT	EXCITATION ENERGY	SOURCE		DETECTOR		ANGLE
			TYPE	RANGE	TYPE	RANGE	
E,P	ABX	12-22	D	16-23	MAG-D		DST

Table 1. Angular distributions of strong proton groups on ^{90}Zr.

E_p (MeV)	E_R (MeV)	E_{ex} (MeV)	W (θ)
6.0	0	14.4	$1 + (0.1\pm0.1)P_1-(0.2\pm0.2)P_2$
6.4	1.5	16.3	$1 + (0.1\pm0.1)P_1-(1.2\pm0.2)P_2$
7.9	0	16.3	$1 + (0.02\pm0.06)P_1-(0.6\pm0.1)P_2$

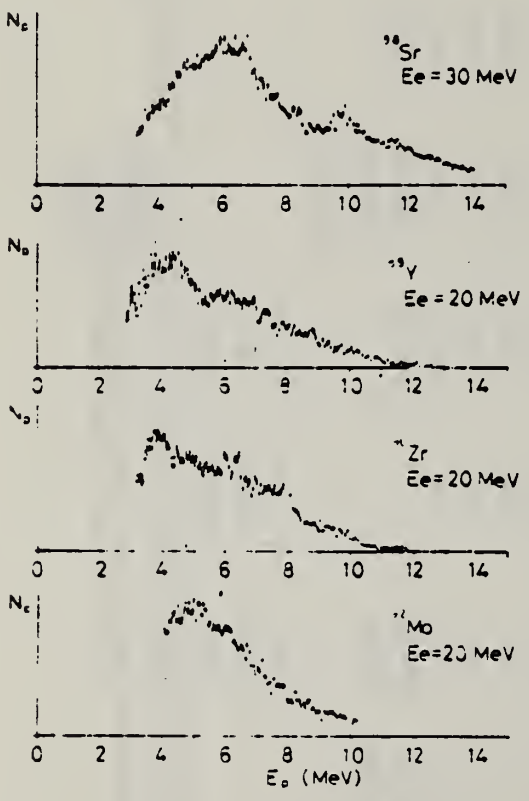

Fig. 1. Energy distributions of photoprotons. Vertical broken lines and solid lines indicate the position of p_o corresponding to the ground IAS and electric dipole IAS (2-/1) respectively.

(over)

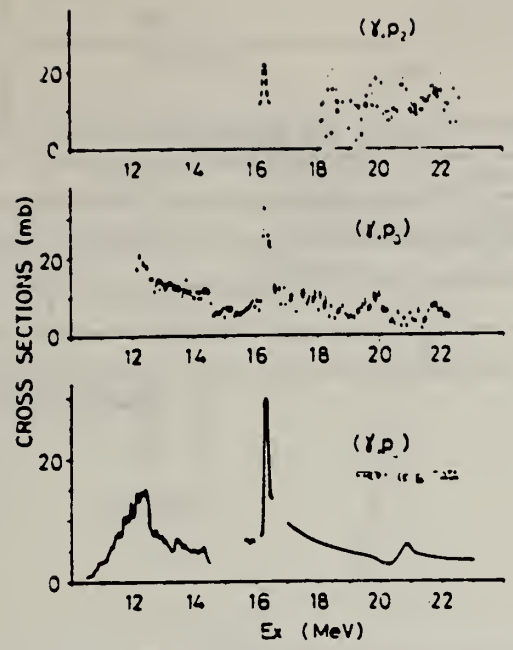

Fig. 2. Cross sections for (γ,p_0), (γ,p_2) of ^{90}Zr. Those of (γ,p_0) obtained from $^{89}Y(p,\gamma_0)^{90}Zr$ experiment(3,5,6) are also shown.

Table 2. The radiative width of main IAS. The result is compared with the single particle unit (W.u.).

Nucleus	E_p (MeV)	E_{ex} (MeV)	Γ_{p0}/Γ	$\Gamma_{\gamma 0}$ (eV)	$2(T+1)\Gamma_{\gamma 0}$ (W.u.)
^{89}Y	7.0	14.0	23/50(a)	60	0.2
	7.5	14.4	18/60(a)	90	0.3
	6.0	14.4	1 (b)	30	0.09
^{90}Zr	6.4	16.3	1/1.4(c)	180	0.4
	7.3				

(a) E. R. Cosman, J. M. Joyce and S. M. Shafroth, Nucl. Phys. A108 519 (1968).

(b) Assumption.

(c) From present data.

(*) The possibility of such method of determination of $\Gamma_{\gamma 0}$ is also suggested by G. M. Temmer (10).

[3] J.L. Black et al., Phys. Lett. 11, 135 (1964).

[5] E. Obst et al., Phys. Lett. 21, 50 (1966).

[6] P. Axel et al., Phys. Rev. Lett. 19, 1343 (1967).

[10] G.M. Temmer, Fundamentals in Nuclear Theory, International Atomic Energy Agency, Vienna p. 237 ('67).

REF.

J. Bellicard, P. Leconte, T. H. Curtis, R. A. Eisenstein, D. Madsen and C. Bockelman
Nucl. Phys. A143, 213 (1970)

Zr	90	40

METHOD

REF. NO. 70 Be 2 egf

REACTION	RESULT	EXCITATION ENERGY	SOURCE		DETECTOR		ANGLE
			TYPE	RANGE	TYPE	RANGE	
E,E/	ABX	0-4	D	42-61	MAG-D	38-61	DST

2.18, 2.74, 3.84

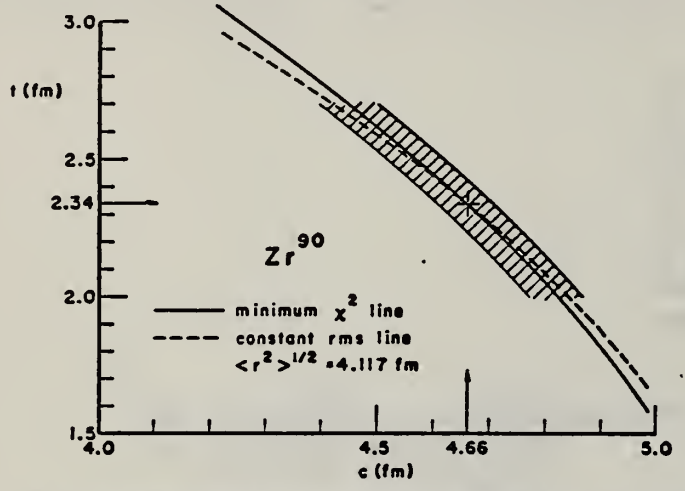

Fig. 2. Values of half-density radius c and skin thickness t consistent with the experimental results lie within the cross-hatched area. The solid line locates the best fit (minimum χ^2), and the dashed line corresponds to a fixed rms radius of 4.12 fm.

TABLE 3
Inelastic scattering results

	$B(EL\uparrow)$ ($e^2 \cdot fm^{2L}$)	$B(EL\uparrow)$ (s.p.u.)	Γ_0^γ (eV)	R^2_{tr} (fm^2)	χ^2/N
2.18 MeV, 2^+					
hydrodynamical model	830±19	6.9	$6.60 \cdot 10^{-3}$	32.5	9.7/6
single-particle model	1000±23	8.3	$8.0 \cdot 10^{-3}$	34.4	9.7/6
2.74 MeV 3^-					
hydrodynamical model	$(1.08 \pm 0.03) \cdot 10^5$	32	$6.71 \cdot 10^{-6}$	37.7	23/5
3.84 MeV, 2^+					
hydrodynamical model	244±9	2.0	$3.29 \cdot 10^{-2}$	32.5	15/5

TABLE 4
Electromagnetic strengths in ^{90}Zr (s.p.u.)

E_{ex} (MeV)	J^π	Present experiment	Coulomb excitation [18]	(α, α') [15]	(p, p') [14]	Theory [25]
2.18	2^+	6.9±1.4	3.5±1.3	5.7±1.7	3.6	1.7
2.74	3^-	32 ±6.4		20.0±1.6	19	17
3.84	2^+	2.0±0.4		1.5±0.5	2.3	

[over]

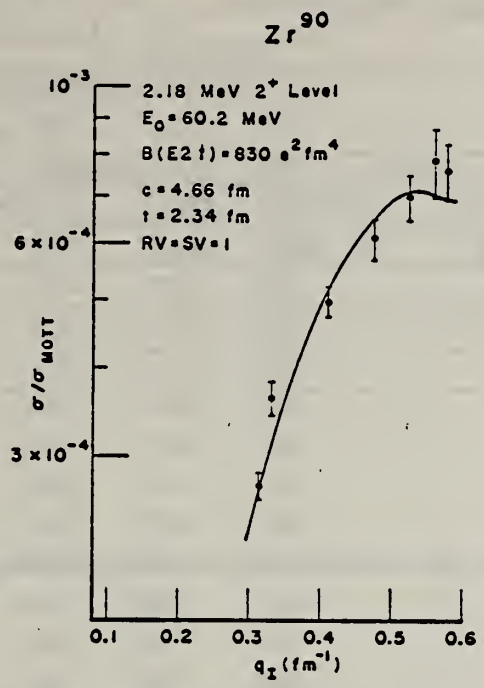

Fig. 3. Inelastic scattering cross sections for excitation of 2.18 MeV level plotted versus momentum transfer. The solid line is the theoretical fit.

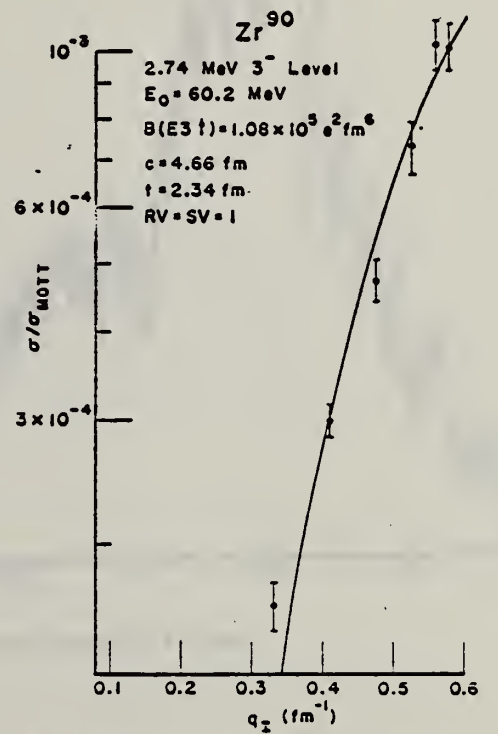

Fig. 4. Inelastic scattering cross sections for excitation of the 2.74 MeV level plotted versus momentum transfer. The solid line is the theoretical fit.

REF. B.I. Goryachev, B.S. Ishkhanov, and V.G. Shevchenko
Proceedings of the Second Symposium on the Problems of Nuclear Physics, Novosibirsk, USSR, June 1970 (Kolybasov, V.M., Ed., Izdatel'stvo Nauka, Moscow 1971), pp. 362-78

ELEM. SYM.	A	Z
Zr	90	40

METHOD

REF. NO. 71 Go 3 egf

REACTION	RESULT	EXCITATION ENERGY	SOURCE		DETECTOR		ANGLE
			TYPE	RANGE	TYPE	RANGE	
G,XN	ABX	12- 28	C	12- 28	MOD-I		4PI

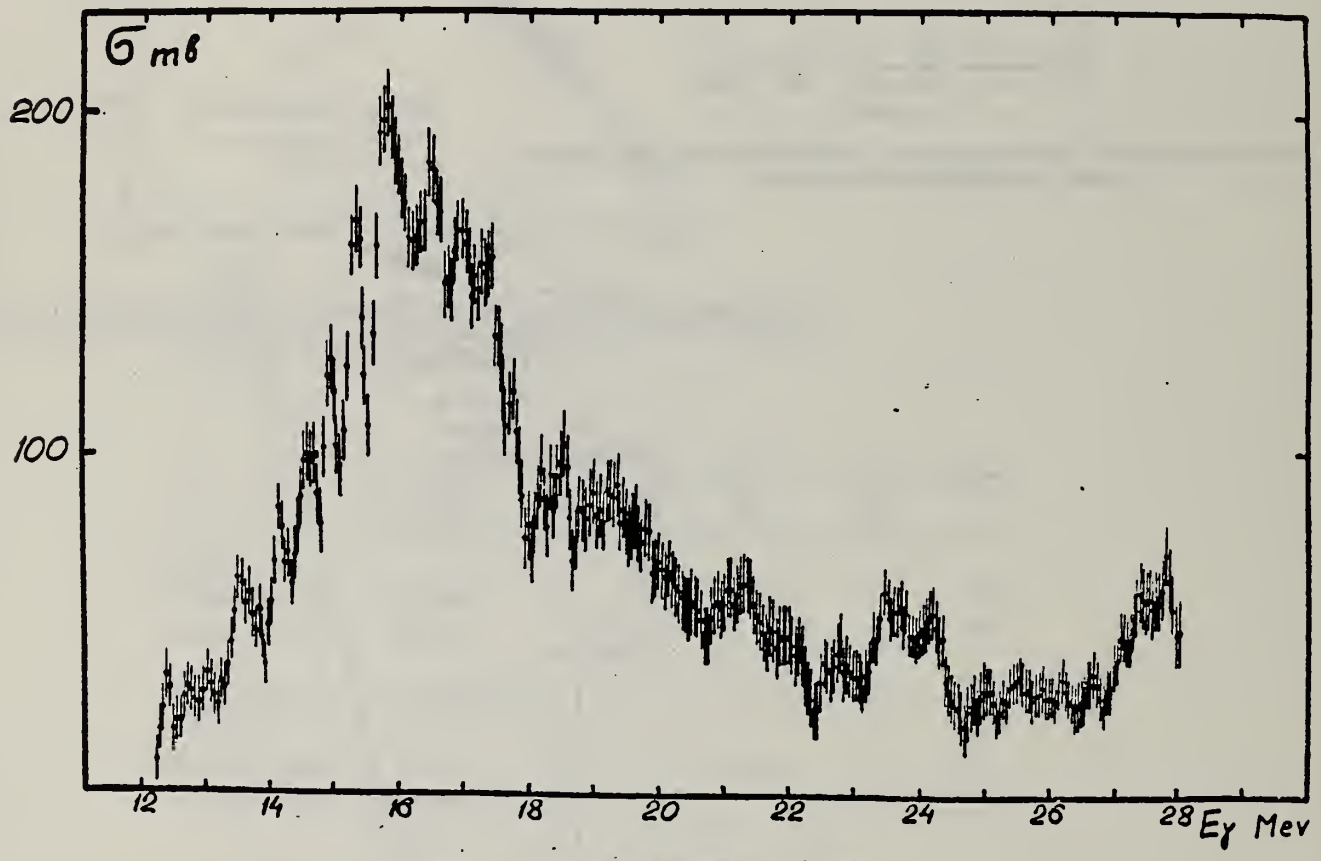

Фиг. 4. Сечение реакции $^{90}Zr(\gamma,n)^{89}Zr$.

(over)

Таблица 2

Zr^{90}	Pb^{208}		
E_∞(Мэв)	E_∞(Мэв)	σ_∞^{int}(Мэв·мбн)	σ_∞^{int} (%)
	7,65	19,5	0,56
	8,06	12,63	0,36
	8,38	16,56	0,47
	8,78	18,61	0,53
	9,03	33,4	0,96
	9,40	34,2	0,98
	9,81	71,1	2,04
	10,29	72,2	2,07
	10,62	63,8	1,83
	10,93	76,6	2,20
	11,24	145,0	4,15
	11,76	247	7,10
12,4	12,3	265	7,61
12,6	12,84	331	9,5
13,1	13,25	344	9,87
13,7	13,78	214	6,14
14,2	14,08	316	9,06
14,6	14,66	245	7,03
14,9	15,13	210	6,02
15,3	15,73	88	2,52
15,8	16,40	114	3,26
16,5	17,13	98	2,81
16,9	17,95	150	4,30
17,3	18,76	78	2,24
18,6	19,52	88	2,52
19,3	20,83	135	3,87
21,3			
22,0			
22,8			
23,5			
24,2			
(25,5)			
27,8			

REF.

B. S. Ishkhanov, I.M. Kapitonov, I.M. Piskarev, O.P. Shevchenko
Yad. Fiz. 14, 27 (1971)
Sov. J. Nucl. Phys. 14, 16 (1972)

ELEM. SYM.	A	Z
Zr	90	40

METHOD

REF. NO.	
71 Is 2	hmg

REACTION	RESULT	EXCITATION ENERGY	SOURCE		DETECTOR		ANGLE
			TYPE	RANGE	TYPE	RANGE	
G,XN	ABX	12-28	C	12-28	BF3-I		4PI

Reaction	Location of resonance peak E_m, MeV	Cross section at the peak σ_m, mb	Resonance width Γ_m, MeV	Integrated cross section $\int_{E_\gamma max}^{\sigma E_\gamma dE_\gamma}$, mb·MeV	$E_{\gamma max}$, MeV	Source of data
$Zr^{90}(\gamma, Tn)$	16.8	150	4.5	1170	28	[9]
	16.0	185	4.1	690	24	[11]
	16.0	200	3.7	950	28	Present work
$Zr^{90}(\gamma, n)$	16.8	180	4.5	960	28	[9]
	16.0	190	2.7	1480	25	[11]
	16.0	200	3.7	930	28	Present work
$Zr^{90}(\gamma, 2n)$				110	28	[9]
				100	28	Present work

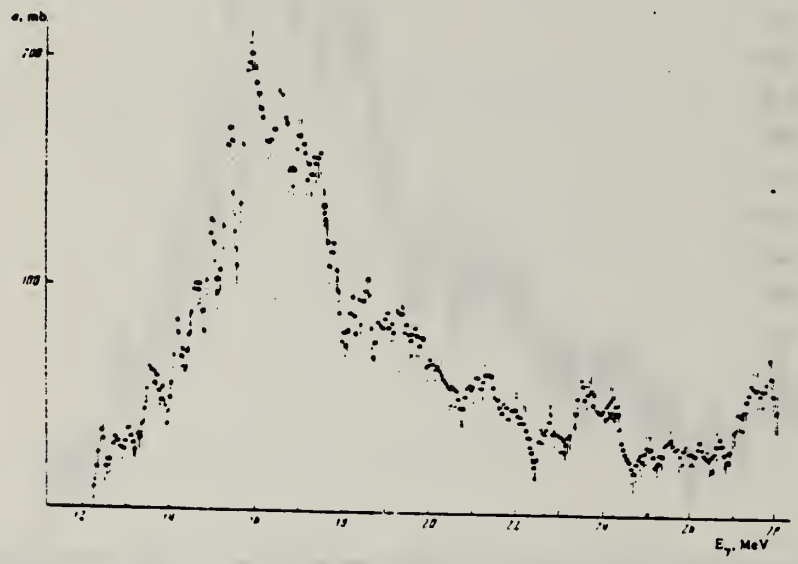

FIG. 1. Cross section for the reaction $Zr^{90}(\gamma, Tn)$.

REF.

A. Lepretre, H. Beil, R. Bergere, P. Carlos, and A. Veyssiere
Nucl. Phys. A175, 609 (1971)

ELEM. STM.		
Zr	90	40

METHOD

REF. NO.	
71 Le 1	egf

REACTION	RESULT	EXCITATION ENERGY	SOURCE		DETECTOR		ANGLE
			TYPE	RANGE	TYPE	RANGE	
G,N	ABX	12-26	D	12-26	MOD-I		4PI
G,2N	ABX	21-26	D	12-26	MOD-I		4PI

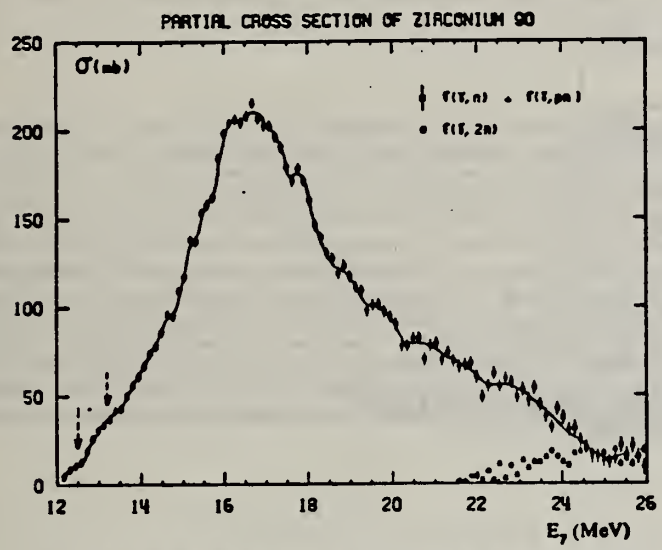

Fig. 4. Partial photoneutron cross sections $\sigma(\gamma, n)$ and $\sigma(\gamma, 2n)$ of ^{90}Zr.

TABLE 1

Lorentz line parameters corresponding to fits shown in fig. 6.

	Rb	Sr	^{89}Y	^{90}Zr	^{93}Nb
σ_1 (mb)	192 ±10	207 ±10	225 ±10	211 ±10	202 ±10
Γ_1 (MeV)	4.1 ± 0.15	4.2± 0.1	4.1± 0.1	4.0 ± 0.1	4.7± 0.2
E_1 (MeV)	16.75± 0.05	16.7± 0.05	16.7± 0.05	16.65± 0.05	16.5± 0.05

TABLE 3

Integrated cross sections (the notation used is defined in the text)

	Rb	Sr	^{89}Y	^{90}Zr	^{93}Nb
σ_0 (MeV · b)	1.14 ±0.06	1.42±0.07	1.36±0.07	1.26±0.07	1.33±0.07
$\frac{\sigma_0}{0.06\,NZ\,A^{-\frac{1}{3}}}$	0.915±0.05	1.09±0.05	1.04±0.05	0.95±0.05	0.97±0.05
σ_{-1} (mb)	67±4	80 ±5	77 ±5	71 ±5	79 ±5
σ_{-2} (mb · MeV^{-1})	4±0.2	4.6 ±0.2	4.4 ±0.2	4 ±0.2	4.8 ±0.2
E_M (MeV)	24	27	27	26	24

(over)

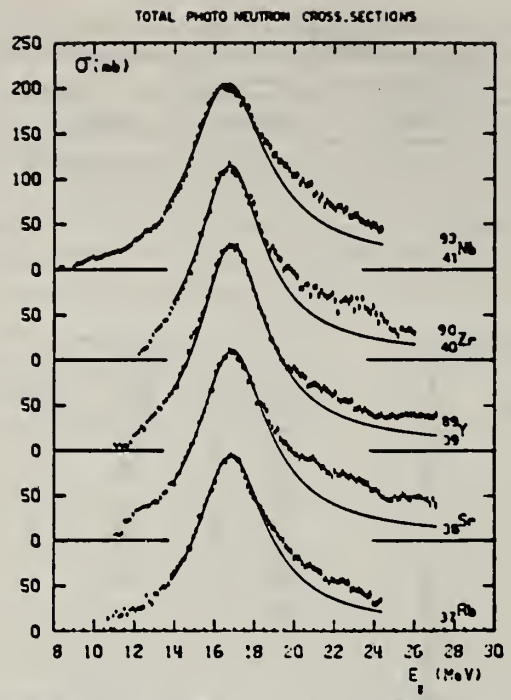

Fig. 6. Total photoneutron cross sections σ_T of Rb, Sr, ^{89}Y, ^{90}Zr and ^{93}Nb and best one Lorentz line fit corresponding to parameters given in table 1.

REF.	ELEM. SYM.	A	Z
C.J. Umbarger, D.A. Close, W.L. Sievers, and R.C. Bearse Phys. Rev. C3, 199 (1971)	Zr	90	40

METHOD	REF. NO.	
	71 Um 1	hmg

REACTION	RESULT	EXCITATION ENERGY	SOURCE		DETECTOR		ANGLE
			TYPE	RANGE	TYPE	RANGE	
P,G	ABX	9-10	D	2-3	SCD-D		C
				(2.3-3.0)			

The $^{88}Sr(p,\gamma)^{89}Y$ and $^{89}Y(p,\gamma)^{90}Zr$ reactions have been investigated in the energy range E_p = 2.3 to 3.0 MeV. Excitation functions for the transition to the ground state, with a total resolution of 2 keV, were determined for each reaction over this energy region. Using thick targets and both a single Ge(Li) detector and a Ge(Li) detector incorporated into a pair spectrometer, total summed spectra for the 700-keV region were obtained. The average total cross section of $^{88}Sr(p,\gamma_0)^{89}Y$ and $^{89}Y(p,\gamma_0)^{90}Zr$ was 12 ± 5 μb and 17 ± 7 μb, respectively. These total summed spectra, which represent the total γ-ray yield in this region, have been examined for a possible dependence of the intensity on the J^π of the final state. The data suggest such a J-dependence hypothesis, but detailed theoretical analysis of the $^{88}Sr(p,\gamma)^{89}Y$ reaction does not completely agree with experiment. A spectrum from a Ge(Li) detector in coincidence with a NaI(Tl) detector was accumulated for the $^{88}Sr(p,\gamma)^{89}Y$ reaction. The decay scheme of the states of ^{89}Y up to an excitation energy of 3.621 MeV was determined and the implications about spins and parities are consistent with accepted assignments.

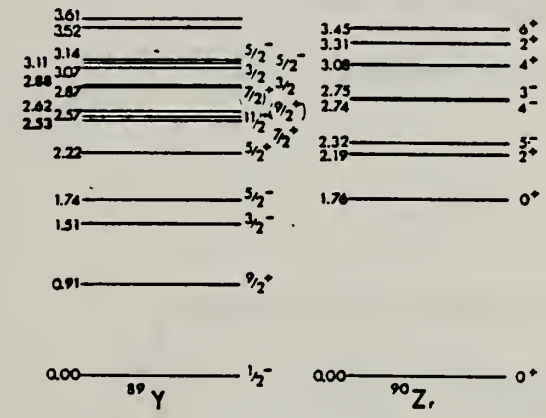

FIG. 1. Presently accepted level schemes for ^{89}Y and ^{90}Zr taken from the data of Van Patter (Ref. 8) and Ball (Ref. 9), respectively.

[8]D. M. Van Patter, Bull. Am. Phys. Soc. 15, 573 (1970).
[9]J. B. Ball, Bull. Am. Phys. Soc. 15, 574 (1970).

[over]

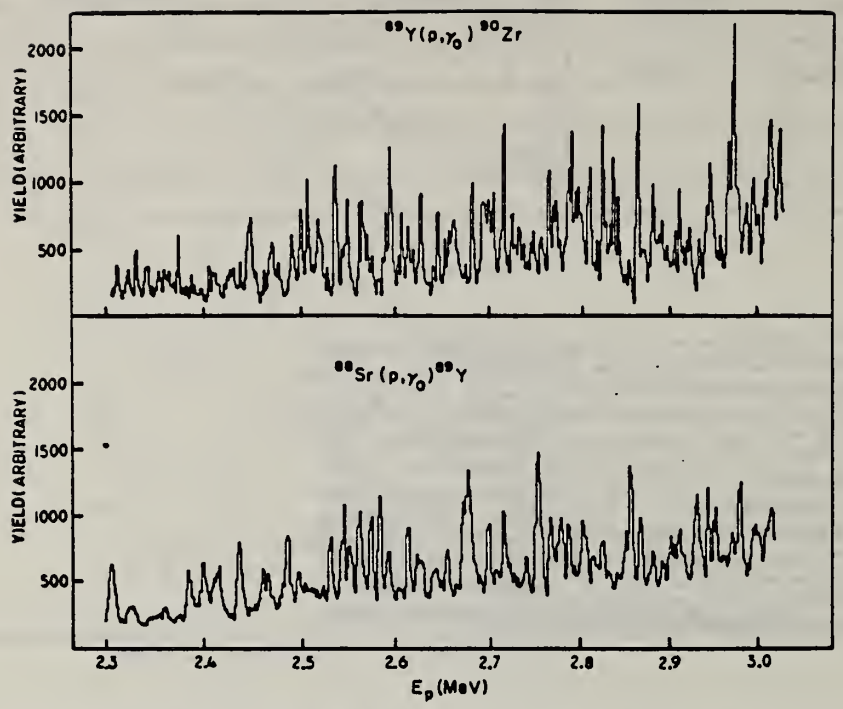

FIG. 2. Excitation functions for $^{88}Sr(p,\gamma_0)^{89}Y$ and $^{89}Y(p,\gamma_0)^{90}Zr$ over the energy region $E_p = 2.3$ to 3.0 MeV.

REF.	ELEM. SYM.	A	Z
H.J. Askin, J.K.F. Allen, R. Hicks, R.J. Petty and M.N. Thompson PICNS-72, 359 (1972) Sendai	Zr	90	40

METHOD	REF. NO.
	72As 10 hvm

REACTION	RESULT	EXCITATION ENERGY	SOURCE TYPE	SOURCE RANGE	DETECTOR TYPE	DETECTOR RANGE	ANGLE
G,P	SPC	13- 30	C	35	SCD-D		90
G,XN	ABX	11- 28	C	11- 28	BF3-I		4PI
G,XN	SPC	12- 15	C	20- 24	SCI-D		4PI

Table 1. Features observed in photoproton and photoneutron measurements.

T=6 states observed in ^{90}Zr (γ,p) (MeV)	14.27	16.15	17.17	19.37	(20.5)*		
Structure observed in ^{90}Zr (γ,n) (MeV)		16.2	17.2	19.3	(20.5)	21.8	23.7

*observed by protons decaying to 2nd excited state in ^{89}Y.

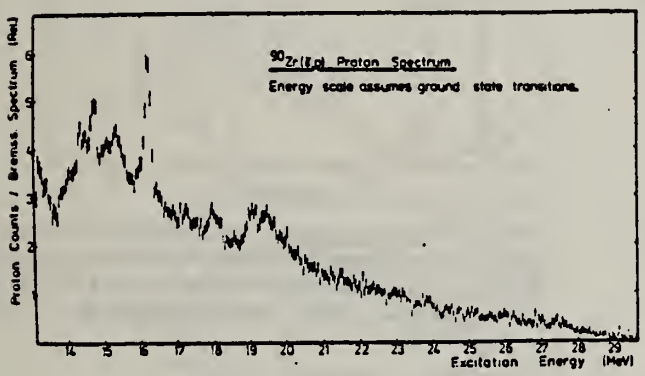

Fig. 2. ^{90}Zr Photoproton spectrum.

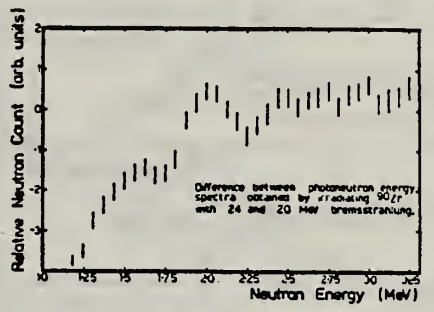

Fig. 4. Photoneutron spectrum from ^{90}Zr.

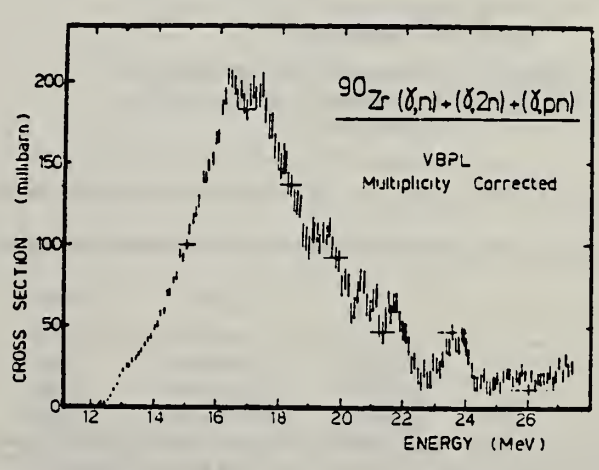

Fig. 3. Total photoneutron cross section of ^{90}Zr.

REF.

S. Fukuda and Y. Torizuka
Phys. Rev. Letters 29, 1109 (1972)

ELEM. SYM.	A	Z
Zr	90	40

METHOD

REF. NO.	
72 Fu 6	hmg

REACTION	RESULT	EXCITATION ENERGY	SOURCE		DETECTOR		ANGLE
			TYPE	RANGE	TYPE	RANGE	
E,E/	FMF	7- 38	D	150-250	MAG-D		DST

B(EL)

Inelastic electron scattering from the giant dipole resonance region in ^{90}Zr was measured. In addition to the usual dipole resonance we have found new resonances at 14.0 MeV and around 28 MeV. The spins and parities and transition strengths of these states are discussed.

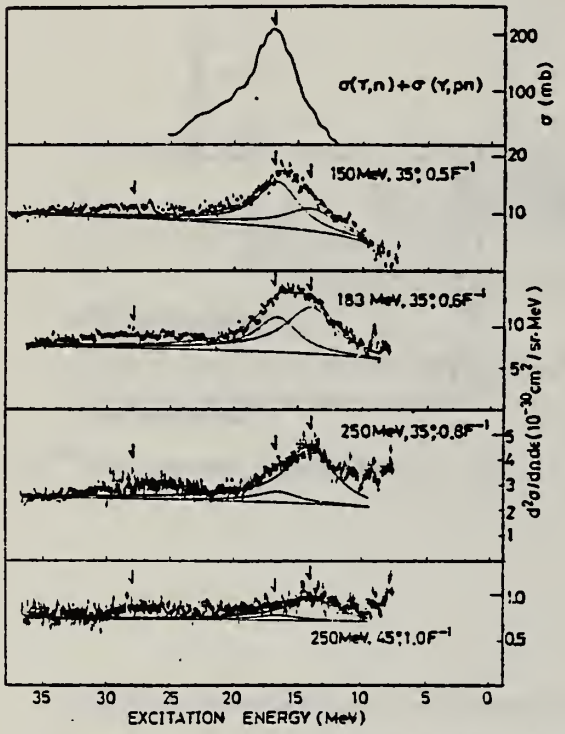

FIG 1. Spectra of photoreaction and electron scattering in ^{90}Zr. The arrows indicate the positions of the 14.0−, 16.65−, and 28-MeV peaks.

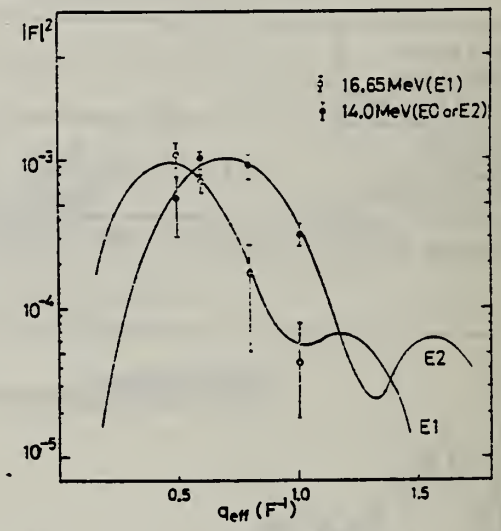

FIG. 2. The experimental form factors for the 14.0- and 16.65-MeV peaks are compared with the $E2$ and $E1$ form factors calculated with the DWBA code written by S. T. Tuan *et al.*, Nucl. Instrum. Methods 60, 70 (1968).

TABLE 1. $B(E1)$, $B(E2)$, and M_{fi}, and energy-weighted sum-rule (EWSR) limits.

E_x (MeV)	J^π	P^a	$E_x P^b$	(EWSR)^b	$\frac{E_x P}{\text{EWSR}}$
16.65	1^-	17.0 ± 5.0	283 ± 86	264	1.07 ± 0.32
14.0	2^+	990 ± 300	13900 ± 4200	24900	0.56 ± 0.17
14.0	0^+	2050 ± 610	28700 ± 8500	28000	1.03 ± 0.3

[a] P is $B(E1)$ in units e^2 F^2 for $J^\pi = 1^-$, $B(E2)$ in e^2 F^4 for $J^\pi = 2^+$, and $|M_{fi}|^2$ in F^4 for $J^\pi = 0^+$.

[b] Units are MeV times units of P.

U.S. DEPARTMENT OF COMMERCE
NATIONAL BUREAU OF STANDARDS
USCOMM-DC 26010-P64

REF.	ELEM. SYM.	A	Z
Stanley S. Hanna PICNS-72, p.453 Sendai	Zr	90	40

METHOD	REF. NO.	
	72 Ha 9	hvm

REACTION	RESULT	EXCITATION ENERGY	SOURCE		DETECTOR		ANGLE
			TYPE	RANGE	TYPE	RANGE	
$ P,G	ABX	13- 25	D	5- 17	NAI-D		DST

POLARIZED PROTONS

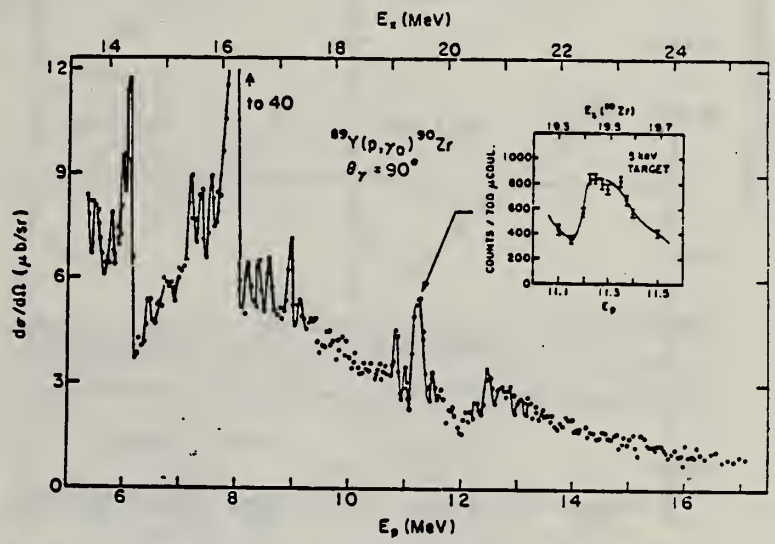

Fig. 4. The 90° yield from the unpolarized reaction $^{89}Y(p,\gamma_0)^{90}Zr$

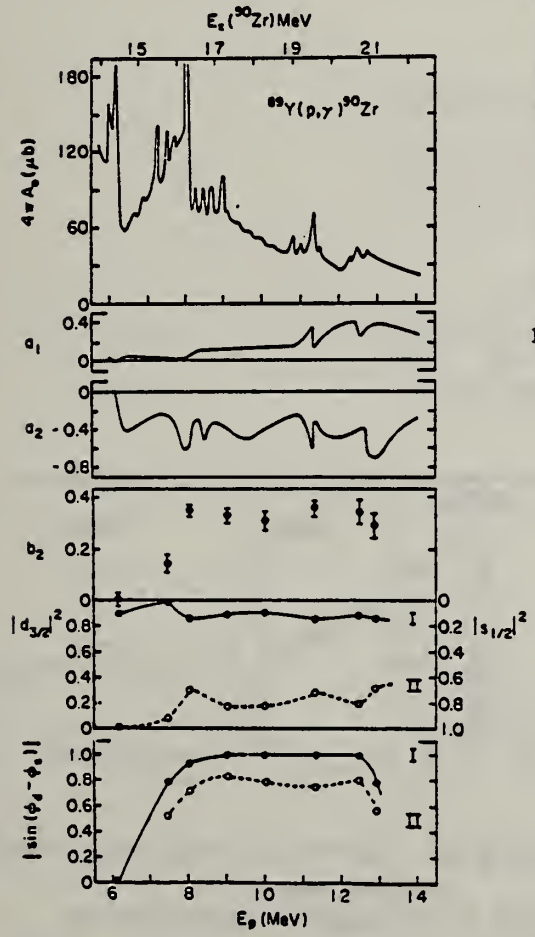

Fig. 7. Summary of the existing information on $^{89}Y(p,\gamma_0)^{90}Zr$. The two solutions for the proton channel are indicated by I and II.

(over)

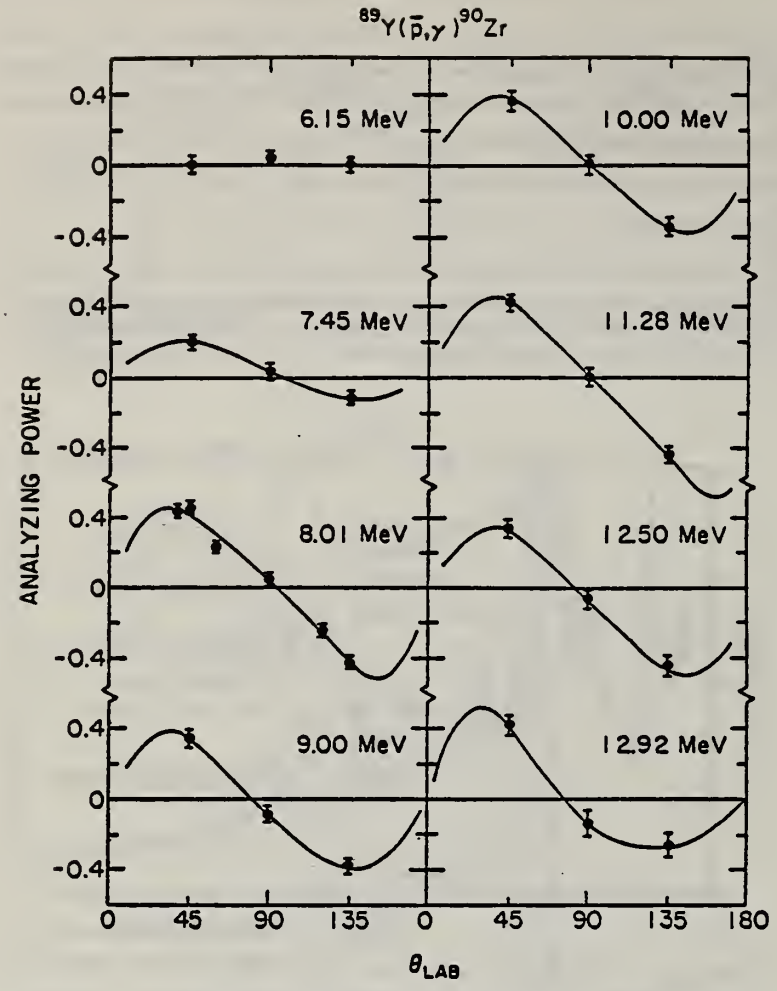

Fig. 6. Measured analyzing powers for the reaction $^{89}Y(p,\gamma_0)^{90}Zr$ plotted vs. angle.

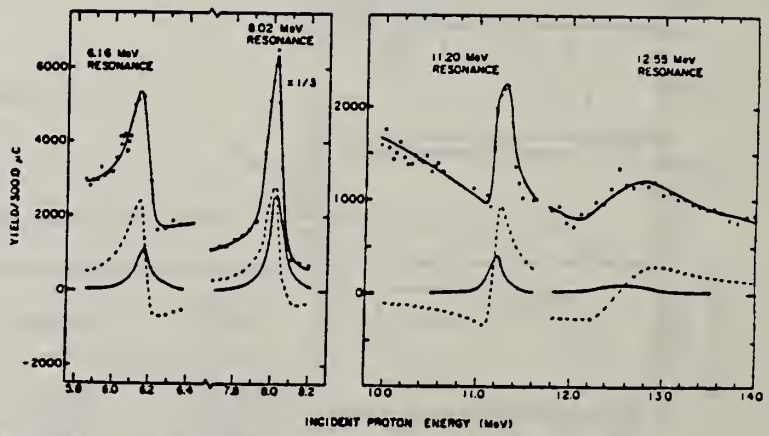

Fig. 5. Analysis of 1^- analogue resonances in $^{89}Y(p,\gamma_0)^{90}Zr$

REF.

F. R. Metzger
Nucl. Phys. A182, 213 (1972)

ELEM. SYM.	A	Z
Zr	90	40

METHOD

REF. NO.	
72 Me 5	egf

REACTION	RESULT	EXCITATION ENERGY	SOURCE		DETECTOR		ANGLE
			TYPE	RANGE	TYPE	RANGE	
G,G	LFT	2	C		SCD-D		DST

2 = 2.186

TABLE 1

Widths of the 2.186 MeV level in ^{90}Zr deduced from the various scattering experiments

Type of scatterer	Γ_0^2/Γ (meV)	
	98°	127°
natural Zr metal	4.90±0.20	4.96±0.28
enr. $^{90}ZrO_2$ single scatt.	4.61±0.19	4.90±0.21
enr. $^{90}ZrO_2$(^{27}Al+^{90}Zr) scatt.	4.84±0.29	5.15±0.46
average	4.77±0.13	4.95±0.16

TABLE 2

Comparison of the $B(E2\uparrow)$ deduced from inelastic electron scattering and from resonance fluorescence experiments for the 2.186 MeV 2$^+$ state in ^{90}Zr

Method		$B(E2\uparrow)e^2 \cdot fm^4$
(e, e') [a]	hydrodyn. model	830±19
	shell model	1000±23
(γ,γ')	present work	608±35
(e, e') [b]	hydrodyn. model	440±20
	shell model	440±30

[a]) Ref. [1]). (J. Bellicard et al., Nucl. Phys. A143 (1970) 213.
[b]) M. T. Mills, private communication, Sept. 1971.

REF.

K. Shoda, M. Sugawara, T. Saito, H. Miyase, A. Suzuki, S. Oikawa, and J. Uegaki
PICNS-72, 321 Sendai

EL.EM. SYM.	A	Z
Zr	90	40

METHOD

REF. NO.	
72 Sh 10	hvm

REACTION	RESULT	EXCITATION ENERGY	SOURCE		DETECTOR		ANGLE
			TYPE	RANGE	TYPE	RANGE	
E,P	SPC	16- 30	C	16- 30	MAG-D		UKN

I A STATES

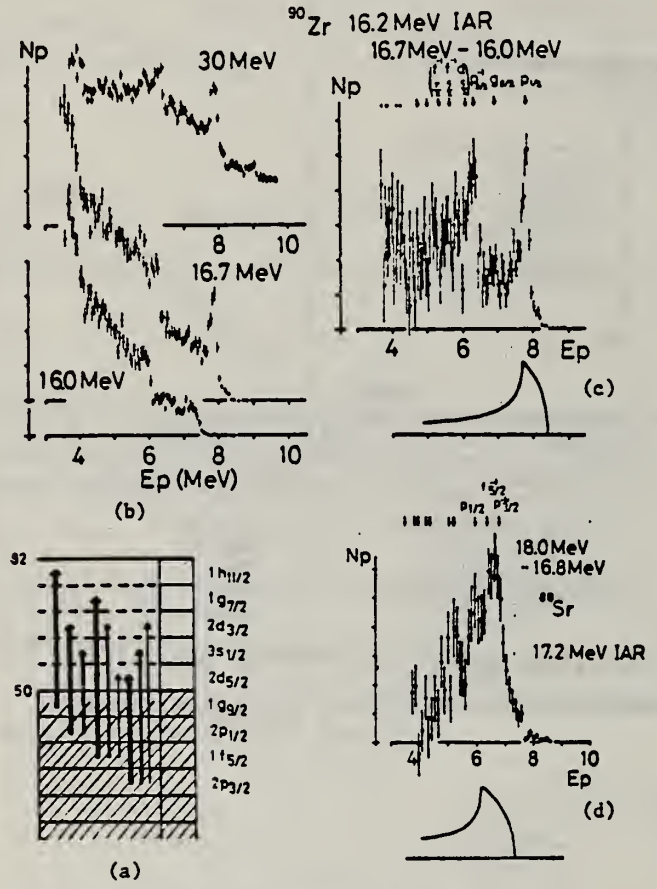

Fig. 7 (a): Shell model diagram of ^{90}Zr and ^{88}Sr.
(b): Energy distributions of ^{90}Zr(e,e'p).
(c): Energy distributions obtained from difference method. Residual states for 16.2 MeV IAR are shown by arrows.
(d): Energy distributions obtained from difference method for ^{88}Sr. Residual states for 17.2 MeV IAR are shown by arrows.

REF. Y. Torizuka, Y. Kojima, T. Saito, K. Itoh, A. Nakada, S. Mitsunobu, M. Nagao, K. Hosoyama, S. Fukuda
PICNS-72, p.171 Sendai

ELEM. SYM.	A	Z
Zr	90	40

METHOD

REF. NO. 72 To 6 hvm

REACTION	RESULT	EXCITATION ENERGY	SOURCE		DETECTOR		ANGLE
			TYPE	RANGE	TYPE	RANGE	
E,E/	FMF	0- 37	D	150-250	MAG-D		DST

LEVELS 14, 16.65

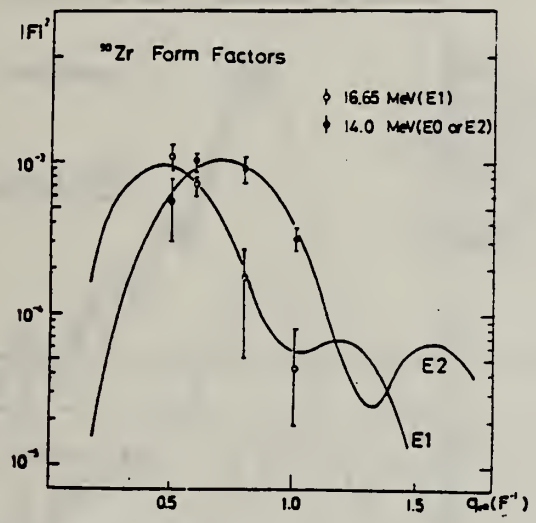

Fig. 5. The experimental form factors for the 14.0- and 16.65-MeV peaks are compared with the DWBA E2 and E1 form factors.

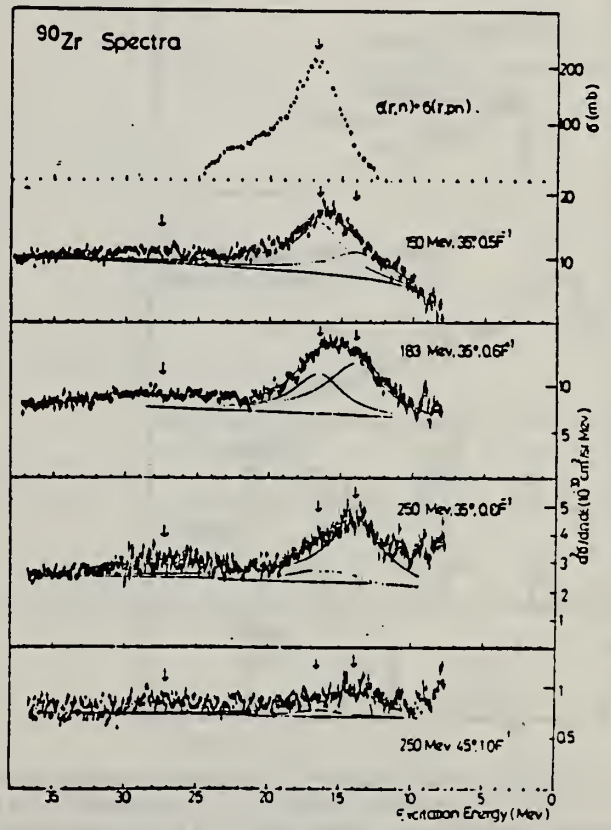

Fig. 4 The spectra of photoreaction and electron scattering

REF. H.J. Askin, R.S. Hicks, K.J.F. Allen, R.J. Petty and M.N. Thompson
Nucl. Phys. A204, 209 (1973)

ELEM. SYM.	A	Z
Zr	90	40

METHOD

REF. NO. 73 As 2 egf

REACTION	RESULT	EXCITATION ENERGY	SOURCE		DETECTOR		ANGLE
			TYPE	RANGE	TYPE	RANGE	
G,P		14- 29	C	31	SCD-D		90
G,XN	ABX	12- 28	C	12- 28	BF3-I		4PI*

*N SPC GIVEN 588

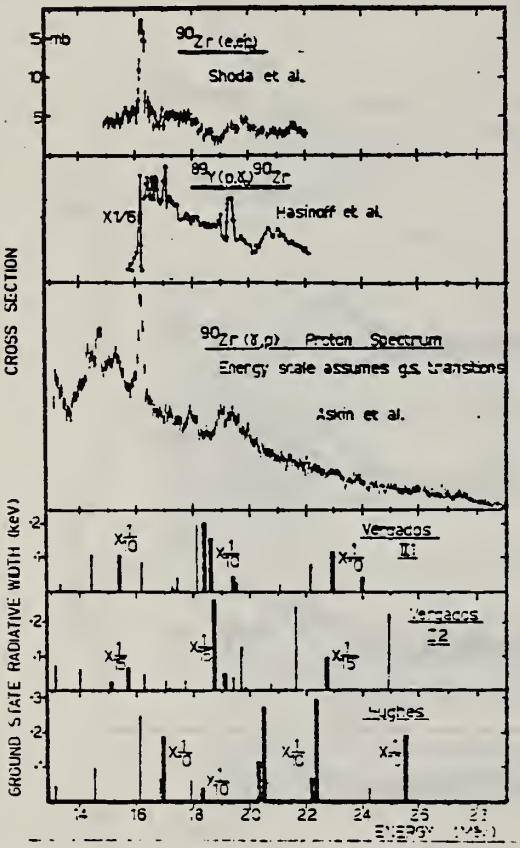

Fig. 3. Comparison of the presented $^{90}Zr(\gamma, p)$ proton spectrum with the $(e, e'p_0)$ data of Shoda [6]) and the (p,γ_0) measurement by Hasinoff *et al.* [5]). Also shown are the results of calculations by Hughes and Fallieros [3]) and Vergados and Kuo [4]) of the excitations and ground state radiative widths of $T_>$ states in ^{90}Zr.

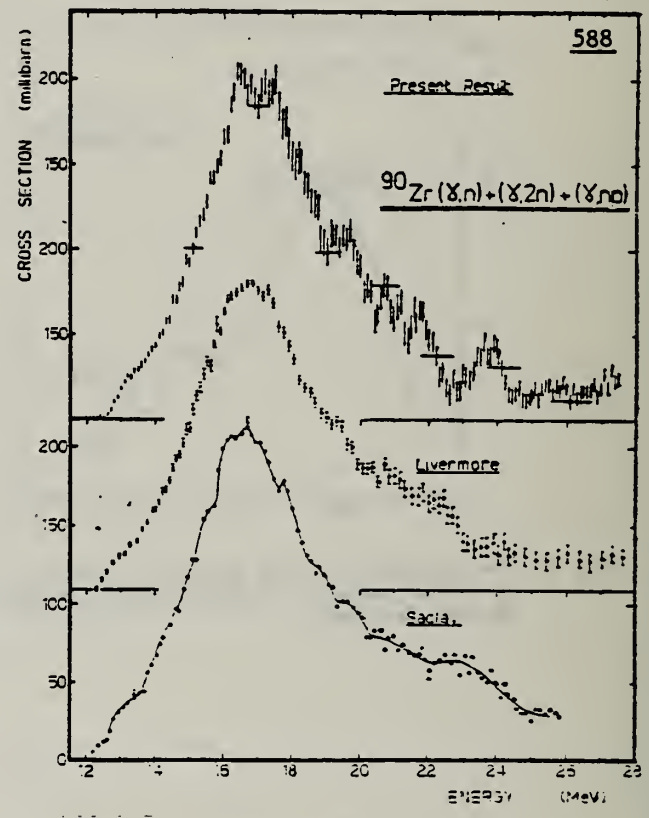

Fig. 4. The measured ^{90}Zr photoneutron cross section and comparison with the work of Berman *et al.* [19]) at Livermore and the Saclay group [20]).

(over)

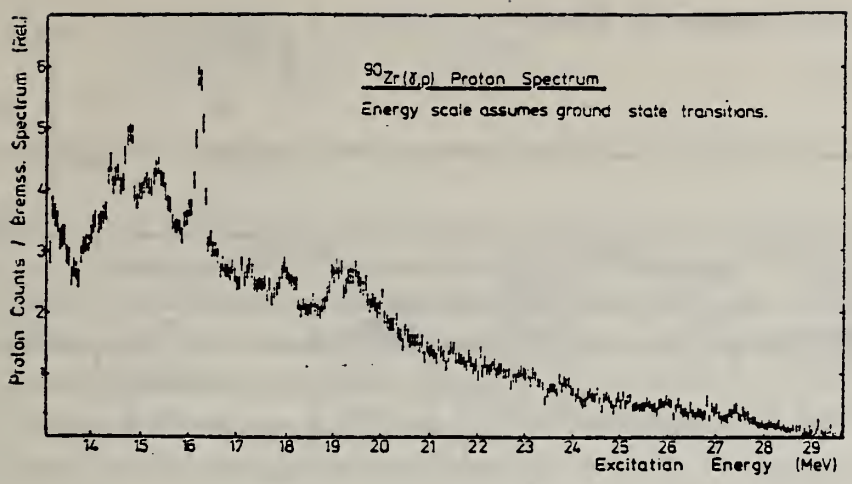

Fig. 2. The ^{90}Zr(γ, p) proton spectrum.

TABLE 1

$T = 6$ states observed in ^{90}Zr(γ, p)(MeV)	14.3	16.2	17.2	19.4	(20.7) [a])		
Structure observed in ^{90}Zr(γ, n) (MeV)		16.2	17.2	19.4	20.7	21.8	23.7

[a]) Observed by protons decaying to excited residual states in ^{89}Y.

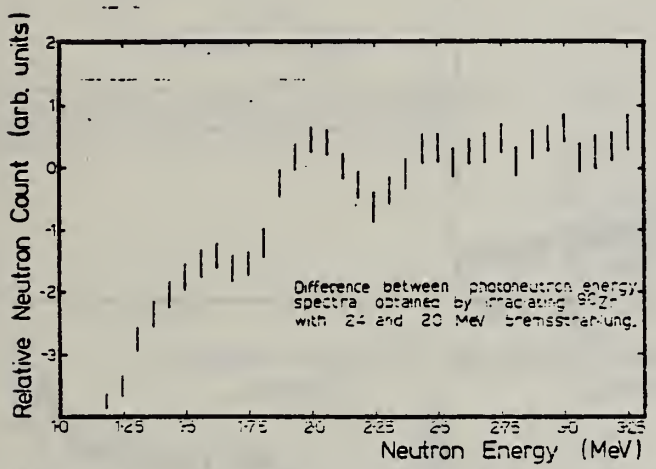

Fig. 5. Difference between the photoneutron energy spectrum measurements obtained using 24 and 20 MeV bremsstrahlung.

[3] T.A. Hughes et al., Nuclear isospin, ed. J.D. Anderson et al. (Academic Press, N.Y. 1969) p.109.

[4] J.D. Vergados et al., Phys. Lett. 35B (1971) 93.

[5] M. Hasinoff et al., Phys. Lett. 30B (1969) 337.

[6] K. Shoda et al., Phys. Rev. Lett. 23 (1969) 800.

[19] B.L. Berman et al., Phys. Rev. 162 (1967) 1098.

[20] A. Lepretre et al., Nucl. Phys. A175 (1971) 609.

REF. H.J. Askin, K.J.F. Allen, M.N. Thompson, K. Shoda, M. Sugawara, H. Miyase, B.N. Sung
PICNS-73, Vol. I, p. 561 Asilomar

ELEM. SYM.	A	Z
Zr	90	40

METHOD

REF. NO. 73 As 9 hmg

REACTION	RESULT	EXCITATION ENERGY	SOURCE TYPE	SOURCE RANGE	DETECTOR TYPE	DETECTOR RANGE	ANGLE
E,P	SPC	THR- 26	D	30	MAG-D		DST

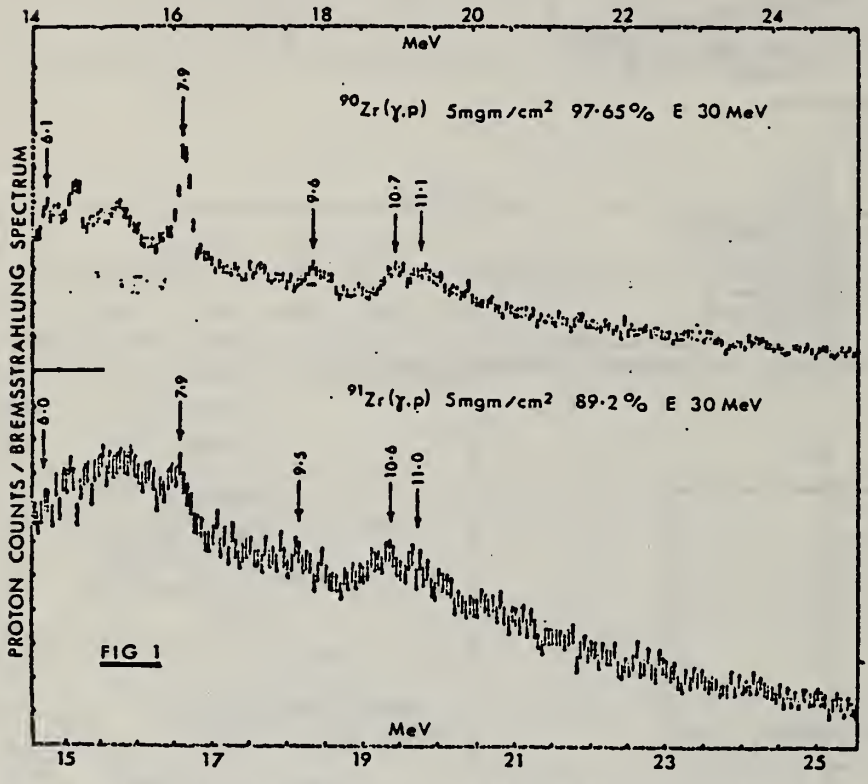

Arrows show proton energies. Horizontal scales indicate excitation energies assuming ground state transitions.

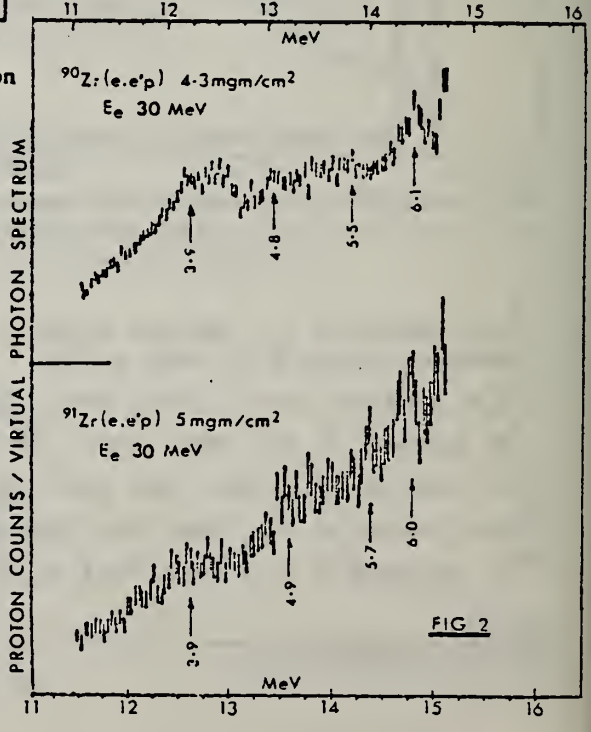

REF. D. Brajnik, D. Jamnik, G. Kernel, M. Korun, U. Miklavzic, B. Pucelj and A. Stanovnik
PICNS-73, Vol.I, p. 539 Asilomar

ELEM. SYM.	A	Z
Zr	90	40

METHOD

REF. NO.	
73 Br 12	hmg

REACTION	RESULT	EXCITATION ENERGY	SOURCE		DETECTOR		ANGLE
			TYPE	RANGE	TYPE	RANGE	
G,P	ABX	8- 24	C	14- 24	SCD-D		DST
G,2N	ABX	21- 28	C	20- 28	ACT-I		UKN
G,NP	ABX	19- 28	C	20- 28	ACT-I		UKN

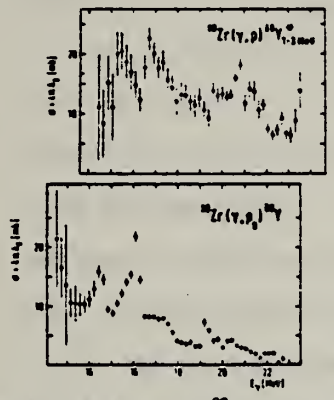

Fig.1. Cross section for the reaction $^{90}Zr(\gamma,p)$ leaving the residual nucleus ^{89}Y in excited states between 1 and 3 MeV (upper diagram). Photoproton cross section to the ground state of ^{89}Y (lower diagram).

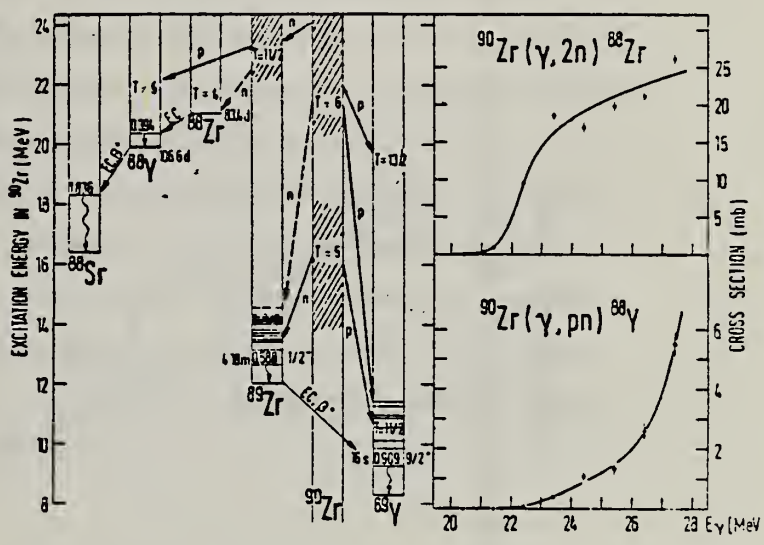

Fig.2. Cross sections for the reactions $^{90}Zr(\gamma,2n)^{88}Zr$ and $^{90}Zr(\gamma,np)^{88}Y$. The decay of the giant resonance is shematically shown in the left diagram.

REF. F.E. Cecil, L.W. Fagg, W.L. Bendel, N. Ensslin, E.C. Jones, Jr.
PICNS-73, Vol.I, p.699 Asilomar

ELEM. SYM.	A	Z
Zr	90	40

METHOD

REF. NO. 73 Ce 3 hmg

REACTION	RESULT	EXCITATION ENERGY	SOURCE		DETECTOR		ANGLE
			TYPE	RANGE	TYPE	RANGE	
E,E/	LFT	9	D	37- 61	MAG-D		180
		(9.1)					

Ground state M1 transition width = 117±23 eV.

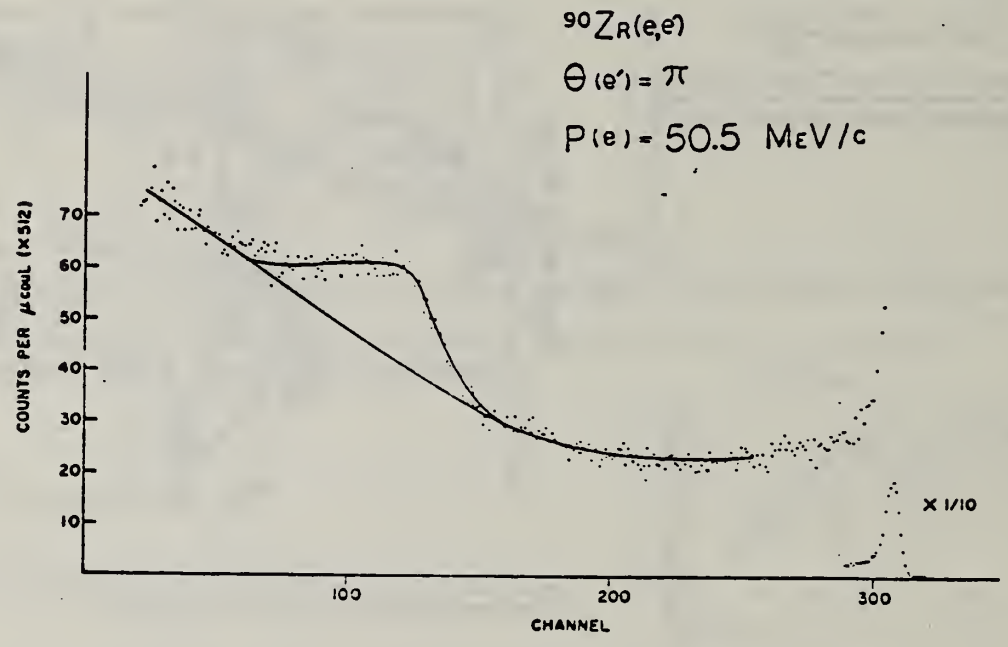

FIG 1

(over)

The giant magnetic dipole resonance recently observed in ^{208}Pb [1] tends to confirm the explanation by Vergados [2] of the deviations from single particle calculations of numerous magnetic dipole measurements in the Lead region. A recent measurement [3] of the M1 width of the 1+ state in ^{88}Sr similarly suggests the existence the giant M1 in ^{90}Zr. This suggestion is supported by an assumed shell model structure of ^{90}Zr of a closed $1g_{9/2}$ neutron shell in the presence of an open $1g_{7/2}$ shell. Within this assumption, the ground state M1 transition strength will be concentrated in the shell model configuration $(g_{9/2}^{-1} - g_{7/2})^{1+}$. In a recent search [4,5], no evidence was found for such a state excited in inelastic proton scattering. As such a non-observance may be attributed to a Serber like nucleon-nucleon effective interaction, a subsequent search has been has been carried out using inelastic electron scattering at 180^{o}.

In this experiment, a self supporting target of isotopically enriched ^{90}Zr, of thickness 66 mg/cm^2 was bombarded with electrons of 37, 50.5, and 60.5 MeV/c incident momentum from the NRL LINAC. The spectrum taken at 50.5 MeV/c is shown in figure 1. The broad peak centered around channel 110 in this figure is also evident in the 37 and 60.5 MeV/c data. This peak lies at an excitation energy of 9.1 MeV and is approximately 2.5 MeV FWHM. A preliminary analysis of the yields for this peak at the three bombarding momenta using the model described by Fagg et. al. [6] together with Coulomb distortion corrections [7] indicates the peak to be magnetic dipole in character. A tentative value of the ground state M1 transition width of this peak is then found to be 117 ± 23 eV. In contrast, the predicted width of an M1 transition from the ground state of ^{90}Zr to a 1+ state at 9.1 MeV whose shell model configuration is $(g_{9/2}^{-1} - g_{7/2})$ is 50 eV. [8]

REF.

M. Hasinoff, G.A. Fisher, and S.S. Hanna
Nucl. Phys. A216, 221 (1973)

ELEM. SYM.	A	Z
Zr	90	40

METHOD

REF. NO.: 73 Ha 13 egf

REACTION	RESULT	EXCITATION ENERGY	SOURCE TYPE	SOURCE RANGE	DETECTOR TYPE	DETECTOR RANGE	ANGLE
P,G	ABX	13- 25	D	5- 17	NAI-D		DST

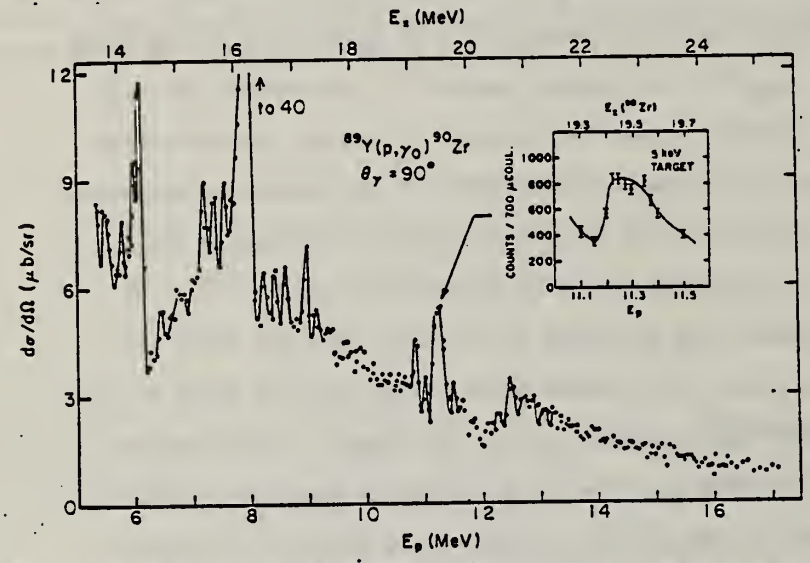

Fig. 3. Excitation curve for the reaction $^{89}Y(p,\gamma_0)^{90}Zr$ at $\theta_\gamma = 90°$. The solid lines indicate the sharp structures in the data. The insert shows the yield in the vicinity of the resonance at $E_p = 11.30$ MeV measured with a thin target.

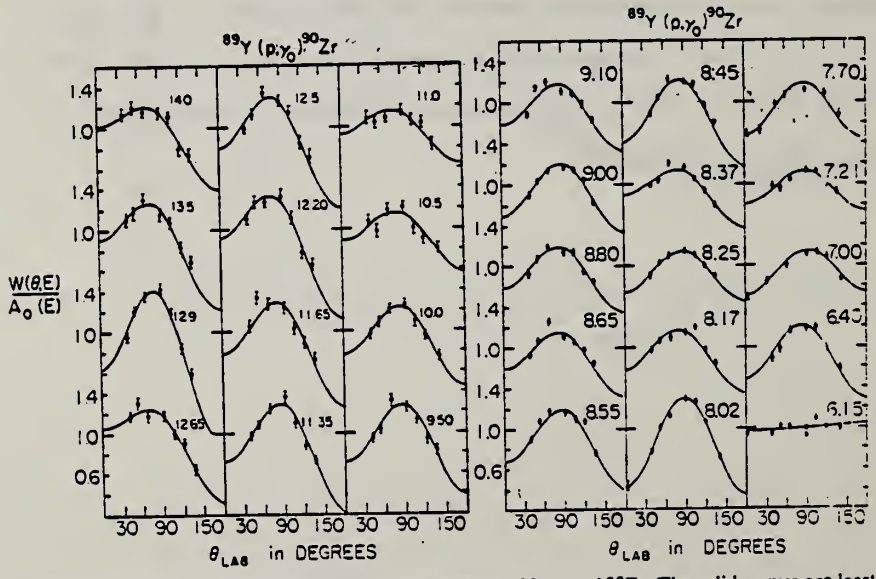

Fig. 4. Normalized angular distributions for the reaction $^{89}Y(p,\gamma_0)^{90}Zr$. The solid curves are least-square fits with Legendre polynomials up to P_2. The incident proton energy (in MeV) is listed in each case.

(over)

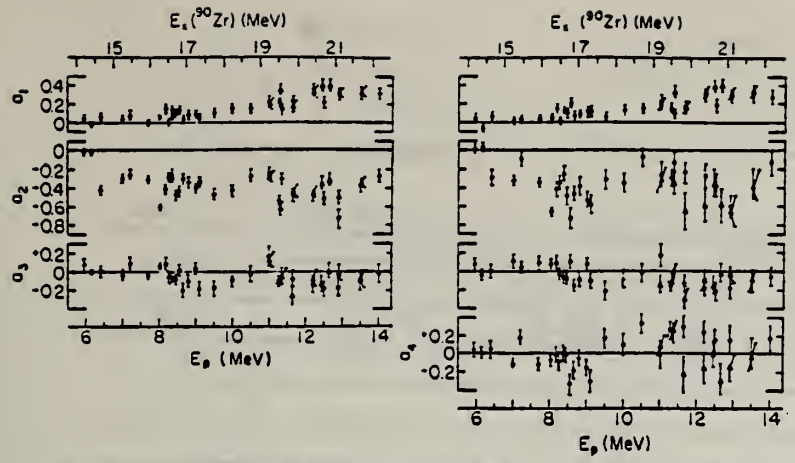

Fig. 6. Legendre polynomial coefficients obtained by fitting the $^{89}Y(p,\gamma_0)^{90}Zr$ angular distributions shown in fig. 4 with the series $W(\theta, E) = A_0[1 + \Sigma_{l=1}^{N} a_l(E)P_l(\cos\theta)]$ where $N = 3, 4$. The triangles represent data measured with a 120 keV thick target.

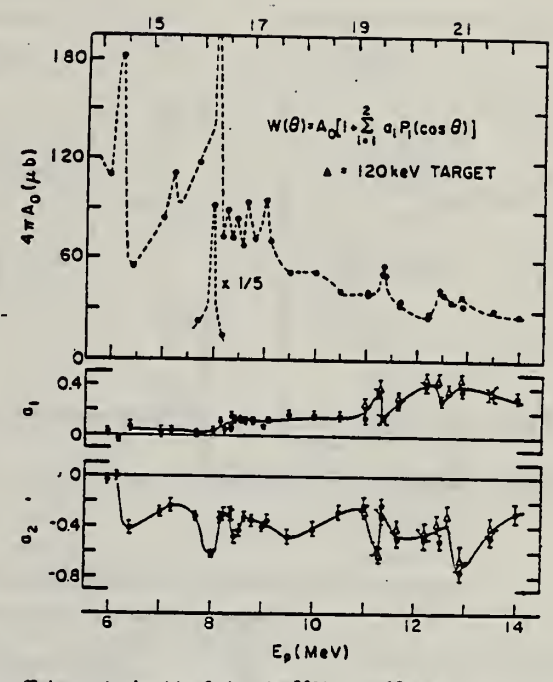

Fig. 5. Legendre polynomial coefficients obtained by fitting the $^{89}Y(p,\gamma_0)^{90}Zr$ angular distributions shown in fig. 4 with the series $W(\theta, E) = A_0[1 + \Sigma_{l=1}^{2} a_l(E)P_l(\cos\theta)]$. The solid lines drawn through the a_1 and a_2 coefficients are visual fits which show the correlation between the structures observed in the A_0, a_1 and a_2 curves. The scale for the total cross section ($4\pi A_0$) should be multiplied by 0.8.

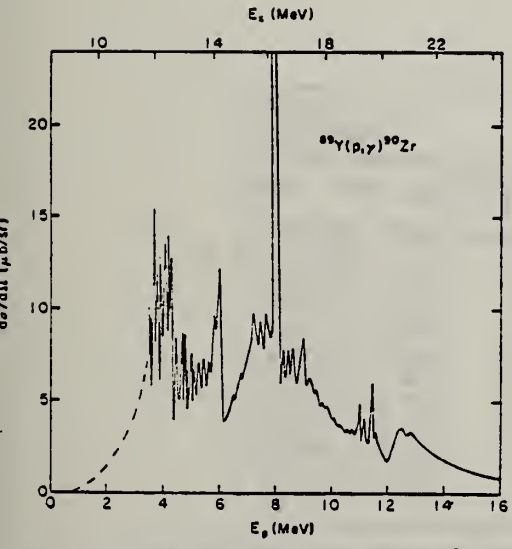

Fig. 14. Complete yield curve for the reaction $^{89}Y(p,\gamma_0)^{90}Zr$ at $\theta_\gamma = 90°$. The curve below $E_p = 5.40$ MeV is a symbolic representation of the data from ref. [23]) which shows a great amount of fine structure.

[23] E. Obst, F. Rauch, E. Rosle, Phys. Lett. 21 (1966) 50;
E. Obst, F. Rauch and H.G. Wahsweiler, Nucl. Phys. A103 (1967) 17. 373

REF. Phan Xuan Ho, J. Bellicard, Ph. Leconte, I. Sick
Nucl. Phys. A210, 189 (1973)

ELEM. SYM.	A	Z
Zr	90	40

METHOD

REF. NO. 73 Ho 4 egf

REACTION	RESULT	EXCITATION ENERGY	SOURCE TYPE	SOURCE RANGE	DETECTOR TYPE	DETECTOR RANGE	ANGLE
E,E/	FMF	2- 3	D	209	MAG-D		DST

2.19, 2.75, 3.08

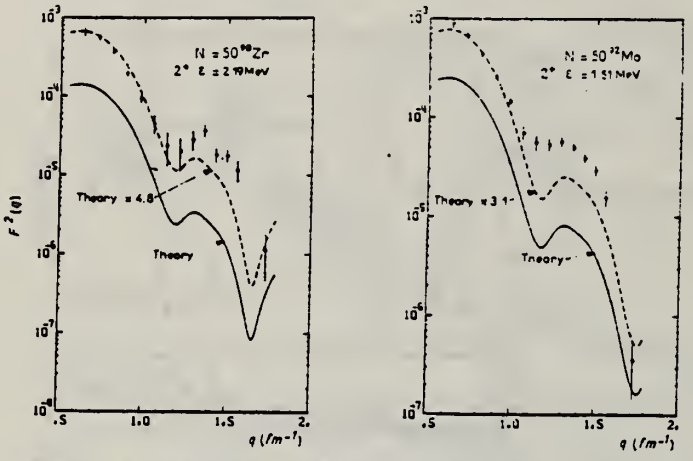

Fig. 5b. Squared inelastic form factor for 2^+ states of the $N = 50$ isotones.

TABLE 5

Inelastic cross sections for $E_e = 209$ MeV on ^{90}Zr

θ (deg.)	$(2^+)\varepsilon = 2.19$ MeV $d\sigma/d\Omega$(mb/sr)	$(3^-)\varepsilon = 2.75$ MeV $d\sigma/d\Omega$(mb/sr)	$(4^+)\varepsilon = 3.08$ MeV $d\sigma/d\Omega$(mb/sr)
35	0.142 E−1±0.170 E−2	0.220 E−1±0.160 E−2	
40	0.686 E−2±0.490 E−3	0.139 E−1±0.800 E−3	
45	0.278 E−2±0.170 E−3	0.846 E−2±0.430 E−3	0.624 E−3±0.176 E−3
50	0.941 E−3±0.610 E−4	0.443 E−2±0.230 E−3	0.419 E−3±0.580 E−4
55	0.307 E−3±0.360 E−4	0.221 E−2±0.130 E−3	0.271 E−3±0.350 E−4
60	0.101 E−3±0.250 E−4	0.984 E−3±0.540 E−4	0.170 E−3±0.240 E−4
65	0.374 E−4±0.165 E−4	0.346 E−3±0.200 E−4	0.115 E−3±0.150 E−4
70	0.232 E−4±0.100 E−4	0.102 E−3±0.900 E−5	0.637 E−4±0.820 E−5
75	0.242 E−4±0.640 E−5	0.242 E−4±0.460 E−5	0.322 E−4±0.450 E−5
80	0.233 E−4±0.350 E−5	0.199 E−4±0.260 E−5	0.161 E−4±0.220 E−5
85	0.892 E−5±0.163 E−5	0.220 E−4±0.150 E−5	0.403 E−5±0.950 E−6
90	0.658 E−5±0.104 E−5	0.216 E−4±0.120 E−5	0.657 E−6±0.353 E−6
95	0.334 E−5±0.950 E−6	0.174 E−4±0.180 E−5	0.378 E−7±0.193 E−7
110	0.155 E−6±0.900 E−7	0.509 E−5±0.370 E−6	0.417 E−6±0.238 E−6

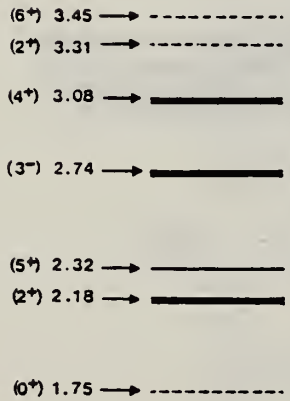

Energy level diagram given by ref. [24]). Levels excited in our experiment are shown with solid lines, dashed lines correspond to other levels. The experimental values are normalized with the elastic cross sections calculated by a phase shift program using a 3-parameter Gaussian model. The parameters ($c = 4.500$, $z = 2.530$, $w = 0.200$) are obtained from ref. [18]).

(over)

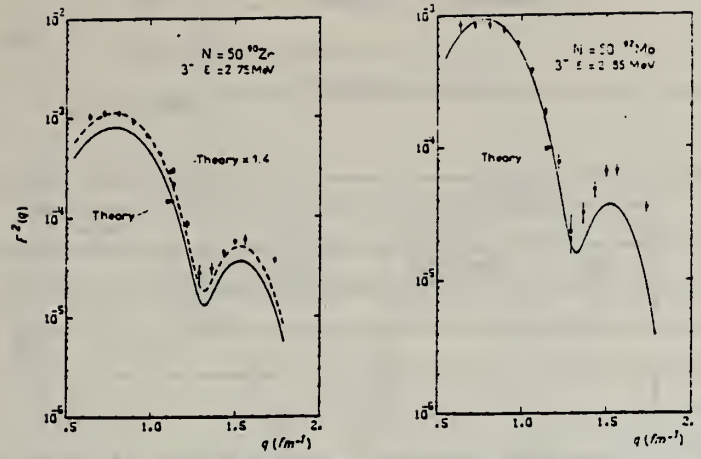

Fig. 6b. Squared inelastic form factor for 3^- states of the $N = 50$ isotones.

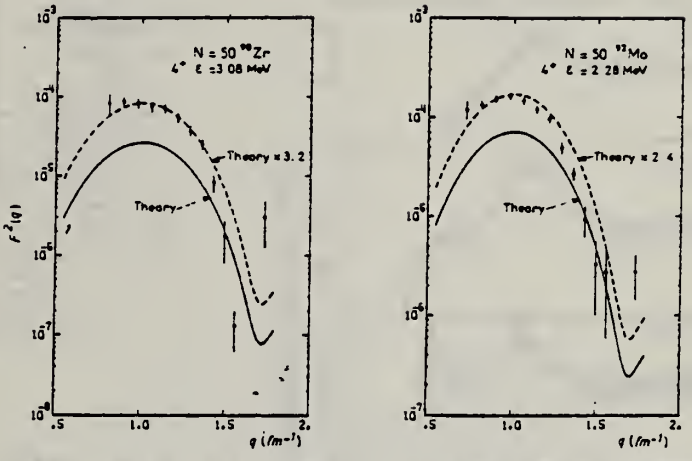

Fig. 7b. Squared inelastic form factor for 4^+ states of the $N = 50$ isotones.

[18] Phan-Xuan Ho, J. Bellicard, A. Bussiere, M. Priou, Nucl. Phys. A179 (1972) 529.
[24] Nuclear Data Sheets B (1970).

REF. Y. Torizuka, Y. Kojima, T. Saito, K. Itoh, A. Nakada, S. Mitsunobu, M. Nagao, K. Hosoyama, S. Fukuda, H. Miura
PICNS-73, Vol.I, p.675 Asilomar

ELEM. SYM.	A	Z
Zr	90	40

METHOD

REF. NO. 73 To 1 hmg

REACTION	RESULT	EXCITATION ENERGY	SOURCE		DETECTOR		ANGLE
			TYPE	RANGE	TYPE	RANGE	
E,E/	FMF	5- 37	D	150-250	MAG-D		DST

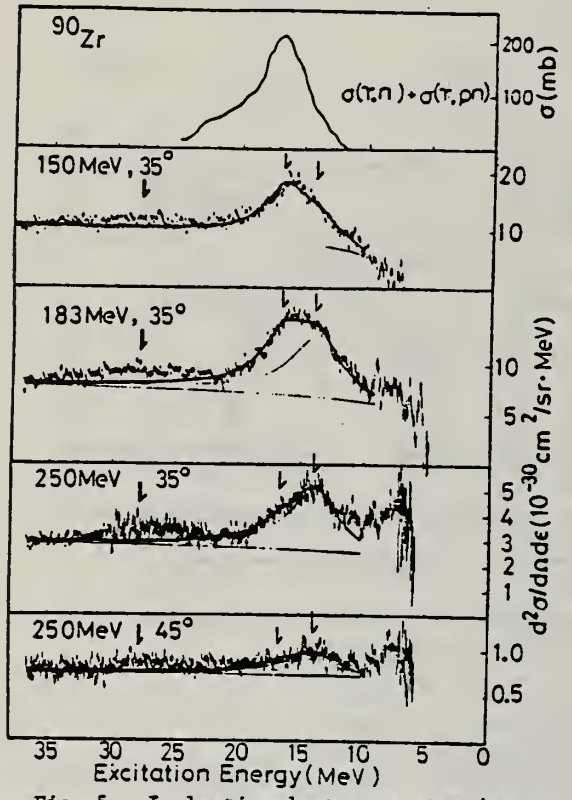

Fig. 5. Inelastic electron scattering spectra of ^{90}Zr from 7 to 35 MeV. The photoreaction spectrum is shown for comparison. The arrows indicate the peaks at 14.0, 16.7, and 27 MeV.

Table III. The B(EL), monopole matrix elements (ME), and fractions of the energy-weighted sum rule (EWSR) for the giant resonances in ^{90}Zr.

	E_x (MeV)	$B(EL)_{or}\|ME\|^2$	fraction of T=0 EWSR	fraction of T=1 EWSR
E2	14.0	990 e^2fm^4	0.522	
	27.0	280.3	0.285	0.228
E0	14.0	2050 fm^4	1.074	
	27.0	547.9	0.594	0.476
E1	16.65	17.0 e^2fm^2 *		0.89

· $\sqrt{\langle r^2 \rangle}$ = 4.255 fm

* B(E1) from (γ,n) is 18.8 e^2fm^2

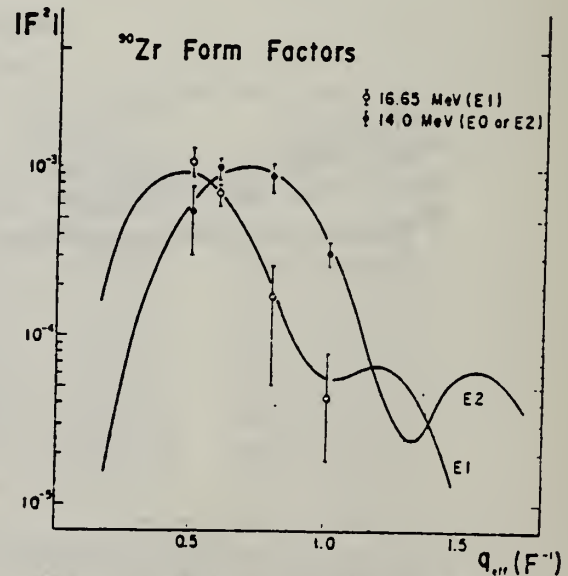

Fig. 6. The form factors for the 14.0- and 16.7-MeV states in ^{90}Zr.

(over)

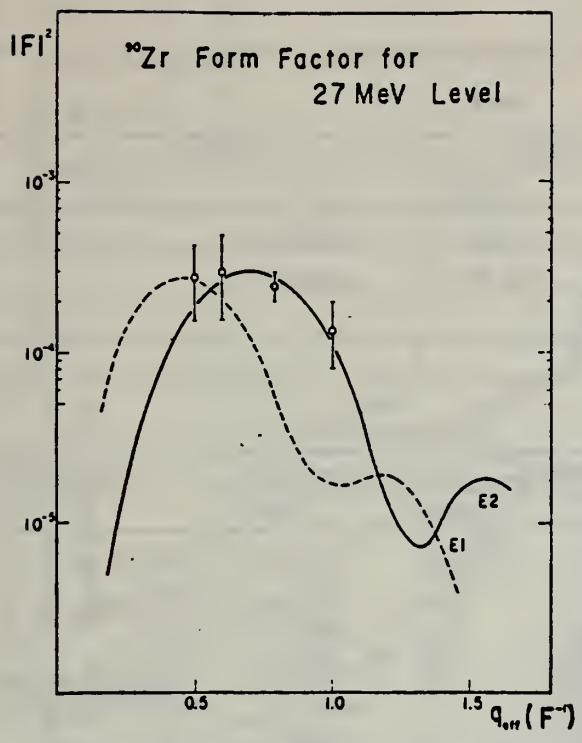

Fig. 8. The form factor for the 27-MeV state in ^{90}Zr.

REF.

H.J. Askin, K.J.F. Allen, M.N. Thompson, K. Shoda, M. Sugawara, H. Miyase, and B.N. Sung
Nucl. Phys. A220, 241 (1974)

ELEM. SYM.	A	Z
Zr	90	40

METHOD

REF. NO.	
74 As 4	egf

REACTION	RESULT	EXCITATION ENERGY	SOURCE		DETECTOR		ANGLE
			TYPE	RANGE	TYPE	RANGE	
G,P	SPC	8- 30	C	30	SCD-D		90
E,P	SPC	8- 30	D	20- 30	MAG-D		90

TABLE 1
Summary of results

Target	Proton energy E_p (MeV)	Excitation energy (MeV)		Residual levels ^{89}Y
		apparent	actual	
^{90}Zr	9.6	17.9	(19.4) [a]	(1.5 MeV, $\frac{3}{2}^-$) [a]
	11.1	19.4	19.4	g.s., $\frac{1}{2}^-$
	10.7	19.0	20.5–20.8 (20.7) [a]	(1.74 MeV, $\frac{3}{2}^-$) [a]
	12.5	20.8	20.8	g.s., $\frac{1}{2}^-$
	11.3	19.6	21.2–21.4	1.5 MeV, $\frac{3}{2}^-$ or 1.74 MeV, $\frac{5}{2}^-$
	10.2	18.5	(21.4) [a]	(2.88 MeV, $\frac{3}{2}^-$) [a]
				^{90}Y:
^{91}Zr	9.5	18.2	19.7 [b]	≈ 1.5 MeV [b]
	11.0	19.7	(19.7–19.9) [a]	g.s., 2$^-$ or 0.2 MeV, 3$^-$
	10.7	19.4	20.8–21.2 (21.1) [a]	1.4–1.8 (1.7) [b]
	12.5	21.2	(21.2) [a]	g.s., 2$^-$ or 0.2 MeV, 3$^-$
	11.3	20.0	21.5–21.8	1.5–1.8
	10.1	18.8	(≈ 21.5) [a]	(≈ 2.7 MeV) [a]

[a]) Most probable.
[b]) Consistent assignment.

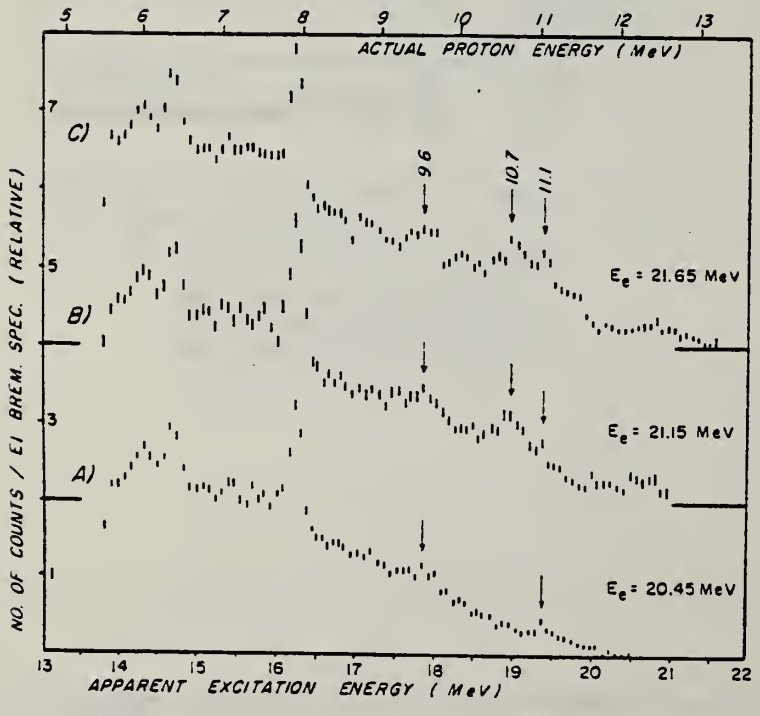

Fig. 3. The ^{90}Zr(e, e'p)^{89}Y spectra: (a) E_e(max) = 20.45 MeV; (b) E_e(max) = 21.15 MeV; (c) E_e(max) = 21.65 MeV.

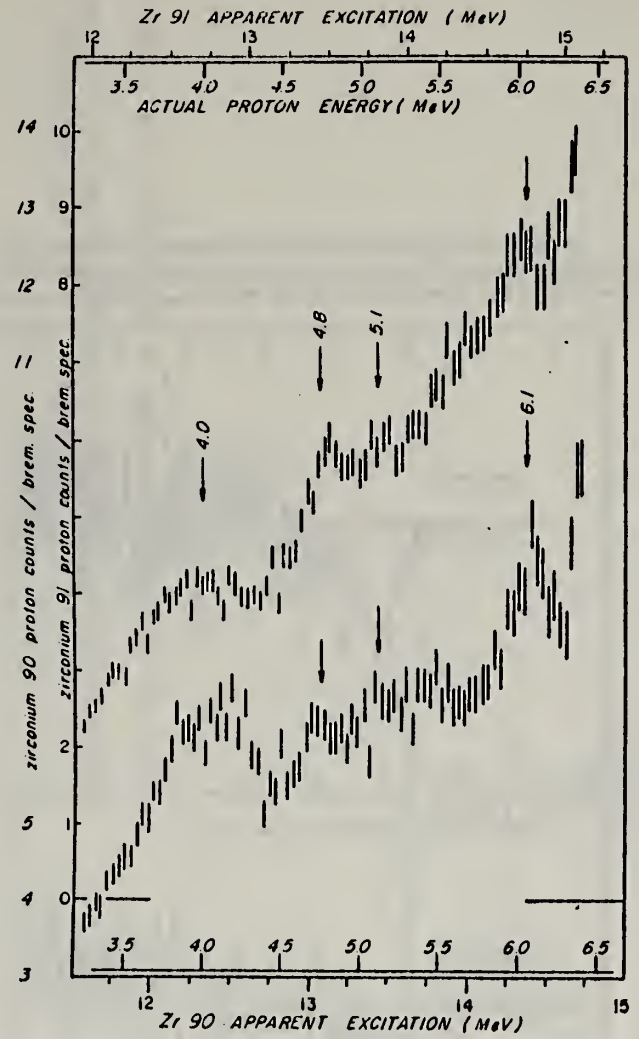

Fig. 1. The $^{91}Zr(e, e'p)^{90}Y$ proton spectrum (upper) and the $^{90}Zr(e, e'p)^{89}Y$ proton spectrum (lower). Bombarding electron energy E_e = 30 MeV. Spectra are plotted with a common proton energy scale.

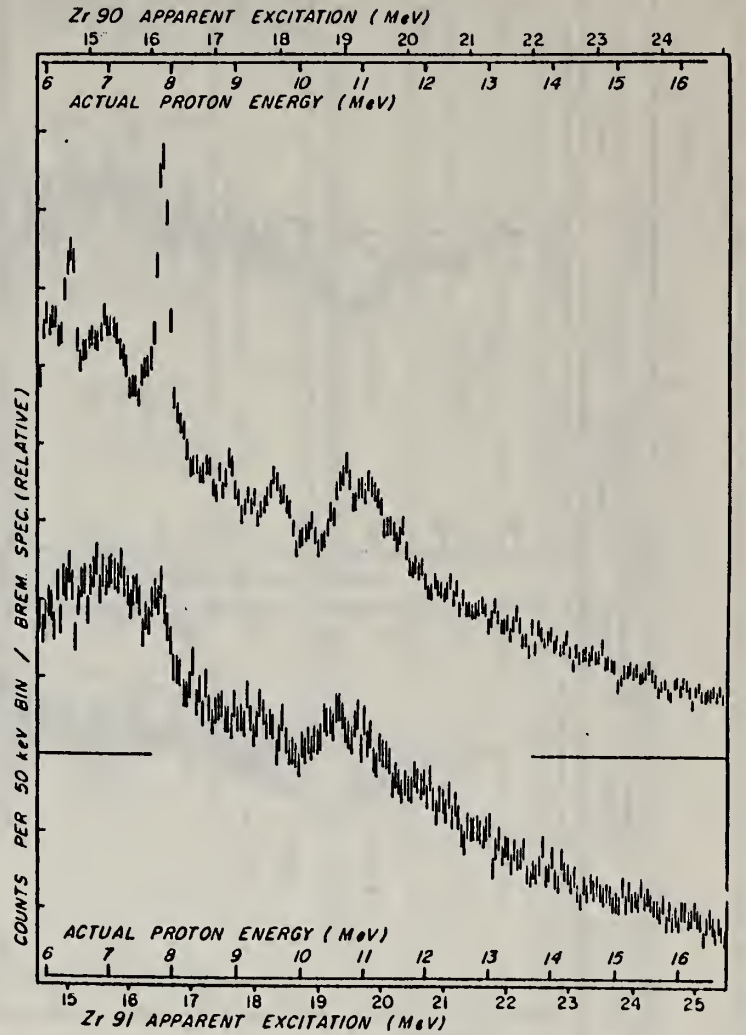

Fig. 2. The $^{90}Zr(\gamma, p)^{89}Y$ proton spectrum (upper) and the $^{91}Zr(\gamma, p)^{90}Y$ proton spectrum (lower). The E_γ endpoint = 30 MeV. Spectra are plotted with a common proton energy scale.

REACTION	RESULT	EXCITATION ENERGY	SOURCE TYPE	SOURCE RANGE	DETECTOR TYPE	DETECTOR RANGE	ANGLE

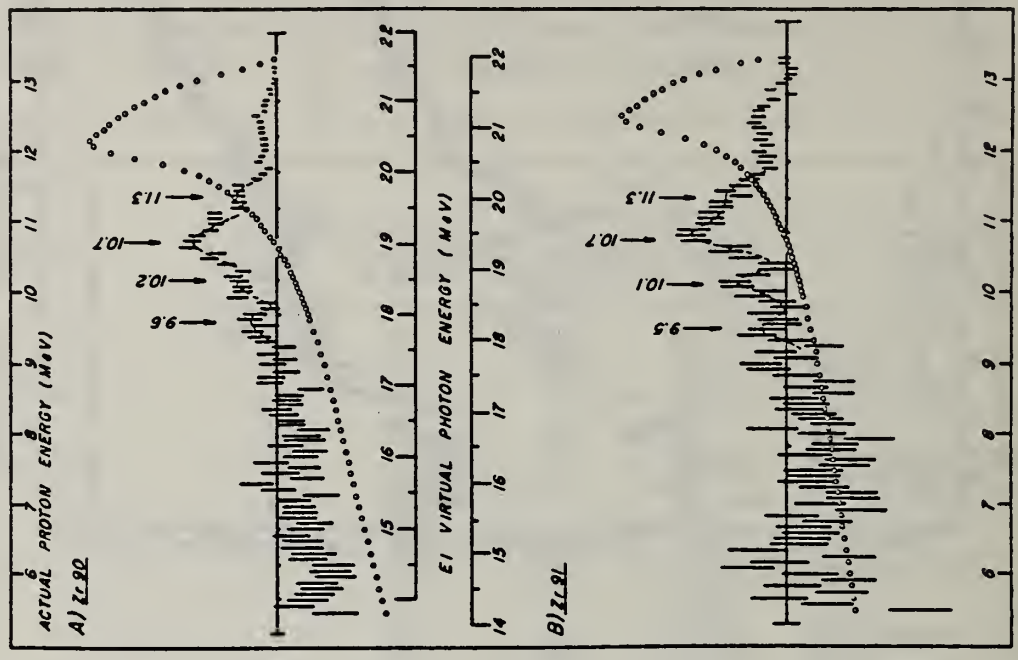

Fig. 7. Comparison of: (a) difference of ^{90}Zr(e, e'p)^{89}Y proton spectra recorded with E_e(max) = 21.65 MeV and 20.45 MeV and (b) difference of ^{91}Zr(e, e'p)^{90}Y spectra recorded with E_e(max) = 22.15 MeV and 21.15 MeV. Both proton difference spectra are plotted on a common proton energy scale. Corresponding E1 virtual photon difference spectra are superimposed.

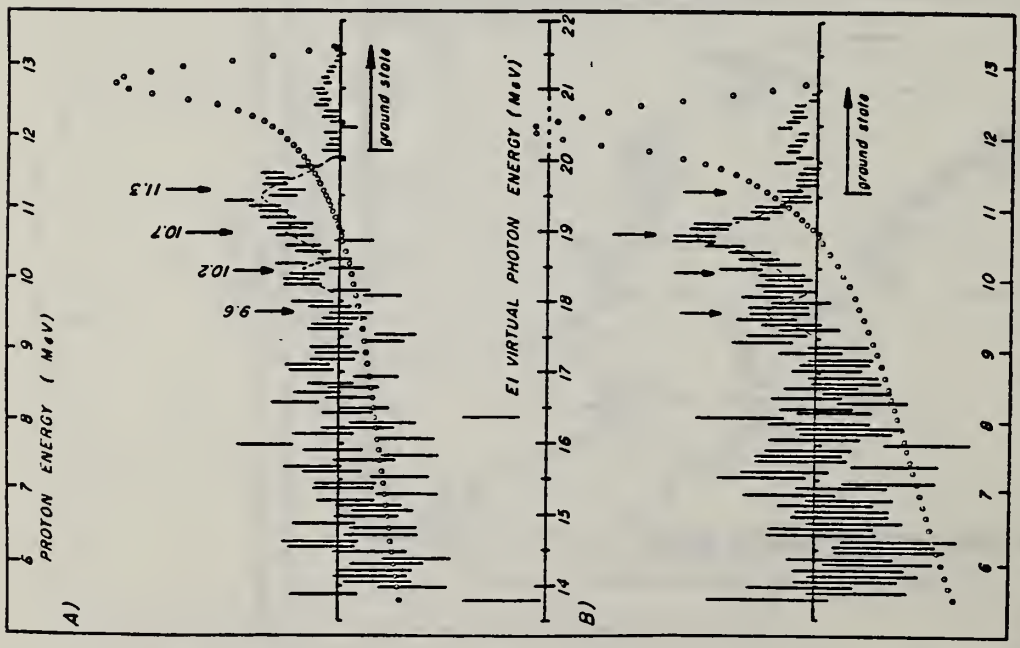

Fig. 5. Differences of ^{90}Zr(e, e'p)^{89}Y proton spectra recorded with: (a) E_e(max) = 21.65 MeV and E_e(max) = 21.15 MeV; (b) E_e(max) = 21.15 MeV and E_e(max) = 20.45 MeV. The corresponding differences in the E1 virtual photon spectra are superimposed (circles).

REF.

F. R. Metzger
Phys. Rev. C9, 1525 (1974)

ELEM. SYM.	A	Z
Zr	90	40

METHOD

REF. NO. 74 Me 2 hmg

REACTION	RESULT	EXCITATION ENERGY	SOURCE TYPE	SOURCE RANGE	DETECTOR TYPE	DETECTOR RANGE	ANGLE
G,G	LFT	2- 6	C	3- 6	SCD-D		DST

5 LEVELS 2-6 MEV

TABLE II. Results of resonance-fluorescence experiments with ^{90}Zr.

Level energy [a] (keV)	I^π	Γ_0^2/Γ (meV)	Γ_0/Γ	Γ_0 (meV)	$\frac{\Gamma_0(\text{expt.})}{\Gamma_0(\text{s.p.})}$
2186	2^+	4.89± 0.28	1.00	4.89± 0.28	5.1
3308±1	2^+	3.45± 0.60	0.75±0.02	4.6 ± 0.8	0.6
3842±1	2^+	24.0 ± 3.4	0.86±0.02	28 ± 4	1.7
4580±2	$1^{(-)}$	24.0 ± 4.0	0.5 ±0.1 [b]	48 ±13	3.7×10^{-4}
5504±2	$1^{(-)}$	48 ±17	0.6 ±0.1	80 ±32	3.5×10^{-4}
4120	2^+	0.3 ± 0.5			
4230	2^+	0.5 ± 0.9			
4680	2^+	<10			

[a] The energies listed for levels two to five are those determined in the present study. The last three energies are those reported in Ref. 4.
[b] Reference 13.

TABLE I. Comparison of experimental and theoretical yield ratios.

Level energy (MeV)	$N_{sc}(98°)/N_{sc}(127°)$ Experiment	Theory Spin 1	Theory Spin 2
3.31	2.2± 0.6	0.74	2.08
3.84	2.0± 0.3		
4.58	0.7± 0.2		

4
J.B. Ball, M.W. Johns, and K. Way, Nucl. Data A8, 407 (1970).
13
B. Seim, Ph.D. thesis, Johann Wolfgang Goethe-Universitaet, 1971 (unpublished).

F. Rauch and B. Seim
Phys. Letters 48B, 33 (1974)

Zr	90	40

METHOD

REF. NO.

74 Ra 3 egf

REACTION	RESULT	EXCITATION ENERGY	SOURCE		DETECTOR		ANGLE
			TYPE	RANGE	TYPE	RANGE	
P,G	ABX	13	D	4	SCD-D		55

4=4.75-4.88 MEV

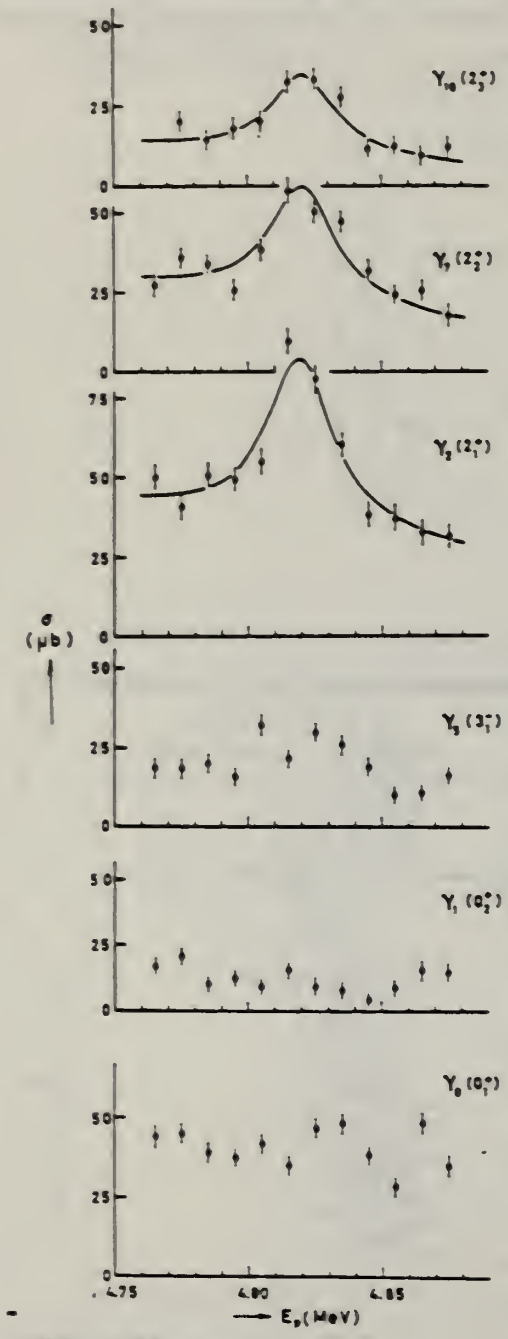

Table 1
Results for the γ decay of the ground state analog in ^{90}Zr.

	γ_2	γ_7	γ_{10}
E_γ(MeV) a)	10.92	9.80	9.26
σ_γ(μb) b)	64 ± 17	43 ± 13	30 ± 10
Γ_γ(eV) c)	15 ± 4	10 ± 3	7 ± 3
Γ_γ^{th}(eV) d)	≲ 4.4	≲ 3.2	≲ 2.9
σ_γ/E_γ^5(μb/MeV^5)	41 x 10^{-5}	47 x 10^{-5}	44 x 10^{-5}
σ_γ^c(μb) e)	84	49	39

a) Transition energy.
b) Experimental resonance cross section.
c) Experimental radiative width.
d) Direct radiative width.
e) Predicted compound resonance cross section.

Fig. 1. The ^{89}Y(p,γ)^{90}Zr excitation functions obtained in the present experiment. The solid lines are Breit–Wigner curves (compare text).

REF.

K. Shoda, M. Sugawara, T. Saito, and H. Miyase
Nucl. Phys. A221, 125 (1974)

ELEM. SYM.	A	Z
Zr	90	40

METHOD

REF. NO.	
74 Sh 6	egf

REACTION	RESULT	EXCITATION ENERGY	SOURCE		DETECTOR		ANGLE
			TYPE	RANGE	TYPE	RANGE	
E,P	ABX	12- 24	D	12- 30	MAG-D		DST

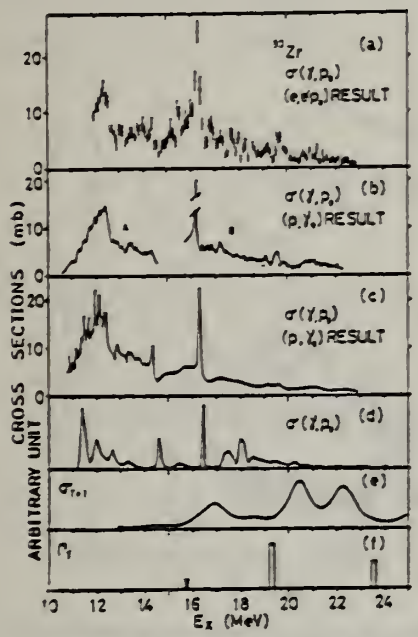

Fig. 11. Comparison of photoproton cross sections of ^{90}Zr. (a) Present result. (b) Curve A, ref. [31]); curve B, ref. [5]); open circles, ref. [32]). (c) Ref. [4]). (d), (e), (f) Theoretical estimates, refs. [12, 14, 15]) respectively.

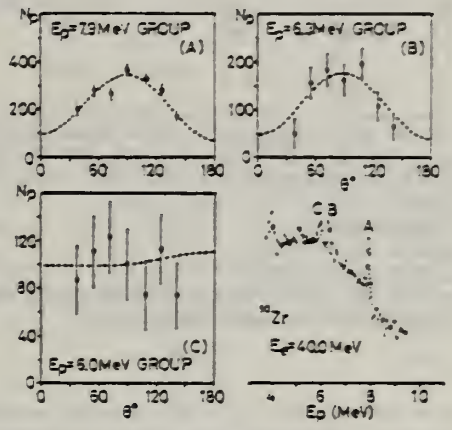

Fig. 14. Angular distributions of proton groups indicated by hatching in the proton spectrum which is summed over various angles. Both the dashed lines in the results of groups A and B are the results of (p, γ$_0$) for group A [ref. [2])]. The dashed line in the result of group C is the (p, γ$_0$) result of this group [2]).

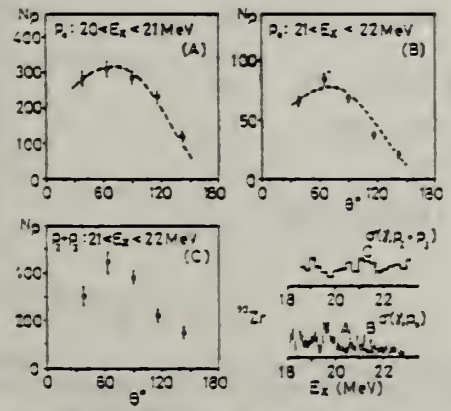

Fig. 15. Angular distributions of proton groups in the $T+1$ coherent resonance region. The groups are indicated by hatching in the cross sections. The dashed line in the figure shows the result of (p, γ$_0$) in the corresponding regions [5]).

(over)

TABLE 5

The radiative width of the narrow E1 IAR obtained from the proton group in the proton spectra

Nucleus	E_x (MeV)	E_p (MeV)	$E_{R1}(J^\pi)$ (MeV)	$\Gamma_\gamma \frac{\Gamma_{p_1}}{\Gamma}$ (eV)	Γ_γ [a] (eV)	$2(T+1)\frac{\Gamma_\gamma}{\Gamma_w}$ [a]	$2(T+1)\frac{\Gamma_\gamma}{\Gamma_{s.p.}}$ [a]	(p,γ_0) data Γ_γ (eV)
^{90}Zr	14.5	6.0	0 ($\frac{1}{2}^-$)	26	26 [b]	0.076		> 30 [a]
	16.3	7.9	0 ($\frac{1}{2}^-$)	74	126 [c]	0.26		> 60 [a]
	16.3	6.3	1.51 ($\frac{3}{2}^-$)	52				
^{89}Y	13.0 [d]	5.9	0 (0^+)	13	13 [b]		-0.13 [f]	18±3 [h]
	14.5 [e]	7.3	0 (0^+)	16	16 [b]		0.14 [f]	11±2 [g]
	15.9 [d]	8.7	0 (0^+)	42	42 [b]		0.68 [f]	40±8 [h]
^{88}Sr	17.1	6.5	0 ($\frac{1}{2}^-$)	9.5	14 [c]	0.029		
	17.1	5.6	0.85(($\frac{1}{2}^-$))	4.9				
	17.3	6.7	0 ($\frac{1}{2}^-$)	30	48 [c]	0.094		
	17.3	5.9	0.85(($\frac{1}{2}^-$))	18				

The available data with the (p,γ_0) experiment are shown in the last column.

[a]) The errors may be ≈ 30% (for ^{90}Zr, ^{88}Sr) and ≈ 50% (for ^{89}Y) including the uncertainty of the process to separate the proton group.

[b]) $\Gamma_{p_0}/\Gamma = 1$ was assumed.

[c]) $(\Gamma_{p_0}+\Gamma_{p_2})/\Gamma = 1$ was assumed.

[d]) $J^\pi = \frac{1}{2}^-$ was assigned as shown in table 3.

[e]) $J^\pi = \frac{3}{2}^-$ was assigned as shown in table 3.

[f]) Correction was made for the spectroscopic factors on the ground state and the excited state with the data of the (He^3, d) and (d, p) reactions respectively.

[g]) Ref. [27]).

[h]) Ref. [6]).

[2] J.L. Black et al., Phys. Lett. 11 (1964) 135; J.L. Black et al., Nucl. Phys. A92 (1967) 365.

[4] W.M. Mason et al., Nucl. Phys. A135 (1969) 193.

[5] M. Hasinoff et al., Phys. Lett. 30B (1969) 337.

[6] P. Paul, nuclear structure studies using electron scattering and photoreaction, ed. K. Shoda and H. Ui (Research report of Lab. Nucl. Sci. Tohoku Univ. vol. 5, 1972) p. 343.

[12] A. Piazza et al., Phys. Lett. 25B (1967) 579.

[14] T.A. Hughes et al., Nuclear isospin, ed. J.D. Anderson et al. (Academic Press, New York, 1969) p. 104.

[15] J.D. Vergados et al., Phys. Lett. 35B (1971) 93.

[27] J.L. Black et al., Nucl. Phys. A92 (1967) 365.

[31] E. Obst et al., Phys. Lett. 21 (1966) 50.

[32] P. Axel, et al., Phys. Rev. Lett. 19 (1967) 1343.

REF. K. Shoda, H. Miyase, M. Sugawara, T. Saito, S. Oikawa, A. Suzuki, J. Uegaki
Nucl. Phys. A239, 397 (1975)

ELEM. SYM.	A	Z
Zr	90	40

METHOD

REF. NO.: 75 Sh 4 egf

REACTION	RESULT	EXCITATION ENERGY	SOURCE TYPE	SOURCE RANGE	DETECTOR TYPE	DETECTOR RANGE	ANGLE
E,P	ABX	14- 24	D	14- 25	MAG-D		90

El virtual photon spectrum used to obtain (γ,p) cross sections.

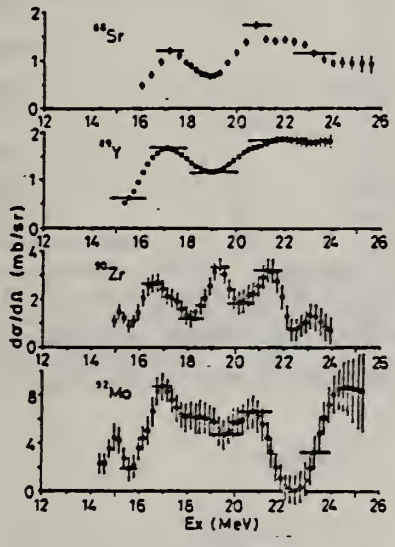

Fig. 3. Differential (γ, p) cross sections at $\theta = 90°$ analysed from (e, e'p) cross sections by the least structure method.

TABLE 2

The parameters of the angular distributions determined by the least-squares fits with $d\sigma/d\Omega = A[1+B\sin^2\theta(1-p\cos\theta)]$

	^{88}Sr	^{90}Zr	^{92}Mo
E_0 (MeV)	21.5	22	20
A a)	1	2.04	6.67
B	0.59	0.69	0.057
p	0.59	0.47	2.3

a) Relative value.

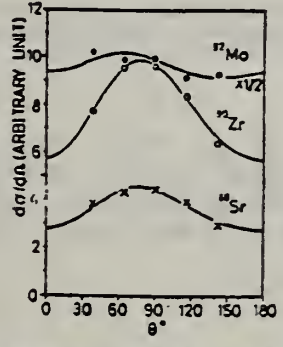

Fig. 4. Angular distributions of protons from the (e, e'p) reaction. The bombarding energies are 21.5, 22 and 20 MeV for ^{88}Sr, ^{90}Zr and ^{92}Mo respectively. The best fit curves obtained with eq. (7) are also shown.

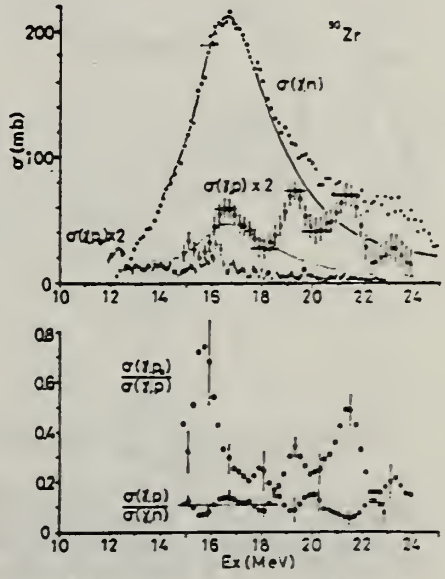

Fig. 7. The caption is the same as in fig. 5.

15
K. Shoda et al., Nucl. Phys. A221 (1974) 125
18
A. Lepretre et al., Nucl. Phys. A175 (1971) 609

REF.	ELEM. SYM.	A	Z
R. P. Singhal, S. W. Brain, C. S. Curran, W. A. Gillespie, A. Johnston, E. W. Lees and A. G. Slight J. Phys. (London) G1, 588 (1975)	Zr	90	40

METHOD	REF. NO.	
	75 Si 11	egf

REACTION	RESULT	EXCITATION ENERGY	SOURCE		DETECTOR		ANGLE
			TYPE	RANGE	TYPE	RANGE	
E,E/	FMF	2- 6	D	53-112	MAG-D		DST

13 STATES,2.18-5.3

Figures 6, 7, and 8 also give form factors for other levels.

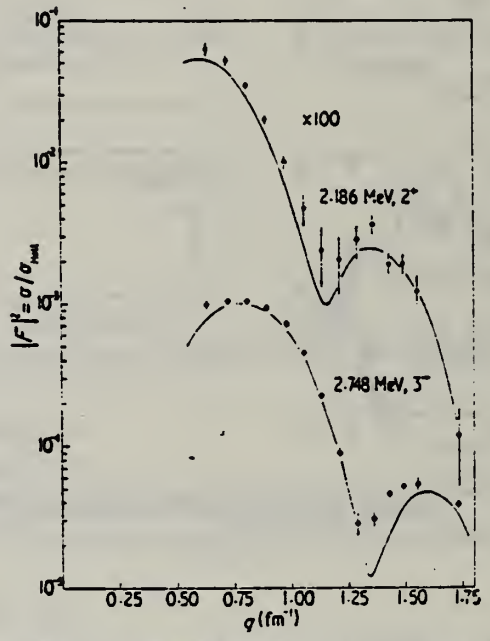

Figure 3. A comparison of the high momentum transfer data of Phan-Xuan-Ho *et al* (1973) with the extrapolation of the fits obtained in the present experiment to 209 MeV. The parameters of the fit are presented in table 3.

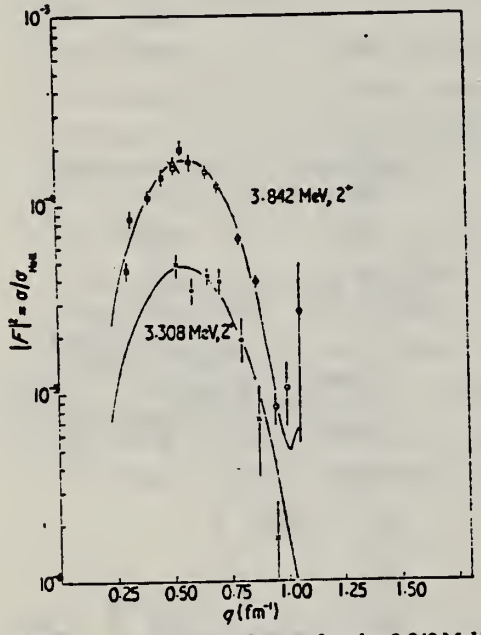

Figure 4. Inelastic form factors for the 3·842 MeV, 2⁺ (□ and ○) and for the 3·308 MeV, 2⁺ (×) levels. The data points □ are those of Bellicard *et al* (1970). The solid lines are the best fits to these levels with the model independent measurements of Metzger (1974) used as constraints (see text).

Bellicard et al., Nucl. Phys. A143, 213 (1970).
Metzger, Phys. Rev. C9, 1525 (1974).
Phan-Xuan-Ho et al., Nucl. Phys. A210, 189 (1973).
Singhal et al., Nucl. Phys. A218, 189 (1974).

(over)

Table 3. Results for the analysis of the present data using the Tassie model.

Excitation energy (MeV)	J^π	χ^2/D	c_{tr} (fm)	t_{tr} (fm)	R_{tr} (fm)	$B(EL\uparrow)$ (e^2fm^{2L})	$B(EL\uparrow)/B(EL\uparrow)_{sp}$
2·186[a]	2^+	1·16	4·32	2·76	5·82±0·11	673±59	5·50±0·48
2·319	5^-	0·79	3·19	2·31	6·75±0·08	(2·12±0·12)×10^{7}[b]	8·37±0·47
2·748	3^-	2·10[c]	4·34	2·54	6·18±0·28	8·74±1·00×10^{6}	25·2±2·9
3·077	4^+	1·03	4·33	2·15	6·15±0·27	2·95±0·80×10^{5}	3·32±0·90
3·308	2^+	1·30	4·52	2·76[d]	5·96	64	0·53
		0·94	4·06	3·22	6·13±0·52	69±18[e]	0·56±0·15
3·842	2^+	1·42	4·45	2·76	5·91	230	1·88
		1·18	4·75	2·15	5·58±0·30	206±36[e]	1·68±0·29
3·97	5^-	0·40	4·14	2·31[d]	7·02±0·60	2·62±1·00×10^{7}	10·4±4·0
4·07	4^+?	0·40	3·15	2·15[d]	5·56±0·34	(4·0±2·4)×10^{6}	0·45±0·27
	5^-?	0·30	4·50	2·31[d]	7·16±0·30	(1·6±0·9)×10^{7}	6·4±3·6
4·34	4^+	0·48	3·98	2·15[d]	5·95±0·16	1·50±0·40×10^{5}	1·69±0·45
4·47	4^+	0·98	4·93	2·15[d]	6·53±0·12	3·45±0·65×10^{5}	3·87±0·73
5·64	3^-	1·61	4·31	2·54[d]	6·16±0·09	6760±950	1·95±0·27
5·78	3^-	0·83	4·13	2·54[d]	6·05±0·13	1450±220	0·42±0·06
5·30 to 5·50 region	4^+?	1·13	4·45	2·15[d]	6·22±0·35	3·1±0·7×10^{5}	3·5±0·8

[a] This is a re-analysis of the level and the numbers are very slightly different from those in Singhal *et al* (1974).
[b] The (n, n′) point was treated as a datum point for the fit. See text.
[c] One datum point (Billicard *et al* 1970) is contributing 15·2 to the χ^2 function.
[d] t_{tr} was fixed (see text).
[e] The (γ, γ') point was treated as a datum point for the fit. See text.

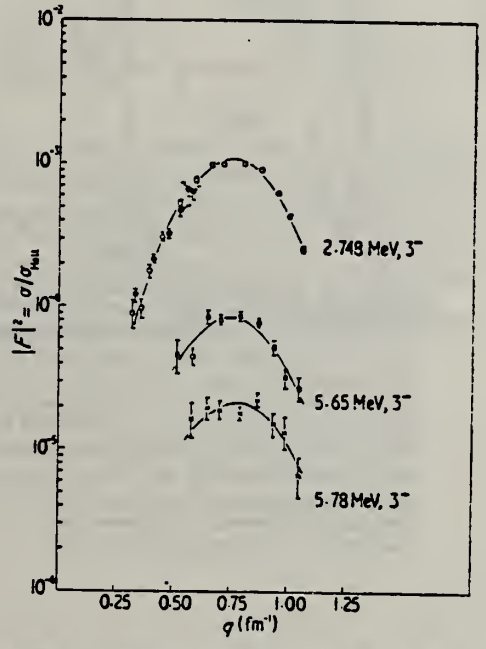

Figure 5. Inelastic form factors for the octupole transitions studied. The transitions shown are to the 2·748 MeV (● and ○), the 5·64 MeV (□) and to the 5·78 MeV (×) levels respectively. The solid circles for the 2·748 MeV level are data points taken from Bellicard *et al* (1970). Solid lines are the fits obtained by using the Tassie model.

REF.

D. Brajnik, D. Jamnik, G. Kernel, M. Korun, U. Miklavzic, B. Pucelj, and A. Stanovnik
Phys. Rev. C13, 1852 (1976)

ELEM. SYM.	A	Z
Zr	90	40

METHOD

REF. NO. 76 Br 5 hmg

REACTION	RESULT	EXCITATION ENERGY	SOURCE		DETECTOR		ANGLE
			TYPE	RANGE	TYPE	RANGE	
G,N	ABX	13- 30	C	13- 32	ACT-I		4PI [1]
G,2N	ABX	20- 31	C	13- 32	ACT-I		4PI
G,NP	ABX	20- 31	C	13- 32	ACT-I		4PI

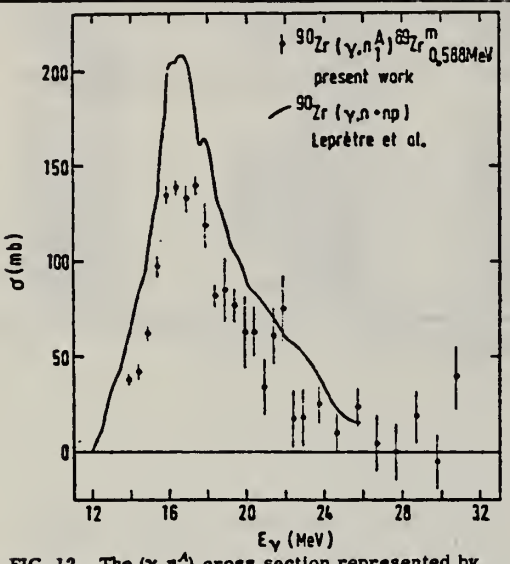

FIG. 12. The (γ, n_1^A) cross section represented by data points contains, in addition to the $^{90}Zr(\gamma, n_1)^{89}Zr_{0.588}$ contribution, also contributions of all photoneutron cross sections involving those residual ^{89}Zr states which subsequently decay to the first-excited state. For comparison the $(\gamma, n+np)$ data of Leprêtre *et al.* (Ref. 6) (continuous curve) are also shown.

TABLE I. Integrated cross sections for various photonuclear reaction channels.

Reactions	Energy region of integration (MeV)	Integrated cross section (MeV mb)
(γ, p_0)	13–23.5	79±7
$(\gamma, p)_{0.5-3\ MeV}$	15–18	35±4
	15–23.5	83±9
$(\gamma, p)_{3-5\ MeV}$	17–23.5	10±5
$(\gamma, p)_{5-7\ MeV}$	18.5–23.5	29±8
(γ, p_{tot})	13–23.5	206±19
	13–18	101±10
(γ, p_1^A)	14–31.5	35±5
	14–23.5	20±3
	14–18	5±1
(γ, n_1^A)	14–31.5	850±70
(γ, n)	14–31.5	1300±100
(γ, np)	20–31	14±6
$(\gamma, 2n)$	21–31	141±15

[1] ISOMER YIELD

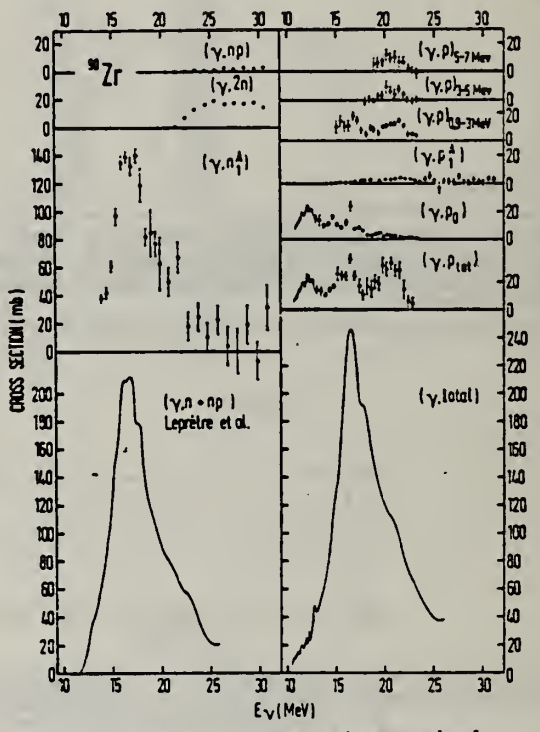

FIG. 14. Cross sections integrated over angles for processes studied in the present work (data points) are displayed with the exception of the total photoneutron cross section (solid curve in the bottom left corner of the diagram) for which the results of Leprêtre *et al.* (Ref. 6) are shown. The low-energy parts of the ground state and total photoproton cross sections are taken from Ref. 3 (solid curves). In the bottom right corner the sum of the total photoproton, the $(\gamma, 2n)$ cross sections from the present experiment and $(\gamma, n+np)$ cross section of Ref. 6, is displayed. It represents to a good accuracy the total photoabsorption cross section.

FIG. 13. Cross sections for the reactions ^{90}Zr(γ,*np*)^{88}Y and ^{90}Zr(γ,2*n*)^{88}Zr. A comparison of present results for the cross section of the reaction ^{90}Zr(γ,2*n*)^{88}Zr with the data of Leprêtre *et al.* (Ref. 6) and Berman *et al.* (Ref. 1) is given in the lower diagram. The solid line is drawn arbitrarily through data points of the present results. The decay scheme shows the decay modes used for the determination of the cross sections (upper diagram).

[1] B. L. Berman, J. T. Caldwell, R. R. Harvey, M. A. Kelly, R. L. Bramblett, and S. C. Fultz, Phys. Rev. 162, 1098 (1967).

[2] P. Axel, D. M. Drake, S. Wheatstone, and S. S. Hanna, Phys. Rev. Lett. 19, 1343 (1967).

[3] W. M. Mason, G. Kernel, J. L. Black, and N. W. Tanner, Nucl. Phys. A135, 193 (1969).

[4] K. Shoda, M. Sugawara, T. Saito, and H. Miyase, Phys. Rev. Lett. 23, 800 (1969).

[5] M. Hasinoff, G. A. Fisher, H. M. Kuan, and S. S. Hanna, Phys. Lett. 30B, 337 (1969).

[6] A. Leprêtre, H. Beil, R. Bergère, P. Carlos, and A. Veyssière, Nucl. Phys. A175, 609 (1971).

[7] H. J. Askin, H. S. Hicks, K. J. F. Allen, R. J. Petty, and M. N. Thompson, Nucl. Phys. A204, 209 (1973).

[8] M. Hasinoff, G. A. Fisher, and S. S. Hanna, Nucl. Phys. A216, 221 (1973).

[9] K. Shoda, H. Miyase, M. Sugawara, T. Saito, S. Oikawa, A. Suzuki, and J. Uegaki, Nucl. Phys. A239, 397 (1975).

[10] S. Fallieros, B. Goulard, and R. H. Venter, Phys. Lett. 19, 398 (1965).

[11] K. Shoda, M. Sugawara, T. Saito, and H. Miyase, Nucl. Phys. A221, 125 (1974).

[12] S. S. Hanna, in *Nuclear Structure Studies Using Electron Scattering and Photoreactions, Sendai, Japan, 1972*, edited by K. Shoda and H. Ui (Tohoku University, Sendai, Japan, 1972), p. 453.

[13] D. Brajnik, D. Jamnik, G. Kernel, U. Miklavžič, and J. Snajder, Nucl. Instrum. 103, 189 (1972).

[14] J. Böhm, U. Miklavžič, B. Pucelj, J. Snajder, and M. Tiringer, Nucl. Instrum. (to be published).

[15] D. Brajnik, D. Jamnik, G. Kernel, U. Miklavžič, and A. Stanovnik, Phys. Rev. C 9, 1901 (1974).

[16] J. L. Black and N. W. Tanner, Phys. Lett. 11, 135 (1964).

REACTION	RESULT	EXCITATION ENERGY	SOURCE		DETECTOR		ANGLE
			TYPE	RANGE	TYPE	RANGE	
G,P	ABX	8- 23	C	14- 24	SCD-D		DST[1]
G,P	ABX	13- 23	C	14- 24	SCD-D		DST[2]
G,P	ABX	14- 31	C	14- 32	ACT-I		4PI[3]

[1] TOT AND EXCIT STATE
[2] GROUND STATE
[3] ISOMER YIELD

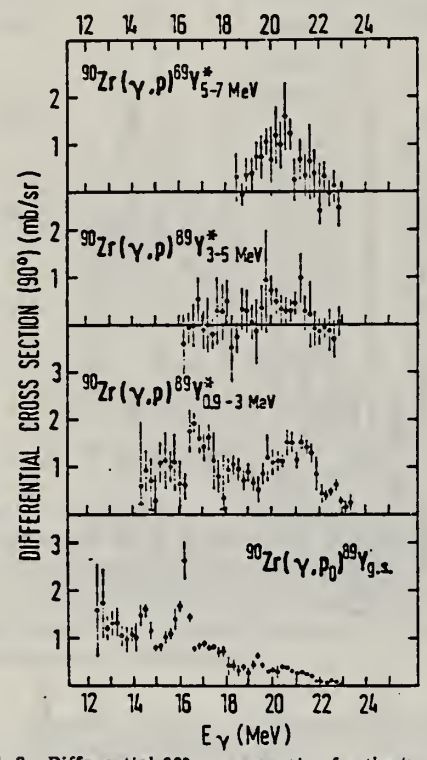

FIG. 3. Differential 90° cross section for the (γ,p_0) reaction and differential summed cross sections for reactions involving various regions of excitations in the residual nucleus ^{89}Y.

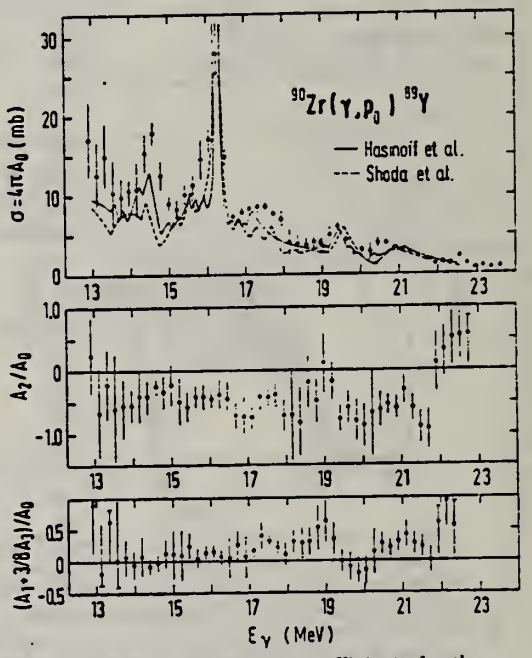

FIG. 4. Legendre polynomial coefficients for the angular distributions of protons in the reaction $^{90}Zr(\gamma,p_0)^{89}Y$ obtained from differential cross sections for the angles 30°, 90°, and 150° assuming an angular dependence of the form $W(\theta)=\sum_{l=0}^{l=3}A_l P_l(\cos\theta)$. Cross sections for particular angles were determined from measured spectra by means of a least-squares-fit analysis (Ref. 13). On the top diagram present results for $\sigma=4\pi A_0$ (data points) are compared to the data of Refs. 11 and 8.

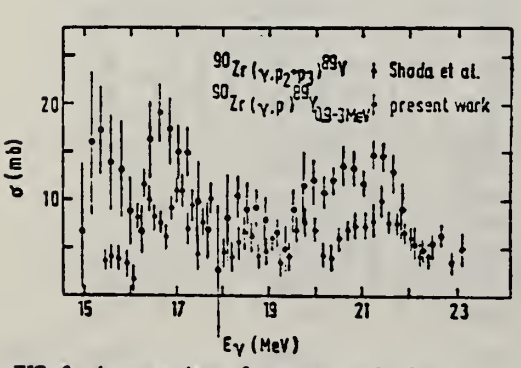

FIG. 8. A comparison of present results for the $^{90}Zr(\gamma,p)^{89}Y_{0.9-3}$ cross section with the data of Shoda *et al.* (Ref. 4).

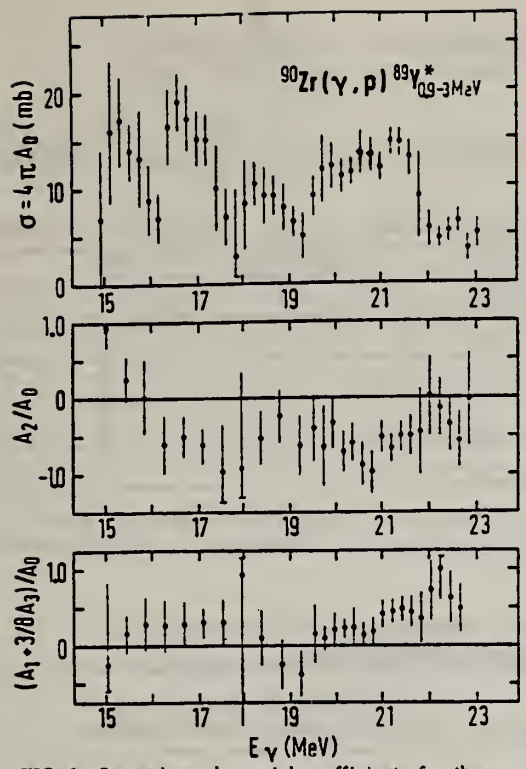

FIG. 6. Legendre polynomial coefficients for the angular distribution of protons in the reaction $^{90}Zr(\gamma,p)$ $^{89}Y^{*}$ involving excited states of ^{89}Y with energies up to 3 MeV. See Fig. 4 for other details.

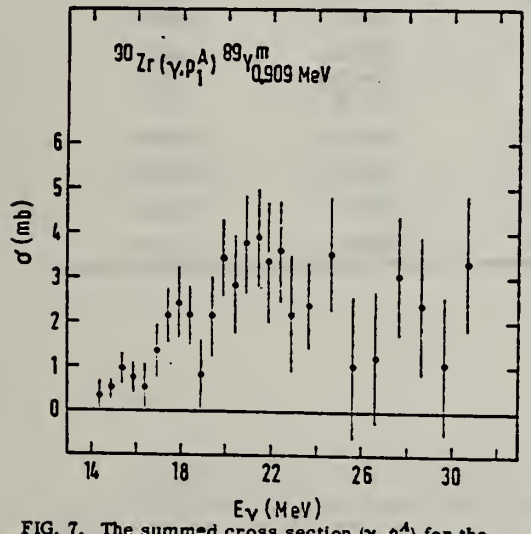

FIG. 7. The summed cross section $(\gamma,p_1^{A_1})$ for the $^{90}Zr(\gamma,p)$ reactions leading to the 0.909 MeV first-excited isomeric state of ^{89}Y. The cross section is obtained from a Penfold-Leiss analysis of the 0.909 MeV γ-ray activation yield. Here, besides the direct (γ,p_1) cross section, also contributions from states decaying to the 0.909 MeV state are contained. In particular, $\sigma(\gamma,p_1^{A_1})$ incorporates $\sigma(\gamma,p_{5+6+7+8})$ and 70% of $\sigma(\gamma,p_4)$, involving ^{89}Y states at 2.529, 2.568, 2.622, 2.871, and 2.220 MeV, respectively.

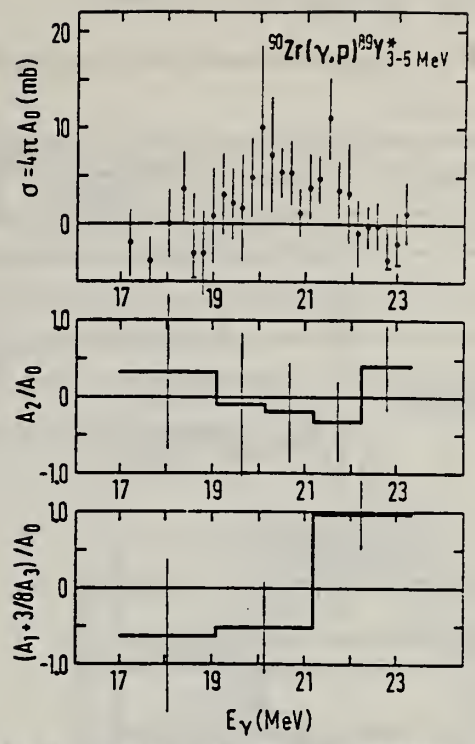

FIG. 9. Integrated cross section over angles and other Legendre polynomial coefficients for the photoproton reaction channels leading to excited states in ^{89}Y of energies 3–5 MeV (see Fig. 4 for other details).

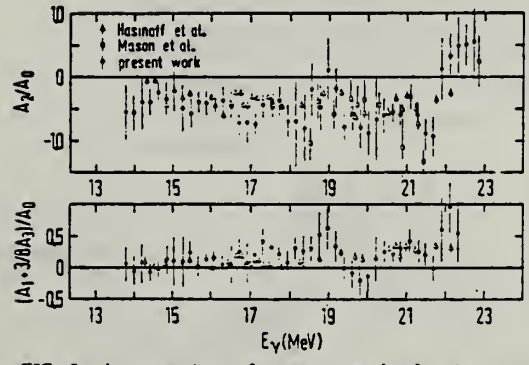

FIG. 5. A comparison of present results for the Legendre polynomial coefficients of the reaction $^{90}Zr-(\gamma,p_0)^{89}Y_{g.s.}$ with the data of Refs. 3 and 8.

REACTION	RESULT	EXCITATION ENERGY	SOURCE		DETECTOR		ANGLE
			TYPE	RANGE	TYPE	RANGE	

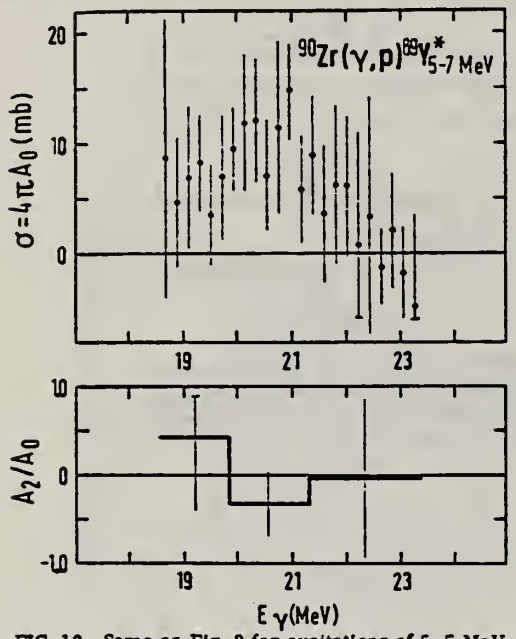

FIG. 10. Same as Fig. 9 for excitations of 5–7 MeV. Odd Legendre polynomial coefficients are not shown due to large errors.

TABLE I. Integrated cross sections for various photonuclear reaction channels.

Reactions	Energy region of integration (MeV)	Integrated cross section (MeV mb)
(γ,p_0)	13–23.5	79±7
$(\gamma,p)_{0.5-3\ MeV}$	15–18	35±4
	15–23.5	88±9
$(\gamma,p)_{3-5\ MeV}$	17–23.5	10±5
$(\gamma,p)_{5-7\ MeV}$	18.5–23.5	29±8
(γ,p_{tot})	13–23.5	206±19
	13–18	101±10
$(\gamma,p_1^{\dagger})$	14–31.5	35±5
	14–23.5	20±3
	14–18	5±1
$(\gamma,n_1^{\dagger})$	14–31.5	850±70
(γ,n)	14–31.5	1300±100
(γ,np)	20–31	14±6
$(\gamma,2n)$	21–31	141±15

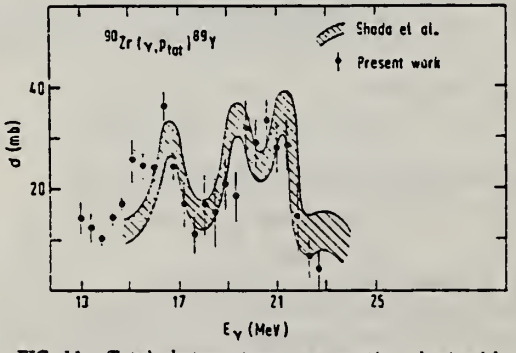

FIG. 11. Total photoproton cross section obtained by summing the contributions shown in Figs. 4, 6, 9, and 10 (data points) is compared to the corresponding data of Shoda *et al.* (Ref. 9). The shaded area represents experimental errors quoted in Ref. 9.

REF.

S. Fukuda and Y. Torizuka
Phys. Lett. 62B, 146 (1976)

ELEM. SYM.	A	Z
Zr	90	40

METHOD

REF. NO.: 76 Fu 1 egf

REACTION	RESULT	EXCITATION ENERGY	SOURCE		DETECTOR		ANGLE
			TYPE	RANGE	TYPE	RANGE	
E,E/	FMF	6- 30	D	150-250	MAG-D		DST

ANALYSIS FOR EO

The multipole expansion of the inelastic electron scattering continuum in ^{90}Zr yields an E2-like structure which involves a giant monopole resonance at 17 MeV with a width of 4 MeV.

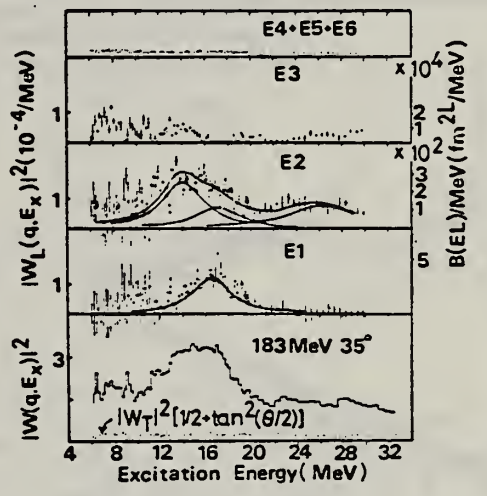

Fig. 1. Differential total form factor $|W(q,E_X)|^2$ at 183 MeV 35°, transverse part $|W_T|^2(1/2 + \tan^2\theta/2)$, and $|W_L(q,E_X)|^2$ corresponding to E1, E2, E3 and E4 + E5 + E6 are shown, where $|W|^2$, $|W_L|^2$, and $|W_T|^2$ are defined in ref. [16]. The scale at the right-hand side indicates $B(EL)$ values in units of fm^{2L}/MeV and at the left-hand side form factors in units of 10^{-4}/MeV.

Table 1
$B(EL)$ values in fm^{2L} and the percentages of the corresponding EWSR in ^{90}Zr.

E_X(MeV)	E1	E2	E3
6–10	2.8±1.8	(3.7±0.9) × 10^3	(4.2±0.4) × 10^4
	(18 ±12)% (T = 1)	(11 ±3)% (T = 0)	(16 ±1)% (T = 0)
10–15	7.3±1.1	(10.9±0.6) × 10^3	(3.9±0.3) × 10^4
	(28 ±4)% (T = 1)	(49 ±3)% (T = 0)	(24 ±2)% (T = 0)
15–20	11.8±1.0	(10.2±0.5) × 10^3	(0.9±0.2) × 10^4
	(61 ±5)% (T = 1)	(64 ±3)% (T = 0)	(14 ±4)% (T = 0)
20–30	2.7±1.4	(12.5±0.7) × 10^3	(4.4±0.4) × 10^4
	(17 ±9)% (T = 1)	(89 ±5)% (T = 1)	(34 ±3)% (T = 1)

REF. F. S. Dietrich, D. W. Heikkinen, K. A. Snover, K. Ebisawa
Phys. Rev. Lett. 38, 156 (1977)

ELEM. SYM.	A	Z
Zr	90	40

METHOD

REF. NO. 77 Di 2 hmg

REACTION	RESULT	EXCITATION ENERGY	SOURCE		DETECTOR		ANGLE
			TYPE	RANGE	TYPE	RANGE	
P,G	ABX	22- 35	C	14- 27	NAI-D		4PI

New detailed angular distribution measurements are presented for $^{89}Y(p,\gamma_0)^{90}Zr$ above the giant dipole resonance (14 MeV $\leq E_p \leq$ 27 MeV), which show pronounced effects of higher multipoles. Direct-semidirect calculations provide a good description of the data by including $E2$ and $E3$ as well as $E1$ radiation. The sensitivity of the reaction to a $T=1$ giant quadrupole resonance is demonstrated.

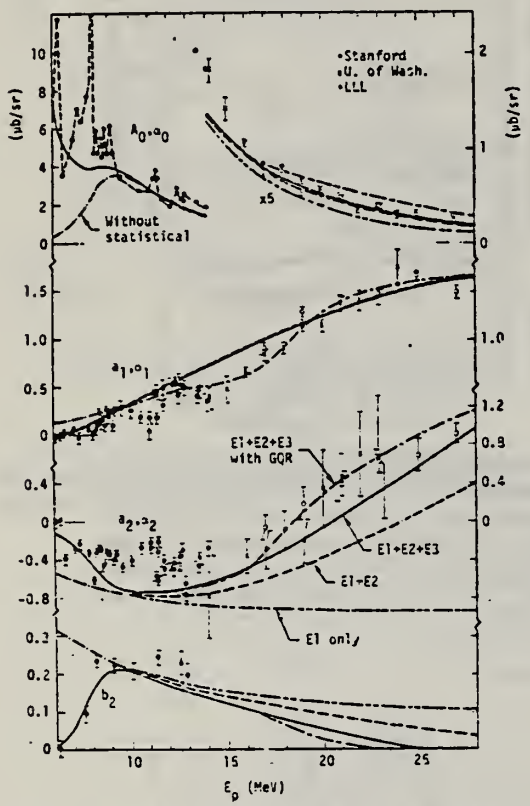

FIG. 1. Angular distribution coefficients for $^{89}Y(p,\gamma_0)^{90}Zr$. Crosses and open circles, present measurements of a_i (see text); solid dots, previous measurements of A_n, a_i, and b_2 (Refs. 14 and 15) ($A_0 \cong a_0$ and $a_i \cong a_i$ for $E_p \leq 14$ MeV). The curves represent calculated a_i; the $E1$ curve includes both direct and semidirect (GDR); $E2$ and $E3$ are direct only, except where semidirect $E2$ (GQR) is indicated.

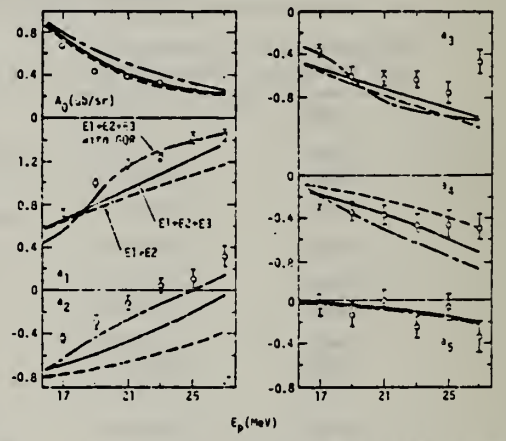

FIG. 2. Angular distribution coefficients extracted from LLL data. See text and Fig. 1 caption for significance of curves.

14 B. L. Berman et al., Phys. Rev. 162, 1098 (1967).
15 M. Hasinoff et al., Nucl. Phys. A216, 221 (1973).

REF. W. Knupfer, Phys. Lett. 77B, 367 (1978)

ELEM. SYM.	A	Z
ZR	90	40

METHOD

REF. NO.: 78 Kn 7 rs

REACTION	RESULT	EXCITATION ENERGY	SOURCE		DETECTOR		ANGLE
			TYPE	RANGE	TYPE	RANGE	
E,E/	RLY	8-10	D	UKN	MAG-D		DST

M2 LEVELS

The location of the M2 giant resonance in ^{28}Si, ^{90}Zr and ^{208}Pb, predicted within the framework of the MSI-RPA particle–hole model, has been confirmed by high-resolution inelastic electron scattering ($E_X \approx 44A^{-1/3}$ MeV). The fragmented M2 strength distribution can only be described assuming a mass-dependent quenching of the intrinsic g_s factor. This has the consequence that the long sought M1 strength is much reduced in heavy nuclei, an effect which is supported experimentally.

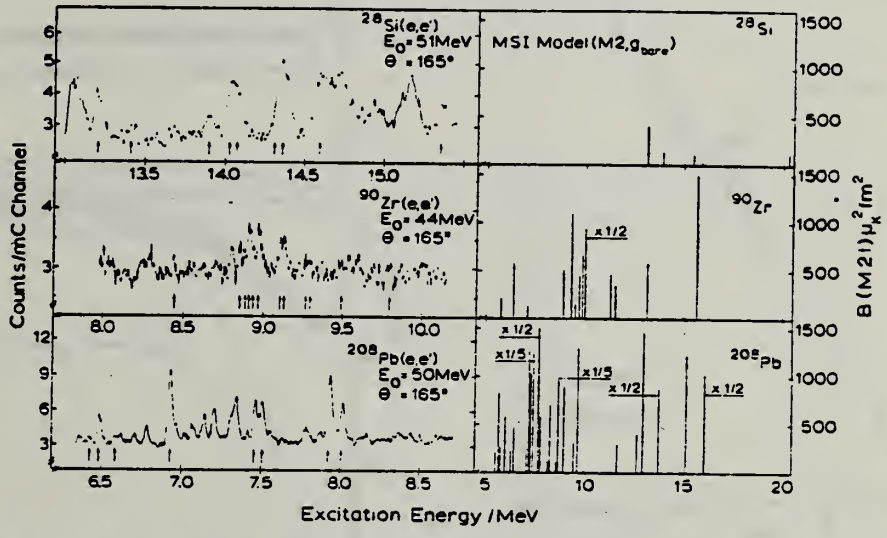

Fig. 1. The left part shows selected (e, e') spectra on ^{28}Si, ^{90}Zr and ^{208}Pb at various energies but all at $\theta = 165°$. The 2^- states are marked by arrows. The right part displays the model prediction for the M2 strength.

REF. K. Masumoto, T. Kato, N. Suzuki
Nucl. Inst. Meth. 157, 567 (1978)

ELEM. SYM.	A	Z
Zr	90	40

METHOD

REF. NO.: 78 Ma 10 hg

REACTION	RESULT	EXCITATION ENERGY	SOURCE		DETECTOR		ANGLE
			TYPE	RANGE	TYPE	RANGE	
G,N	ABY	12-68	C	30-68	ACT		4PI
G,PN	ABY	20-68	C	30-68	ACT		4PI

Analysis is made of reactions interfering with photon activation analysis procedures.

The activation yield curves have been presented for a number of photonuclear reactions in the energy range from 30 to 68 MeV, in order to evaluate quantitatively the interferences due to competing reactions in multielement photon activation analysis. The general features of the yields as functions of both target mass number and excitation energy were elucidated from the data obtained, discussion being given on the results in terms of the reaction mechanism.

Simultaneous neutron activation due to appreciable neutron production from the converter and surrounding materials has also been studied, and, finally, the magnitudes of interferences in real multielement analysis were given in the form of their energy dependences.

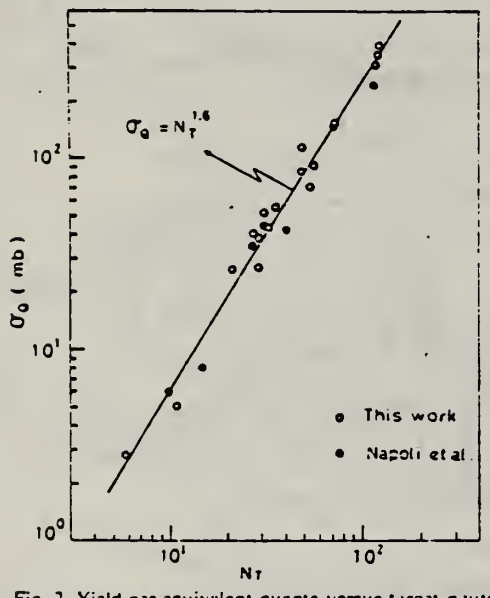

Fig. 2. Yield per equivalent quanta versus target neutron number.

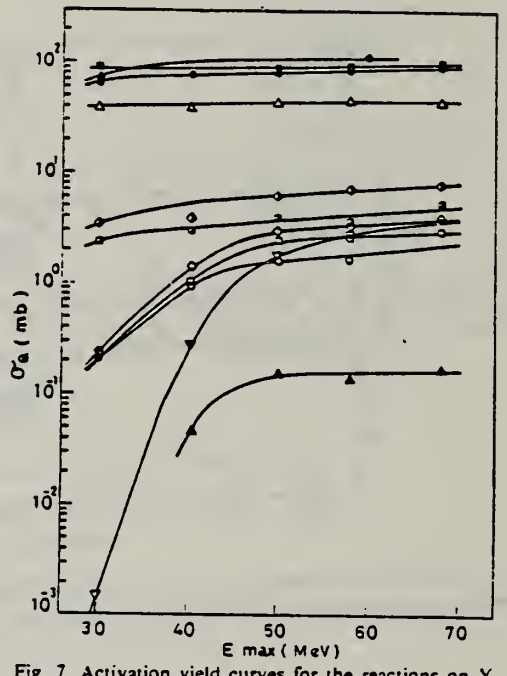

Fig. 7. Activation yield curves for the reactions on Y, Zr, Nb and Mo.
◆ $^{89}Y(\gamma, n)^{88}Y$, ● $^{90}Zr(\gamma, n)^{89}Zr$, ○ $^{90}Zr(\gamma, pn)^{88}Y$,
△ $^{93}Nb(\gamma, n)^{92m}Nb$, ▲ $^{93}Nb(\gamma, xn)^{88}Y$, ■ $^{100}Mo(\gamma, n)^{99}Mo$,
◆ $^{97}Mo(\gamma, p)^{96}Nb$, ◪ $^{96}Mo(\gamma, p)^{95m}Nb$, ◇ $^{94}Mo(\gamma, pn)^{92m}Nb$,
□ $^{92}Mo(\gamma, 2n)^{90}Mo$, ▽ $^{94}Mo(\gamma, xn)^{89}Zr$.

(over)

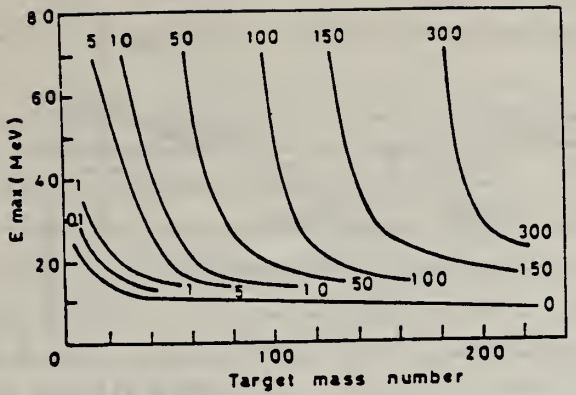

Fig. 9. Yields of the (γ, n) reactions as a function of bremsstrahlung maximum energy and target mass number. The numerical values in the figure are yields per equivalent quanta in mb.

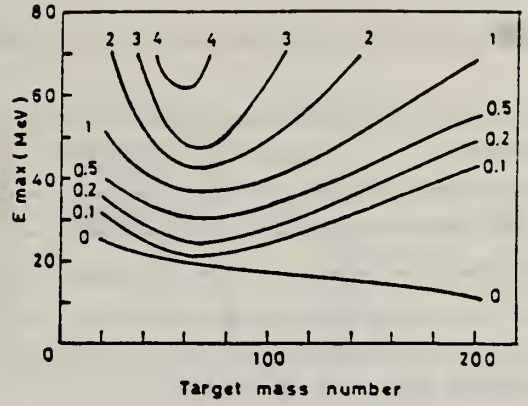

Fig. 11. Yields of the (γ, pn) reactions as a function of bremsstrahlung maximum energy and target mass number. The numerical values in the figure are yields per equivalent quanta in mb.

REF. D. Meuer, R. Frey, D.H.H. Hoffmann, A. Richter, E. Spamer, O. Titze, W. Knüpfer
Nucl. Phys. A349, 309 (1980)

ELEM. SYM.	A	Z
Zr	90	40

METHOD

REF. NO. 80 Me 7 hg

REACTION	RESULT	EXCITATION ENERGY	SOURCE		DETECTOR		ANGLE
			TYPE	RANGE	TYPE	RANGE	
E,E/	FMF	8-10	D	24-66	MAG-D		DST

Spectra shown in the paper

BML, 21 LEVELS

Abstract: High-resolution (FWHM ≈ 30 keV) inelastic electron scattering on ^{90}Zr at low momentum transfer ($0.20 < q < 0.62$ fm^{-1}) has been used to study magnetic transitions at excitation energies $E_x = 8$–10 MeV. The experimental data were analyzed in the distorted-wave Born approximation (DWBA) with wave functions calculated in the random phase approximation (RPA). Three $J^\pi = 1^+$ states have been identified $E_x = 8.233$, 9.000 and 9.371 MeV. There is some indication of further very fragmented dipole strength and the upper limit for the total M1 strength in the investigated energy region is $\Sigma B(\mathrm{M1})\uparrow \lesssim 2.5\ \mu_K^2$. It is much smaller than any theoretical prediction. Furthermore, a large number of 2^- states has been observed, with the center of gravity located at $E_x = 9$ MeV. These states carry a total strength of $\Sigma B(\mathrm{M2})\uparrow = 1000\ \mu_K^2 \cdot \mathrm{fm}^2$. Their strong fragmentation is in qualitative agreement with theoretical calculations, but the deduced strength is much smaller than theoretically predicted. In addition the distributions of spacings and radiative widths of the 2^- states are consistent with a Wigner and a Porter–Thomas distribution, respectively.

E NUCLEAR REACTIONS ^{90}Zr(e, e'), $E = 24$–66 MeV; measured $\sigma(E, \theta)$. ^{90}Zr deduced levels, transition strengths. Shell-model calculations.

TABLE 2

Levels observed in the present experiment and multipole assignment due to comparison with the theoretical calculations described in the text

E_x (MeV)	J^π	E_x (MeV)	J^π
7.774	$(1^+, 2^-)$	8.882	2^-
7.806	(2^-)	8.911	2^-
7.868	$(1^+, 2^-)$	8.934	2^-
7.907	$((3^-))$	8.971	2^-
7.996	(3^-)	9.000	1^+
8.032	2^-	9.061	2^-
8.113	$1^+(2^-)$	9.101	2^-
8.142	$1^+(2^-)$	9.127	2^-
8.233	1^+	9.150	$1^+(2^-)$
8.291	2^-	9.265	2^-
8.316	(2^-)	9.294	2^-
8.366	(1^+)	9.327	2^-
8.400	(2^-)	9.371	1^+
8.442	2^-	9.439	$1^+(2^-)$
8.494	$1^+(2^-)$	9.489	2^-
8.542	2^-	9.520	$(1^+, 2^-)$
8.602	(1^+)	9.541	2^-
8.627	2^-	9.601	$(1^+, 2^-)$
8.701	(2^-)	9.694	2^-
8.809	(2^-)	9.863	$(1^+, 2^-)$
8.853	2^-		

The excitation energies are uncertain to 3–10 keV and the number of parentheses around J^π values indicate the ambiguity in the assignments.

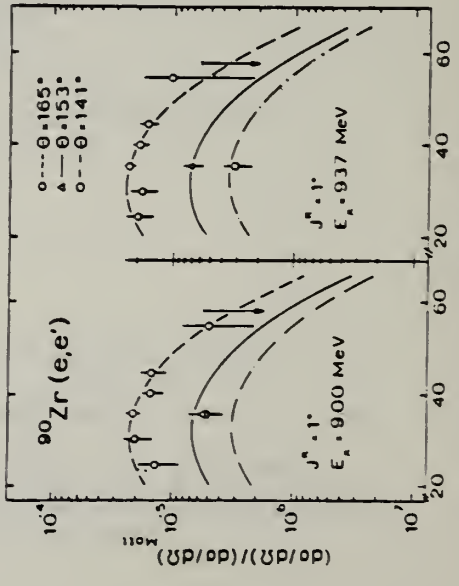

Fig. 7. Experimentally derived form factors for the two states at $E_x = 9.000$ MeV and $E_x = 9.371$ MeV compared to the shape of the theoretically predicted M1 form factor. This leads to a $J^\pi = 1^+$ assignment.

(OVER)

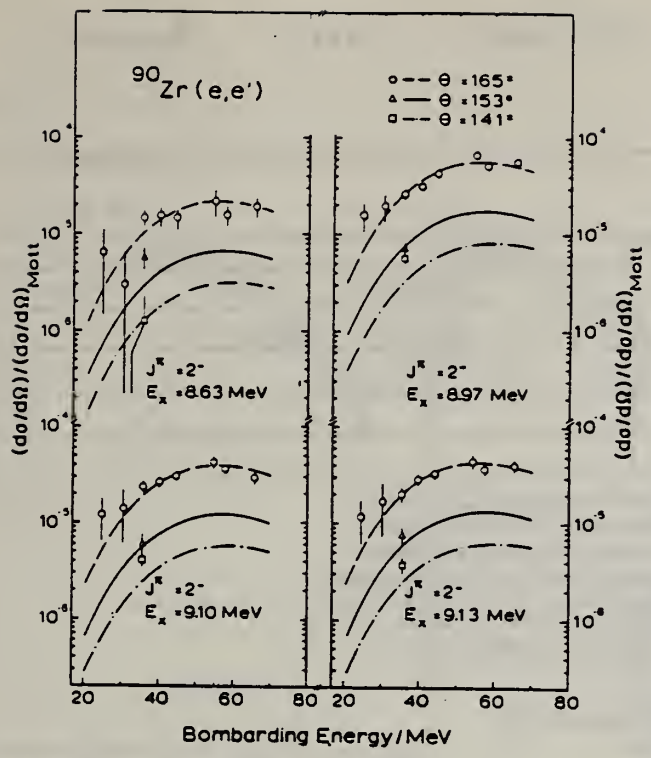

Fig. 8. Excitation function of four $J^\pi = 2^-$ states. The experimental data are compared to MSI model calculations.

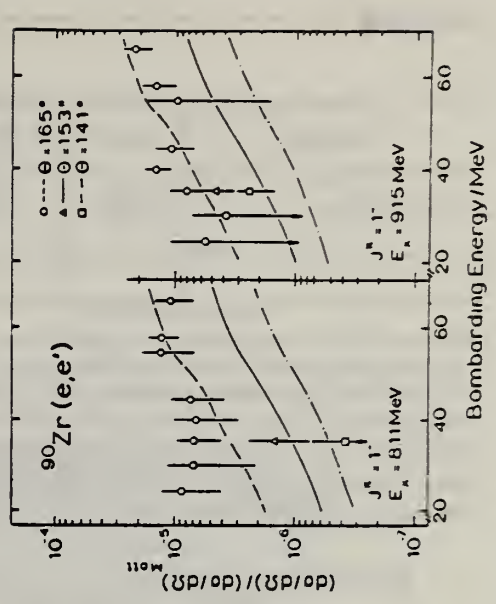

Fig. 10. Comparison between experimentally determined and calculated E1 form factors.

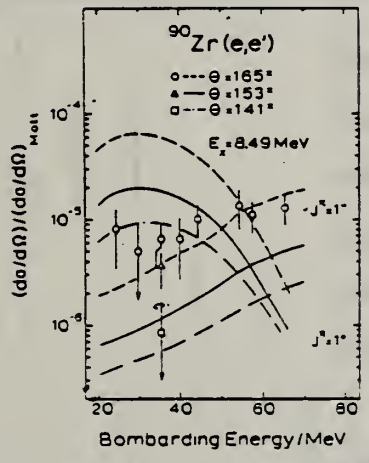

Fig. 11. Experimental form factor for the state at $E_x = 8.494$ MeV compared to the different shapes of the theoretical form factor predictions for $J^\pi = 1^-$ and $J^\pi = 1^+$ states, respectively. The theoretical M1 form factor is scaled to obtain a ground-state radiative width of $\Gamma_\gamma^0 = 1.6$ eV as quoted in ref. [42]), obviously in disagreement with the experimental finding which is consistent with an E1 assignment to the transition.

REF. K. Raghunathan, L.L. Rutledge, R.E. Segel, L. Meyer-Schützmeister
Phys. Rev. C22, 2409 (1980)

ELEM. SYM.	A	Z
Zr	90	40

METHOD

REF. NO. 80 Ra 3 hg

REACTION	RESULT	EXCITATION ENERGY	SOURCE TYPE	SOURCE RANGE	DETECTOR TYPE	DETECTOR RANGE	ANGLE
A,G	ABX	15-19	D	9-13 (9.-12.5)	NAI-D		DST

The $^{86}Sr(\alpha,\gamma_0)^{90}Zr$ reaction has been studied over the energy range $9.0 \leq E_\alpha \leq 12.5$ MeV; there was no detectable yield below 9 MeV. Data were taken at three angles, thus making it possible to decompose the radiation into its $E1$ and $E2$ components. The $E1$ yield, which is at least 85% of the total, shows a broad peak centered at an excitation energy of about 17 MeV. Utilizing Hauser-Feshbach calculations, the magnitude and shape of the $E1$ yield is shown to be consistent with the $E1$ capture proceeding entirely through the compound nucleus. The $E2$ yield is small at the lower bombarding energies, but appears to be significant above about $E(^{90}Zr^*) = 16.5$ MeV. Any observed $E2$ cross section is shown to be much too large for the reaction to proceed mainly through the compound nucleus.

[NUCLEAR REACTIONS $^{86}Sr(\alpha,\gamma_0)^{90}Zr$, $9 \leq E_\alpha \leq 12.5$ MeV; measured E_γ, $d\sigma/d\Omega(\theta, E_\alpha)$; deduced $\sigma_{E1}(\gamma,\alpha_0)$, $\sigma_{E2}(\gamma,\alpha_0)$.]

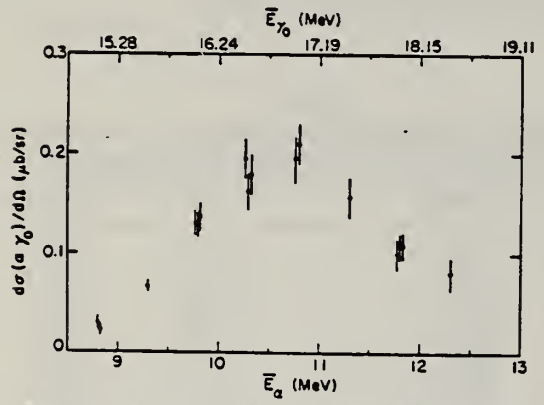

FIG. 3. Yield curve at 90°. The alpha energy is the mean energy in the target. Data are from different runs spread over about a year and the error bars indicate the estimated uncertainties in the absolute cross sections. The estimated errors in the relative cross sections, as far as angular distributions are concerned, are about one half of the absolute errors.

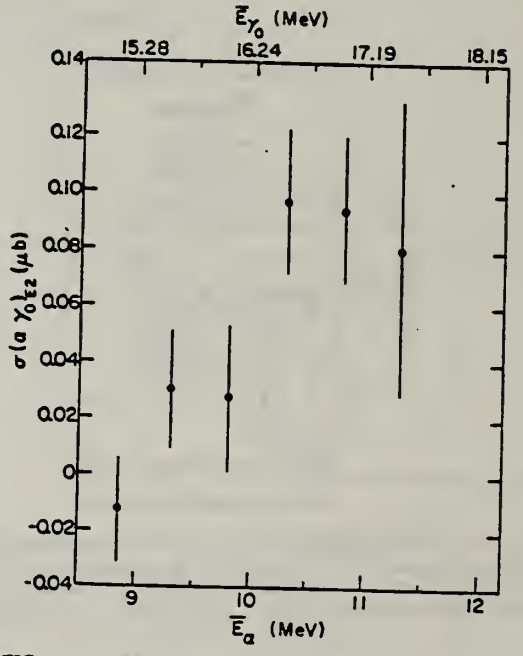

FIG. 4. Cross section for producing $E2$ radiation.

(OVER)

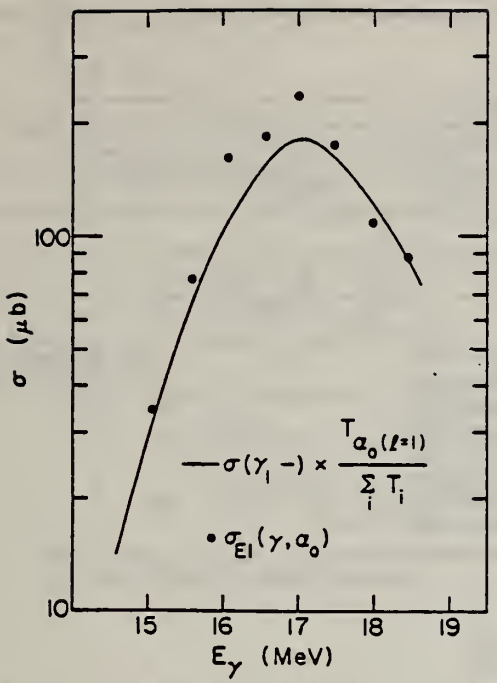

FIG. 5. Total $E1$ absorption cross section calculated from the measured $E1$ capture under the assumption that the entire reaction proceeds through the compound nucleus. Also shown is the measured total absorption given in Ref. 10.

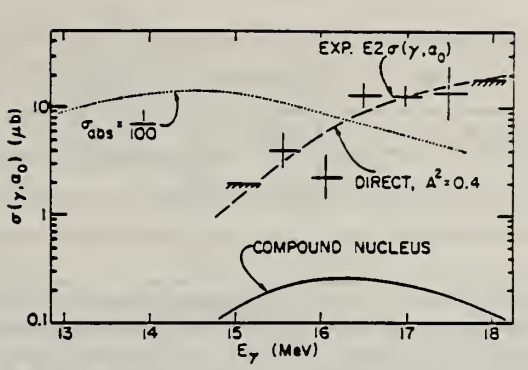

FIG. 6. Solid lines are the $E2$ (γ,α_0) cross section, obtained from the observed $E2$ capture by detailed balance. The cross hatching indicates an upper limit. Solid curve is the compound nucleus $E2$ (γ,α_0) expected from a 4-MeV wide resonance centered at 14.5 MeV. The broken curve is that calculated for a direct reaction proceeding through a giant quadrupole state that has a 40% $^{88}Sr+\alpha$ component. Dotted curve is the gamma-ray absorption cross section, divided by 100, expected for a 4-MeV wide resonance centered at 14.5 MeV.

REF. T. Tamae, T. Urano, M. Hirooka, M. Sugawara
Phys. Rev. C21, 1758 (1980)

ELEM. SYM.	A	Z
Zr	90	40

METHOD

REF. NO. 80 Ta 2 hg

REACTION	RESULT	EXCITATION ENERGY	SOURCE		DETECTOR		ANGLE
			TYPE	RANGE	TYPE	RANGE	
E,A	ABX	7-67	D	13-67	SPK-D		DST

The (e,α) cross section in ^{90}Zr has been measured at incident electron energies from 13.5 MeV to 66.5 MeV for α particles between 6.9 and 16.8 MeV. The (γ,α) cross section was deduced from it assuming both $E1$ interaction and $E2$ interaction. The angular distribution of the (γ,α_0) cross section and an experiment using the bremsstrahlung plus electron beam make it clear that the $E1$ interaction is dominant over all the present energy range. The (γ,α) cross section extracted by using $E1$ virtual photon spectra has a large bump above the excitation energy of 30 MeV in addition to a bump in the giant dipole resonance region. The (γ,α_0) cross section also has a bump at the giant dipole resonance which exhausts most of the (γ,α) cross section in that region. The compound nucleus model was used successfully to explain the bump at the giant dipole resonance. The cross section above 30 MeV is discussed in terms of the pre-equilibrium α emission process combined with the quasi-deuteron model.

VIRT. PHOTON ANAL.

[NUCLEAR REACTIONS $^{90}Zr(e,\alpha)$, E_e=13.5–66.5 MeV; measured $d\sigma(e,\alpha)/d\Omega$, deduced $d\sigma(\gamma,\alpha)/d\Omega$ and $d\sigma(\gamma,\alpha_0)/d\Omega$. Angular distributions; (γ,α_0) at E_e=17.5 MeV and (e,α) at E_e=40.0 MeV, θ_α=45–135°. Experiment using electron plus bremsstrahlung at E_e=60.0 MeV. Calculations, compound nucleus model, and pre-equilibrium exciton model combined with quasi-deuteron model.]

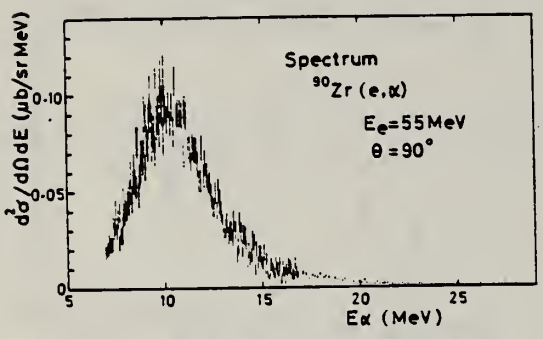

FIG. 4. (e,α) energy spectrum of ^{90}Zr at θ=90°, for E_e=55 MeV. Alpha-particle energy was corrected for energy loss in half target thickness.

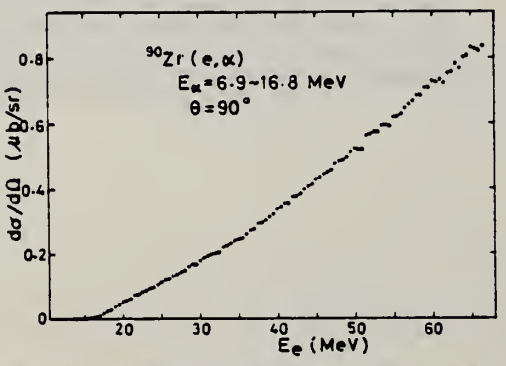

FIG. 5. Differential cross section of the (e,α) reaction at θ=90°.

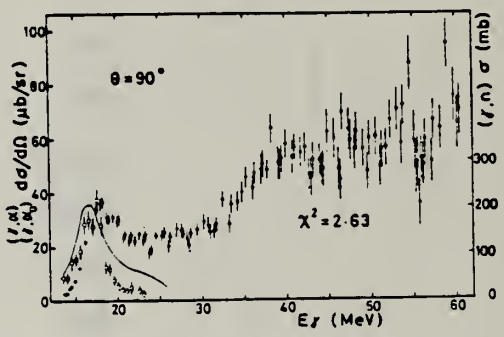

FIG. 6. Photoalpha differential cross section of ^{90}Zr (closed points) analyzed from the (e,α) cross section in Fig. 5 and $^{90}Zr(\gamma,\alpha_0)$ differential cross section (open circles), at θ=90°. $E1$ interaction only was considered in these analyses. The value of χ^2 for the total (γ,α) cross section was calculated for the cross section smoothed by eye. Solid line shows $^{90}Zr(\gamma,n)$ cross section.

(OVER)

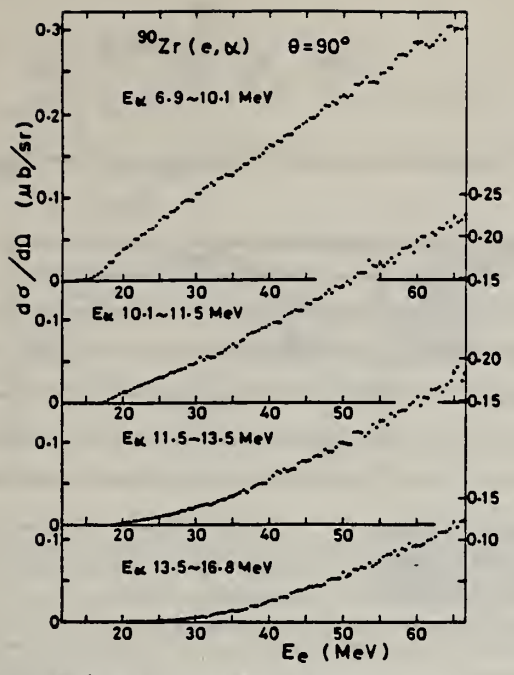

FIG. 9. ^{90}Zr(e, α) cross sections divided into four parts with particular α-particle energies.

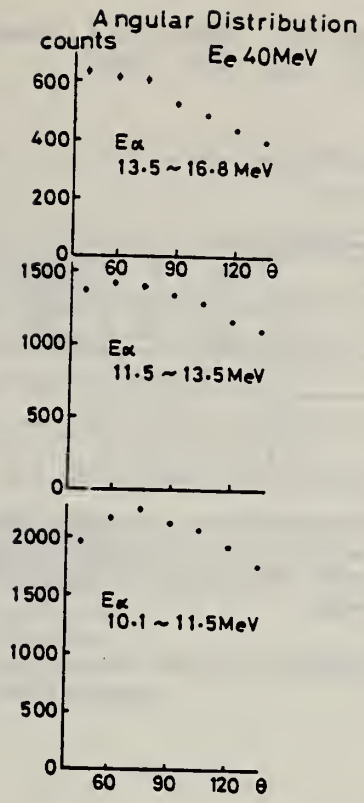

FIG. 13. Alpha-particle angular distributions at E_e = 40 MeV.

REF. L.W. Fagg, W.L. Bendel, E.C. Jones,Jr.
Phys. Rev. C26, 1304 (1982)

ELEM. SYM.	A	Z
Zr	90	40

METHOD

REF. NO. 82 Fa 2 egf

REACTION	RESULT	EXCITATION ENERGY	SOURCE		DETECTOR		ANGLE
			TYPE	RANGE	TYPE	RANGE	
E,E/	ABX	0-12	D	37,61	MAG-D		180

Spectra of 37.2 and 60.6 MeV electrons scattered at 180° constitute evidence for very low observable $M1$ transition strength and significant $M2$ transition strength in the 9 MeV excitation energy region of ^{90}Zr. This is consistent with recent high resolution results of other workers at more forward angles.

NUCLEAR REACTIONS ^{90}Zr(e,e'), E_0=37.2, 60.6 MeV; measured $d\sigma/d\Omega$ at θ=180°.

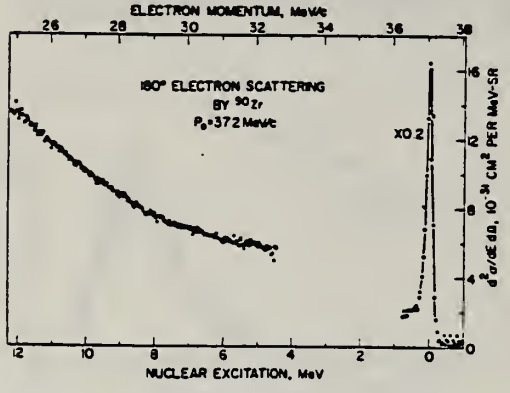

FIG. 1. Inelastic cross section spectrum of 37.2 MeV electrons scattered at 180° from ^{90}Zr.

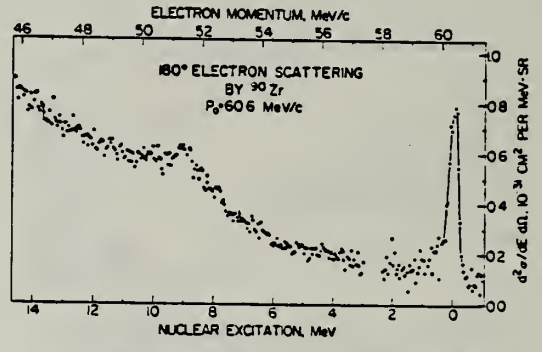

FIG. 2. Inelastic cross section spectrum of 60.6 MeV electrons scattered at 180° from ^{90}Zr.

REF. F.Z. Khien, N.K. Zui, N.T. An
Yad. Fiz. 35, 257 (1982)
Sov. J. Nucl. Phys. 35, 145 (1982)

ELEM. SYM.	A	Z
Zr	90	40

METHOD

REF. NO. 82 Kh 2 egf

REACTION	RESULT	EXCITATION ENERGY	SOURCE		DETECTOR		ANGLE
			TYPE	RANGE	TYPE	RANGE	
G,N	NOX	12-14	C	14	ACT-I		4PI

ISOMERIC RATIO

The method is developed for calculation of the isomeric ratio for the case of low excitation energy of the residual nucleus, and the isomeric ratio is measured in the $(n, 2n)$ and (γ, n) reactions in the neutron-deficient nuclei ^{92}Mo, ^{90}Zr, ^{86}Sr, and ^{74}Se. The good agreement between the experimental and theoretical results on the (γ, n) reaction has confirmed the reliability of the characterstics of the residual nuclei, the transmission coefficients of the emitted neutrons, etc., used in the calculations. From study of the $(n, 2n)$ reaction we have obtained values of the parameters of the spin dependence of the level density of the nucleus in the excitation-energy region ~ 14 MeV.

PACS numbers: 25.20. + y, 25.40.Gr, 27.50. + e, 27.60. + j

TABLE III. Isomeric ratio in the (γ, n) reaction.

Target nucleus	σ_{exp}	σ_{theor}	Published data[1]
^{92}Mo	1.54±0.15	1.36	1.82±0.15 (70) [9] 1.03±0.21 [10] 0.85±0.07 (30) [15]
^{90}Zr	1.52±0.04	1.49	0.50±0.15 (30) [15]
^{86}Sr	0.70±0.07	0.86	0.68±0.14 (30) [15]
^{74}Se	7.5±1.0	10.5[2] 8.5[3]	

[1] In parentheses we have given the values of the bremsstrahlung maximum energy.
[2] In the calculations we used the ^{73}Se level scheme of Ref. 2, $I_g = 7/2^+$ and $I_m = 1/2^-$.
[3] In the calculations we used the level scheme of ^{73}Se in Ref. 3, $I_g = 9/2^+$ and $I_m = 3/2^-$.

ZR
A=91

ZR
A=91

Ref. R. Nathans, P.F. Yergin
Phys. Rev. 98, 1296 (1955)

Elem. Sym.	A	Z
Zr	91	40

Method BF_3 counters; 24 MeV Bremss; Betatron

Ref. No. 55 Na 1 EGF

Reaction	E or ΔE	E_o	Γ	$\int \sigma dE$	Jπ	Notes
(γ,xn)	5.0-24	16.2	5.4	1.27 MeV-mb		E_{th} = 7.2 MeV; σ_{max} = 200 mb. No Corrections. [NOTE: Figure 3 - Ref 8: Katz, Baker, Montalbetti, Can. J. Phys. 31, 250 (1953)]

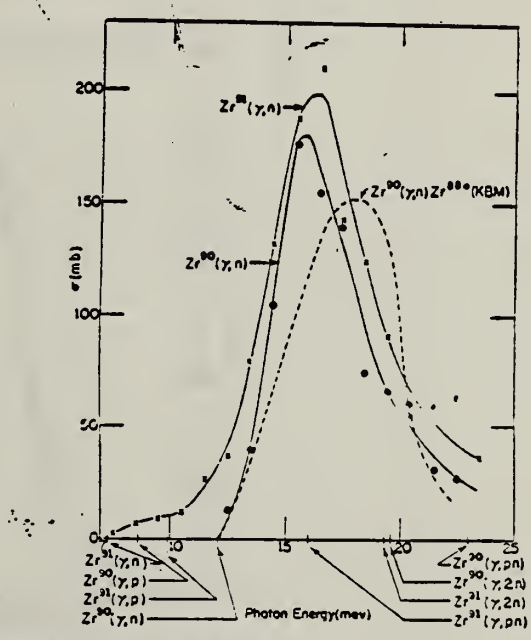

FIG. 3. (γ,n) cross sections for Zr^{90} and Zr^{91}. The ordinate scale is in millibarns (10^{-27} cm^2). The points shown are those calculated from the yield data. The solid curves are drawn to fit the points. The dashed curve is the cross section reported (see reference 8) for the production of the isomeric state of Zr^{89} by photon bombardment of natural Zr. The locations of the thresholds for various reactions in the two isotopes are indicated by the arrows.

Ref. P.F. Yergin, B.P. Fabricand
Phys. Rev. 104, 1334 (1956)

Elem. Sym.	A	Z
Zr	91	40

Method: 24 MeV betatron; 250r Victoreen in 3.75 cm Lucite; neutron detector

Ref. No.: 56 Ye 2 — EGF

Reaction	E or ΔE	E_0	Γ	$\int \sigma dE$	Jπ	Notes
$Zr^{91}(\gamma,xn)$	Bremss. 24	16.5	5.0 MeV	$\int_0^{23}$ = 1.22 MeV-b		

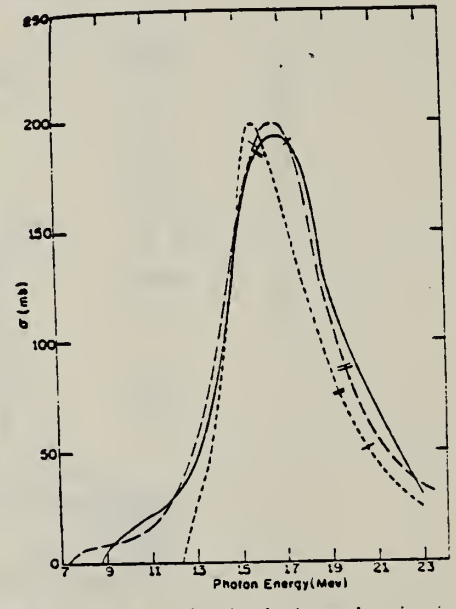

FIG. 5. Cross sections for the (γ,n) reactions in zirconium isotopes. Short dashes Zr^{90}, long dashes Zr^{91}, full curve Zr^{92}. The previously published Zr^{90} and Zr^{91} results have been recomputed, taking into account the present Zr^{92} measurements. The single and double slash marks on each curve represent the locations of the (γ,pn) and $(\gamma,2n)$ thresholds respectively. The units of the ordinate are 10^{-27} cm².

TABLE III. Parameters of giant-resonance cross-section curves for (γ,n) reactions in nuclei near 50 neutrons. Nuclides $_{33}As^{75}$, $_{41}Nb^{93}$, and $_{45}Rh^{103}$ from reference 4, $_{40}Zr^{90}$ and $_{40}Zr^{91}$ from reference 5 recomputed in present work. Neutron number is shown in column 2, location of peak cross-section value in column 3, peak cross-section value in column 4, half-height width of curve in column 5, and area under curve from threshold to 23 Mev in column 6.

Nuclide	N	E_m (Mev)	σ_m (millibarns)	Γ (Mev)	$\int_0^{23}\sigma dE$ (Mev-barns)
$_{33}As^{75}$	42	17.3	90.3	9.0	0.80
$_{38}Sr^{86}$	48	15.9	160	5.0	0.92
$_{38}Sr^{87}$	49	15.8	146	5.3	1.00
$_{38}Sr^{88}$	50	16.3	201	4.0	1.05
$_{39}Y^{89}$	50	16.3	191	3.8	0.87
$_{40}Zr^{90}$	50	15.8	199	4.3	0.98
$_{40}Zr^{91}$	51	16.5	200	5.0	1.22
$_{40}Zr^{92}$	52	16.9	193	5.5	1.24
$_{41}Nb^{93}$	52	17.0	195	6.8	1.46
$_{45}Rh^{103}$	58	16.5	205	8.9	1.94

REF. S. C. Fultz, R. L. Bramblett, B. L. Berman, J. T. Caldwell, and M. A. Kelly
Proc. Gatlinburg Conference 397 (1966)

ELEM. SYM.	A	Z
Zr	91	40

METHOD

REF. NO. 66 Fu 2 hmg

REACTION	RESULT	EXCITATION ENERGY	SOURCE		DETECTOR		ANGLE
			TYPE	RANGE	TYPE	RANGE	
G,XN	ABI	THR-30	D	THR-30	BF3-I		4PI
G,2N	ABI	THR-30	D	THR-30	BF3-I		4PI

TABLE 1

Integrated Cross Sections for Zirconium and Yttrium

Isotope	E_{max} $a = \int \sigma_{\gamma n} dE$ (MeV - barns)	E_{max} $b = \int \sigma_{\gamma 2n} dE$ (MeV - barns)	b/a	E_{max} (MeV)
^{90}Zr	0.980	0.108	0.110	28
^{91}Zr	1.078	0.202	0.187	30
^{92}Zr	1.096	0.447	0.408	28
^{94}Zr	1.041	0.577	0.554	30
^{89}Y	0.991	0.095	0.096	28

REF.	ELEM. SYM.	A	Z
B.L. Berman, J.T. Caldwell, R.R. Harvey, M.A. Kelly, R.L. Bramblett, and S.C. Fultz Phys. Rev. 162, 1098 (1967)	Zr	91	40

METHOD	REF. NO.	
	67 Be 2	hmg

REACTION	RESULT	EXCITATION ENERGY	SOURCE		DETECTOR		ANGLE
			TYPE	RANGE	TYPE	RANGE	
G,N 7+	ABX	THR-30	D	THR-30	BF3-I		4PI
G,2N 8+	ABX	THR-30	D	THR-30	BF3-I		4PI

TABLE IV. Integrated cross sections.

Nucleus	$\sigma_{int}[(\gamma,n)+(\gamma,pn)]$ (MeV-b)[a]	$\sigma_{int}(\gamma,2n)$ (MeV-b)[a]	$E_{\gamma max}$ (MeV)	$\frac{\sigma_{int}(\gamma,2n)}{\sigma_{int}(\gamma,\text{total})}$[b]	$(\frac{1}{2}\pi)\sigma_m\Gamma$ (MeV-b)	$0.06NZ/A$ (MeV-b)
Y^{89}	0.94	0.10	28	0.10	1.14	1.31
Zr^{90}	0.96	0.10	28	0.09	1.16	1.33
Zr^{91}	0.88	0.20	30	0.19	1.22	1.35
Zr^{92}	0.65	0.45	28	0.41	1.23	1.36
Zr^{94}	0.43	0.58	30	0.56[c]	1.32	1.38

[a] All measured integrated cross-section values are given for an energy region from threshold to $E_{\gamma max}$. For the Zr^{91} and Zr^{92} cases, it was necessary to extrapolate the low-energy part of the total photoneutron cross section down to threshold; the error introduced in this process, however, is less than 0.5%.
[b] The word "total" in this table refers to the total photoneutron cross section $\sigma([\gamma,n)+(\gamma,pn)+(\gamma,2n)+(\gamma,3n)]$, and excludes the (γ,γ) and (γ,p) cross sections.
[c] This value includes the contribution of $\sigma_{int}(\gamma,3n)$, which equals 0.03 MeV-b from threshold to 30 MeV.

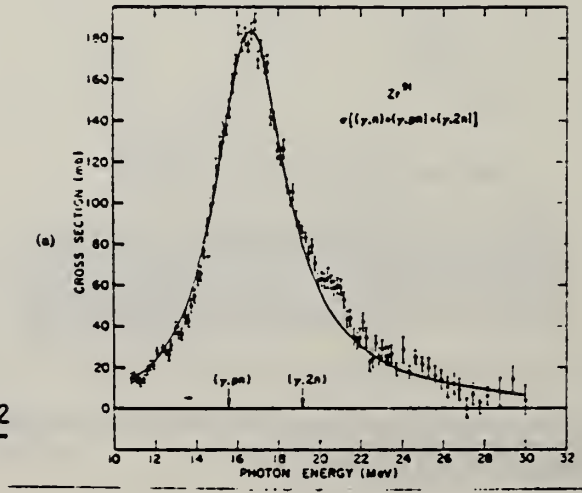

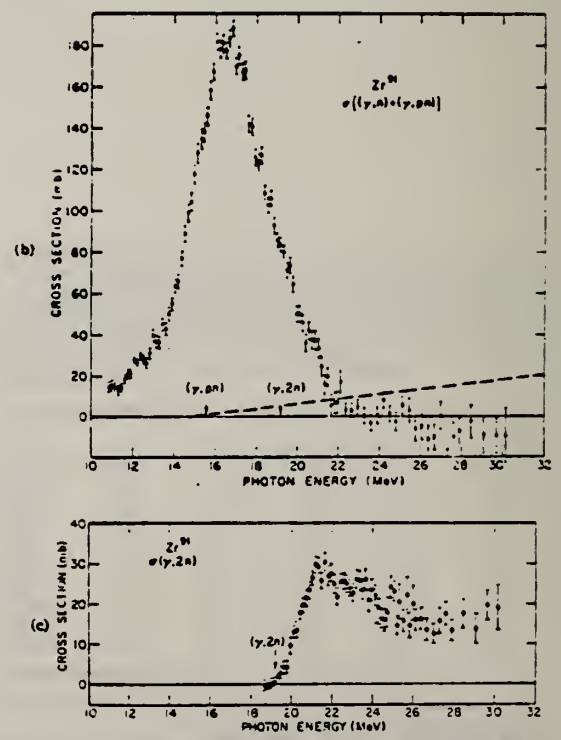

FIG. 10. (a) Total photoneutron cross section for Zr^{94}. (b) Single photoneutron cross section for Zr^{94}. (c) The $(\gamma,2n)$ cross section for Zr^{91}.

FORM NBS-418
(REV. 7-14-64)
USCOMM-DC 26010-P64

REF. G. P. Antropov, I. E. Mitrofanov, A. I. Prokof'ev and V. S. Russkikh
Izv. Akad. Nauk Fiz. 33, 700 (1969)
Bull. Acad. Sci. USSR-Phys. 33, 645 (1969)

ELEM. SYM.	A	Z
Zr	91	40

METHOD

REF. NO. 69 An 7 egf

REACTION	RESULT	EXCITATION ENERGY	SOURCE		DETECTOR		ANGLE
			TYPE	RANGE	TYPE	RANGE	
G,XN	ABX	12-23	C	12-23	BF3-I		4PI

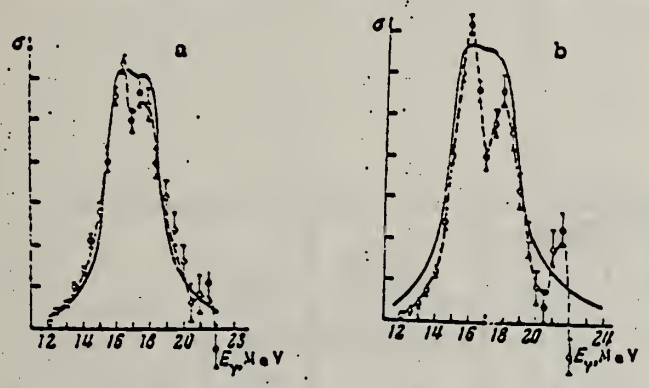

Fig.1. Cross section for the (γ,n) reaction in ^{90}Zr (a) and ^{91}Zr (b). The points and the dashed curve are experimental; the full curve is the sum of two Lorentz curves.

Table 1

Nucleus	0.06 NZ/A	$\int_{22,5\,MeV} \sigma(E)\,dE$,	Γ_{exp}, MeV	$\sigma_{-n} 0.00225 A^{5/3}$
^{90}Zr	1,33	1,27	4,0	0,91
^{91}Zr	1,35	1,42	4,2	1,02

REF. H. J. Askin, K. J. F. Allen, M. N. Thompson, K. Shoda, M. Sugawara, H. Miyase, B. N. Sung
PICNS-73, Vol. I, p. 561 Asilomar

ELEM. SYM.	A	Z
Zr	91	40

METHOD

REF. NO.	
73 As 9	hmg

REACTION	RESULT	EXCITATION ENERGY	SOURCE		DETECTOR		ANGLE
			TYPE	RANGE	TYPE	RANGE	
E,P	SPC	THR- 26	D	30	MAG-D		DST

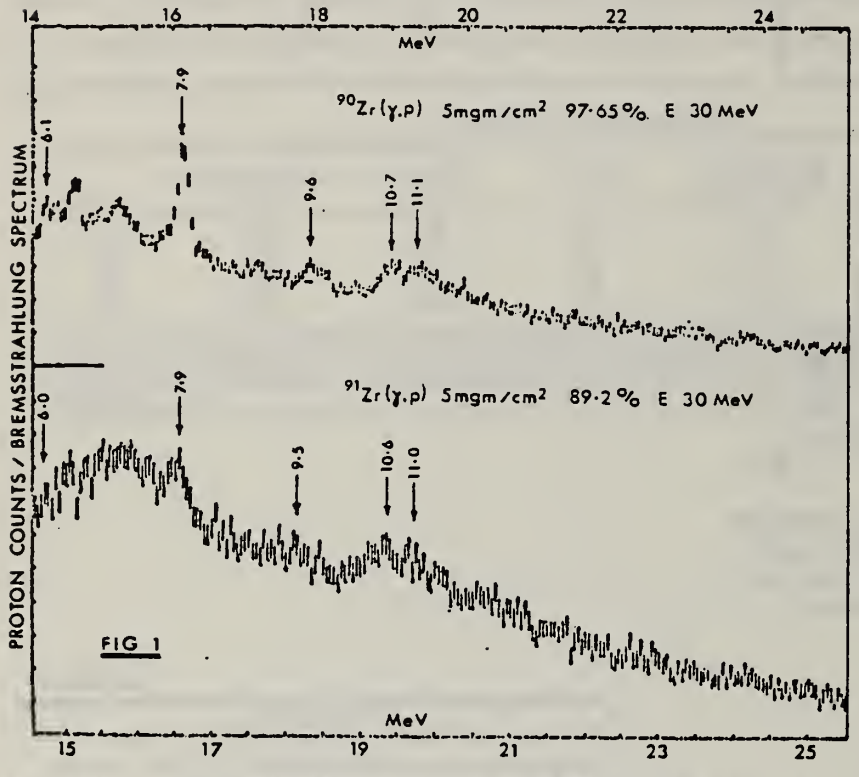

FIG 1

Arrows show proton energies. Horizontal scales indicate excitation energies assuming ground state transitions.

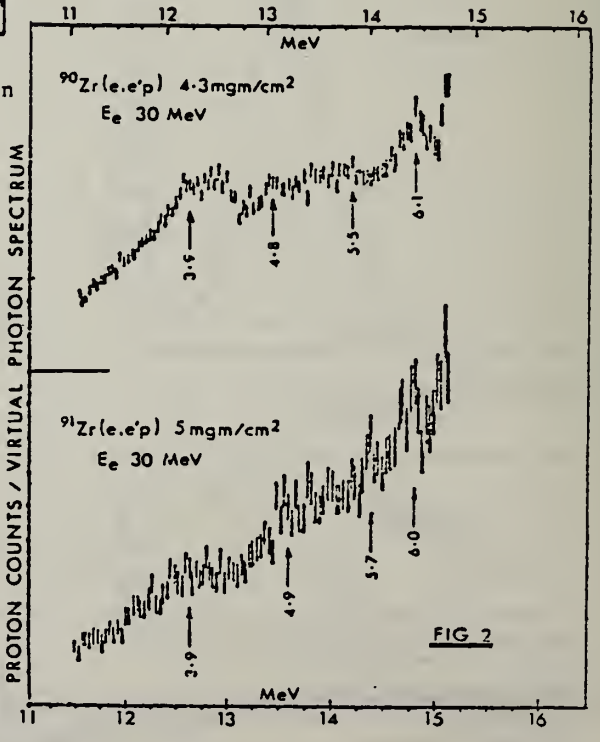

FIG 2

REF. E.J. Winhold, B.H. Patrick, E.M. Bowey, and D.B. Gaythe
PICNS-73, Vol. I, p. 701 Asilomar

ELEM. SYM.	A	Z
Zr	91	40

METHOD

REF. NO. 73 Wi 6 hmg

REACTION	RESULT	EXCITATION ENERGY	SOURCE		DETECTOR		ANGLE
			TYPE	RANGE	TYPE	RANGE	
G,N	ABX	7- 11	C	7- 11	TOF-D		130

PEAK AT 9.1 MEV

Table I

Reaction	Thres-hold (MeV)	Energy Range of Experiment (MeV)	Observed Peaks		
			Peak Energy (MeV)	$\frac{d\sigma}{d\omega}$ at peak (mb/ster.)	$4\pi \int_{\text{peak}} \left(\frac{d\sigma}{d\omega}\right)_{130^\circ} dE_\gamma$
$^{87}Sr(\gamma,n_o)$	8.44	9.4-11.1			(MeV-mb)
$^{87}Sr(\gamma,n_1)$	9.52	10.5-11.1			
$^{91}Zr(\gamma,n_o)$	7.19	7.8-10.3	9.1	1.2	20
$^{97}No(\gamma,n_o)$	6.82	7.8-9.2	8.1	0.3	3
$^{113}Cd(\gamma,n_o)$	6.54	7.4-9.3	7.7	0.9	7
$^{117}Sn(\gamma,n_o)$	6.94	7.6-8.8	7.8	2.5	20
$^{119}Sn(\gamma,n_o)$	6.48	7.1-9.0	7.8	1.6	18

REF.

H.J. Askin, K.J.F. Allen, M.N. Thompson, K. Shoda, M. Sugawara, H. Miyase, and B.N. Sung
Nucl. Phys. A220, 241 (1974)

Zr	91	40

METHOD

REF. NO. 74 As 4 egf

REACTION	RESULT	EXCITATION ENERGY	SOURCE TYPE	SOURCE RANGE	DETECTOR TYPE	DETECTOR RANGE	ANGLE
G,P	SPC	8- 30	C	30	SCD-D		90
E,P	SPC	8- 30	D	20- 30	MAG-D		90

TABLE I
Summary of results

Target	Proton energy E_p (MeV)	Excitation energy (MeV) apparent	Excitation energy (MeV) actual	Residual levels ^{90}Y
^{90}Zr	9.6	17.9	(19.4) [a]	(1.5 MeV, $\frac{1}{2}^-$) [a]
	11.1	19.4	19.4	g.s., $\frac{1}{2}^-$
	10.7	19.0	20.5–20.8 (20.7) [a]	(1.74 MeV, $\frac{1}{2}^-$) [a]
	12.5	20.8	20.8	g.s., $\frac{1}{2}^-$
	11.3	19.6	21.2–21.4	1.5 MeV, $\frac{1}{2}^-$ or 1.74 MeV, $\frac{1}{2}^-$
	10.2	18.5	(21.4) [a]	(2.88 MeV, $\frac{3}{2}^-$) [a]
				^{90}Y:
^{91}Zr	9.5	18.2	19.7 [b]	≈ 1.5 MeV [b]
	11.0	19.7	(19.7–19.9) [a]	g.s., 2$^-$ or 0.2 MeV, 3$^-$
	10.7	19.4	20.8–21.2	1.4–1.8
			(21.1) [a]	(1.7) [b]
	12.5	21.2	(21.2) [a]	g.s., 2$^-$ or 0.2 MeV, 3$^-$
	11.3	20.0	21.5–21.8	1.5–1.8
	10.1	18.8	(≈ 21.5) [a]	(≈ 2.7 MeV) [a]

[a]) Most probable.
[b]) Consistent assignment.

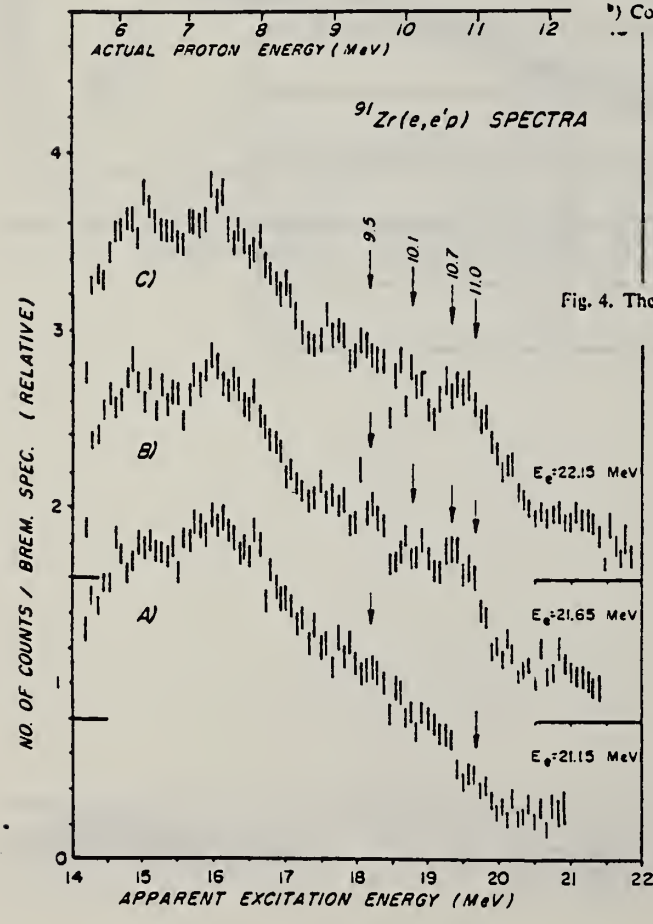

Fig. 4. The ^{91}Zr(e, e'p)^{90}Y spectra: (a) E_e(max) = 21.15 MeV; (b) E_e(max) = 21.65 MeV; (c) E_e(max) = 22.15 MeV.

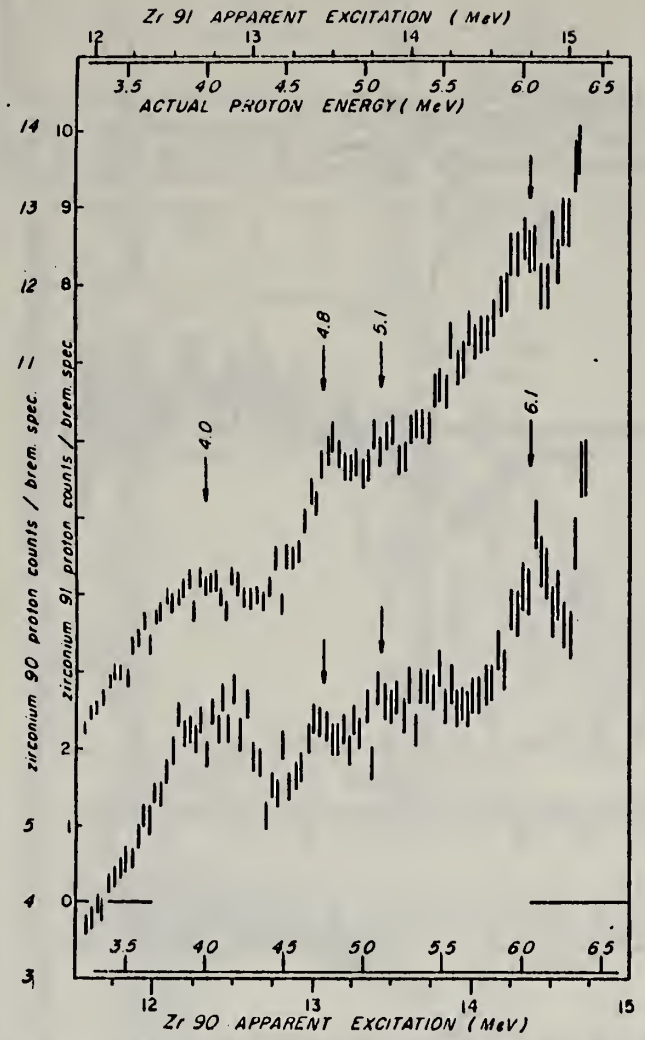

Fig. 1. The $^{91}Zr(e, e'p)^{90}Y$ proton spectrum (upper) and the $^{90}Zr(e, e'p)^{89}Y$ proton spectrum (lower). Bombarding electron energy E_e = 30 MeV. Spectra are plotted with a common proton energy scale.

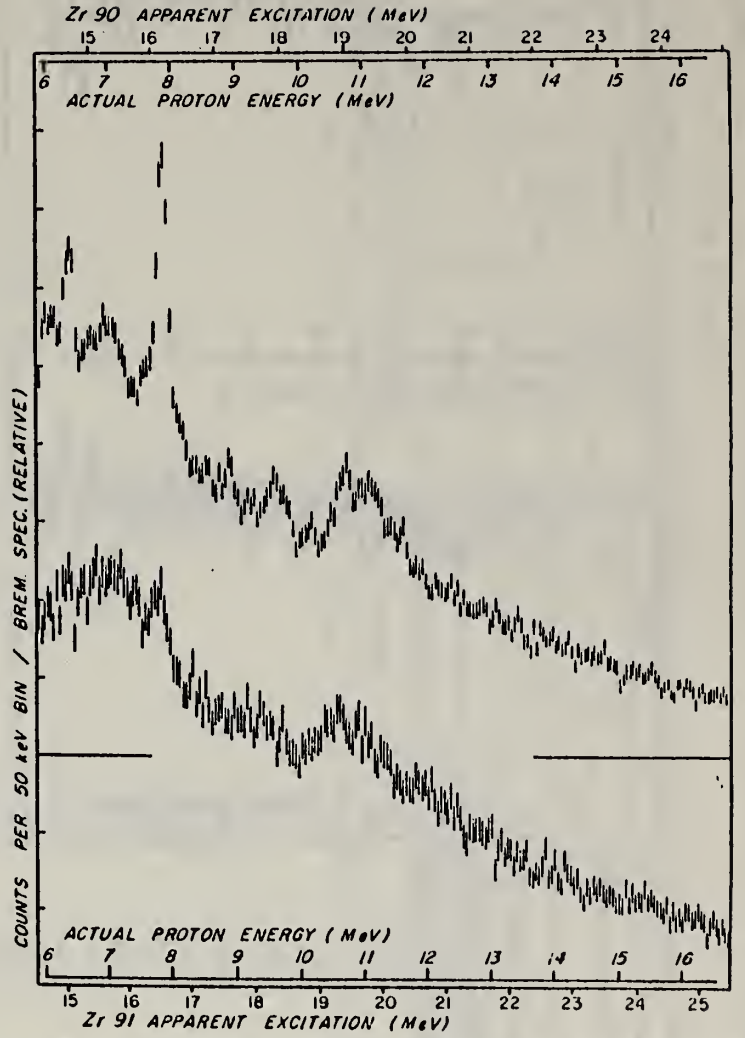

Fig. 2. The $^{90}Zr(\gamma, p)^{89}Y$ proton spectrum (upper) and the $^{91}Zr(\gamma, p)^{90}Y$ proton spectrum (lower). The E_γ endpoint = 30 MeV. Spectra are plotted with a common proton energy scale.

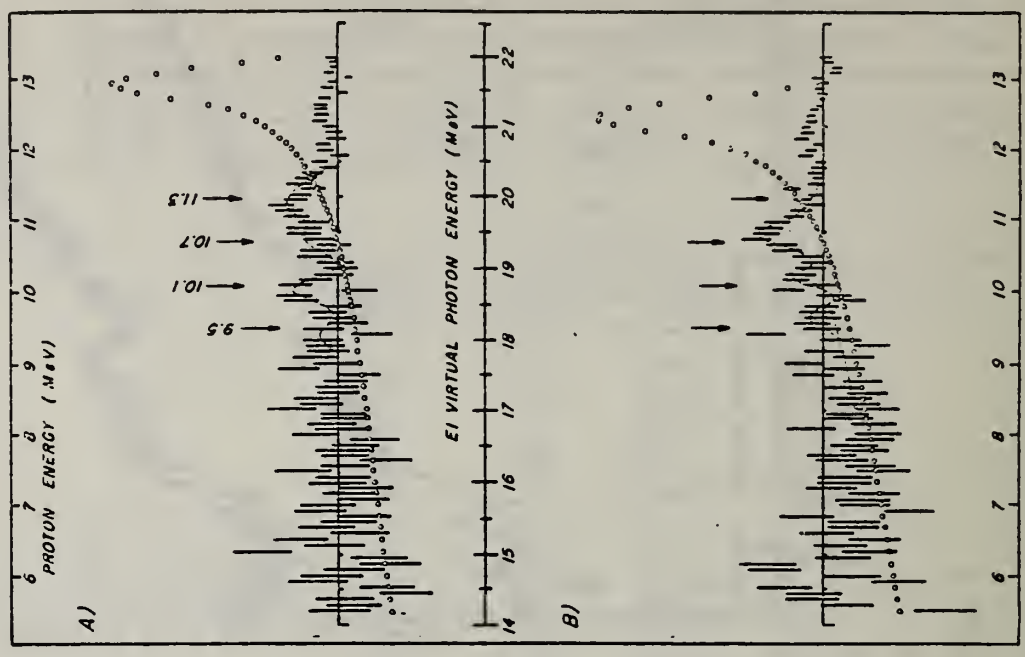

Fig. 6. Differences of $^{91}Zr(e,e'p)^{90}Y$ proton spectra recorded with: (a) $E_e(max) = 22.15$ MeV and $E_e(max) = 21.65$ MeV; (b) $E_e(max) = 21.65$ MeV and $E_e(max) = 21.15$ MeV. The corresponding differences in the EI virtual photon spectra are superimposed (circles).

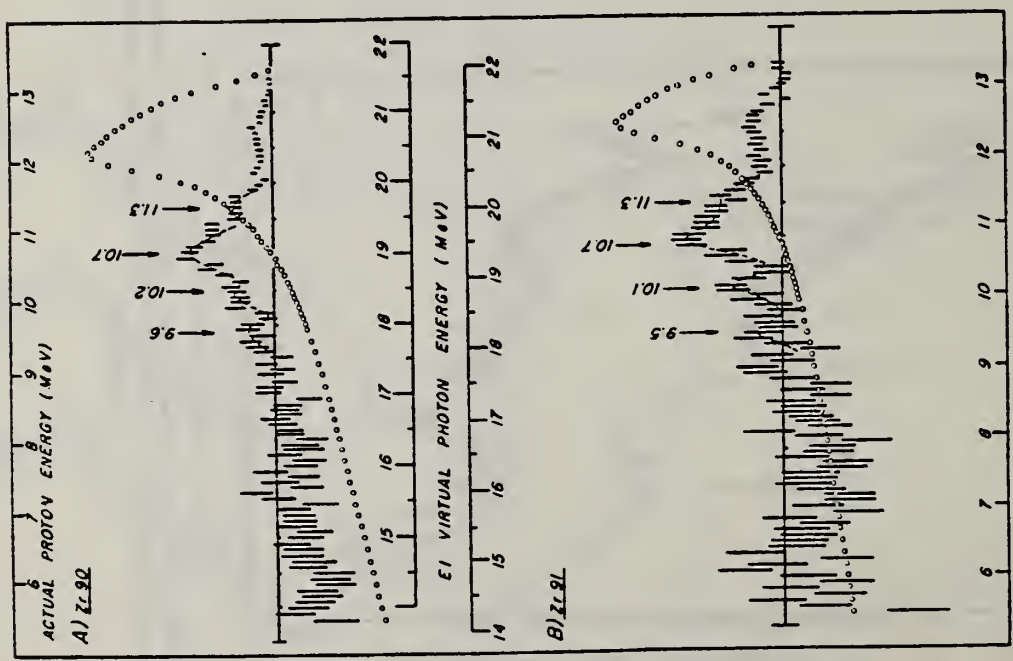

Fig. 7. Comparison of: (a) difference of $^{90}Zr(e,e'p)^{89}Y$ proton spectra recorded with $E_e(max) = 21.65$ MeV and 20.45 MeV and (b) difference of $^{91}Zr(e,e'p)^{90}Y$ spectra recorded with $E_e(max) = 22.15$ MeV and 21.15 MeV. Both proton difference spectra are plotted on a common proton energy scale. Corresponding EI virtual photon difference spectra are superimposed.

REF.

R.E. Toohey and H.E. Jackson
Phys. Rev. C9, 346 (1974)

ELEM. SYM.	A	Z
Zr	91	40

METHOD

REF. NO. 74 To 2 hmg

REACTION	RESULT	EXCITATION ENERGY	SOURCE TYPE	SOURCE RANGE	DETECTOR TYPE	DETECTOR RANGE	ANGLE
G,N	LFT	7- 9	C	9	TOF-D		135

Gamma ray widths correlate with neutron widths for p 3/2 resonances.

TABLE I. $^{91}Zr(\gamma,n)^{90}Zr$ resonance parameters obtained from threshold photoneutron measurements at Argonne National Laboratory. $j^{\pi}=\frac{1}{2}^{-}$ except as noted.

E (keV)	E_n (RC) (keV)	E_n (exp) (keV)	$\Gamma_{\gamma 0}$ (eV)
6.82	7.23	7.25	0.10
25.2	26.46	26.46	0.12
27.7	28.7	28.8	0.02
34.0[a]	35.2	35.4	0.06
38.0	39.3	39.5	0.05
39.1[b]	40.5	40.4	0.21
39.9[b]	41.3	41.3	0.63
43.2	44.7	44.6	0.05
59.7	61.7	61.9	0.05
63.1	65.1	65.3	0.16
66.3	68.4	68.5	0.11
70.6	72.8	72.5	0.02
73.5	75.8	74.5	0.04
79.7	82.2	82.1	0.07
84.5[a]	87.1	85.8	0.07
89.8	92.5	92.9	0.05
93.0[b]	95.7	95.8	0.03
94.3[b]	97.2	97.3	0.10
97.4	100.4	99.1	0.03
102.0	105.1	105.6	0.28
105.9	109.0	109.3	0.04
106.8	110.0	110.3	0.33
116.4	119.6	119.0	0.05
124.5	126.3	127.3	0.05
126.3[a]	130.0	129.8	0.23
129.9	133.7	134.2	0.33
134.9	138.8	139.0	0.12
141.1	145.2	145.3	0.08
151.3	155.6	156.1	0.17
157.4	161.8	163.4	0.11
161.3	165.9	166.5	0.26
166.9	171.6	172.6	0.28
171.8	176.7	177.7	0.57
175.7	180.7	181.6	0.01
179.0	184.1	184.3	0.11
184.2	189.4	190.1	0.11
193.7[a]	199.1	198.7	0.21
204.2	209.9	211.4	0.11
207.6	213.4	215.2	0.09
214.4	220.4	220.3	0.37

[a] An s-wave resonance; $j^{\pi}=\frac{1}{2}^{+}$.
[b] Not well resolved

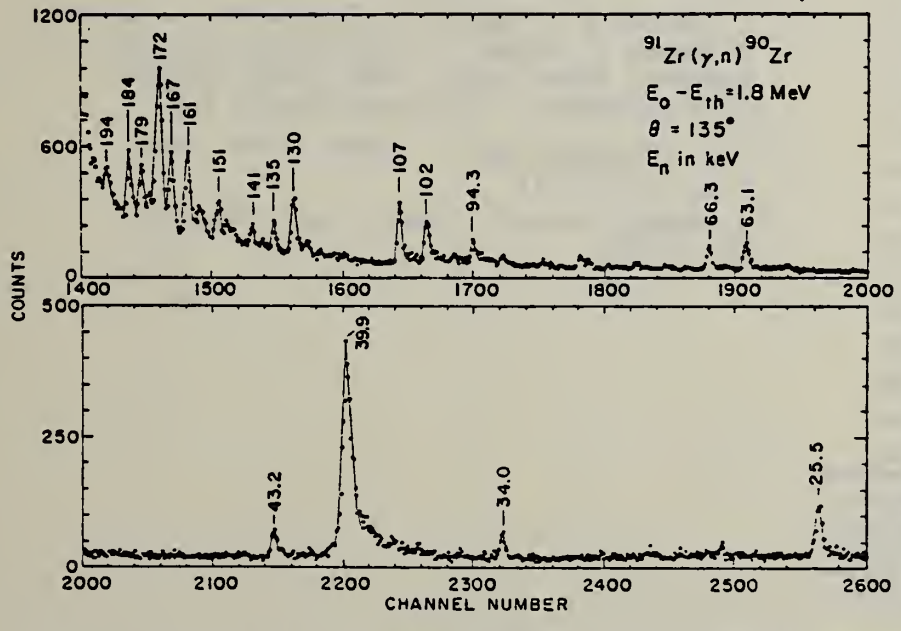

FIG. 3. A portion of the threshold photoneutron spectrum of ^{91}Zr. Prominent resonances are labeled with their energies in keV.

REF. F.R. Metzger
Phys. Rev. C 16, 597 (1977)

ELEM. SYM.	A	Z
Zr	91	40

METHOD

REF. NO. 77 Me 6 hmg

REACTION	RESULT	EXCITATION ENERGY	SOURCE TYPE	SOURCE RANGE	DETECTOR TYPE	DETECTOR RANGE	ANGLE
G,G	LFT	1 - 5	C	1 - 5	SCD-D		DST
		(1.205-4.704)		(1.85-5.0)			

Using electron bremsstrahlung with up to 5-MeV end point energy, the resonant scattering of γ rays by an enriched sample of ^{91}Zr has been studied. Substantial resonant scattering was observed from 14 levels. An additional 17 known levels were found to give rise to marginal peaks or to no observable scattering. In a few instances, the transition strengths corresponding to the resonance fluorescence yields could be compared with the results of other lifetime measurements and with the strengths expected under different assumptions concerning the nature of the levels involved.

14 LEVELS 1.2-4.7 MeV

TABLE II. Properties of the ^{91}Zr levels studied with bremsstrahlung of energy ≤5 MeV.

E_{level} [a] (MeV)	J^{π}_{exc} [b]	Γ_0/Γ [c]	$g\Gamma_0^2/\Gamma$ [d] (meV)
(1.205)	$\frac{1}{2}^+$	1.0	0.07 ±0.11
1.466 (1)	$\frac{5}{2}^+$	1.0	1.3 ±0.4
1.882 (1)	$\frac{7}{2}^+$	1.0	8.0 ±1.1
2.042 (1)	$\frac{3}{2}^+$	1.0	27.3 ±2.6
2.132 (1)	$\frac{9}{2}^+$	1.0	6.3 ±0.9
(2.190)	$\frac{5}{2}^-$	1.0	0.5 ±0.5
(2.201)	$\frac{7}{2}^+$	1.0	1.5 ±0.8
2.367 (1)	$(\frac{5}{2}, \frac{7}{2})^-$	1.0	6.5 ±0.1
(2.557)	$\frac{1}{2}^+$	0.8	0.8 ±0.6
2.577 (2)	$(\frac{5}{2})^-$	1.0	3.6 ±0.9
(2.641)	$(\frac{3}{2})^-$	1.0	4 ±2
2.694 (1)	$(\frac{5}{2})^-$	1.0	24 ±4
(2.776)	$(\frac{3}{2})^-$	1.0	4 ±3
2.811 (1)	$(\frac{7}{2})^-$	0.78	23 ±4
3.108 (3)	$\frac{9}{2}^+$		8 ±3
(3.235)	$\frac{1}{2}^-, \frac{3}{2}^-$		1 ±3
(3.317)	$\frac{7}{2}^+, \frac{9}{2}^+$		3 ±3
3.476 (1)	$\frac{1}{2}^-, \frac{3}{2}^-$	1.0	90 ±10
3.576 (1)	$\frac{1}{2}^-, \frac{3}{2}^-$		40 ±7
3.681 (3)	$(\frac{3}{2})^+$	1.0	46 ±18 [e]
3.704 (3)			25 ±9
4.322 (2)	$\frac{1}{2}^-, \frac{3}{2}^-$		70 ±30
(4.674)	$\frac{1}{2}^+, \frac{3}{2}^-$		50 ±30
(4.704)			80 ±40

[a] For weak excitations, the energies, given in parentheses, were taken from the literature (Refs. 2, 3, 5, 17, and 18). For well-defined excitations, the energies determined in the (γ,γ) experiments are listed, with the uncertainties in units of the last digits given in parentheses.

[b] From Refs. 5 and 18.

[c] Based on Refs. 2, 16, and 17.

[d] Results of the (γ,γ) experiments described in this paper.

[e] The larger error reflects the fact that a contribution from the 3.684-MeV level in ^{13}C had to be subtracted.

[2] J.E. Glenn, H.W. Baer, and J.J. Kraushaar, Nucl. Phys. A165, 533 (1970)

[3] A. Graue, L.H. Herland, K.J. Lervik, J.T.Nesse, and E.R. Cosman, Nucl. Phys. A187, 141 (1972)

[5] H.P. Blok, L. Hulstman, E.J. Kaptein, and J. Blok, Nucl. Phys. A273, 142 (1976)

[16] C. Borcea, E.R. Cosman, W. Duennweber, E. Grosse, M. Maier, K. Pingel, D. Proetel, and P. von Brentano, Annual report, Max Planck Institut fuer Kernphysik, 1970 (unpublished), p.52

[17] S.S. Glickstein and G. Tessler, Phys. Rev. C 10, 173 (1974)

[18] H. Verheul and W.B. Ewbank, Nucl. Data B8, 477 (1972)

ZR
A=92

ZR
A=92

ZR
A=92

Ref. P.F. Yergin, B.P. Fabricand
Phys. Rev. 104, 1334 (1956)

Elem. Sym.	A	Z
Zr	92	40

Method: 24 MeV betatron; 250r Victoreen in 3.75 cm Lucite; neutron detector

Ref. No.: 56 Ye 2 | EGF

Reaction	E or ΔE	E_0	Γ	$\int \sigma dE$	Jπ	Notes
$Zr^{92}(\gamma,xn)$	Bremss. 24	16.9	5.5 MeV	$\int_0^{23}$ = 1.24 MeV-b		

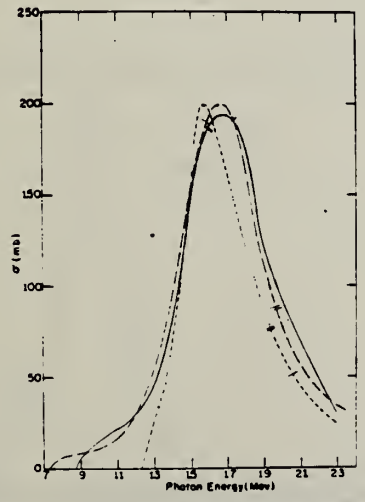

FIG. 5. Cross sections for the (γ,n) reactions in zirconium isotopes. Short dashes Zr^{90}, long dashes Zr^{91}, full curve Zr^{92}. The previously published Zr^{90} and Zr^{91} results have been recomputed, taking into account the present Zr^{92} measurements. The single and double slash marks on each curve represent the locations of the (γ,pn) and $(\gamma,2n)$ thresholds respectively. The units of the ordinate are 10^{-27} cm^2.

TABLE III. Parameters of giant-resonance cross-section curves for (γ,n) reactions in nuclei near 50 neutrons. Nuclides $_{33}As^{75}$, $_{41}Nb^{93}$, and $_{45}Rh^{103}$ from reference 4, $_{40}Zr^{90}$ and $_{40}Zr^{91}$ from reference 5 recomputed in present work. Neutron number is shown in column 2, location of peak cross-section value in column 3, peak cross-section value in column 4, half-height width of curve in column 5, and area under curve from threshold to 23 Mev in column 6.

Nuclide	N	E_m (Mev)	σ_m (millibarns)	Γ (Mev)	$\int_0^{23}\sigma dE$ (Mev-barns)
$_{33}As^{75}$	42	17.3	90.3	9.0	0.80
$_{38}Sr^{88}$	48	15.9	160	5.0	0.92
$_{38}Sr^{87}$	49	15.8	146	5.3	1.00
$_{38}Sr^{86}$	50	16.3	201	4.0	1.05
$_{39}Y^{89}$	50	16.3	191	3.8	0.87
$_{40}Zr^{90}$	50	15.8	199	4.3	0.98
$_{40}Zr^{91}$	51	16.5	200	5.0	1.22
$_{40}Zr^{92}$	52	16.9	193	5.5	1.24
$_{41}Nb^{93}$	52	17.0	195	6.8	1.46
$_{45}Rh^{103}$	58	16.5	205	8.9	1.94

REF. S. C. Fultz, R. L. Bramblett, B. L. Berman, and J. T. Caldwell and M. A. Kelly
Proc. Gatlinburg Conference 397 (1966)

ELEM. SYM.	A	Z
Zr	92	40

METHOD

REF. NO. 66 Fu 2 hmg

REACTION	RESULT	EXCITATION ENERGY	SOURCE		DETECTOR		ANGLE
			TYPE	RANGE	TYPE	RANGE	
G,XN	ABI	THR-28	D	THR-28	BF3-I		4PI
G,2N	ABI	THR-28	D	THR-28	BF3-I		4PI

TABLE 1

Integrated Cross Sections for Zirconium and Yttrium

Isotope	E_{max} $a = \int \sigma_{tot}\, dE$ (MeV - barns)	E_{max} $b = \int \sigma_{\gamma,2n} dE$ (MeV - barns)	b/a	E_{max} (MeV)
^{90}Zr	0.980	0.108	0.110	28
^{91}Zr	1.078	0.202	0.187	30
^{92}Zr	1.096	0.447	0.408	28
^{94}Zr	1.041	0.577	0.554	30
^{89}Y	0.991	0.095	0.096	28

REF. B.L. Berman, J.T. Caldwell, R.R. Harvey, M.A. Kelly, R.L. Bramblett, and S.C. Fultz
Phys. Rev. 162, 1098 (1967)

ELEM. SYM.	A	Z
Zr	92	40

METHOD

REF. NO. 67 Be 2 hmg

REACTION	RESULT	EXCITATION ENERGY	SOURCE TYPE	SOURCE RANGE	DETECTOR TYPE	DETECTOR RANGE	ANGLE
G,N 11+	ABX	THR-28	D	THR-28	BF3-I		4PI
G,2N 10	ABX	THR-28	D	THR-28	BF3-I		4PI

TABLE IV. Integrated cross sections.

Nucleus	$\sigma_{int}[(\gamma,n)+(\gamma,p\pi)]$ (MeV-b)[a]	$\sigma_{int}(\gamma,2n)$ (MeV-b)[a]	$E_{\gamma max}$ (MeV)	$\frac{\sigma_{int}(\gamma,2n)}{\sigma_{int}(\gamma,\text{total})}$[b]	$(\frac{1}{2}\pi)\sigma_m\Gamma$ (MeV-b)	$0.06NZ/A$ (MeV-b)
Y^{89}	0.94	0.10	28	0.10	1.14	1.31
Zr^{90}	0.96	0.10	28	0.09	1.16	1.33
Zr^{91}	0.88	0.20	30	0.19	1.22	1.35
Zr^{92}	0.65	0.45	28	0.41	1.23	1.36
Zr^{94}	0.43	0.58	30	0.56[c]	1.32	1.38

[a] All measured integrated cross-section values are given for an energy region from threshold to $E_{\gamma max}$. For the Zr^{92} and Zr^{94} cases, it was necessary to extrapolate the low-energy part of the total photoneutron cross section down to threshold; the error introduced in this process, however, is less than 0.5%.
[b] The word "total" in this table refers to the total photoneutron cross section $\sigma([\gamma,n)+(\gamma,pn)+(\gamma,2n)+(\gamma,3n)]$, and excludes the (γ,γ) and (γ,p) cross sections.
[c] This value includes the contribution of $\sigma_{int}(\gamma,3n)$, which equals 0.03 MeV-b from threshold to 30 MeV.

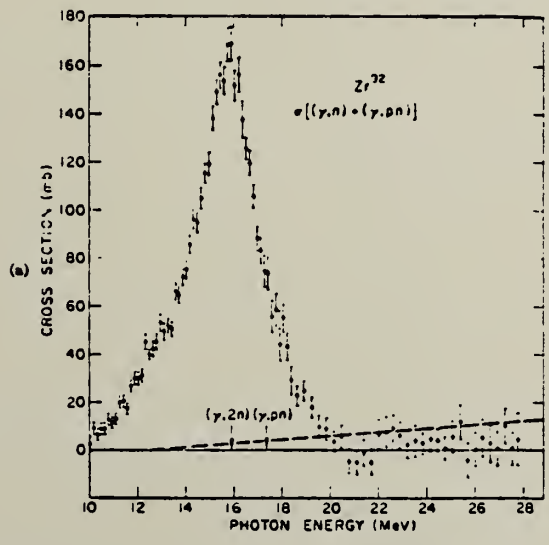

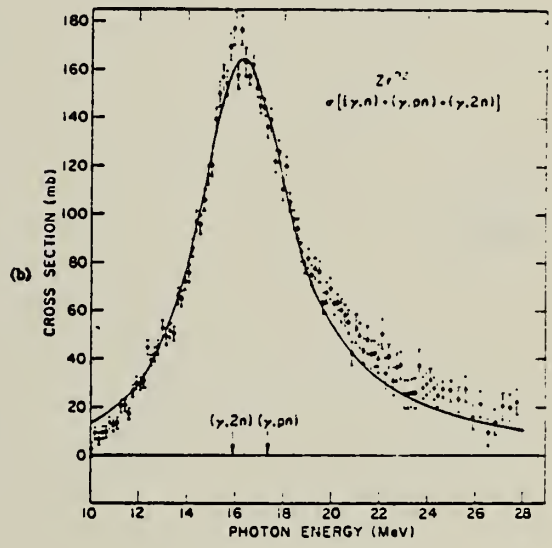

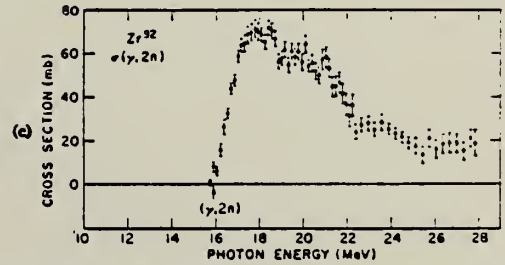

FIG. 11. (a) Total photoneutron cross section for Zr^{92}. (b) Single photoneutron cross section for Zr^{92}. (c) The $(\gamma,2n)$ cross section for Zr^{92}.

ZR
A=94

ZR
A=94

REF. S. C. Fultz, R. L. Bramblett, B. L. Berman, J. T. Caldwell, and M. A. Kelly
Proc. Gatlinburg Conference 397 (1966)

ELEM. SYM.	A	Z
Zr	94	40

METHOD

REF. NO. 66 Fu 2 hmg

REACTION	RESULT	EXCITATION ENERGY	SOURCE		DETECTOR		ANGLE
			TYPE	RANGE	TYPE	RANGE	
G,XN	ABI	THR-30	D	THR-30	BF3-I		4PI
G,2N	ABI	THR-30	D	THR-30	BF3-I		4PI

TABLE 1

Integrated Cross Sections for Zirconium and Yttrium

Isotope	E_{max} $a = \int \sigma_{tot}\, dE$ (MeV - barns)	E_{max} $b = \int \sigma_{Y_{2n}} dE$ (MeV - barns)	b/a	E_{max} (MeV)
^{90}Zr	0.980	0.108	0.110	28
^{91}Zr	1.078	0.202	0.187	30
^{92}Zr	1.096	0.447	0.408	28
^{94}Zr	1.041	0.577	0.554	30
^{89}Y	0.991	0.095	0.096	28

REF. B. L. Berman, J. T. Caldwell, R.R. Harvey, M.A. Kelly, R.L. Bramblett and S.C. Fultz

ELEM. SYM.	A	Z
Zr	94	40

METHOD

REF. NO. 67 Be 2 hmg

REACTION	RESULT	EXCITATION ENERGY	SOURCE TYPE	SOURCE RANGE	DETECTOR TYPE	DETECTOR RANGE	ANGLE
G,N	ABX	THR-30	D	THR-30	BF3-I		4PI
G,2N	ABX	THR-30	D	THR-30	BF3-I		4PI

TABLE IV. Integrated cross sections.

Nucleus	$\sigma_{int}[(\gamma,\pi)+(\gamma,p\pi)]$ (MeV-b)[a]	$\sigma_{int}(\gamma,2\pi)$ (MeV-b)[a]	$E_{\gamma max}$ (MeV)	$\frac{\sigma_{int}(\gamma,2\pi)}{\sigma_{int}(\gamma,\text{total})}$[b]	$(\frac{1}{2}\pi)\sigma_m\Gamma$ (MeV-b)	$0.06NZ/A$ (MeV-b)
Y^{89}	0.94	0.10	28	0.10	1.14	1.31
Zr^{90}	0.96	0.10	28	0.09	1.16	1.33
Zr^{91}	0.88	0.20	30	0.19	1.22	1.35
Zr^{92}	0.65	0.45	28	0.41	1.23	1.36
Zr^{94}	0.43	0.58	30	0.56[c]	1.32	1.38

[a] All measured integrated cross-section values are given for an energy region from threshold to $E_{\gamma max}$. For the Zr^{94} and Zr^{92} cases, it was necessary to extrapolate the low-energy part of the total photoneutron cross section down to threshold; the error introduced in this process, however, is less than 0.5%.
[b] The word "total" in this table refers to the total photoneutron cross section $\sigma([\gamma,\pi)+(\gamma,p\pi)+(\gamma,2\pi)+(\gamma,3\pi)]$, and excludes the (γ,γ) and (γ,p) cross sections.
[c] This value includes the contribution of $\sigma_{int}(\gamma,3\pi)$, which equals 0.03 MeV-b from threshold to 30 MeV.

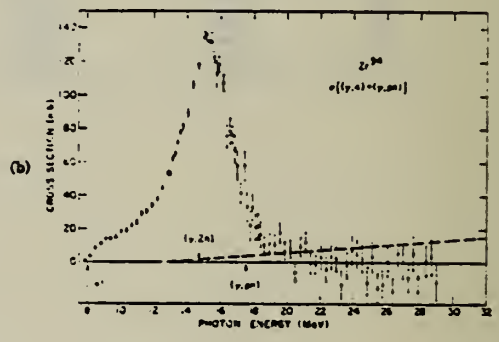

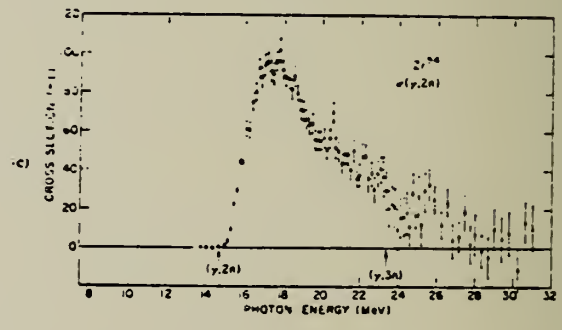

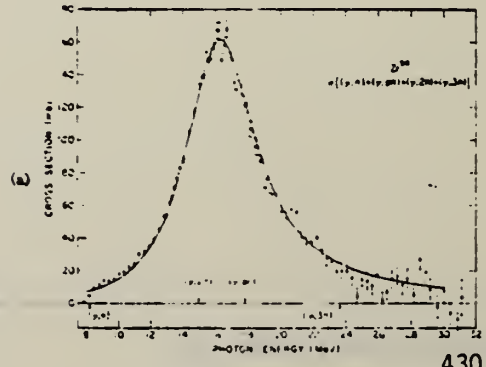

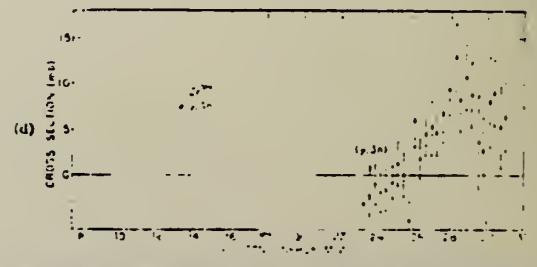

FIG. 12. (a) Total photoneutron cross section $\sigma[(\gamma,\pi)+(\gamma,p\pi)+(\gamma,2\pi)+(\gamma,3\pi)]$ for Zr^{94}. (b) Single photoneutron cross section for Zr^{94}; (c) The $(\gamma,2\pi)$ cross section for Zr^{94}. (d) The $(\gamma,3\pi)$ cross section for Zr^{94}.

# NIOBIUM
Z=41

Niobium is a metallic element closely associated with tantalum in ores and in properties; it was named in 1844 by the German chemist Heinrich Rose after the goddess Niobe, daughter of Tantalus. It was first discovered in 1801 in a New England mineral by the British chemist Charles Hatchett, who called the element columbium. By international agreement in 1949, chemists established the name niobium but the name columbium persisted strongly in the U.S. metallurgical industry.

Nb
A=93

Nb
A=93

B.G. Chidley, L. Katz, S. Kowalski
Can. J. Phys. 36, 407 (1958)

ELEM. SYM.	A	Z
Nb	93	41

Betatron

REF. NO.	
58 Ch 2	NVB

REACTION	RESULT	EXCITATION ENERGY	SOURCE		DETECTOR		ANGLE
			TYPE	RANGE	TYPE	RANGE	
G,N	RLY	THR	C	THR	BF3-I		4PI

THRESHOLD

TABLE I

MEASURED PHOTONEUTRON THRESHOLDS

Reaction	Measured Q value, Mev.	Other Q values, Mev.	Method	Reference
$Nb^{93}(\gamma, n)Nb^{92}$	8.86±0.05			
		8.70 ±0.20	Threshold	Sher *et al.* (1951)
		8.69 ±0.40	Mass data	Wapstra (1955)

See 58 Ka 1 for cross sections.

L. Katz, G.B. Chidley
Nuclear Reactions at Low and Medium Energies (Academy of Science, USSR: 1958) 371

CLASSIFICATION			
	Nb	93	41

METHOD: Betatron; neutron cross section; BF_3 counters; ion chamber monitor

REF. NO.: 58 Ka 1 | NVB

REACTION	RESULT	EXCITATION ENERGY	SOURCE		DETECTOR		ANGLE
			TYPE	RANGE	TYPE	RANGE	
G,XN	ABX	9-22	C	9-22	BF3-I		4PI

Таблица 2

Пороги испускания фотонейтронов

Изотоп	B_n, *Мэв*	B_m, *Мэв*	Изотоп	B_n, *Мэв*	B_m, *Мэв*
V^{51}	11,16	20,5	La^{139}	8.81	16,1
Mn^{55}	10.14	19,2	Pr^{141}	9.46	17,6
Co^{59}	10.44	18,6	Tb^{159}	8.16	14,8
As^{75}	10.24	18,1	Ho^{165}	8.10	14,6
Y^{89}	11,82	20,7	Tm^{169}	8.00	14,7
Nb^{93}	8,86	17,1	Lu^{175}	7,77	14,2
Rh^{103}	9,46	16,8	Ta^{181}	7,66	13,8
J^{127}	9,14	16,2	Au^{197}	7,96	13,3
Cs^{133}	9,11	16,5	Bi^{209}	7,43	14,5

THRESHOLDS

не приведены, поскольку они превышают 22 *Мэв* во всех случаях, кроме золота, для которого B_m=21 *Мэв*. Свойства сечения $\sigma_c(\gamma)$ сведены в табл. 3.

Таблица 1

Изотоп	$E_{макс}$, *Мэв*	$\sigma_n(E_\gamma)$, барн	Γ, *Мэв*	Γ^{int}, *Мэв·барн*	$Y(22)$, 10^{-3} нейтрон/100 р·моль
V^{51}	18,4	0,062	5,2	0,33	1,62
Mn^{55}	20,2	0,060	7,0	0,39	2,01
Co^{59}	18,3	0,068	6,3	0,44	2,30
As^{75}	16,4	0,090	9,5	0,74	4,25
Y^{89}	17,1	0,172	5,2	0,93	5,33
Nb^{93}	18,0	0,156	7,5	1,17	6,80
Rh^{103}	17,5	0,160	9,4	1,40	8,28
J^{127}	15,2	0,273	6,8	1,76	11,9
Cs^{133}	16,5	0,238	7,7	1,59	10,7
La^{139}	15,5	0,325	3,8	1,55	11,2
Pr^{141}	15,0	0,320	4,9	1,93	13,1
Tb^{159}	15,6	0,274	9,8	2,49	18,1
Ho^{165}	13,5	0,305	8,9	2,52	18,7
Tm^{169}	16,4	0,250	8,4	1,91	14,9
Lu^{175}	16,0	0,225	8,4	1,90	23,0
Ta^{181}	14,5	0,380	8,5	3,15	22,0
Au^{197}	13,8	0,475	4,7	3,04	22,6
Bi^{209}	13,2	0,455	5,9	2,89	23,2

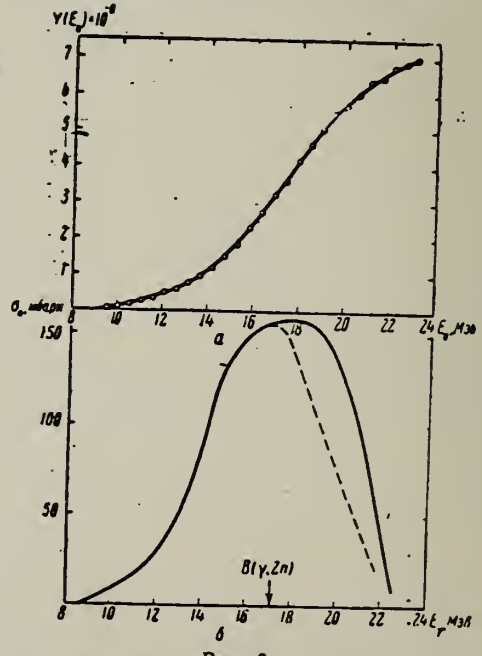

Рис. 6.

а — Выход фотонейтронов для Nb; б — $\sigma_n(E_\gamma)$ и $\sigma_c(\gamma)$ для Nb

Ref. E. Silva, J. Goldemberg, P.B. Smith, L. Marquez
Il Nuovo Cimento 9, 17 (1958)

Elem. Sym.	A	Z
Nb	93	41

Method: 22 MeV Betatron; activation; NaI

Ref. No.: 58 Si 2 | EH

Reaction	E or ΔE	E_o	Γ	$\int \sigma dE$	Jπ	Notes
(γ,n)	8-22	~ 17		1.25 MeV-b		

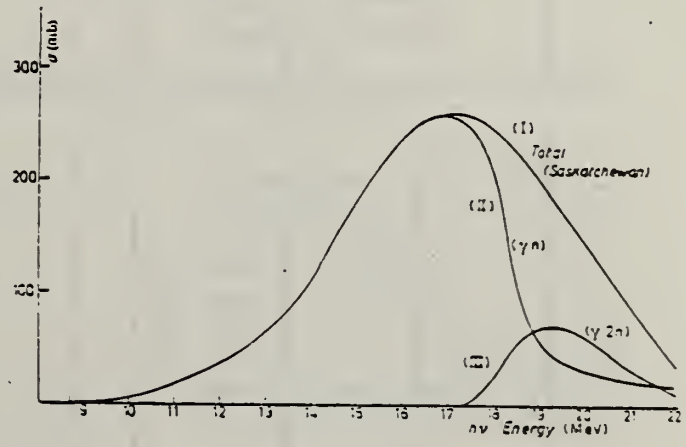

Fig. 3.

Ref. M.E. Toms, J. McElhinney
Phys. Rev. 111, 561 (1958)

Elem. Sym.	A	Z
Nb	93	41

Method: Betatron; alpha yield; nuclear emulsion

Ref. No.: 58 To 2 | NVB

Reaction	E or ΔE	E_o	Γ	$\int \sigma dE$	Jπ	Notes
$Nb^{93}(\gamma,\alpha)$	Bremss. 22					Yield = 0.5×10^4 alpha/mole/roentgen

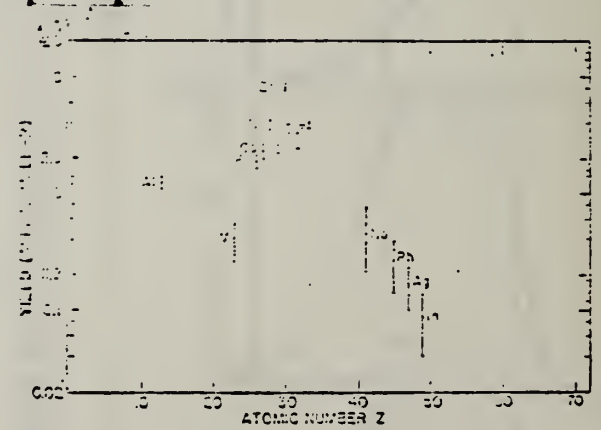

FIG. 8. Photo-alpha yields plotted against atomic numbers for the exposures of the survey.

Ref. W.C. Barber, V.J. Vanhuyse
Nuclear Phys. 16, 381 (1960)

Elem. Sym.	A	Z
Nb	93	41

Method: Stanford Mark II accelerator; virtual and real photon spectrum from electrons; magnetic spectrum; KI scintillator crystals.

Ref. No.: 60 Ba 5 JHH

Reaction	E or ΔE	E_0	Γ	$\int \sigma dE$	Jπ	Notes
$Nb^{93}(\gamma,p)$	$E_{e^-} = \leq 40$			$\int_0^{40} = 230 \pm 25\%$ MeVmb		$\int \sigma dE$ from calculated real and virtual photon spectrum.

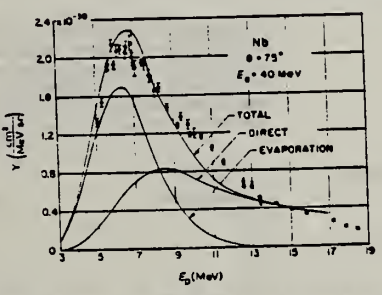

Fig. 4. Energy distribution of protons from Nb. The curves are calculated distributions arbitrarily normalized.

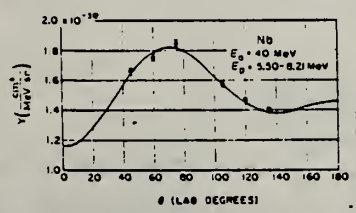

Fig. 9. Angular distribution of protons from Nb. The curve is a plot of the expression $(1.31-0.15\cos\theta+0.41\sin^2\theta+0.65\cos\theta\sin^2\theta)\times 10^{-30}$, which is a four-parameter least-squares fit to the data.

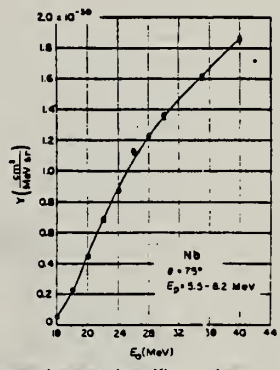

Fig. 14. Excitation of a group of protons from Nb as a function of primary electron energy. The curve was drawn arbitrarily.

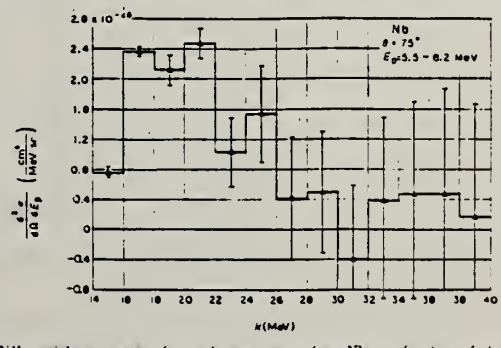

Fig. 17. Differential cross section for producing protons from Nb as a function of photon energy The histogram was drived by a photon-difference analysis of fig. 14.

W.C. Barber, V.J. Vanhuyse
J. Phys. Radium 21, 299 (1960)

Nb	93	41

METHOD: Linac; proton spectrum; angular distribution; magnetic spectrometer

REF. NO.: 60 Ba 6 | NVB

REACTION	RESULT	EXCITATION ENERGY	SOURCE		DETECTOR		ANGLE
			TYPE	RANGE	TYPE	RANGE	
G,P	SPC	17-40	C	10-40	MAG-D	5-18	DST

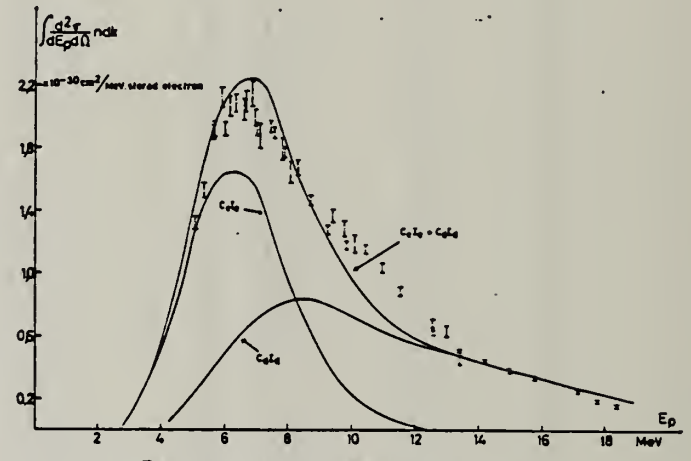

FIG. 2. — Distribution d'énergie. $E_0 = 40$ MeV, $\theta = 75°$.
$C_e I_e$ = distribution des protons évaporés. $C_d I_d$ = distribution des protons directs.

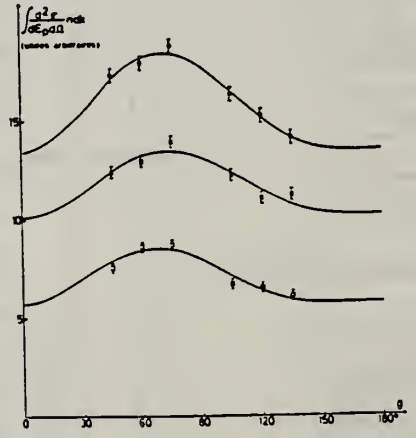

FIG. 3. — Distributions angulaires. $E_0 = 40$ MeV.
× $E_p = 5,05 - 6,55$ MeV ;
$1 + 0,28 \sin^2\theta(1 + 0,80 \cos\theta)$.
○ $E_p = 5,75 - 7,45$ MeV ;
$1 + 0,31 \sin^2\theta(1 + 0,99 \cos\theta)$.
☑ $E_p = 7,05 - 8,45$ MeV ;
$1 + 0,37 \sin^2\theta(1 + 1,29 \cos\theta)$

de photons réels n_γ (produits par le rayonnement de freinage dans l'émetteur secondaire, les fenêtres et la cible) et du nombre de photons virtuels n_v dans la cible. Il a été tenu compte de n_γ et de n_v dans le calcul de $n(E_0, k)$. Pour le calcul de n_v on a supposé qu'on avait des transitions E_1.

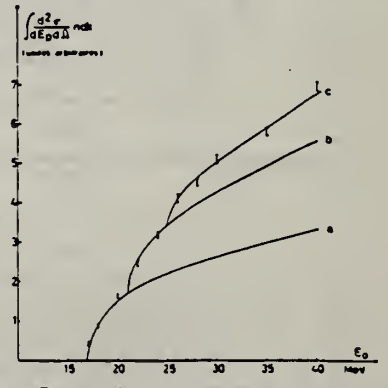

FIG. 4. — Fonction d'excitation. $\theta = 75°$.
a = isochromate de 17 MeV ;
b = somme d'isochromates de 17 et 21 MeV ;
c = somme d'isochromates de 17,21 et 25 MeV ;

REF.

K. N. Geller, J. Halpern, and E. G. Muirhead
Phys. Rev. 118, 1302-12 (1960)

Nb	93	41

METHOD

Betatron; neutron threshold; ion chamber

REF. NO. 60 Ge 3 NVB

REACTION	RESULT	EXCITATION ENERGY	SOURCE		DETECTOR		ANGLE
			TYPE	RANGE	TYPE	RANGE	
G,N	NØX	THR	C THR		BF3-I		4 PI

THRESHØLD

TABLE I. Summary and comparison of neutron separation energies inferred from present threshold measurements with values predicted from mass data and reaction energies. All energies are expressed in the center-of-mass system in Mev.

Reaction	No. runs	Present results	Other results	Method	Reference
$Nb^{93}(\gamma,n)Nb^{92}$	2	8.78±0.06	≥8.61 ±0.52	mass data	m
			$Q(\alpha)$		n
			8.86 ±0.05	threshold	f

[m] Henry E. Duckworth, *Mass Spectroscopy* (Cambridge University Press, New York, 1958), p. 177.
[n] L. J. Lidofsky, Revs. Modern Phys. 29, 773 (1957).

Ref.		Elem. Sym.	A	Z
	R.E. Welsh, D.J. Donahue Phys. Rev. 121, 880 (1961)	Nb	93	41

Method	Ref. No.	
Monoergic γ's from thermal n-capture; activation	61 We 1	JHH

Reaction	E or ΔE	E_o	Γ	$\int \sigma dE$	Jπ	Notes
(γ,n)	8.997 9.30 9.73					Measurement of 0.930 MeV γ from decay of Nb^{92}. Data in Table II (millibarns), Fig. 6 $E_{\gamma\ thresh.}$ = 8.99 ± 0.04 MeV.

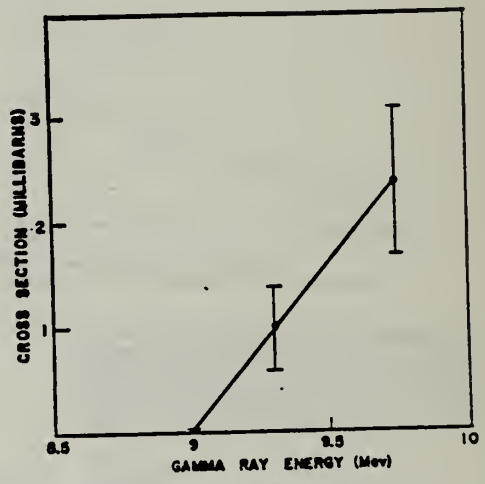

FIG. 6. Cross section vs energy $Nb^{93}(\gamma,n)Nb^{92}$(10 day). The line indicates a possible extrapolation to threshold.

TABLE II. Summary of measured cross sections.

γ-ray source / Energy (Mev) / Reaction	Co 7.49	Fe 7.64	Al 7.73	Cu 7.91	Cl 8.56	Ni 8.997	Fe 9.30	Cr 9.72	Fe 10.16	N 10.83
$Ta^{181}(\gamma,n)Ta^{180m}$	0±0.05	0.5±1	4.8±1.6	14±5	32±16	44±15	···	83±33	···	120±48
$Au^{197}(\gamma,n)Au^{196}$	···	···	···	0±2	34±17	44±11	64±30	80±30	···	···
$Ho^{165}(\gamma,n)Ho^{164}$	···	···	···	0±0.1	29±15	30±18	46±21	86±31	···	260±93
$Nb^{93}(\gamma,n)Nb^{92}$	···	···	···	···	···	0.008±0.005	1.0±0.4	2.4±0.7	···	···
$Ag^{107}(\gamma,n)Ag^{106}$	···	···	···	···	···	0±0.1	···	4.4±1.5	22±16	23±7.5

Ref. O.M.M. Mitchell, K.G. McNeill
Can. J. Phys. 41, 871 (1963)

Elem. Sym.	A	Z
Nb	93	41

Method: Betatron; proton yield; angular distribution; scintillator; ion chamber

Ref. No.: 63 Mi 5 NVB

Reaction	E or ΔE	E_o	Γ	$\int \sigma dE$	Jπ	Notes
$Nb^{93}(\gamma,xp)$	Bremss. 22					Angular distribution: $Y(\theta) = a + b \sin^2\theta (1 + p \cos\theta)^2$ where a = 23±8; b = 71±13; p = 0.1±0.1; and b/a = 3.0±1.2. Yield (E_p > 8 MeV): (2.8±0.7) 10^5 protons/mole-r. Yield (3.7 < E_p < 14): (21±2) 10^5

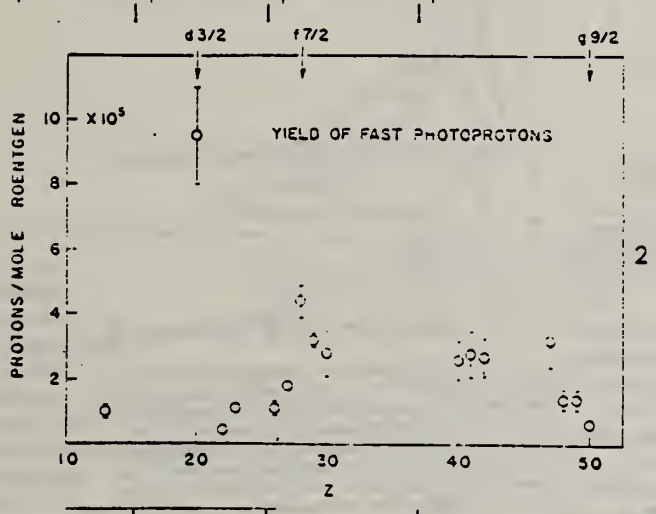

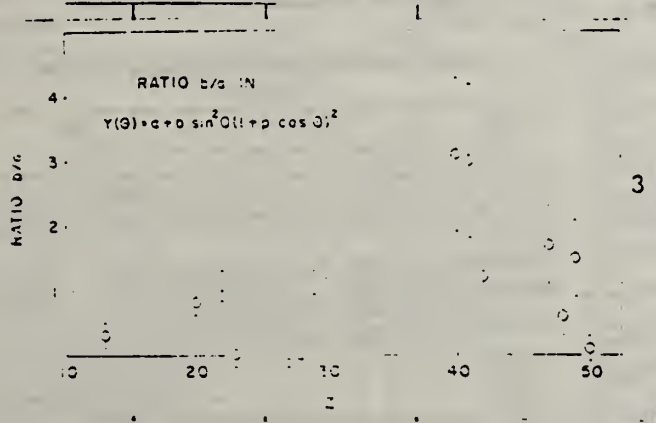

FIG. 2. The yields of fast photoprotons ($E_p \geq 8$ MeV) obtained from targets of various elements when irradiated with 22 MeV bremsstrahlung. The target thicknesses range from 24 to 372 mg/cm² (one about 8 MeV for protons). The errors noted are statistical.

FIG. 3. The anisotropy coefficient b/a for fast photoprotons ($E_p \geq 8$ MeV) from the elements. The errors noted are statistical.

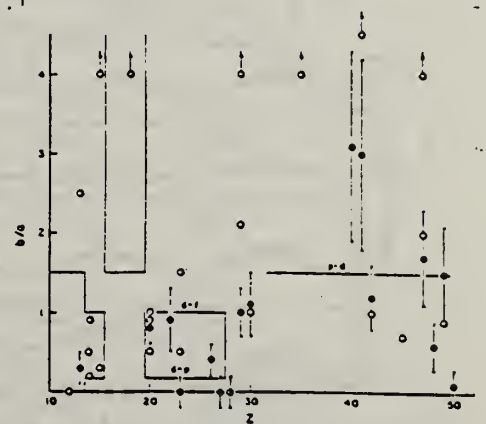

FIG. 4. The values of the fast photoproton anisotropy coefficient b/a found by the present authors (●) and other workers (○) in the region of the periodic table 10 < Z < 50. Arrows indicate sub-shell points. The references to the results of other workers are given in Table II. The demarcations are explained in the text.

FORM NBS-41
18-1-63)
USCOMM-DC 18556-P63

U.S. DEPARTMENT OF COMMERCE
NATIONAL BUREAU OF STANDARDS

Ref. R.M. Osokina
Zhur. Eksp. i Teoret. Fiz. 44, 444 (1963)
Soviet Phys. JETP 17, 303 (1963)

Elem. Sym.	A	Z
Nb	93	41

Method 30 MeV Synchrotron; emulsions

Ref. No. 63 Os 1 JHH

Reaction	E or ΔE	E_0	Γ	$\int \sigma dE$	Jπ	Notes
(γ,p)				Relative yields: (Ep > 3 MeV)		Measured yeilds > by factor of 10 than statistical theory including effects of nuclear pair correlation predicts.
	19.5			1.00 ± 0.04		
	23.5			1.58 ± 0.04		
	27.5			2.22 ± 0.10		

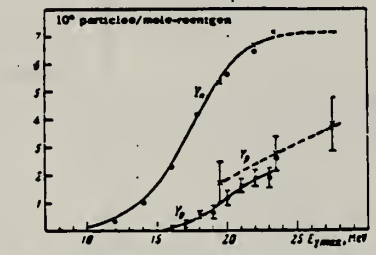

FIG. 4. Dependence of photoproton yield Y_p and photoneutron yield Y_n from Nb^{93} on $E_{\gamma max}$. For Y_p: x – present work, ∘ – [9], ∘ – [8]; the yields have been multiplied by the factor S. For Y_n: x and ∘ – measured in [11] and [12], respectively; the smooth curve was obtained in [10].

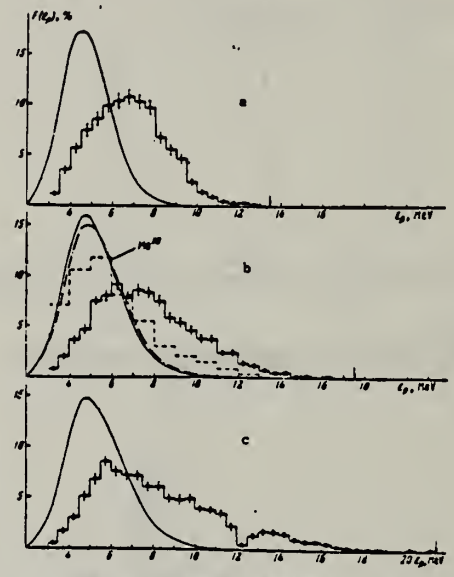

FIG. 2. Energy distributions of photoprotons from Nb^{93} for $E_{\gamma max}$ = 19.5 MeV (a), 23.5 MeV (b), and 27.5 MeV (c). The histograms are the experimental spectra. The dashed histogram in Fig. 2b is the photoproton spectrum of Mo^{98}.[9] The smooth curves are spectra computed from the evaporation model for level density ω, taking account of pair correlations. The dashed curve in Fig. 2b is the same, neglecting pair correlations. Arrows indicate the maximum possible proton energy $\epsilon_{p\,max} = E_{\gamma max} - B_p$.

FIG. 3. Angular distributions of photoprotons from Nb^{93} for $E_{\gamma max}$ = 19.5 MeV (a), 23.5 MeV (b), and 27.5 MeV (c). The histograms are the experimental results. The smooth curves represent distributions of the forms $I(\theta) = a + b \sin^2\theta$ and $I(\theta) = a + b \sin^2\theta + c \sin^2\theta \cos\theta$. The parameters a, b, and c obtained by least squares are given in Table II.

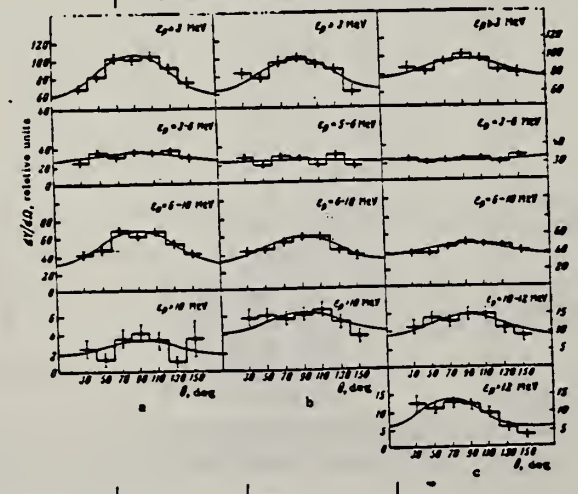

Table II. Angular distribution parameters obtained by least squares

$E_{\gamma max}$, MeV / $\Delta\epsilon_p$	19.5 a	19.5 b	19.5 b/a	23.5 a	23.5 b	23.5 b/a	27.5 a	27.5 b	27.5 c	27.5 b/a	27.5 c/a
All protons >3 MeV	60.0± ±5.1	45.1± ±7.3	0.75± ±0.18	63.7± ±4.7	34.4± ±6.5	0.54± ±0.15	73.1± ±5.3	21.3± ±6.8	—	0.25± ±0.11	—
3—6 MeV	26.5± ±3.2	8.5± ±4.4	0.32± ±0.20	22.1± ±2.8	3.0± ±2.7	0.14± ±0.13	25.4± ±2.8	−3.1± ±3.8	—	−0.12± ±0.14	—
6—10 MeV	29.9± ±3.9	37.3± ±5.6	1.25± ±0.34	31.1± ±3.3	26.2± ±4.9	0.84± ±0.25	35.5± ±3.2	12.8± ±4.5	—	0.36± ±0.17	—
>10 MeV	3.6± ±1.3	−0.7± ±1.7	−0.19± ±0.53	10.5± ±1.8	5.2± ±2.5	0.49± ±0.33	14.3± ±2.2	11.6± ±3.2	10.6± ±3.1	0.81± ±0.34	0.74± ±0.22
10—12 MeV	—	—	—	—	—	—	8.4± ±1.6	6.1± ±2.2	2.2± ±2.1	0.72± ±0.39	0.26± ±0.29
>12 MeV	—	—	—	—	—	—	5.9± ±1.5	5.6± ±2.1	7.8± ±1.9	0.94± ±0.58	1.31± ±0.39

REF.

J. A. Scheer, K. Schlupmann und F. Triantafyllidis
Nucl. Phys. 56, 113-116 (1964)

ELEM. SYM.	A	Z
Nb	93	41

METHOD: Betatron

REF. NO.: 64 Sc 1 JOC

REACTION	RESULT	EXCITATION ENERGY	SOURCE		DETECTOR		ANGLE
			TYPE	RANGE	TYPE	RANGE	
G,A	SPC	THR - 33	C	33	SCD	6-14	90

ABS YIELD

Tabelle 1
Meßdaten und Ergebnisse

	Ti	Ni	Cu	Nb
Targetdicke (mg/cm²)	2.08	1.52	9.90	8.87
Bestrahlungsdauer (h)	52.5	55.5	18.0	84.5
Registrierte Teilchenanzahl ($4 \leqq E_\alpha \leqq 12.6$ MeV)	1861	2376	2333	1987
Lage des Maximums E_{max} der Energieverteilung (MeV)	6.4	8.2	8.5	11
Halbwertsbreite des Maximums (MeV)	2.8	2.8	4.0	3.5
Mittlerer Energieverlust im Target bei $E_\alpha = E_{max}$ (MeV)	0.4	0.25	1.7	1.1
Ausbeute in μb/MeV [a]	22±3.5	45±7	23±3.5	5.5±0.8

[a]) Vgl. Bemerkung [a]) in Tabelle 2.

Tabelle 2
Vergleich der Ergebnisse verschiedener Autoren

	E_α(MeV)	Ti	Ni	Cu	Nb
Ausbeute ($10^3 \times N_\alpha$/Mol. r)					
Boulègue	31		58.7	50.8	
Diese Arbeit [a])	32.5	48±7	98±15	50±7.5	12±1.8
Toms und McElhinney	21.5		39.4	26	4.6 [b])
Relative Ausbeute					
Boulègue	31		1	0.87	
Kregar und Povh	30		1	0.54	
Diese Arbeit	32.5	0.49±0.08	1	0.51±0.08	0.12±0.02
Toms und McElhinney	21.5		1	0.66	0.12 [b])

[a]) Die Fehlerangaben beinhalten auch die Unsicherheit in der Absoluteichung der Intensität des γ-Strahles.

[b]) Dieser Wert wurde aus nur 14 beobachteten Ereignissen bestimmt.

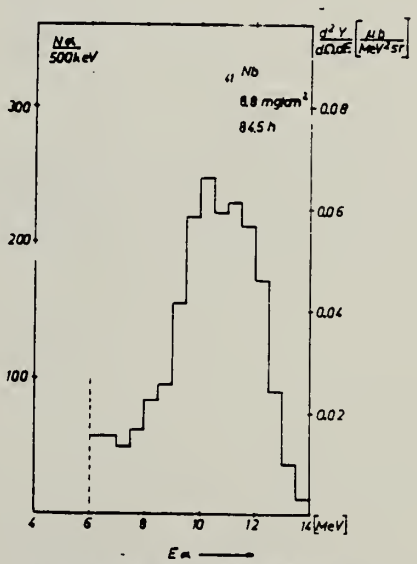

Abb. 1. Die erhaltenen Energie-Spektren der Photoalphateilchen aus Ti, Ni, Cu und Nb.

REF.

K. Schlupmann, R. Wendling
Naturwissenschaften 16, 380 (1964)

ELEM. SYM.	A	Z
Nb	93	41

METHOD

Betatron

REF. NO.

64 Sc 3 NVB

REACTION	RESULT	EXCITATION ENERGY	SOURCE		DETECTOR		ANGLE
			TYPE	RANGE	TYPE	RANGE	
G,XP	SPC		C	32	SCI-D	2-15	90

ABY

$$\left(\frac{dY}{d\Omega}\right)_{90^\circ} = 18 \frac{\mu b}{\text{MeV-ster}} \pm 25\%$$

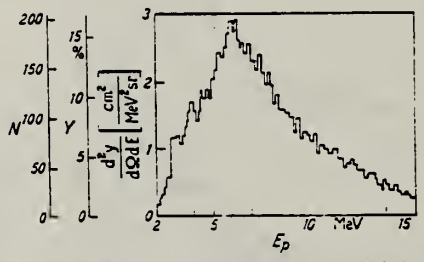

Fig. 1. Energieverteilung der bei dem Prozeß $^{93}Nb(\gamma, p)^{92}Zr$ entstehenden Protonen.

REF.

W. B. Walters and J. P. Hummel
Phys. Rev. 150, 867 (1966)

ELEM. SYM.	A	Z
Nb	93	41

METHOD

Betatron

REF. NO.	
66 Wa 1	JDM

REACTION	RESULT	EXCITATION ENERGY	SOURCE		DETECTOR		ANGLE
			TYPE	RANGE	TYPE	RANGE	
G,2P4N	RLY	THR-280	C	150,280	ACT-I		4PI

Measured isomeric yield ratios.

TABLE IV. Summary of the results for the photoproduction of the Y^{87} isomers (spins $\frac{1}{2}$ and $\frac{9}{2}$).

Target isotope and spin	Bremsstrahlung energy (MeV)	Fraction of yield to high-spin isomer
Y^{89} ($I=\frac{1}{2}$)	150	0.42±0.05
	280	0.42±0.05
Nb^{93} ($I=\frac{9}{2}$)	150	0.71±0.13
	280	0.69±0.13

REF.

R. R. Hurst and D. J. Donahue
Nucl. Phys. A91, 365 (1967)

ELEM. SYM.	A	Z
Nb	93	41

METHOD

Neutron capture gamma rays

REF. NO.

67 Hu 1 EGF

REACTION	RESULT	EXCITATION ENERGY	SOURCE		DETECTOR		ANGLE
			TYPE	RANGE	TYPE	RANGE	
G,N	ABX	9-11	D	9-11	BF3-I		4PI

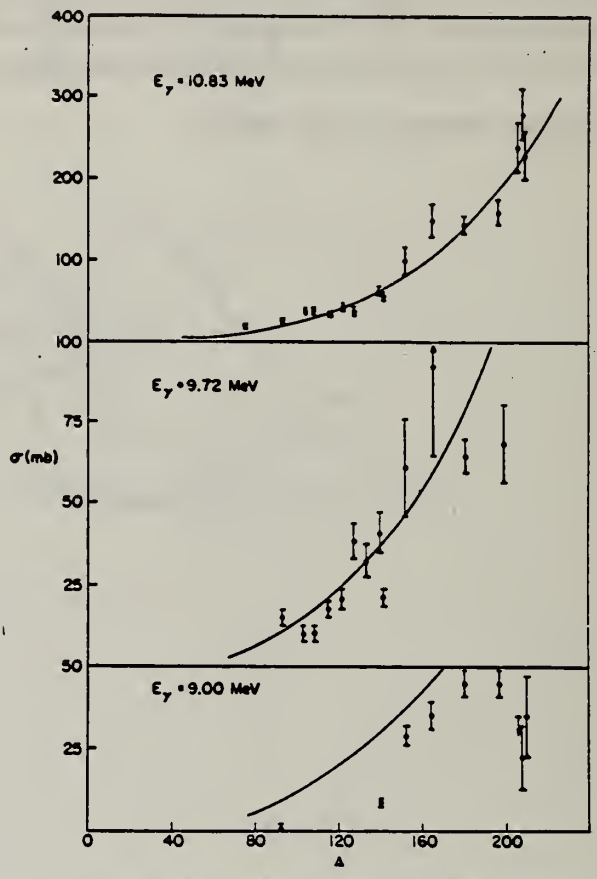

Fig. 1. Cross section (in mb) versus mass number of the target for gamma-ray energies of 9.00 9.72 and 10.83 MeV. The solid lines are plots of eq. (1) in the text.

TABLE I

Photoneutron cross sections (mb)

Target	7.72 MeV	9.00 MeV	9.72 MeV	10.83 MeV
^{59}Co				9.0± 0.8
^{75}As				20.4± 1.7
^{93}Nb		0.53± 0.10	14.6± 2.2	25.8± 2.1
^{103}Rh			10.6± 1.7	38.8± 3.1
^{107}Ag, ^{109}Ag			10.0± 1.5	37.6± 2.9
^{115}In			17.1± 2.6	33.3± 2.7
^{121}Sb, ^{123}Sb			20.7± 3.1	42.5± 3.6
^{127}I			38.7± 5.8	38.8± 3.1
^{133}Cs			31.7± 4.8	52.5± 3.8
^{139}La		8.61± 0.86	40.8± 6.5	63.0± 5.0
^{141}Pr			21.5± 3.2	58.3± 4.1
^{151}Eu, ^{153}Eu		28.9 ± 3.2	61.3±14.7	102 ±18
^{165}Ho		35.6 ± 4.3	92.2±27.6	150 ±20
^{181}Ta	4.14±0.36	45.4 ± 3.7	65.0 ± 5.5	146 ±12
^{197}Au		44.5 ± 3.6	68.4±13.5	160 ±15
^{206}Pb		<34.3		238 ±29
^{208}Pb		22.6 ±11.3		280 ±31
^{209}Bi		36.1 ±12.0		226 ±27

REF. S. M. Hussain and K. G. McNeill
Can. J. Phys. 45, 2851 (1967)

ELEM. SYM.	A	Z
Nb	93	41

METHOD

REF. NO. 67 Hu 2 EGF

REACTION	RESULT	EXCITATION ENERGY	SOURCE		DETECTOR		ANGLE
			TYPE	RANGE	TYPE	RANGE	
G,N	ABY	THR-22	C	22	THR	4-	DST

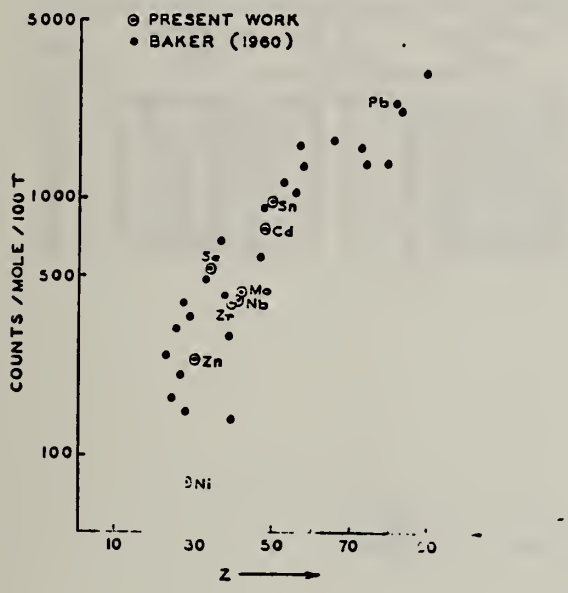

FIG. 3. The yields of fast photoneutrons from various elements as measured in the present work and by Baker. The present results have been normalized to Baker's measurements for lead.

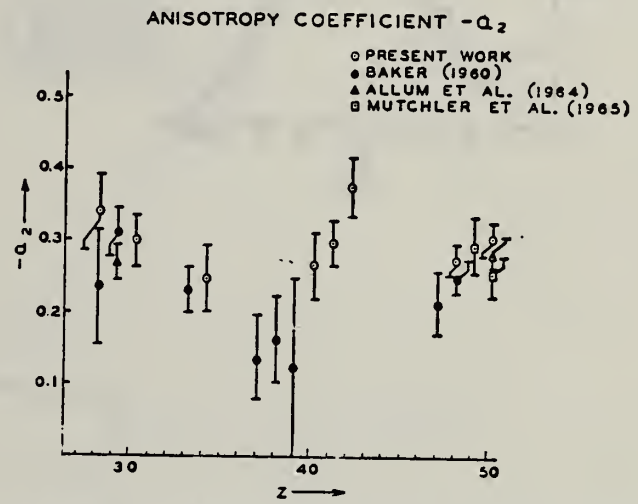

FIG. 2. The anisotropy coefficients a_2, in the formula $W(\theta) = a_0(1 + a_1P_1 + a_2P_2)$, obtained in the present work, and those obtained by other workers in the same part of the Periodic Table.

TABLE I

Element	a_0*	a_1	a_2
Nickel	77 (1.0±0.05)	0.14±0.04	−0.34±0.0[illegible]
Zinc	236 (1.0±0.04)	0.06±0.03	−0.30±0.04
Selenium	525 (1.0±0.05)	0.10±0.04	−0.25±0.05
Zirconium	380 (1.0±0.05)	0.03±0.04	−0.27±0.05
Niobium	392 (1.0±0.03)	0.01±0.02	−0.30±0.03
Molybdenum	410 (1.0±0.03)	0.05±0.03	−0.41±0.04
Cadmium	755 (1.0±0.02)	0.05±0.01	−0.28±0.02
Tin	935 (1.0±0.02)	0.08±0.02	−0.30±0.02
Lead	2274 (1.0±0.02)	0.06±0.02	−0.48±0.02

*For comparison purposes the experimental value of a_0 for Pb has been normalized to coincide with that obtained by Baker and McNeill (1961) and is the yield per mole per 100 roentgen. All other values of a_0 have also been quoted with the same normalization.

REF.

G. Kraft and R. Kosiek
Natur., Heft 13, 337 (1967)

ELEM. SYM.	A	Z
Nb	93	41

METHOD

REF. NO.	
67 Kr 1	EGF

REACTION	RESULT	EXCITATION ENERGY	SOURCE		DETECTOR		ANGLE
			TYPE	RANGE	TYPE	RANGE	
G,A	SPC	2-31	C	31	SCD-D	6-15	90
				(30.5)			

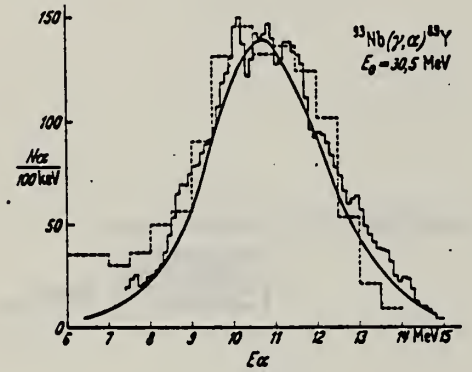

Fig. 1

REF. N. G. Shevchenko, N. G. Afanas'ev, G. A. Savitskii, V. M. Khvastunov, V. D. Kovalev, A. S. Omelaenko, and I. S. Gul'karov
J. Nucl. Phys. (USSR) 5, 948 (1967)
Sov. J. Nucl. Phys. 5, 676 (1967)

ELEM. SYM.	A	Z
Nb	93	41

METHOD

REF. NO. 67 Sh 1 HMG

REACTION	RESULT	EXCITATION ENERGY	SOURCE TYPE	SOURCE RANGE	DETECTOR TYPE	DETECTOR RANGE	ANGLE
E,E/	FMF	2-3	D	225	MAG-D		DST
		(2.5)					

G-WIDTH, J-PI

Table IV
Absolute differential cross section for inelastic scattering of electrons with energy 225 ± 1 MeV by Nb^{93} with excitation of levels at 2.2 ± 0.2 MeV

θ, deg	Cross section, cm²/sr	θ, deg	Cross section, cm²/sr	θ, deg	Cross section, cm²/sr
30	$(0.245\pm0.040)\cdot10^{-28}$	57	$(5.89\pm0.53)\cdot10^{-31}$	82	$(4.07\pm0.76)\cdot10^{-32}$
40	$(1.54\pm1.14)\cdot10^{-29}$	60	$(4.09\pm0.62)\cdot10^{-31}$	84	$(3.23\pm0.72)\cdot10^{-32}$
43	$(1.00\pm0.08)\cdot10^{-29}$	65	$(3.11\pm0.37)\cdot10^{-31}$	85	$(2.25\pm0.59)\cdot10^{-32}$
45	$(6.54\pm0.65)\cdot10^{-30}$	67	$(2.42\pm0.276)\cdot10^{-31}$	87	$(2.97\pm0.48)\cdot10^{-32}$
47	$(6.10\pm0.43)\cdot10^{-30}$	67	$(2.42\pm0.276)\cdot10^{-31}$	90	$(2.62\pm0.52)\cdot10^{-32}$
50	$(2.94\pm0.26)\cdot10^{-30}$	70	$(2.25\pm0.29)\cdot10^{-31}$	95	$(2.06\pm0.37)\cdot10^{-32}$
52	$(2.86\pm0.29)\cdot10^{-30}$	75	$(1.08\pm0.16)\cdot10^{-31}$	95	$(1.45\pm0.31)\cdot10^{-32}$
55	$(1.37\pm0.12)\cdot10^{-30}$	80	$(4.95\pm0.97)\cdot10^{-32}$		

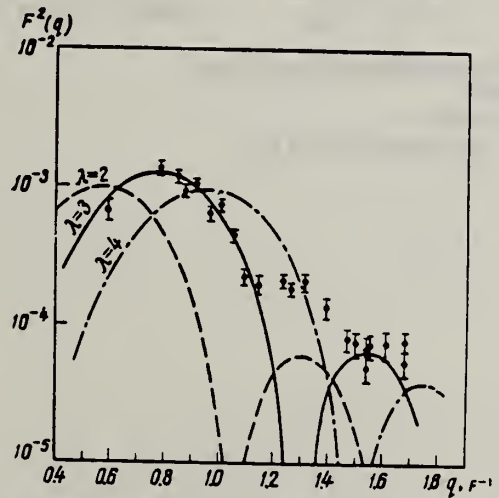

Fig. 6. Squared form factor as a function of momentum transfer for the 2.2 ± 0.2 MeV inelastic peak from Nb^{93}. The curves are calculated in the Born approximation for different values of multipolarity λ.

REF. G. Kraft, R. Kosiek, R. Mundhenke and J. Winter
Nucl. Phys. A118, 25 (1968)

ELEM. SYM.	A	Z
Nb	93	41

METHOD

REF. NO. 68 Kr 2 egf

REACTION	RESULT	EXCITATION ENERGY	SOURCE		DETECTOR		ANGLE
			TYPE	RANGE	TYPE	RANGE	
G,A	ABX	THR-33	C	33	SCD-D	7-14	90
				(32.5)			

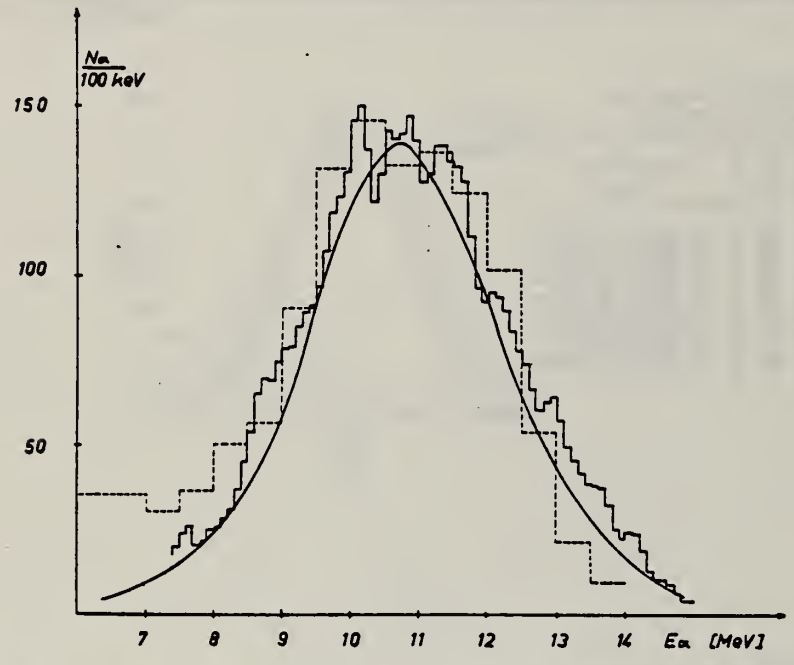

Fig. 4. Histogram: energy distribution of α-particles from Nb. Dashed histogram: results of Scheer *et al.* [2]). Curve: statistical-model calculation.

[2] J. A. Scheer, K. Schlüpmann and F. Triantafyllidis, Nucl. Phys. 56, 113 (1964).

REF. N.V. Goncharov, A.I. Derebchinskii, O.P. Konovalov, S.G. Tonapetyan, and V.M. Khvorostyan
Yad. Fiz. 14, 31 (1971)
Sov. J. Nucl. Phys. 14, 18 (1972)

ELEM. SYM.	A	Z
Nb	93	41

METHOD

REF. NO. 71 Go 2 hmg

REACTION	RESULT	EXCITATION ENERGY	SOURCE		DETECTOR		ANGLE
			TYPE	RANGE	TYPE	RANGE	
G,PI+	RLY	150-500	C	500	CCH-D		DST

PI-/PI+ YIELD RATIO

Measurements are reported of the relative yield of π^+ mesons and the π^-/π^+ yield ratio for mesons with energy 40 ± 10 MeV emitted in the angular range θ_{lab} = 50–160° in photon-induced reactions with E_γ^{max} = 500 MeV with light and medium nuclei. The charged π-meson detector was a 34-cm Freon bubble chamber with a tube for the beam. The π^-/π^+ yield ratio for He^4, Li^7, C^{12}, Si^{28}, S^{32}, Ca^{40}, and Nb^{93} was found to be respectively 0.94 ± 0.14, 2.15 ± 0.31, 1.22 ± 0.21, 1.25 ± 0.15, 1.0 ± 0.13, 1.11 ± 0.13, and 1.53 ± 0.25. It was established that the π^+-meson yield follows a $ZA^{-1/3}$ law.

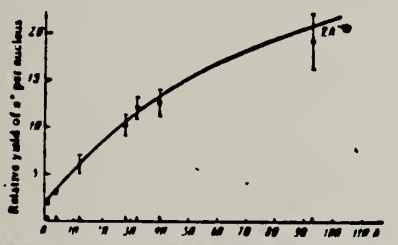

FIG. 2. Relative yield of π^+ mesons per nucleus as a function of mass number A.

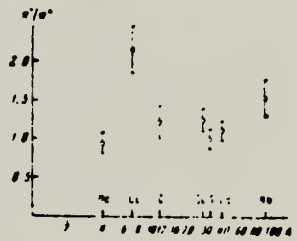

FIG. 3. π^-/π^+ yield ratio as a function of mass number A.

A. Lepretre, H. Beil, R. Bergere, P. Carlos, and A. Veyssiere
Nucl. Phys. A175, 609 (1971)

Nb	93	41

METHOD

REF. NO. 71 Le 1 egf

REACTION	RESULT	EXCITATION ENERGY	SOURCE		DETECTOR		ANGLE
			TYPE	RANGE	TYPE	RANGE	
G,N 369	ABX	9-24	D	9-24	MOD-I		4PI
G,2N 370+	ABX	16-24	D	9-24	MOD-I		4PI

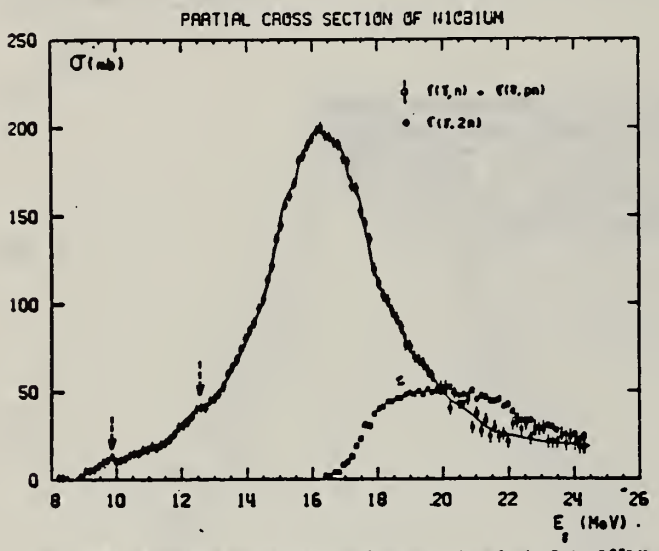

Fig. 5. Partial photoneutron cross sections $\sigma(\gamma, n)$ and $\sigma(\gamma, 2n)$ of ^{93}Nb.

TABLE 1

Lorentz line parameters corresponding to fits shown in fig. 6.

	Rb	Sr	^{89}Y	^{90}Zr	^{93}Nb
σ_1 (mb)	192 ±10	207 ±10	225 ±10	211 ±10	202 ±10
Γ_1 (MeV)	4.1 ± 0.15	4.2± 0.1	4.1± 0.1	4.0 ± 0.1	4.7± 0.2
E_1 (MeV)	16.75± 0.05	16.7± 0.05	16.7± 0.05	16.65± 0.05	16.5± 0.05

TABLE 3

Integrated cross sections (the notation used is defined in the text)

	Rb	Sr	^{89}Y	^{90}Zr	^{93}Nb
σ_0 (MeV · b)	1.14 ±0.06	1.42±0.07	1.36 0.07	1.26±0.07	1.33 ±0.07
$\frac{\sigma_0}{0.06\,NZ\,A^{-\frac{1}{3}}}$	0.915±0.05	1.09±0.05	1.04 ±0.05	0.95±0.05	0.97±0.05
σ_{-1} (mb)	67±4	80 ±5	77 ±5	71 ±5	79 ±5
σ_{-2} (mb · MeV^{-1})	4±0.2	4.6 ±0.2	4.4 ±0.2	4 ±0.2	4.8 ±0.2
E_M (MeV)	24	27	27	26	24

(over)

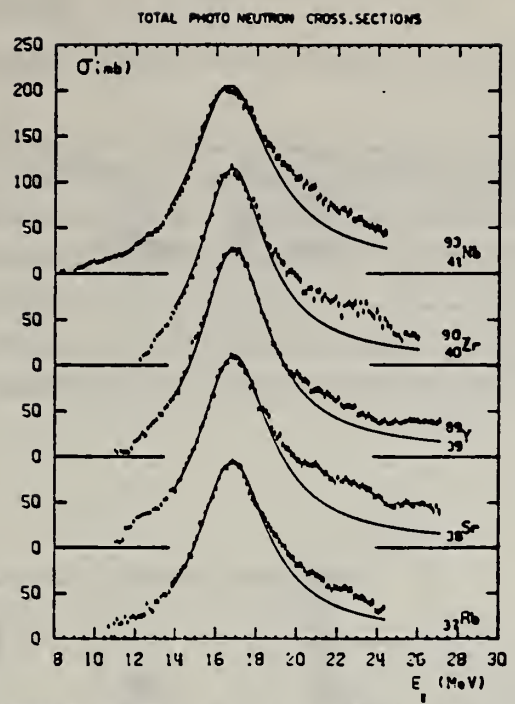

Fig. 6. Total photoneutron cross sections σ_T of Rb, Sr, ^{89}Y, ^{90}Zr and ^{93}Nb and best one Lorentz line fit corresponding to parameters given in table I.

REF.

Tatsuya Saito
Nippon Kagaku Zasshi 92, 164 (1971)

ELEM. SYM.	A	Z
Nb	93	41

METHOD

REF. NO. 71 Sa 1 egf

REACTION	RESULT	EXCITATION ENERGY	SOURCE		DETECTOR		ANGLE
			TYPE	RANGE	TYPE	RANGE	
G,N	ABY	8-68	C	10-68	ACT-I		4PI

Nippon Kagaku Zasshi, 92, 164~168(1971)

The Yields of Radioactivities Induced by (γ, n) Reactions with Bremsstrahlung up to 68 MeV

by Tatsuya SAITO

The (γ, n) yields of 12 target nuclides have been measured at 10, 13, 16, 30, 45 and 68 MeV bremsstrahlung by observing the induced activities.

The energy dependence of the yields has been investigated extensively in the same way as in the previous work at 20 MeV bremsstrahlung.

In the case of heavy nuclides, the yields rise greatly as a function of maximum bombarding energy up to 20 MeV, and rise gradually from 20 MeV up to 68 MeV. However, in the case of light nuclides, the yields rise greatly up to 30 MeV, because the neutron separation energies of light ones are larger than those of heavy ones, and the bremsstrahlung spectrum covers the giant resonance and so the yields rise gradually from 30 MeV up to 68 MeV.

The yields have approximately been estimated from the parameter of the giant resonance, that is the peak cross section and the half width, in order to compare with the experimental data. As a result, the experimental data of light nuclides and heavy ones are nearly in agreement with the estimated data of Nathans et al., Johns et al. and Montalbetti et al., but those of medium weight ones are relatively lower values.

Department of Chemistry, Faculty of Science, Tohoku University; Katahira-cho, Sendai-shi, Japan

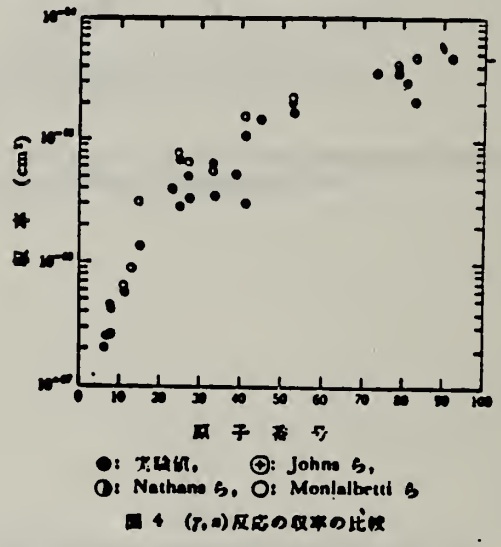

図 4 (γ, n)反応の収率の比較

REF.

R.F. Barrett, J.R. Birkelund, B.J. Thomas, K.S. Lam, and H.H. Thies
Nucl. Phys. A210, 355 (1973)

ELEM. SYM.	A	Z
Nb	93	41

METHOD

REF. NO. 73 Ba 20 egf

REACTION	RESULT	EXCITATION ENERGY	SOURCE TYPE	SOURCE RANGE	DETECTOR TYPE	DETECTOR RANGE	ANGLE
G,N	NOX	THR- 27	C	10- 27	BF3-I		4PI

MEAN NEUT ENERGY

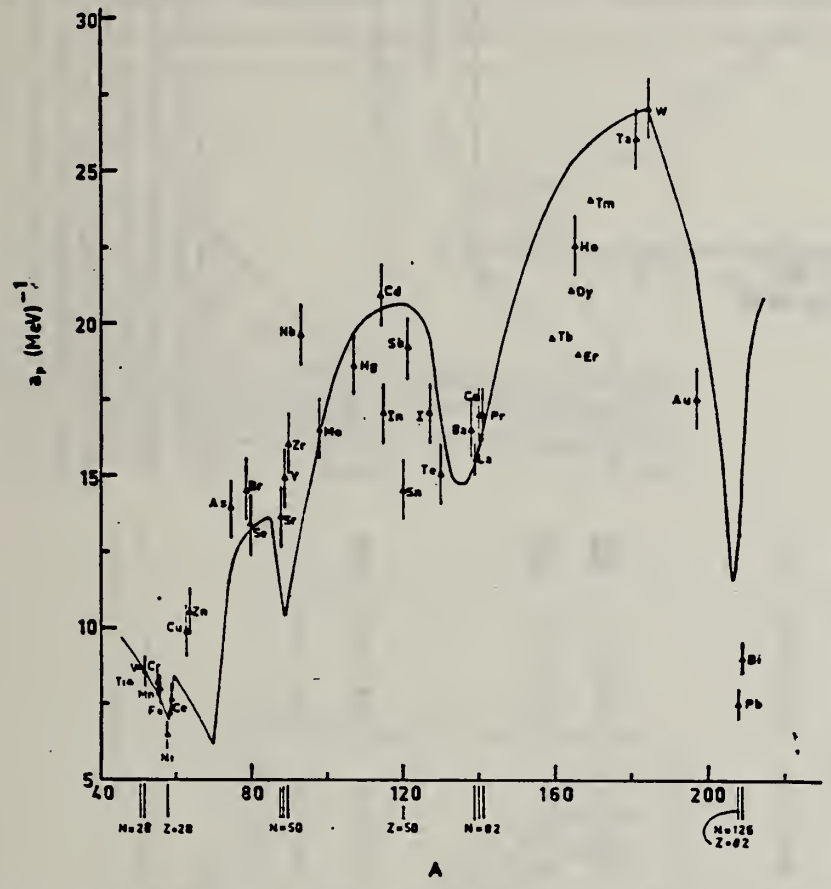

Fig. 12. Experimental values of the level density parameter a_p (Fermi gas formula plus pairing correction) versus atomic number A. The continuous curve is a least-squares fit to the data of a theoretical calculation from Newton [15].

1
H. Baba and S. Baba, Japan Atomic Energy Research Institute report JAERI-1183 (1969).
2
H. Baba, Nucl. Phys. A159, 625 (1970).
15
T.D. Newton, Can. J. Phys. 34, 804 (1956).

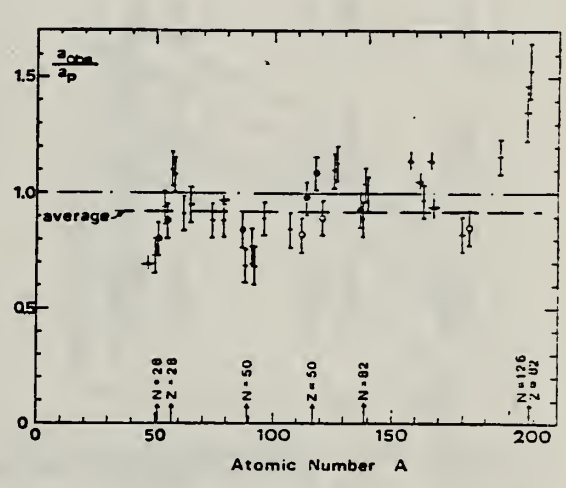

Fig. 15. Ratio a_{obs}/a_p versus atomic number A. Here a_{obs} is the level density parameter taken from the neutron resonance work of refs. [1,2]), and a_p is the level density parameter derived from the present (γ, n) work. Filled circles represent points where nuclei in the neutron resonance and in the (γ, n) experiment were the same. Open circles represent points where the respective nuclei were approximately matched. Triangles represent points which are based on measurement of neutron mean energies at two bremsstrahlung energies only.

(over)

TABLE 3 (continued)

Target	N (residual nucleus) [a]		Goodness of fit [b] no p.c.	Goodness of fit [b] with p.c.	$\hat{E}_a(24)$ (MeV) [c]	T (MeV) [d]	a_p (MeV^{-1}) [e]	a_{obs} (MeV^{-1}) [f]	a_{obs}/a_p
Y	49	100%	G	G	1.30		14.9–^{88}Y	10.17–^{90}Y	0.68
Zr	49	52%	F	F	1.28		16.0–^{90}Zr	12.2 –^{91}Zr	0.77
	50	11%							
	51	17%							
	53	17%							
	55	3%							
Nb	51	100%	F	F	1.28		19.6–^{92}Nb	13.15–^{94}Nb	0.68
Mo	49	16%	G	G	1.27		16.5–^{95}Mo	14.7 –^{97}Mo	0.89
	51	9%							
	52	16%							
	53	17%							
	54	10%							
	55	24%							
	57	8%							
Ag	59	51%	V.P.	F	1.27	0.55	18.6–^{107}Ag	15.61–^{108}Ag	0.84
	61	49%							
Cd	57	1%	V.P.	F	1.24	0.54	20.9–$^{111.4}$Cd	17.0 –^{112}Cd	0.82
	61	12%							
	62	13%							
	63	24%							
	64	12%							
	65	29%							
	67	8%							
In	63	4%	V.P.	F	1.26	0.57	17.0–^{114}In	16.66–^{114}In	0.98
	65	96%							
Sn	65	14%	V.P.	V.P.	1.38	0.73	14.5–^{116}Sn	15.9 –^{118}Sn	1.09
($Z = 50$)	66	8%							
	67	24%							
	68	9%							
	69	33%							
	71	5%							
	73	6%							
Sb	69	57%	V.P.	P	1.2	0.68	19.2–^{121}Sb	17.0 –^{121}Sb	0.89
	71	43%							
Te	69	2%	V.P.	F	1.36	0.83	15.0–^{127}Te	17.0 –^{127}Te	1.13
	71	5%							
	72	7%							
	73	19%							
	75	32%							
	77	34%							
I	73	100%	F	G	1.23	0.70	17.0–^{126}I	17.02–^{128}I	1.00

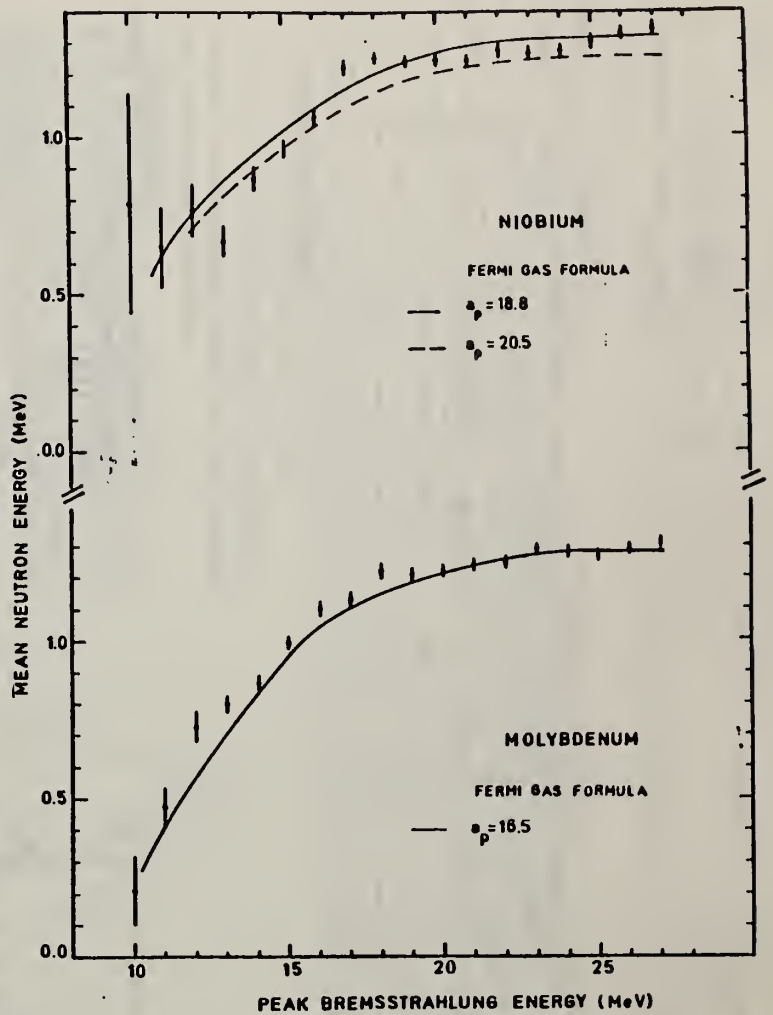

Fig. 8. Same as fig. 5, for niobium and molybdenum.

[a]) Neutron numbers and abundances of respective residual nuclei in (γ, n) experiments.

[b]) These give an assessment of the goodness of fit of a calculated $\hat{E}_a$ versus E_0 curve to the observed data, using the Fermi gas level density formula both without and with pairing corrections.

[c]) Bremsstrahlung photoneutron mean energies $\hat{E}_a$ for peak bremsstrahlung energy E_0 = 24 MeV.

[d]) Nuclear temperature from fit with constant-temperature formula.

[e]) Level density parameter a_p derived from the present (γ, n) experiment, using a Fermi gas formula plus pairing correction, and corresponding residual nucleus (the atomic weight shown is the weighted average of atomic weights of the respective isotopes present).

[f]) As column 7, but using data on n-resonance absorption from refs. [1,2]).

[g]) Measurements of $\hat{E}_a(E_0)$ for these nuclei were made only for E_0 = 21, 23 and 24 MeV.

REF. N.V. Goncharov, A.I. Derebchinskii, O.G. Konovalov, S.G. Tonapetyan, and V.M. Khvorostyan
Yad. Fiz. 17, 242 (1973)
Sov. J. Nucl. Phys. 17, 124 (1973)

ELEM. SYM.	A	Z
Nb	93	41

METHOD

REF. NO. 73 Go 5 hmg

REACTION	RESULT	EXCITATION ENERGY	SOURCE		DETECTOR		ANGLE
			TYPE	RANGE	TYPE	RANGE	
G,PI+	ABY	170-400	C	400	BBL-D		90
G,PI-	ABY	170-400	C	400	BBL-D		90
G,P	ABY	76-400	C	400	BBL-D		90

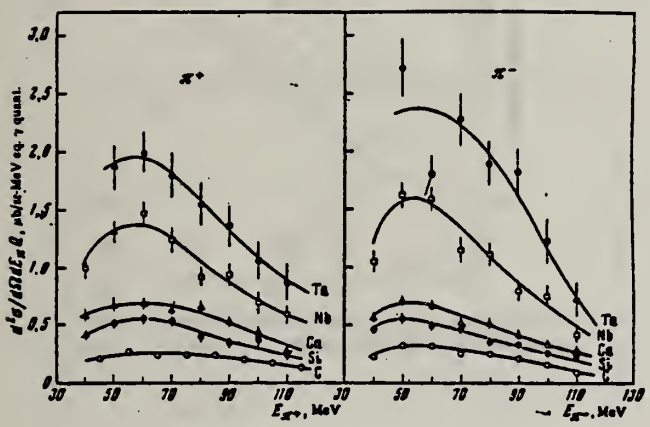

FIG. 2. Energy spectra of π^+ and π^- mesons, $E_\gamma^{max} = 400$ MeV, $\theta_{lab} = (90 \pm 7)°$.

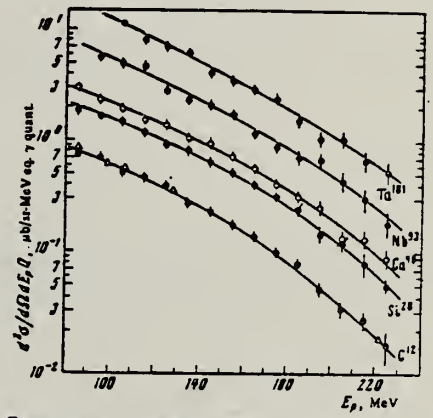

FIG. 3. Energy spectra of protons, $E_\gamma^{max} = 400$ MeV, $\theta_{lab} = (90 \pm 7)°$. Circles—present data, triangles—from [18].

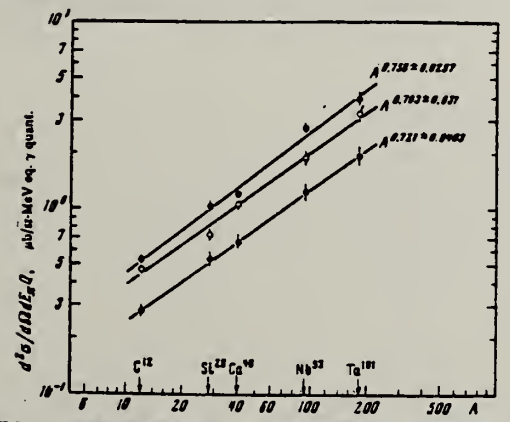

FIG. 4. Charged pion yield vs. the mass number of the nucleus: ●—$E_\pi = 105 \pm 10$ MeV, ○—$E_\pi = 85 \pm 10$ MeV, ◐—$E_\pi = 65 \pm 10$ MeV.

18 P. Dougan, W. Stiefler, LUSY Preprint, 1001-1003, 1970.

(over).

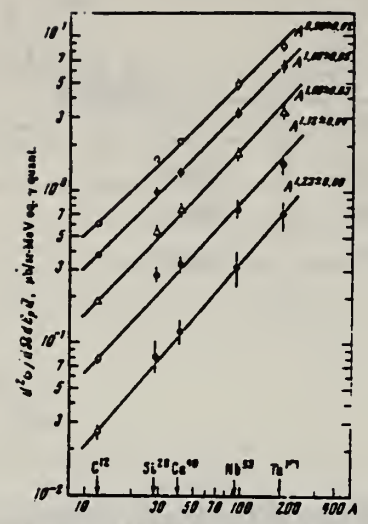

FIG. 5. Proton yields vs. mass number of the nucleus: ○–E_p = 100 ± 10 MeV, ●–E_p = 125 ± 15 MeV, Δ–E_p = 155 ± 15 MeV, ◐–E_p = 185 ± 15 MeV, ⊖–E_p = 215 ± 15 MeV.

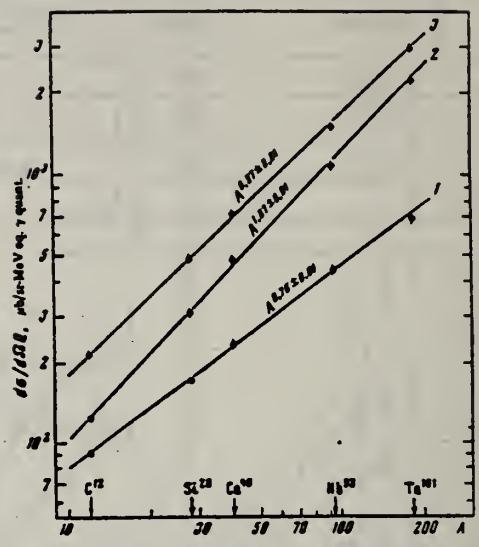

FIG. 6. Pion yield (1), proton yield (2), and summary pion and proton yield (3) vs. the mass number of the nucleus.

REF. S. Sugiyama and T. Tomimasu
PICNS-73, Vol.I, p.563 Asilomar

ELEM. SYM.	A	Z
Nb	93	41

METHOD

REF. NO. 73 Su 12 hmg

REACTION	RESULT	EXCITATION ENERGY	SOURCE		DETECTOR		ANGLE
			TYPE	RANGE	TYPE	RANGE	
G,MU-T	ABX	10- 26	C	18, 26	MGP-D		4PI

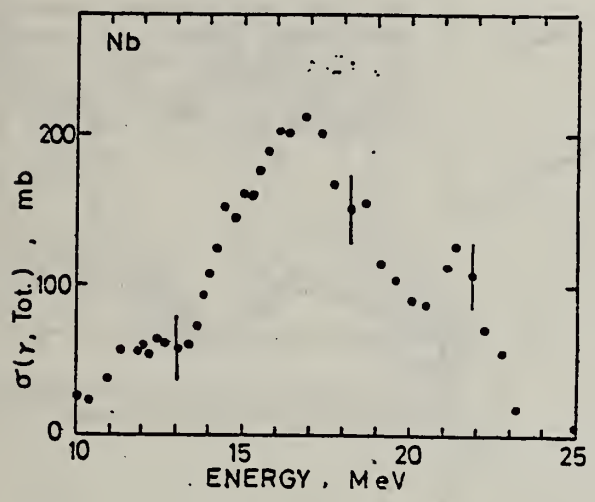

Fig. 2
Total photonuclear cross section for Nb

REF.	ELEM. SYM.	A	Z
P. David, J. Debrus, F. Lubke, H. Mommsen, R. Schoenmackers, and G. Stein Nucl. Phys. A221, 145 (1974)	Nb	93	41

METHOD	REF. NO.
	74 Da 2 egf

REACTION	RESULT	EXCITATION ENERGY	SOURCE		DETECTOR		ANGLE
			TYPE	RANGE	TYPE	RANGE	
G,A	ABY	10-450	C	450	TEL-D		90

Data measured for p,t, and He3, but not given in paper.

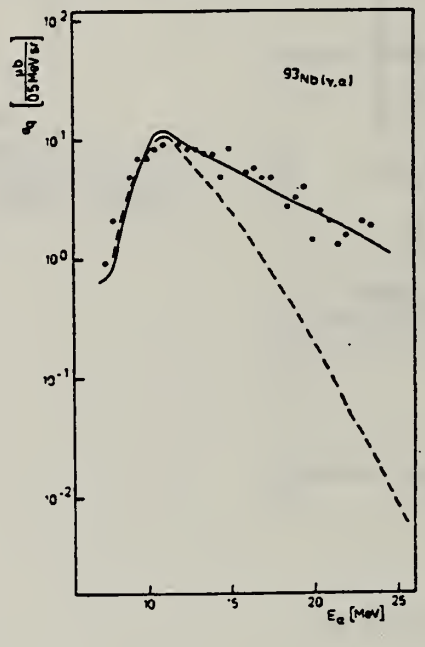

Fig. 7. Experimental data with statistical model calculations for the reaction ^{93}Nb(γ,α). Broken line for E_γ^{max} = 50 MeV (calculation). Full line for E_γ^{max} = 450 MeV (fit).

TABLE 4

The integrated absorption cross sections and the percentage values of compound nucleus formation

ΔE_γ (MeV)	50–150	150–250	250–350	350–450	$\int\sigma_{\gamma\,tot}dE_\gamma$, $\int\sigma_{c\gamma}dE_\gamma$ [a]) (b · MeV)	$\sigma_{c\gamma}/\sigma_{\gamma\,tot}$ (%)
^{27}Al $\sigma_{\gamma\,tot}$	6	10	15	12	4.3	
$\sigma'_{\gamma\,tot} = \sigma_{c\gamma}$	6.2		7.6		2.9	69
^{40}Ca $\sigma_{\gamma\,tot}$	8	15	22	17	6.2	
$\sigma_{c\gamma}$	7.2		10.1		3.75	60
^{51}V $\sigma_{\gamma\,tot}$	11	19	27	22	7.9	
$\sigma_{c\gamma}$	13		0.01		1.3	16.5
^{93}Nb $\sigma_{\gamma\,tot}$	19	35	50	39	15.3	
$\sigma_{c\gamma}$	5.8		5.9		2.3	15
^{nat}Ag $\sigma_{\gamma\,tot}$	22	40	58	47	16.7	
$\sigma_{c\gamma}$	15		7.6		3.81	23

The $\sigma_{\gamma\,tot}$ values (in mb) used in the evaporation calculation in the γ-energy range E_γ = 50–450 MeV and corresponding best fit values $\sigma'_{\gamma\,tot}$ are given. The formation cross section of the compound nucleus $\sigma_{c\gamma}$ is assumed to be equal to $\sigma_{\gamma\,tot}$ or $\sigma'_{\gamma\,tot}$.

[a]) E_γ = 50–450 MeV.

U.S. DEPARTMENT OF COMMERCE
NATIONAL BUREAU OF STANDARDS

REF. S. G. Tonapetyan, N. V. Goncharov, and V. M. Khvorostyan
Yad. Fiz. 22, 440 (1975)
Sov. J. Nucl. Phys. 22, 226 (1976)

ELEM. SYM.	A	Z
Nb	93	41

METHOD

REF. NO. 75 To 4 hmg

REACTION	RESULT	EXCITATION ENERGY	SOURCE		DETECTOR		ANGLE
			TYPE	RANGE	TYPE	RANGE	
G,PI+	ABY	150-400	C	300,400	BBL-D		90
G,PI-	ABY	150-400	C	300,400	BBL-D		90
G,P	ABY	86-400	C	300,400	BBL-D		90

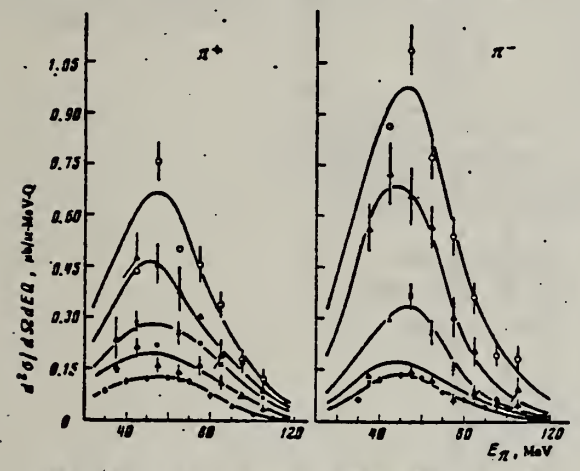

FIG. 1. Energy spectra of π^+ and π^- mesons. E_γ^{max} = 300 MeV, θ_{lab} = 90 ± 7°. Points: ●—^{12}C, ▲—^{28}Si, X—^{40}Ca, △—^{93}Nb, ○—^{181}Ta.

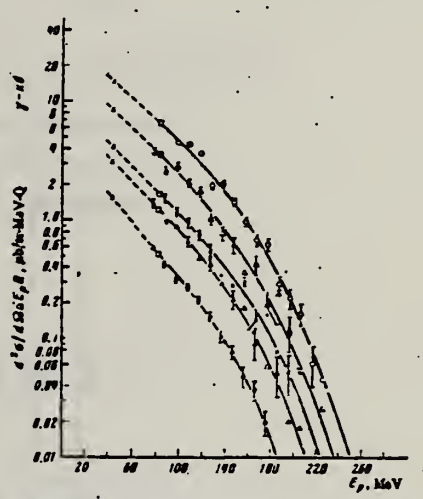

FIG. 3. Energy spectra of protons, E_γ^{max} = 300 MeV. θ_{lab} = 90 ± 7°. Points: ●—^{12}C, ▲—^{28}Si, X—^{40}Ca, △—^{93}Nb, ○—^{181}Ta, □—data from ref. 5, *—data from ref. 6.

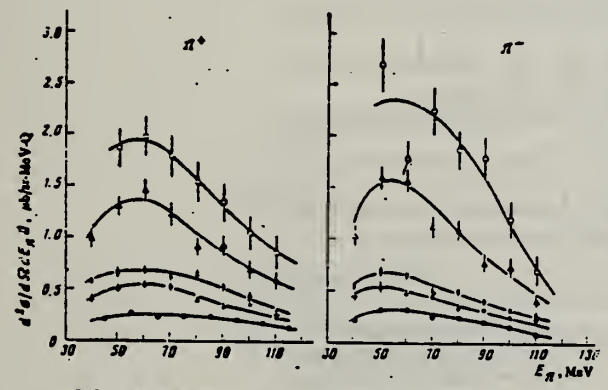

FIG. 2. Energy spectra of π^+ and π^- mesons. E_γ^{max} = 400 MeV, θ_{lab} = 90 ± 7°. The points are the same as in Fig. 1.

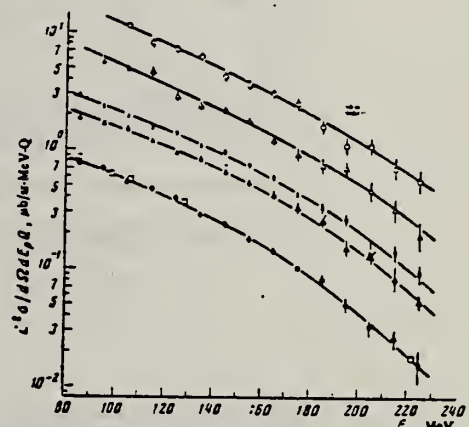

FIG. 4. Energy spectra of protons, E_γ^{max} = 400 MeV, θ_{lab} = 90 ± 7°. The points are the same as in Fig. 1; □—data from ref. 7.

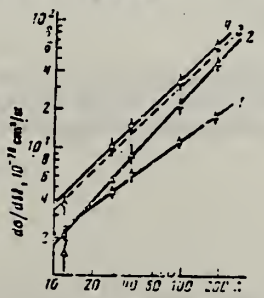

FIG. 5. Dependence of yields of π mesons 1, protons 2, and the sum of π-meson and proton yields 4 as a function of mass number of the nucleus. The dashed line 3 is the theory. Points: □—experimental differential cross sections for pions of all signs, △—differential cross sections for protons emitted at the same angle θ_{lab} = 90°, ○—combined values of these differential cross sections. The statistical errors are shown.

[5] P.C.Murray et al., Phys.Rev. 94, 764 (54).
[6] C.Levinthal et al., Phys.Rev. 82,822 (51).
[7] P.Dougan et al., LUSY Prep.1002 (1970).

REF. Z. Berant, J. Tenenbaum, A. Wolf and R. Moreh
Nucl. Phys. A306, 101 (1978)

ELEM. SYM.	A	Z
Nb	93	41

METHOD

REF. NO. 78 Be 2 rs

REACTION	RESULT	EXCITATION ENERGY	SOURCE		DETECTOR		ANGLE
			TYPE	RANGE	TYPE	RANGE	
G,G	LFT	1- 6	D	4- 6	SCD-D		DST

ALSO G,G/ DATA

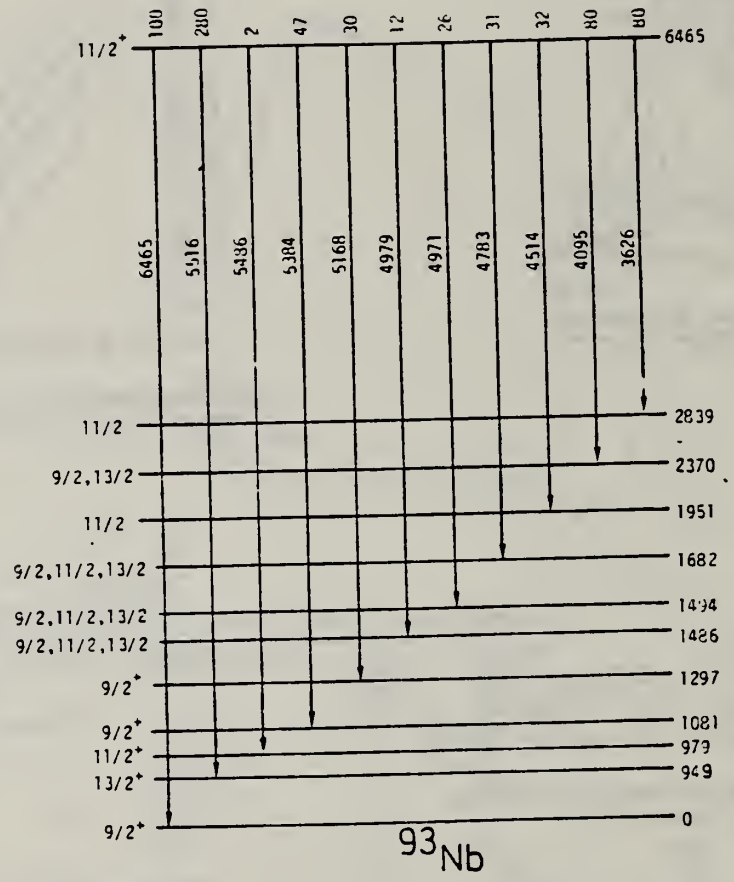

Fig. 3. Decay scheme of the 6465 keV level of ^{93}Nb showing level energies and relative intensities normalized so that the intensity of the ground-state transition is taken to be 100. The level spins are those obtained by combining the results of the present work (table 1) and those reported in refs. [3, 7]).

over

TABLE 1

γ-line energies E_γ, level energies E_x of ^{93}Nb, angular distribution coefficients A and spins J^π

Present work					Refs. [3, 7] [a])	
E_γ ($\mp$3 keV)	intensity	A (exp)	E_x ($+$3 keV)	J^π	E_x	J^π
5516	280 ± 5	0.06 ± 0.04	949	$\frac{13}{2}^+$	949.6	$\frac{13}{2}^+$
5486	2 ± 2		979	$\frac{9}{2}, \frac{11}{2}, \frac{13}{2}$	979	$\frac{11}{2}^+$
5384	47 ± 2	0.02 ± 0.07	1081	$\frac{9}{2}, \frac{11}{2}$	1082.5	$\frac{9}{2}^+$
5168	30 ± 2	0.14 ± 0.08	1297	$\frac{9}{2}, \frac{13}{2}$	1298	$\frac{9}{2}^+$
4979	12 ± 3		1486	$\frac{9}{2}, \frac{11}{2}, \frac{13}{2}$	1481	$\frac{1}{2}^-, \frac{3}{2}^-$
4971	26 ± 1		1494	$\frac{9}{2}, \frac{11}{2}, \frac{13}{2}$	1491	$\frac{9}{2}^-, \frac{11}{2}^-, \frac{13}{2}^+$
4783	31 ± 1		1682	$\frac{9}{2}, \frac{11}{2}, \frac{13}{2}$	1682.6	$\frac{7}{2}^-, \frac{9}{2}^-, \frac{11}{2}^-$
4514	32 ± 3	−0.19 ± 0.12	1951	$\frac{11}{2}^-$	1950.5	$\frac{7}{2}^-, \frac{9}{2}^-$
4095	80 ± 25	0.07 ± 0.10	2370	$\frac{9}{2}, \frac{13}{2}$	2360 [b])	
3626	80 ± 25	−0.17 ± 0.11	2839	$\frac{13}{2}^-$	2810 [b])	
6465	100 ± 2	0.04 ± 0.05	6465	$\frac{11}{2}^-$		

The spins J^π are based either on the values of A or on the assumption that the resonance level is deexcited by dipole transitions.

[a]) Only those levels of refs. [3, 7] are listed which were also observed in the present work.

[b]) The reported energy uncertainty of these levels is ±20 keV.

[3] I. J. van Heerden, W. R. McMurray and R. Saayman, Z. Phys. 260 (1973) 9

[7] D. C. Kocher, Nucl. Data B8 (1972) 527

TABLE 3

Values of R_T, R, δ, σ_r, Γ_0/Γ and Γ_0 of the 6465 keV level in ^{93}Nb

R_T [a])	R [b])	δ [c]) (eV)	σ_r [d]) (mb)	Γ_0/Γ	Γ (meV)
1.022 ± 0.011	0.004 ± 0.003	6 ± 2	1.6 ± 0.7	0.12 ± 0.03	38 ± 17

[a]) R_T is the ratio of scattering cross sections at T = 78°K and room temperature T = 293°K given for a 13 g.cm^{-2} thick scatterer placed at an angle of 60° and a detector angle of 135° with respect to the incident beam.

[b]) R is the self-absorption ratio and is given for the same scatterer-detector geometry as that of R_T and for an absorber thickness of 18.4 g.cm^{-2}.

[c]) δ is the energy separation between the peak of the incident γ-line and the peak of the resonance level.

[d]) σ_r is the elastic scattering cross section.

REF. D.J.S. Findlay, D.J. Gibson, R.O. Owens, J.L. Matthews
Phys. Lett. 79B, 356 (1978)

ELEM. SYM.	A	Z
Nb	93	41

METHOD

REF. NO. 78 Fi 7 hg

REACTION	RESULT	EXCITATION ENERGY	SOURCE		DETECTOR		ANGLE
			TYPE	RANGE	TYPE	RANGE	
G,P	NOX	45-85	C	60-100	MAG-D		DST

Experimental data on the (γ, p) reaction at $E_\gamma = 60-100$ MeV for targets in the range $A = 7-93$ are compared with predictions based on a single-particle knock-out mechanism using shell model wavefunctions. The results show that this mechanism is more important than has generally been believed

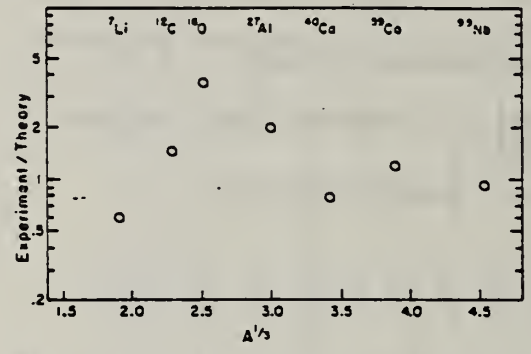

Fig. 2. The ratio of the measured photoproton emission populating low-lying states to the single-particle direct knock-out predictions is shown as a function of nuclear mass A for 80 MeV bremsstrahlung. Errors in the ratio, due to uncertainties in our calculations, are estimated to be a factor of ≈ 1.5. Errors in the experimental data are negligible.

REF. K. Masumoto, T. Kato, N. Suzuki
Nucl. Inst. Meth. 157, 567 (1978)

ELEM. SYM.	A	Z
NB	93	41

METHOD

REF. NO.	
78 Ma 10	hg

REACTION	RESULT	EXCITATION ENERGY	SOURCE		DETECTOR		ANGLE
			TYPE	RANGE	TYPE	RANGE	
G,N	ABY	9-68	C	30-68	ACT		4PI
G,AN	ABY	13-68	C	30-68	ACT		4PI

Analysis is made of reactions interfering with photon activation analysis procedures.

The activation yield curves have been presented for a number of photonuclear reactions in the energy range from 30 to 68 MeV, in order to evaluate quantitatively the interferences due to competing reactions in multielement photon activation analysis. The general features of the yields as functions of both target mass number and excitation energy were elucidated from the data obtained, discussion being given on the results in terms of the reaction mechanism.

Simultaneous neutron activation due to appreciable neutron production from the converter and surrounding materials has also been studied, and, finally, the magnitudes of interferences in real multielement analysis were given in the form of their energy dependences.

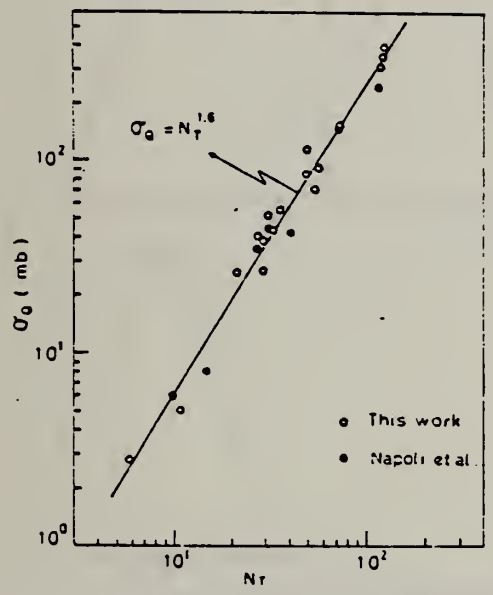

Fig. 2. Yield per equivalent quanta versus target neutron number.

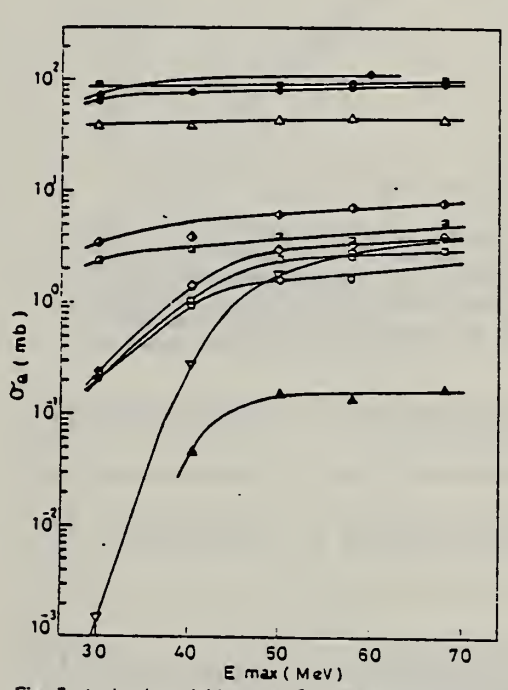

Fig. 7. Activation yield curves for the reactions on Y, Zr, Nb and Mo.
◆ $^{89}Y(\gamma, n)^{88}Y$, ● $^{90}Zr(\gamma, n)^{89}Zr$, ○ $^{90}Zr(\gamma, pn)^{88}Y$,
△ $^{93}Nb(\gamma, n)^{92m}Nb$, ▲ $^{93}Nb(\gamma, xn)^{88}Y$, ■ $^{100}Mo(\gamma, n)^{99}Mo$,
◑ $^{97}Mo(\gamma, p)^{96}Nb$, ◪ $^{96}Mo(\gamma, p)^{95m}Nb$, ◇ $^{94}Mo(\gamma, pn)^{92m}Nb$,
□ $^{92}Mo(\gamma, 2n)^{90}Mo$, ▽ $^{94}Mo(\gamma, xn)^{89}Zr$.

(over)

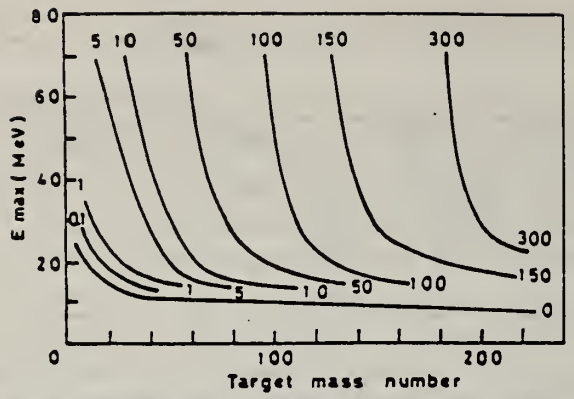

Fig. 9. Yields of the (γ, n) reactions as a function of bremsstrahlung maximum energy and target mass number. The numerical values in the figure are yields per equivalent quanta in mb.

REF. G.A. Vartapetyan, E.O. Grigoryan, A.S. Danagulyan, N.A. Demëkhina, A.G. Khudaverdyan
Yad. Fiz. 34, 289 (1981)
Sov. J. Nucl. Phys. 34, 163 (1981)

ELEM. SYM.	A	Z
Nb	93	41

METHOD

REF. NO. 81 Va 2 egf

REACTION	RESULT	EXCITATION ENERGY	SOURCE TYPE	SOURCE RANGE	DETECTOR TYPE	DETECTOR RANGE	ANGLE
$G,SPL	ABY	THR*4	C	4*	ACT-I		4PI

The charge distribution of residual nuclei has been studied in the disintegration of ^{93}Nb by bremsstrahlung with $E_{\gamma\,max} = 4.5$ GeV. Identification of the residual nuclei and determination of their yields were carried out by detecting the induced activity by means of a semiconductor Ge(Li) detector. Study of the charge distribution of isobars and comparison of the data obtained with the results of hadron-nucleus reactions permitted us to determine some regularities of the nuclear disintegration and to predict the probability of formation of residual nuclei which are hard to measure by the activation method. For quantitative estimates of the yields of the reaction products we used the five-parameter Rudstam formula. The nature and properties of the isobar and mass yields are discussed in comparison with calculations in terms of a two-step cascade-evaporative model.

*4.5 GEV 39 FINAL Z,A

PACS numbers: 25.20. + y, 27.60. + j

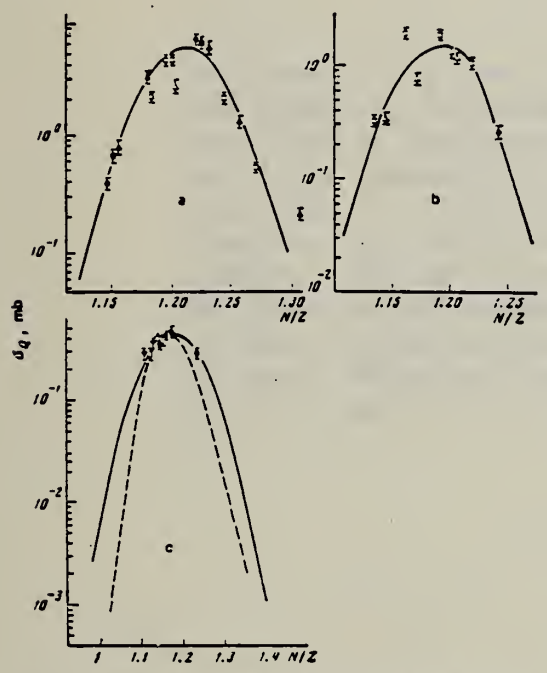

FIG. 1. Curves of the charge distribution of products of the reaction Nb + γ for the following mass intervals: a) 90–84, b) 83–75, c) 74–65. Points: ●–Nb, ■–Zr, ▲–Y, □–Sr, ○–Rb, Δ–Br, ▼–Se, ◆–As, ◇–Ga, ×–Zn, ▽–Co; c) calculation with the cascade-evaporative model[4] for the reaction Mo + p (in relative units); the dashed curve is for a proton energy 1800 MeV.

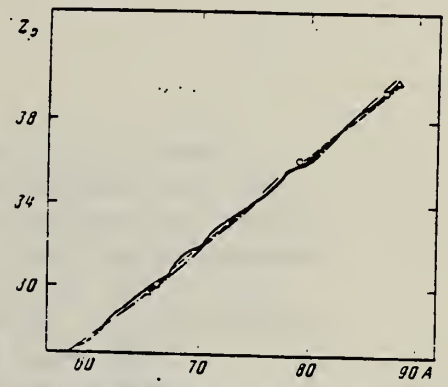

FIG. 2. Most probable charge of the charge distribution, as a function of the mass number of the product. Calculations of the cascade-evaporative model[13] for the reaction Nb + p with the following proton energies: 462 MeV (solid curve), 944 MeV (dashed curve), 1844 MeV (dot-dash curve). Points: ○—data of the present work, Δ—data of Ref. 13.

TABLE I.

Residual nucleus	Type of yield	σ_Q, mb (experiment)	σ_Q, mb (theory)	σ_Q exp / σ_Q theo
^{89m}Nb	–	3.3±0.9	5.01	9.56
^{89g}Nb	–	0.8±0.1	7.36	0.91
^{90}Nb	–	1.4±0.3	1.56	0.90
^{90m}Nb	–	0.22±0.1	2.08	0.17
^{91}Nb	–	0.72±0.05	1.28	0.57
^{95}Zr	–	0.72±0.05	1.63	1.31
^{97}Zr	–	1.4±0.2	1.61	0.97
^{97}Zr	–	2.3±0.1	2.18	1.03
^{88}Y	–	0.6±0.05	0.67	0.90
^{88}Y	–	0.21±0.05	0.22	0.94
^{89}Y	–	1.3±0.25	1.55	0.84
^{90}Y	–	0.66±0.17	0.78	0.85
^{90m}Y	–	2.7±0.6	2.99	1.19
^{91}Y	–	1.06±0.12	3.99	0.93
^{91m}Y	–	2.65±0.14	2.18	2.44
^{92}Y	–	1.92±0.2	0.85	0.93
^{92}Y	–	3.35±0.35	2.12	2.12
^{93}Y	–	0.79±0.08	0.90	1.03
^{93}Y	–	2.17±0.3	0.43	2.32
^{93}Y	–	2.08±0.21	0.99	1.31
^{93}Y	–	0.52±0.06	1.77	0.65
^{93}Y	–	2.1±0.3	1.87	1.06
^{94}Y	–	1.16±0.15	0.33	1.03
^{94}Y	–	1.97±0.39	1.05	1.13
^{94}Y	–	0.33±0.05	0.82	0.95
^{95}Y	–	1.18±0.29	0.36	1.00
^{95}Y	–	0.78±0.20	0.67	1.79
^{95}Y	–	<0.96±0.05	0.36	1.07
^{95m}Y	–	1.21±0.15	0.13	2.38
^{95m}Y	–	0.38±0.08	0.21	1.40
^{96}Y	–	0.29±0.06	0.30	0.87
^{96}Y	–	0.51±0.05	0.34	1.06
^{96}Y	–	0.36±0.08	0.24	1.45
^{96}Y	–	0.40±0.02	0.13	2.15
^{96}Y	–	0.28±0.04	0.23	1.89
^{96}Y	–	0.61±0.05	0.09	4.4
^{96}Y	–	0.90±0.12	0.06	10.5
^{96}Y	–	0.41±0.06	0.05	2.4
^{96}Y	–	0.12±0.04	0.05	15.4
^{96}Y	–	0.11±0.05	0.049	

# MOLYBDENUM
Z=42

Molybdos is the term first applied by the Greeks and Romans to describe minerals that were soft and lead-like in appearance. The word molybdenum itself was first introduced around 1816. Native molybdenum disulfide is a soft black mineral that looks like graphite. Up until the later part of the eighteenth century, both were sold under the same name: Molybdan, or molybdenum. The German writers called molybdenite "Wasserbley," a name suggestive of lead. Molybdenite was first identified by the Swedish chemist, Karl Wilhelm Scheele in 1778.

REF.

Sven A. E. Johansson
Phys. Rev. 97, 434-43 (1955)

ELEM.		
Mo		42

METHOD

Synchrotron; ZnS counter; ion chamber

REF. NO. 55 Jo 1 NVB

REACTION	RESULT	EXCITATION ENERGY	SOURCE		DETECTOR		ANGLE
			TYPE	RANGE	TYPE	RANGE	
G,P	RLY	THR - 65	C 65		SCI-D	14 - +	DST

TABLE I. Target thickness and the constants a and b in the angular distribution curve $a+(\sin\theta+b\sin\theta\cos\theta)^2$.

Element	Target thickness mg/cm²	a	b
Carbon	182	0.32	0.80
Aluminum	274	0.58	1.35
Nickel	352	0.94	1.45
Molybdenum	295	0.62	2.00

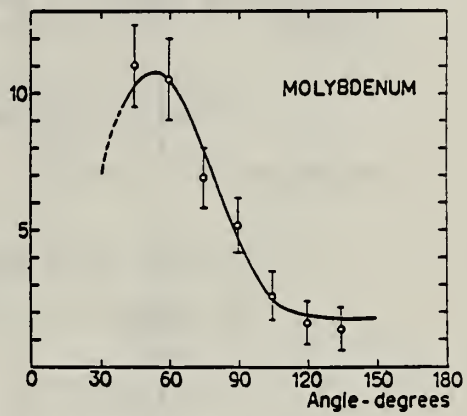

FIG. 5. The angular distributions of protons with an energy above 14 Mev.

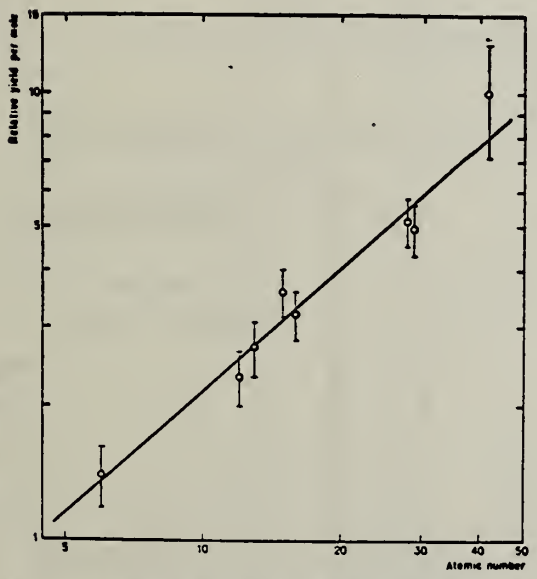

FIG. 10. The relative yield per mole for protons above 14 Mev as a function of the atomic number.

Ref. E. Seibel, A.K. Mann
Phys. Rev. 118, 701 (1960)

Elem. Sym.	A	Z
Mo		42

Method: γ's from $F^{19}(p,\alpha\gamma)$ reaction; protons from Van de Graaff; Re I.

Ref. No. 60 Re 1 JHH

Reaction	E or ΔE	E_o	Γ	$\int \sigma dE$	Jπ	Notes
(γ,γ)	$E_\gamma = \sim 7$					$\langle\sigma\rangle$ (E_p = 2.05 MeV) = 1.4 ± 0.2 mb

Ref. O.M.M. Mitchell, K.G. McNeill
Can. J. Phys. 41, 871 (1963)

Elem. Sym.	A	Z
Mo		42

Method: Betatron; proton yield; angular distribution; scintillator; ion chamber

Ref. No.: 63 Mi 5 NVB

Reaction	E or ΔE	E_o	Γ	$\int \sigma dE$	Jπ	Notes
Mo(γ,xp)	Bremss. 22					Angular distribution: $Y(\theta) = a + b \sin^2\theta (1 + p \cos\theta)^2$ where a = 46±10; b = 55 ± 15; p = 0.2±0.2 and b/a = 1.2±0.4. Yield (E_p > 8 MeV): (2.7±0.6) 10^5 protons/mole-r. Yield (3.7 < E_p < 14): (26±3) 10^5

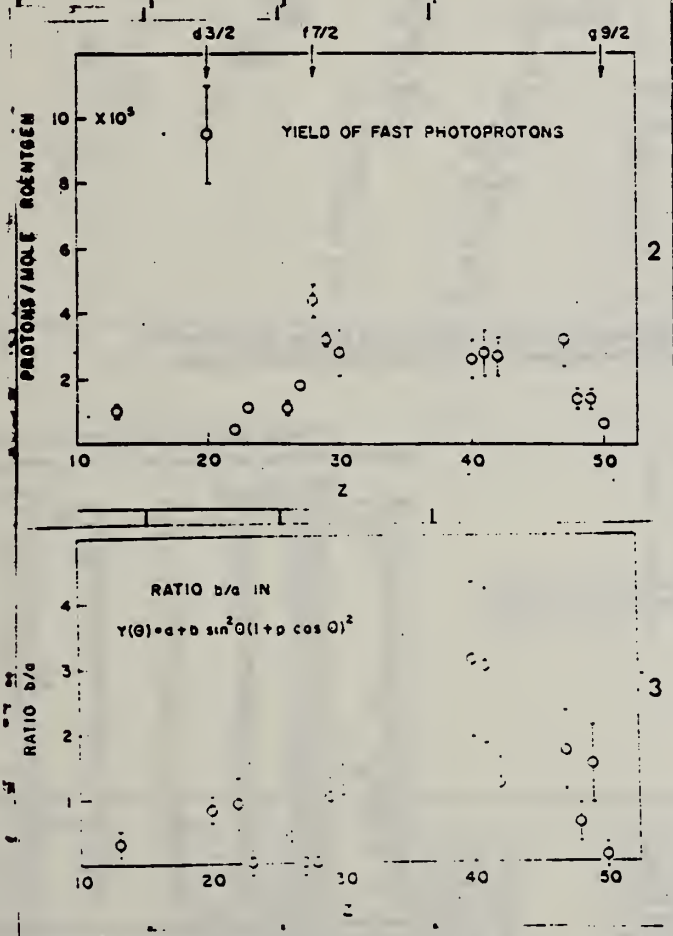

Fig. 2. The yields of fast photoprotons (E_p > 8 Mev) obtained from targets of various elements when irradiated with 22 Mev bremsstrahlung. The target thicknesses range from 251 to 572 mg/cm² (about 8 Mev for protons). The errors noted are statistical.

Fig. 3. The anisotropy coefficient b/a for fast photoprotons (E_p > 8 Mev) from 16 elements. The errors noted are statistical.

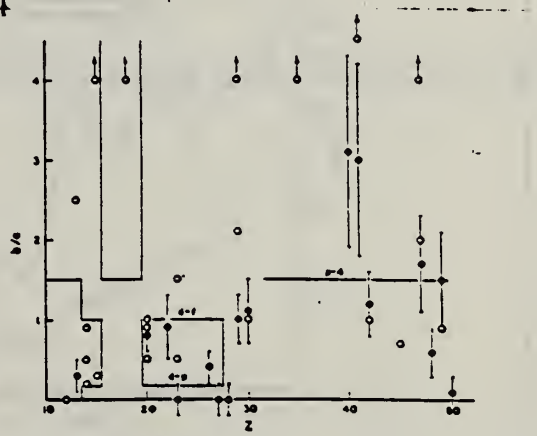

Fig. 4. The values of the fast photoproton anisotropy coefficient b/a found by the present authors (●) and other workers (○) in the region of the periodic table 10 ≤ Z ≤ 50. Arrows indicate isotopic points. The references to the results of other workers are given in Table II. The demarcations are explained in the text.

REF.	ELEM. SYM.	A	Z
G. Ben-David, B. Arad, J. Balderman, and Y. Schlesinger Phys. Rev. 146, B852 (1966)	Mo		42

METHOD	REF. NO.	
Nuclear Resonance Scattering using N,G reactions.	66 Be 3	JDM

REACTION	RESULT	EXCITATION ENERGY	SOURCE		DETECTOR		ANGLE
			TYPE	RANGE	TYPE	RANGE	
G,G	RLX	5 - 10	D	5 - 10	NAI-D	5 - 10	135

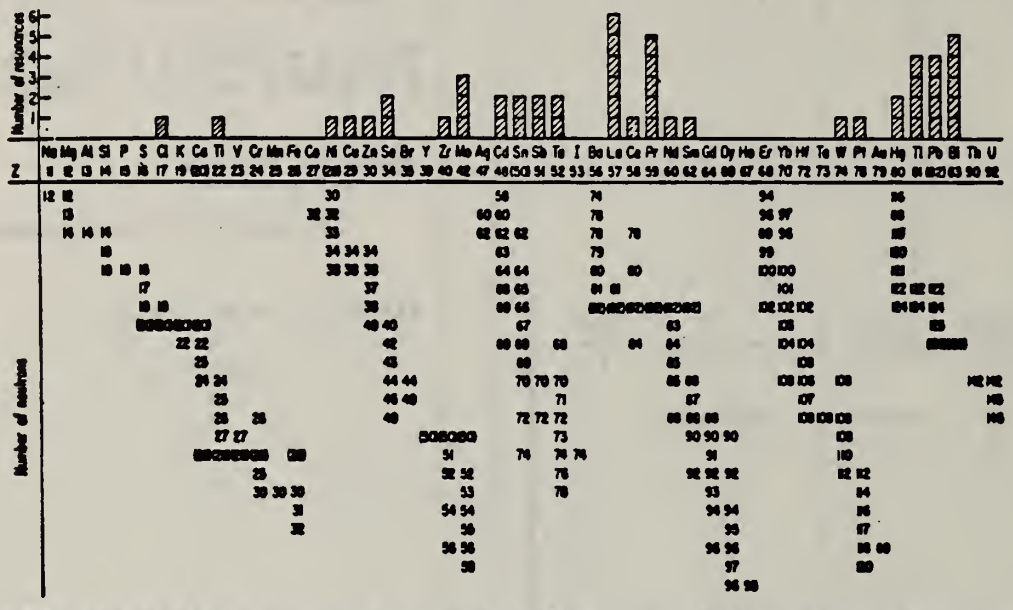

FIG. 3. Histogram of distribution of observed resonances among the different targets. The atomic number is given directly beneath the chemical symbol followed by the neutron numbers of the naturally occurring isotopes. Magic numbers are shown in brackets.

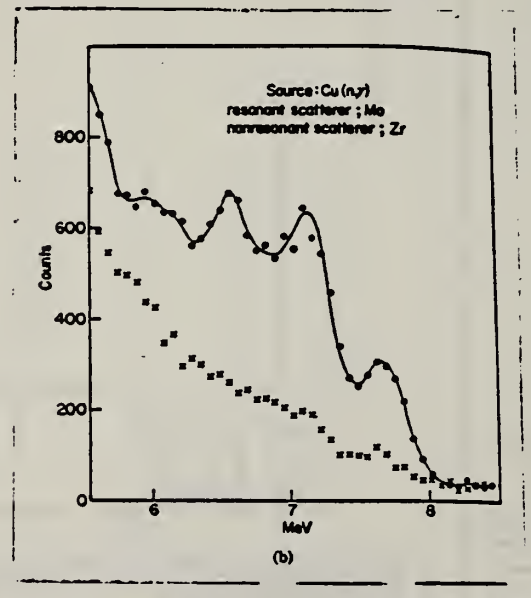

Fig.1.(b) Complex scattered spectrum from Mo excited by Cu capture rays (with Zr background).

TABLE III. List of effective cross sections.

Scatterer	Energy (MeV)	Gamma source	δ (mb)	Scatterer	Energy (MeV)	Gamma source	δ (mb)
Sm^{144}	8.997	Ni	100	Sn	7.01	Cu	110
Pr^{141}	8.881	Cr	9	Nd	6.867	Co	30
La	8.532	Ni	6	Pr^{141}	6.867	Co	3
Te	8.532	Ni	3[b]	Te	6.7	Ni	...
Cu	8.499	Cr	24	La	6.54	Ag	12
Zr	8.496	Se	3050	Cd	6.474	Co	110
Zn	8.119	Ni	13	Mo	6.44	Hg	25[a]
Se	7.817	Ni	50	La	6.413	Ti	72
Se	7.76	K	90	Mo	6.413	Ti	10
Sb	7.67	V	...[b]	Tl	6.413	Ti	25
Cd	7.64	Fe	40[a]	W	~6.3	Ti	...[b]
Ni	7.64	Fe	7[a]	Sb	6.31	Hg	6[a]
Pr^{141}	7.64	Fe	12[a]	Tl	6.31	Hg	2[a]
Tl	7.64	Fe	370[a]	Sn	6.27	Ag	75
La	7.634	Cu	7	Pb^{208}	6.15	Gd	...[c]
Mo	7.634	Cu	11	Te	5.8	Ni	...[f]
Bi^{209}	7.634	Cu	4	La	6.12	Cl	35
Te	7.528	Ni	66[d]	Pr^{141}	6.12	Cl	110
Bi^{209}	7.416	Se	100	Pt	5.99	Hg	40[a,e]
Bi^{209}	7.300	As	80[a]	Tl	5.99	Hg	5[e]
Pb^{208}	7.285	Fe	4100	Pb^{208}	5.9	Sr	...[b]
Cl	7.285	Fe	34	Ce	5.646	Co	17
Pr^{141}	7.185	Se	80	Bi^{209}	5.646	Co	55
Tl	7.16	Cu	120	Pb^{208}	5.53	Ag	70
La	7.15	Mn	50	Hg	5.44	Hg	75[e]
Bi^{209}	7.149	Tl	2000	Hg	4.903	Co	385

[a] High-energy component of a complex spectrum.
[b] A broad scattered spectrum with no observable peak structure.
[c] There are actually two lines of energies 7.647 and 7.633 MeV having equal intensities in the iron capture gamma spectrum. The cross section has therefore been corrected, although there is no possibility at present of deciding which line is responsible for each resonance.
[d] Is probably an independent level in the complex spectrum of Ni + rays on Te.
[e] Rough estimate.
[f] May be inelastic component from 7.528 level in Te.
[g] The relative line intensities in this case are due to Groshev and co-workers.
[h] No line is known for the source at this energy.
[i] Difficult to resolve among the many source lines present at this energy.

REF. S. M. Hussain and K. G. McNeill
Can. J. Phys. 45, 2851 (1967)

ELEM. SYM.	A	Z
Mo		42

METHOD

REF. NO. 67 Hu 2 EGF

REACTION	RESULT	EXCITATION ENERGY	SOURCE		DETECTOR		ANGLE
			TYPE	RANGE	TYPE	RANGE	
G,N	ABY	THR-22	C	22	THR	4-	DST

YIELD AT Eo = 22 MeV
^{28}Si (n,p) ACTIVATION BY PHOTONEUTRONS

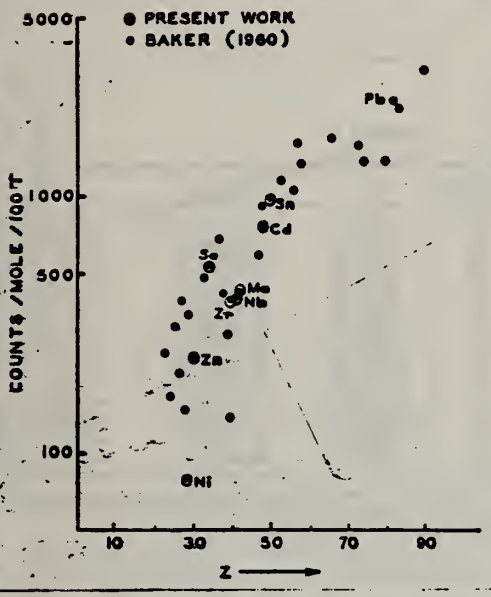

FIG. 3. The yields of fast photoneutrons from various elements as measured in the present work and by Baker. The present results have been normalized to Baker's measurements for lead.

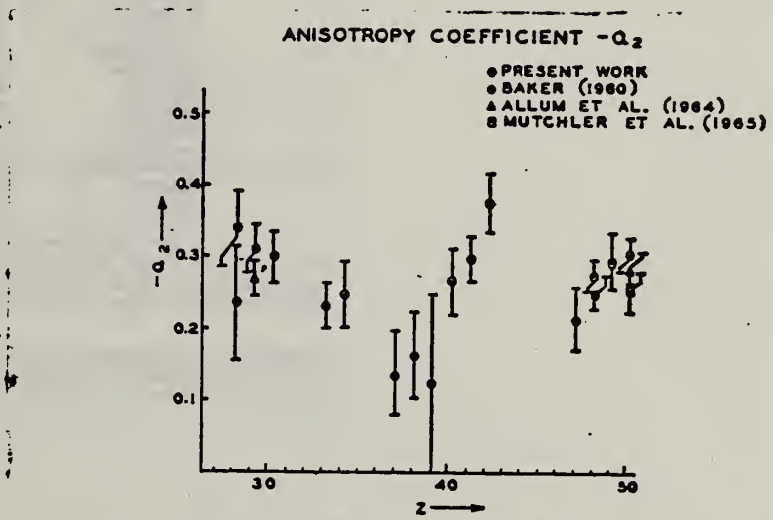

FIG. 2. The anisotropy coefficients a_2, in the formula $W(\theta) = a_0(1 + a_1P_1 + a_2P_2)$, obtained in the present work, and those obtained by other workers in the same part of the Periodic Table.

TABLE I

Element	a_0*	a_1	a_2
Nickel	77 (1.0±0.05)	0.14±0.04	−0.34±0.06
Zinc	236 (1.0±0.04)	0.06±0.03	−0.30±0.04
Selenium	525 (1.0±0.05)	0.10±0.04	−0.25±0.05
Zirconium	380 (1.0±0.05)	0.03±0.04	−0.27±0.05
Niobium	392 (1.0±0.03)	0.04±0.02	−0.30±0.03
Molybdenum	410 (1.0±0.03)	0.05±0.03	−0.41±0.04
Cadmium	755 (1.0±0.02)	0.05±0.01	−0.28±0.02
Tin	955 (1.0±0.02)	0.08±0.02	−0.30±0.02
Lead	2274 (1.0±0.02)	0.06±0.02	−0.48±0.02

*For comparison purposes the experimental value of a_0 for Pb has been normalized to coincide with that obtained by Baker and McNeill (1961) and is the yield per mole per 100 roentgen. All other values of a_0 have also been quoted with the same normalization.

REF.

J. W. Jury, J. S. Hewitt, and K. G. McNeill
Can. J. Phys. 46, 1823 (1968)

ELEM. SYM.	A	Z
Mo		42

METHOD

REF. NO. 68 Ju 1 EGF

REACTION	RESULT	EXCITATION ENERGY	SOURCE		DETECTOR		ANGLE
			TYPE	RANGE	TYPE	RANGE	
G,N	NOX	THR-22	C	22	THR	5-	DST

$$W(\theta) = a_o + a_1 P_1 + a_2 P_2$$

TABLE I

Target element	Z	Energy	a_0*	a_1/a_0	a_2/a_0
Vanadium	23	32	640±50	0.11±0.10	−0.09±0.11
Chromium	24	22	365±39	0.02±0.08	0.00±0.10
Manganese	25	22	450±33	0.07±0.05	−0.11±0.06
Bromine	35	27	874±54	0.05±0.06	−0.15±0.08
Molybdenum	42	22	610±60	0.09±0.05	−0.35±0.06
Ruthenium	44	27	1100±25	0.12±0.02	−0.29±0.03
Rhodium	45	27	1270±47	0.06±0.03	−0.14±0.03
Palladium	46	27	1350±29	0.26±0.02	−0.12±0.02
Antimony	51	27	2140±62	0.04±0.08	−0.25±0.11
Lanthanum	57	27	1940±70	0.12±0.10	−0.52±0.14
Praseodymium	59	30	1800±58	0.20±0.08	−0.40±0.09
Platinum	78	27	2600±52	0.17±0.02	−0.15±0.03
Lead	82	22	2274±59	0.08±0.08	−0.46±0.09

*The yield per mole per 100 r was normalized to a yield of 2274 for the lead sample at the same energy.

REF.

S. Costa, L. Ferrero, L. Pasqualini, and E. Mancini
Lettere al Nuovo Cimento 2, 665 (1971)

ELEM. SYM.	A	Z
Mo		42

METHOD

REF. NO. 71 Co 2 egf

REACTION	RESULT	EXCITATION ENERGY	SOURCE		DETECTOR		ANGLE
			TYPE	RANGE	TYPE	RANGE	
G,XN	ABI	36-64	C	10-64	BF3-I		4PI

FAST N YIELD

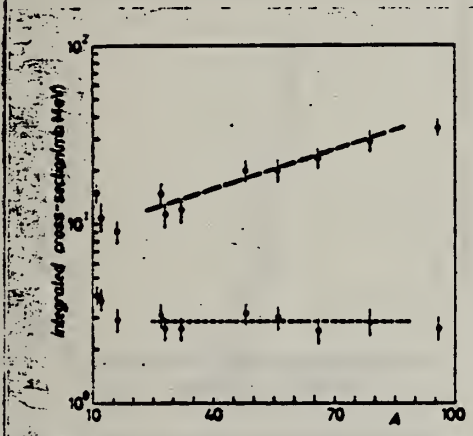

Fig. 2.

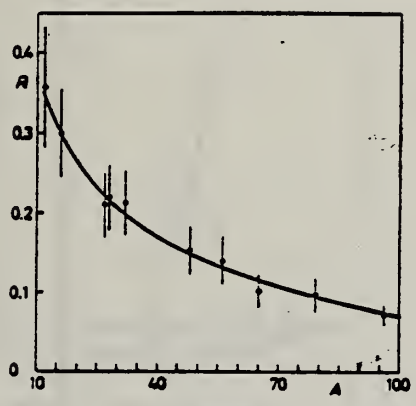

Fig. 3.

Fig 2. – Experimental photoneutron cross-sections integrated over photon energy between 36 and 64 MeV and divided by NZ/A are plotted as a function of the mass number. Black dots are total cross-sections not corrected for neutron multiplicity; open circles represent fast neutron cross-sections (see text). The dashed lines are drawn only to guide the eye.

Fig. 3. – The ratio between «fast» and total photoneutron integrated cross-sections as a function of the mass number A. The solid line represents a fit of the ratios calculated for some nuclei by taking into account the theoretical neutron energy spectra given by GABRIEL and ALEXANDER (*) and the efficiencies of our detector (see Fig. 1).

REF. T. Methasiri and S. A. E. Johansson
Nucl. Phys. A167, 97 (1971)

ELEM. SYM.	A	Z
Mo		42

METHOD

REF. NO. 71 Me 1 egf

REACTION	RESULT	EXCITATION ENERGY	SOURCE		DETECTOR		ANGLE
			TYPE	RANGE	TYPE	RANGE	
G,F	ABY	THR-900	C	300-900	FRG-I		4PI

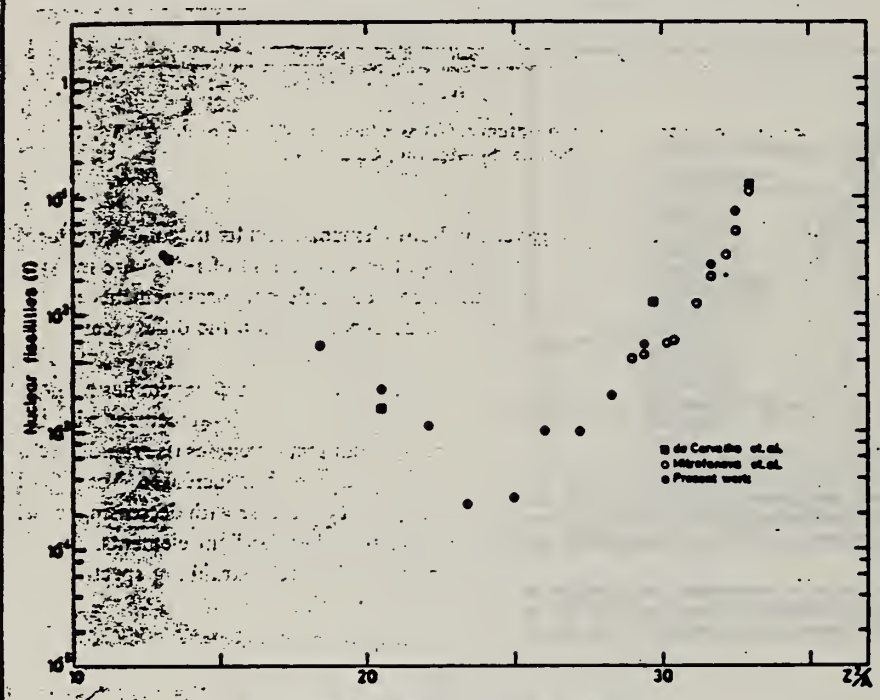

Fig. 2. Nuclear fissilities as a function of Z^2/A.

TABLE 1

The constant fission cross sections above the threshold

Element	σ_f (cm^2)	Element	σ_f (cm^2)
Pb	$(5.0\pm0.2)\times10^{-27}$	La	$(1.1\pm0.1)\times10^{-29}$
Au	$(1.7\pm0.1)\times10^{-27}$	Sn	$(4.3\pm1.1)\times10^{-29}$
Ta	$(3.3\pm0.2)\times10^{-28}$	Ag	$(8.4\pm2.0)\times10^{-29}$
Yb	$(1.2\pm0.2)\times10^{-28}$	Mo	$(1.7\pm0.4)\times10^{-28}$
Ho	$(5.5\pm0.3)\times10^{-29}$	Cu	$(6.6\pm1.2)\times10^{-28}$
Gd	$(5.3\pm0.8)\times10^{-29}$	Ni	$(5.8\pm0.1)\times10^{-28}$
Nd	$(1.3\pm0.2)\times10^{-29}$		

[over]

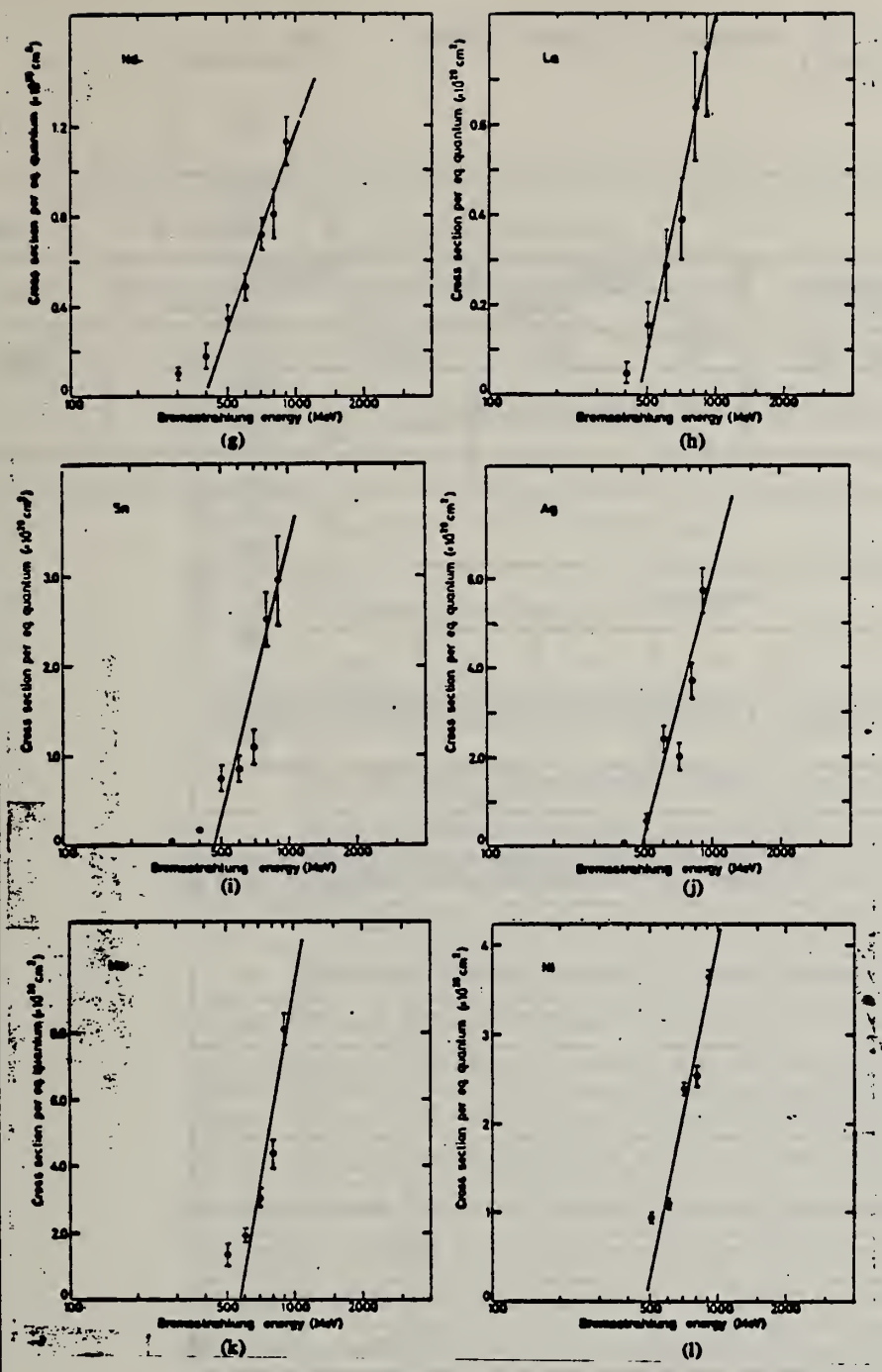

Fig. 1. Cross sections per equivalent quantum $\sigma_q(E)$ as a function of log E.

REF. V.P. Kovalev, V.P. Kharitz, V.V. Gordeev, V.I. Isaev (USSR)
Atomnaya Energiya 32, 496 (1972)

EL EM. SYM.	A	Z
Mo		42

METHOD

REF. NO. 72 Ko 8 hmg

REACTION	RESULT	EXCITATION ENERGY	SOURCE		DETECTOR		ANGLE
			TYPE	RANGE	TYPE	RANGE	
G,N	NCY	6- 22	C	22	THR-I		DST

Мишень	Энергия электронов, Мэв	Детектор	Угол, *град*							В/А
			30	50	70	90	110	130	150	
Al	22,5	$P^{31}(n,p)$	1,05±0,08	1,03±0,08	0,97±0,08	1,0±0,08	0,98±0,08	1,02±0,08	1,04±0,08	Изотропное
	22,5	$Al^{27}(n,p)$	0,90±0,15	0,95±0,15	1,02±0,15	1,00±0,14	0,96±0,13	1,07±0,13	1,01±0,13	»
Ti	22,5	$P^{31}(n,p)$	1,04±0,07	0,96±0,07	1,03±0,07	1,00±0,07	0,98±0,07	1,05±0,07	1,03±0,07	»
	22,5	$Al^{27}(n,p)$	1,06±0,13	0,94±0,13	1,04±0,12	1,00±0,12	0,95±0,11	0,98±0,11	1,02±0,10	»
Ca	12,8	$P^{31}(n,p)$	0,97±0,10	1,04±0,10	1,02±0,10	1,00±0,10	1,01±0,10	0,90±0,10	0,96±0,10	»
	17,0	$P^{31}(n,p)$	1,03±0,07	0,97±0,07	1,00±0,07	1,00±0,07	1,06±0,07	0,95±0,07	0,88±0,07	»
	22,5	$P^{31}(n,p)$	0,87±0,05	0,94±0,05	0,97±0,05	1,00±0,05	0,99±0,05	0,93±0,05	0,91±0,05	0,18±0,04
	22,5	$Al^{27}(n,p)$	0,75±0,09	0,86±0,07	0,93±0,06	1,00±0,05	1,02±0,05	0,94±0,04	0,90±0,04	0,28±0,06
Mo	22,5	$P^{31}(n,p)$	0,90±0,05	0,93±0,05	0,98±0,05	1,00±0,05	0,99±0,05	0,92±0,05	0,84±0,05	0,21±0,04
	22,5	$Al^{27}(n,p)$	0,80±0,08	0,95±0,08	0,95±0.07	1,00±0,06	0,94±0,05	0,83±0,04	0,72±0,04	0,44±0,08
	22,5	$Al^{27}(n,\alpha)$	0,72±0,08	0,84±0,08	0,89±0,08	1,00±0,08	0,95±0,08	0,87±0,08	0,63±0,08	0,78±0,18
W	22,5	$P^{31}(n,p)$	0,85±0,04	0,90±0,04	0,98±0,04	1,00±0,04	0,98±0,04	0,92±0,04	0,087±0,04	0,25±0,04
	22,5	$Al^{27}(n,p)$	0,78±0,06	0,84±0,06	0,89±0,05	1,00±0,05	0,97±0,04	0,86±0,04	0,75±0,04	0,54±0,06
Pb	22,5	$P^{31}(n,p)$	0,79±0,04	0,85±0,04	0,96±0,04	1,00±0,04	0,98±0,04	0,88±0,04	0,84±0,04	0,36±0,05
	22,5	$Al^{27}(n,p)$	0,70±0,09	0,81±0,08	0,94±0,07	1,00±0,06	0,94±0,06	0,80±0,05	0,69±0,05	0,69±0,12

(over)

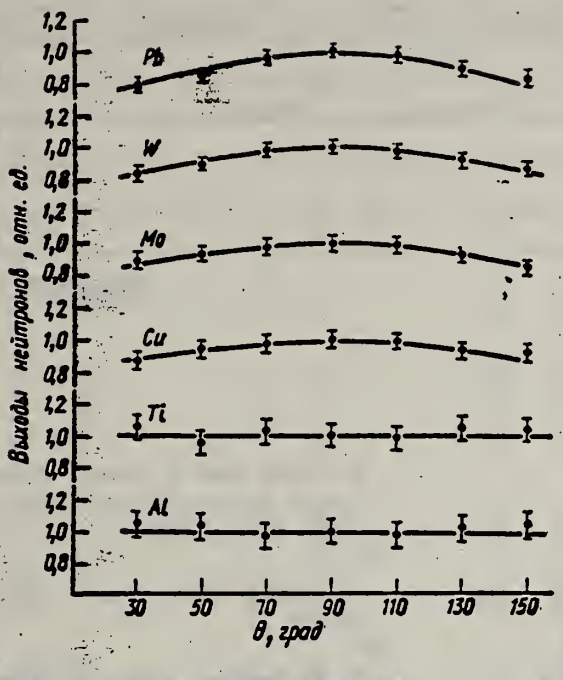

Угловые распределения быстрых фотонейтронов из Al, Ti, Cu, Mg, W, Pb, облученных электронами с энергией 22,5 *Мэв*. Детектор P^{31} (n, p) Si^{31}.

REF.

R.F. Barrett, J.R. Birkelund, B.J. Thomas, K.S. Lam, and H.H. Thies
Nucl. Phys. A210, 355 (1973)

ELEM. SYM.	A	Z
Mo		42

METHOD

REF. NO.	
73 Ba 20	egf

REACTION	RESULT	EXCITATION ENERGY	SOURCE		DETECTOR		ANGLE
			TYPE	RANGE	TYPE	RANGE	
G,N	NOX	THR- 27	C	10- 27	BF3-I		4PI

MEAN NEUT ENERGY

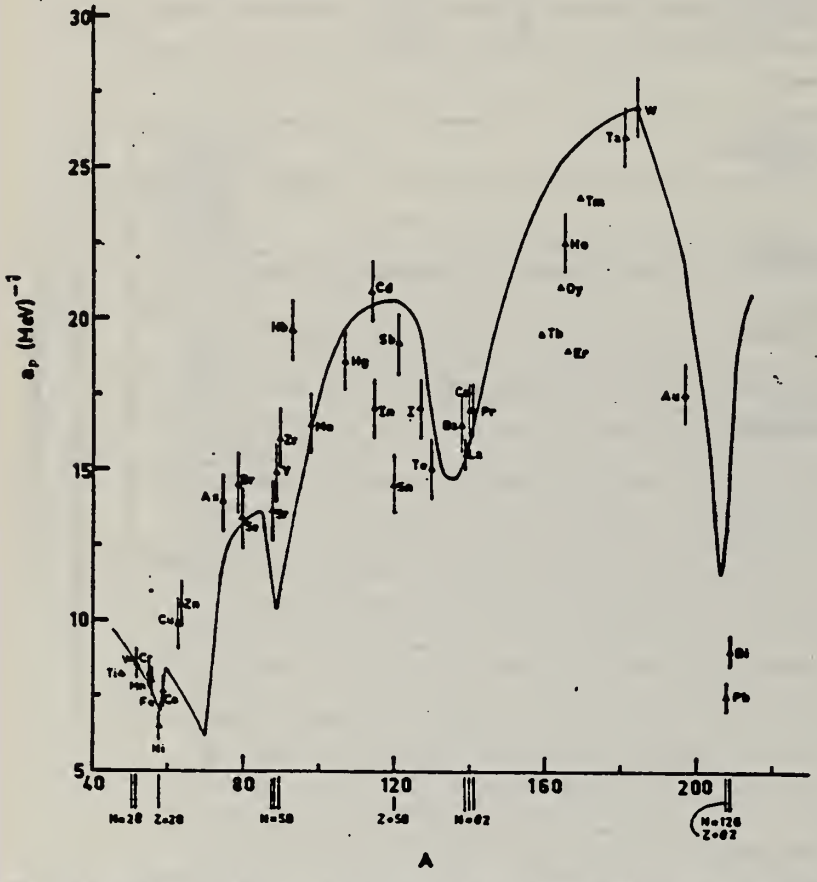

Fig. 12. Experimental values of the level density parameter a_p (Fermi gas formula plus pairing correction) versus atomic number A. The continuous curve is a least-squares fit to the data of a theoretical calculation from Newton [15]).

1
H. Baba and S. Baba, Japan Atomic Energy Research Institute report JAERI-1183 (1969).
2
H. Baba, Nucl. Phys. A159, 625 (1970).
15
T.D. Newton, Can. J. Phys. 34, 804 (1956).

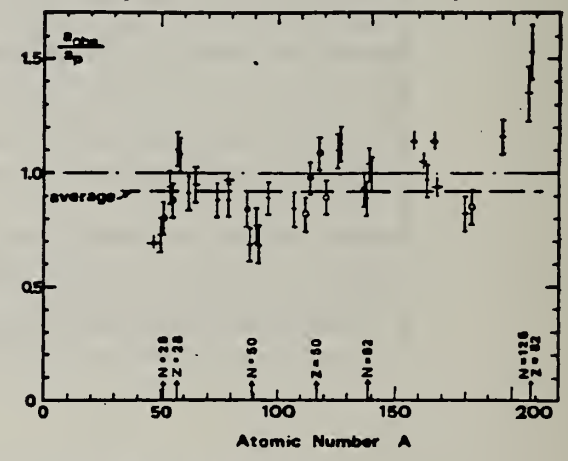

Fig. 15. Ratio a_{obs}/a_p versus atomic number A. Here a_{obs} is the level density parameter taken from the neutron resonance work of refs. [1,2]), and a_p is the level density parameter derived from the present (γ, n) work. Filled circles represent points where nuclei in the neutron resonance and in the (γ, n) experiment were the same. Open circles represent points where the respective nuclei were approximately matched. Triangles represent points which are based on measurement of neutron mean energies at two bremsstrahlung energies only.

(over)

TABLE 3 (continued)

Target	N (residual nucleus) [a]		Goodness of fit [b]		$\hat{E}_n(24)$ (MeV) [c]	T (MeV) [d]	a_p (MeV^{-1}) [e]	a_{obs} (MeV^{-1}) [f]	a_{obs}/a_p
			no p.c.	with p.c.					
Y	49	100%	G	G	1.30		14.9–^{88}Y	10.17–^{90}Y	0.68
Zr	49	52%	F	F	1.28		16.0–^{90}Zr	12.2 –^{91}Zr	0.77
	50	11%							
	51	17%							
	53	17%							
	55	3%							
Nb	51	100%	F	F	1.28		19.6–^{92}Nb	13.15–^{94}Nb	0.68
Mo	49	16%	G	G	1.27		16.5–^{95}Mo	14.7 –^{97}Mo	0.89
	51	9%							
	52	16%							
	53	17%							
	54	10%							
	55	24%							
	57	8%							
Ag	59	51%	V.P.	F	1.27	0.55	18.6–^{107}Ag	15.61–^{108}Ag	0.84
	61	49%							
Cd	57	1%	V.P.	F	1.24	0.54	20.9–$^{111.4}$Cd	17.0 –^{112}Cd	0.82
	61	12%							
	62	13%							
	63	24%							
	64	12%							
	65	29%							
	67	8%							
In	63	4%	V.P.	F	1.26	0.57	17.0–^{114}In	16.66–^{114}In	0.98
	65	96%							
Sn ($Z = 50$)	65	14%	V.P.	V.P.	1.38	0.73	14.5–^{118}Sn	15.9 –^{118}Sn	1.09
	66	8%							
	67	24%							
	68	9%							
	69	33%							
	71	5%							
	73	6%							
Sb	69	57%	V.P.	P	1.2	0.68	19.2–^{121}Sb	17.0 –^{121}Sb	0.89
	71	43%							
Te	69	2%	V.P.	F	1.36	0.83	15.0–^{127}Te	17.0 –^{127}Te	1.13
	71	5%							
	72	7%							
	73	19%							
	75	32%							
	77	34%							
I	73	100%	F	G	1.23	0.70	17.0–^{126}I	17.02–^{128}I	1.00

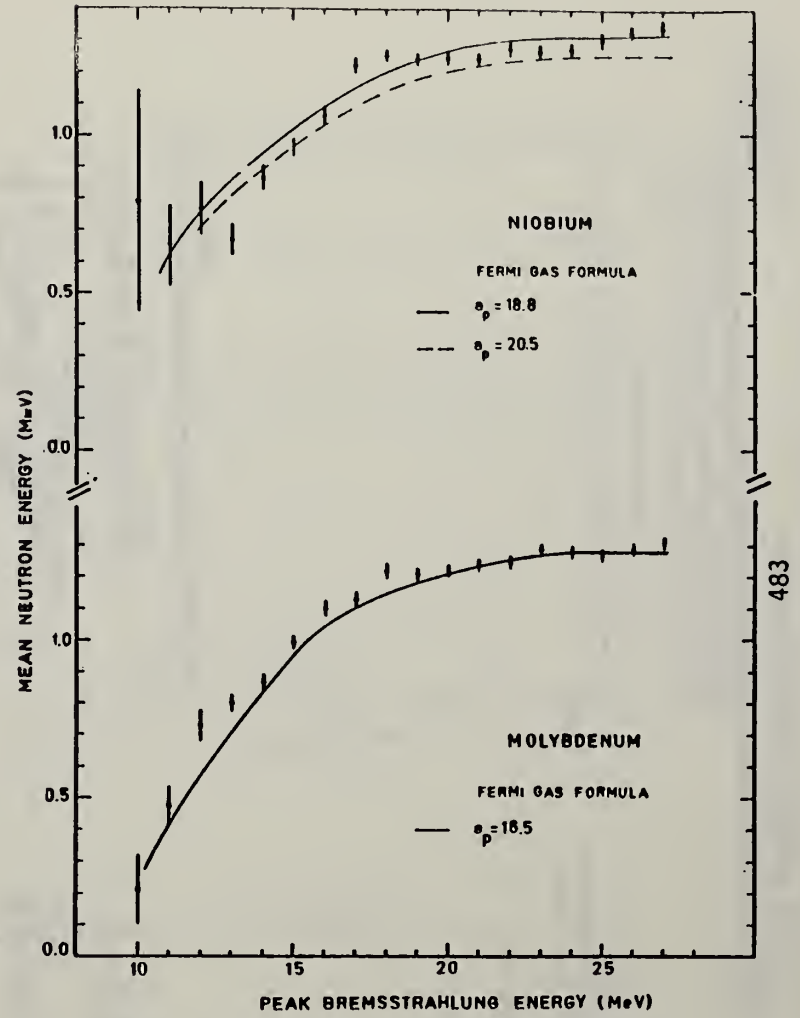

Fig. 8. Same as fig. 5, for niobium and molybdenum.

[a]) Neutron numbers and abundances of respective residual nuclei in (γ, n) experiments.
[b]) These give an assessment of the goodness of fit of a calculated $\hat{E}_n$ versus E_0 curve to the observed data, using the Fermi gas level density formula both without and with pairing corrections.
[c]) Bremsstrahlung photoneutron mean energies $\hat{E}_n$ for peak bremsstrahlung energy $E_0 = 24$ MeV.
[d]) Nuclear temperature from fit with constant-temperature formula.
[e]) Level density parameter a_p derived from the present (γ, n) experiment, using a Fermi gas formula plus pairing correction, and corresponding residual nucleus (the atomic weight shown is the weighted average of atomic weights of the respective isotopes present).
[f]) As column 7, but using data on n-resonance absorption from refs. [1, 2]).
[g]) Measurements of $\hat{E}_n(E_0)$ for these nuclei were made only for $E_0 = 21$, 23 and 24 MeV.

REF.	ELEM. SYM.	A	Z
V.G. Vlasenko, V.A. Gol'dshtein, A.V. Mitrofanova, V.I. Noga, Yu.N. Ranuuk, V.I. Startsev, P.V. Sorokin, Yu.N. Telegin Yad. Fiz. 23, 504 (1976) Sov. J. Nucl. Phys. 23, 265 (1976)	Mo		42

METHOD	REF. NO.	
	76 V1 1	hmg

REACTION	RESULT	EXCITATION ENERGY	SOURCE		DETECTOR		ANGLE
			TYPE	RANGE	TYPE	RANGE	
E,E/	ABX	100-500	D	1* 2	MAG-D		DST

Inelastic electron scattering has been used to measure the total hadronic cross sections for absorption of photons with energy 150–500 MeV by nuclei of C, Al, Ni, Mo, and W. The results obtained are compared with calculations carried out in the impulse approximation.

*E IN GEV,1.2,1.36

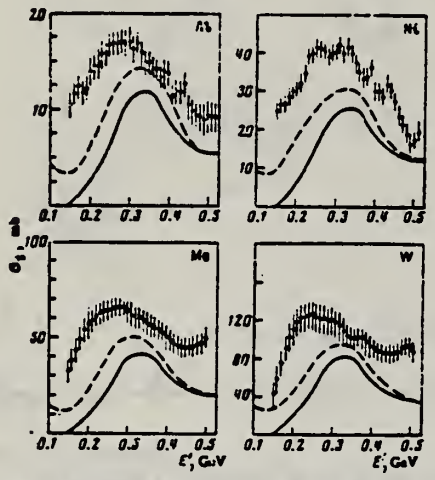

FIG. 5. Total hadronic cross sections for absorption of photons by nuclei.

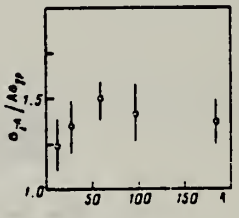

FIG. 6. The ratio $\sigma_{\gamma A}/A\sigma_{\gamma p}$ as a function of A for $k = 0.32$ GeV.

A. Järund and B. Forkman
Z. Physik A281, 39 (1977)

						Mo		42
						REF. NO.		
						77 Ja 2		egf
REACTION	RESULT	EXCITATION ENERGY	SOURCE		DETECTOR		ANGLE	
			TYPE	RANGE	TYPE	RANGE		
G,NA24	ABY	THR-999	C	400-999	ACT-I		4PI	

999=1 GEV

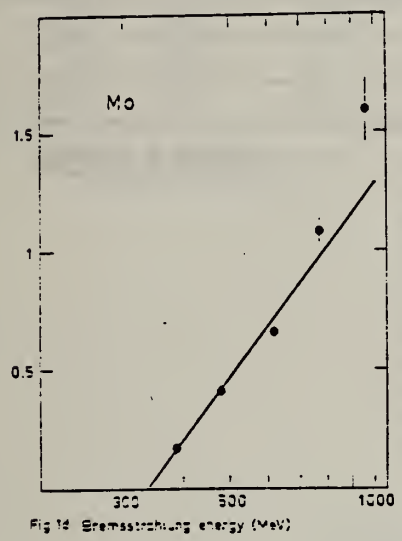

Fig 1d Bremsstrahlung energy (MeV)

Fig. 1a–j. The measured yield as a function of bremsstrahlung end point energy. The error bars give the statistical errors in the numbers of γ-quanta detected. The solid lines are fitted to the yield points with the least-squares method. The yield from Cu (Fig. 1a) is measured in [1] and has been recalculated using the monitor curve of [3]

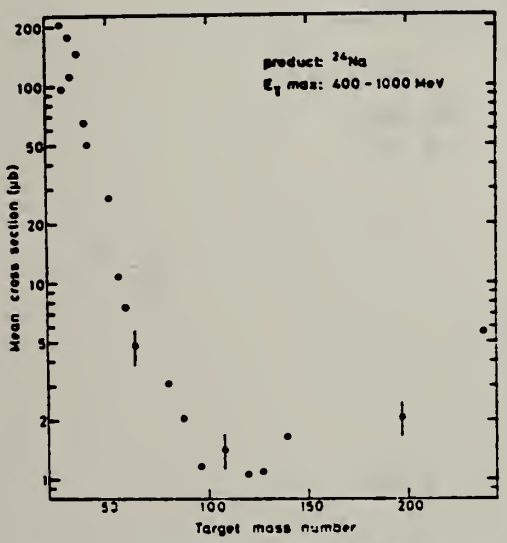

Fig. 2. The mean cross section in the energy range 400 to 1000 MeV calculated from the yields of Figure 1 in this work and of Figures 1 to 6 in [3]. The error is given by bars in some points

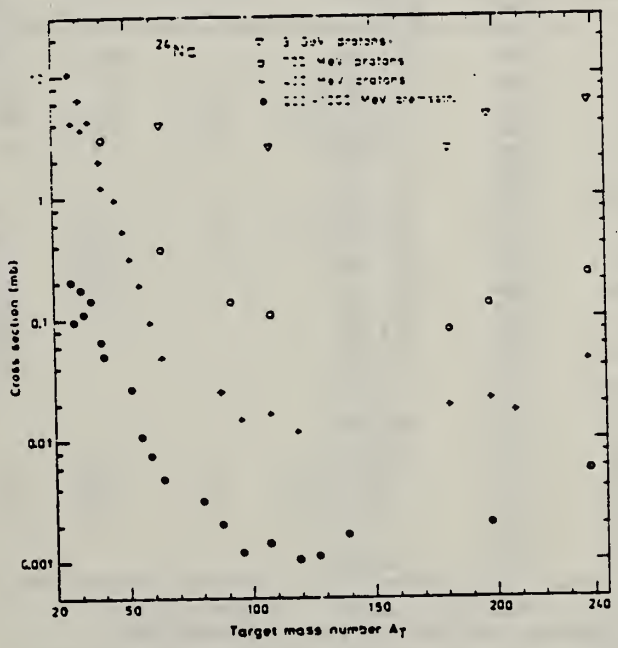

Fig. 4. Mean cross sections of the present work and of [1] (●) compared with the cross sections in proton irradiations: + 400 MeV from [4], ○ 700 MeV from [16] and an extrapolated value from [17], ▽ 3 GeV from [18]

REF. M. Schumacher, F. Smend, W. Mückenheim, P. Rullhusen, H.G. Börner
Z. Phys. A300, 193 (1981)

EL EM. SYM.	A	Z
Mo		42

METHOD

REF. NO. 81 Sc 6 egf

REACTION	RESULT	EXCITATION ENERGY	SOURCE TYPE	SOURCE RANGE	DETECTOR TYPE	DETECTOR RANGE	ANGLE
G,G	ABX	7.7		7.7	SCD-D		90

6.759,7.168 MEV

Elastic scattering by nuclei in the range of mass numbers between 64 and 238 has been studied with monochromatic photons in the energy range between 2 and 8 MeV. These photons were provided either by a Ti(n,γ) source installed in the tangential through channel of the Grenoble high flux reactor, or by ^{24}Na and ^{56}Co sources produced by deuteron bombardment of Al or Fe at the Göttingen cyclotron. The photoexcitation of 23 nuclear levels has been observed and the decay properties and groundstate widths of the majority of these levels have been determined. For the lead scattering target the coherent elastic differential cross section has been studied in detail. There is evidence that below the photo-neutron threshold the elastic scattering via virtual photoexcitation of the nucleus can be approximated by extrapolating the real part of the Giant Dipole Resonance amplitude along a Lorentzian curve. Coulomb corrections to Delbrück scattering seem to play a small role at 6.5 MeV.

Table 4. Properties of levels observed by photoexcitation. $(d\sigma/d\Omega)^{NRF}$: experimental differential cross section per identified isotope or element for resonance scattering through $\Theta = 90°$. I^π: spin-parity of excited level; $W(\Theta)$: angular correlation function; $g = (2I_{ex}+1)/(2I_g+1)$; Γ_0: radiative groundstate transition width, Γ: total level width. Errors in the last digits are given in parentheses

Isotope	E_γ (MeV)	$(d\sigma/d\Omega)^{NRF}$ (μb/sr)	I^π	Γ_0/Γ [a]	$W(\Theta)g\Gamma_0^2/\Gamma$ (meV)	Γ_0^f (meV)	Γ_0^g (meV)
^{238}U	2.754	13 (4)	(1)	0.77	0.145	0.084	-
^{238}U	3.254	421 (5)	1^-	0.24	0.83	1.5	0.52(15)[d]
^{209}Bi	6.555	2.1 (4)·10^2	-	-	0.74	0.74[b]	-
^{209}Bi	7.168	1.7 (3)·10^5	9/2^{-}[a]	1.00	710	786	820 (40)[a]
^{203}Tl	6.418	8.75(30)·10^3	1/2[a]	0.28	30	102	82 (15)[a]
Tl	6.759	7 (3)	-	-	-	-	-
Hg	6.555	68 (17)	-	-	-	-	-
^{186}W	6.418	5.2 (3)·10^2	1^-[a]	0.32	1.75	2.4	-
^{184}W	6.555	9.8 (10)·10^2	(1)	0.52	3.44	2.9	-
^{184}W	6.759	46 (10)	(1)	0.58	0.17	0.13	-
^{181}Ta	3.010	174 (17)	-	0.72	0.42	0.59	-
^{181}Ta	6.418	62 (4)	-	0.73	0.2	0.27[c]	-
^{181}Ta	6.759	4.8 (12)	-	-	0.018	0.018[b]	-
^{165}Ho	6.418	10.3 (30)	-	-	0.035	0.035[b]	-
^{165}Ho	6.759	5.6 (14)	-	-	0.021	0.021[b]	-
Nd	2.754	2.6 (5)	-	-	-	-	-
Nd	3.254	14.0 (10)	-	-	-	-	-
Ce	6.759	13.4 (10)	-	-	-	-	-
^{121}Sb	3.452	2.20 (5)·10^3	-	0.60	2.9	4.9[b]	-
^{100}Mo	6.418	1.53 (4)·10^4	1^-[a]	0.88	52	26	25 (8)[a]
^{94}Mo	6.555	4.4 (4)·10^3	(1)	0.33	15	21	-
Mo	6.759	6.2 (15)	-	-	-	-	-
Mo	7.168	8.2 (26)·10^2	-	-	-	-	-

[a] [11] [b] $W(\Theta)g\Gamma_0/\Gamma = 1$ assumed [c] $W(\Theta)g = 1$ assumed
[d] [28] (a small correction has been applied to the data of [28])
[e] Upper limits in case not all the transitions to lower levels were observed
[f] Present work [g] Previous work

(OVER)

Table 2. Elastic differential cross sections $d\sigma/d\Omega(\Theta=90°)$ in μb/sr measured with the Ti(n,γ) source and compared with theoretical predictions. n: predicted number of levels in a $\Delta E=25$ eV interval at 6.5 MeV. Errors in the last digits are given in parentheses

Scattering target	6.418 MeV		6.555 MeV		6.759 MeV		7.168 MeV		n
	exp.	th.	exp.	th.	exp.	th.	exp.	th.	
^{238}U	23 (12)	10.3	-	-	-	-	-	-	45
^{209}Bi	-	-	219(39)[b,c]	8.0	12 (4)	7.4	$1.5(3)\cdot10^{5}$[b,c]	5.7	0.1
^{nat}Pb	7.0(15)	8.6	-	-	6.5(11)	7.4	-	-	0.05
^{nat}Tl	2,586 (92)[a,c]	7.5	-	-	13 (3)[b]	6.0	-	-	0.4
^{nat}Hg	12 (3)	7.8	74(17)[b]	6.5	6.7(15)	6.4	-	-	3.4
^{nat}W	159 (10)[a,c]	6.6	306(33)[a,c]	6.3	20 (2)[a,c]	5.6	-	-	13
^{181}Ta	68 (4)[a,c]	6.3	-	-	10.1(12)[b,c]	5.3	-	-	28
^{165}Ho	15 (3)[b]	4.7	-	-	9.5(14)[b]	3.9	-	-	18
^{nat}Ce	4.1(21)	4.1	-	-	17 (1)[b,c]	3.6	-	-	0.04
^{nat}Sn	4.2(13)	3.0	-	-	2.5 (5)	2.7	-	-	1.9
^{nat}Mo	1,474 (44)[a,c]	2.5	407(39)[a,c]	2.5	8.5(15)[b,c]	2.3	817(258)[b,c]	2.0	0.5
^{nat}Zn	2.4 (8)	1.6	-	-	1.8 (5)	1.5	-	-	0.3

[a] Transitions to excited states observed
[b] Photoexcitation identified from size of differential cross section
[c] Photoexcitation reported in [11]

^{92}Nb

A=92

^{92}Nb

A=92

^{92}Nb

A=92

REF. A. El Sioufi, P. Erdos and P. Stoll
Helv. Phys. Acta 30, 265 (1957)

ELEM. SYM.	A	Z
Mo	92	42

METHOD

REF. NO. 57 El 1 egf

REACTION	RESULT	EXCITATION ENERGY	SOURCE		DETECTOR		ANGLE
			TYPE	RANGE	TYPE	RANGE	
G,NP	ABI	19- 30	C	32	ACT-I		4PI

Tabelle 1.
Zusammenstellung der gem. W. Q.

Reaktion	Q-Wert MeV	MeV barn	Verhältnis der Querschnitte
$Zn^{66}(\gamma, np)Cu^{64*)}$	18,65	0,02	$\frac{\sigma_{Zn^{66}(\gamma, p)}}{\sigma_{Zn^{66}(\gamma, np)}} = 3,6 \pm 0,5$
$Zn^{66}(\gamma, p)Cu^{67**)}$	10,01	0,08	
$Zn^{64}(\gamma, 2n)Zn^{62}$	20,82	0,08	$\frac{\sigma_{Zn^{66}(\gamma, np)}}{\sigma_{Zn^{64}(\gamma, 2n)}} = 0,25$
$Mo^{92}(\gamma, np)Nb^{90}$	19,5	0,02	
$Mo^{98}(\gamma, p)Nb^{97}$		0,09	$\frac{\sigma_{Mo^{98}(\gamma, p)}}{\sigma_{Mo^{92}(\gamma, np)}} = 4,5$

*) σ_{max}: 5,3 mb bei $E_\gamma = 27 \pm 0,5$ MeV $\Gamma = 3,7$ MeV.
**) σ_{max}: 11,5 mb bei $E_\gamma = 22 \pm 0,5$ MeV $\Gamma = 6,4$ MeV.

REF.

A. Hofmann, P. Stoll
Helv. Phys. Acta 31, 591 (1958)

ELEM. SYM.	A	Z
Mo	92	42

METHOD

REF. NO.	
58 Ho 1	egf

REACTION	RESULT	EXCITATION ENERGY	SOURCE		DETECTOR		ANGLE
			TYPE	RANGE	TYPE	RANGE	
G,NP	ABI	19- 32	C	32	ACT-I		4PI

(γ,np) yields include (γ,d).

Tabelle I

Reaktion	Q-Wert MeV	I.W.Q. $\bar{\sigma}$ MeV barn	σ_{max} mb	E_{max} MeV	Γ MeV
$Ca^{40}(\gamma, pn)\ K^{39}$	− 24,3	0,005	2,4	30 ± 1	2,1
$Zn^{64}(\gamma, pn)\ Cu^{63}$	− 18,36	0,03			
$Zn^{66}(\gamma, pn)\ Cu^{65}$	− 18,65	0,031	7,2	28 ± 1	4
$Zn^{68}(\gamma, p)\ Cu^{67}$	− 10,01	0,19	11,4	22,7 ± 1	6
$Sc^{80}(\gamma, pn)\ As^{74}$	− 20,43	0,02			
$Zn^{64}(\gamma, 2n)\ Zn^{62}$	− 20,82	0,08			
$Mo^{92}(\gamma, pn)\ Nb^{90}$	− 19,5	0,02			
$Sb^{122}(\gamma, pn)Sn^{121}$	− 18,2	0,0006			

Ref. N. Mutsuro, Y. Ohnuki, K. Sato, M. Kimura
J. Phys. Soc. Japan 14, 1649 (1959)

Elem. Sym.	A	Z
Mo	92	42

Method: Betatron; neutron yield; radioactivity; r-chamber

Ref. No.: 59 Mu 2 | NVB

Reaction	E or ΔE	E_0	Γ	$\int \sigma dE$	Jπ	Notes
$Mo^{92}(\gamma,n)$	Bremss. 0-25	16.0	2.7 MeV	1.48 MeV-b		

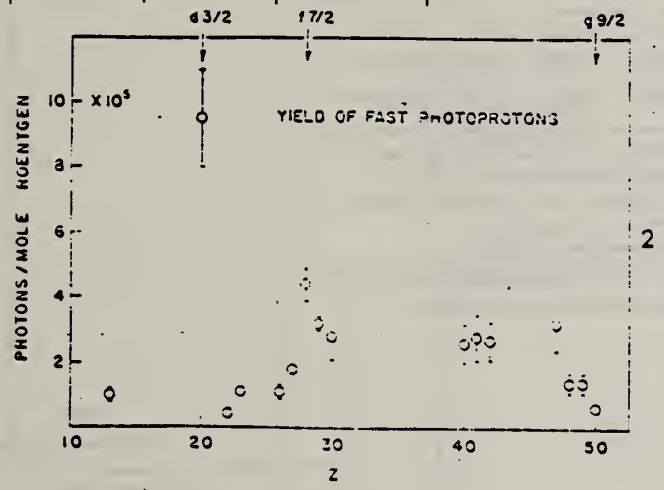

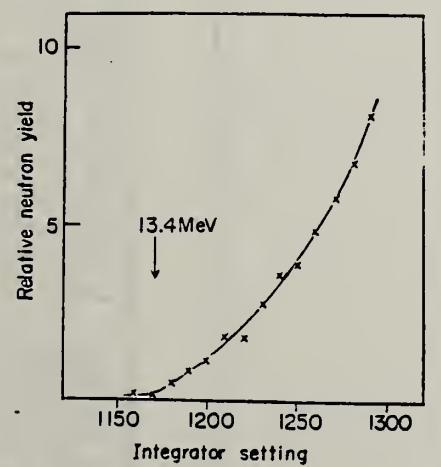

Fig. 3-2. Activation curve near threshold for $Mo^{92}(\gamma, n)Mo^{91}$.

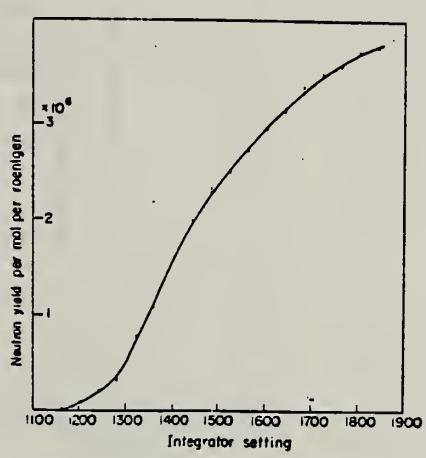

Fig. 4-2. Activation curve for $Mo^{92}(\gamma, n)Mo^{91}$.

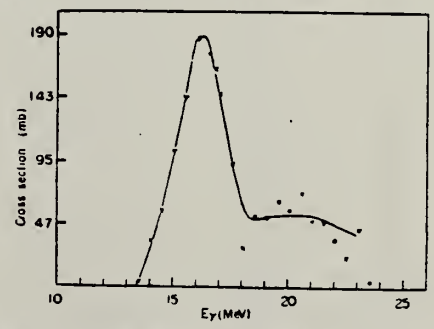

Fig. 5-2. Cross section curve for $Mo^{92}(\gamma, n)Mo^{91}$.

Ref. J.H. Carver, G.E. Coote, T.R. Sherwood
Nuclear Phys. 35, 449 (1962)

Elem. Sym.	A	Z
Mo	92	42

Method: 30 MeV electron synchrotron; activation; NaI

Ref. No.: 62 Ca 1 JHH

Reaction	E or ΔE	E_0	Γ	$\int \sigma dE$	Jπ	Notes
$Mo^{92}(\gamma,n)$	Bremss. 30					

REFERENCES

1) J. H. Huizenga and L. Vandenbosch, Phys. Rev. 120 (1960) 1305
2) T. Erlesom, Advances in Physics, 9 (1960) 425
3) D. L. Allan, Nuclear Physics 24 (1961) 274
4) C. T. Hibdon, Phys. Rev. 114 (1959) 179
5) C. T. Hibdon, Phys. Rev. 122 (1961) 1235
6) T. Erlesom, Nuclear Physics 11 (1959) 481
7) J. H. Carver and G. A. Jones, Nuclear Physics 19 (1960) 184
8) A. C. Douglas and H. Macdonald, Nuclear Physics 13 (1959) 382
9) T. Erlesom and V. M. Scrutinski, Nuclear Physics 8 (1958) 284
10) L. Katz, L. Peaco and E. Hoody, Can. J. Phys. 30 (1952) 476
11) L. Katz, E. G. Baker and E. Mantalbetti, Can. J. Phys. 31 (1953) 25
12) E. Silva and J. Goldemberg, An. Acad. Brasil Ciencs 28 (1956) 275
13) J. H. Carver and D. C. Peaslee, Phys. Rev. 120 (1960) 2155
14) J. M. Blatt and V. F. Weisskopf "Theoretical Nuclear Physics" New York: Wiley (1952)
15) M. M. Voguro, L. L. Marsden and R. L. Heath, U.S. Atomic Energy Commission Report IDO-16370 (1958)
16) Nuclear Data Sheets, National Research Council, Washington (1960, up to and including Set 5)
17) L. Vandenbosch and J. R. Huizenga, Phys. Rev. 120 (1960) 1313
18) E. Weigold and E. Glover, Nuclear Physics (in press)
19) K. J. Le Couteur and D. W. Lang, Nuclear Physics 13 (1959) 32
20) T. D. Newton, Can. J. Phys. 34 (1956) 804
21) D. W. Lang, Nuclear Physics 26 (1961) 434
22) M. E. Rose, "Internal Conversion Coefficients", Amsterdam: North Holland Publishing Co. (1958)
23) J. Goldemberg and L. Katz, Phys. Rev. 90 (1955) 308

TABLE 1

Isomeric Ratios from (γ,n) reactions

Target Nucleus	J_0	Residual Nucleus: Ground state Spin	Ground state Half-life	Metastable state Spin	Metastable state Half-life	Excited State Spin	Isomer ratio $Y_1/(Y_1+Y_2)$	Notes
Co^{59}	7/2⁻	Co^{58} 2⁺	71.3d	5⁺	9.2h		0.44 ± 0.02	5.2 ± 0.2
Ge^{76}	0⁺	Ge^{75} 1/2⁻	82m	7/2⁺	49s		0.48 ± 0.07	2.8 ± 0.5
Br^{81}	3/2⁻	Br^{80} 1⁺	18m	5⁻	4.4h	2⁻	0.52 ± 0.02	6.5 ± 1.0
Zr^{96}	0⁺	Zr^{95} 9/2⁺	64d	1/2⁻	70m	7/2⁺	0.36 ± 0.07	2.2 ± 0.4
Zr^{90}	0⁺	Zr^{89} 9/2⁺	77h	1/2⁻	4.4m		0.55 ± 0.10	2.8 ± 0.7
Se^{82}	0	Se^{81} 9/2⁺	15.7m	1/2⁻	56s		0.46 ± 0.04	6^{+4}_{-2}
Ag^{107}	1/2⁻	Ag^{106} 1⁺	24m	6	9.5d		0.04 ± 0.02	2.0 ± 0.3
In^{115}	9/2⁺	In^{112} 1⁺	14.5m	4⁺	20.7m	7⁻	0.8 ± 0.1	5.1 ± 0.7
Cd^{116}	0⁺	Cd^{115} 1/2⁺	53h	11/2⁻	43d		≤ 0.2	≤ 5
Ce^{140}	0⁺	Ce^{139} 5/2⁻	140d	11/2⁻	55s		0.08 ± 0.01	2.5 ± 0.2
Hg^{198}	0⁺	Hg^{197} 1/2⁻	65h	13/2⁺	24h	3/2⁻ 5/2⁻	0.05 ± 0.01	5.4 ± 0.5
Previous work								
Br^{81} [10]	3/2⁻	Br^{80} 1⁺	18m	5⁻	4.4h	2⁻	0.35	6.5
Se^{82} [12]	0⁺	Se^{81} 1/2⁻	18m	7/2⁺	57d		0.5	5.0
Zr^{90} [11]	0⁺	Zr^{89} 9/2⁺	79h	1/2⁻	4.5m		0.44 ± 0.06	4.5 ± 1
In^{115} [23]	9/2⁺	In^{114} 1⁻	72s	5⁺	50d	a ($T_{1/2}$ = 2.5h)	0.85	5.0

The yields, Y_1 and Y_2, are for (γ,n) reactions ending in the isomeric - or ground - state. The yield Y_1 is for the shortest-lived state.

Ref. W.E. Del Bianco, W.E. Stephens
Phys. Rev. 126, 709 (1962)

Elem. Sym.	A	Z
Mo	92	42

Method Electrostatic generator, $H^3(p,\gamma)He^4$ reaction; activation of positron emitter; 2 NaI in coincidence.

Ref. No. 62 De 1 JHH

Reaction	E or ΔE	E_o	Γ	$\int \sigma dE$	Jπ	Notes
(γ,n)	20.48					$\sigma(\gamma,n)$ = 35.4±2.3 mb (branch leaving Mo^{91} nucleus in ground state).

REF.
R. W. Gellie, K. H. Lokan
Nucl. Phys. 60, 343-348 (1964)

ELEM. SYM.	A	Z
Mo	92	42

METHOD
Betatron; ion chamber monitor

REF. NO.
64 Ge 1 JOC

	REACTION	RESULT	EXCITATION ENERGY	SOURCE TYPE	SOURCE RANGE	DETECTOR TYPE	DETECTOR RANGE	ANGLE
1)	G,N	ABX	THR - 22	C	THR -33	ACT-I		4 PI
2)	G,2N	ABX	THR - 33	C	THR -33	ACT-I		4 PI
3)	G,NP	ABX	THR - 33	C	THR -33	ACT-I		4 PI

2) MIXED WITH G,NP
3) MIXED WITH G,2N

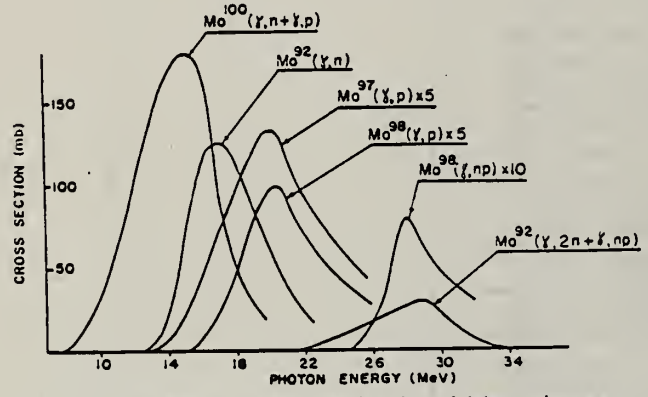

Fig. 2. Cross sections for photoreactions in molybdenum isotopes.

TABLE 2
Reaction parameters

Reaction	Peak energy (MeV)	$\int \sigma dE$ (MeV · mb)
$Mo^{100}(\gamma, n+\gamma, p)$	15	1110 ± 200
$Mo^{92}(\gamma, n)$	17	750 ± 70
$Mo^{97}(\gamma, p)$	20	215 ± 50
$Mo^{98}(\gamma, p)$	20	140 ± 15
$Mo^{98}(\gamma, np)$	28	30 ± 10
$Mo^{92}(\gamma, np+\gamma, 2n)$	29	160 ± 25

REF.
S. Costa, F. Ferrero, S. Ferroni, L. Pasquallini and E. Silva - also Istituto Nazionale di Fisica Nucleare - Sezione di Torino
Nuclear Phys. 72, 158 (1965)

ELEM. SYM.	A	Z
Mo	92	42

METHOD

REF. NO. 65 Co 1 EGF

REACTION	RESULT	EXCITATION ENERGY	SOURCE		DETECTOR		ANGLE
			TYPE	RANGE	TYPE	RANGE	
G,N	RLX	THR - 70	C	12 - 70	ACT-I		4PI

Measured isomer production ratio.
Spin cut off < 1.5

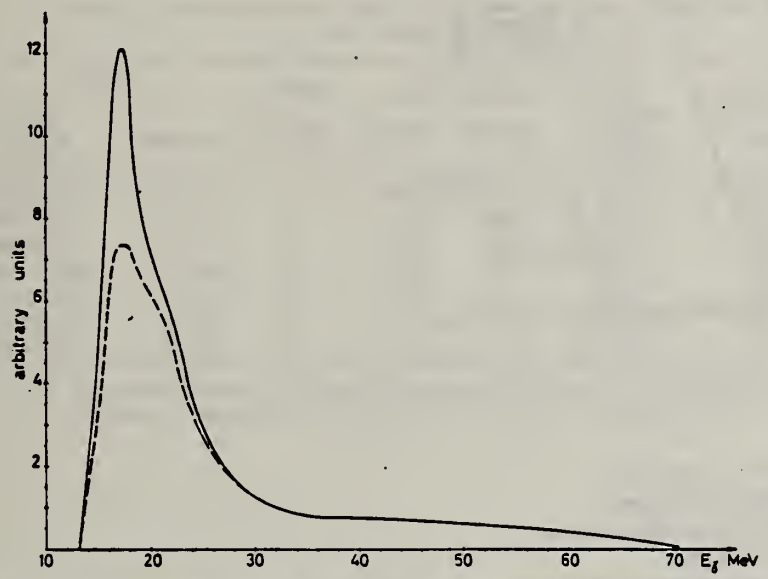

Fig. 3. (γ, n) reaction in ^{92}Mo, total (solid line) and $\frac{1}{2}^-$ state (dashed line) cross sections.

TABLE 1
Spins and half-lives of isomeric states

Target nucleus	Spin of isomeric states	Half-life	Modes of decay (used for detection)	Detection method
^{38}K	0+	0.95 sec	β^+ (100 %)	γ–γ fast-slow coincidence (resolving time 0.2 and 2 μsec)
$J = \frac{1}{2}$	3+	7.7 min	β^+ (> 99 %)	γ–γ coincidence
^{90}Zr	$\frac{1}{2}^-$	4.3 min	γ (93 %)	NaI (well type) spectrometer centered on the 0.588 MeV γ ray line
			β^+ (1.7 %)	γ–γ coincidence
$J = 0$	$\frac{1}{2}^+$	79 h	β^+ (30 %)	γ–γ coincidence
^{92}Mo	$\frac{1}{2}^-$	66 sec	γ (57 %)	NaI (well type) spectrometer centered on the 0.658 MeV γ ray line
			β^+ (38 %)	γ–γ coincidence
$J = 0$	$\frac{1}{2}^+$	16 min	β^+ (94 %)	γ–γ coincidence

R. W. Gellie
Aust. J. Phys. 21, 765 (1968)

Mo	92	42

METHOD

REF. NO. 68 Ge 1 egf

REACTION	RESULT	EXCITATION ENERGY	SOURCE		DETECTOR		ANGLE
			TYPE	RANGE	TYPE	RANGE	
G,N	ABX	12-26	C	THR-26	ACT-I		4PI

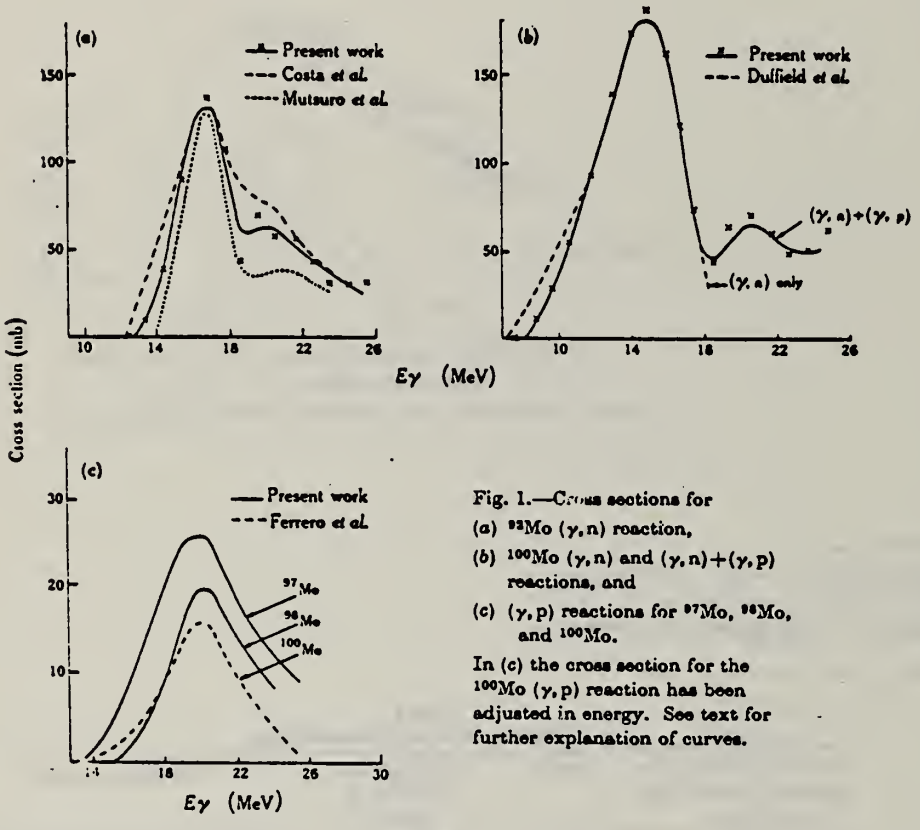

Fig. 1.—Cross sections for
(a) ^{92}Mo (γ, n) reaction,
(b) ^{100}Mo (γ, n) and (γ, n)+(γ, p) reactions, and
(c) (γ, p) reactions for ^{97}Mo, ^{98}Mo, and ^{100}Mo.
In (c) the cross section for the ^{100}Mo (γ, p) reaction has been adjusted in energy. See text for further explanation of curves.

REF. Y. Oka, T. Kato and A. Yamadera
Bull. Chem. Soc. Japan 41, 1606 (1968)

ELEM. SYM.	A	Z
Mo	92	42

METHOD

REF. NO. 68 Ok 2 egf

REACTION	RESULT	EXCITATION ENERGY	SOURCE		DETECTOR		ANGLE
			TYPE	RANGE	TYPE	RANGE	
G,N	ABY	THR-20	C	20	ACT-I		4PI

ISOMERIC YIELI

TABLE 1. THE PARTICULARS OF THE (γ,n) REACTION PRODUCTS AND THE DATA OBTAINED WITH 20 MeV BREMSSTRAHLUNG

Nuclide		Half-life of product (sec)	Gamma-ray determined			Limit of detection (μg)	Yield ($mol^{-1} \cdot R^{-1}$)
Parent (Natural abundance, %)	Residual		Energy (MeV)	Branching ratio (%)	Photopeak activity (cpm/mg)[a]		
^{24}Mg(78.60)	^{23}Mg	9.9	0.511	200	2.04×10^{6}	0.49	8.1×10^{4}
^{76}Ge(7.67)	^{73m}Ge	48	0.139	100	6.37×10^{5}	1.6	1.1×10^{4}
^{78}Se(23.52)	^{77m}Se	17	0.162	100	1.82×10^{6}	0.55	1.2×10^{6}
^{92}Mo(15.86)	^{91m}Mo	65	0.650	57	2.22×10^{5}	4.5	2.7×10^{6}
^{140}Ce(88.48)	^{139m}Ce	58	0.745	100	1.06×10^{6}	0.95	1.3×10^{6}
^{142}Nd(27.13)	^{141m}Nd	64	0.760	100	3.19×10^{5}	3.1	1.4×10^{6}
^{159}Tb(100)	^{158m}Tb	11	0.111	100	2.56×10^{5}	3.8	2.2×10^{6}

a) The value corrected at the end of one-minute irradiation with the dose rate of 10^{7} R/min; Counting geometry is 20% with a 3"dia.×3"NaI(Tl) detector.

REF.

K. Shoda, M. Sugawara, T. Saito & H. Miyase
PICNS-69 Proceedings of the Conference on Nuclear Isospin. Asilomar-Pacific Grove, California 1969 (Academic Press, New York & London 1969) p. 125.

ELEM. SYM.	A	Z
Mo	92	42

METHOD

REF. NO. 69 Sh 6 egf

REACTION	RESULT	EXCITATION ENERGY	SOURCE		DETECTOR		ANGLE
			TYPE	RANGE	TYPE	RANGE	
E,P	SPC	11-18	D	20	D	20	UKN

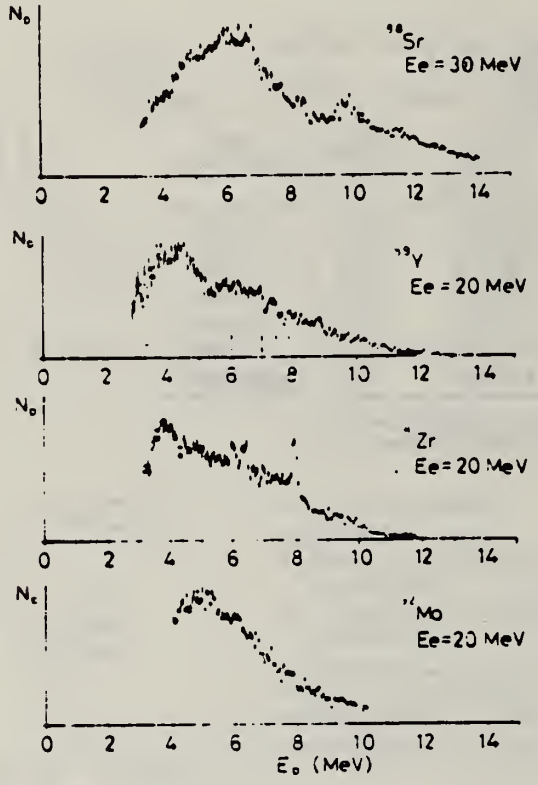

Fig. 1. Energy distributions of photoprotons. Vertical broken lines and solid lines indicate the position of p_0 corresponding to the ground IAS and electric dipole IAS (2^-_4) respectively.

REF.	ELEM. SYM.	A	Z
B.S. Ishkhanov, I.M. Kapitonov, E.V. Lazutin, I.M. Piskarev, and O.P. Shevchenko Yad. Fiz. 11, 702 (1970) Sov. J. Nucl. Phys. 11, 394 (1970)	Mo	92	42

METHOD	REF. NO.	
	70 Is 1	hmg

REACTION	RESULT	EXCITATION ENERGY	SOURCE		DETECTOR		ANGLE
			TYPE	RANGE	TYPE	RANGE	
G,XN	ABX	THR-30	C	THR-30	BF3-I		4PI

We used the 35-MeV betatron of our institute to investigate photoneutron reactions on the isotopes Mo^{92} and Mo^{98}. The yield curves of the reactions (γ, Tn) were measured in the energy range from 7 to 30 MeV in steps of 100 keV. The targets were prepared from metallic Mo. The content of the investigated isotopes was not less than 97%. The use of a highly efficient neutron detector ($\epsilon \approx 45\%$) and of a multichannel method of measurements has made it possible to obtain the yield curves with high accuracy (0.1% in the region 25–30 MeV) and to observe, for the first time, the intermediate structure of the giant resonance on the isotopes of Mo. The statistical reduction of the experimental information and the determination of the cross sections of the photoneutron reactions was carried out in accordance with a program prepared by the Computational Center of the Moscow State University[1].

The obtained cross section of the reactions $\sigma(\gamma, Tn) = \sigma(\gamma, n) + 2\sigma(\gamma, 2n) + \sigma(\gamma, np)$ are shown in the figure, from which it is seen that approximately 15 resonances are observed in each cross section.

The widths of the giant resonances in the reaction (γ, Tn) on Mo^{92} and Mo^{98} are 5 and 7 MeV respectively (curves a in the figure). After taking into account the multiplicity in accordance with the data of[2] for this region of nuclei, the cross sections obtained were $\sigma_n = \sigma(\gamma, n) + \sigma(\gamma, 2n) + \sigma(\gamma, np)$ (curves b). The widths of these cross sections for Mo^{92} and Mo^{98} are the same and equal 5 MeV. The curves c correspond to the cross sections $\sigma(\gamma, n) + \sigma(\gamma, np)$. The widths for them are 5 and 3.5 MeV respectively for Mo^{92} and Mo^{98}.

The widths σ_n of the integral cross sections of the reactions for Mo^{92} and Mo^{98} are 1.29 ± 0.13 and 2.0 ± 0.2 MeV-b. The integral cross section σ_n increases with increasing N − Z for isotopes of a given element. It is interesting to note, however, that in the case of Mo the increase of σ_n and of the width of the giant resonance is due to the cross section of the reaction $(\gamma, 2n)$. Thus, for Mo^{92} we have $\sigma(\gamma, 2n) = 0.17$ ± 0.02 MeV-b, whereas for Mo^{98} we have $\sigma(\gamma, 2n)$ = 0.83 ± 0.08 MeV-b, i.e., the cross section of the reaction $(\gamma, 2n)$ increases by almost five times. Such a sharp increase of the cross section of the reaction $Mo^{98}(\gamma, 2n)$ is connected with the low threshold of the $(\gamma, 2n)$ reaction, namely $E^{thr}_{Mo^{98}}(\gamma, 2n) = 15.5$ MeV. For comparison, we point out that $E^{thr}_{Mo^{92}}(\gamma, 2n)$ = 22.8 MeV.

For the reaction $(\gamma, n) + (\gamma, np)$, the integral cross sections for Mo^{92} and Mo^{98} are respectively 1.12 ± 0.11 and 1.10 ± 0.11 MeV-b.

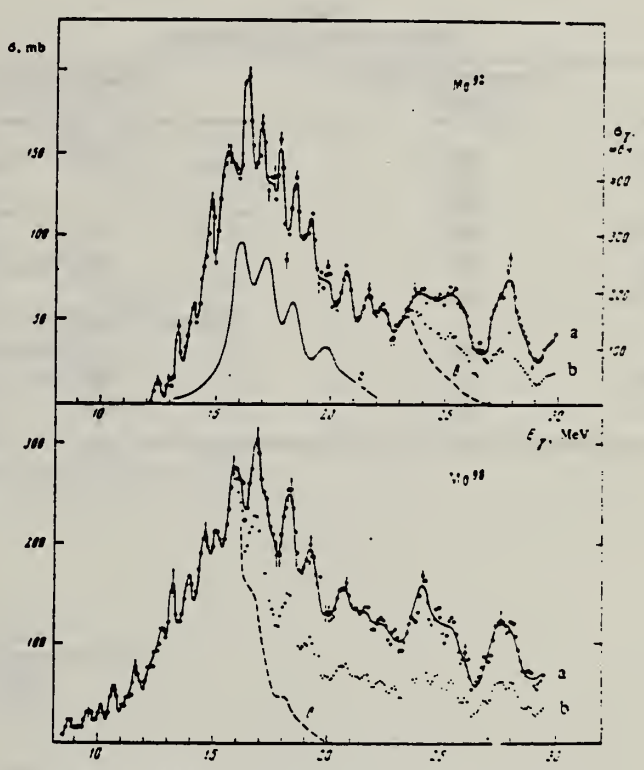

Effective cross sections for Mo^{92} and Mo^{98}: a – $\sigma(\gamma, Tn)$; b – $\sigma(\gamma, n) + \sigma(\gamma, 2n) + \sigma(\gamma, np)$; c – $\sigma(\gamma, n) + \sigma(\gamma, np)$; d – total-absorption cross section σ_γ, obtained in [4] for Mo^{94} (right-hand scale).

There are at present no published data on the structure of the photoneutron cross sections on the Mo isotopes. Such general characteristics of the giant resonance as the position and magnitude of the integral cross section are known only for the reaction $Mo^{92}(\gamma, n)$[3-5]. Even these results, however, are highly contradictory. Thus, data on the width of the giant resonance, obtained in[3], exceed the data of[4] by a factor of 2.

In conclusion, let us compare the experimental results obtained by us with the calculations performed on the basis of the collective dynamic theory[6]. The photodisintegration of the Mo^{94} was calculated within the framework of this theory, and the result is shown in the figure (curve d). We see that the theoretical calculation agrees only roughly with the experimental data. The experimentally measured cross sections re-

REF. W. B. Walters, J. R. Van Hise, W. L. Switzer, J. P. Hummel
Nucl. Phys. A157, 73 (1970)

ELEM. SYM.	A	Z
Mo	92	42

METHOD

REF. NO.	
70 Wa 3	egf

REACTION	RESULT	EXCITATION ENERGY	SOURCE		DETECTOR		ANGLE
			TYPE	RANGE	TYPE	RANGE	
G,2N	RLY	THR-305	C	150-305	ACT-I		4PI
G,PN	RLY	THR-305	C	150-305	ACT-I		4PI

TABLE 1
Summary of measured yield ratios

Target	Bremsstrahlung energy (MeV)	Measured yield ratio
natural Cr	150	$^{48}Cr/^{48}V = 0.043 \pm 0.002$
	250	0.047 ± 0.009
	305	0.042 ± 0.002
enriched ^{52}Cr	250	0.025 ± 0.005
natural Fe	250	$^{52}Fe/^{52}Mn = 0.037 \pm 0.003$
enriched ^{56}Fe	250	0.024 ± 0.005
		$^{52g}Mn/(^{52m}Mn + ^{52g}Mn) = 0.47 \pm 0.02$
natural Y	150	$^{87}Y/^{87m}Sr = 12.9 \pm 1.6$
natural Mo	150	$^{90}Mo/^{90}Nb = 0.41 \pm 0.05$
	280	0.49 ± 0.05

TABLE 2
Summary of experimental and theoretical ratios of $(\gamma, 2n)$ to (γ, pn) yields

Target isotope	Bremsstrahlung energy (MeV)	Experimental $(\gamma, 2n)/(\gamma, pn)$ yield ratio	Calculated $(\gamma, 2n)/(\gamma, pn)$ yield ratio
^{50}Cr	250	0.095 ± 0.025	0.14
^{54}Fe	250	0.10 ± 0.03	0.07
^{89}Y	150	7.4 ± 1.0	6.7
^{92}Mo	150	0.41 ± 0.05	0.15
	280	0.49 ± 0.05	0.16

REF.

P. E. Haustein and A. F. Voigt
J. inorg. nucl. Chem. 33, 289 (1971)

ELEM. SYM.	A	Z
Mo	92	42

METHOD

REF. NO.: 71 Ha 2 egf

REACTION	RESULT	EXCITATION ENERGY	SOURCE		DETECTOR		ANGLE
			TYPE	RANGE	TYPE	RANGE	
G,N	RLY	13-70	C	70	ACT-I		4PI

Isomer ratio = (yield to low spin state)/(yield to high spin state)

ISOMER RATIO

Table 2. Isomer ratio measurements for ^{92}Mo, ^{137}Ce, and ^{141}Nd

Reaction	Isomer ratio	I^π Target	I^π Ground state	I^π Isomer	Threshold (MeV)	$41A^{-1/3}$ (MeV)
^{92}Mo(γ, n)^{91}Mo	1·92 ± 0·15	0$^+$	9/2$^+$	1/2$^-$	13·13	16·60
^{92}Mo($\gamma, 3n$)^{89}Mo	1·59 ± 0·16	0$^+$			30·72	16·52
^{138}Ce(γ, n)^{137}Ce	3·1	0$^+$	3/2$^+$	11/2$^+$	10·31	15·30
^{140}Ce($\gamma, 3n$)^{137}Ce	1·10 ± 0·12	0$^+$			26·34	15·26
^{142}Nd(γ, n)^{141}Nd	5·2 ± 0·3	0$^+$	3/2$^+$	11/2$^+$	9·79	15·22
^{144}Nd($\gamma, 3n$)^{141}Nd	1·80 ± 0·25	0$^+$			23·67	15·17

REF. Phan Xuan Ho, J.B. Bellicard, Ph. Leconte and I. Sick
PICNS-72, 125 (1972) Sendai

ELEM. SYM.	A	Z
Mo	92	42

METHOD

REF. NO. 72 Ho 6 hvm

REACTION	RESULT	EXCITATION ENERGY	SOURCE		DETECTOR		ANGLE
			TYPE	RANGE	TYPE	RANGE	
E,E/	ABX	1, 2	D	209	MAG-D		DST

1=1.51, 2=2.85 MEV

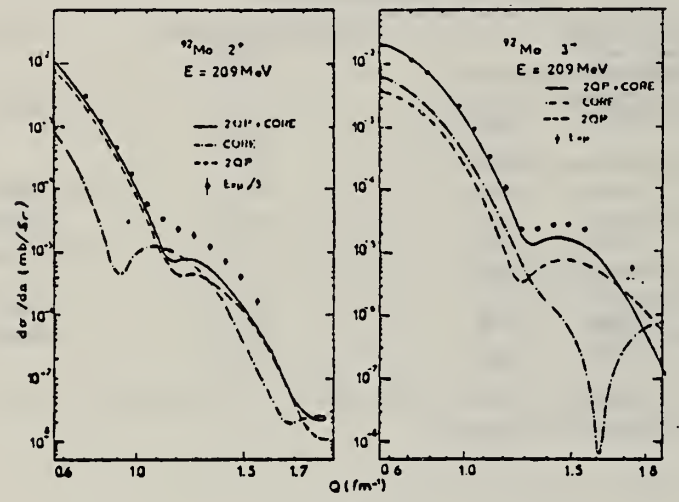

Fig. 5

REF.

Phan Xuan Ho, J. B. Bellicard, Ph. Leconte and I. Sick
J. Phys. (Paris) Colloq. 5, 167 (1972)

ELEM. SYM.	A	Z
Mo	92	42

METHOD

REF. NO. 72 Ho 10 egf

REACTION	RESULT	EXCITATION ENERGY	SOURCE		DETECTOR		ANGLE
			TYPE	RANGE	TYPE	RANGE	
E,E/	ABX	1, 2	D	209	MAG-D		DST

1.5, 2.85 MEV

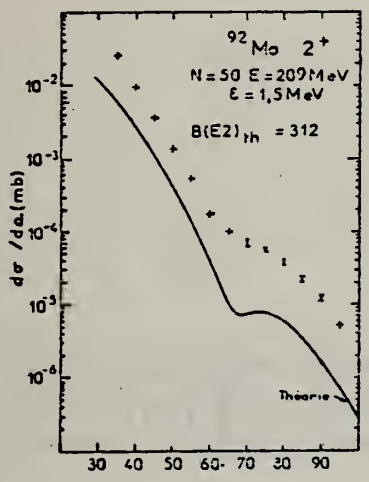

Fig. 1

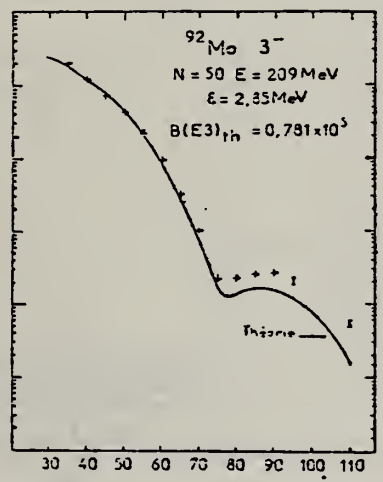

Fig. 2

REF. R. Bergere, H. Beil, P. Carlos, A. Lepretre, A. Veyssiere
PICNS-73, Vol. I, p. 525 Asilomar

ELEM. SYM.	A	Z
Mo	92	42

METHOD

REF. NO. 73 Be 10 hmg

REACTION	RESULT	EXCITATION ENERGY	SOURCE		DETECTOR		ANGLE
			TYPE	RANGE	TYPE	RANGE	
G,SN	ABX	12- 28	D	12- 28	BF3-I		4PI

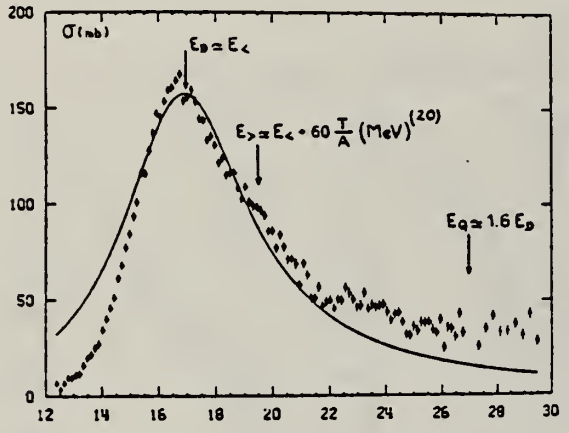

Fig. 14 Total $\sigma(\gamma,n) + \sigma(\gamma,pn) + \sigma(\gamma,2n)$ cross section of ^{92}Mo.

Table I

Isotopes	^{92}Mo	^{94}Mo	^{96}Mo	^{98}Mo	^{100}Mo
σ_{on}	0.83	0.98	1.08	1.11	1.08

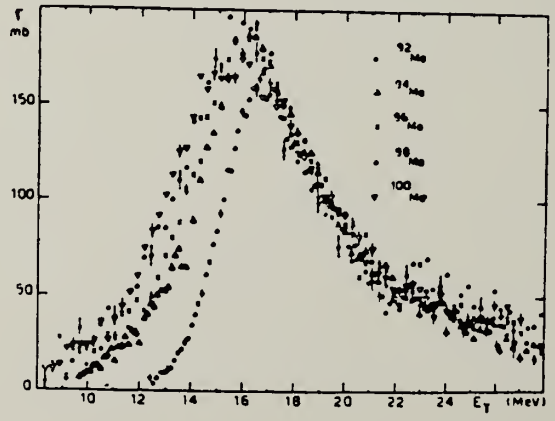

Fig. 15 Comparison of the total photoneutron cross sections of ^{92}Mo ^{94}Mo ^{96}Mo ^{98}Mo and ^{100}Mo

REF.	Phan Xuan Ho, J. Bellicard, Ph. Leconte, I. Sick Nucl. Phys. A210, 189 (1973)	ELEM. SYM.	A	Z
		Mo	92	42

METHOD	REF. NO.
	73 Ho 4 egf

REACTION	RESULT	EXCITATION ENERGY	SOURCE		DETECTOR		ANGLE
			TYPE	RANGE	TYPE	RANGE	
E,E/	FMF	1- 3	D	209	MAG-D		DST

1.51, 2.28, 2.85

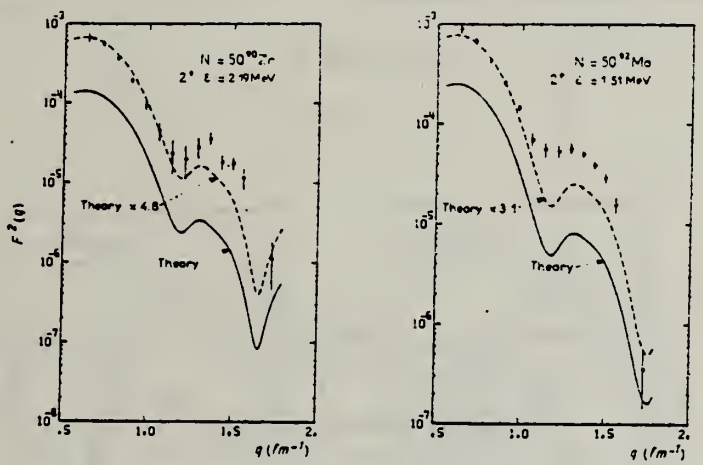

Fig. 5b. Squared inelastic form factor for 2^+ states of the $N = 50$ isotones.

TABLE 6

Inelastic cross sections for $E_e = 209$ MeV on ^{92}Mo

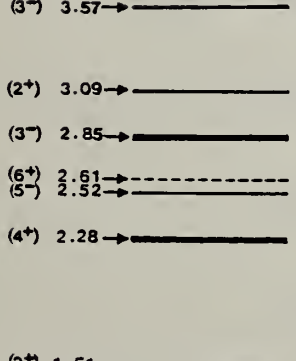

θ (deg.)	$(2^+)\varepsilon = 1.51$ MeV $d\sigma/d\Omega$(mb/sr)	$(3^-)\varepsilon = 2.85$ MeV $d\sigma/d\Omega$(mb/sr)	$(4^+)\varepsilon = 2.28$ MeV $d\sigma/d\Omega$(mb/sr)
35	0.209 E−1±0.220 E−2	0.197 E−1±0.220 E−2	
40	0.916 E−2±0.630 E−3	0.114 E−1±0.700 E−3	0.161 E−2±0.300 E−3
45	0.363 E−2±0.200 E−3	0.708 E−2±0.440 E−3	0.112 E−2±0.100 E−3
50	0.139 E−2±0.800 E−4	0.418 E−2±0.230 E−3	0.829 E−3±0.630 E−4
55	0.533 E−3±0.400 E−4	0.221 E−2±0.140 E−3	0.593 E−3±0.410 E−4
60	0.175 E−3±0.250 E−4	0.957 E−3±0.470 E−4	0.367 E−3±0.280 E−4
65	0.996 E−4±0.153 E−4	0.330 E−3±0.220 E−4	0.215 E−3±0.180 E−4
70	0.697 E−4±0.880 E−5	0.100 E−3±0.120 E−4	0.124 E−3±0.110 E−4
75	0.549 E−4±0.560 E−5	0.223 E−4±0.710 E−5	0.469 E−4±0.600 E−5
80	0.362 E−4±0.280 E−5	0.232 E−4±0.400 E−5	0.193 E−4±0.250 E−5
85	0.214 E−4±0.170 E−5	0.260 E−4±0.330 E−5	0.509 E−5±0.169 E−5
90	0.122 E−4±0.130 E−5	0.270 E−4±0.250 E−5	0.137 E−5±0.940 E−6
95	0.501 E−5±0.900 E−6	0.215 E−4±0.220 E−5	0.877 E−6±0.687 E−6
110	0.546 E−7±0.325 E−7	0.536 E−5±0.440 E−6	0.422 E−6±0.210 E−6

Energy level diagram given by ref. [24]). Levels excited in our experiment are shown with solid lines, dashed lines correspond to other levels. The experimental values are normalized with the elastic cross sections calculated by a phase shift program using a 3-parameter Gaussian model. The parameters ($c = 4.610$, $z = 2.520$, $w = 0.190$) are obtained from ref. [18]).

(over)

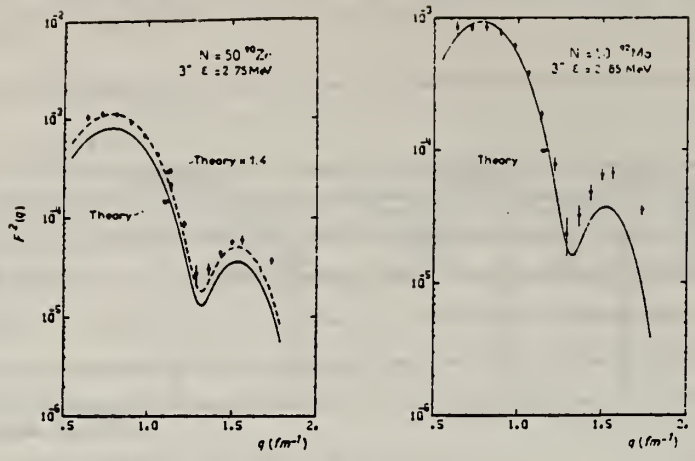

Fig. 6b. Squared inelastic form factor for 3^- states of the $N = 50$ isotones.

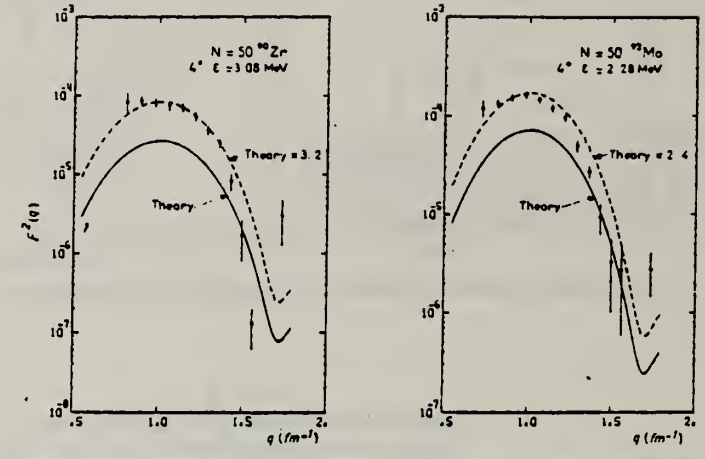

Fig. 7b. Squared inelastic form factor for 4^+ states of the $N = 50$ isotones.

[18] Phan-Xuan Ho, J. Bellicard, A. Bussiere, M. Priou, Nucl. Phys. A179 (1972) 529.

[24] Nuclear Data Sheets B (1970).

REF. H. Beil, R. Bergere, P. Carlos, A. Lepretre, A. De Miniac, and A. Veyssiere
Nucl. Phys. A227, 427 (1974)

ELEM. SYM.	A	Z
Mo	92	42

METHOD

REF. NO. 74 Be 3 egf

REACTION	RESULT	EXCITATION ENERGY	SOURCE TYPE	SOURCE RANGE	DETECTOR TYPE	DETECTOR RANGE	ANGLE
G,N *	ABX	12- 30	D	12- 30	BF3-I		4PI
G,2N **	ABX	22- 30	D	22- 30	BF3-I		4PI

* 693
** 694+

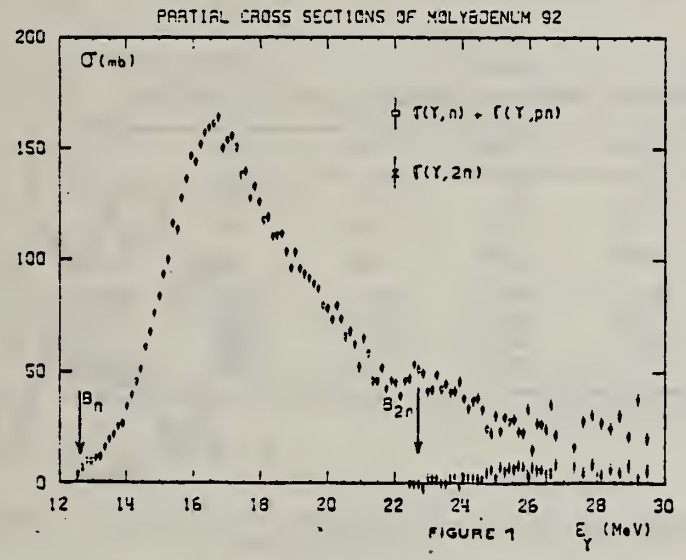

Fig. 1. Partial photoneutron cross sections $\sigma(\gamma, n)+\sigma(\gamma, pn)$ and $\sigma(\gamma, 2n)$ of ^{92}Mo. Arrows B_n and B_{2n} indicate theoretical threshold values for (γ, n) and $(\gamma, 2n)$ reactions respectively.

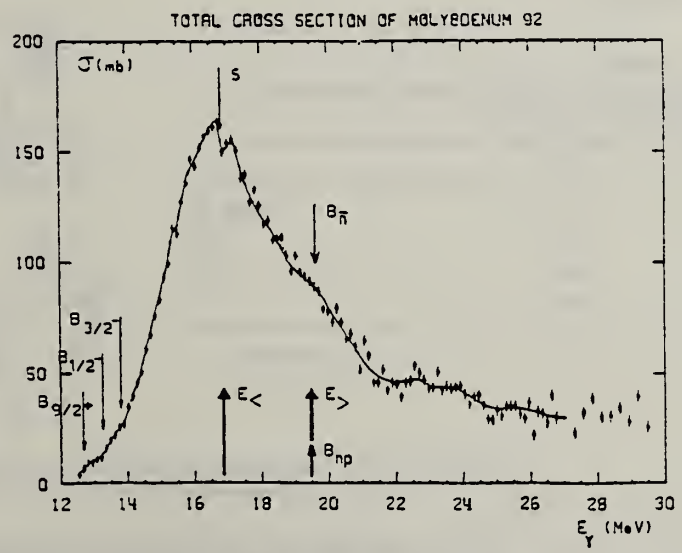

Fig. 7. Total photoneutron cross section $\sigma_{T,n}(E)$ of ^{92}Mo. The solid line is merely to guide the eye.

(over)

TABLE 3

Lorentz line parameters E_1, σ_1 and Γ_1 corresponding to the best single Lorentz line fits to the experimental $\sigma_{T,n}(E)$ curves shown in fig. 12

	E_1 (MeV)	σ_1 (mb)	Γ_1 (MeV)
^{92}Mo	16.9±0.1	154±10	5.4±0.2
^{94}Mo	16.4±0.1	184±10	5.7±0.2
^{96}Mo	16.2±0.1	184±10	6.3±0.2
^{98}Mo	15.8±0.1	189±15	6.0±0.2
^{100}Mo	15.7±0.1	170±10	7.9±0.2

TABLE 4

Integrated photoneutron cross sections and sum rules of the Mo isotopes

Nucleus	^{92}Mo	^{94}Mo	^{96}Mo	^{98}Mo	^{100}Mo
E_M (MeV)	29	29	29.5	29	28.5
σ_{0n} (MeV · b)	1.10	1.37	1.53	1.60	1.58
$\frac{\sigma_{0n}}{0.06\,NZA^{-1}}$	0.804	0.98	1.08	1.11	1.08
σ_{-1n} (mb)	60	79.3	89.2	95.4	95.4
$\sigma_{-1n}A^{-\frac{1}{3}}$ (mb)	0.145	0.186	0.203	0.211	0.206
σ_{-2n} (mb · MeV^{-1})	3.3	4.8	5.1	6.0	6.1
$\sigma_{-2n}A^{-\frac{1}{3}}$ (μb · MeV^{-1})	1.77	2.48	2.55	2.91	2.86

The notation used is defined in the text.

REF. K. Shoda, H. Miyase, M. Sugawara, T. Saito, S. Oikawa, A. Suzuki, J. Uegaki
Nucl. Phys. A239, 397 (1975)

ELEM. SYM.	A	Z
Mo	92	42

METHOD

REF. NO. 75 Sh 4 egf

REACTION	RESULT	EXCITATION ENERGY	SOURCE TYPE	SOURCE RANGE	DETECTOR TYPE	DETECTOR RANGE	ANGLE
E,P	ABX	14- 26	D	14- 25	MAG-D		90

El virtual photon spectrum used to obtain (γ,p) cross sections.

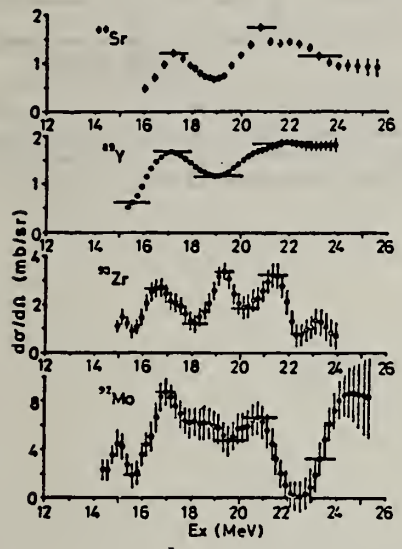

Fig. 3. Differential (γ, p) cross sections at $\theta = 90°$ analysed from (e, e'p) cross sections by the least structure method.

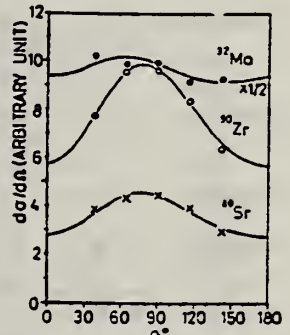

Fig. 4. Angular distributions of protons from the (e, e'p) reaction. The bombarding energies are 21.5, 22 and 20 MeV for ^{88}Sr, ^{90}Zr and ^{92}Mo respectively. The best fit curves obtained with eq. (7) are also shown.

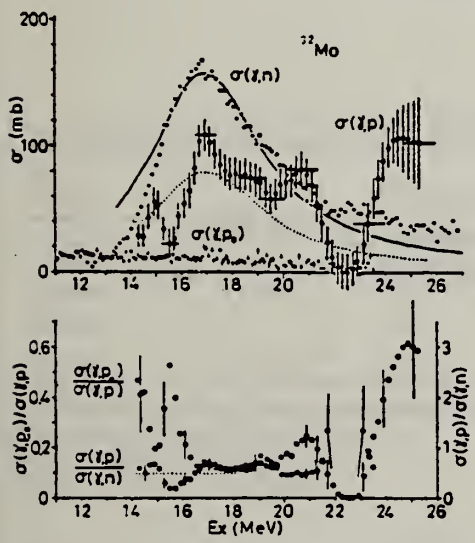

Fig. 8. The caption is the same as in fig. 5, but $\sigma(\gamma, p_0)$ is the present result while the plots and Lorentz line for the (γ, n) reaction are from ref. [22]).

Fig. 5. Upper figure: open circles, $\sigma(\gamma, p)$; closed circles, $\sigma(\gamma, n)$ [ref. [18])]; closed points, $\sigma(\gamma, p_0)$ [ref. [15])]; solid line, Lorentz line fit to the $T_<$ region of $\sigma(\gamma, n)$ [ref. [18])]; dotted line, Lorentz line fit to the $T_<$ region of $\sigma(\gamma, p)$ with Γ_i and E_R equal to those of $\sigma(\gamma, n)$. Lower figure: ratio between cross sections. Dotted line: constant for $\sigma(\gamma, p)/\sigma(\gamma, n)$ determined around $T_<$ GDR.

TABLE 2

The parameters of the angular distributions determined by the least-squares fits with $d\sigma/d\Omega = A[1 + B\sin^2\theta(1 + p\cos\theta)]$

	^{88}Sr	^{90}Zr	^{92}Mo
E_0 (MeV)	21.5	22	20
A *)	1	2.04	6.67
B	0.59	0.69	0.057
p	0.59	0.47	2.3

*) Relative value.

[15] K. Shoda et al., Nucl. Phys. A221 (1974) 125

[18] A. Lepretre et al., Nucl. Phys. A175 (1971) 609

FORM NBS-418 (REV. 7-14-64) USCOMM-NBS-DC

REF.

H. Bartsch, K. Huber, U. Kneissl, H. Krieger
Nucl. Phys. A256, 243 (1976)

ELEM. SYM.	A	Z
Mo	92	42

METHOD

REF. NO.: 76 Ba 1 egf

REACTION	RESULT	EXCITATION ENERGY	SOURCE TYPE	SOURCE RANGE	DETECTOR TYPE	DETECTOR RANGE	ANGLE
G,N	RLY	THR-UKN	C	UKN	SCD-D		4PI

ISOMER RATIO

TABLE 1
Experimental and theoretical results

Process	Target-spin	E_γ (keV)	$T_{\frac{1}{2}}$	Spin high	Spin low	$R_{exp} = \frac{\sigma_{high}}{\sigma_{low}}$	SCOP (ħ)
$^{181}Ta(\gamma, 3n)$	$\frac{7}{2}^+$	93	2.2 h 9.31 min 8.15 h	7^-	1^+	0.51 ±0.09	3.6 ±0.2
$^{142}Nd(\gamma, n)$	0^+	755 1100–1300, 145	63 s 2.5 h	$\frac{11}{2}^-$	$\frac{3}{2}^+$	0.055±0.006 0.19 ±0.01 [a]	2.20±0.06
$^{92}Mo(\gamma, n)$	0^+	652.9 1208, 1508, 1581, 1637	66 s 15.49 min	$\frac{1}{2}^+$	$\frac{1}{2}^-$	1.03 ±0.21 0.85 ±0.07 [b] 1.92 ±0.15 [a]	5.03±0.75 4^{+6}_{-2}
$^{100}Mo(\gamma, n)$	0^+	97.3 140.5	16.8 μs 66.02 h	$\frac{1}{2}^+$	$\frac{1}{2}^+$	0.85 ±0.24	1.72±0.25
$^{108}Pd(\gamma, n)$	0^+	214.5 115	22 s 850 ns	$\frac{11}{2}^-$	$\frac{1}{2}^+$	0.5 ±0.2	3.4 ±0.5
$^{110}Pd(\gamma, n)$	0^+	188 113 87.7	4.7 min 390 ns 13.47 h	$\frac{11}{2}^-$ $\frac{11}{2}^-$ $\frac{1}{2}^+$	$\frac{1}{2}^+$ $\frac{1}{2}^+$ $\frac{1}{2}^+$	0.11 ±0.02 0.41 ±0.09 3.2 ±0.7	3.14±0.15 3.0 ±0.25 3.3 ±0.4
$^{89}Y(\gamma, n)$	$\frac{1}{2}^-$	231.7 442.3 392.5	14.2 ms 300 μs	8^+	1^+	0.056±0.008	

[a]) Ref. [14]). [b]) Ref. [15]).

[14] P.E. Haustein et al., J. Inorg. Nucl. Chem. 33, 289 (1971)

[15] J.H. Carver et al., Nucl. Phys. 37, 449 (1962)

REF. F. R. Metzger
Phys. Rev. C15, 193 (1977)

ELEM. SYM.	A	Z
Mo	92	42

METHOD

REF. NO. 77 Me 2 hmg

REACTION	RESULT	EXCITATION ENERGY	SOURCE TYPE	SOURCE RANGE	DETECTOR TYPE	DETECTOR RANGE	ANGLE
G,G	LFT	1- 5	C	2- 6	SCD-D		DST
		(1.509-4.634)		(2.0-5.1)			

5 STATES 1.509-4.634

Levels in ^{92}Mo at 1.509 (2^+), 3.091 (2^+), 3.925 (2^+), 3.942, and 4.634 MeV have been excited by bremsstrahlung. Based on the angular distributions of the resonantly scattered γ lines, spin one can be unambiguously assigned to the 3.942- and 4.634-MeV levels. The lifetimes deduced from the scattering yields are compared with the results of two sets of Doppler shift attenuation experiments which had been analyzed using different theories for the attenuation factor $F(\tau)$.

TABLE II. Comparison of the lifetimes derived for the ^{92}Mo states from the resonance fluorescence experiments with DSAM results.

	Mean lifetimes (fs)		
		Doppler shift attenuation	
E_{Level}[a] (MeV)	Resonance fluorescence	Winterbon $F(\tau)$	Blaugrund $F(\tau)$
1.509	582 ± 37	520^{+120}_{-70} [b]	420^{+80}_{-60} [b]
3.091	46.3 ± 4.0	50^{+5}_{-4} [b]	31^{+3}_{-3} [c]
3.925	15.3 ± 3.6	24^{+23}_{-15} [b]	29^{+29}_{-17} [c]
3.942	16.5 ± 2.5	14^{+15}_{-4} [b]	30^{+29}_{-17} [c]

[a] Energies according to Ref. 3 (rounded off).
[b] Ref. 1.
[c] Ref. 3.

TABLE I. Properties of the ^{92}Mo levels excited with bremsstrahlung of energy ≤5.1 MeV.

E_{Level}[a] (MeV)	J^π	Γ_0/Γ	Γ_0^2/Γ (meV)	Γ_0 (meV)	Γ (meV)
1.509(1)	2^+	1	1.13 ± 0.07	1.13 ± 0.07	1.13 ± 0.07
3.092(2)	2^+	0.82(2) [b]	9.3 ± 0.6	11.3 ± 0.8	13.8 ± 1.2
3.925(2)	2^+	0.65(5) [b]	18 ± 3	28 ± 5	43 ± 10
3.944(2)	1^+	1 [b]	40 ± 6	40 ± 6 60 ± 20 [c]	40 ± 6
4.634(2)	1^+	0.59 ± 0.19 [d]	86 ± 13	145 ± 40 [c]	250 ± 110

[a] Energies deduced from the resonance fluorescence data.
[b] Combining the results of Refs. 3 and 10.
[c] From a self-absorption experiment.
[d] From a comparison of columns 4 and 5.

[1] R. Doerr, F. Rauch, et al., Proc. Int. Conf. on Nucl. Struc. and Spectroscopy, Amsterdam, 1974, ed. by H.P. Blok and A.E.L. Dieperink (Scholar's Press, Amsterdam, 1974), Vol.1, p.130.
[3] C.T. Papadopoulos et al., Nucl. Phys. A254, 93 (1975).
[10] R. Doerr et al., Jahresbericht 1973 (IKF-32), Inst. fur Kernphysik, Frankfurt/Main (unpublished) p.22.

REF. H. Bartsch, K. Huber, U. Kneissl and H. Krieger
Z. Physik A285, 273 (1978)

ELEM. SYM.	A	Z
Mo	92	42

METHOD

REF. NO. 78 Ba 11 | hmg 11/17/80

REACTION	RESULT	EXCITATION ENERGY	SOURCE		DETECTOR		ANGLE
			TYPE	RANGE	TYPE	RANGE	
G,NPG	LFT	*123(122.6)	C	20,40	SCD-D	---	135

*KeV, Isomer LFT

Short-lived isomers in the nuclei ^{90,92}Nb, ^{99}Mo, ^{98,100,101}Tc and ^{101}Ru populated in photonuclear reactions were studied by pulsed beam techniques. Energy and half-life of the γ-rays deexciting the isomeric levels were measured by recording energy-time spectra. The delayed γ-rays and K X-rays were detected by means of an intrinsic Ge-detector of high resolution. From the measured intensity ratios internal conversion coefficients were determined. The multipolarities of the isomeric transitions could be deduced in most cases. A classification of the observed isomers has been tried on the basis of the obtained experimental results and most recent literature data.

Table 1. Experimental results. E: energy, $T_{1/2}$: halflife, I_{rel}: relative intensity, L: multipolarity, H: hindrance factor

	Line	E [keV]	$T_{1/2}$ [μs]	$T_{1/2}$ [μs] (weighted average)	I_{rel}	α_K	Intensity ratios	L	H
^{90}Nb	K X-rays	–	–		1	–		–	–
	123	122.6±0.2	63 ±2		2.5	0.56±0.22		$E2$	120
^{92}Nb	K X-rays	–	–		1	–		–	–
	90	90.4±0.2	5.9 ±0.2		10.3	0.14±0.01		$E1$	$1.5\cdot10^7$
^{99}Mo	K X-rays	–	15.2 ±0.4	15.5 ±0.2	1	–		–	–
	98	97.8±0.1	15.6 ±0.2		0.95	1.45±0.27		$E2$	20
	138	137.7±0.2	0.79±0.09	0.76±0.06	1		$I_{450}/I_{138}=$	$M1$	–
	449	449.2±0.2	0.74±0.08		0.97		0.97±0.08	($M2$)	(37)
^{98}Tc	K X-rays	–	14.8 ±0.5	14.6 ±0.4	1			–	–
	22	21.8±0.2	16.4 ±2.7	from	0.036		$I_{43}/I_{22}=$	$E1+1\%\,M2$	10^7
	26	–	–	X, 43	–		5.1±0.5	($E2$)	–
	43	43.5±0.2	14.4 ±0.5		0.18			$M1$	–
^{100}Tc	K X-rays	–	8.2 ±0.7	8.2 ±0.3	1			–	–
	29	28.7±0.3	–	from	0.027		$I_{172}/I_{29}=$	$E2$	1
	172	172.3±0.3	8.2 ±0.3	X, 172	2.2		82±40	($M1$, $E2$)	–
^{101}Tc	K X-rays	–	–		1	–		–	–
	192	192.0±0.3	636 ±8		5.0	0.26±0.06		$M2$	560
^{101}Ru	K X-rays	–	16.1 ±3.9	17.5 ±0.4	1			–	–
	220	220.7±0.2	17.4 ±0.5	from	7.5		$I_{306}/I_{220}=$	$M2$	28
	306	306.6±0.3	17.7 ±0.6	220, 306	9.1		1.2±0.1	–	–

REF. K. Masumoto, T. Kato, N. Suzuki
Nucl. Inst. Meth. 157, 567 (1978)

ELEM. SYM.	A	Z
Mo	92	42

METHOD

REF. NO.	
78 Ma 10	hg

REACTION	RESULT	EXCITATION ENERGY	SOURCE		DETECTOR		ANGLE
			TYPE	RANGE	TYPE	RANGE	
G,2N	ABY	23-68	C	30-68	ACT - I		4PI

Analysis is made of reactions interfering with photon activation analysis procedures.

The activation yield curves have been presented for a number of photonuclear reactions in the energy range from 30 to 68 MeV, in order to evaluate quantitatively the interferences due to competing reactions in multielement photon activation analysis. The general features of the yields as functions of both target mass number and excitation energy were elucidated from the data obtained, discussion being given on the results in terms of the reaction mechanism.

Simultaneous neutron activation due to appreciable neutron production from the converter and surrounding materials has also been studied, and, finally, the magnitudes of interferences in real multielement analysis were given in the form of their energy dependences.

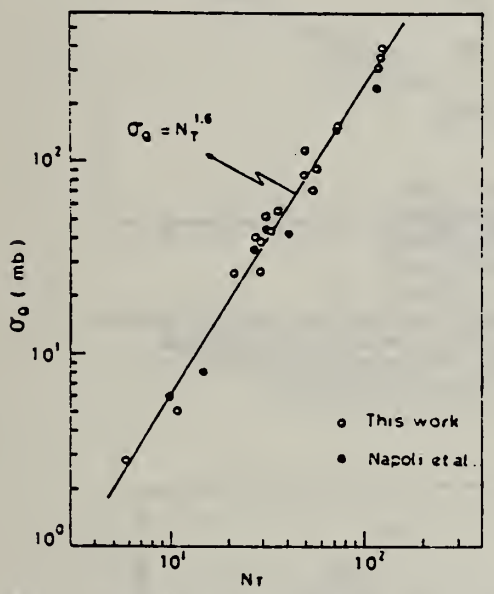

Fig. 2. Yield per equivalent quanta versus target neutron number.

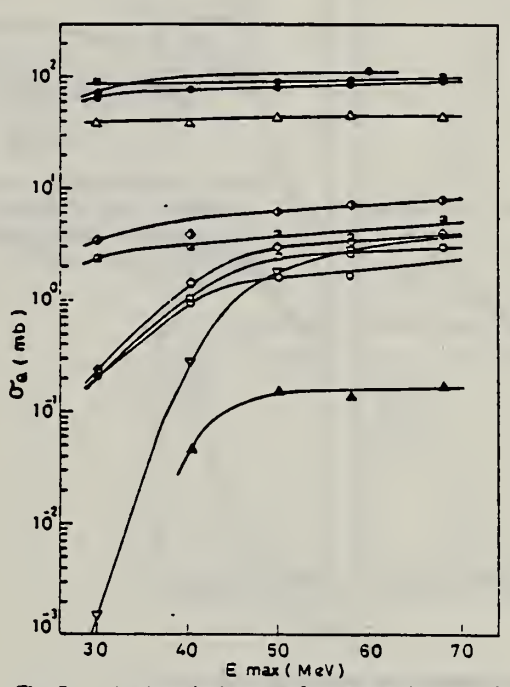

Fig. 7. Activation yield curves for the reactions on Y, Zr, Nb and Mo.
◆ $^{89}Y(\gamma, n)^{88}Y$, ● $^{90}Zr(\gamma, n)^{89}Zr$, ○ $^{90}Zr(\gamma, pn)^{88}Y$,
△ $^{93}Nb(\gamma, n)^{92m}Nb$, ▲ $^{93}Nb(\gamma, xn)^{88}Y$, ■ $^{100}Mo(\gamma, n)^{99}Mo$,
◈ $^{97}Mo(\gamma, p)^{96}Nb$, ◪ $^{96}Mo(\gamma, p)^{95m}Nb$, ◇ $^{94}Mo(\gamma, pn)^{92m}Nb$,
□ $^{92}Mo(\gamma, 2n)^{90}Mo$, ▽ $^{94}Mo(\gamma, xn)^{89}Zr$.

REF. J.J. Murphy, II, D.M. Skopik, J. Asai, and J. Uegaki
Phys. Rev. C 18, 736 (1978)

ELEM. SYM.	A	Z
Mo	92	42

METHOD

REF. NO. 78 Mu 9 hg

REACTION	RESULT	EXCITATION ENERGY	SOURCE		DETECTOR		ANGLE
			TYPE	RANGE	TYPE	RANGE	
E,A	ABX	5-100	D	100	MAG-D		DST

α particles from the electrodisintegration of seven nuclei with Z between 29 and 79 have been observed. Energy spectra at 50° in the laboratory for six nuclei and angular distributions for five nuclei are reported. The cross sections exhibit a broad peak whose magnitude decreases with increasing Z; the energy of the peak increases as Z increases. Angular distributions at the highest energies measured become increasingly forward peaked suggesting a direct-reaction process.

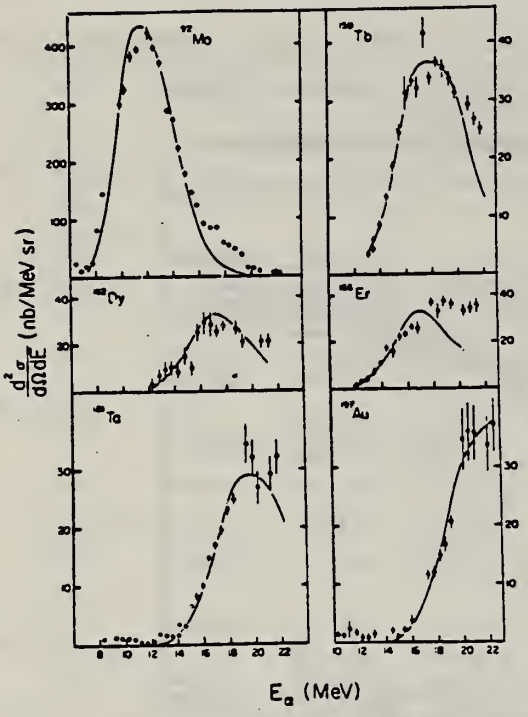

FIG. 2. The α-particle energy spectra at 50° in the laboratory for the four new nuclei studied as well as for two nuclei in which additional data have been obtained. The solid curves are the evaporation model fits described in text.

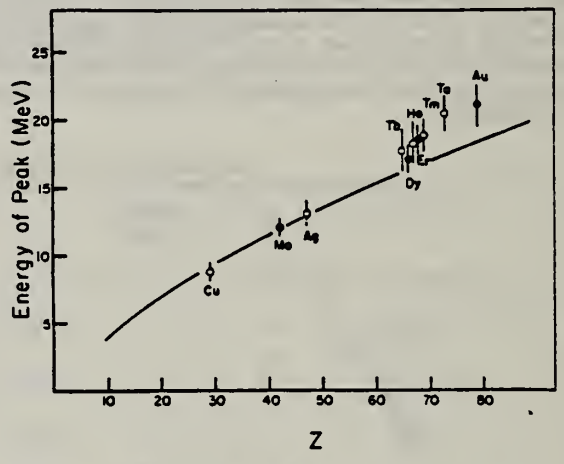

FIG. 3. Energy of the cross section peak as a function of Z. The solid line is the energy of the classical Coulomb barrier. The closed circles are the current work; the open circles are from Ref. 1.

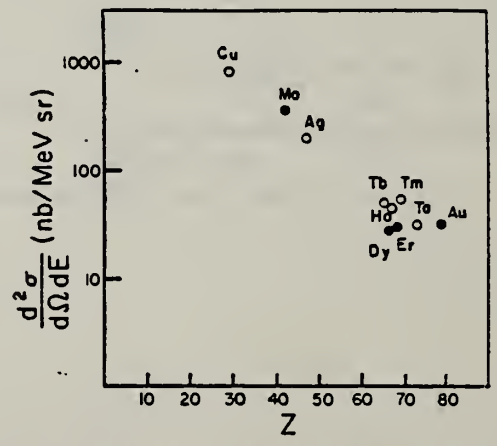

FIG. 4. Magnitude of cross section peak as a function of Z. The closed circles are the current work; the open circles are from Ref. 1.

over

[1] J.J. Murphy, II, H.J. Gehrhardt, and D.M. Skopik, Nucl. Phys. A277, 69 (1977)

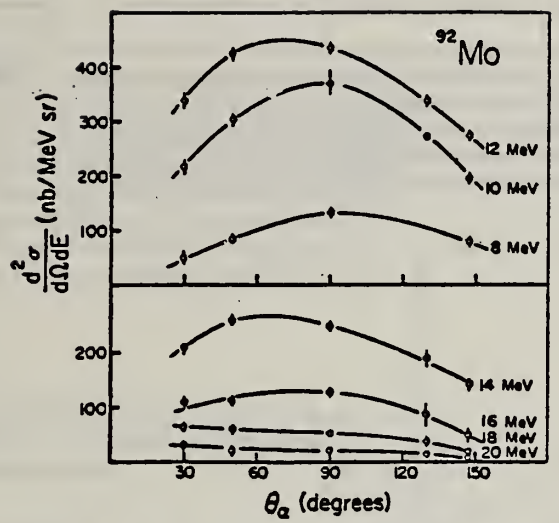

FIG. 5. Angular distributions for molybdenum. Errors are statistical; curves are to guide the eye. Increased forward peaking with increasing energy is taken as evidence for the importance of the direct process at higher energies.

REF. A. G. Flowers, D. Branford, J. C. McGeorge, A. C. Shotter, P. Thorley
C. H. Zimmerman, R. O. Owens, J. S. Pringle
Phys. Rev. Lett. 43, 323 (1979)

ELEM. SYM.	A	Z
Mo	92	42

METHOD

REF. NO. 79F12 hg

REACTION	RESULT	EXCITATION ENERGY	SOURCE		DETECTOR		ANGLE
			TYPE	RANGE	TYPE	RANGE	
E,A	SPC	UKN	D	120	MAG-D		30

This paper presents energy spectra of α particles emitted following the bombardment of ^{27}Al, ^{nat}Ni, ^{92}Mo, ^{94}Mo, and ^{197}Au with 120-MeV electrons, together with α-particle angular distributions from ^{197}Au and ^{nat}Ni for E_α = 30 and 50 MeV. The data are compared with preequilibrium exciton-model and statistical-model calculations. It is concluded that few-step processes are dominant in the production of α particles with energies above 20 MeV.

PREEQUILIB A EMISS

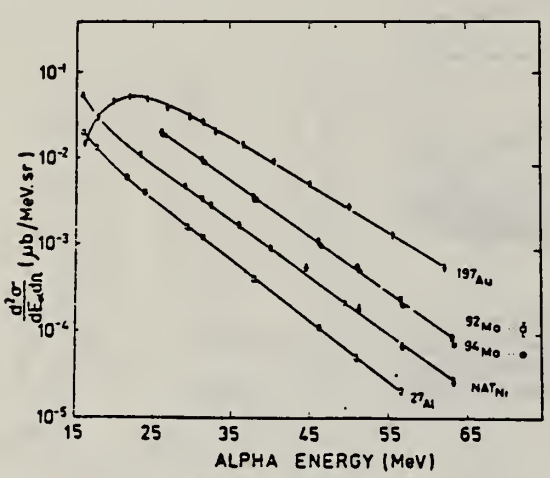

FIG. 1. α-particle energy spectra at θ_α = 30°, for E_e = 120 MeV. Errors shown are the sum of statistical and systematic contributions. The solid lines are a guide to the eye.

TABLE I. Temperatures corresponding to the preequilibrium component of the (e,α) reaction, derived from energy spectra at θ_α = 30° for E_e = 120 MeV.

Target	Temperature[a] (MeV)
^{27}Al	5.3
^{nat}Ni	5.5
^{68}Zn	5.4
^{92}Mo	5.6
^{94}Mo	5.4
^{197}Au	6.1

[a] Error is ± 0.2 MeV.

REF. T.J. Bowles, R.J. Holt, H.E. Jackson, R.M. Laszewski, R.D. McKeown, A.M. Nathan, J.R. Specht
Phys. Rev. C24, 1940 (1981)

ELEM. SYM.	A	Z
Mo	92	42

METHOD

REF. NO. 81 Bo 5 hg

REACTION	RESULT	EXCITATION ENERGY	SOURCE		DETECTOR		ANGLE
			TYPE	RANGE	TYPE	RANGE	
G,G	ABX	15-23	D	15-23	NAI-D		90

Quasimonochromatic photons have been used to measure elastic and inelastic photon scattering cross sections in the giant dipole resonance region of ^{52}Cr, Fe, ^{60}Ni, ^{92}Mo, and ^{96}Mo in an experiment in which the elastic and inelastic scattering are resolved. The elastic scattering cross sections show clear evidence for isospin splitting of the giant dipole resonance. The inelastic scattering to low-lying vibrational levels, which is a measure of the coupling between the giant dipole resonance and collective surface vibrations, is in qualitative agreement with the predictions of the dynamic collective model. However, when examined in detail, this model does not provide an adequate description of the scattering data.

[NUCLEAR REACTIONS ^{52}Cr, Fe, ^{60}Ni, ^{92,96}Mo (γ,γ'), $14 \leq E_\gamma \leq 22$ MeV; measured E_γ, $E_{\gamma'}$, $d\sigma/d\Omega$ for γ_0,γ_1. Compared to DCM predictions. Tagged photons.]

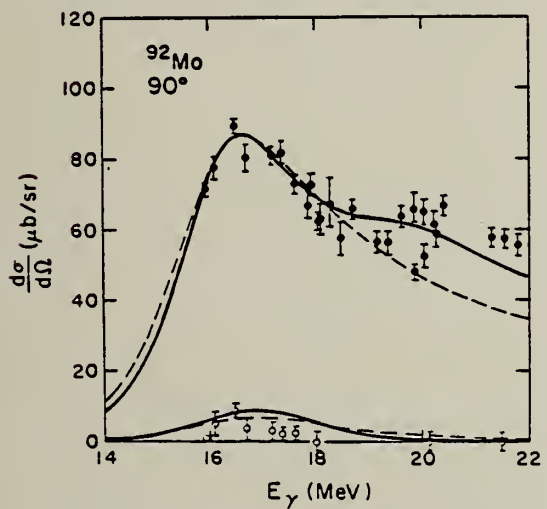

FIG. 5. Elastic (closed circles) and inelastic (open circles) scattering cross sections at $\theta = 90°$ on ^{92}Mo. The error bars represent statistical uncertainties only. The solid (dashed) lines are DCM calculations for the elastic and inelastic cross sections including (not including) the effect of isospin splitting.

REF. F.Z. Khien, N.K. Zui, N.T. An
Yad. Fiz. 35, 257 (1982)
Sov. J. Nucl. Phys. 35, 145 (1982)

ELEM. SYM.	A	Z
Mo	92	42

METHOD

REF. NO. 82 Kh 2 egf

REACTION	RESULT	EXCITATION ENERGY	SOURCE		DETECTOR		ANGLE
			TYPE	RANGE	TYPE	RANGE	
G,N	NOX	13-14	C	14	ACT-I		4PI

ISOMERIC RATIO

The method is developed for calculation of the isomeric ratio for the case of low excitation energy of the residual nucleus, and the isomeric ratio is measured in the $(n, 2n)$ and (γ, n) reactions in the neutron-deficient nuclei ^{92}Mo, ^{90}Zr, ^{86}Sr, and ^{74}Se. The good agreement between the experimental and theoretical results on the (γ, n) reaction has confirmed the reliability of the characteristics of the residual nuclei, the transmission coefficients of the emitted neutrons, etc., used in the calculations. From study of the $(n, 2n)$ reaction we have obtained values of the parameters of the spin dependence of the level density of the nucleus in the excitation-energy region ~14 MeV.

PACS numbers: 25.20. + y, 25.40.Gr, 27.50. + e, 27.60. + j

TABLE III. Isomeric ratio in the (γ, n) reaction.

Target nucleus	σ_{exp}	σ_{theor}	Published data[1]
^{92}Mo	1.54±0.15	1.36	1.82±0.15 (70) [9] 1.03±0.21 [10] 0.85±0.07 (30) [15]
^{90}Zr	1.52±0.04	1.49	0.50±0.15 (30) [15]
^{86}Sr	0.70±0.07	0.86	0.63±0.14 (30) [15]
^{74}Se	7.5±1.0	10.5[2] 8.8[3]	

[1] In parentheses we have given the values of the bremsstrahlung maximum energy.
[2] In the calculations we used the ^{73}Se level scheme of Ref. 2, $I_g = 7/2^+$ and $I_m = 1/2^-$.
[3] In the calculations we used the level scheme of ^{73}Se in Ref. 3, $I_g = 9/2^+$ and $I_m = 3/2^-$.

Mo
A=94

Mo
A=94

Mo
A=94

REF.

P. E. Haustein and A. F. Voigt
J. inorg. nucl. Chem. 33, 289 (1971)

ELEM. SYM.	A	Z
Mo	94	42

METHOD

REF. NO.	
71 Ha 2	egf

REACTION	RESULT	EXCITATION ENERGY	SOURCE		DETECTOR		ANGLE
			TYPE	RANGE	TYPE	RANGE	
G,3N	RLY	31-70	C	70	ACT-I		4PI

Isomer ratio = (yield to low spin state)/(yield to high spin state) ISOMER RATIO

Table 2. Isomer ratio measurements for ^{94}Mo, ^{137}Ce, and ^{141}Nd

Reaction	Isomer ratio	I^π Target	I^π Ground state	I^π Isomer	Threshold (MeV)	$41A^{-1/3}$ (MeV)
^{92}Mo(γ, n)^{91}Mo	1·92 ± 0·15	0⁺	9/2⁺	1/2⁻	13·13	16·60
^{94}Mo(γ, 3n)^{91}Mo	1·59 ± 0·16	0⁺			30·72	16·52
^{136}Ce(γ, n)^{135}Ce	3·1	0⁺	3/2⁺	11/2⁺	10·31	15·30
^{140}Ce(γ, 3n)^{137}Ce	1·10 ± 0·12	0⁺			26·34	15·26
^{142}Nd(γ, n)^{141}Nd	5·2 ± 0·3	0⁺	3/2⁺	11/2⁺	9·79	15·22
^{144}Nd(γ, 3n)^{141}Nd	1·80 ± 0·25	0⁺			23·67	15·17

REF. R. Bergere, H. Beil, P. Carlos, A. Lepretre, A. Veyssiere
PICNS-73, Vol.I, p.525 Asilomar

ELEM. SYM.	A	Z
Mo	94	42

METHOD

REF. NO. 73 Be 10 hmg

REACTION	RESULT	EXCITATION ENERGY	SOURCE		DETECTOR		ANGLE
			TYPE	RANGE	TYPE	RANGE	
G,SN	ABX	9- 28	D	9- 28	BF3-I		4PI

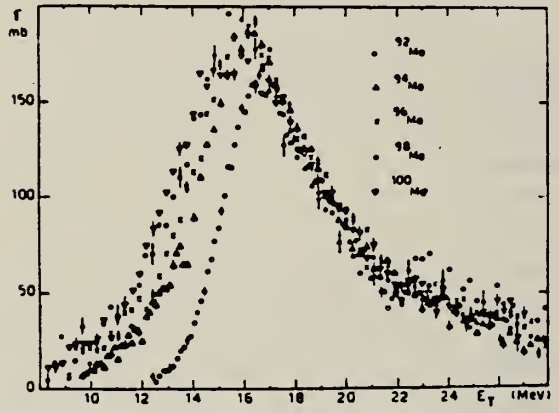

Fig. 15 Comparison of the total photoneutron cross sections of ^{92}Mo ^{94}Mo ^{96}Mo ^{98}Mo and ^{100}Mo

Table I

Isotopes	^{92}Mo	^{94}Mo	^{96}Mo	^{98}Mo	^{100}Mo
σ_{on}	0.83	0.98	1.08	1.11	1.08

REF.

H. Beil, R. Bergere, P. Carlos, A. Lepretre, A. De Miniac, and A. Veyssiere
Nucl. Phys. A227, 427 (1974)

EL EM. SYM.	A	Z
Mo	94	42

METHOD

REF. NO.: 74 Be 3 egf

REACTION	RESULT	EXCITATION ENERGY	SOURCE TYPE	SOURCE RANGE	DETECTOR TYPE	DETECTOR RANGE	ANGLE
* G,N	ABX	9- 28	D	9- 28	BF3-I		4PI
** G,2N	ABX	15- 28	D	15- 28	BF3-I		4PI
							* 696+
							**697+

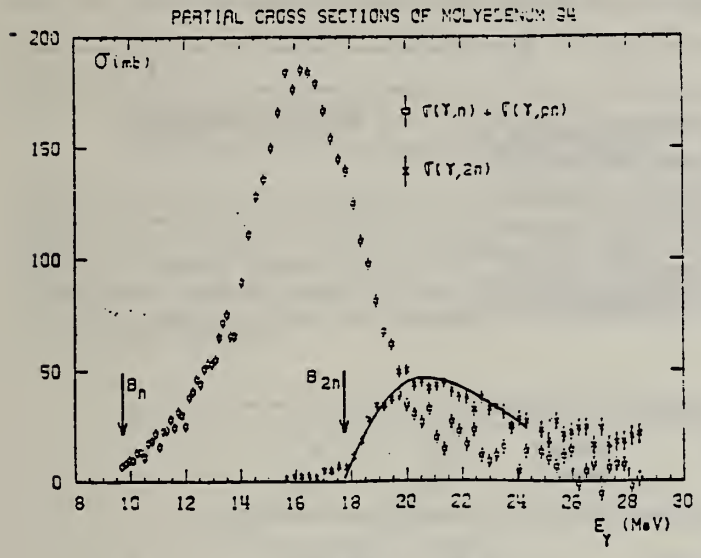

Fig. 2. Same as fig. 1, for ^{94}Mo.

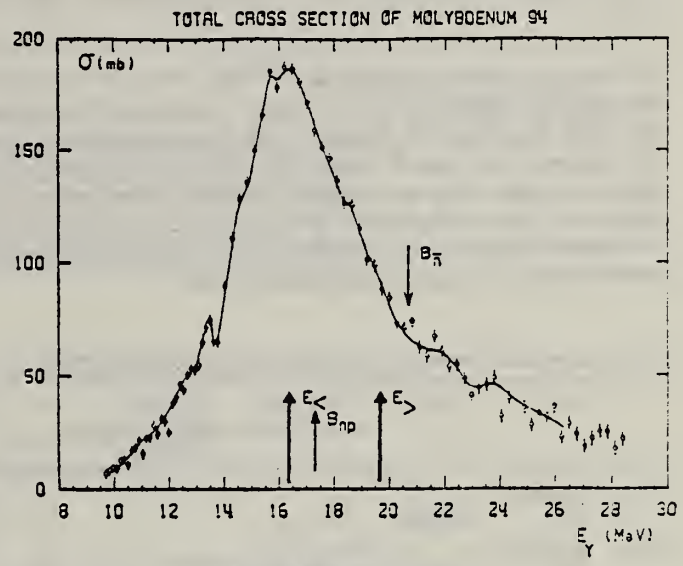

Fig. 8. Same as fig. 7, for ^{94}Mo.

TABLE 3

Lorentz line parameters E_1, σ_1 and Γ_1 corresponding to the best single Lorentz line fits to the experimental $\sigma_{T,a}(E)$ curves shown in fig. 12

	E_1 (MeV)	σ_1 (mb)	Γ_1 (MeV)
^{92}Mo	16.9±0.1	154±10	5.4±0.2
^{94}Mo	16.4±0.1	184±10	5.7±0.2
^{96}Mo	16.2±0.1	184±10	6.3±0.2
^{98}Mo	15.8±0.1	189±15	6.0±0.2
^{100}Mo	15.7±0.1	170±10	7.9±0.2

TABLE 4

Integrated photoneutron cross sections and sum rules of the Mo isotopes

Nucleus	^{92}Mo	^{94}Mo	^{96}Mo	^{98}Mo	^{100}Mo
E_M (MeV)	29	29	29.5	29	28.5
σ_{0a} (MeV · b)	1.10	1.37	1.53	1.60	1.58
$\frac{\sigma_{0a}}{0.06\,NZA^{-1}}$	0.804	0.98	1.08	1.11	1.08
σ_{-1a} (mb)	60	79.3	89.2	95.4	95.4
$\sigma_{-1a}A^{-\frac{1}{3}}$ (mb)	0.145	0.186	0.203	0.211	0.210
σ_{-2a} (mb · MeV^{-1})	3.3	4.8	5.1	6.0	6.1
$\sigma_{-2a}A^{-\frac{1}{3}}$ (μb · MeV^{-1})	1.77	2.48	2.55	2.91	2.86

The notation used is defined in the text.

PH

REF. H. Bartsch, K. Huber, U. Kneissl and H. Krieger
Z. Physik A285, 273 (1978)

ELEM. SYM.	A	Z
Mo	94	42

METHOD

REF. NO. 78 Ba 11 | hmg 11/17/80

REACTION	RESULT	EXCITATION ENERGY	SOURCE		DETECTOR		ANGLE
			TYPE	RANGE	TYPE	RANGE	
G,NPG	LFT	*91(90.4)	C	20,40	SCD-D	---	135

*KeV, Isomer LFT

Short-lived isomers in the nuclei ^{90,92}Nb, ^{99}Mo, ^{98,100,101}Tc and ^{101}Ru populated in photonuclear reactions were studied by pulsed beam techniques. Energy and half-life of the γ-rays deexciting the isomeric levels were measured by recording energy-time spectra. The delayed γ-rays and K X-rays were detected by means of an intrinsic Ge-detector of high resolution. From the measured intensity ratios internal conversion coefficients were determined. The multipolarities of the isomeric transitions could be deduced in most cases. A classification of the observed isomers has been tried on the basis of the obtained experimental results and most recent literature data.

Table 1. Experimental results. E: energy, $T_{1/2}$: halflife, I_{rel}: relative intensity, L: multipolarity, H: hindrance factor

	Line	E [keV]	$T_{1/2}$ [μs]	$T_{1/2}$ [μs] (weighted average)	I_{rel}	α_K	Intensity ratios	L	H
^{90}Nb	K X-rays	–	–		1	–		–	–
	123	122.6±0.2	63 ±2		2.5	0.56±0.22		$E2$	120
^{92}Nb	K X-rays	–	–		1	–		–	–
	90	90.4±0.2	5.9 ±0.2		10.3	0.14±0.01		$E1$	$1.5\cdot10^7$
^{99}Mo	K X-rays	–	15.2 ±0.4	15.5 ±0.2	1	–		–	–
	98	97.8±0.1	15.6 ±0.2		0.95	1.45±0.27		$E2$	20
	138	137.7±0.2	0.79±0.09	0.76±0.06	1		I_{449}/I_{138} =	$M1$	–
	449	449.2±0.2	0.74±0.08		0.97		0.97±0.08	($M2$)	(37)
^{98}Tc	K X-rays	–	14.8 ±0.5	14.6 ±0.4	1			–	–
	22	21.8±0.2	16.4 ±2.7	from	0.036		I_{43}/I_{22} =	$E1+1\%M2$	10^7
	26	–	–	X, 43	–		5.1±0.5	($E2$)	–
	43	43.5±0.2	14.4 ±0.5		0.18			$M1$	–
^{100}Tc	K X-rays	–	8.2 ±0.7	8.2 ±0.3	1			–	–
	29	28.7±0.3	–	from	0.027		I_{172}/I_{29} =	$E2$	1
	172	172.3±0.3	8.2 ±0.3	X, 172	2.2		82±40	($M1, E2$)	–
^{101}Tc	K X-rays	–	–		1	–		–	–
	192	192.0±0.3	636 ±8		5.0	0.26±0.06		$M2$	560
^{101}Ru	K X-rays	–	16.1 ±3.9	17.5 ±0.4	1			–	–
	220	220.7±0.2	17.4 ±0.5	from	7.5		I_{306}/I_{220} =	$M2$	28
	306	306.6±0.3	17.7 ±0.6	220, 306	9.1		1.2±0.1	–	–

REF. K. Masumoto, T. Kato, N. Suzuki
Nucl. Inst. Meth. 157, 567 (1978)

ELEM. SYM.	A	Z
Mo	94	42

METHOD

REF. NO. 78 Ma 10 hg

REACTION	RESULT	EXCITATION ENERGY	SOURCE		DETECTOR		ANGLE
			TYPE	RANGE	TYPE	RANGE	
G,PN	ABY	17-68	C	30-68	ACT - I		4PI
G,AN	ABY	14-68	C	30-68	ACT - I		4PI

Analysis is made of reactions interfering with photon activation analysis procedures.

(G,PN) TO NB-92M
(G,AN) TO ZR-89M

The activation yield curves have been presented for a number of photonuclear reactions in the energy range from 30 to 68 MeV, in order to evaluate quantitatively the interferences due to competing reactions in multielement photon activation analysis. The general features of the yields as functions of both target mass number and excitation energy were elucidated from the data obtained, discussion being given on the results in terms of the reaction mechanism.

Simultaneous neutron activation due to appreciable neutron production from the converter and surrounding materials has also been studied, and, finally, the magnitudes of interferences in real multielement analysis were given in the form of their energy dependences.

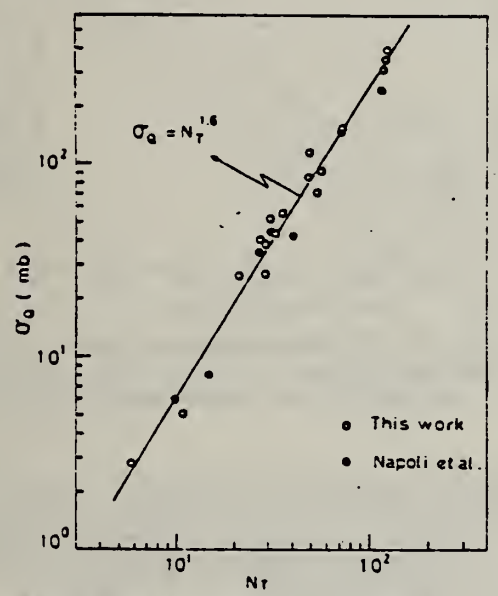

Fig. 2. Yield per equivalent quanta versus target neutron number.

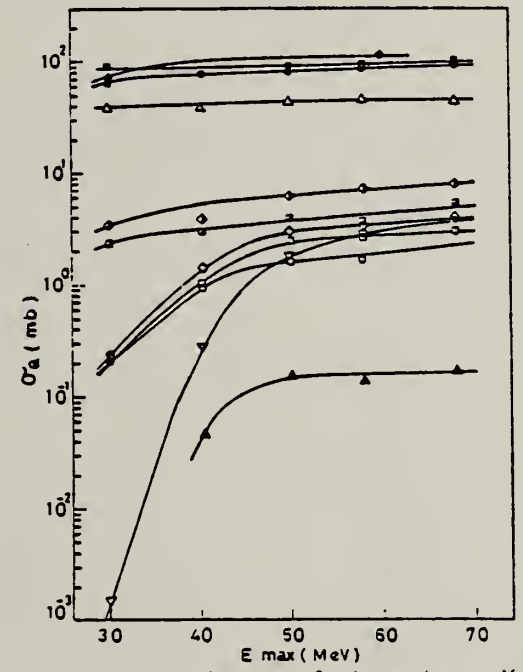

Fig. 7. Activation yield curves for the reactions on Y, Zr, Nb and Mo.
◆ $^{89}Y(\gamma, n)^{88}Y$, ● $^{90}Zr(\gamma, n)^{89}Zr$, ○ $^{90}Zr(\gamma, pn)^{88}Y$,
△ $^{93}Nb(\gamma, n)^{92m}Nb$, ▲ $^{93}Nb(\gamma, \alpha n)^{88}Y$, ■ $^{100}Mo(\gamma, n)^{99}Mo$,
◈ $^{97}Mo(\gamma, p)^{96}Nb$, ◪ $^{96}Mo(\gamma, p)^{95m}Nb$, ◇ $^{94}Mo(\gamma, pn)^{92m}Nb$,
□ $^{92}Mo(\gamma, 2n)^{90}Mo$, ▽ $^{94}Mo(\gamma, \alpha n)^{89}Zr$.

(over)

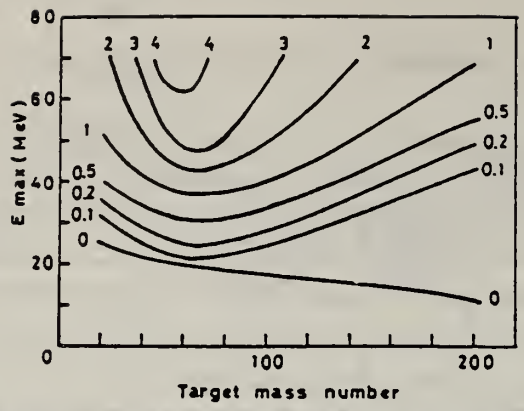

Fig. 11. Yields of the (γ, pn) reactions as a function of bremsstrahlung maximum energy and target mass number. The numerical values in the figure are yields per equivalent quanta in mb.

REF. A. G. Flowers, D. Branford, J. C. McGeorge, A. C. Shotter, P. Thorley, C. H. Zimmerman, R. O. Owens, J. S. Pringle
Phys. Rev. Lett. 43, 323 (1979)

ELEM. SYM.	A	Z
Mo	94	42

METHOD

REF. NO. 79F12 hg

REACTION	RESULT	EXCITATION ENERGY	SOURCE		DETECTOR		ANGLE
			TYPE	RANGE	TYPE	RANGE	
E,A	SPC	UKN	D	120	MAG-D		30

This paper presents energy spectra of α particles emitted following the bombardment of ^{27}Al, ^{nat}Ni, ^{92}Mo, ^{94}Mo, and ^{197}Au with 120-MeV electrons, together with α-particle angular distributions from ^{197}Au and ^{nat}Ni for E_α = 30 and 50 MeV. The data are compared with preequilibrium exciton-model and statistical-model calculations. It is concluded that few-step processes are dominant in the production of α particles with energies above 20 MeV.

PREEQUILIB A EMISS

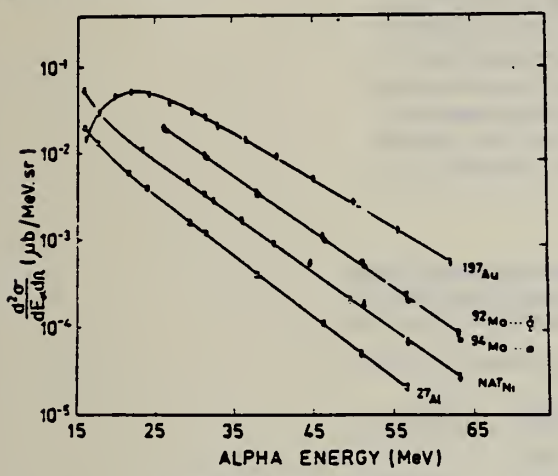

FIG. 1. α-particle energy spectra at $\theta_\alpha = 30°$, for E_e = 120 MeV. Errors shown are the sum of statistical and systematic contributions. The solid lines are a guide to the eye.

TABLE I. Temperatures corresponding to the preequilibrium component of the (e,α) reaction, derived from energy spectra at $\theta_\alpha = 30°$ for E_e = 120 MeV.

Target	Temperature[a] (MeV)
^{27}Al	5.3
^{nat}Ni	5.5
^{68}Zn	5.4
^{92}Mo	5.6
^{94}Mo	5.4
^{197}Au	6.1

[a] Error is ± 0.2 MeV.

REF. M. Schumacher, F. Smend, W. Mückenheim, P. Rullhusen, H.G. Börner
Z. Phys. A300, 193 (1981)

ELEM. SYM.	A	Z
Mo	94	42

METHOD

REF. NO. 81 Sc 6 egf

REACTION	RESULT	EXCITATION ENERGY	SOURCE		DETECTOR		ANGLE
			TYPE	RANGE	TYPE	RANGE	
G,G	ABX	6		6	SCD-D		90

Elastic scattering by nuclei in the range of mass numbers between 64 and 238 has been studied with monochromatic photons in the energy range between 2 and 8 MeV. These photons were provided either by a Ti(n,γ) source installed in the tangential through channel of the Grenoble high flux reactor, or by ^{24}Na and ^{56}Co sources produced by deuteron bombardment of Al or Fe at the Göttingen cyclotron. The photoexcitation of 23 nuclear levels has been observed and the decay properties and groundstate widths of the majority of these levels have been determined. For the lead scattering target the coherent elastic differential cross section has been studied in detail. There is evidence that below the photo-neutron threshold the elastic scattering via virtual photoexcitation of the nucleus can be approximated by extrapolating the real part of the Giant Dipole Resonance amplitude along a Lorentzian curve. Coulomb corrections to Delbrück scattering seem to play a small role at 6.5 MeV.

6.555 MEV

Table 4. Properties of levels observed by photoexcitation. $(d\sigma/d\Omega)^{NRF}$: experimental differential cross section per identified isotope or element for resonance scattering through $\Theta = 90°$. I^π: spin-parity of excited level; $W(\Theta)$: angular correlation function; $g = (2I_{ex}+1)/(2I_g+1)$; Γ_0: radiative groundstate transition width, Γ: total level width. Errors in the last digits are given in parentheses

Isotope	E_γ (MeV)	$(d\sigma/d\Omega)^{NRF}$ (μb/sr)	I^π	Γ_0/Γ [a]	$W(\Theta)g\Gamma_0^2/\Gamma$ (meV)	Γ_0^f (meV)	Γ_0^s (meV)
^{238}U	2.754	13 (4)	(1)	0.77	0.145	0.084	-
^{238}U	3.254	421 (5)	1^-	0.24	0.83	1.5	0.52(15)[d]
^{209}Bi	6.555	2.1 (4)·10^2	-	-	0.74	0.74[b]	-
^{209}Bi	7.168	1.7 (3)·10^5	$9/2^{+}$[e]	1.00	710	786	820 (40)[s]
^{203}Tl	6.418	8.75(30)·10^3	$1/2^+$[a]	0.28	30	102	82 (15)[s]
Tl	6.759	7 (3)	-	-	-	-	-
Hg	6.555	68 (17)	-	-	-	-	-
^{186}W	6.418	5.2 (3)·10^2	1^-[a]	0.32	1.75	2.4	-
^{184}W	6.555	9.8 (10)·10^2	(1)	0.52	3.44	2.9	-
^{184}W	6.759	46 (10)	(1)	0.58	0.17	0.13	-
^{181}Ta	3.010	174 (17)	-	0.72	0.42	0.59	-
^{181}Ta	6.418	62 (4)	-	0.73	0.2	0.27[c]	-
^{181}Ta	6.759	4.8 (12)	-	-	0.018	0.018[b]	-
^{165}Ho	6.418	10.3 (30)	-	-	0.035	0.035[b]	-
^{165}Ho	6.759	5.6 (14)	-	-	0.021	0.021[b]	-
Nd	2.754	2.6 (5)	-	-	-	-	-
Nd	3.254	14.0 (10)	-	-	-	-	-
Ce	6.759	13.4 (10)	-	-	-	-	-
^{121}Sb	3.452	2.20 (5)·10^3	-	0.60	2.9	4.9[b]	-
^{100}Mo	6.418	1.53 (4)·10^4	1^-[a]	0.88	52	26	25 (8)[s]
^{94}Mo	6.555	4.4 (4)·10^3	(1)	0.33	15	21	-
Mo	6.759	6.2 (15)	-	-	-	-	-
Mo	7.168	8.2 (26)·10^2	-	-	-	-	-

[a] [11] [b] $W(\Theta)g\Gamma_0/\Gamma = 1$ assumed [c] $W(\Theta)g = 1$ assumed
[d] [28] (a small correction has been applied to the data of [28])
[e] Upper limits in case not all the transitions to lower levels were observed
[f] Present work [s] Previous work

^{95}Nb
A=95

^{95}Nb
A=95

^{95}Mo
A=95

REF. H. Langhoff, R. Cesareo and A. Flammersfeld
Z. Physik 205, 1 (1967)

ELEM. SYM.	A	Z
Mo	95	42

METHOD

REF. NO.	
67 La 3	egf

REACTION	RESULT	EXCITATION ENERGY	SOURCE		DETECTOR		ANGLE
			TYPE	RANGE	TYPE	RANGE	
G,G	LFT	1	D	1	NAI-D	0-1	DST
		(766 keV)					

1=0.766 MEV

Lifetime $2.9 \pm {}^{1.6}_{1.0}$ psec.

$W(\theta) = 1 + A_2 P_2(\cos\theta)$ $\quad A_2 = 0.5\ {}^{+0.3}_{-0.2}$

Mo
A=96

Mo
A=96

Ref. H. E. Jackson

Phys. Rev. 127, 1687 (1962)

Elem. Sym.	A	Z
Mo	96	42

Method

reactor, Argonne fast chopper - NaI(Tl)

Ref. No. 62Jal

BG

Reaction	E or ΔE	E_o	Γ	$\int \sigma dE$	Jπ	Notes
$Mo^{95}(n,\gamma)Mo^{96}$	E_n up to 700eV.	107 eV			1^-	Resonance due to capture of p wave neutron; E1 transition Capture of γ-ray spectrum studied in order to identify individual resonances due to pwave neutron capture. Detector at 90°

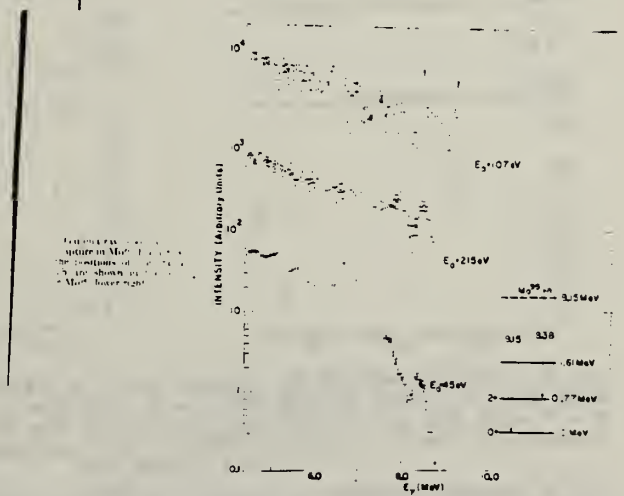

FORM NBS-418
(8-1-63)
USCOMM-DC 18556-P83

U.S. DEPARTMENT OF COMMERCE
NATIONAL BUREAU OF STANDARDS

REF. Yu. P. Antuf'ev, V. L. Agranovich, V. B. Ganenko, V. S. Kuzmenko, I. I. Miroshnichenko, and P. V. Sorokin
Ukr. Fiz. Zh. 14, 248 (1969)

ELEM. SYM.	A	Z
Mo	96	42

METHOD

REF. NO. 69 An 6 egf

REACTION	RESULT	EXCITATION ENERGY	SOURCE		DETECTOR		ANGLE
			TYPE	RANGE	TYPE	RANGE	
G,P	ABY	106-999	C	700,999	TEL-D	97-230	DST
G,D	ABY	113-999	C	700,999	TEL-D	97-205	DST

999 = 1.2 GEV

Summary

The cross-sections of the (γ, p) (γ, d) reactions were investigated. Li^7, Be^9, C^{12}, Si^{28}, Cu^{63}, Mo^{96} and Ta^{181} targets were irradiated with the bremsstrahlung of 700 and 1200 MeV maximum energy from the Kharkov PhTI Ac. Sci. UkrSSR linear accelerator. The photoprotons and deuterons were detected by the scintillation telescope at 30°, 60°, and 120° with the beam. Possible mechanisms of the proton and deuteron photoproduction are discussed. The qualitative agreement of A dependence of the cross-sections is observed with a suggestion on the meson mechanism for these reactions.

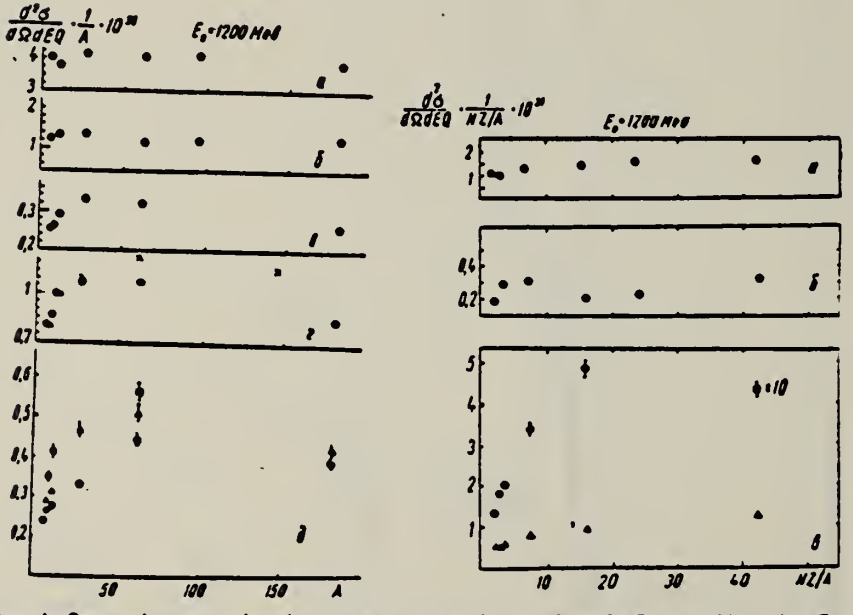

Рис. 1. Залежність перерізу (γ, p)-реакції від A: $а$ — ϑ=30°, E_p=97 *Мев*; $б$ — E_p=205 *Мев*; $в$ — ϑ=60°, E_p=230 *Мев*; $г$ — E_p=157 *Мев* (× — дані [3]); $д$ — ϑ=120°, ○ — E_p=120 *Мев*, △ — E_p=157 *Мев*, ■ — E_p=230 *Мев*. Абсолютне значення перерізу наведено при енергії протонів E_p=120 *Мев*. Інші дані нормовані до перерізу для Li^7 при E_p=120 *Мев*.

Рис. 2. Залежність перерізу (γ, d)-реакції від NZ/A: $а$ — ϑ=30°, E_d=97 *Мев*; $б$ — ϑ=30°, E_d=205 *Мев*; $в$: △ — ϑ=60°, E_d=97 *Мев*, ○ — ϑ=120°, E_d=97 *Мев* (перерізи наведені в одиницях 10^{-32} *см²/стер·Мев·Q*).

R. B. Begzhanov and S. M. Akhrarov
ZhETF Pis. Red. 10, 39 (1969)
JETP Letters 10, 26 (1969)

Mo	96	42

METHOD

REF. NO.

69 Be 7 hmg

REACTION	RESULT	EXCITATION ENERGY	SOURCE TYPE	SOURCE RANGE	DETECTOR TYPE	DETECTOR RANGE	ANGLE
G,G	LFT	6.0	D	6.0	D		DST
		(6.41,6.44)		(6.41,6.44)			(90,135)

Self-Absorption. 6.41, 6.44 MEV

Results of determination of the resonance-level parameters

Source-scatterer	E_γ, MeV	$\langle\sigma_{pp}\rangle$, mb	Γ_{γ_0}, eV	D, keV	Reference
Pb → Zn^{64}	7.38	33±4.5	0.58±0.12	53.70±10.13	This work
Ti → Mo^{96}	6.413	11.2 ±1.4	0.11±0.02	8.68± 1.57	"
Ti → La^{139}	6.413	16 04±2.10	0.28±0.05	8.03± 1.42	"
Ti → Bi^{209}	7.15	1200±230	0.32 ±0.07	1.84± 0.40	"
	6.996	1560	–	–	[1]
	7.15	2600±800	0.42±0.14	–	[5]
Ti → Cu^{65}	6.07	423 ±108	0.34±0.06	99.1±17.4	This work
	6.07	440 ±130	0.36±0.07		[5]
Ti → Cu^{63}	6.07	215± 71	0.18 ±0.04	57.14±12 70	This work
	6.07	200± 60	0.16± 0.03	–	[6]
Cr → Cu^{63}	8.50	22 ± 7	0.26±0.08	130 ±40	This work
	8.499	35	75	–	[1]
	8.50	19 ±6	0.28±0.09	–	[6]
Cr → Cu^{65}	8.50	36 ±9	0.47±0.10	21.36 ±4.54	This work
	8.499	80	10.5	–	[1]
	8.50	42 ±13	0.94±0.29	–	[6]
Cu → Sn^{117}	7.01	1150 ±240	0.15±0.04	0.44 ±0.12	This work
	7.01	1000	–	–	[1]
	7.01	1200 ±400	0.3 ±0.3	–	[5]
Hg → Mo^{96}	6.44	201 ±37	0.12 ±0.04	0.23 ±3.07	This work

REF. R. Bergere, H. Beil, P. Carlos, A. Lepretre, A. Veyssiere
PICNS-73, Vol.I, p.525 Asilomar

ELEM. SYM.	A	Z
Mo	96	42

METHOD

REF. NO. 73 Be 10 hmg

REACTION	RESULT	EXCITATION ENERGY	SOURCE		DETECTOR		ANGLE
			TYPE	RANGE	TYPE	RANGE	
G,SN	ABX	9- 28	D	9- 28	BF3-I		4PI

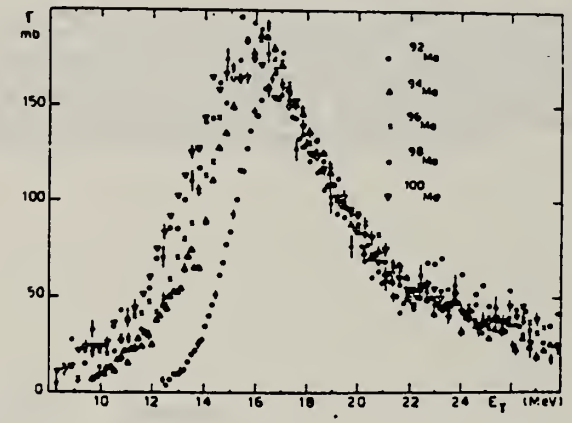

Fig. 15 Comparison of the total photoneutron cross sections of ^{92}Mo ^{94}Mo ^{96}Mo ^{98}Mo and ^{100}Mo

Table I

Isotopes	^{92}Mo	^{94}Mo	^{96}Mo	^{98}Mo	^{100}Mo
σ_{on}	0.83	0.98	1.08	1.11	1.08

REF.

H. Beil, R. Bergere, P. Carlos, A. Lepretre, A. De Miniac, and A. Veyssiere
Nucl. Phys. A227, 427 (1974)

ELEM. SYM.	A	Z
Mo	96	42

METHOD

REF. NO.	
74 Be 3	egf

REACTION	RESULT	EXCITATION ENERGY	SOURCE		DETECTOR		ANGLE
			TYPE	RANGE	TYPE	RANGE	
* G,N	ABX	9- 28	D	9- 28	BF3-I		4PI
** G,2N	ABX	16- 28	D	16- 28	BF3-I		4PI
*** G,3N	ABX	26- 29	D	26- 29	BF3-I		4PI

*699 +
**700
***701+

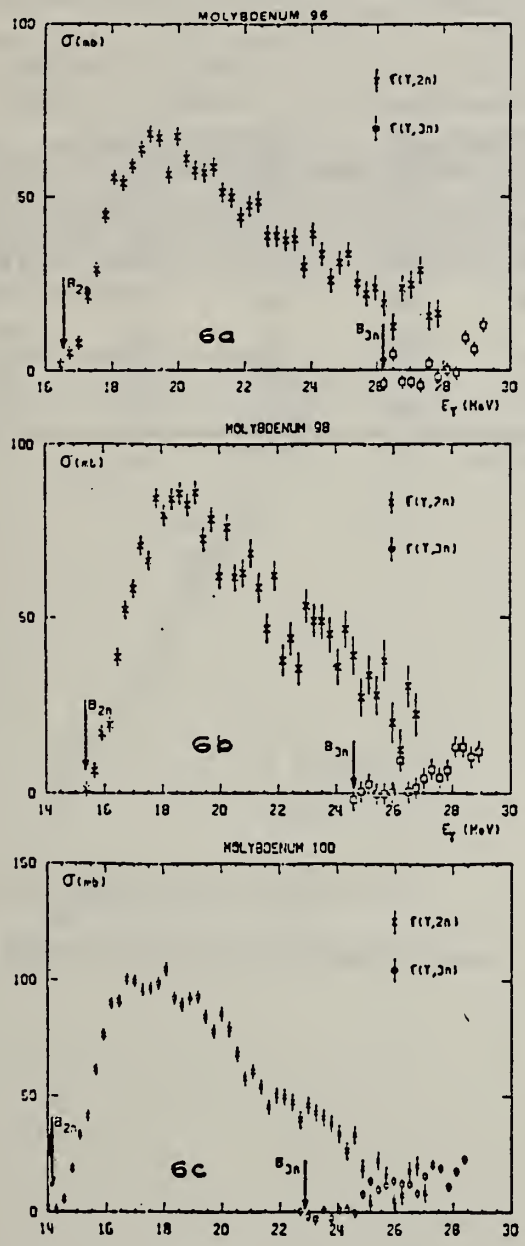

Fig. 6. Partial photoneutron cross sections $\sigma(\gamma, 2n)$ and $\sigma(\gamma, 3n)$ of ^{96}Mo, ^{98}Mo and ^{100}Mo. Arrows indicate theoretical threshold values given in table 2.

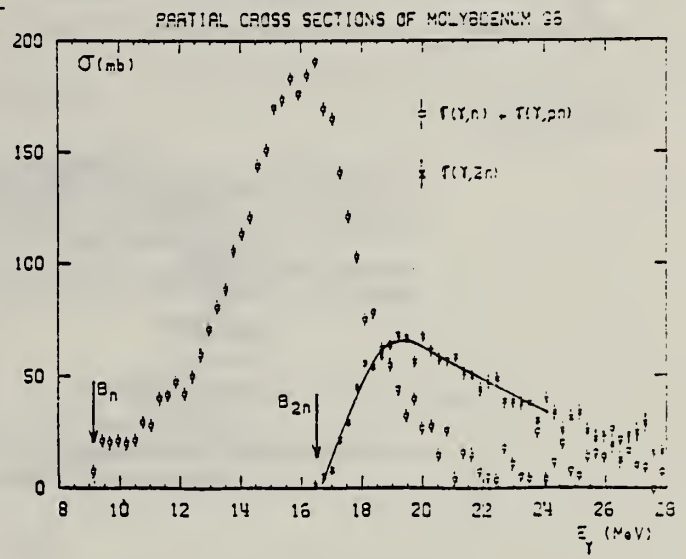

Fig. 3. Same as fig. 1, for ^{96}Mo.

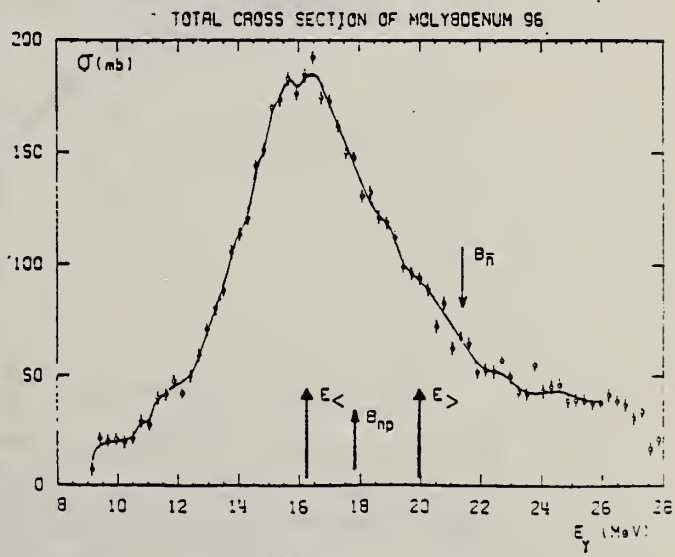

Fig. 9. Same as fig. 7. for ^{96}Mo.

(over)

TABLE 3

Lorentz line parameters E_1, σ_1 and Γ_1 corresponding to the best single Lorentz line fits to th. experimental $\sigma_{\gamma,n}(E)$ curves shown in fig. 12

	E_1 (MeV)	σ_1 (mb)	Γ_1 (MeV)
^{92}Mo	16.9±0.1	154±10	5.4±0.2
^{94}Mo	16.4±0.1	184±10	5.7±0.2
^{96}Mo	16.2±0.1	184±10	6.3±0.2
^{98}Mo	15.8±0.1	189±15	6.0±0.2
^{100}Mo	15.7±0.1	170±10	7.9±0.2

TABLE 4

Integrated photoneutron cross sections and sum rules of the Mo isotopes

Nucleus	^{92}Mo	^{94}Mo	^{96}Mo	^{98}Mo	^{100}Mo
E_M (MeV)	29	29	29.5	29	23.5
σ_{0n} (MeV · b)	1.10	1.37	1.53	1.60	1.58
$\frac{\sigma_{0n}}{0.06\,NZA^{-1}}$	0.804	0.98	1.08	1.11	1.08
σ_{-1n} (mb)	60	79.3	89.2	95.4	95.4
$\sigma_{-1n}A^{-\frac{1}{3}}$ (mb)	0.145	0.186	0.203	0.211	0.206
σ_{-2n} (mb · MeV^{-1})	3.3	4.8	5.1	6.0	6.1
$\sigma_{-2n}A^{-\frac{1}{3}}$ (μb · MeV^{-1})	1.77	2.48	2.55	2.91	2.86

The notation used is defined in the text.

REF. K. Masumoto, T. Kato, N. Suzuki
Nucl. Inst. Meth. 157, 567 (1978)

ELEM. SYM.	A	Z
Mo	96	42

METHOD

REF. NO. 78 Ma 10 hg

REACTION	RESULT	EXCITATION ENERGY	SOURCE		DETECTOR		ANGLE
			TYPE	RANGE	TYPE	RANGE	
G,P	ABY	9-68	C	30-68	ACT -I		4PI

Analysis is made of reactions interfering with photon activation analysis procedures.

TO NB-95M

The activation yield curves have been presented for a number of photonuclear reactions in the energy range from 30 to 68 MeV, in order to evaluate quantitatively the interferences due to competing reactions in multielement photon activation analysis. The general features of the yields as functions of both target mass number and excitation energy were elucidated from the data obtained, discussion being given on the results in terms of the reaction mechanism.

Simultaneous neutron activation due to appreciable neutron production from the converter and surrounding materials has also been studied, and, finally, the magnitudes of interferences in real multielement analysis were given in the form of their energy dependences.

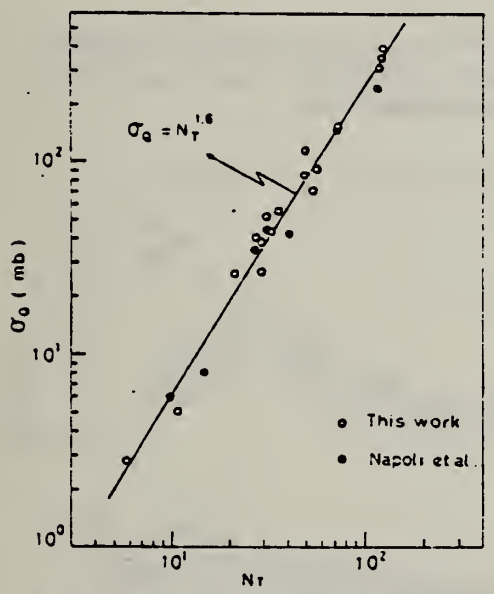

Fig. 2. Yield per equivalent quanta versus target neutron number.

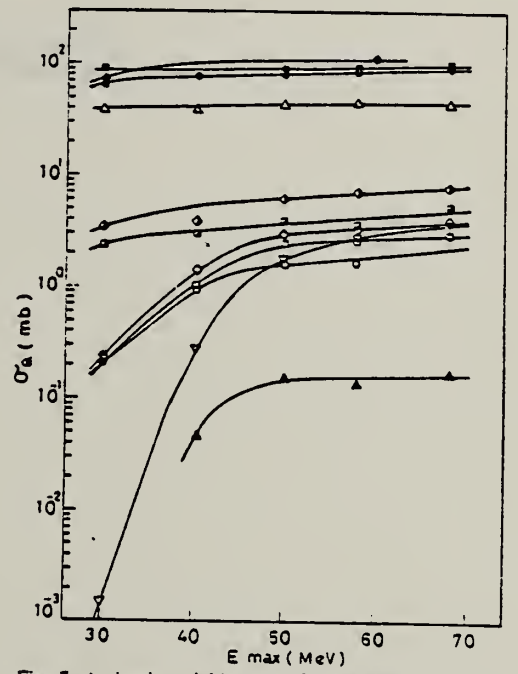

Fig. 7. Activation yield curves for the reactions on Y, Zr, Nb and Mo.
◆ $^{89}Y(\gamma, n)^{88}Y$, ● $^{90}Zr(\gamma, n)^{89}Zr$, ○ $^{90}Zr(\gamma, pn)^{88}Y$,
△ $^{93}Nb(\gamma, n)^{92m}Nb$, ▲ $^{93}Nb(\gamma, 2n)^{88}Y$, ■ $^{100}Mo(\gamma, n)^{99}Mo$,
◈ $^{97}Mo(\gamma, p)^{96}Nb$, ◪ $^{96}Mo(\gamma, p)^{95m}Nb$, ◇ $^{94}Mo(\gamma, pn)^{92m}Nb$,
□ $^{92}Mo(\gamma, 2n)^{90}Mo$, ▽ $^{94}Mo(\gamma, 2n)^{89}Zr$.

(over)

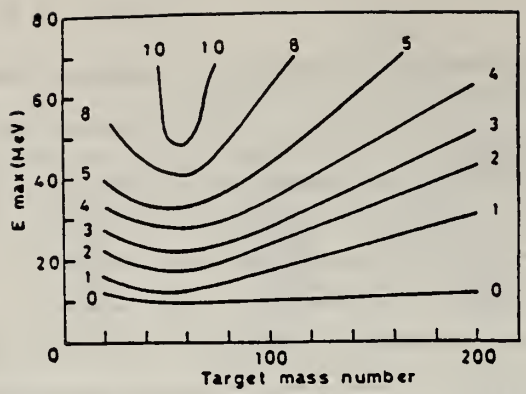

Fig. 10. Yields of the (γ, p) reactions as a function of bremsstrahlung maximum energy and target mass number. The numerical values in the figure are yields per equivalent quanta in mb.

REF. T.J. Bowles, R.J. Holt, H.E. Jackson, R.M. Laszewski, R.D. McKeown, A.M. Nathan, J.R. Specht
Phys. Rev. C24, 1940 (1981)

ELEM. SYM.	A	Z
Mo	96	42

METHOD

REF. NO. 81 Bo 5 hg

REACTION	RESULT	EXCITATION ENERGY	SOURCE		DETECTOR		ANGLE
			TYPE	RANGE	TYPE	RANGE	
G,G	ABX	14-23	D	14-23	NAI-D		90

Quasimonochromatic photons have been used to measure elastic and inelastic photon scattering cross sections in the giant dipole resonance region of ^{52}Cr, Fe, ^{60}Ni, ^{92}Mo, and ^{96}Mo in an experiment in which the elastic and inelastic scattering are resolved. The elastic scattering cross sections show clear evidence for isospin splitting of the giant dipole resonance. The inelastic scattering to low-lying vibrational levels, which is a measure of the coupling between the giant dipole resonance and collective surface vibrations, is in qualitative agreement with the predictions of the dynamic collective model. However, when examined in detail, this model does not provide an adequate description of the scattering data.

[NUCLEAR REACTIONS ^{52}Cr, Fe, ^{60}Ni, ^{92,96}Mo (γ,γ'), $14 \leq E_\gamma \leq 22$ MeV; measured E_γ, $E_{\gamma'}$, $d\sigma/d\Omega$ for γ_0,γ_1. Compared to DCM predictions. Tagged photons.]

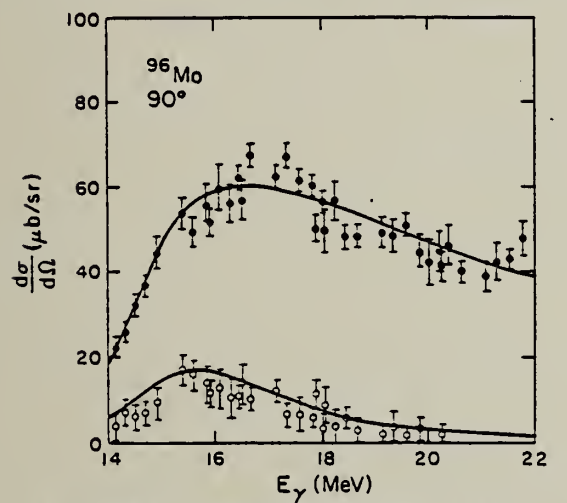

FIG. 4. Elastic (closed circles) and inelastic (open circles) scattering cross sections at $\theta = 90°$ on ^{96}Mo. The error bars represent statistical uncertainties only. The solid lines are the DCM calculations for the elastic and inelastic cross sections. The curves corresponding to calculations with and without isospin splitting are indistinguishable.

Nb
A=97

Nb
A=97

R. W. Gellie, K. H. Lokan
Nucl. Phys. 60, 343-348 (1964)

Mo	97	42

METHOD
Betatron; ion chamber monitor

REF. NO.
64 Ge 1

JOC

REACTION	RESULT	EXCITATION ENERGY	SOURCE		DETECTOR		ANGLE
			TYPE	RANGE	TYPE	RANGE	
G,P	ABX	THR - 26	C	THR - 33	ACT - I		4 PI

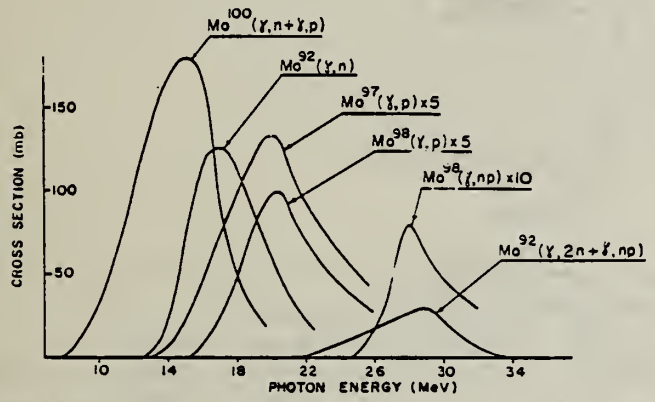

Fig. 2. Cross sections for photoreactions in molybdenum isotopes.

TABLE 2
Reaction parameters

Reaction	Peak energy (MeV)	$\int \sigma dE$ (MeV · mb)
$Mo^{100}(\gamma, n-\gamma, p)$	15	1110 ± 200
$Mo^{92}(\gamma, n)$	17	750 ± 70
$Mo^{97}(\gamma, p)$	20	215 ± 50
$Mo^{98}(\gamma, p)$	20	140 ± 15
$Mo^{98}(\gamma, np)$	28	30 ± 10
$Mo^{92}(\gamma, np-\gamma, 2n)$	29	160 ± 25

R. W. Gellie
Aust. J. Phys. 21, 765 (1968)

Mo	97	42

METHOD

REF. NO. 68 Ge 1 egf

REACTION	RESULT	EXCITATION ENERGY	SOURCE		DETECTOR		ANGLE
			TYPE	RANGE	TYPE	RANGE	
G,P	ABX	13-26	C	THR-26	ACT-I		4PI

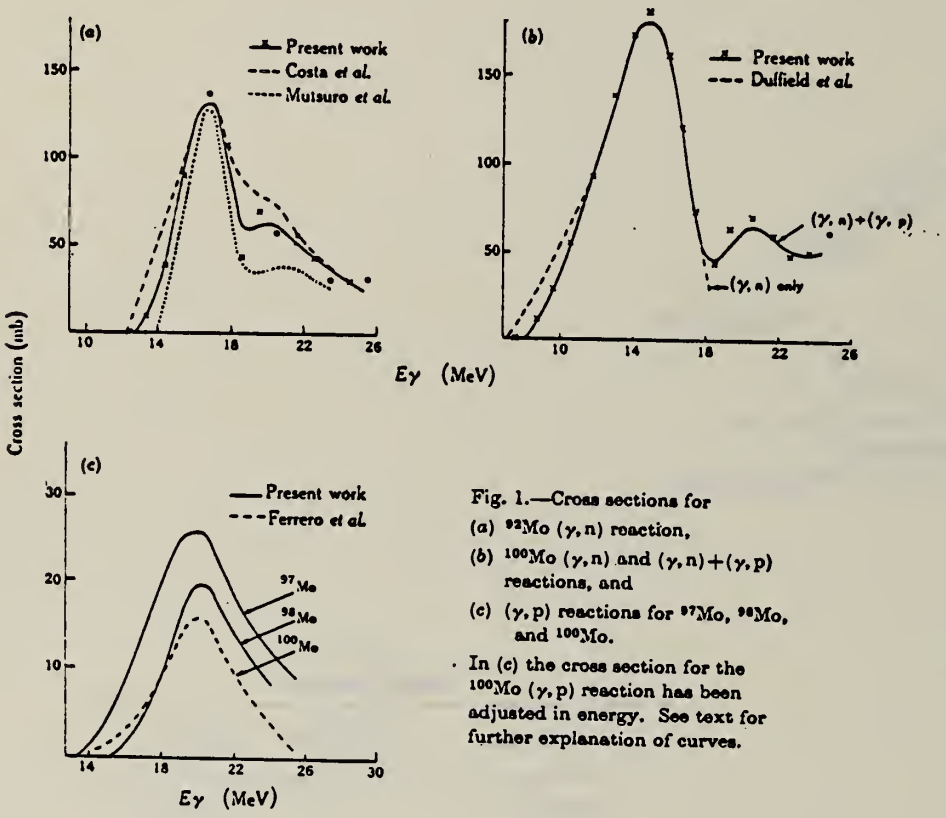

Fig. 1.—Cross sections for
(a) ^{92}Mo (γ, n) reaction,
(b) ^{100}Mo (γ, n) and (γ, n)+(γ, p) reactions, and
(c) (γ, p) reactions for ^{97}Mo, ^{98}Mo, and ^{100}Mo.

In (c) the cross section for the ^{100}Mo (γ, p) reaction has been adjusted in energy. See text for further explanation of curves.

REF. E.J. Winhold, B.H. Patrick, E.M. Bowey, and D.B. Gayther
PICNS-73, Vol.I, p.701 Asilomar

ELEM. SYM.	A	Z
Mo	97	42

METHOD

REF. NO.	
73 Wi 6	hmg

REACTION	RESULT	EXCITATION ENERGY	SOURCE		DETECTOR		ANGLE
			TYPE	RANGE	TYPE	RANGE	
G,N	ABX	6- 10	G	7- 10	TOF-D		130

PEAK AT 8.1 MEV

Table I

Reaction	Threshold (MeV)	Energy Range of Experiment (MeV)	Observed Peaks		
			Peak Energy (MeV)	$\frac{d\sigma}{d\omega}$ at peak (mb/ster.)	$4\pi \int \left(\frac{d\sigma}{d\omega}\right)_{130^\circ} dE_\gamma$ peak
$^{87}Sr(\gamma,n_o)$	8.44	9.4-11.1	.		(MeV-mb)
$^{87}Sr(\gamma,n_1)$	9.52	10.5-11.1			
$^{91}Zr(\gamma,n_o)$	7.19	7.8-10.3	9.1	1.2	20
$^{97}No(\gamma,n_o)$	6.82	7.8-9.2	8.1	0.3	3
$^{113}Cd(\gamma,n_o)$	6.54	7.4-9.3	7.7	0.9	7
$^{117}Sn(\gamma,n_o)$	6.94	7.6-8.8	7.8	2.5	20
$^{119}Sn(\gamma,n_o)$	6.48	7.1-9.0	7.8	1.6	18

REF. K. Masumoto, T. Kato, N. Suzuki
Nucl. Inst. Meth. 157, 567 (1978)

ELEM. SYM.	A	Z
Mo	97	42

METHOD

REF. NO. 78 Ma 10 hg

REACTION	RESULT	EXCITATION ENERGY	SOURCE		DETECTOR		ANGLE
			TYPE	RANGE	TYPE	RANGE	
G,P	ABY	9-68	C	30-68	ACT - I		4PI

Analysis is made of reactions interfering with photon activation analysis procedures.

The activation yield curves have been presented for a number of photonuclear reactions in the energy range from 30 to 68 MeV, in order to evaluate quantitatively the interferences due to competing reactions in multielement photon activation analysis. The general features of the yields as functions of both target mass number and excitation energy were elucidated from the data obtained, discussion being given on the results in terms of the reaction mechanism.

Simultaneous neutron activation due to appreciable neutron production from the converter and surrounding materials has also been studied, and, finally, the magnitudes of interferences in real multielement analysis were given in the form of their energy dependences.

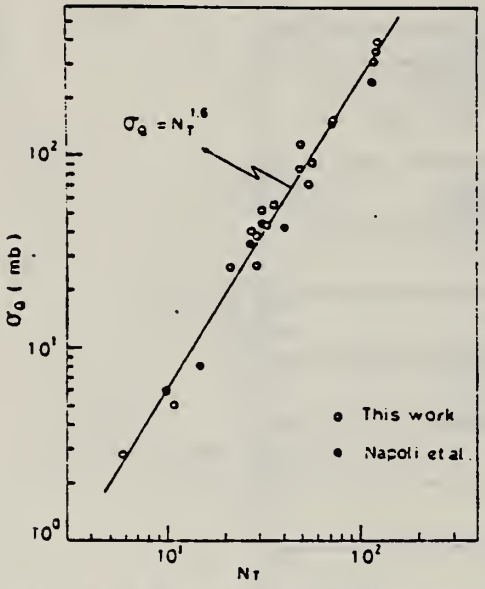

Fig. 2. Yield per equivalent quanta versus target neutron number.

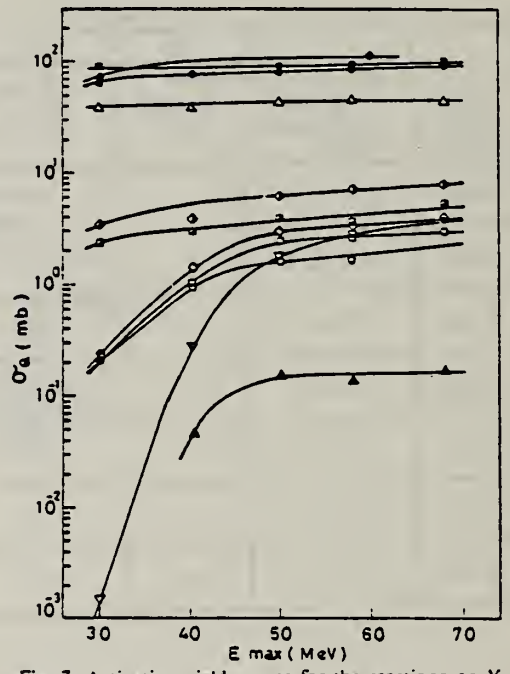

Fig. 7. Activation yield curves for the reactions on Y, Zr, Nb and Mo.
◆ $^{89}Y(\gamma, n)^{88}Y$, ● $^{90}Zr(\gamma, n)^{89}Zr$, ○ $^{90}Zr(\gamma, pn)^{88}Y$,
△ $^{93}Nb(\gamma, n)^{92m}Nb$, ▲ $^{93}Nb(\gamma, 2n)^{88}Y$, ■ $^{100}Mo(\gamma, n)^{99}Mo$,
◈ $^{97}Mo(\gamma, p)^{96}Nb$, ◪ $^{96}Mo(\gamma, p)^{95m}Nb$, ◇ $^{94}Mo(\gamma, pn)^{92m}Nb$,
□ $^{92}Mo(\gamma, 2n)^{90}Mo$, ▽ $^{94}Mo(\gamma, \alpha n)^{89}Zr$.

(over)

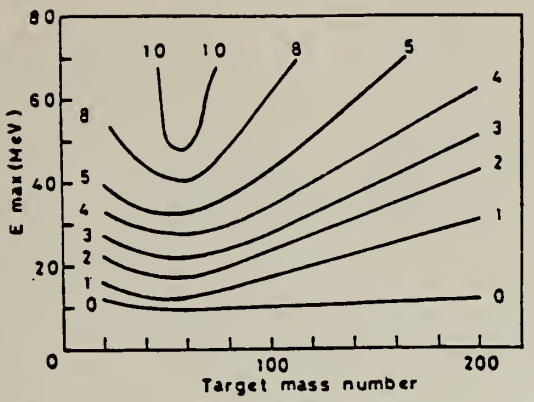

Fig. 10. Yields of the (γ, p) reactions as a function of bremsstrahlung maximum energy and target mass number. The numerical values in the figure are yields per equivalent quanta in mb.

:b
A=98

:C
A=98

REF. A. El Sioufi, P. Erdos and P. Stoll
Helv. Phys. Acta 30, 265 (1957)

ELEM. SYM.	A	Z
Mo	98	42

METHOD

REF. NO. 57 E1 1 egf

REACTION	RESULT	EXCITATION ENERGY	SOURCE		DETECTOR		ANGLE
			TYPE	RANGE	TYPE	RANGE	
G,P	ABI	10- 30	C	32	ACT-I		4PI

Tabelle 1.
Zusammenstellung der gem. W. Q.

Reaktion	Q-Wert MeV	MeV barn	Verhältnis der Querschnitte
$Zn^{66}(\gamma, np)Cu^{64*}$)	18,65	0,02	$\frac{\sigma_{Zn^{66}(\gamma, p)}}{\sigma_{Zn^{66}(\gamma, np)}} = 3{,}6 \pm 0{,}5$
$Zn^{66}(\gamma, p)Cu^{67**}$)[5])	10,01	0,08	
$Zn^{64}(\gamma, 2n)Zn^{62}$	20,82	0,08	$\frac{\sigma_{Zn^{66}(\gamma, np)}}{\sigma_{Zn^{64}(\gamma, 2n)}} = 0{,}25$
$Mo^{92}(\gamma, np)Nb^{90}$	19,5	0,02	
$Mo^{98}(\gamma, p)Nb^{97}$		0,09	$\frac{\sigma_{Mo^{98}(\gamma, p)}}{\sigma_{Mo^{92}(\gamma, np)}} = 4{,}5$

*) σ_{max}: 5,3 mb bei $E_\gamma = 27 \pm 0{,}5$ MeV $\Gamma = 3{,}7$ MeV.
**) σ_{max}: 11,5 mb bei $E_\gamma = 22 \pm 0{,}5$ MeV $\Gamma = 6{,}4$ MeV.

R. W. Gellie, K. H. Lokan
Nucl. Phys. 60, 343-348 (1964)

Mo	98	42

METHOD

Betatron; ion chamber monitor

REF. NO.

64 Ge 1 JOC

REACTION	RESULT	EXCITATION ENERGY	SOURCE		DETECTOR		ANGLE
			TYPE	RANGE	TYPE	RANGE	
G,P	ABX	THR - 26	C	THR-33	ACT - I		4 PI
G,NP	ABX	THR - 32	C	THR-33	ACT - I		4 PI

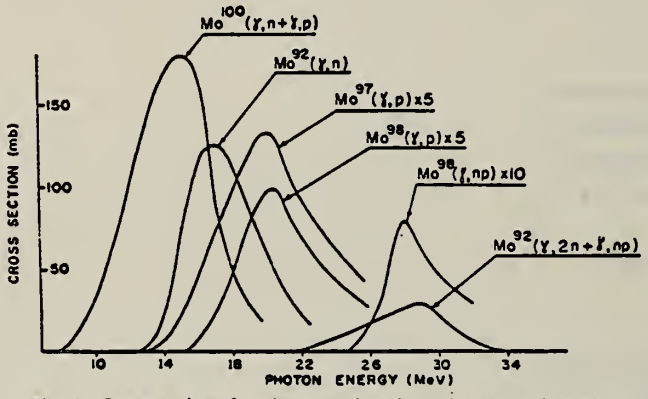

Fig. 2. Cross sections for photoreactions in molybdenum isotopes.

TABLE 2

Reaction parameters

Reaction	Peak energy (MeV)	$\int \sigma dE$ (MeV · mb)
$Mo^{100}(\gamma, n+\gamma, p)$	15	1110 ± 200
$Mo^{92}(\gamma, n)$	17	750 ± 70
$Mo^{97}(\gamma, p)$	20	215 ± 50
$Mo^{98}(\gamma, p)$	20	140 ± 15
$Mo^{98}(\gamma, np)$	28	30 ± 10
$Mo^{92}(\gamma, np+\gamma, 2n)$	29	160 ± 25

R. W. Gellie
Aust. J. Phys. 21, 765 (1968)

Mo	98	42

METHOD

REF. NO. 68 Ge 1 egf

REACTION	RESULT	EXCITATION ENERGY	SOURCE		DETECTOR		ANGLE
			TYPE	RANGE	TYPE	RANGE	
G,P	ABX	13-26	C	THR-26	ACT-I		4PI

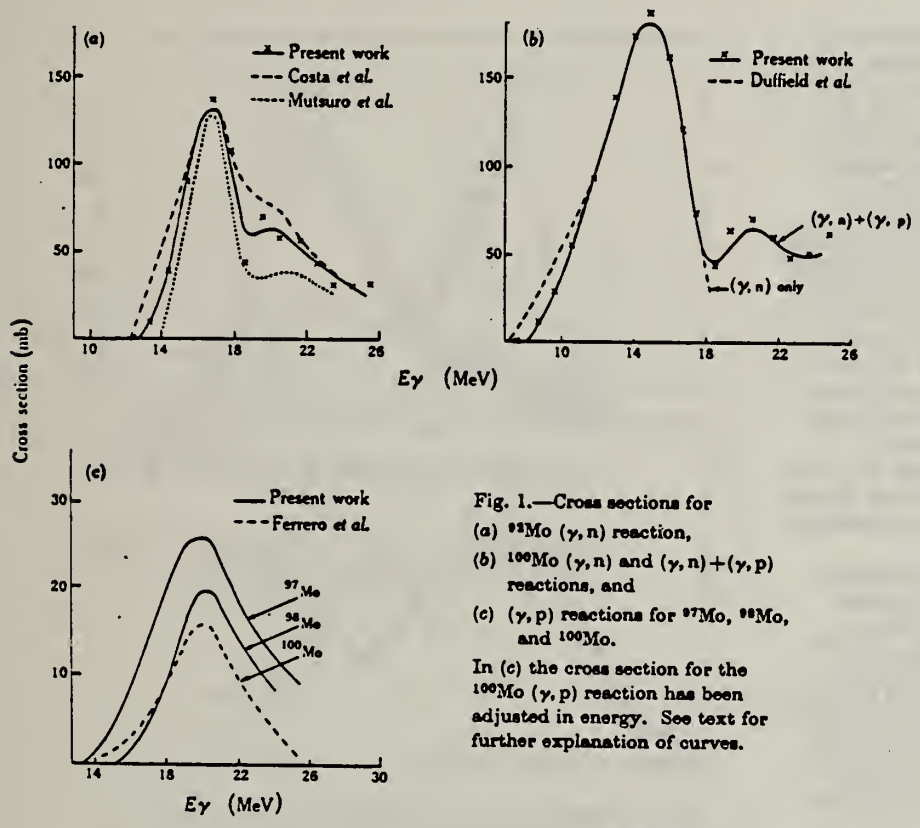

Fig. 1.—Cross sections for
(a) ^{92}Mo (γ, n) reaction,
(b) ^{100}Mo (γ, n) and (γ, n)+(γ, p) reactions, and
(c) (γ, p) reactions for ^{97}Mo, ^{98}Mo, and ^{100}Mo.

In (c) the cross section for the ^{100}Mo (γ, p) reaction has been adjusted in energy. See text for further explanation of curves.

REF.		ELEM. SYM.	A	Z
	B.S. Ishkhanov, I.M. Kapitonov, E.V. Lazutin, I.M. Piskarev, and O.P. Shevchenko Yad. Fiz. 11, 702 (1970) Sov. J. Nucl. Phys. 11, 394 (1970)	Mo	98	42

METHOD	REF. NO.
	70 Is 1 hmg

REACTION	RESULT	EXCITATION ENERGY	SOURCE		DETECTOR		ANGLE
			TYPE	RANGE	TYPE	RANGE	
G,XN	ABX	THR-30	C	THR-30	BF3-I		4PI

We used the 35-MeV betatron of our institute to investigate photoneutron reactions on the isotopes Mo^{92} and Mo^{98}. The yield curves of the reactions (γ, Tn) were measured in the energy range from 7 to 30 MeV in steps of 100 keV. The targets were prepared from metallic Mo. The content of the investigated isotopes was not less than 97%. The use of a highly efficient neutron detector ($\epsilon \approx 45\%$) and of a multichannel method of measurements has made it possible to obtain the yield curves with high accuracy (0.1% in the region 25–30 MeV) and to observe, for the first time, the intermediate structure of the giant resonance on the isotopes of Mo. The statistical reduction of the experimental information and the determination of the cross sections of the photoneutron reactions was carried out in accordance with a program prepared by the Computational Center of the Moscow State University[1].

The obtained cross section of the reactions $\sigma(\gamma, Tn) = \sigma(\gamma, n) + 2\sigma(\gamma, 2n) + \sigma(\gamma, np)$ are shown in the figure, from which it is seen that approximately 15 resonances are observed in each cross section.

The widths of the giant resonances in the reaction (γ, Tn) on Mo^{92} and Mo^{98} are 5 and 7 MeV respectively (curves a in the figure). After taking into account the multiplicity in accordance with the data of[2] for this region of nuclei, the cross sections obtained were $\sigma_n = \sigma(\gamma, n) + \sigma(\gamma, 2n) + \sigma(\gamma, np)$ (curves b). The widths of these cross sections for Mo^{92} and Mo^{98} are the same and equal 5 MeV. The curves c correspond to the cross sections $\sigma(\gamma, n) + \sigma(\gamma, np)$. The widths for them are 5 and 3.5 MeV respectively for Mo^{92} and Mo^{98}.

The widths σ_n of the integral cross sections of the reactions for Mo^{92} and Mo^{98} are 1.29 ± 0.13 and 2.0 ± 0.2 MeV-b. The integral cross section σ_n increases with increasing $N - Z$ for isotopes of a given element. It is interesting to note, however, that in the case of Mo the increase of σ_n and of the width of the giant resonance is due to the cross section of the reaction $(\gamma, 2n)$. Thus, for Mo^{92} we have $\sigma(\gamma, 2n) = 0.17 \pm 0.02$ MeV-b, whereas for Mo^{98} we have $\sigma(\gamma, 2n) = 0.83 \pm 0.08$ MeV-b, i.e., the cross section of the reaction $(\gamma, 2n)$ increases by almost five times. Such a sharp increase of the cross section of the reaction $Mo^{98}(\gamma, 2n)$ is connected with the low threshold of the $(\gamma, 2n)$ reaction, namely $E^{thr}_{Mo^{98}}(\gamma, 2n) = 15.5$ MeV. For comparison, we point out that $E^{thr}_{Mo^{92}}(\gamma, 2n) = 22.8$ MeV.

For the reaction $(\gamma, n) + (\gamma, np)$, the integral cross sections for Mo^{92} and Mo^{98} are respectively 1.12 ± 0.11 and 1.10 ± 0.11 MeV-b.

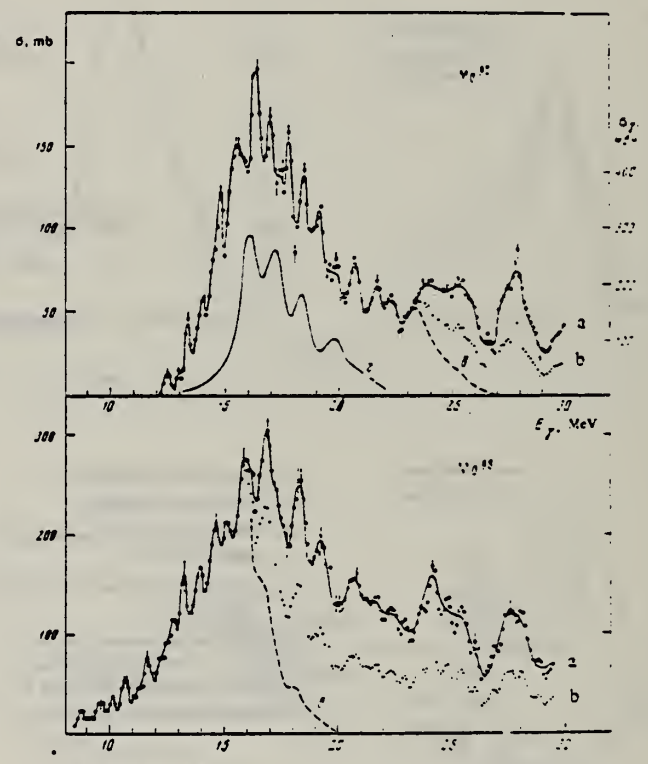

Effective cross sections for Mo^{92} and Mo^{98}: a – $\sigma(\gamma, Tn)$; b – $\sigma(\gamma, n) + \sigma(\gamma, 2n) + \sigma(\gamma, np)$; c – $\sigma(\gamma, n) + \sigma(\gamma, np)$; d – total-absorption cross section σ_γ, obtained in [4] for Mo^{94} (right-hand scale).

There are at present no published data on the structure of the photoneutron cross sections on the Mo isotopes. Such general characteristics of the giant resonance as the position and magnitude of the integral cross section are known only for the reaction $Mo^{92}(\gamma, n)$[3-5]. Even these results, however, are highly contradictory. Thus, data on the width of the giant resonance, obtained in[3], exceed the data of[4] by a factor of 2.

In conclusion, let us compare the experimental results obtained by us with the calculations performed on the basis of the collective dynamic theory[6]. The photodisintegration of the Mo^{94} was calculated within the framework of this theory, and the result is shown in the figure (curve d). We see that the theoretical calculation agrees only roughly with the experimental data. The experimentally measured cross sections re-

REF. R. Bergere, H. Beil, P. Carlos, A. Lepretre, A. Veyssiere
PICNS-73, Vol.I, p.525 Asilomar

ELEM. SYM.	A	Z
Mo	98	42

METHOD

REF. NO.	
73 Be 10	hmg

REACTION	RESULT	EXCITATION ENERGY	SOURCE		DETECTOR		ANGLE
			TYPE	RANGE	TYPE	RANGE	
G,SN	ABX	8- 28	D	8- 28	BF3-I		4PI

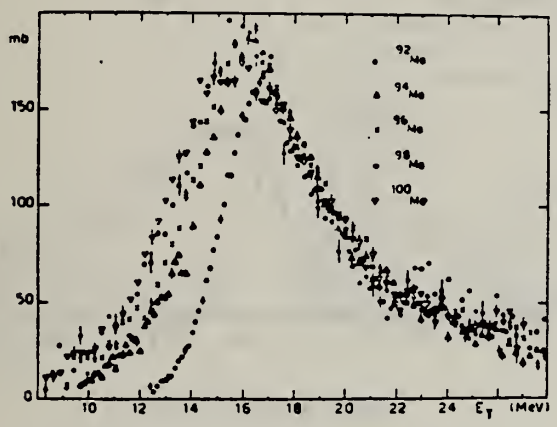

Fig. 15 Comparison of the total photoneutron cross sections of ^{92}Mo ^{94}Mo ^{96}Mo ^{98}Mo and ^{100}Mo

Table I

Isotopes	^{92}Mo	^{94}Mo	^{96}Mo	^{98}Mo	^{100}Mo
σ_{on}	0.83	0.98	1.08	1.11	1.08

REF.

H. Beil, R. Bergere, P. Carlos, A. Lepretre, A. De Miniac, and A. Veyssiere
Nucl. Phys. A227, 427 (1974)

Mo	98	42

METHOD

REF. NO.

74 Be 3 egf

REACTION	RESULT	EXCITATION ENERGY	SOURCE TYPE	SOURCE RANGE	DETECTOR TYPE	DETECTOR RANGE	ANGLE
* G,N	ABX	8- 28	D	8- 28	BF3-I		4PI
** G,2N	ABX	15- 28	D	15- 28	BF3-I		4PI
*** G,3N	ABX	24- 29	D	24- 29	BF3-I		4PI

*703 +
**704
***705+

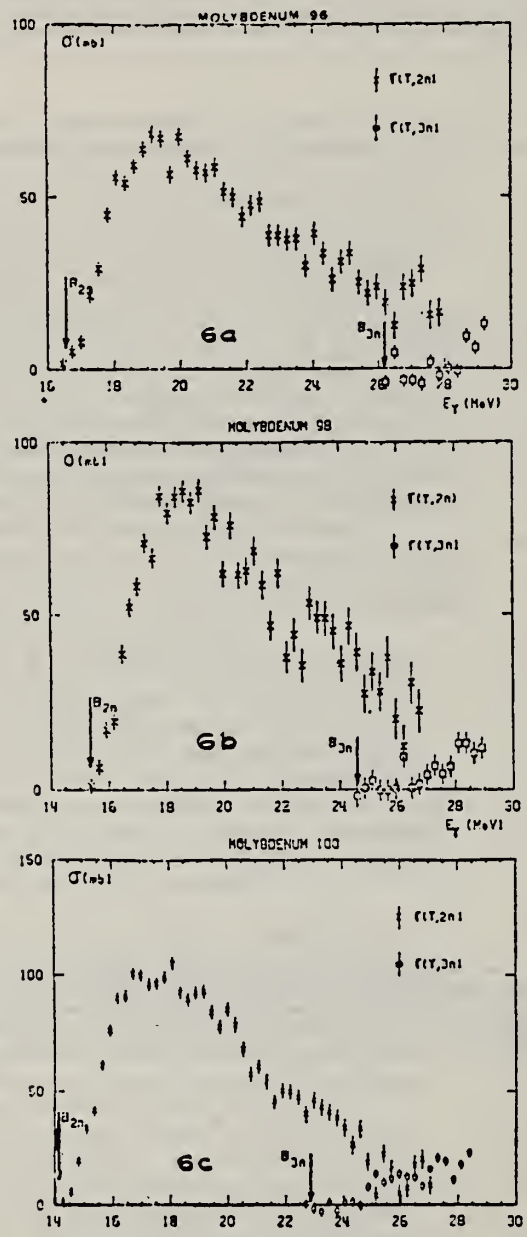

Fig. 6. Partial photoneutron cross sections $\sigma(\gamma, 2n)$ and $\sigma(\gamma, 3n)$ of ^{96}Mo, ^{98}Mo and ^{100}Mo. Arrows indicate theoretical threshold values given in table 2.

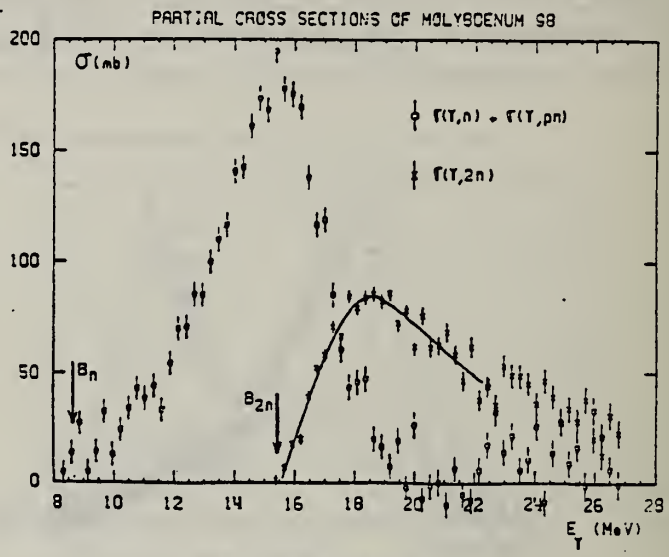

Fig. 4. Same as fig. 1, for ^{98}Mo.

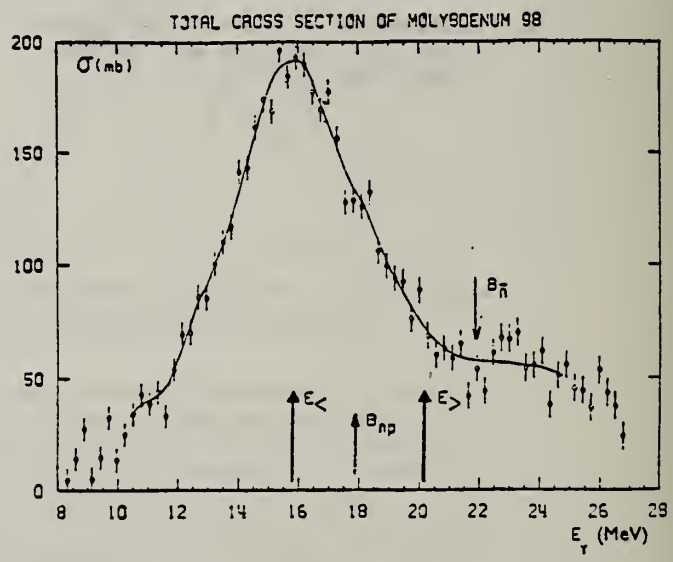

Fig. 10. Same as fig. 7, for ^{98}Mo.

(over)

TABLE 3

Lorentz line parameters E_1, σ_1 and Γ_1 corresponding to the best single Lorentz line fits to the experimental $\sigma_{T,a}(E)$ curves shown in fig. 12

	E_1 (MeV)	σ_1 (mb)	Γ_1 (MeV)
^{92}Mo	16.9±0.1	154±10	5.4±0.2
^{94}Mo	16.4±0.1	184±10	5.7±0.2
^{96}Mo	16.2±0.1	184±10	6.3±0.2
^{98}Mo	15.8±0.1	189±15	6.0±0.2
^{100}Mo	15.7±0.1	170±10	7.9±0.2

TABLE 4

Integrated photoneutron cross sections and sum rules of the Mo isotopes

Nucleus	^{92}Mo	^{94}Mo	^{96}Mo	^{98}Mo	^{100}Mo
E_M (MeV)	29	29	29.5	29	28.5
σ_{0a} (MeV · b)	1.10	1.37	1.53	1.60	1.58
$\frac{\sigma_{0a}}{0.06\,NZA^{-1}}$	0.804	0.98	1.08	1.11	1.08
σ_{-1a} (mb)	60	79.3	89.2	95.4	95.4
$\sigma_{-1a}A^{-\frac{1}{3}}$ (mb)	0.145	0.186	0.203	0.211	0.206
σ_{-2a} (mb · MeV^{-1})	3.3	4.8	5.1	6.0	6.1
$\sigma_{-2a}A^{-\frac{1}{3}}$ (μb · MeV^{-1})	1.77	2.48	2.55	2.91	2.86

The notation used is defined in the text.

Mo
A=100

Mo
A=100

Mo
A=100

Ref. F. Ferrero, A.O. Hanson, R. Malvano, C. Tribuno
Nuovo Cimento 6, 585 (1957)

Elem. Sym.	A	Z
Mo	100	42

Method: Betatron; proton yield; radioactivity; ion chamber

Ref. No.: 57 Fe 3 | NVB

Reaction	E or ΔE	E_o	Γ	$\int \sigma dE$	Jπ	Notes
$Mo^{100}(\gamma,p)$	Bremss. 14-30			$\int_{14}^{30} = 0.10 \pm 0.2$ MeV-b		

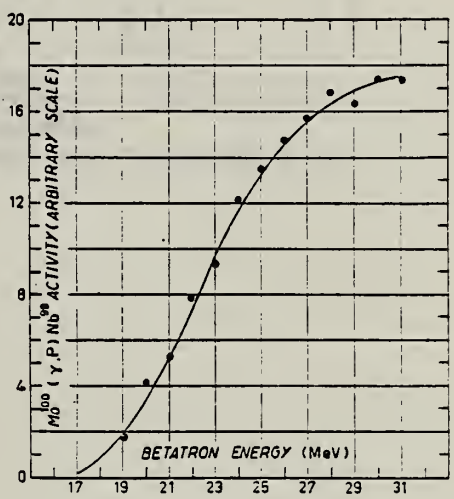

Fig. 1.

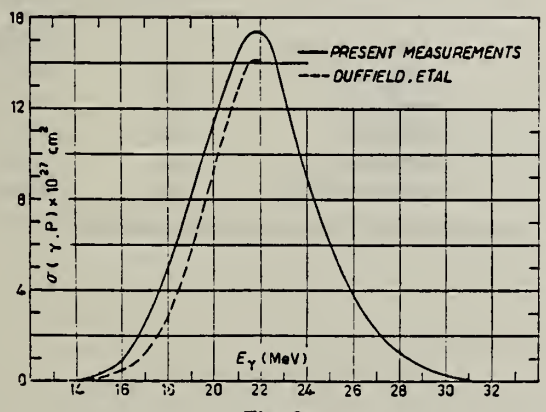

Fig. 2.

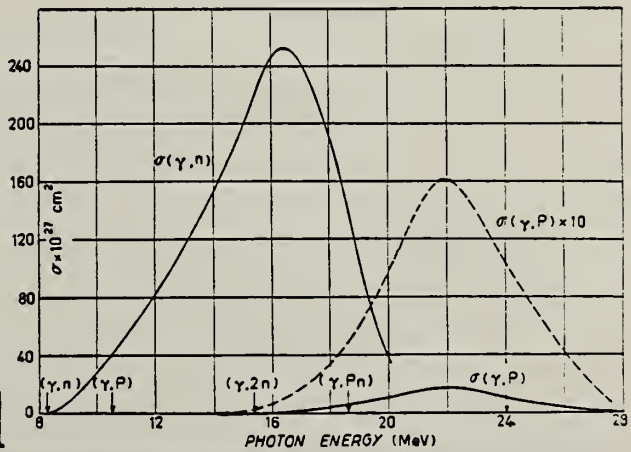

Fig. 3.

FORM NBS-418
(8-1-63)
USCOMM-DC 18858-P63

REF.

R. W. Gellie, K. H. Lokan
Nucl. Phys. 60, 343-348 (1964)

ELEM. SYM.	A	Z
Mo	100	42

METHOD

Betatron; ion chamber monitor

REF. NO. 64 Ge 1 JOC

REACTION	RESULT	EXCITATION ENERGY	SOURCE TYPE	SOURCE RANGE	DETECTOR TYPE	DETECTOR RANGE	ANGLE
1) G,N	ABX	THR - 20	C	THR-33	ACT - I		4 PI
2) G,P	ABX	THR - 20	C	THR-33	ACT - I		4 PI

1) MIXED WITH G,P
2) MIXED WITH G,N

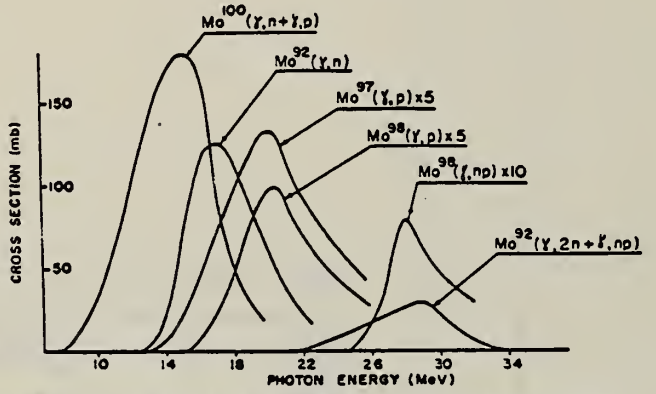

Fig. 2. Cross sections for photoreactions in molybdenum isotopes.

TABLE 2
Reaction parameters

Reaction	Peak energy (MeV)	$\int \sigma dE$ (MeV · mb)
$Mo^{100}(\gamma, n+\gamma, p)$	15	1110±200
$Mo^{92}(\gamma, n)$	17	750± 70
$Mo^{97}(\gamma, p)$	20	215± 50
$Mo^{98}(\gamma, p)$	20	140± 15
$Mo^{98}(\gamma, np)$	28	30± 10
$Mo^{92}(\gamma, np+\gamma, 2n)$	29	160± 25

R. W. Gellie
Aust. J. Phys. 21, 765 (1968)

ELEM. SYM.	A	Z
Mo	100	42

METHOD

REF. NO. 68 Ge 1 egf

REACTION	RESULT	EXCITATION ENERGY	SOURCE		DETECTOR		ANGLE
			TYPE	RANGE	TYPE	RANGE	
G,N+P	ABX	7-26	C	THR-26	ACT-I		4PI

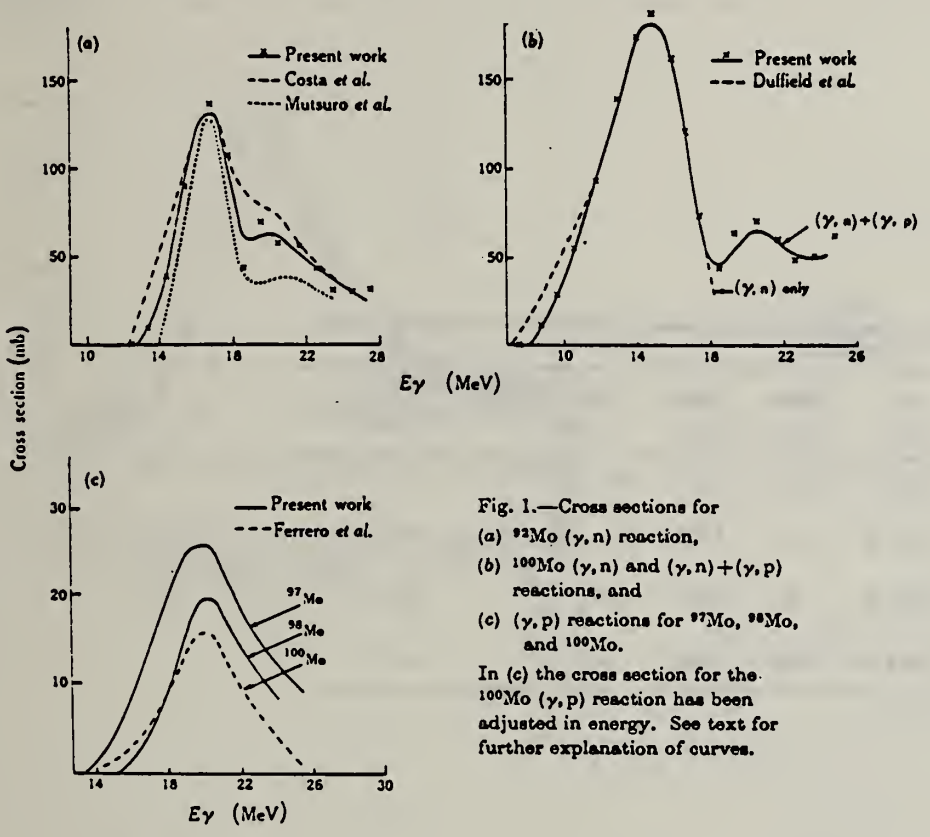

Fig. 1.—Cross sections for
(a) ^{92}Mo (γ, n) reaction,
(b) ^{100}Mo (γ, n) and (γ, n)+(γ, p) reactions, and
(c) (γ, p) reactions for ^{97}Mo, ^{98}Mo, and ^{100}Mo.
In (c) the cross section for the ^{100}Mo (γ, p) reaction has been adjusted in energy. See text for further explanation of curves.

R. Moreh, A. Nof, O. Shahal and A. Wolf
Phys. Letters 36B, 71 (1971)

Mo	100	42

METHOD

REF. NO. 71 Mo 2 egf

REACTION	RESULT	EXCITATION ENERGY	SOURCE		DETECTOR		ANGLE
			TYPE	RANGE	TYPE	RANGE	
G,G/	LFT	6	D	6,8	SCD-D		DST

6.418 MEV

Table 1
Summary of the experimental and theoretical decay properties of the resonance levels excited by nuclear photo-excitation.

Scatterer	Transition $1^- \rightarrow 2^+$ (keV)	A $(1^- \rightarrow 2^+)$	Γ_γ (meV)	Γ(M2) (μeV)	Γ(M2) (W.u.)	δ^2(M2/E1) ($\times 10^3$)	δ^2(M2/E1) Weisskopf estimate ($\times 10^6$)
^{74}Ge	6018 → 2200	0.14 ± 0.04	120 ± 15	190	0.89	17^{+23}_{-12}	3.2
^{100}Mo	6418 → 1064	0.20 ± 0.08	50 ± 45	110	0.079	46^{+53}_{-33}	6.3
^{112}Cd	7632 → 617	0.09 ± 0.02	86 ± 15	36	0.006	$3.6^{+4.5}_{-2.7}$	10.8
^{186}W	6418 → 122	-0.011 ± 0.014	46 ± 35	110	0.023	$9.0^{+5.4}_{-4.1}$	8.7

REF. R. Bergere, H. Beil, P. Carlos, A. Lepretre, A. Veyssiere
PICNS-73, Vol. I, p. 525 Asilomar

ELEM. SYM.	A	Z
Mo	100	42

METHOD

REF. NO. 73 Be 10 hmg

REACTION	RESULT	EXCITATION ENERGY	SOURCE		DETECTOR		ANGLE
			TYPE	RANGE	TYPE	RANGE	
G,SN	ABX	8- 28	D	8- 28	BF3-I		4PI

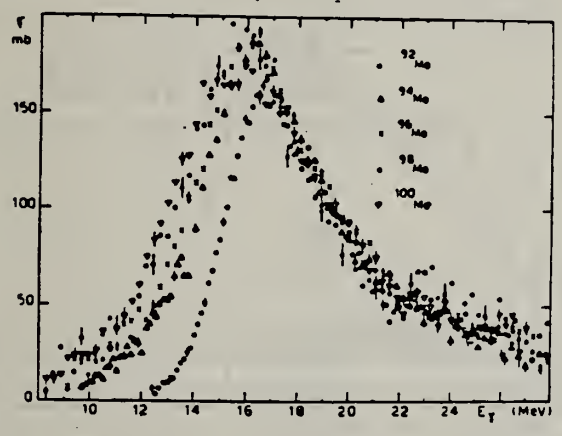

Fig. 15 Comparison of the total photoneutron cross sections of ^{92}Mo ^{94}Mo ^{96}Mo ^{98}Mo and ^{100}Mo

Table I

Isotopes	^{92}Mo	^{94}Mo	^{96}Mo	^{98}Mo	^{100}Mo
σ_{on}	0.83	0.98	1.08	1.11	1.08

REF.

R. Moreh, A. Wolf, O. Shahal, J. Tenenbaum, A. Nof
Nucl. Phys. A217, 477 (1973)

ELEM. SYM.	A	Z
Mo	100	42

METHOD

REF. NO. 73 Mo 12 egf

REACTION	RESULT	EXCITATION ENERGY	SOURCE TYPE	SOURCE RANGE	DETECTOR TYPE	DETECTOR RANGE	ANGLE
G,G	LFT	5- 8	D	5- 8	SCD-D		DST

Fig. 2. Decay scheme of four resonance levels in ^{100}Mo showing the relative intensities for de-excitation to low-lying levels. Most probable spins and parities for some levels assigned from angular distribution results are given. Parentheses indicate uncertainties.

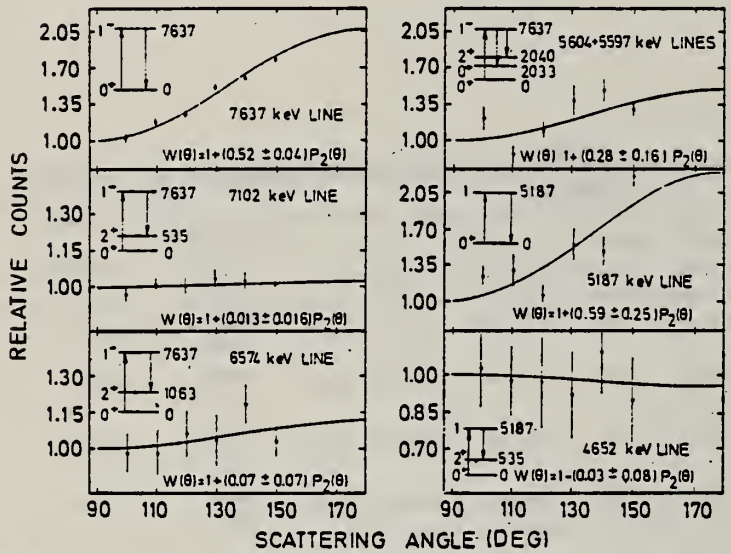

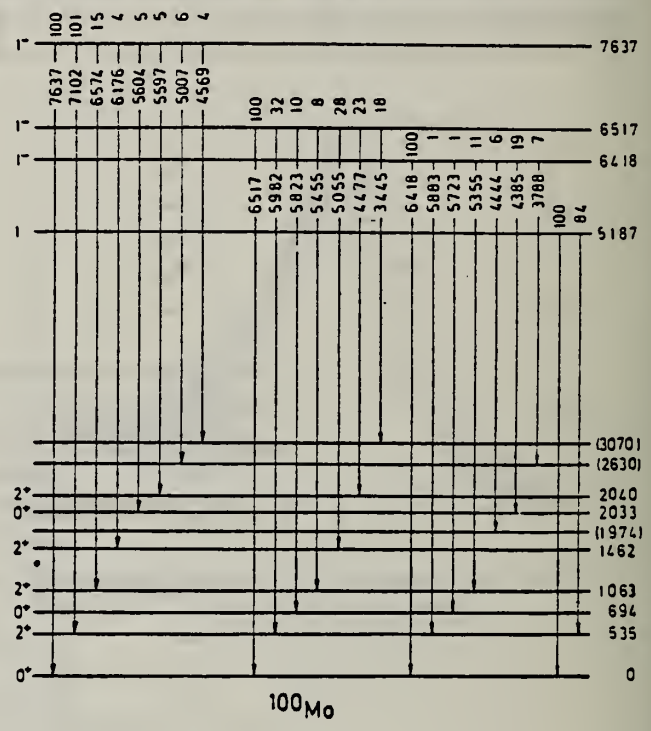

Fig. 3. Angular distributions of the elastic and some inelastic transitions de-exciting the 7637 keV level in ^{100}Mo as measured using a 20 cm^3 Ge(Li) detector. The solid lines have the form $W(0) = 1+AP_2(\cos 0)$ and are least square fits to the experimental distributions. In each case the corresponding γ-γ cascade is indicated.

TABLE 6

Summary of the parameters of the resonance levels in ^{100}Mo

Energy (keV)	(n,γ) source	Γ_0 (meV)	Γ (meV)	$\langle\sigma_\gamma\rangle$ (mb)	δ (eV)
6418	Ti	25±8	50± 35	150±15	4.7±0.3
6517	V	72^{+68}_{-48}	180±100	110±30	12.8±1.2
7637	Cu	40±5	140± 40	98±15	4.5±0.5

REF.

H. Beil, R. Bergere, P. Carlos, A. Lepretre, A. De Miniac, and A. Veyssiere
Nucl. Phys. A227, 427 (1974)

ELEM. SYM.	A	Z
Mo	100	42

METHOD

REF. NO. 74 Be 3 egf

REACTION	RESULT	EXCITATION ENERGY	SOURCE		DETECTOR		ANGLE
			TYPE	RANGE	TYPE	RANGE	
* G,N	ABX	8- 27	D	8- 27	BF3-I		4PI
** G,2N	ABX	14- 27	D	14- 27	BF3-I		4PI
*** G,3N	ABX	21- 28	D	21- 28	BF3-I		4PI

*707 +
**708
***709+

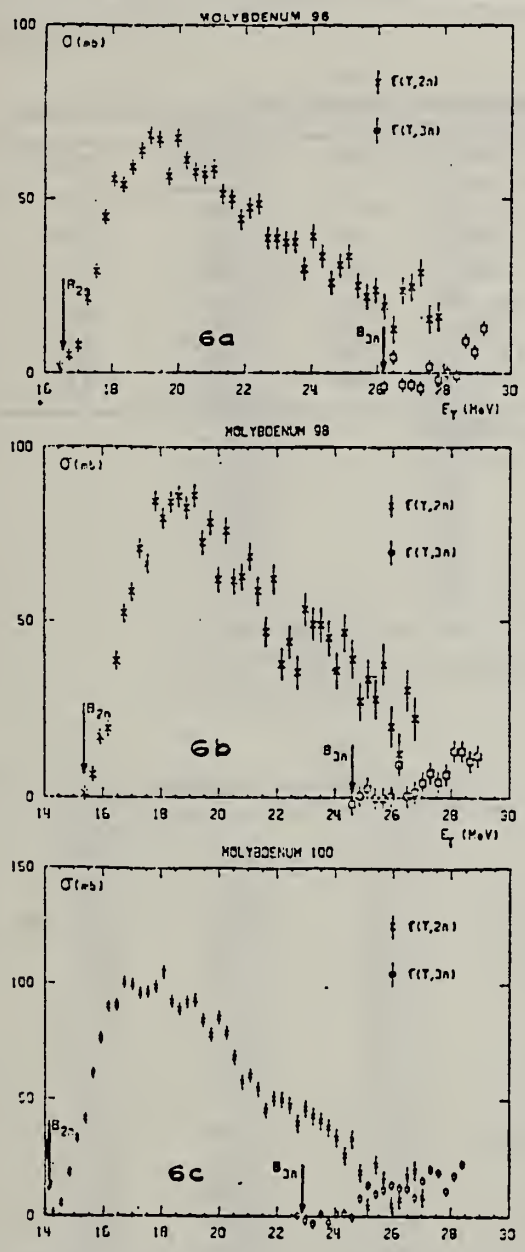

Fig. 6. Partial photoneutron cross sections $\sigma(\gamma, 2n)$ and $\sigma(\gamma, 3n)$ of ^{96}Mo, ^{98}Mo and ^{100}Mo. Arrows indicate theoretical threshold values given in table 2.

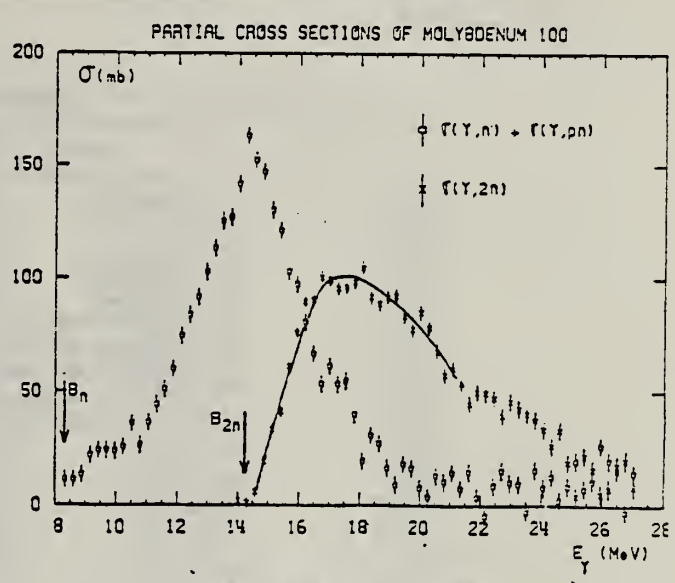

Fig. 5. Same as fig. 1, for ^{100}Mo.

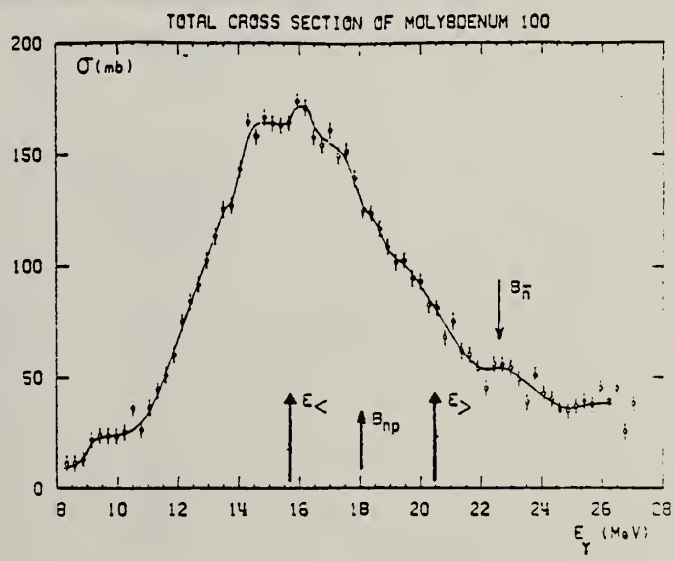

Fig. 11. Same as fig. 7, for ^{100}Mo.

(over)

TABLE 3

Lorentz line parameters E_1, σ_1 and Γ_1 corresponding to the best single Lorentz line fits to the experimental $\sigma_{\gamma,n}(E)$ curves shown in fig. 12

	E_1 (MeV)	σ_1 (mb)	Γ_1 (MeV)
^{92}Mo	16.9±0.1	154±10	5.4±0.2
^{94}Mo	16.4±0.1	184±10	5.7±0.2
^{96}Mo	16.2±0.1	184±10	6.3±0.2
^{98}Mo	15.8±0.1	189±15	6.0±0.2
^{100}Mo	15.7±0.1	170±10	7.9±0.2

TABLE 4

Integrated photoneutron cross sections and sum rules of the Mo isotopes

Nucleus	^{92}Mo	^{94}Mo	^{96}Mo	^{98}Mo	^{100}Mo
E_M (MeV)	29	29	29.5	29	23.5
σ_{0a} (MeV · b)	1.10	1.37	1.53	1.60	1.53
$\frac{\sigma_{0a}}{0.06\,NZA^{-1}}$	0.804	0.98	1.08	1.11	1.08
σ_{-1a} (mb)	60	79.3	89.2	95.4	95.4
$\sigma_{-1a}A^{-\frac{2}{3}}$ (mb)	0.145	0.186	0.203	0.211	0.226
σ_{-2a} (mb · MeV^{-1})	3.3	4.8	5.1	6.0	6.1
$\sigma_{-2a}A^{-\frac{2}{3}}$ (μb · MeV^{-1})	1.77	2.48	2.55	2.91	2.86

The notation used is defined in the text.

REF.

A. Wolf, R. Moreh, and O. Shahal
Nucl. Phys. A227, 373 (1974)

ELEM. SYM.	A	Z
Mo	100	42

METHOD

REF. NO. 74 Wo 2 egf

REACTION	RESULT	EXCITATION ENERGY	SOURCE TYPE	SOURCE RANGE	DETECTOR TYPE	DETECTOR RANGE	ANGLE
$ G,G	LFT	6- 8	D	6- 8	SCD-D		DST

δ = Doppler width

6.418, 7.637

TABLE 4

Upper limit of Γ_0/Γ, the temperature variation ratio R_T, and the self-absorption ratio R

Scatterer (γ-source)	E_0 (MeV)	Γ_0/Γ (±15%)	R_T [a]	R(%) [b]
^{65}Cu(Ti)	6.556	0.80	0.94 ±0.02	1.1±0.5
^{69}Ga(Cu)	7.306	0.52	1.035±0.004	3.5±0.5
^{100}Mo(Cu)	7.637	0.28	1.043±0.007	0.8±0.3
^{100}Mo(Ti)	6.418	0.85	1.032±0.003	0.6±0.3
^{118}Sn(Cu)	6.988	0.84	1.020±0.009	5.7±0.2
^{126}Te(Cu)	7.915	0.4 ±0.1	0.95 ±0.05	6 ±5
^{130}Te(Cu)	7.637	0.45±0.10	0.84 ±0.05	0.9±1.5
^{139}La(Cu)	7.637	0.55	0.95 ±0.01	2.2±0.3
^{139}La(Ti)	6.418	0.78	0.968±0.008	6.4±0.8
^{141}Pr(Cu)	7.915	0.25	1.02 ±0.01	0.9±0.9
^{141}Pr(Cu)	7.252	0.51	1.005±0.003	5.9±0.4
^{144}Nd(Cu)	7.915	0.27	0.89 ±0.05	< 0.5
^{186}W(Ti)	6.418	0.31	1.030±0.004	< 0.5
^{203}Tl(Ti)	6.418	0.28	1.03 ±0.01	1.6±0.3
^{205}Tl(Cu)	7.252	0.58	1.02 ±0.01	1.6±0.7
^{209}Bi(Cu)	7.637	1.00	1.00 ±0.02	2 ±1
^{209}Bi(Ti)	7.168	1.00	0.971±0.005	28.0±0.6

[a]) The values of R_T are given for 10 g/cm² thick scatterers placed at an angle of 60° and a detector angle of 135°.

[b]) The values of R are given for the same scatterer-detector geometry as that of R_T and a 20 g/cm² thick absorber.

TABLE 7

Summary of Γ, Γ_0 and δ of resonance levels measured in the present work and in earlier works [8, 16, 17])

Isotope	Energy (MeV)	Γ (meV)	Γ_0 (meV)	δ (eV)	Ground state transition
^{65}Cu	6.556	70^{+60}_{-20}	28^{+15}_{-5}	11.2 ±0.8	
^{69}Ga [a])	7.306	105±40	48± 7	6.2 ±0.5	E1
^{100}Mo [c])	7.637	140±40	40± 5	4.5 ±0.5	E1
^{100}Mo [c])	6.418	50±35	25± 8	4.25±0.25	E1
^{118}Sn	6.988	152± 5	128± 3	5.5 ±0.5	E1
^{126}Te	7.915	12± 6	5± 2	11 ±2	M1
^{130}Te	7.637	60±30	30±10	15 ±2	E1
^{139}La [b])	7.637	170±40	47± 6	10.5 ±0.5	E1
^{139}La [b])	6.418	85^{+13}_{-7}	67± 8	9.5 ±0.5	E1
^{141}Pr [b])	7.915	7± 3	2± 1	6.6 ±1.0	M1
^{141}Pr [b])	7.252	290±30	110±10	6.4 ±0.5	E1
^{144}Nd [b])	7.915	30±10	8± 3	14.0 ±0.5	M1
^{186}W	6.418	46±35	6± 3	1 ±1	E1
^{203}Tl [b])	6.418	350±60	82±15	0.5 ±0.5	
^{205}Tl [b])	7.252	50±30	25± 6	5.2 ±1.5	M1
^{209}Bi	7.637	> 500	> 30		
^{209}Bi [b])	7.168	820±40	820±40	5.8 ±0.8	E1

[a]) Ref. [16]). [b]) Ref. [8]). [c]) Ref. [17]).

(over)

TABLE 6

Values of A_2, $N_\parallel/N_\perp$, spins, and mixing amplitudes x

Scatterer (γ-source)	E_0 (MeV)	A_2	$N_\parallel/N_\perp$	J_0^π	J^π	J_f^π	x
^{63}Cu(Ti)	6.556	0		$\frac{1}{2}^-$	$\frac{1}{2}$	$\frac{3}{2}^-$	0
^{69}Ga(Cu)	7.306	0.14 ±0.01	1.046±0.022	$\frac{3}{2}^-$	$\frac{3}{2}^+$	$\frac{3}{2}^-$	0
^{100}Mo(Cu)	7.637	0.49 ±0.05	1.17 ±0.05	0^+	1^-	0^+	0
^{100}Mo(Cu)	7.102 [a])	0.013±0.016		0^+	1^-	2^+	−0.06±0.02 [b])
^{100}Mo(Ti)	6.418	0.52 ±0.02	1.15 ±0.03	0^+	1^-	0^+	0
^{100}Mo(Ti)	5.355 [a])	0.19 ±0.08		0^+	1^-	2^+	0.21±0.12 [b])
^{118}Sn(Cu)	6.988	0.48 ±0.02	1.12 ±0.05	0^+	1^-	0^+	0
^{126}Te(Cu)	7.915	0.46 ±0.11	0.86 ±0.10	0^+	1^+	0^+	0
^{130}Te(Cu)	7.637	0.48 ±0.04	1.12 ±0.04	0^+	1^-	0^+	0
^{139}La(Cu)	7.637	0.16 ±0.02	1.024±0.015	$\frac{7}{2}^+$	$\frac{5}{2}^-$	$\frac{5}{2}^+$	0
^{139}La(Ti)	6.418	0.093±0.004	1.018±0.006	$\frac{7}{2}^+$	$\frac{5}{2}^-$	$\frac{5}{2}^+$	0
^{141}Pr(Cu)	7.915	0.41 ±0.06	0.94 ±0.03	$\frac{5}{2}^+$	$\frac{5}{2}^+$	$\frac{5}{2}^+$	$0.26^{+0.13}_{-0.09}$
^{141}Pr(Cu)	7.252	0.23 ±0.06	1.03 ±0.02	$\frac{5}{2}^+$	$\frac{3}{2}^-$	$\frac{3}{2}^+$	0
^{144}Nd(Cu)	7.915	0.50 ±0.03	0.92 ±0.09	0^+	1^+	0^+	0
^{186}W(Ti)	6.418	0.49 ±0.05	1.15 ±0.06	0^+	1^-	0^+	0
^{186}W(Ti)	6.296 [a])	−0.011±0.014		0^+	1^-	2^+	−0.10±0.05 [c])
^{203}Tl(Ti)	6.418	0	1.01 ±0.01	$\frac{1}{2}^+$	$\frac{1}{2}$	$\frac{1}{2}^-$	0
^{205}Tl(Cu)	7.252	0.71 ±0.08	0.90 ±0.02	$\frac{1}{2}^+$	$\frac{3}{2}^+$	$\frac{1}{2}^+$	−0.25±0.05
^{205}Tl(Cu)	7.047 [a])	−0.69 ±0.03		$\frac{1}{2}^+$	$\frac{3}{2}^+$	$\frac{1}{2}^+$	0.33 ±0.04
^{209}Bi(Cu)	7.637	0.24 ±0.04		$\frac{9}{2}^-$	$(\frac{9}{2})$	$\frac{9}{2}^-$	
^{209}Bi(Ti)	7.168	0.20 ±0.02	1.040±0.015	$\frac{9}{2}^-$	$\frac{7}{2}^+$	$\frac{9}{2}^-$	

Errors refer to one standard deviation.
[a]) Inelastic transitions.
[b]) Ref. [17]).
[c]) Ref. [15]).

1) R. Moreh et al., Phys. Rev. C2 (1970) 1144
8) A. Wolf, et al., Phys. Rev. C6 (1972) 2276
15) R. Moreh et al., Phys. Lett. 36B (1971) 71
16) R. Moreh et al., Phys. Rev. C7 (1973) 1885
17) R. Moreh et al., Nucl. Phys. A217 (1973) 477
29) R. Moreh et al., Phys. Rev. C4 (1971) 2265
30) R. Moreh et al., Phys. Rev. 178 (1969) 1961

TABLE 8

Values of Γ_f, D, k_{E1} and k_{M1}

E1 transitions					M1 transitions				
scatterer (γ-source)	$E_0 \to E_f$ (MeV)	Γ_f (meV)	D (eV)	k_{E1} (10^{-9} MeV^{-3})	scatterer (γ-source)	$E_0 \to E_f$ (MeV)	Γ_f (meV)	D (eV)	k_{M1} (10^{-9} MeV^{-3})
^{62}Ni(Fe) [a])	7.646		12300		^{126}Te(Cu)	7.915		260	
	→ 1.172	24		0.5		→ 0.666	2.3		23
^{69}Ga(Cu)	7.306		660			→ 1.421	1.7		6
	→ 0.572	3.2		1.0	^{141}Pr(Cu)	7.915		90	
	→ 0.872	2.7		0.9		→ 1.298	1.3		30
^{100}Mo(Cu)	7.637		670			→ 1.437	0.8		32
	→ 0.535	40		7.7		→ 1.580	1.4		44
	→ 1.063	5.7		1.4		→ 1.655	1.0		42
	→ 1.461	1.4		0.4	^{141}Pr(Fe) [c])	7.632		170	
^{112}Cd(Fe) [b])	7.632		350			→ 0.145	5.6		73
	→ 0.617	11		4		→ 1.130	6.4		130
	→ 1.223	7.3		3.4		→ 1.293	0.4		9
	→ 1.429	2		1		→ 1.437	5.6		140
	→ 1.468	1.7		0.9		→ 1.451	6.8		170
^{130}Te(Cu)	7.637		360			→ 1.532	1.1		29
	→ 0.837	16		5.5	^{144}Nd(Cu)	7.915		380	
	→ 1.589	18		8.8		→ 0.697	13		91
^{139}La(Cu)	7.637		190			→ 1.041	2.7		22
	→ 1.384	3		2.5		→ 1.564	6.2		54
	→ 1.538	3		2.7	^{205}Tl(Cu)	7.252		1200	
^{141}Pr(Cu)	7.252		220			→ 0.205	4		9
	→ 0.146	82		38					
	→ 1.120	8.6		6.5					
^{186}W(Cu)	6.418		110						
	→ 0.122	12		14					

The values of D refer to an excitation energy E_0.
[a]) Ref. [1]). [b]) Ref. [29]). [c]) Ref. [30]).

REF.

H. Bartsch, K. Huber, U. Kneissl, H. Krieger
Nucl. Phys. A256, 243 (1976)

ELEM. SYM.	A	Z
Mo	100	42

METHOD

REF. NO.: 76 Ba 1 egf

REACTION	RESULT	EXCITATION ENERGY	SOURCE		DETECTOR		ANGLE
			TYPE	RANGE	TYPE	RANGE	
G,N	RLY	THR-UKN	C	UKN	SCD-D		4PI

ISOMER RATIO

TABLE 1
Experimental and theoretical results

Process	Target-spin	E_γ (keV)	$T_{\frac{1}{2}}$	Spin high	Spin low	$R_{exp} = \frac{\sigma_{high}}{\sigma_{low}}$	SCOP ($\hbar$)
^{181}Ta(γ, 3n)	$\frac{7}{2}^+$	93	2.2 h 9.31 min 8.15 h	7^-	1^+	0.51 ±0.09	3.6 ±0.2
^{142}Nd(γ, n)	0^+	755 1100–1300, 145	63 s 2.5 h	$\frac{11}{2}^-$	$\frac{3}{2}^+$	0.055±0.006 0.19 ±0.01 [a])	2.20±0.06
^{92}Mo(γ, n)	0^+	652.9 1208, 1508, 1581, 1637	66 s 15.49 min	$\frac{5}{2}^+$	$\frac{1}{2}^-$	1.03 ±0.21 0.85 ±0.07 [b]) 1.92 ±0.15 [a])	5.03±0.75 4^{+6}_{-2}
^{100}Mo(γ, n)	0^+	97.3 140.5	16.8 μs 66.02 h	$\frac{5}{2}^+$	$\frac{1}{2}^+$	0.85 ±0.24	1.72±0.25
^{108}Pd(γ, n)	0^+	214.5 115	22 s 850 ns	$\frac{11}{2}^-$	$\frac{1}{2}^+$	0.5 ±0.2	3.4 ±0.5
^{110}Pd(γ, n)	0^+	188 113 87.7	4.7 min 390 ns 13.47 h	$\frac{11}{2}^-$ $\frac{11}{2}^-$ $\frac{5}{2}^+$	$\frac{5}{2}^+$ $\frac{1}{2}^+$ $\frac{1}{2}^+$	0.11 ±0.02 0.41 ±0.09 3.2 ±0.7	3.14±0.15 3.0 ±0.25 3.3 ±0.4
^{89}Y(γ, n)	$\frac{1}{2}^-$	231.7 442.3 392.5	14.2 ms 300 μs	8^+	1^+	0.056±0.008	

[a]) Ref. [14]). [b]) Ref. [15]).

[14] P.E. Hausteing et al., J. Inorg. Nucl. Chem. 33, 289 (1971)
[15] J.H. Carver et al., Nucl. Phys. 37, 449 (1962)

REF. H. Bartsch, K. Huber, U. Kneissl and H. Krieger
Z. Physik A285, 273 (1978)

ELEM. SYM.	A	Z
Mo	100	42

METHOD

REF. NO. 78 Ba 11 | hmg 11/17/80

REACTION	RESULT	EXCITATION ENERGY	SOURCE TYPE	SOURCE RANGE	DETECTOR TYPE	DETECTOR RANGE	ANGLE
G,NG	LFT	98(97,8)*450(499.2)	C	20,40	SCD-D	---	135

Short-lived isomers in the nuclei ^{90,92}Nb, ^{99}Mo, ^{98,100,101}Tc and ^{101}Ru populated in photonuclear reactions were studied by pulsed beam techniques. Energy and half-life of the γ-rays deexciting the isomeric levels were measured by recording energy-time spectra. The delayed γ-rays and K X-rays were detected by means of an intrinsic Ge-detector of high resolution. From the measured intensity ratios internal conversion coefficients were determined. The multipolarities of the isomeric transitions could be deduced in most cases. A classification of the observed isomers has been tried on the basis of the obtained experimental results and most recent literature data.

*KeV, Isomer LFT

Table 1. Experimental results. E: energy, $T_{1/2}$: halflife, I_{rel}: relative intensity, L: multipolarity, H: hindrance factor

	Line	E [keV]	$T_{1/2}$ [μs]	$T_{1/2}$ [μs] (weighted average)	I_{rel}	α_K	Intensity ratios	L	H
^{90}Nb	K X-rays	–	–		1	–		–	–
	123	122.6±0.2	63 ±2		2.5	0.56±0.22		$E2$	120
^{92}Nb	K X-rays	–	–		1	–		–	–
	90	90.4±0.2	5.9 ±0.2		10.3	0.14±0.01		$E1$	$1.5\cdot10^7$
^{99}Mo	K X-rays	–	15.2 ±0.4	15.5 ±0.2	1	–		–	–
	98	97.8±0.1	15.6 ±0.2		0.95	1.45±0.27		$E2$	20
	138	137.7±0.2	0.79±0.09	0.76±0.06	1		I_{450}/I_{138} =	$M1$	–
	449	449.2±0.2	0.74±0.08		0.97		0.97±0.08	($M2$)	(37)
^{98}Tc	K X-rays	–	14.8 ±0.5	14.6 ±0.4	1			–	–
	22	21.8±0.2	16.4 ±2.7	from	0.036		I_{43}/I_{22} =	$E1+1\%\,M2$	10^7
	26	–	–	X, 43	–		5.1±0.5	($E2$)	–
	43	43.5±0.2	14.4 ±0.5		0.18			$M1$	–
^{100}Tc	K X-rays	–	8.2 ±0.7	8.2 ±0.3	1			–	–
	29	28.7±0.3	–	from	0.027		I_{172}/I_{29} =	$E2$	1
	172	172.3±0.3	8.2 ±0.3	X, 172	2.2		82±40	($M1, E2$)	–
^{101}Tc	K X-rays	–	–		1	–		–	–
	192	192.0±0.3	636 ±8		5.0	0.26±0.06		$M2$	560
^{101}Ru	K X-rays	–	16.1 ±3.9	17.5 ±0.4	1			–	–
	220	220.7±0.2	17.4 ±0.5	from	7.5		I_{306}/I_{220} =	$M2$	28
	306	306.6±0.3	17.7 ±0.6	220, 306	9.1		1.2±0.1	–	–

REF. H. Bartsch, W. Günther, K. Huber, U. Kneissl & H. Krieger
Z. Physik A285, 71 (1978)

ELEM. SYM.	A	Z
Mo	100	42

METHOD

REF. NO. 78 Ba 14 hg

REACTION	RESULT	EXCITATION ENERGY	SOURCE		DETECTOR		ANGLE
			TYPE	RANGE	TYPE	RANGE	
G,N	RLY	8-65	C	65	SCD-D		4PI

Isomeric cross section ratios were measured for the photonuclear reactions $^{100}Mo(\gamma,n)$ $^{99m_1,m_2,g}Mo$ and $^{102}Ru(\gamma,p)$ $^{101m,g}Tc$. Using the Huizenga-Vandenbosch-method spin cut-off parameters were deduced. The applicability of this statistical procedure is discussed. A systematic analysis of all known (γ,xn) isomeric ratio-measurements shows a linear correlation between derived spin cut-off parameters and the mean value of the spins of the isomeric pair.

ISOMER YIELD, DE-EX G

Table 1. Experimental and theoretical results

Process	Targetspin ($\hbar$)	E_γ(keV)	$t_{1/2}$	Spin high ($\hbar$)	Spin low ($\hbar$)	R_{exp}	SCOP($\hbar$)
$^{100}Mo(\gamma,n)$	0^+	449.2	760 ns	$11/2^-$	$5/2^+$	0.11 ± 0.02	4.3 ± 0.4
		137.7		$11/2^-$	$1/2^+$	0.10 ± 0.02	4.3 ± 0.4
		97.8	15.5 μs	$5/2^+$	$1/2^+$	0.94 ± 0.25	1.8 ± 0.3
$^{102}Ru(\gamma,p)$	0^+	191.9	636 μs	$9/2^+$	$1/2^-$	1.33 ± 0.30	1.65 ± 0.35
		306.6					

$$Rexp = \frac{Y \text{ high spin}}{Y \text{ low spin}}$$

REF. K. Masumoto, T. Kato, N. Suzuki
Nucl. Inst. Meth. 157, 567 (1978)

ELEM. SYM.	A	Z
Mo	100	42

METHOD

REF. NO. 78 Ma 10 hg

REACTION	RESULT	EXCITATION ENERGY	SOURCE		DETECTOR		ANGLE
			TYPE	RANGE	TYPE	RANGE	
G,N	ABY	8-68	C	30-68	ACT - I		4PI

Analysis is made of reactions interfering with photon activation analysis procedures.

The activation yield curves have been presented for a number of photonuclear reactions in the energy range from 30 to 68 MeV, in order to evaluate quantitatively the interferences due to competing reactions in multielement photon activation analysis. The general features of the yields as functions of both target mass number and excitation energy were elucidated from the data obtained, discussion being given on the results in terms of the reaction mechanism.

Simultaneous neutron activation due to appreciable neutron production from the converter and surrounding materials has also been studied, and, finally, the magnitudes of interferences in real multielement analysis were given in the form of their energy dependences.

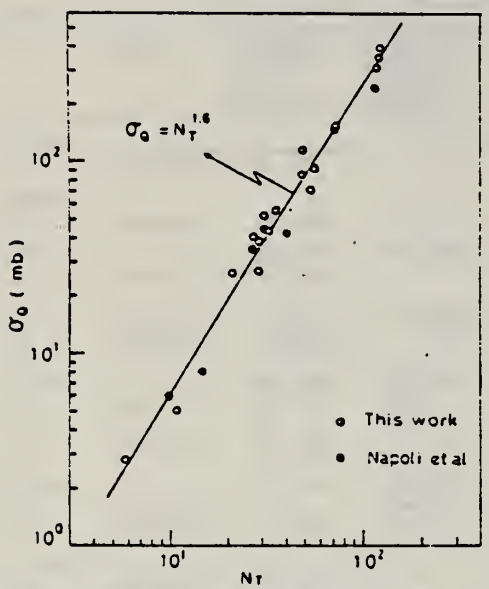

Fig. 2. Yield per equivalent quanta versus target neutron number.

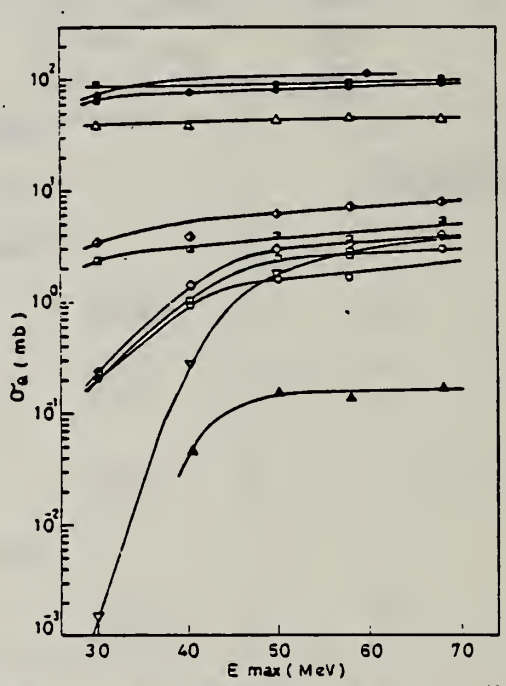

Fig. 7. Activation yield curves for the reactions on Y, Zr, Nb and Mo.
◆ $^{89}Y(\gamma, n)^{88}Y$, ● $^{90}Zr(\gamma, n)^{89}Zr$, ○ $^{90}Zr(\gamma, pn)^{88}Y$,
△ $^{93}Nb(\gamma, n)^{92m}Nb$, ▲ $^{93}Nb(\gamma, xn)^{88}Y$, ■ $^{100}Mo(\gamma, n)^{99}Mo$,
◈ $^{97}Mo(\gamma, p)^{96}Nb$, ◪ $^{96}Mo(\gamma, p)^{95m}Nb$, ◇ $^{94}Mo(\gamma, pn)^{92m}Nb$,
□ $^{92}Mo(\gamma, 2n)^{90}Mo$, ▽ $^{94}Mo(\gamma, xn)^{89}Zr$.

(over)

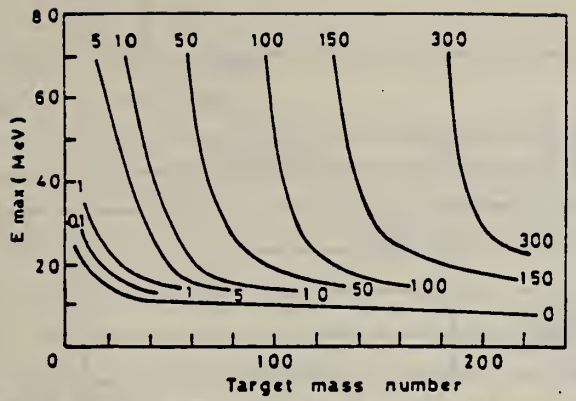

Fig. 9. Yields of the (γ, n) reactions as a function of bremsstrahlung maximum energy and target mass number. The numerical values in the figure are yields per equivalent quanta in mb.

REF. M. Schumacher, F. Smend, W. Mückenheim, P. Rullhusen, H.G. Börner
Z. Phys. A300, 193 (1981)

ELEM. SYM.	A	Z
Mo	100	42

METHOD

REF. NO. 81 Sc 6 egf

REACTION	RESULT	EXCITATION ENERGY	SOURCE TYPE	SOURCE RANGE	DETECTOR TYPE	DETECTOR RANGE	ANGLE
G,G	ABX	6		6	SCD-D		90

6.418 MEV

Elastic scattering by nuclei in the range of mass numbers between 64 and 238 has been studied with monochromatic photons in the energy range between 2 and 8 MeV. These photons were provided either by a Ti(n,γ) source installed in the tangential through channel of the Grenoble high flux reactor, or by ^{24}Na and ^{56}Co sources produced by deuteron bombardment of Al or Fe at the Göttingen cyclotron. The photoexcitation of 23 nuclear levels has been observed and the decay properties and groundstate widths of the majority of these levels have been determined. For the lead scattering target the coherent elastic differential cross section has been studied in detail. There is evidence that below the photo-neutron threshold the elastic scattering via virtual photoexcitation of the nucleus can be approximated by extrapolating the real part of the Giant Dipole Resonance amplitude along a Lorentzian curve. Coulomb corrections to Delbrück scattering seem to play a small role at 6.5 MeV.

Table 4. Properties of levels observed by photoexcitation. $(d\sigma/d\Omega)^{NRF}$: experimental differential cross section per identified isotope or element for resonance scattering through $\Theta = 90°$. I^π: spin-parity of excited level; $W(\Theta)$: angular correlation function; $g = (2I_{ca}+1)/(2I_g+1)$; Γ_0: radiative groundstate transition width, Γ: total level width. Errors in the last digits are given in parentheses

Isotope	E_γ (MeV)	$(d\sigma/d\Omega)^{NRF}$ (μb/sr)	I^π	Γ_0/Γ^c	$W(\Theta)g\Gamma_0^2/\Gamma$ (meV)	Γ_0^f (meV)	Γ_0^g (meV)
^{238}U	2.754	13 (4)	(1)	0.77	0.145	0.084	-
^{238}U	3.254	421 (5)	1^-	0.24	0.83	1.5	0.52(15)[d]
^{209}Bi	6.555	2.1 (4)·10^2	-	-	0.74	0.74[b]	-
^{209}Bi	7.168	1.7 (3)·10^5	9/2$^+$[a]	1.00	710	786	820 (40)[e]
^{203}Tl	6.418	8.75(30)·10^3	1/2[a]	0.28	30	102	82 (15)[e]
Tl	6.759	7 (3)	-	-	-	-	-
Hg	6.555	68 (17)	-	-	-	-	-
^{186}W	6.418	5.2 (3)·10^2	1^-[a]	0.32	1.75	2.4	-
^{184}W	6.555	9.8 (10)·10^2	(1)	0.52	3.44	2.9	-
^{184}W	6.759	46 (10)	(1)	0.58	0.17	0.13	-
^{181}Ta	3.010	174 (17)	-	0.72	0.42	0.59	-
^{181}Ta	6.418	62 (4)	-	0.73	0.2	0.27[c]	-
^{181}Ta	6.759	4.8 (12)	-	-	0.018	0.018[b]	-
^{165}Ho	6.418	10.3 (30)	-	-	0.035	0.035[b]	-
^{165}Ho	6.759	5.6 (14)	-	-	0.021	0.021[b]	-
Nd	2.754	2.6 (5)	-	-	-	-	-
Nd	3.254	14.0 (10)	-	-	-	-	-
Ce	6.759	13.4 (10)	-	-	-	-	-
^{121}Sb	3.452	2.20 (5)·10^3	-	0.60	2.9	4.9[b]	-
^{100}Mo	6.418	1.53 (4)·10^4	1^-[a]	0.88	52	26	25 (8)[e]
^{94}Mo	6.555	4.4 (4)·10^3	(1)	0.33	15	21	-
Mo	6.759	6.2 (15)	-	-	-	-	-
Mo	7.168	8.2 (26)·10^2	-	-	-	-	-

[a] [11] [b] $W(\Theta)g\Gamma_0/\Gamma = 1$ assumed [c] $W(\Theta)g = 1$ assumed
[d] [28] (a small correction has been applied to the data of [28])
[e] Upper limits in case not all the transitions to lower levels were observed
[f] Present work [g] Previous work

RUTHENIUM
Z=44

Ruthenium, the last of the platinum metals to be discovered, was found in the insoluble residues arising from the refining of the extensive alluvial deposits of native platinum found in the Ural Mountain region of Russia. G. W. Osann announced in 1828 that he found three new elements in the residues; he called them pluran, ruthen, and polin. His work, discredited by the great Berzelius, later was a stimulus to the real discovery of ruthenium in 1844 by K. K. Klaus from the University of Kazan. This Russian chemist showed that Osann's ruthenium oxide was very impure but did contain a small amount of a new metal. Klaus adopted the name ruthenium, a latinized name for Russia, partly for patriotic reasons and partly in recognition of the earlier work of Osann.

REF. J. W. Jury, J. S. Hewitt, and K. G. McNeill
Can. J. Phys. 46, 1823 (1968)

ELEM. SYM.	A	Z
Ru		44

METHOD

REF. NO.	
68 Ju 1	EGF

REACTION	RESULT	EXCITATION ENERGY	SOURCE		DETECTOR		ANGLE
			TYPE	RANGE	TYPE	RANGE	
G,N	NOX	THR-27	C	27	THR	5-	DST

$$W(\theta) = a_o + a_1 P_1 + a_2 P_2$$

TABLE I

Target element	Z	Energy	a_0*	a_1/a_0	a_2/a_0
Vanadium	23	32	640 ± 50	0.11 ± 0.10	−0.09 ± 0.11
Chromium	24	22	365 ± 39	0.02 ± 0.08	0.00 ± 0.10
Manganese	25	22	450 ± 33	0.07 ± 0.05	−0.11 ± 0.06
Bromine	35	27	874 ± 54	0.05 ± 0.06	−0.15 ± 0.08
Molybdenum	42	22	610 ± 60	0.09 ± 0.05	−0.35 ± 0.06
Ruthenium	44	27	1160 ± 25	0.12 ± 0.02	−0.29 ± 0.03
Rhodium	45	27	1270 ± 47	0.06 ± 0.03	−0.14 ± 0.03
Palladium	46	27	1350 ± 29	0.26 ± 0.02	−0.12 ± 0.02
Antimony	51	27	2140 ± 62	0.04 ± 0.08	−0.25 ± 0.11
Lanthanum	57	27	1940 ± 70	0.12 ± 0.10	−0.52 ± 0.14
Praseodymium	59	30	1800 ± 58	0.20 ± 0.08	−0.40 ± 0.09
Platinum	78	27	2600 ± 52	0.17 ± 0.02	−0.15 ± 0.03
Lead	82	22	2274 ± 59	0.08 ± 0.08	−0.46 ± 0.09

*The yield per mole per 100 r was normalized to a yield of 2274 for the lead sample at the same energy.

RU
A=99

RU
A=99

REF. H. Bartsch, K. Huber, U. Kneissl and H. Krieger
Z. Physik A285, 273 (1978)

ELEM. SYM.	A	Z
Ru	99	44

METHOD

REF. NO. 78 Ba 11 hmg 11/17/80

REACTION	RESULT	EXCITATION ENERGY	SOURCE		DETECTOR		ANGLE
			TYPE	RANGE	TYPE	RANGE	
G,PG	LFT	22(21.8)*44(43.5)	C	20,40	SCD-D	---	135

Short-lived isomers in the nuclei ^{90,92}Nb, ^{99}Mo, ^{98,100,101}Tc and ^{101}Ru populated in photonuclear reactions were studied by pulsed beam techniques. Energy and half-life of the γ-rays deexciting the isomeric levels were measured by recording energy-time spectra. The delayed γ-rays and K X-rays were detected by means of an intrinsic Ge-detector of high resolution. From the measured intensity ratios internal conversion coefficients were determined. The multipolarities of the isomeric transitions could be deduced in most cases. A classification of the observed isomers has been tried on the basis of the obtained experimental results and most recent literature data.

*KeV, Isomer LFT

Table 1. Experimental results. E: energy. $T_{1/2}$: halflife, I_{rel}: relative intensity, L: multipolarity, H: hindrance factor

	Line	E [keV]	$T_{1/2}$ [μs]	$T_{1/2}$ [μs] (weighted average)	I_{rel}	α_K	Intensity ratios	L	H
^{90}Nb	K X-rays	–	–		1	–		–	–
	123	122.6±0.2	63 ±2		2.5	0.56±0.22		$E2$	120
^{92}Nb	K X-rays	–	–		1	–		–	–
	90	90.4±0.2	5.9 ±0.2		10.3	0.14±0.01		$E1$	$1.5\cdot10^7$
^{99}Mo	K X-rays	–	15.2 ±0.4	15.5 ±0.2	1	–		–	–
	98	97.8±0.1	15.6 ±0.2		0.95	1.45±0.27		$E2$	20
	138	137.7±0.2	0.79±0.09	0.76±0.06	1		I_{450}/I_{138} =	$M1$	–
	449	449.2±0.2	0.74±0.08		0.97		0.97±0.08	($M2$)	(37)
^{98}Tc	K X-rays	–	14.8 ±0.5	14.6 ±0.4	1			–	–
	22	21.8±0.2	16.4 ±2.7	from	0.036		I_{43}/I_{22} =	$E1+1\%\,M2$	10^7
	26	–	–	X, 43	–		5.1±0.5	($E2$)	–
	43	43.5±0.2	14.4 ±0.5		0.18			$M1$	–
^{100}Tc	K X-rays	–	8.2 ±0.7	8.2 ±0.3	1			–	–
	29	28.7±0.3	–	from	0.027		I_{172}/I_{29} =	$E2$	1
	172	172.3±0.3	8.2 ±0.3	X, 172	2.2		82±40	($M1$, $E2$)	–
^{101}Tc	K X-rays	–	–		1	–		–	–
	192	192.0±0.3	636 ±8		5.0	0.26±0.06		$M2$	560
^{101}Ru	K X-rays	–	16.1 ±3.9	17.5 ±0.4	1			–	–
	220	220.7±0.2	17.4 ±0.5	from	7.5		I_{306}/I_{220} =	$M2$	28
	306	306.6±0.3	17.7 ±0.6	220, 306	9.1		1.2±0.1	–	–

Ru
A=101

Ru
A=101

REF. H. Bartsch, K. Huber, U. Kneissl and H. Krieger
Z. Physik A285, 273 (1978)

ELEM. SYM.	A	Z
Ru	101	44

METHOD

REF. NO. 78 Ba 11 hmg 11/17/80

REACTION	RESULT	EXCITATION ENERGY	SOURCE TYPE	SOURCE RANGE	DETECTOR TYPE	DETECTOR RANGE	ANGLE
G,PG	LFT	29(28.7)*173(172.3)	C	20,40	SCD-D	---	135

*KeV, Isomer LFT

Short-lived isomers in the nuclei ^{90,92}Nb, ^{99}Mo, ^{98,100,101}Tc and ^{101}Ru populated in photonuclear reactions were studied by pulsed beam techniques. Energy and half-life of the γ-rays deexciting the isomeric levels were measured by recording energy-time spectra. The delayed γ-rays and *K* X-rays were detected by means of an intrinsic Ge-detector of high resolution. From the measured intensity ratios internal conversion coefficients were determined. The multipolarities of the isomeric transitions could be deduced in most cases. A classification of the observed isomers has been tried on the basis of the obtained experimental results and most recent literature data.

Table 1. Experimental results. *E*: energy, $T_{1/2}$: halflife, I_{rel}: relative intensity, *L*: multipolarity, *H*: hindrance factor

	Line	*E* [keV]	$T_{1/2}$ [μs]	$T_{1/2}$ [μs] (weighted average)	I_{rel}	α_K	Intensity ratios	*L*	*H*
^{90}Nb	*K* X-rays	–	–		1	–		–	–
	123	122.6 ± 0.2	63 ± 2		2.5	0.56 ± 0.22		*E*2	120
^{92}Nb	*K* X-rays	–	–		1	–		–	–
	90	90.4 ± 0.2	5.9 ± 0.2		10.3	0.14 ± 0.01		*E*1	$1.5 \cdot 10^7$
^{99}Mo	*K* X-rays	–	15.2 ± 0.4	15.5 ± 0.2	1	–		–	–
	98	97.8 ± 0.1	15.6 ± 0.2		0.95	1.45 ± 0.27		*E*2	20
	138	137.7 ± 0.2	0.79 ± 0.09	0.76 ± 0.06	1		I_{450}/I_{138} =	*M*1	–
	449	449.2 ± 0.2	0.74 ± 0.08		0.97		0.97 ± 0.08	(*M*2).	(37)
^{98}Tc	*K* X-rays	–	14.8 ± 0.5	14.6 ± 0.4	1			–	–
	22	21.8 ± 0.2	16.4 ± 2.7	from	0.036		I_{43}/I_{22} =	*E*1 + 1 % *M*2	10^7
	26	–	–	X, 43	–		5.1 ± 0.5	(*E*2)	–
	43	43.5 ± 0.2	14.4 ± 0.5		0.18			*M*1	–
^{100}Tc	*K* X-rays	–	8.2 ± 0.7	8.2 ± 0.3	1			–	–
	29	28.7 ± 0.3	–	from	0.027		I_{172}/I_{29} =	*E*2	1
	172	172.3 ± 0.3	8.2 ± 0.3	X, 172	2.2		82 ± 40	(*M*1, *E*2)	–
^{101}Tc	*K* X-rays	–	–		1	–		–	–
	192	192.0 ± 0.3	636 ± 8		5.0	0.26 ± 0.06		*M*2	560
^{101}Ru	*K* X-rays	–	16.1 ± 3.9	17.5 ± 0.4	1			–	–
	220	220.7 ± 0.2	17.4 ± 0.5	from	7.5		I_{306}/I_{220} =	*M*2	28
	306	306.6 ± 0.3	17.7 ± 0.6	220, 306	9.1		1.2 ± 0.1	–	–

Pu
A=102

Pu
A=102

Pu
A=102

REF. H. Bartsch, K. Huber, U. Kneissl and H. Krieger
Z. Physik A285, 273 (1978)

ELEM. SYM.	A	Z
Ru	102	44

METHOD

REF. NO. 78 Ba 11 | hmg 11/17/80

REACTION	RESULT	EXCITATION ENERGY	SOURCE TYPE	SOURCE RANGE	DETECTOR TYPE	DETECTOR RANGE	ANGLE
G,NG	LFT	221(220.7)*307(306.6)	C	20,40	SCD-D	---	135

*KeV, Isomer LFT

Short-lived isomers in the nuclei ^{90,92}Nb, ^{99}Mo, ^{98,100,101}Tc and ^{101}Ru populated in photonuclear reactions were studied by pulsed beam techniques. Energy and half-life of the γ-rays deexciting the isomeric levels were measured by recording energy-time spectra. The delayed γ-rays and K X-rays were detected by means of an intrinsic Ge-detector of high resolution. From the measured intensity ratios internal conversion coefficients were determined. The multipolarities of the isomeric transitions could be deduced in most cases. A classification of the observed isomers has been tried on the basis of the obtained experimental results and most recent literature data.

Table 1. Experimental results. E: energy. $T_{1/2}$: halflife, I_{rel}: relative intensity, L: multipolarity, H: hindrance factor

	Line	E [keV]	$T_{1/2}$ [μs]	$T_{1/2}$ [μs] (weighted average)	I_{rel}	α_K	Intensity ratios	L	H
^{90}Nb	K X-rays	–	–		1	–		–	–
	123	122.6±0.2	63 ±2		2.5	0.56±0.22		$E2$	120
^{92}Nb	K X-rays	–	–		1	–		–	–
	90	90.4±0.2	5.9 ±0.2		10.3	0.14±0.01		$E1$	$1.5\cdot10^7$
^{99}Mo	K X-rays	–	15.2 ±0.4	15.5 ±0.2	1	–		–	–
	98	97.8±0.1	15.6 ±0.2		0.95	1.45±0.27		$E2$	20
	138	137.7±0.2	0.79±0.09	0.76±0.06	1		I_{450}/I_{138} =	$M1$	–
	449	449.2±0.2	0.74±0.08		0.97		0.97±0.08	$(M2)$	(37)
^{98}Tc	K X-rays	–	14.8 ±0.5	14.6 ±0.4	1			–	–
	22	21.8±0.2	16.4 ±2.7	from	0.036		I_{43}/I_{22} =	$E1+1\%\,M2$	10^7
	26	–	–	X, 43	–		5.1±0.5	$(E2)$	–
	43	43.5±0.2	14.4 ±0.5		0.18			$M1$	–
^{100}Tc	K X-rays	–	8.2 ±0.7	8.2 ±0.3	1			–	–
	29	28.7±0.3	–	from	0.027		I_{172}/I_{29} =	$E2$	1
	172	172.3±0.3	8.2 ±0.3	X, 172	2.2		82±40	$(M1, E2)$	–
^{101}Tc	K X-rays	–	–		1	–		–	–
	192	192.0±0.3	636 ±8		5.0	0.26±0.06		$M2$	560
^{101}Ru	K X-rays	–	16.1 ±3.9	17.5 ±0.4	1			–	–
	220	220.7±0.2	17.4 ±0.5	from	7.5		I_{306}/I_{220} =	$M2$	28
	306	306.6±0.3	17.7 ±0.6	220, 306	9.1		1.2±0.1	–	–

REF. H. Bartsch, W. Günther, K. Huber, U. Kneissl & H. Krieger
Z. Phys. A285, 71 (1978)

ELEM. SYM.	A	Z
Ru	102	44

METHOD

REF. NO. 78 Ba 14 hg

REACTION	RESULT	EXCITATION ENERGY	SOURCE		DETECTOR		ANGLE
			TYPE	RANGE	TYPE	RANGE	
G,P	RLY	9-65	C	65	SCD-D		4PI

Isomeric cross section ratios were measured for the photonuclear reactions ^{100}Mo(γ, n) ^{99m_1,m_2,g}Mo and ^{102}Ru(γ, p) ^{101m,g}Tc. Using the Huizenga-Vandenbosch-method spin cut-off parameters were deduced. The applicability of this statistical procedure is discussed. A systematic analysis of all known ($\gamma, x n$) isomeric ratio-measurements shows a linear correlation between derived spin cut-off parameters and the mean value of the spins of the isomeric pair.

ISOMER YIELD, DE-EX G

Table 1. Experimental and theoretical results

Process	Targetspin ($\hbar$)	E_γ(keV)	$t_{1/2}$	Spin high ($\hbar$)	Spin low ($\hbar$)	R_{exp}	SCOP($\hbar$)
^{100}Mo(γ, n)	0^+	449.2	760 ns	$11/2^-$	$5/2^+$	0.11 ± 0.02	4.3 ± 0.4
		137.7		$11/2^-$	$1/2^+$	0.10 ± 0.02	4.3 ± 0.4
		97.8	15.5 μs	$5/2^-$	$1/2^+$	0.94 ± 0.25	1.8 ± 0.3
^{102}Ru(γ, p)	0^+	191.9	636 μs	$9/2^+$	$1/2^-$	1.33 ± 0.30	1.65 ± 0.35
		306.6					

$$Rexp = \frac{Y \text{ high spin}}{Y \text{ low spin}}$$

# RHODIUM
Z=45

Rhodium was discovered in 1803-04 by W. H. Wollaston (1766-1828) while working in London. He was investigating methods to improve the technology for the refining and fabrication of platinum. Some 7000 ounces of native platinum from South America had been dissolved in aqua regia to remove the platinum. Wollaston discovered the new element when he decomposed the substance precipitated by the addition of mercurous cyanide. He choose the name rhodium (from the Greek *rhodon*, rose) in recognition of the beautiful color of the chloro salt and its aqueous solutions.

Rh
A=103

Rh
A=103

Ref. W.K. Dawson
Can. J. Phys. 34, 1480 (1956)

Elem. Sym.	A	Z
Rh	103	45

Method: Synchrotron; proton yield, spectrum; angular distribution; nuclear emulsion; ion chamber.

Ref. No.: 56 Da 2 | NVB

Reaction	E or ΔE	E_0	Γ	$\int \sigma dE$	Jπ	Notes
$Rh^{103}(\gamma,xp)$	70					Yield = 2.6×10^5 protons(up to 16 MeV)/r-mole ± 30% for 70 MeV Bremss.

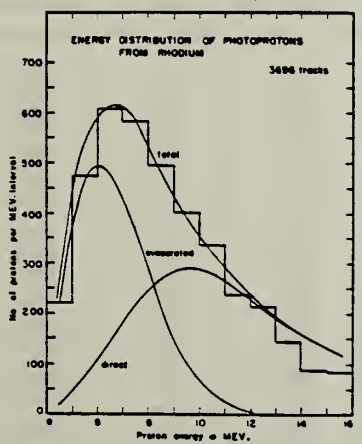

FIG. 4. The calculated energy distribution (smooth curve marked total) contains both evaporated and direct protons in a 1 to 1 ratio. The separate distributions are also shown. A constant nuclear temperature of 1.0 Mev. was used for the evaporated proton energy distribution.

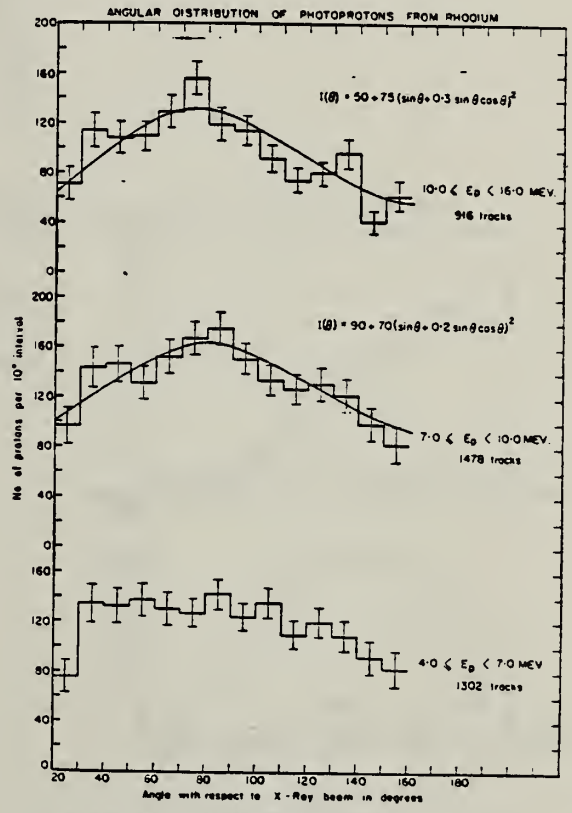

FIG. 8. The angular distributions of photoprotons of various energies from rhodium. Standard deviations are shown. The smooth curves were calculated from equation (6).

B.G. Chidley, L. Katz, S. Kowalski
Can. J. Phys. 36, 407 (1958)

ELEM. SYM.	A	Z
Rh	103	45

Betatron

REF. NO.	
58 Ch 2	NVB

REACTION	RESULT	EXCITATION ENERGY	SOURCE		DETECTOR		ANGLE
			TYPE	RANGE	TYPE	RANGE	
G,N	RLY	THR	C	THR	BF3-I		4PI

See 58 Ka 1 for cross sections.

THRESHØLD

TABLE I

MEASURED PHOTONEUTRON THRESHOLDS

Reaction	Measured Q value, Mev.	Other Q values, Mev.	Method	Reference
$Rh^{103}(\gamma, n)Rh^{102}$	9.46±0.08			
		9.35 ±0.20	Threshold	Sher *et al.* (1951)
		9.45 ±0.30	Mass data	Duckworth (unpublished)
			Q^- value	Kochendorfer and Farmer (1954)
		9.41 ±0.34	Mass data	Duckworth (unpublished)
			Q^+ value	Kochendorfer and Farmer (1954)

L. Katz, G.B. Chidley Nuclear Reactions at Low and Medium Energies (Academy of Science, USSR: 1958) 371	Rh	103	45
METHOD: Betatron; neutron cross section; BF_3 counters; ion chamber monitor	REF. NO. 58 Ka 1		NVB

REACTION	RESULT	EXCITATION ENERGY	SOURCE		DETECTOR		ANGLE
			TYPE	RANGE	TYPE	RANGE	
G,XN	ABX	9-22	C	9-22	BF3-I		4PI

Таблица 2

Пороги испускания фотонейтронов

Изотоп	B_n, *Мэв*	B_{2n}, *Мэв*	Изотоп	B_n, *Мэв*	B_{2n}, *Мэв*
V^{51}	11,16	20,5	L^{139}	8,81	16,1
Mn^{55}	10,14	19,2	Pr^{141}	9,46	17,6
Co^{59}	10,44	18,6	Tb^{159}	8,16	14,8
As^{75}	10,24	18,1	Ho^{165}	8,10	14,6
Y^{89}	11,82	20,7	Tm^{169}	8,00	14,7
Nb^{93}	8,86	17,1	Lu^{175}	7,77	14,2
Rh^{103}	9,46	16,8	Ta^{181}	7,66	13,8
J^{127}	9,14	16,2	Au^{197}	7,96	13,3
Cs^{133}	9,11	16,5	Bi^{209}	7,43	14,5

THRESHOLDS

не приведены, поскольку они превышают 22 *Мэв* во всех случаях, кроме золота, для которого $B_{2n}=21$ *Мэв*. Свойства сечений $\sigma_C(\gamma)$ сведены в табл. 3.

Таблица 1

Изотоп	$E_{макс}$, *Мэв*	$\sigma_n(E_\gamma)$, барн	T, *Мэв*	$\int\sigma_C d\gamma$, *Мэв·барн*	$Y(22)$, 10^{-6} нейтрон/100 р·моль
V^{51}	18,4	0,062	5,2	0,33	1,62
Mn^{55}	20,2	0,060	7,0	0,39	2,01
Co^{59}	18,3	0,068	6,3	0,44	2,30
As^{75}	16,4	0,090	9,5	0,74	4,25
Y^{89}	17,1	0,172	5,2	0,93	5,33
Nb^{93}	18,0	0,156	7,5	1,17	6,80
Rh^{10}	17,5	0,160	9,4	1,40	8,28
J^{127}	15,2	0,273	6,8	1,76	11,9
Cs^{133}	16,5	0,238	7,7	1,59	10,7
La^{139}	15,5	0,325	3,8	1,55	11,2
Pr^{141}	15,0	0,320	4,9	1,93	13,1
Tb^{159}	15,6	0,274	9,8	2,49	18,1
Ho^{165}	13,5	0,305	8,9	2,52	18,7
Tm^{169}	16,4	0,250	8,4	1,91	14,9
Lu^{175}	16,0	0,225	8,4	1,90	23,0
Ta^{181}	14,5	0,380	8,5	3,15	22,0
Au^{197}	13,8	0,475	4,7	3,04	22,6
Bi^{209}	13,2	0,455	5,9	2,89	23,2

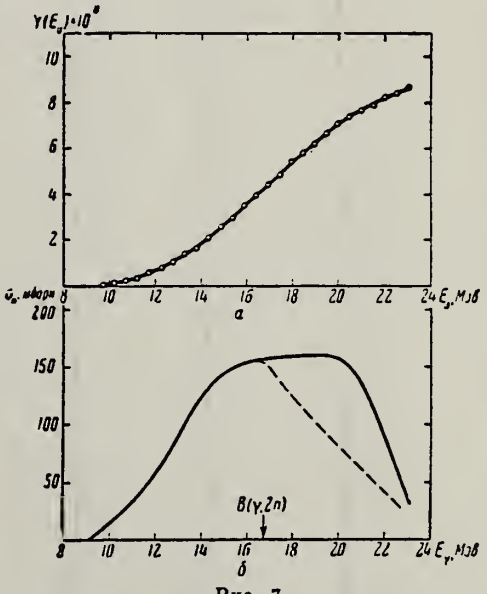

Рис. 7.

а — Выход фотонейтронов для Rh; б — $\sigma_n(E_\gamma)$ и $\sigma_C(\gamma)$ для Rh

Ref. M.E. Toms, J. McElhinney
Phys. Rev. 111, 561 (1958)

Elem. Sym.	A	Z
Rh	103	45

Method: Betatron; alpha spectrum; nuclear emulsion

Ref. No.: 58 To 2 | NVB

Reaction	E or ΔE	E_o	Γ	$\int \sigma dE$	Jπ	Notes
$Rh^{103}(\gamma,\alpha)$	Bremss. 22					Yield = 0.3×10^{4} alpha/mole/roentgen

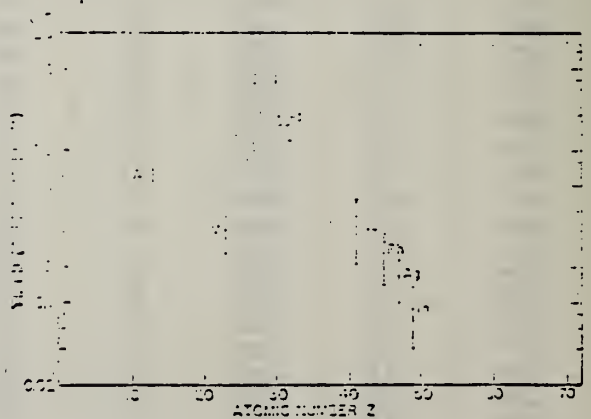

FIG. 8. Photo-alpha yields plotted against atomic numbers for the exposures of the survey.

REF.

N. Ikeda and K. Yoshihara
Radioisotopes (Tokyo) 8, 24 (1959)

ELEM. SYM.	A	Z
Rh	103	45

METHOD

REF. NO. 59 Ik 1 EGF

REACTION	RESULT	EXCITATION ENERGY	SOURCE		DETECTOR		ANGLE
			TYPE	RANGE	TYPE	RANGE	
G,G/	ABX	1.3	D	1.3	ACT-I		4PI

Source was 10 kc ^{60}Co.

Activation cross section 3×10^{-32} cm^2.

Activation of 57m 40 keV state.

Ref. R.W. Parsons
Can. J. Phys. 37, 1344 (1959)

Elem. Sym.	A	Z
Rh	103	45

Method: 24 MeV betatron; neutron yield; BF_3 chamber, Lucite ionization chamber

Ref. No.: 59 Pa 2 | EH

Reaction	E or ΔE	E_o	Γ	$\int \sigma dE$	Jπ	Notes
$Rh^{103}(\gamma,n)$	Bremss. 24	14.5	3.4 MeV			σ_a = 104 mb
		17	4.5 MeV			σ_b = 164 mb
						Q_o = 2.1b compared to 2.2 b found in Coulomb excitation experiments of Heydenburg and Temmer [Phys. Rev. 95, 861 (1954)].

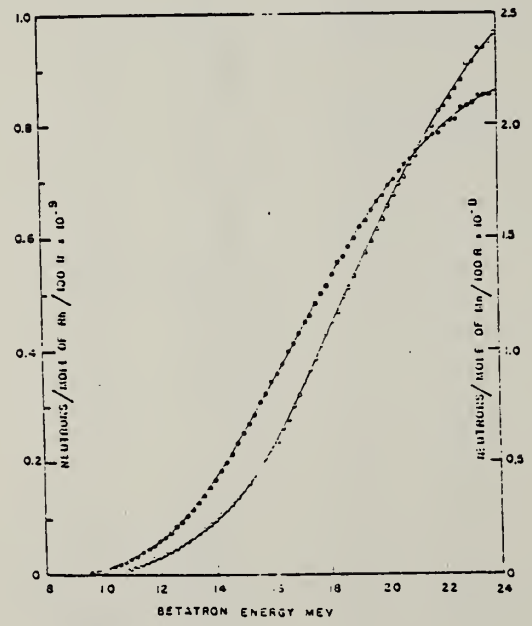

FIG. 1. Photoneutron yield versus betatron energy. ○ manganese; ○ rhodium.

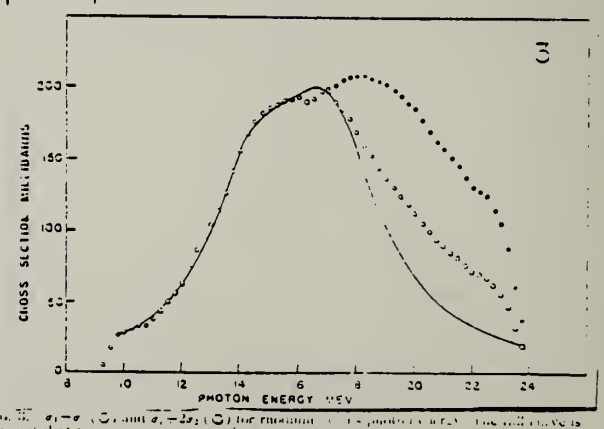

FIG. 3. $\sigma_1 = \sigma_a$ (○) and $\sigma_2 = \sigma_b$ (○) for rhodium [illegible]. The full curves is compounded of two resonance curves whose parameters are given in the text.

FORM NBS-418
(6-1-63)
USCOMM-DC 16556-P63

U.S. DEPARTMENT OF COMMERCE
NATIONAL BUREAU OF STANDARDS

Ref. O.V. Bogdankevich, L.E. Lazareva, A.M. Moiseev
Zhur, Eksp. i Teoret. Fiz. 39, 1224 (1960)
Soviet Phys. JETP 12, 853 (1961)

Elem. Sym.	A	Z
Rh	103	45

Method: 30-MeV synchrotron; activation

Ref. No.: 60 Bo 2 | JHH

Reaction	E or ΔE	E_o	Γ	$\int \sigma dE$	Jπ	Notes
$Rh^{103}(\gamma,\gamma^1)Rh^{103m}$	5.9-25.5 Bremss.	9.3 ~ 20				In Table II, below, (γ,γ^1) is compared with $_n = (\gamma,n)+(\gamma,2n)$ as measured by Parsons [Can. J. Phys. 37, 1344 (1959)].

Table II

E. Mev	σ (γ, γ'), mb	σ_n, mb	σ (γ, γ')/σ_n	E. Mev	σ (γ, γ'), mb	σ_n, mb	σ (γ, γ')/σ_n
5	1.8	—	—	12	0.6	62.1	0.01
7	8.5	—	—	14	1.2	155.2	~0.01
9.3	21.2	—	—	16	2.7	193.1	~0.01
9.35	21.1	10.3	2.04	18	6.1	169.0	0.04
9.5	14.8	17.2	0.86	19	9.2	136.2	0.07
9.75	4.4	25.2	0.18	20	10.3	111.0	0.09
10	2.6	27.6	0.09	21	8.7	87.9	0.10
11	1.0	37.2	0.03	22	4.4	71.7	0.06

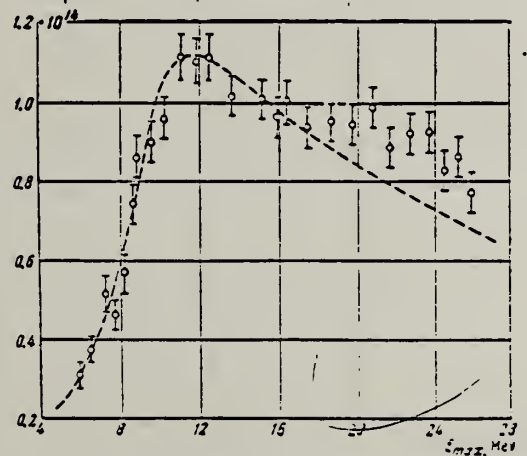

FIG. 1. Yield of the reaction $Rh^{103}(\gamma,\gamma')Rh^{103m}$ at various maximum x-ray energies E_{max}. Ordinates – saturated activity per second per mole per ampere of ionization current of the absolute chamber. The dashed curve is the yield curve calculated under the assumption that the reaction cross section is zero at energies above 12.5 Mev.

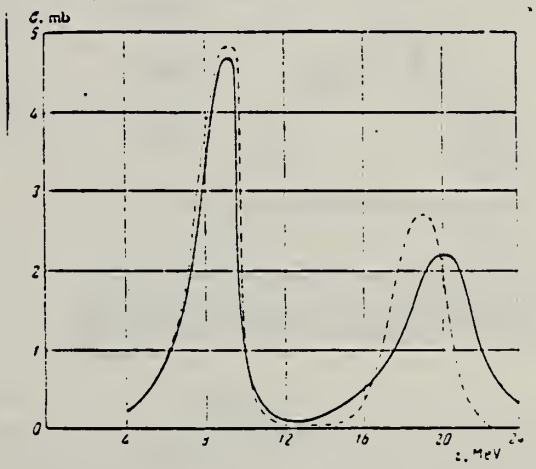

FIG. 2. Cross section of the reaction $Rh^{103}(\gamma,\gamma')Rh^{103m}$. Two versions of the calculation are given; other versions yield intermediate values.

REF.
K.N. Geller, J. Halpern, E.G. Muirhead
Phys. Rev. 118, 1302 (1960)

ELEM. SYM.	A	Z
Rh	103	45

METHOD
Betatron; neutron threshold; ion chamber

REF. NO.
60 Ge 3 NVB

REACTION	RESULT	EXCITATION ENERGY	SOURCE		DETECTOR		ANGLE
			TYPE	RANGE	TYPE	RANGE	
G,N	NØX	THR	C	THR	BF3-I		4PI

THRESHØLD

TABLE I. Summary and comparison of neutron separation energies inferred from present threshold measurements with values predicted from mass data and reaction energies. All energies are expressed in the center-of-mass system in Mev.

Reaction	No. runs	Present results	Other results	Method	Reference
$Rh^{103}(\gamma,n)Rh^{102}$	2	9.307±0.032	9.40 ±0.33	mass data	m
				$Q(\beta^+)$	n
			9.46 ±0.30	mass data	m
				$Q(\beta^-)$	n
			9.46 ±0.08	threshold	f

[m] Henry E. Duckworth, *Mass Spectroscopy* (Cambridge University Press, New York, 1958), p. 177.
[n] L. J. Lidofsky, Revs. Modern Phys. 29, 773 (1957).

Ref. O.V.Bogdankevich, B.I.Goryachev, V.A.Zapevalov Zhur.Eksptl. i Teoret.Riz. 42, 1502 (1962); Soviet Phys.JETP 15, 1044 (1962)	Elem. Sym.	A	Z
	Rh	103	45

Method 30 MeV Synchrotron - BF_3	Ref. No.
	62Bo1

Reaction	E or ΔE	E_o	Γ	$\int \sigma dE$	Jπ	Notes
(γ,n)	threshold 23 MeV	Fig.3 fitted with smooth curve which is superposition of 2 Lorentz lines - Data for Lorentz lines given in Table 1 ($\sigma_{int} = \int_0 \gamma dE_\gamma$ $E = R_1 - R_2/R_o$, R_1 and R_2 are axes of nuclear ellipsoid. R_o radius of sphere with volume equal to nuclear ellipsoid).				

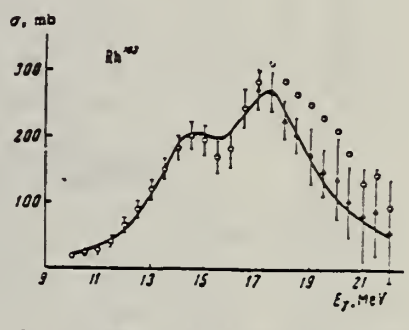

FIG. 3. Photoneutron production cross section of Rh^{103}. Here and in the other graphs we denote the experimental values of σ_n by circles, the computed values of σ_γ by triangles.

Table I

	Ta^{181}	Rh^{103}	In^{115}		Ta^{181}	Rh^{103}	In^{115}
σ_1^{max}, mb	350	150	166	σ_{int2}, MeV·b	2.38	1.43	1.43
E_{01}, MeV	12.4	14.25	14	$\sigma_{int2}/\sigma_{int1}$	1.8	2.0	1.8
Γ_1, MeV	2.4	3.0	3.0	σ_{int}, MeV·b	3.70	2.13	2.21
σ_{int1}, MeV·b	1.32	0.706	0.78	$\sigma_{int}/(0.058NZ/A)$	1.46	1.44	1.36
σ_2^{max}, mb	400	240	240	s	0.23	0.21	0.15
E_{02}, MeV	15.5	17.5	16.25	ε_0	0.22	0.20	0.14
Γ_2, MeV	3.8	3.8	3.8	Q_0, b	7.1±0.8	2.7±0.3	2.3±0.4

Ref. V.G.Shevchenko, B.A.Yur'ev

Zhur.Eksptl. i Teoret.Fiz. 42, 707 (1962)
Soviet Phys.JETP 15, 492 (1962)

Elem. Sym.	A	Z
Rh	103	45

Method
35 MeV Betatron ; nuclear emulsions

Ref. No.
62Sh2

Reaction	E or ΔE	E_o	Γ	$\int \sigma dE$	Jπ	Notes
(γ, p)	$E_{\gamma max}$= 22.5 33.5					Angular distribution of photoprotons fitted to $a \pm b\sin^2\theta(1 + p\cos\theta)^2$ where a, b and p are given in the article. Quadrapole absorption is estimated to be about 20%.

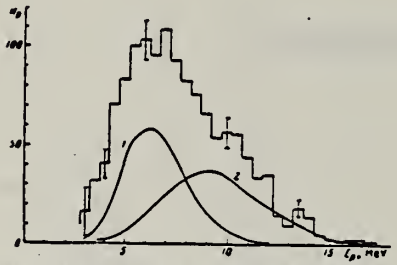

FIG. 1. Energy distribution of 1287 photoprotons from for $E_{\gamma max}$ = 22.5 MeV. Calculated spectra: curve 1 for ev: rated protons; curve 2 for protons from the direct photoeff

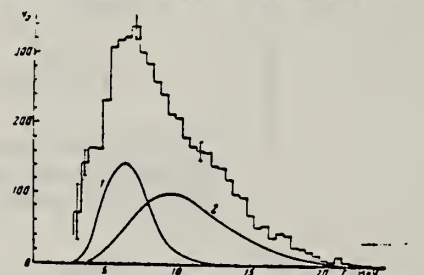

FIG. 2. Energy distribution of 5222 photoprotons from Rh^{103} for $E_{\gamma max}$ = 33.5 MeV. Same notation as in Fig. 1.

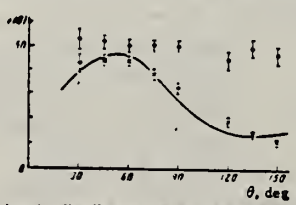

FIG. 6. Angular distributions of photoprotons from Rh^{103} for $E_{\gamma max}$ = 33.5 MeV. ●–E_p = 3.25–9.25 MeV; x–E_p > 9.25 MeV.

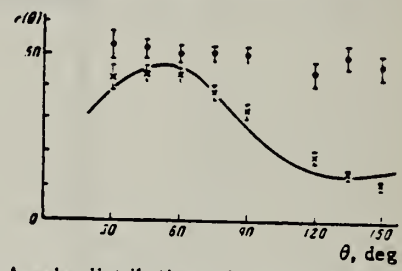

FIG. 6. Angular distributions of photoprotons from Rh^{103} for $E_{\gamma max}$ = 33.5 MeV. ●–E_p = 3.25–9.25 MeV; x–E_p > 9.25 MeV.

Table I. Parameters of curves of $a + b\sin^2\theta(1 + p\cos\theta)^2$ and estimated contributions of E2 transitions

Element	Z	$E_{\gamma max}$, MeV	E_p, MeV	a	b	p	$\sigma_{E2}/\sigma_{E1+E2}$, %
Rh	45	22.5	3.25–9.25	97	0	0	0
			>9.25	28	19	0.2	~1
		33.5	3.25–9.25	49	0	0	0
			>9.25	14.5	16	1.2	~20
Pt	78	33.5	7.25–14.25	34.5	15.5	2.6	~60
			>14.25	3	8	3.8	~75
Pb	82	22.5	>5.25	15.5	13	1.8	~40
			>10.25	6.5	8	2.2	~50

Table II. Measured yields Y of photoprotons from Rh, Pt, and Pb, and estimates based on the evaporation model and on the direct photoeffect

Element	Rh		Pt	Pb
$E_{\gamma max}$, MeV	22.5	33.5	33.5	22.5
Y_{exp}, protons/mole-roentgen	$1.3 \cdot 10^5$	$2.8 \cdot 10^5$	$9.6 \cdot 10^4$	$2.9 \cdot 10^4$
Y_{exp}/Y_{evap}	~3	~6	~2000	~1500
Y_{exp}/Y_{direct}	~3	~4.5	~20	~11

Ref. V.G. Shevchenko. B.A. Yurev
Nuclear Phys. 37, 495 (1962)

Elem. Sym.	A	Z
Rh	103	45

Method: 35 - MeV betatron; emulsions

Ref. No.: 62 Sh 4 — JHH

Reaction	E or ΔE	E_o	Γ	$\int \sigma dE$	Jπ	Notes
$Rh^{103}(\gamma,p)$	Bremss. 22.5 33.5					Parameters a, b and p for $\omega(\theta_p) = a + b \sin^2\theta(1 + p\cos\theta)^2$ in Table I.

Coefficients of expressions of type [illegible]

Element	Z	$E_{\gamma max}$ (MeV)	E_p (MeV)	a	b	p	[illegible]
Rh	45	22.5	3.25-9.25	1.0	0	0	[illegible]
			> 9.25	[illegible]	1.0	0.2	[illegible]
		33.5	3.25-9.25	12.2	0	0	[illegible]
			> 9.25	4.5	[illegible]	1.2	[illegible]
Pr	59	22.5	[illegible]-7.25	1.4	0.7	0.42	[illegible]
			7.25-11.25	2.9	4.4	[illegible]	[illegible]
			> 11.25	1.5	3.4	[illegible]	
		33.5	4.5-7.25	3.3	1.2	[illegible]	[illegible]
			7.25-11.25	4.2	1.35	2.2	[illegible]
			> 11.25	0.8	1.2	1.5	[illegible]
W	74	22.5	[illegible]	[illegible]	[illegible]	[illegible]	[illegible]
			[illegible]-12.75	2.5	[illegible]	[illegible]	[illegible]
			> 12.75	2.2	[illegible]	[illegible]	[illegible]
		33.5	[illegible]	1.2	[illegible]	[illegible]	[illegible]
			[illegible]-12.75	1.3	0.35	2.0	[illegible]
			> 12.75	[illegible]	[illegible]	[illegible]	[illegible]
Pt	78	22.5	[illegible]	0.6	1.0	[illegible]	[illegible]
			[illegible]-11.75	2.5	[illegible]	1.2	[illegible]
			> 11.75	1.4	[illegible]	[illegible]	[illegible]
		33.5	7.25-14.25	2.1	[illegible]	[illegible]	[illegible]
			[illegible]	[illegible]	[illegible]	[illegible]	[illegible]
Pb	82	22.5	[illegible]	1.05	[illegible]	[illegible]	[illegible]
			[illegible]	0.75	[illegible]	[illegible]	[illegible]
		33.5	[illegible]	1.0	1.2	[illegible]	[illegible]
			[illegible]-14.25	1.15	[illegible]	2.0	[illegible]
			[illegible]	[illegible]	[illegible]	[illegible]	[illegible]

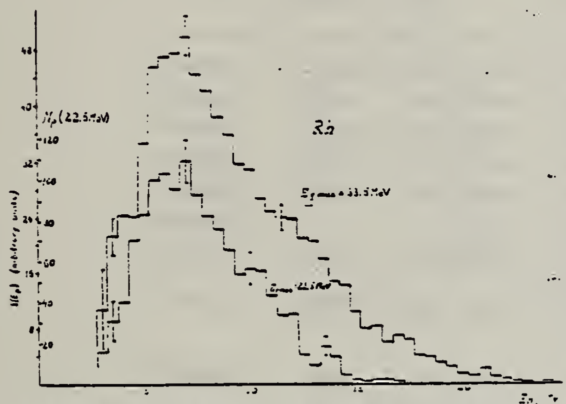

Fig. 2. Energy distributions of photoprotons from Rh^{103} when irradiated with $E_{\gamma max}$ = 22.5 and 33.5 MeV. N_p is the number of protons in the spectrum interval [illegible] MeV. Relative scale [illegible] $I(E_p)$ are chosen the same for all spectra in figs. [illegible] statistical errors are given.

Table 2

Measured photoproton yields and [illegible]

Element	$E_{\gamma max}$ (MeV)	[illegible]	[illegible]	[illegible]
Rh^{103}	[illegible]	[illegible]	[illegible]	[illegible]
	33.5	[illegible]	[illegible]	[illegible]
[illegible]	[illegible]	[illegible]	[illegible]	[illegible]
	33.5	[illegible]	[illegible]	[illegible]
W	22.5	[illegible]	[illegible]	[illegible]
	[illegible]	[illegible]	[illegible]	≈ 11
Pt	[illegible]	[illegible]	[illegible]	[illegible]
	33.5	[illegible]	[illegible]	[illegible]
Pb	[illegible]	[illegible]	[illegible]	[illegible]
	[illegible]	[illegible]	[illegible]	[illegible]

[illegible]

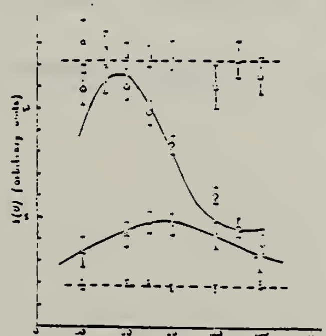

Fig. 7. Angular distributions of photoprotons from Rh^{103}. Experimental points for irradiation with bremsstrahlung γ-spectrum with $E_{\gamma max}$ = 22.5 MeV are designated by solid dots for E_p 3.25-9.25 MeV and by crosses for E_p > 9.25 MeV. For the case of $E_{\gamma max}$ = 33.5 MeV squares denote E_p = 3.25-9.25 MeV and centred circles E_p > 9.25 MeV. Curves plotted through experimental points are described by expressions of the type (1), the coefficients for which are given in table 1.

References

1) M. E. Toms and W. E. Stephens, Phys. Rev. 98 (1955) 626
2) M. M. Hoffman and A. G. W. Cameron, Phys. Rev. 92 (1953) 1184
3) W. C. Barber and V. J. Vanhuyse, Nuclear Physics 16 (1960) 381
4) M. E. Toms and W. E. Stephens, Phys. Rev. 92 (1953) 362
5) E. D. Makhnovsky, JETP 38 (1960) 95
6) R. B. Taylor, Nuclear Physics 19 (1960) 453
7) A. G. W. Cameron, W. Harms and L. Katz, Phys. Rev. 83 (1951) 1264
8) V. G. Neudachin, V. G. Shevchenko and N. P. Yudin, Report at the Second All-Union Conf. for Nuclear Reactions at Low and Medium Energies, Moscow, 1960
9) E. D. Courant, Phys. Rev. 82 (1951) 703
10) V. V. Balashov, V. G. Shevchenko and N. P. Yudin, JETP 41 (1961) 1929

REF.

B.S. Ishkanov, E.N. Kornienko, Yu.I. Sorokin, V.G. Shevchenko, B.A. Yur'ev
Zhur. Eksp. i Teoret. Fiz. 45, 38 (1963); Soviet Phys. JETP 18, 29 (1964)

ELEM. SYM.	A	Z
Rh	103	45

METHOD

Betatron; proton cross section; CsI; ion chamber

REF. NO. 63 Is 2 NVB

REACTION	RESULT	EXCITATION ENERGY	SOURCE		DETECTOR		ANGLE
			TYPE	RANGE	TYPE	RANGE	
G,XP	ABX	13-32	C	14-32	SCI-D	3-+	DST
				(14.5-32.5)		(3.5-+)	

E peak	σ peak	half width
19±0.5 MeV	8±1.5 mb	~ 5.5 MeV

$$\int_{13}^{32} \sigma dE = 85 \pm 15 \text{ MeV-mb}$$

Discuss quadrupole resonance.

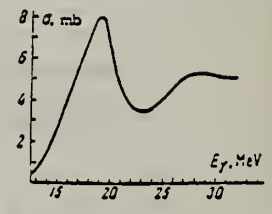

FIG. 3. Plot of the $Rh^{103}(\gamma, p)$ reaction cross section against the energy E_γ.

A. Veres
Acta Phys. Acad. Sci.Hung. 16, 261-73 (1963)

Rh	103	45

METHOD: Radioactive source

REF. NO.: 63 Ve 2 | NVB

REACTION	RESULT	EXCITATION ENERGY	SOURCE TYPE	SOURCE RANGE	DETECTOR TYPE	DETECTOR RANGE	ANGLE
G,G/	ABX	0-1	D	0-1	NAI-D		

Activation by ^{60}Co radiation.

ISOMERS

Таблица II

Измеренные значения после облучения, сравниваемые с другими литературными данными

Элемент	Активность облучения после первого измерения (имп/мин.)	Активн. экстрп. в конце облуч. (имп/мин.)	Литературные данные $T_{1/2}$	Литературные данные E (кэв)	Данные измерений $T_{1/2}$	Данные измерений E (кэв)	σ_m (10^{-28} см^2)	Γ_{ym} (10^{-3} эв)
Se-77m	3842±96	5400	17,5 сек.	160	18,1±1 сек.	160±10	9,5	1,75
Sr-87m	191±5	200	2,8 ч.	390	2,9±0,1 ч.	365±25	0,85	0,2
Y-89m	96±20	170	16 сек.	910	16,7±5 сек.		0,08	0,02
Rh-103m	28±5	31	57 мин.	40	58±2 мин.	20,5±0,5	0,08	0,01
Ag-107m	220±14	250	44 сек.	93	43,8±0,6 сек	91±10	0,8	0,2
Ag-109m			39 сек.	88				
Hf-179m	80±18	155	19 сек.	160; 215	19±2 сек.		1	0,2
Ir-191m	90±20	250	4,9 сек.	42; 130	5±2 сек.		5,6	1
Pt-195m	90±9	100	3,5 д.	31; 100; 130;	3,5±0,2 д.	32±3 67,5±5 96±5 130±10	0,2	0,04
Au-197m	240±16	520	7,2 сек.	130; 277; 407	7,2±1 сек.	68:130: 280±20 390±20	0,07	0,01
Hg-199m	9,6±3,2		42 мин.	160; 370			0,005	0,001

Acta Phys. Hung. Tom. XVI. Fasc. 3.

REF.

P. Kruger, T. M. Crawford, J. Goldemberg and W. C. Barber
Nuclear Phys. 62, 584 (1965)

ELEM. SYM.	A	Z
Rh	103	45

METHOD

REF. NO.	
65 Kr 1	EGF

REACTION	RESULT	EXCITATION ENERGY	SOURCE		DETECTOR		ANGLE
			TYPE	RANGE	TYPE	RANGE	
G,2P	ABX	15-40	C	15-40	ACT-I		4PI
G,G/	RLY	7-18	C	7-18	ACT-I		4PI
E,E/	RLY	7-18	D	7-18	ACT-I		4PI

(Last two cards) E/G ISOMER YIELD

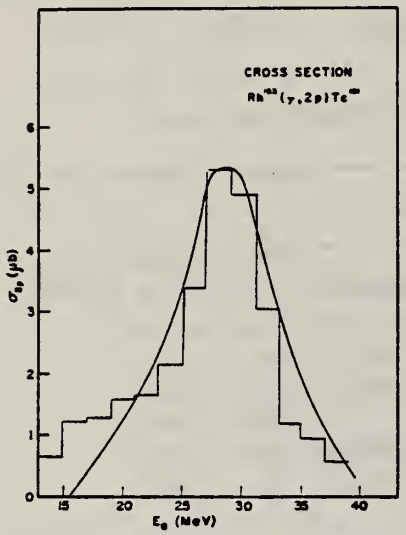

Fig. 4. Cross section for the reaction $Rh^{103}(\gamma, 2p)Tc^{101}$.

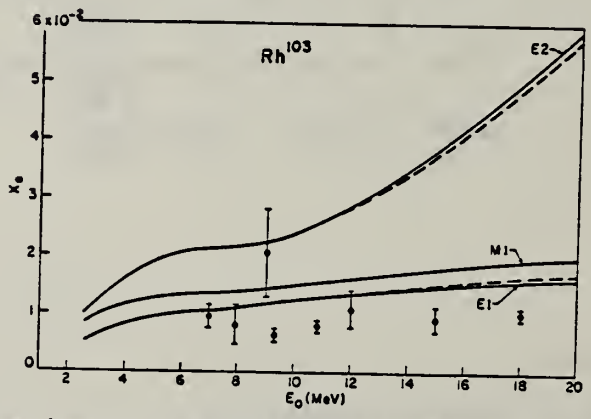

Fig. 5. Experimental results for the ratio of electron/photon yields in Rh^{103m} and the theoretical predictions under the assumptions that the cross section is made up entirely of either E1, M1, or E2 transitions (solid curves). The dashed curve lying near the E1 curve was computed under the assumption that the first peak in the cross section curve is E1 while the second peak is E2. The dashed curve lying near the E2 curve was computed under the assumption that the first peak is E2 and the second is E1.

REF. R. R. Hurst and D. J. Donahue
Nucl. Phys. A91, 365 (1967)

ELEM. SYM.	A	Z
Rh	103	45

METHOD: Neutron capture gamma rays

REF. NO.: 67 Hu 1 EGF

REACTION	RESULT	EXCITATION ENERGY	SOURCE TYPE	SOURCE RANGE	DETECTOR TYPE	DETECTOR RANGE	ANGLE
G,N	ABX	10,11	D	10,11	BF3-I		4PI

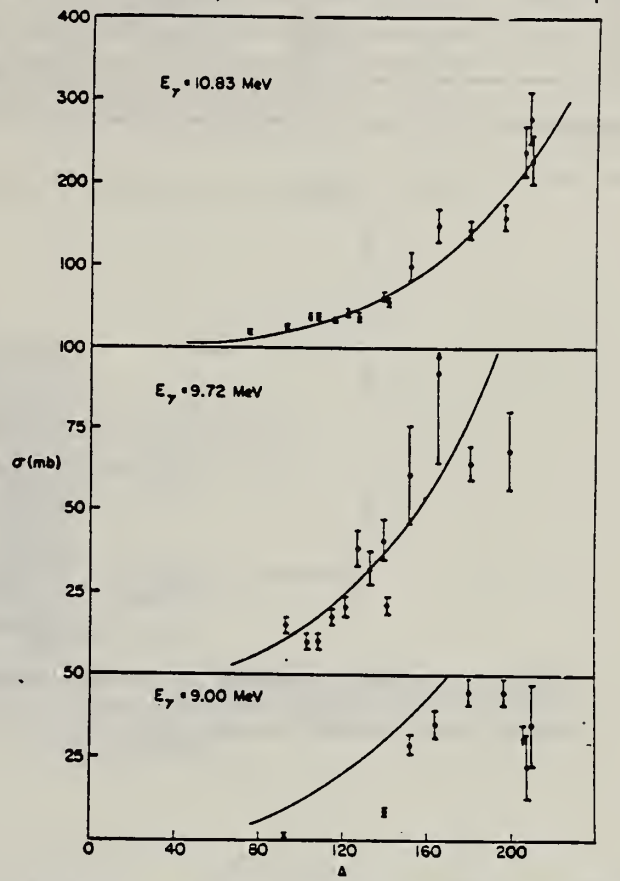

Fig. 1. Cross section (in mb) versus mass number of the target for gamma-ray energies of 9.00, 9.72 and 10.83 MeV. The solid lines are plots of eq. (1) in the text.

TABLE I
Photoneutron cross sections (mb)

Target	7.72 MeV	9.00 MeV	9.72 MeV	10.83 MeV
^{59}Co				9.0± 0.8
^{75}As				20.4± 1.7
^{93}Nb		0.53± 0.10	14.6± 2.2	25.8± 2.1
^{103}Rh			10.6± 1.7	38.8± 3.1
^{107}Ag, ^{109}Ag			10.0± 1.5	37.6± 2.9
^{115}In			17.1± 2.6	33.3± 2.7
^{121}Sb, ^{123}Sb			20.7± 3.1	42.5± 3.6
^{127}I			38.7± 5.8	38.8± 3.1
^{133}Cs			31.7± 4.8	52.5± 3.8
^{139}La		8.61± 0.86	40.8± 6.5	63.0± 5.0
^{141}Pr			21.5± 3.2	58.3± 4.1
^{151}Eu, ^{153}Eu		28.9 ± 3.2	61.3±14.7	102 ±18
^{165}Ho		35.6 ± 4.3	92.2±27.6	150 ±20
^{181}Ta	4.14±0.36	45.4 ± 3.7	65.0± 5.5	146 ±12
^{197}Au		44.5 ± 3.6	68.4±13.5	160 ±15
^{206}Pb		<34.3		238 ±29
^{208}Pb		22.6 ±11.3		280 ±31
^{209}Bi		36.1 ±12.0		226 ±27

REF. J. W. Jury, J. S. Hewitt, and K. G. McNeill
Can. J. Phys. 46, 1823 (1968)

ELEM. SYM.	A	Z
Rh	103	45

METHOD

REF. NO.	
68 Ju 1	EGF

REACTION	RESULT	EXCITATION ENERGY	SOURCE		DETECTOR		ANGLE
			TYPE	RANGE	TYPE	RANGE	
G,N	NOX	THR-27	C	27	THR	5-	DST

$$W(\theta) = a_o + a_1 P_1 + a_2 P_2$$

TABLE I

Target element	Z	Energy	a_0*	a_1/a_0	a_2/a_0
Vanadium	23	32	640±50	0.11±0.10	−0.09±0.11
Chromium	24	22	365±39	0.02±0.08	0.00±0.10
Manganese	25	22	450±33	0.07±0.05	−0.11±0.06
Bromine	35	27	874±54	0.05±0.06	−0.15±0.08
Molybdenum	42	22	610±60	0.09±0.05	−0.35±0.06
Ruthenium	44	27	1100±25	0.12±0.02	−0.29±0.03
Rhodium	45	27	1270±47	0.06±0.03	−0.14±0.03
Palladium	46	27	1350±29	0.26±0.02	−0.12±0.02
Antimony	51	27	2140±62	0.04±0.08	−0.25±0.11
Lanthanum	57	27	1940±70	0.12±0.10	−0.52±0.14
Praseodymium	59	30	1800±58	0.20±0.08	−0.40±0.09
Platinum	78	27	2600±52	0.17±0.02	−0.15±0.03
Lead	82	22	2274±59	0.08±0.08	−0.46±0.09

*The yield per mole per 100 r was normalized to a yield of 2274 for the lead sample at the same energy.

REF.	ELEM. SYM.	A	Z
H. G. De Carvalho, V. Di Napoli, D. Margadonna, F. Salvetti and K. Tesch Nucl. Phys. A126, 505 (1969)	Rh	103	45

METHOD	REF. NO.	
	69 De 1	egf

REACTION	RESULT	EXCITATION ENERGY	SOURCE		DETECTOR		ANGLE
			TYPE	RANGE	TYPE	RANGE	
G,N	ABY	THR-999	C	1-6	ACT-I		4PI
				(1.0-5.5)			
G,2N	ABY	THR-999	C	2-6	ACT-I		4PI
				(2.0-5.5)			

Yield per equivalent quantum.

999 = 5.5 GEV

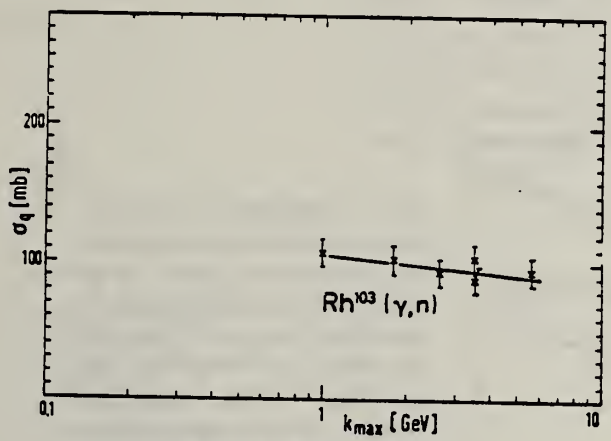

Fig. 2. See caption to fig. 1.

Cross sections per equivalent quantum for (γ, n) reactions as a function of the maximum bremsstrahlung energy. A straight line is adjusted to the experimental points by means of a least-squares fit. The indicated errors are due to the γ-ray spectroscopy. The dashed line gives the result of simple estimates.

In addition to the reactions mentioned above, we measured in the energy range 2-5.5 GeV, the following reactions: $^{55}Mn(\gamma, n)$, $^{55}Mn(\gamma, 3n)$, $^{103}Rh(\gamma, 2n)$ and $^{127}I(\gamma, 3n)$. The resulting cross sections per equivalent quantum are 43 mb, 0.55 mb, 21 mb and 9.5 mb, respectively. Within the experimental error of 20 %, we found no variation of these cross sections with the maximum bremsstrahlung energy.

REF.

C. Aurisicchio, V. diNapoli, F. Salvetti, and M.L. Terranova
Gazz. Chim. Ital. 102, 378 (1972)

ELEM. SYM.	A	Z
Rh	103	45

METHOD

REF. NO. 72 Au 13 egf

REACTION	RESULT	EXCITATION ENERGY	SOURCE		DETECTOR		ANGLE
			TYPE	RANGE	TYPE	RANGE	
G,N	ABY	9-900	C	400-900	ACT-I		4PI
G,2N	ABY	17-900	C	400-900	ACT-I		4PI
G,6P9N	ABY	THR-900	C	400-900	ACT-I		4PI

Yield = Cross section per equivalent quantum

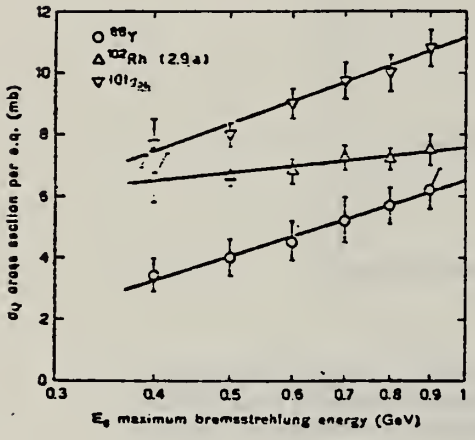

FIG. 7. - Behaviour of cross sections per equivalent quantum σ_Q, as a function of $\log_e E_o$ (maximum bremsstrahlung energy) for reactions ^{102}Rh (γ, n) ^{102}Rh ($t_{\frac{1}{2}}$ 2,9 y), ^{102}Rh $(\gamma, 2n)$ ^{101g}Rh and ^{103}Rh $(\gamma, 6p\ 9n)$ ^{88}Y. The straight lines through the experimental points were obtained by using the least-squares method

TABLE III.

Bremsstrahlung energy E_o (GeV)	σ_q(mb)		
	^{102}Rh(2.9 y)	^{101g}Rh	^{88}Y
0.4	6.6 ± 0.8	7.7 ± 0.8	3.4 ± 0.6
0.5	6.6 ± 0.3	8.0 ± 0.4	4.0 ± 0.6
0.6	6.8 ± 0.4	9.0 ± 0.5	4.5 ± 0.6
0.7	7.3 ± 0.4	9.8 ± 0.6	5.2 ± 0.6
0.8	7.2 ± 0.4	10.0 ± 0.6	5.7 ± 0.6
0.9	7.5 ± 0.5	10.8 ± 0.6	6.2 ± 0.6

REF.

L.E. Lazareva, A.I. Lepestkin, and V.I. Sidorov
Yad. Fiz. 20, 242 (1974)
Sov. J. Nucl. Phys. 20, 128 (1975)

ELEM. SYM.	A	Z
Rh	103	45

METHOD

REF. NO.: 74 La 5 hmg

REACTION	RESULT	EXCITATION ENERGY	SOURCE		DETECTOR		ANGLE
			TYPE	RANGE	TYPE	RANGE	
G,XN	SPC	8- 29	C	29	EMU-D		DST
				(28.5)			

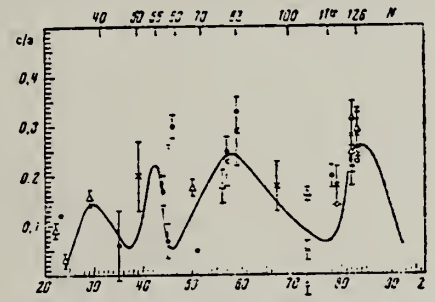

FIG. 2. Assymetry coefficients c/a obtained for nuclei with various Z in the following studies: ref. 10–$E_{\gamma\,max}$ = 25.5 MeV, $E_n > 7.4$ MeV (•); ref. 11–$E_{\gamma\,max}$ = 27–32 MeV, $E_n > \sim 5$ MeV (●); ref. 12–$E_{\gamma\,max}$ = 34 MeV, $E_n > \sim 8$ MeV (△); ref. 13–$E_{\gamma\,max}$ = 55 MeV, $E_n > \sim 5$ MeV (X); present work–$E_{\gamma\,max}$ = 28.5 MeV, $E_n > 5$ MeV (▽). The smooth curve shows the coefficient b/a characterizing the photoneutron angular distribution anisotropy as a function of atomic number Z. (This has been converted from the curve given in ref. 11 and and is for the distribution $I(\vartheta) = a + b\sin^2\vartheta + c\cos\vartheta$, normalized at the points Z_i = 82–83.)

[11] J.W. Jury, J.S. Hewitt, K.G. McNeill, Can. J. Phys. 46, 1823 (1968).

[12] F.R. Allum, T.W. Quirk, B.M. Spicer, Nucl. Phys. 53, 545 (1964).

[13] G.C. Reinhardt and W.D. Whitehead, Nucl. Phys. 30, 201 (1962).

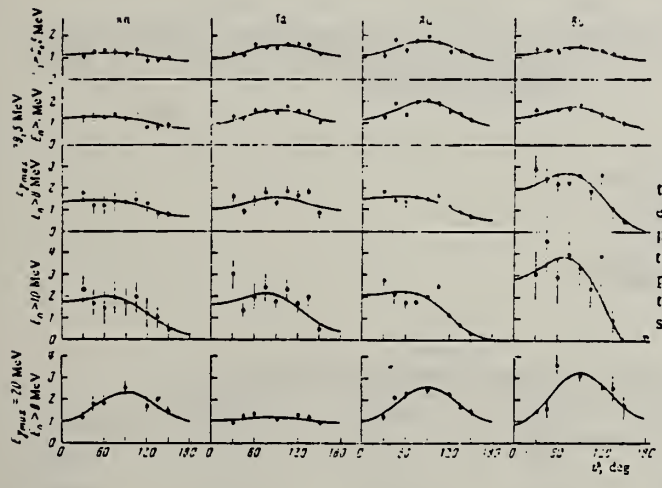

FIG. 1. Angular distributions of photoneutrons obtained in irradiation of Rh, Ta, Au, and Bi samples by bremsstrahlung with maximum energy $E_{\gamma\,max}$ = 28.5 MeV. The curves were calculated from the experimental points by the method of least squares for a distribution of the form $I(\vartheta) = a + b\sin^2\vartheta + c\cos\vartheta$ and normalized (a = 1). For comparison we have shown below the angular distributions of photoneutrons with energy $E_n > 8$ MeV obtained in irradiation of the same samples by bremsstrahlung with $E_{\gamma\,max}$ = 20 MeV.

(over)

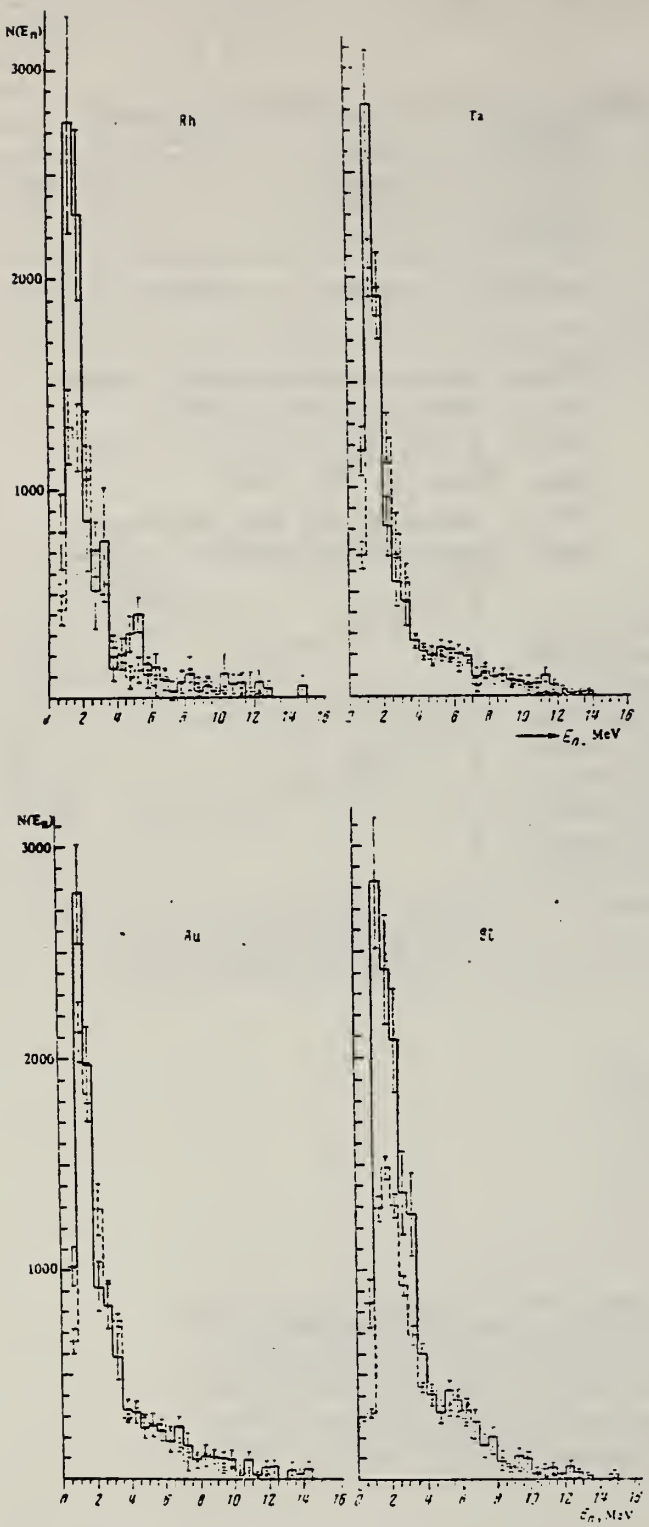

FIG. 3. Photoneutron energy spectra from Rh, Ta, Au, and Bi for irradiation of the samples by bremsstrahlung with maximum energy $E_{\gamma\,max}$ = 20 (dashed line) and 28.5 (solid line) MeV for angles θ with maximum neutron yield. For each nucleus the histograms given for $E_{\gamma\,max}$ = 20 and 28.5 MeV have been combined in the interval E_n = 4–4.5 MeV.

REF. A. Lepretre, H. Beil, R. Bergere, P. Carlos, A. De Miniac, A. Veyssiere, and K. Kernbach
Nucl. Phys. A219, 39 (1974)

ELEM. SYM.	A	Z
Rh	103	45

METHOD

REF. NO. 74 Le 1 egf

REACTION	RESULT	EXCITATION ENERGY	SOURCE		DETECTOR		ANGLE
			TYPE	RANGE	TYPE	RANGE	
G,N	ABX	9- 24	D	9- 24	MOD-I		4PI
G,2N	ABX	16- 24	D	9- 24	MOD-I		4PI

617+
618+

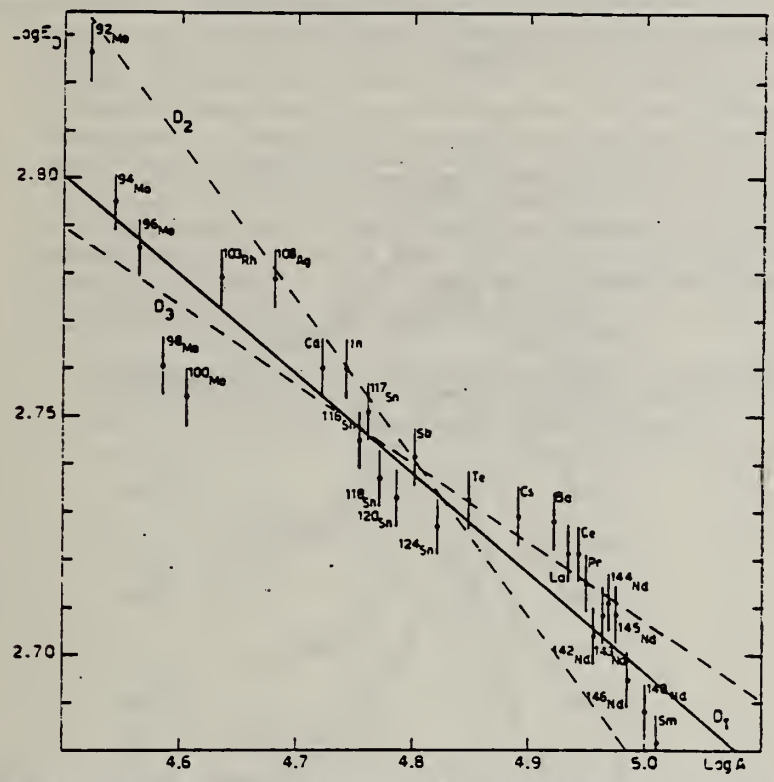

Fig. 13. Experimental results of the average energy E_D of the GDR versus the mass number A with the best fit $E_D = 41.8\,A^{-1/4.8}$ (line D_1). Two fits with $A^{-\frac{1}{3}}$ and $A^{-\frac{1}{6}}$ laws are also shown as lines D_2 and D_3 respectively.

TABLE 7

Lorentz line parameters for a two-Lorentz-line fit of the GDR of rhodium

σ_1 (mb)	E_1 (MeV)	Γ_1 (MeV)	σ_2 (mb)	E_2 (MeV)	Γ_2 (MeV)
88	15	4.94±0.1	126	17.05	6.90±0.1

Errors are the same as in table 4.

TABLE 6

Lorentz line parameters for a single Lorentz line fit

	$^{103}_{45}$Rh	$_{46}$Pd	$_{47}$Ag	$_{48}$Cd	$^{115}_{49}$In
σ_0 (mb)	191	199	198	226	243
Γ_0 (MeV)	7.4±0.1	7.1±0.1	7.7±0.1	6.3±0.1	6.1±0.1
E_0 (MeV)	16.15	15.9	16.1	15.8	15.8

Errors are the same as in table 4.

(over)

Integrated cross sections ... text

	^{103}Rh	Pd	Ag	Cd	^{115}In	^{116}Sn	^{117}Sn	^{118}Sn	^{120}Sn	^{124}Sn	Sb	Te	^{133}Cs
E_{s1} (MeV)	30	21.3	29.7	26.5	29.7	29.7	21.6	23	29.7	23	29.7	26	24.1
σ_0 (MeV · b)	1.75	1.38	1.90	1.75	2.1	1.86	1.57	1.69	2.14	1.62	2.1	2.05	2.15
0.06 NZ/A (MeV · b)	1.53	1.567	1.59	1.65	1.69	1.71	1.72	1.73	1.75	1.79	1.78	1.85	1.93
$\sigma'_0/(0.06\ NZ/A)$	1.45	1.41	1.50	1.35	1.39	1.29	1.25	1.25	1.34	1.17	1.39	1.37	1.38
σ_{-1} (mb)	96	88.2	109	107	121	113	102	107	128	104	125	125	136.9
σ_{-2} (mb · MeV^{-1})	6.2	5.8	6.6	6.8	7.4	7.15	6.80	7.0	8.1	6.9	7.9	7.9	9.05
$\sigma_{-1}/A1$	0.212	0.175	0.215	0.200	0.220	0.203	0.181	0.188	0.220	0.171	0.210	0.198	0.205
$\sigma_{-2}/A1$	2.83×10^{-3}	2.44×10^{-3}	2.78×10^{-3}	2.68×10^{-3}	2.81×10^{-3}	2.67×10^{-3}	2.51×10^{-3}	2.55×10^{-3}	2.86×10^{-3}	2.31×10^{-3}	2.72×10^{-3}	2.52×10^{-3}	2.70×10^{-3}

The average errors $\Delta\sigma_0$ and $\Delta\sigma_0'$ are ±0.1 MeV · mb.

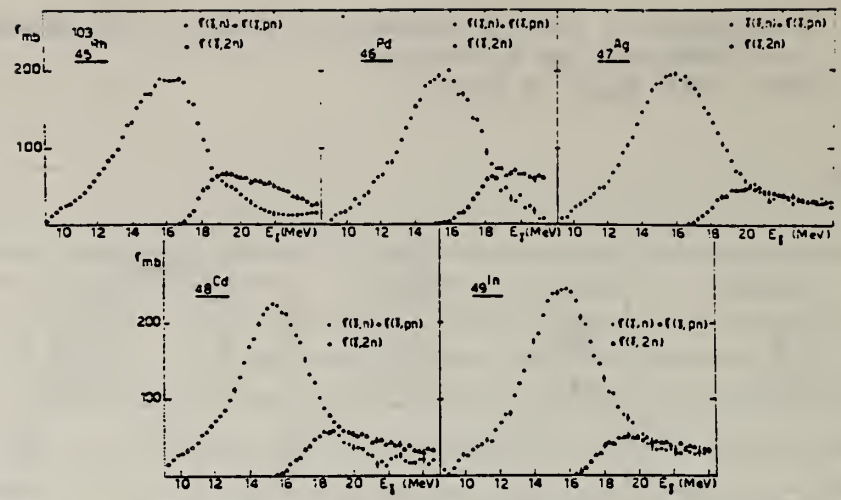

Fig. 7. Partial photoneutron cross sections $[\sigma(\gamma, n)+\sigma(\gamma, np)]$ and $\sigma(\gamma, 2n)$ for $_{45}$Rh, $_{46}$Pd, $_{47}$Ag, $_{48}$Cd and $_{49}$In.

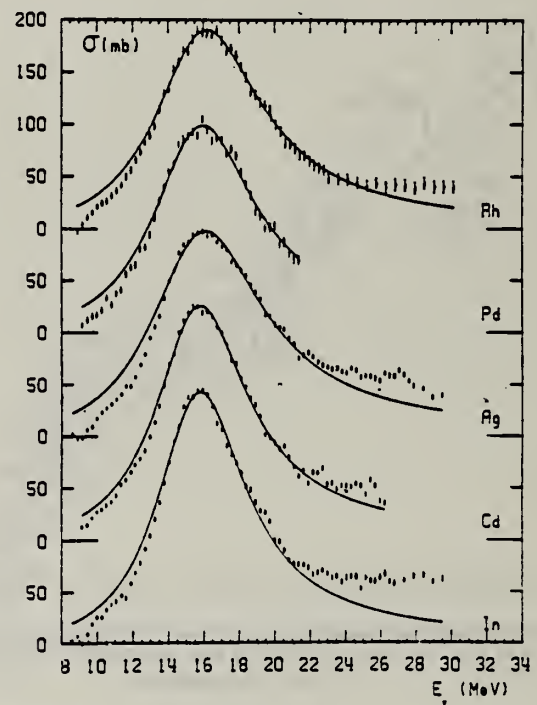

Fig. 8. Best single Lorentz line fit to $\sigma_{exp}(\gamma, \text{tot}) = \sigma(\gamma, n)+\sigma(\gamma, np)+\sigma(\gamma, 2n)$ for $_{45}$Rh, $_{46}$Pd, $_{47}$Ag, $_{48}$Cd and $_{49}$In.

REF. Y. Cauchois, H. Ben Abdelaziz, R. Khérouf, C. Schloesing-Mőller
J. Phys. G7, 1539 (1981)

ELEM. SYM.	A	Z
Rh	103	45

METHOD

REF. NO. 81 Ca 2 hg

REACTION	RESULT	EXCITATION ENERGY	SOURCE TYPE	SOURCE RANGE	DETECTOR TYPE	DETECTOR RANGE	ANGLE
G,G	I FT	0,2	C	0 - 2	SCD-D		
		(.803,1.277)					

.803, 1.277 MEV

Abstract. Lifetimes of 49 excited states below 1.65 MeV have been measured in ^{24}Mg, ^{27}Al, ^{48}Ti, ^{58}Ni, ^{59}Co, ^{61,62}Ni, ^{63,65}Cu, ^{64,66,68}Zn, ^{75}As, ^{103}Rh, ^{113,115}In, ^{116,118,120}Sn and ^{121,123}Sb by means of nuclear resonance fluorescence experiments. The levels are excited by bremsstrahlung x-ray photons. The self-absorption technique applied to suitable cases provides nuclear absorption cross sections, widths and lifetimes from which the x-ray spectral distributions are also obtained. Scattering experiments are performed for all other cases in order to obtain widths and lifetimes from these x-ray photon curves. The Compton effect in the sample is taken into account. Self-absorption provides $g\Gamma_0$ from which Γ is deduced using adopted J^π and Γ_0/Γ values; scattering provides $u = g(\Gamma_0^2/\Gamma)W(\theta)$ from which Γ is also deduced with J, Γ_0/Γ and mixing ratios taken from the literature. Thanks to simultaneous determination of the x-ray spectra all the lifetimes as given by our programs with their statistical errors form an unusually coherent set of values.

NUCLEAR REACTIONS (γ, γ'), bremsstrahlung excitation; natural isotopes: ^{24}Mg, ^{27}Al, ^{48}Ti, ^{58}Ni, ^{59}Co, ^{61,62}Ni, ^{63,65}Cu, ^{64,66,68}Zn, ^{75}As, ^{103}Rh, ^{113,115}In, ^{116,118,120}Sn and ^{121,123}Sb; $E \simeq 0.5$–1.65 MeV; measured $g\Gamma_0$ or $g(\Gamma_0^2/\Gamma)W(\theta)$; deduced $T_{1/2}$.

(OVER)

Tableau 3. Résultats des mesures des niveaux étudiés par diffusion.

Table 3. Results obtained using the diffusion method.

Isotope	Energie (keV)	J^π	J_0^π	Γ_0/Γ	δ	$u=g(\Gamma_0^2/\Gamma)W(\theta)$ (meV)	τ (ps) ce travail	$\tau_{réf}$ (ps)	Références †
^{24}Mg	1368.59(4)	2^+	0^+	1	E2	1,08(13)	1,76(21)	1,98(4)	Endt et van der Leun (1978)
^{27}Al	1014.45(3)	$\frac{3}{2}^+$	$\frac{1}{2}^+$	0,971	+0.351(12)	0,186(13)	2,20(16)	2,12(8)	Endt et van der Leun (1978)
^{48}Ti	983.512(3)	2^+	0^+	1	E2	0,282(23)	6,74(55)	6,1(13)	Been (1978)
^{58}Ni	1454.45(15)	2^+	0^+	1	E2	2,11(26)	0,90(11)	0,92(3)	Kocher et Auble (1976)
^{59}Co	1099,224(25)	$\frac{3}{2}^-$	$\frac{7}{2}^-$	1	(E2)	0,069(8)	4,79(55)	3,17(58)	Kim (1976)
^{59}Co	1458.8(3)	$\frac{5}{2}^-$	$\frac{7}{2}^-$	0,91	(E2)	0,68(8)	1,17(14)	1,52(16)	Kim (1976)
^{59}Co	1480.9(3)	$\frac{5}{2}^-$	$\frac{7}{2}^-$	0.8	$<0.35^a$	1,23(15)	0,254(31)	0,31(3)	Kim (1976)
^{61}Ni	1185.7(6)	$\frac{3}{2}^-$	$\frac{3}{2}^-$	0.77(8)[i]	$\lvert 0.14\rvert$	1,88(49)	0,21(5)	0,16(3)	Andreev *et al* (1974)
^{62}Ni	1172,91(9)	2^+	0^+	1	E2	0,88(17)	2,15(42)	2,09(3)	Halbert (1979a)
^{63}Cu	1327,00(7)	$\frac{7}{2}^-$	$\frac{3}{2}^-$	0,84	(E2)	1,04(14)	0,84(11)	0,88(4)	Auble (1979b)
^{63}Cu	1412.05(4)	$\frac{5}{2}^-$	$\frac{3}{2}^-$	0,72	$+0.61\{^{+9}_{-8}\}$	0,260(38)	1,90(28)	1,61(3)	Auble (1979b)
^{64}Zn	991.54(7)	2^+	0^+	1	E2	0,640(54)	2,97(25)	2,60(13)	Halbert (1979b)
^{65}Cu	1481,83(5)	$\frac{7}{2}^-$	$\frac{3}{2}^-$	0,85	(E2)	1,13(19)	0,79(13)	0,49(5)	Auble (1975a)
^{66}Zn	1039,37(6)	2^-	0^+	1	E2	0,70(6)	2,71(23)	2,25(15)	Auble (1975b)
^{68}Zn	1077,38(5)	2^+	0^+	1	E2	0,70(6)	2,71(23)	2,34(23)	Lewis (1975)
^{75}As	572.5(10)	$\frac{1}{2}^-$	$\frac{3}{2}^-$	1[d]	0,39[b]	0.236(26)	4,14(46)	3,5(9)	Horen et Lewis (1975)
^{75}As	823,0(10)	$\frac{7}{2}^-$	$\frac{3}{2}^-$	0,86[d]	(E2)	0.214(22)	4,27(43)	3,5(3)	Robinson *et al* (1967)
^{75}As	865.5(10)	$\frac{5}{2}^+$	$\frac{3}{2}^-$	0,83[d]	—[c]	0,78(6)	0,863(68)	0,60(12)	Celliers *et al* (1977)
^{75}As	1076,0(10)	$\frac{5}{2}^-$	$\frac{3}{2}^-$	0,94[d]	0,38[d]	1,97(13)	0,287(19)	0,32(7)	Celliers *et al* (1977)
^{75}As	1128,5(10)	$\frac{1}{2}^+$	$\frac{3}{2}^-$	1	E1[d]	0,224(24)	1,47(16)	—	
^{75}As	1349,0(10)	$\frac{3}{2}^-$	$\frac{3}{2}^-$	0.67[d]	0.20[d]	1.61(29)	0.180(32)	0.12(3)	Wilson (1970)
^{75}As	1370.0(10)	$\frac{1}{2}^-$	$\frac{3}{2}^-$	0.47[d]	0.47[d]	0.64(13)	0,218(44)	—	
^{103}Rh	803.1(2)	$\frac{1}{2}^-$	$\frac{1}{2}^-$	0.70	M1	1.85(16)	0.174(15)	—	Harmatz (1979)
^{103}Rh	1277.0(2)	$\frac{3}{2}^-$	$\frac{1}{2}^-$	0.75	−0.62(30)[e]	0.81(9)	0.87(10)	1.3(9)	Harmatz (1979)
^{113}In	1177(1)	$\frac{11}{2}^+$	$\frac{9}{2}^+$	1	+0.5(2)	9,1(8)	0,086(8)	0,10(6)	Tuttle *et al* (1976)
^{113}In	1510(1)	$\frac{7}{2}^+$	$\frac{9}{2}^+$	0,935	$-0.5\{^{+1}_{-2}\}$	6,4(9)	0,071(10)	$0.11\{^{+4}_{-2}\}$	Tuttle *et al* (1976)
^{115}In	1077.7(10)	$\frac{5}{2}^+$	$\frac{9}{2}^+$	0.81[j]	(E2)	0.159(24)	1.61(24)	1.23(7)	Tuttle *et al* (1976)
^{115}In	1290.59(3)	$\frac{11}{2}^+$	$\frac{9}{2}^+$	0.98[j]	(E2)	1.31(11)	0.66(6)	0.55(4)	Tuttle *et al* (1976)
^{115}In	1448.78(3)	$\frac{13}{2}^+$	$\frac{9}{2}^+$	0.86	−8[f]	0.90(11)	0.50(6)	0.52(20)	Tuttle *et al* (1976)
^{115}In	1486.1(1)	$\frac{9}{2}^+$	$\frac{9}{2}^+$	0,787	−0.8[f]	0,63(9)	0,63(9)	0,4(3)	Tuttle *et al* (1976)
^{115}In	1497,2(4)	$(\frac{1}{2}^+)$	$\frac{9}{2}^+$	< 1	(E2)	1,33(16)	< 0,30(4)	—	
^{115}In	1607.8(15)	$(\frac{1}{2}^+)$	$\frac{9}{2}^+$	⩽ 1	(E2)	1,54(24)	⩽ 0,26(4)	—	
^{116}Sn	1293.54(2)	2^+	0^+	1	E2	3,58(37)	0,53(6)	0,522(14)	Carlson *et al* (1975)
^{118}Sn	1229.64(4)	2^+	0^+	1	E2	2,75(28)	0,69(7)	0,67(2)	Carlson *et al* (1976)
^{120}Sn	1171,6(2)	2^+	0^+	1	E2	1,83(16)	1,04(9)	0,91(2)	Kocher (1976)
^{121}Sb	1023,5(10)	$\frac{7}{2}^+$	$\frac{5}{2}^+$	1	$\lvert 0.57\rvert$[g]	3.69(34)	0.228(21)	0.20(7)[h]	Tamura *et al* (1979)
^{121}Sb	1105,5(10)	$\frac{9}{2}^+$	$\frac{7}{2}^+$	0.4	—	0,47(4)	0,42(4)	—	
^{121}Sb	1142,5(10)	$\frac{9}{2}^+$	$\frac{5}{2}^+$	0.6	(E2)	0.85(8)	0,449(40)	0,41(8)[h]	Booth *et al* (1973)
^{121}Sb	1384,0(10)	$\frac{7}{2}^-$	$\frac{5}{2}^+$	1	$\lvert 0.45\rvert$[g]	4,7(5)	0.092(10)	0.088(14)[h]	Booth *et al* (1973)
^{123}Sb	1029,5(10)	$\frac{9}{2}^+$	$\frac{7}{2}^+$	1	$\lvert 0.57\rvert$[g]	2,96(27)	0.272(25)	0.26(4)[h]	Booth *et al* (1973)
^{123}Sb	1086.5(10)	$\frac{9}{2}^+$	$\frac{7}{2}^+$	1	$\lvert\delta\rvert > 1.26$[g]	1.06(9)	0.67(6)	0.72(15)[h]	Booth *et al* (1973)

† Références pour les colonnes 3, 4, 5, 6 et 9 de chaque ligne, sauf indication appelée au bas de ce tableau. Pour les autres données se reporter au texte.

Remarque. Pour calculer δ^2 quand nous ne disposons que de $B(E2)$, pour un mélange (E2) + (M1), nous déduisons $g\Gamma_0(E2) \propto B(E2)E_\gamma^5$; en admettant $W(\theta)=1$ et connaissant Γ_0/Γ, notre détermination de a donne une première approximation de $g\Gamma_0$ d'où une valeur de $\delta^2=(g\Gamma_0(E2))/(g\Gamma_0 - g\Gamma_0(E2))$ qui permet d'améliorer $W(\theta)$ et $g\Gamma_0$ de proche en proche.

[a] Swann (1971); [b] Robinson *et al* (1967); [c] $W(\theta)=0.99$ calculé d'après la formule de Celliers *et al* (1977); [d] Abbondanno *et al* (1978); [e] Sayer *et al* (1972); [f] Tuttle *et al* (1976); [g] d'après $B(E2)$ de Barnes *et al* (1966); [h] calculé d'apres Booth *et al* (1973); [i] Williams *et al* (1975); [j] Dietrich *et al* (1970).

# PALLADIUM
Z=46

William Wollaston first isolated palladium from crude platinum; in 1803 he announced the discovery by circulating an anonyomous advertisement of the new metal for sale. Because of this unorthodox announcement, it was widely thought that the new metal was not an element but an alloy of platinum and mercury. A year later, however, Wollaston explained his source of the palladium along with an announcement of his discovery of yet another new element, rhodium.

REF.

P. Kneisel, A. Goldmann and H. v. Buttlar
Z. Physik 199, 440 (1967)

ELEM. SYM.	A	Z
Pd		46

METHOD

Linac

REF. NO. 67 Kn 1 JDM

REACTION	RESULT	EXCITATION ENERGY	SOURCE		DETECTOR		ANGLE
			TYPE	RANGE	TYPE	RANGE	
G,T	RLY	THR-49	C	36,49	ACT-I		4PI

Tabelle. *Zusammenstellung der Meßergebnisse*

	E_m = 36,2 MeV	E_m = 49,2 MeV
$Y[Ni(\gamma, t)]/Y[C(\gamma, n)C^{11}]$	$(2,2 \pm 0,2)\ 10^{-3}$	$(4,6 \pm 0,4)\ 10^{-3}$
$Y[Pd(\gamma, t)]/Y[C(\gamma, n)C^{11}]$	—	$(6,1 \pm 1,0)\ 10^{-3}$
$\sigma_y[Ni(\gamma, t)]$	$(4,0 \pm 0,4)$ µbarn	$(10,5 \pm 1,0)$ µbarn
$\sigma_y[Pd(\gamma, t)]$	—	$(13,8 \pm 2,3)$ µbarn

REF. J. W. Jury, J. S. Hewitt, and K. G. McNeill
Can. J. Phys. 46, 1823 (1968)

ELEM. SYM.	A	Z
Pd		46

METHOD

REF. NO.	
68 Ju 1	EGF

REACTION	RESULT	EXCITATION ENERGY	SOURCE		DETECTOR		ANGLE
			TYPE	RANGE	TYPE	RANGE	
G,N	NOX	THR-27	C	27	THR	5-	DST

$$W(\theta) = a_o + a_1 P_1 + a_2 P_2$$

TABLE I

Target element	Z	Energy	a_0*	a_1/a_0	a_2/a_0
Vanadium	23	32	640 ± 50	0.11 ± 0.10	−0.09 ± 0.11
Chromium	24	22	365 ± 39	0.02 ± 0.08	0.00 ± 0.10
Manganese	25	22	450 ± 33	0.07 ± 0.05	−0.11 ± 0.06
Bromine	35	27	874 ± 54	0.05 ± 0.06	−0.15 ± 0.08
Molybdenum	42	22	610 ± 60	0.09 ± 0.05	−0.35 ± 0.06
Ruthenium	44	27	1100 ± 25	0.12 ± 0.02	−0.29 ± 0.03
Rhodium	45	27	1270 ± 47	0.06 ± 0.03	−0.14 ± 0.03
Palladium	46	27	1350 ± 29	0.26 ± 0.02	−0.12 ± 0.02
Antimony	51	27	2140 ± 62	0.04 ± 0.08	−0.25 ± 0.11
Lanthanum	57	27	1940 ± 70	0.12 ± 0.10	−0.52 ± 0.14
Praseodymium	59	30	1800 ± 58	0.20 ± 0.08	−0.40 ± 0.09
Platinum	78	27	2600 ± 52	0.17 ± 0.02	−0.15 ± 0.03
Lead	82	22	2274 ± 59	0.08 ± 0.08	−0.46 ± 0.09

*The yield per mole per 100 r was normalized to a yield of 2274 for the lead sample at the same energy.

REF.	ELEM. SYM.	A	Z
A. Lepretre, H. Beil, R. Bergere, P. Carlos, A. De Miniac, A. Veyssiere, and K. Kernbach Nucl. Phys. A219, 39 (1974)	Pd		46

METHOD	REF. NO.
	74 Le 1

e2f

REACTION	RESULT	EXCITATION ENERGY	SOURCE		DETECTOR		ANGLE
			TYPE	RANGE	TYPE	RANGE	
G,N	ABX	9- 22	D	9- 22	MOD-I		4PI
G,2N	ABX	15- 22	D	9- 22	MOD-I		4PI

620+
621+

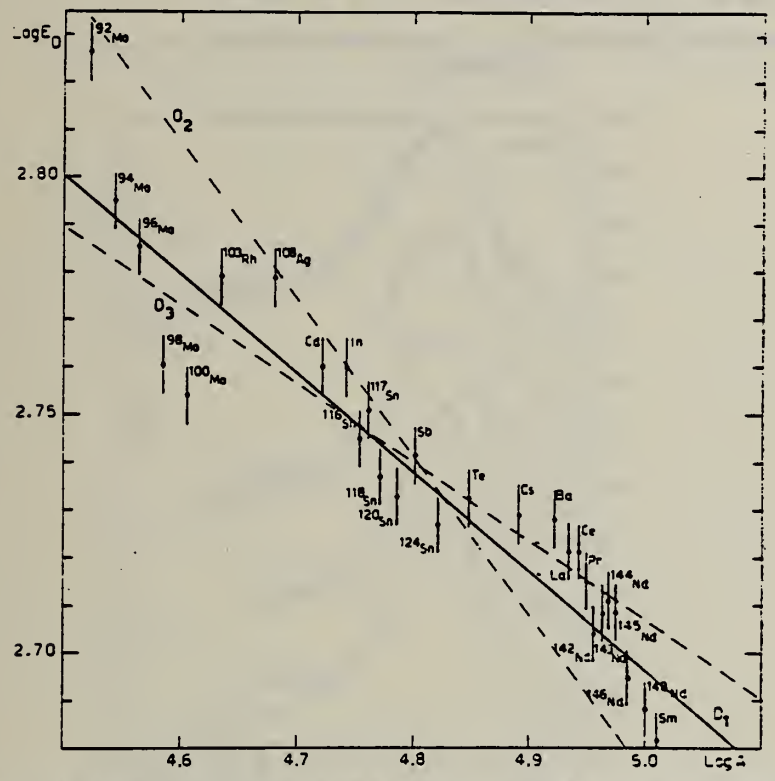

Fig. 13. Experimental results of the average energy E_D of the GDR versus the mass number A with the best fit $E_D = 41.8\,A^{-1/4.8}$ (line D_1). Two fits with $A^{-\frac{1}{3}}$ and $A^{-\frac{1}{4}}$ laws are also shown as lines D_2 and D_3 respectively.

TABLE 6

Lorentz line parameters for a single Lorentz line fit

	$^{103}_{45}$Rh	$_{46}$Pd	$_{47}$Ag	$_{48}$Cd	$^{115}_{49}$In
σ_0 (mb)	191	199	198	226	243
Γ_0 (MeV)	7.4±0.1	7.1±0.1	7.7±0.1	6.3±0.1	6.1±0.1
E_0 (MeV)	16.15	15.9	16.1	15.8	15.3

Errors are the same as in table 4.

(over)

TABLE II

Integrated cross sections as defined in the text

	^{103}Rh	Pd	Ag	Cd	^{115}In	^{116}Sn	^{117}Sn	^{118}Sn	^{120}Sn	^{124}Sn	Sb	Te	^{133}Cs
E_{th} (MeV)	30	21.3	29.7	26.5	29.7	29.7	21.6	23	29.7	23	29.7	26	24.1
σ_0 (MeV · b)	1.75	1.38	1.90	1.75	2.1	1.86	1.57	1.69	2.14	1.62	2.1	2.05	2.15
$0.06\,NZ/A$ (MeV · b)	1.53	1.567	1.59	1.65	1.69	1.71	1.72	1.73	1.75	1.79	1.78	1.85	1.93
$\sigma'_0/(0.06\,NZ/A)$	1.45	1.41	1.50	1.35	1.39	1.29	1.25	1.25	1.34	1.17	1.39	1.37	1.38
σ_{-1} (mb)	96	88.2	109	107	121	113	102	107	128	104	125	125	136.9
σ_{-2} (mb · MeV^{-1})	6.2	5.8	6.6	6.8	7.4	7.15	6.80	7.0	8.1	6.9	7.9	7.9	9.05
σ_{-1}/A	0.212	0.175	0.215	0.200	0.220	0.203	0.181	0.188	0.220	0.171	0.210	0.198	0.205
σ_{-2}/A	2.83×10^{-3}	2.44×10^{-3}	2.78×10^{-3}	2.68×10^{-3}	2.81×10^{-3}	2.67×10^{-3}	2.51×10^{-3}	2.55×10^{-3}	2.86×10^{-3}	2.31×10^{-3}	2.72×10^{-3}	2.52×10^{-3}	2.70×10^{-3}

The average errors $\Delta\sigma_0$ and $\Delta\sigma_0'$ are ±0.1 MeV · mb.

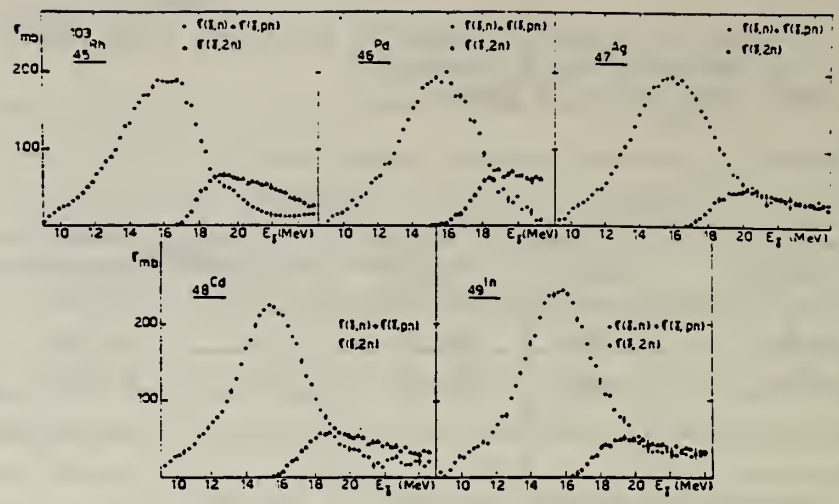

Fig. 7. Partial photoneutron cross sections $[\sigma(\gamma, n)+\sigma(\gamma, np)]$ and $\sigma(\gamma, 2n)$ for $_{45}$Rh, $_{46}$Pd, $_{47}$Ag, $_{48}$Cd and $_{49}$In.

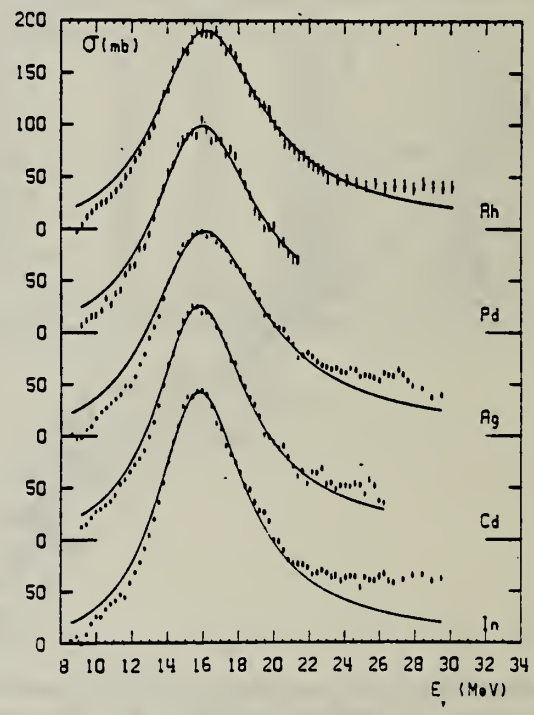

Fig. 8. Best single Lorentz line fit to $\sigma_{exp}(\gamma, tot) = \sigma(\gamma, n)+\sigma(\gamma, np)+\sigma(\gamma, 2n)$ for $_{45}$Rh, $_{46}$Pd, $_{47}$Ag, $_{48}$Cd and $_{49}$In.

P_D
A=104

P_D
A=104

REF.

Y. Oka, T. Kato, K. Nomura, T. Saito, Hui-Tuh Tsai
Bull. Chem. Soc. Japan 41, 380 (1968)

Pd	104	46

METHOD

REF. NO. 68 Ok 3 egf

REACTION	RESULT	EXCITATION ENERGY	SOURCE		DETECTOR		ANGLE
			TYPE	RANGE	TYPE	RANGE	
G,NP	ABY	THR-20	C	20	ACT-I		4PI

TABLE 2. THE YIELDS OF SOME (γ, pn) REACTIONS WITH 20 MeV BREMSSTRAHLUNG

Reaction	Half-life of product	Specific activity[a] (μCi/mg)	Yield ($mol^{-1} \cdot R^{-1}$)
$^{56}Fe(\gamma, pn)^{55}Mn$	314 d	2.5×10^{-6}	3.6×10^{2}
$^{64}Zn(\gamma, pn)^{63}Cu$	13 hr	7.2×10^{-3}	7.5×10^{3}
$^{104}Pd(\gamma, pn)^{103}Rh$	210 d	1.1×10^{-6}	1.7×10^{3}

a) The value corrected at the end of 1 hr irradiation (9.4×10^{6} R/min).

Pd
A=105

Pd
A=105

Ref. F.R. Metzger
Phys. Rev. 128, 2332 (1962)

Elem. Sym.	A	Z
Pd	105	46

Method
Rh^{105} source on ultra centrifuge rotor to compensate for Doppler shift; NaI.

Ref. No. 62 Me 1 JHH

Reaction	E or ΔE	E_o	Γ	$\int \sigma dE$	Jπ	Notes
$Pd^{105}(\gamma,\gamma)$	319 keV	319 keV			$7/2^+$	Spins 1/2 and 3/2 eliminated; spin 5/2 possible, but less probable than 7/2. E2/M1 mixing amplitude (I = 7/2) is S = -0.11. Gamma transition probability (I = 7/2) is $\tau_\gamma = (1.37 \pm 0.07)\ 10^{10}\ sec^{-1}$. $\omega(\theta) = 1+(0.25\pm0.05)P_2(\cos\theta)$.

REF.

Yu. K. Shubnyi, Yu. A. Lysikov
Izv. Akad. Nauk SSSR Fiz. 35, 1651 (1971)

ELEM. SYM.	A	Z
Pd	105	46

METHOD

REF. NO. 71 Sh 6 egf

REACTION	RESULT	EXCITATION ENERGY	SOURCE		DETECTOR		ANGLE
			TYPE	RANGE	TYPE	RANGE	
G,G	LFT	1	D	1	NAI-D		UKN

$6.9 \pm 1.0 \times 10^{-11}$ s

1=.319 MEV

Pd
A=106

Pd
A=106

A. V. Davydov, G. R. Kartashov, I. N. Vishnevsky
Phys. Letters 30B, 616 (1969)

Pd	106	46

METHOD

REF. NO. 69 Da 1 egf

REACTION	RESULT	EXCITATION ENERGY	SOURCE		DETECTOR		ANGLE
			TYPE	RANGE	TYPE	RANGE	
G,G	ABY	1	D	1	NAI-D	0-1	120

$d\sigma/d\Omega = 0.27 \pm 0.05$ mb/sr.

1=.5117 MEV

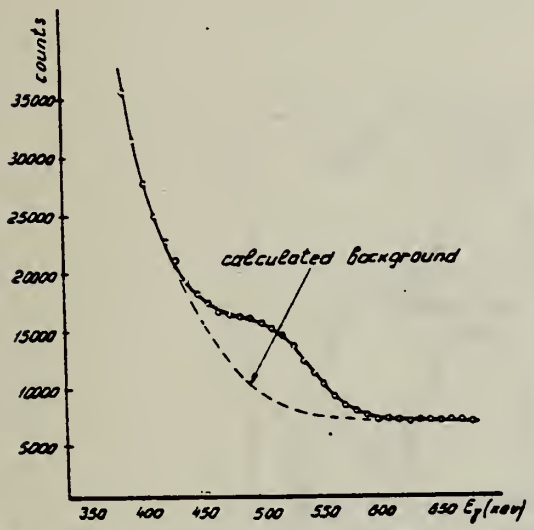

Fig. 1. Scintillation counter pulse spectrum of ^{64}Cu annihilation radiation scattered at $\theta = 120^0$ by palladium which includes the 511 keV γ-line corresponding to elastic processes (Rayleigh and resonant γ-ray scattering.

REF. K. Hosoyama, Y. Torizuka, Y. Kawazoe, H. Ui
PICNS-72, 139 (1972) Sendai

ELEM. SYM.	A	Z
Pd	106	46

METHOD

REF. NO. 72 Ho 7 hvm

REACTION	RESULT	EXCITATION ENERGY	SOURCE		DETECTOR		ANGLE
			TYPE	RANGE	TYPE	RANGE	
E,E/	FMF	0, 1	D	250	MAG-D		DST

0=.51; 1=1.13 MEV

	$\frac{B(E2)}{B_{sp}(E2)}$	Ω_n	α	Q_2(b)	$\frac{B(E2)}{B_{sp}(E2)}$	Q_2(b)
^{114}Cd	29	0.18	0.21	-0.39±0.07	34	-0.38 a)
					31.2	-0.32±0.08 b)
^{106}Pd	50	0.23	0.25	-0.53±0.07	48±3	c)
					42±3	-0.458±0.059 d)

a) S.G.Steadman et.al. N.P.A155(1970)1
b) A.M.Kleinfeld et.al. N.P.A158(1970)81
c) R.L.Robinson et.al. N.P.A124(1963)553
d) R.Beyer et.al. P.R. C2(1970)1469

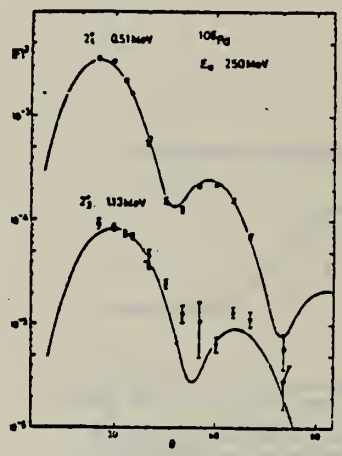

fig.3

REF. Y. Torizuka, Y. Kojima, T. Saito, K. Itoh, A. Nakada, S. Mitsunobu, M. Nagao, K. Hosoyama, S. Fukuda
PICNS-72, p.171 Sendai

ELEM. SYM.	A	Z
Pd	106	46

METHOD

REF. NO.	
72 To 6	hvm

REACTION	RESULT	EXCITATION ENERGY	SOURCE		DETECTOR		ANGLE
			TYPE	RANGE	TYPE	RANGE	
E,E/	SPC	0- 37	D	183	MAG-D		35

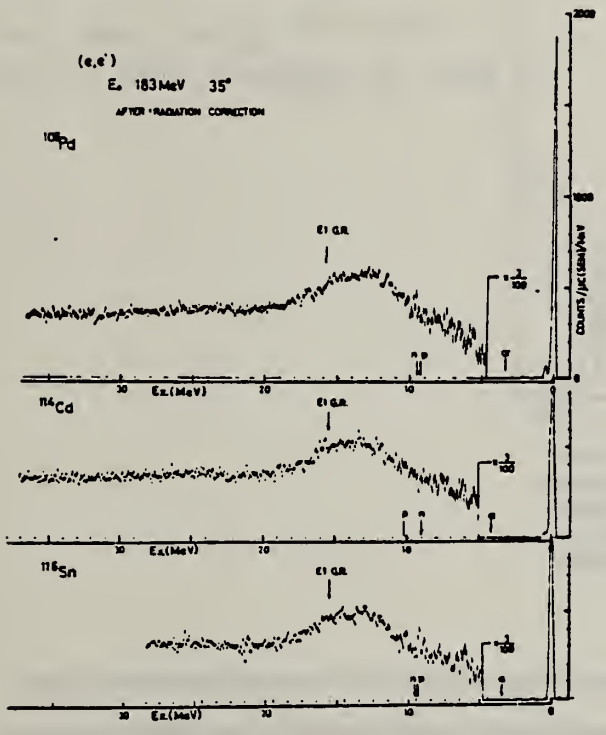

Fig. 6. Spectra of ^{116}Sn, ^{114}Cd and ^{106}Pb obtained at 183 MeV and 35°.

REF. K. Hosoyama, Y. Torizuka, Y. Kawazoe, and H. Ui
Phys. Rev. Letters 30, 388 (1973)

ELEM. SYM.	A	Z
Pd	106	46

METHOD

REF. NO. 73 Ho 2 hmg

REACTION	RESULT	EXCITATION ENERGY	SOURCE		DETECTOR		ANGLE
			TYPE	RANGE	TYPE	RANGE	
E,E/	FMF	0- 2	D	183,250	MAG-D		DST

LEVEL .51, 1.13 COMPLEX

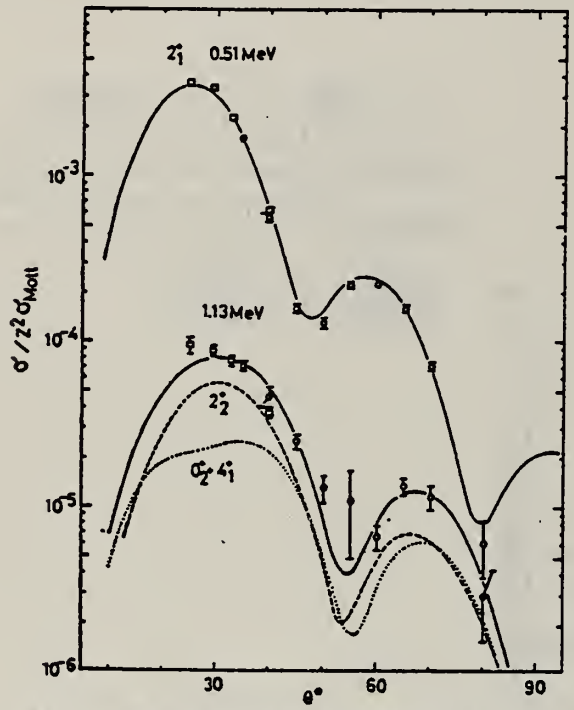

FIG. 1. Inelastic electron scattering form factors for the 2_1^+ and unresolved 0_2^+, 2_2^+, and 4_1^+ levels in ^{106}Pd at an incident energy of 250 MeV. The triplet form factors are compared with the sum of the 0_2^+ and 4_1^+ form factor (dotted line) and 2_2^+ form factor (dashed line).

TABLE II. Values of the radiative transition rates for the crossover and cascade transitions from the 2_2^+ state.

	^{106}Pd		^{114}Cd	
	Present	Experimental	Present	Experimental
$\frac{B(E2,2_2^+ \to 2_1^+)}{B(E2,2_1^+ \to 0^+)}$	$1.39^{+0.06}_{-0.14}$	0.96 ± 0.13[a]	$1.56^{+0.08}_{-0.13}$	0.75 ± 0.20[b]
$\frac{B(E2,2_2^+ \to 0^+)}{B(E2,2_1^+ \to 0^+)}$	$(0.82^{+0.92}_{-0.72}) \times 10^{-2}$	$(2.51^{+0.43}_{-0.33}) \times 10^{-2}$ [a]	$0.75^{+1.05}_{-0.59}$	$(1.6 \pm 0.3) \times 10^{-2}$ [b]

[a]Ref. 2. [b]Ref. 6.

(over)

TABLE I. Values of c, t, β, and α (the parameters of ρ_{tr}), $B(E2)$ in single-particle units, and the 2_1^+ state static quadrupole moment.

					Present		Coulomb excitation	
	c	t	β	α	$\frac{B(E2)}{B_{sp}(E2)}$	Q_2 (b)	$\frac{B(E2)}{B_{sp}(E2)}$	Q_2 (b)
^{106}Pd	$0.97c_0$ [a]	$1.05t_0$ [b]	0.23	0.23	50 ± 5	-0.51 ± 0.07	48 ± 3 [c]	
							42 ± 3 [d]	-0.458 ± 0.059 [d]
^{114}Cd	$0.95c_0$ [e]	$t = t_0$ [f]	0.18	0.19	29 ± 3	-0.36 ± 0.07	31 ± 2 [g]	-0.32 ± 0.08 [g]
							34 [h]	-0.38 [h]

[a] $c_0 = 5.14$ fm. [c] Ref. 2. [e] $c_0 = 5.43$ fm. [g] Ref. 3.
[b] $t_0 = 2.59$ fm. [d] Ref. 5. [f] $t_0 = 2.50$ fm. [h] Ref. 4.

[2] R. L. Robinson et al., Nucl. Phys. A124, 553 (1969).

[3] S.G. Steadman et al., Nucl. Phys. A155, 1 (1970).

[4] A.M. Kleinfeld et al., Nucl. Phys. A158, 81 (1970).

[5] R. Beyer et al., Phys. Rev. C2, 1469 ('70).

[6] W.T. Milner et al., Nucl. Phys. A129, 687 ('69).

Pd
A=108

REF. T. K. Deague, E. G. Muirhead, B. M. Spicer

Contributions Montreal Conference 350 (1969)

ELEM. SYM.	A	Z
Pd	108	46

METHOD

REF. NO. 69 De 2 egf

REACTION	RESULT	EXCITATION ENERGY	SOURCE		DETECTOR		ANGLE
			TYPE	RANGE	TYPE	RANGE	
G,XN	ABX	9-25	C	9-25	BF3-I		4PI
G,P	ABX	9-25	C	9-25	ACT-I		4PI

[illegible] SPIN SPLITTING OF THE $^{108}_{46}Pd$ GIANT DIPOLE RESONANCE

T. K. Deague, E. G. Muirhead and B. M. Spicer, School of Physics, University of Melbourne, Parkville, Victoria 3052, Australia

The ^{108}Pd photoneutron production cross section, and the $^{108}Pd(\gamma,p)^{107}Rh$ cross section have been measured by direct neutron detection, and by counting the 305 keV γ-ray in the residual ^{107}Rh, respectively. Both cross sections were unfolded from yield curves by the method of Penfold and Leiss. Correction was made to the neutron production cross section for the double weighting of the (γ,2n) reaction. The two cross sections are shown in the figure.

The low energy spectrum of ^{108}Pd is a good approximation to that of a spherical vibrator, the vibrations having comparatively large amplitude. Hence ^{108}Pd is a good test for the dynamic collective model of the giant resonance (Huber, Danos, Weber and Greiner, Phys.Rev. 155 (1967) 1073), in which quadrupole surface vibrations are coupled to the giant dipole vibration. A fit to the predicted dipole spectrum, using Lorentz line shapes, is shown in the figure. Reasonable agreement is evident, although the theoretical peak at 16.75 MeV is not matched in the experiment. The additional strength at lower energies is attributed tentatively to single particle effects.

Fallieros, Goulard and Venter (Phys.Lett. 19 (1965) 398) have suggested that the giant dipole resonance should be split into two components with isospins T_0 (= N-Z/2) and $T_0 + 1$. In a sufficiently heavy nucleus, these components are represented by the (γ,n) and (γ,p) cross sections respectively. Accepting this break-up, the separation of the T-components in ^{108}Pd is ~ 6 MeV. The ratio of the strengths in the two components is 0.0235; this is to be compared with Macfarlane's estimate of this ratio (in "Isobaric Spin in Nuclear Physics", eds. J. D. Fox and D. Robson, Academic Press, 1966) of D/T_0 where the dynamical factor, D, is less than unity.

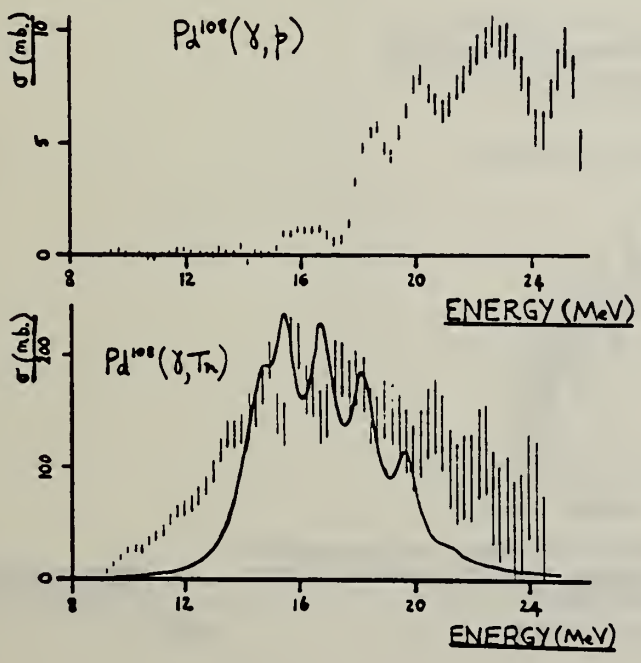

T. K. Deague, E. G. Muirhead, and B. M. Spicer
Nucl. Phys. A139, 501 (1969)

Pd	108	46

METHOD

REF. NO. 69 De 5 egf

REACTION	RESULT	EXCITATION ENERGY	SOURCE TYPE	SOURCE RANGE	DETECTOR TYPE	DETECTOR RANGE	ANGLE
G,XN	ABX	8-25	C	8-25	BF3-I		4PI
G,P	ABX	15-28	C	8-28	ACT-I		4PI

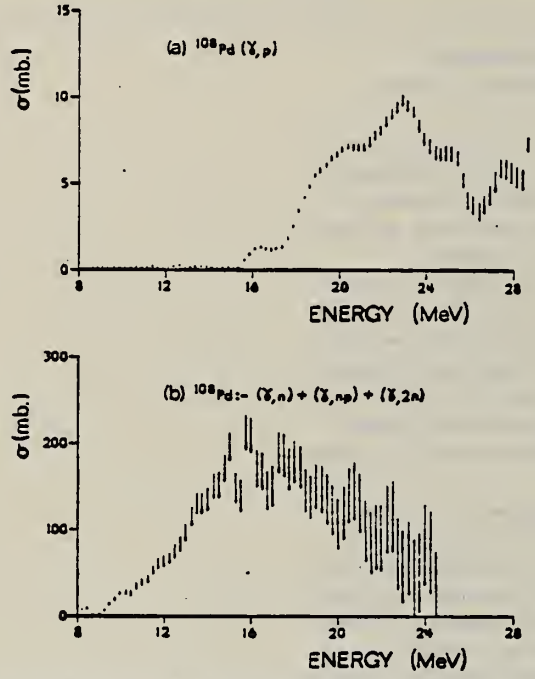

Fig. 2. (a) The (γ, p) cross section in ^{108}Pd, obtained using an analysis bin width of 1.5 MeV. (b) The (γ, n)+(γ, np)+(γ, 2n) cross section in ^{108}Pd, obtained using an analysis bin width of 0.5 MeV.

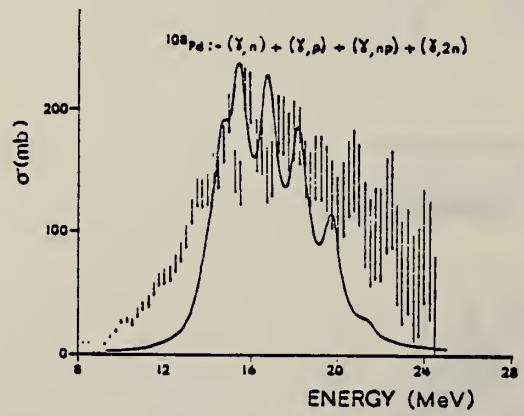

Fig. 3. The (γ, n)+(γ, p)+(γ, np)+(γ, 2n) cross section in ^{108}Pd, obtained using an analysis bin width of 0.5 MeV, compared with a fit of Lorentz line shapes with widths 1.0 MeV, to the ^{108}Pd dipole spectrum predicted by Huber [6]).

[6] M. G. Huber, private communication (1967)

[over]

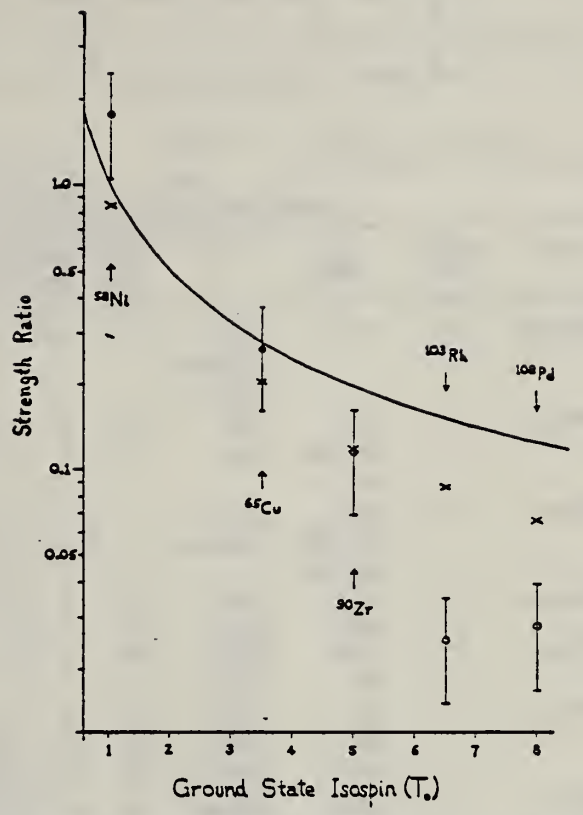

Fig. 7. The ratio, for five nuclei, of the "bremsstrahlung weighted" cross sections for proton and neutron production, respectively (circles with error bars), as a function of the ground state isospin, T_0. Crosses represent theoretical estimates of the relative strengths of the T_0+1 and T_0 giant dipole resonances. The continuous curve gives the "geometric factor", $1/T_0$.

REF.

H. Bartsch, K. Huber, U. Kneissl, H. Krieger
Nucl. Phys. A256, 243 (1976)

ELEM. SYM.	A	Z
Pd	108	46

METHOD

REF. NO.: 76 Ba 1 egf

REACTION	RESULT	EXCITATION ENERGY	SOURCE		DETECTOR		ANGLE
			TYPE	RANGE	TYPE	RANGE	
G,N	RLY	THR-UKN	C	UKN	SCD-D		4PI

ISOMER RATIO

TABLE 1
Experimental and theoretical results

Process	Target-spin	E_γ (keV)	$T_{\frac{1}{2}}$	Spin high	Spin low	$R_{exp} = \frac{\sigma_{high}}{\sigma_{low}}$	SCOP (ñ)
^{181}Ta(γ, 3n)	$\frac{7}{2}^+$	93	2.2 h 9.31 min 8.15 h	7^-	1^+	0.51 ±0.09	3.6 ±0.2
^{142}Nd(γ, n)	0^+	755 1100–1300, 145	63 s 2.5 h	$\frac{11}{2}^-$	$\frac{3}{2}^+$	0.055±0.006 0.19 ±0.01 [a])	2.20±0.06
^{92}Mo(γ, n)	0^+	652.9 1208, 1508, 1581, 1637	66 s 15.49 min	$\frac{9}{2}^+$	$\frac{1}{2}^-$	1.03 ±0.21 0.85 ±0.07 [b]) 1.92 ±0.15 [a])	5.03±0.75 4^{+6}_{-2}
^{100}Mo(γ, n)	0^+	97.3 140.5	16.8 μs 66.02 h	$\frac{5}{2}^+$	$\frac{1}{2}^+$	0.85 ±0.24	1.72±0.25
^{108}Pd(γ, n)	0^+	214.5 115	22 s 850 ns	$\frac{11}{2}^-$	$\frac{1}{2}^+$	0.5 ±0.2	3.4 ±0.5
^{110}Pd(γ, n)	0^+	188 113 87.7	4.7 min 390 ns 13.47 h	$\frac{11}{2}^-$ $\frac{11}{2}^-$ $\frac{5}{2}^+$	$\frac{3}{2}^+$ $\frac{1}{2}^+$ $\frac{1}{2}^+$	0.11 ±0.02 0.41 ±0.09 3.2 ±0.7	3.14±0.15 3.0 ±0.25 3.3 ±0.4
^{89}Y(γ, n)	$\frac{1}{2}^-$	231.7 442.3 392.5	14.2 ms 300 μs	8^+	1^+	0.056±0.008	

[a]) Ref. [14]). [b]) Ref. [15]).

[14] P.E. Haustein et al, J. Inorg. Nucl. Chem. 33, 289 (1971)

[15] J.H. Carver et al., Nucl. Phys. 37, 449 (1962)

REF. R.G. Arthur, R.P. Singhal, S.W. Brain, W.A. Gillespie, A. Johnston, E.W. Lees and M.W.S. Macauley J. Phys. G4, 961 (1978)

ELEM. SYM.	A	Z
Pd	108	46

METHOD

REF. NO. 78 Ar 4 rs

REACTION	RESULT	EXCITATION ENERGY	SOURCE		DETECTOR		ANGLE
			TYPE	RANGE	TYPE	RANGE	
E,E/	FMF	0-2	D	21-121	MAG-D		140

Abstract. The elastic electron-scattering form factor, and inelastic form factors for the 2_1^+ (0·434 MeV), 2_2^+ (0·931 MeV) and 3^- (2·046 MeV) states in ^{108}Pd were measured. The ground-state charge distribution parameters were obtained from a phase-shift analysis of the elastic form factor. Analysis of the 2_1^+ and 2_2^+ form factors in the anharmonic vibrator model yields the reduced transition probabilities and the 2_1^+ quadrupole moment ($Q_{2_1^+}$) which is in excellent agreement with recent Coulomb reorientation measurements. The 3^- form factor is well described by the assumption that this state is a pure octupole vibration.

Comment: Elastic & inelastic scattering data given in two tables.

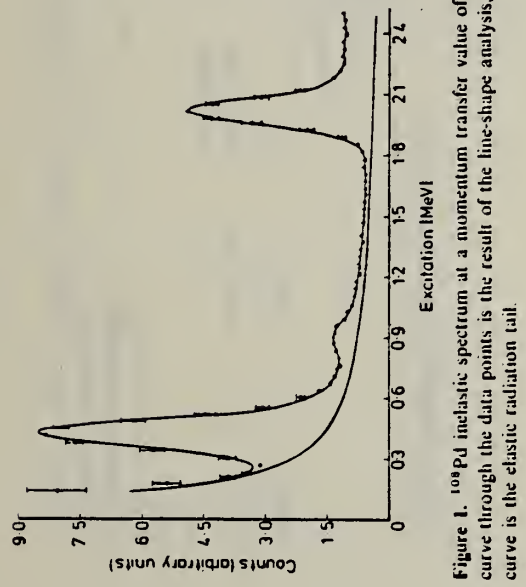

Figure 1. ^{108}Pd inelastic spectrum at a momentum transfer value of 0·75 fm^{-1}. The full curve through the data points is the result of the line-shape analysis, and the underlying curve is the elastic radiation tail.

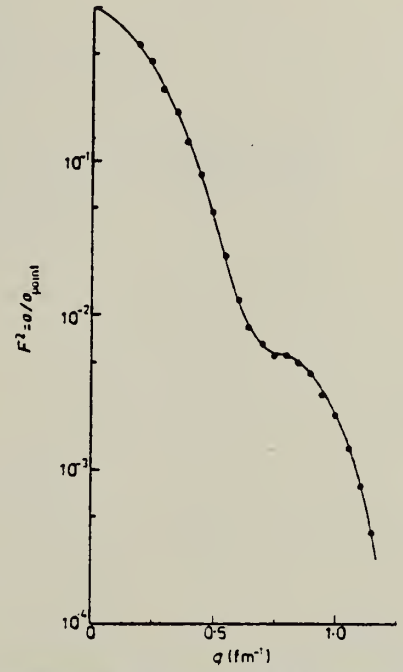

Figure 3. ^{108}Pd elastic form factor. The full curve is the phase-shift best fit. The error bars are smaller than the data points.

(over)

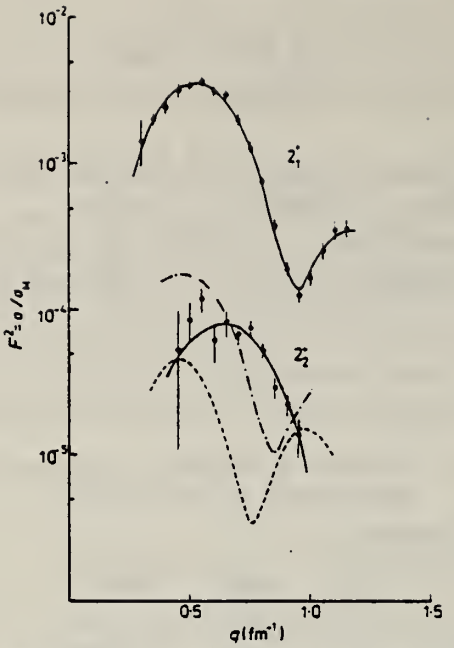

Figure 4. 2_1^+ and 2_2^+ form factors—anharmonic model fits. The fits to the 2_2^+ are respectively $\cos\phi = -1$ (——), $\cos\phi = +1$ (——) and pure harmonic two-phonon (---).

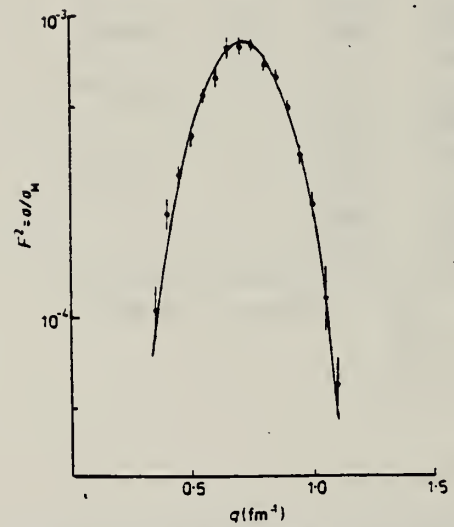

Figure 5. 3^- form factor. The full curve is the best fit assuming the level to be a single octupole phonon vibration.

Table 4. Quadrupole moment and $B(EL,1)$ values.

E_x (MeV)	J^π	Q_2 (eb)			$B(EL,1)$ (e^2fm^{2L})	
		Coulomb excitation		Reorientation precession	Coulomb excitation	
		(e,e')	(i) (ii)		(e,e')	
0·434	2_1^+	−0·58 ± 0·04	−0·58 ± 0·13[a] −0·51 ± 0·06[c]	−0·37 ± 0·12[b] −0·30 ± 0·06[c]	−0·66 ± 0·18[d]	8049 ± 290
0·931	2_2^+					7600 ± 500[e] 7000 ± 700[e]
2·046	3^-					170 ± 15[e] (9·3 ± 2·6) × 10^4
					58·2 ± 9·6 (11·3 ± 1·5) × 10^4	

(i) Constructive interference.
(ii) Destructive interference.
[a] Robinson *et al* (1969); [b] Harper *et al* (1971); [c] Lutz *et al* (1972); [d] Hasselgren *et al* (1976)

Pd
A=110

Pd
A=110

T. K. Deague, E. G. Muirhead, and B. M. Spicer
Nucl. Phys. A139, 501 (1969)

Pd	110	46

METHOD

REF. NO. 69 De 5 egf

REACTION	RESULT	EXCITATION ENERGY	SOURCE		DETECTOR		ANGLE
			TYPE	RANGE	TYPE	RANGE	
G,N	ABX	8-28	C	8-28	ACT-I		4PI

ISOMER YIELD ONLY

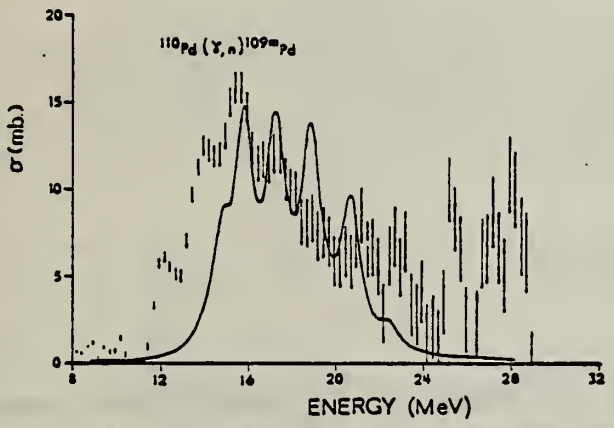

Fig. 4. The ^{110}Pd(γ, n)^{109m}Pd cross section, obtained using an analysis bin width of 1.0 MeV, compared with a fit of Lorentz line shapes with widths 1.0 MeV, to the ^{110}Pd dipole spectrum predicted by Huber [6].

[6] M. G. Huber, private communication (1967).

REF. S. Penner, J.W. Lightbody,Jr., S.P. Fivozinsky, H. Crannell, P.L. Hallowell, and M. Finn
PICNS-72, 49 (1972) Sendai

ELEM. SYM.	A	Z
Pd	110	46

METHOD

REF. NO. 72 Pe 2 hvm

REACTION	RESULT	EXCITATION ENERGY	SOURCE TYPE	SOURCE RANGE	DETECTOR TYPE	DETECTOR RANGE	ANGLE
E,E/	FMF	0, 0	D	40-110	MAG-D		128

0=.374, 0=.81 MEV

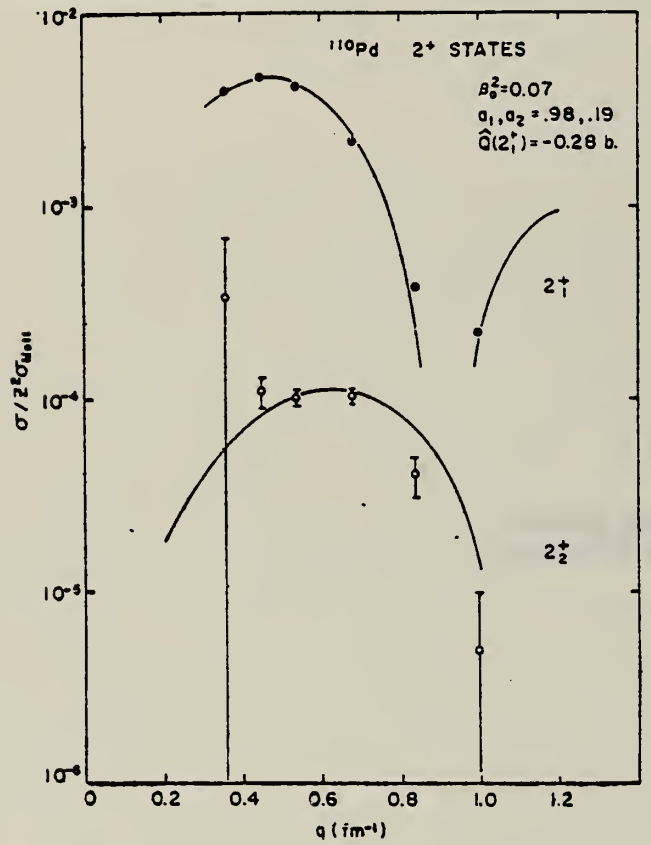

Fig. 2. Form factors for excitation of the first and second 2^+ states in ^{110}Pd. The smooth curves are the best fits of the anharmonic vibrator model.

Table 2. First Excited State Static Quadrupole Moments

Nucleus	Q, barns electron scattering	Q, barns reorientation effect
^{48}Ti	-.177 ± .008 [b]	-.22 ± .08 [c]
		-.135± .082 [d]
		-.38 ± .13 [e]
^{52}Cr	-.082 ± .016 [a]	-.07 ± .13 [f]
^{60}Ni	-.104 ± .018 [b]	0 ± .13 [g]
^{64}Zn	-.135 ± .016 [b]	-
^{70}Zn	-.21 ± .03 [b]	-
^{110}Pd	-.28 ± .03 [a]	(-.27 OR -.48)±.05 [h] (-.45 OR -.72)±.12 [i]
^{114}Cd	-.29 ± .03 [a]	-.32 ± .08 [j]
^{116}Sn	-.14 ± .03 [a]	+.09 ± .13 [k]

a) New preliminary values
b) From Ref. (1)
c) O. Hausser, et al., Nucl. Phys. A150, 417 (1970)
d) P.M.S. Lesser, et al., University of Rochester Annual Report, 1970 (unpublished)
e) N.V. deCastro-Faria, et al., Nucl. Phys. A174, 37 (1971)
f) D. Cline, University of Rochester Report UR-NSRL-40, 1971 (unpublished)
g) D. Cline, et al., Nucl. Phys. A133, 445 (1969)
h) R. Beyer, et al., Phys. Rev. C2, 1469 (1970)
i) R.P. Harper, et al., Nucl. Phys. A162, 161 (1971)
j) Z. Berant, et al., Phys. Rev. Letters 27, 110 (1971)
k) A.M. Kleinfeld, et al., Nucl. Phys. A154, 499 (1970)

REF. H. Bartsch, K. Huber, U. Kneissl, H. Krieger
Nucl. Phys. A256, 243 (1976)

ELEM. SYM.	A	Z
Pd	110	46

METHOD

REF. NO. 76 Ba 1 egf

REACTION	RESULT	EXCITATION ENERGY	SOURCE		DETECTOR		ANGLE
			TYPE	RANGE	TYPE	RANGE	
G,N	RLY	THR-UKN	C	UKN	SCD-D		4PI

ISOMER RATIO

TABLE 1
Experimental and theoretical results

Process	Target-spin	E_γ (keV)	$T_{\frac{1}{2}}$	Spin high	Spin low	$R_{exp} = \frac{\sigma_{high}}{\sigma_{low}}$	SCOP ($\hbar$)
^{181}Ta(γ, 3n)	$\frac{7}{2}^+$	93	2.2 h 9.31 min 8.15 h	7^-	1^+	0.51 ±0.09	3.6 ±0.2
^{142}Nd(γ, n)	0^+	755 1100–1300, 145	63 s 2.5 h	$\frac{11}{2}^-$	$\frac{3}{2}^+$	0.055±0.006 0.19 ±0.01 [a])	2.20±0.06
^{92}Mo(γ, n)	0^+	652.9 1208, 1508, 1581, 1637	66 s 15.49 min	$\frac{3}{2}^+$	$\frac{1}{2}^-$	1.03 ±0.21 0.85 ±0.07 [b]) 1.92 ±0.15 [a])	5.03±0.75 4^{+6}_{-3}
^{100}Mo(γ, n)	0^+	97.3 140.5	16.8 μs 66.02 h	$\frac{1}{2}^+$	$\frac{1}{2}^+$	0.85 ±0.24	1.72±0.25
^{108}Pd(γ, n)	0^+	214.5 115	22 s 850 ns	$\frac{11}{2}^-$	$\frac{1}{2}^+$	0.5 ±0.2	3.4 ±0.5
^{110}Pd(γ, n)	0^+	188 113 87.7	4.7 min 390 ns 13.47 h	$\frac{11}{2}^-$ $\frac{11}{2}^-$ $\frac{1}{2}^+$	$\frac{1}{2}^+$ $\frac{1}{2}^+$ $\frac{1}{2}^+$	0.11 ±0.02 0.41 ±0.09 3.2 ±0.7	3.14±0.15 3.0 ±0.25 3.3 ±0.4
^{89}Y(γ, n)	$\frac{1}{2}^-$	231.7 442.3 392.5	14.2 ms 300 μs	8^+	1^+	0.056±0.008	

[a]) Ref. [14]). [b]) Ref. [15]).

14 P.E. Haustein et al., J. Inorg. Nucl. Chem. 33, 289 (1971)
15 J. H. Carver et al., Nucl. Phys. 37, 449 (1962)

REF. J.W. Lightbody, Jr., S. Penner, S.P. Fivozinsky, P.W. Hallowell and Hall Crannell
Phys. Rev. C14, 952 (1976)

ELEM. SYM.	A	Z
Pd	110	46

METHOD

REF. NO. 76 Li 5 hmg

REACTION	RESULT	EXCITATION ENERGY	SOURCE		DETECTOR		ANGLE
			TYPE	RANGE	TYPE	RANGE	
E,E/	FMF	0, 1	D	39-111	MAG-D		127
		(.374,.81)					

LEVEL .374,.81

TABLE VI. Anharmonic vibrator model parameters.

	^{110}Pd	^{114}Cd	^{116}Sn
c_{tr} (fm)	5.169 ± 0.022	5.214 ± 0.021	5.446 ± 0.048
z_{tr} (fm)	0.529 ± 0.039	0.593 ± 0.040	0.550 ± 0.047
β_0	0.277 ± 0.012	0.218 ± 0.009	0.124 ± 0.004
a	0.2011 ± 0.0044	0.1749 ± 0.0060	0.14 ± 0.02 [a]
$B(E2_1^+)$ (e^2fm^4)	7966 ± 682	5753 ± 475	2288 ± 148
$\chi^2(2_1^+)/(N-P)$	1.3	1.5	1.2
$N-P$	3	3	4
$B(E2_2^+)$ (e^2fm^4)	72.9 ± 8.0	50.2 ± 7.6	19.8^{+10}_{-7}
$\chi^2(2_2^+)/(N-P)$	3.0	3.0	1.0
$N-P$	5	5	6

[a] Fit estimated by eye.

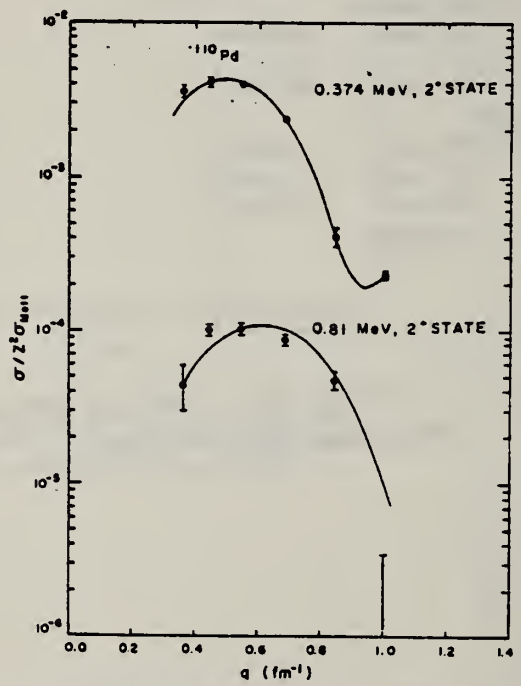

FIG. 5. Cross sections for ^{116}Fd in units of $Z^2\,\sigma_{Mott}$ for the 0.374 and 0.81 MeV, σ_{Mott} 2^+ states. The solid curves are fits based on the anharmonic vibrator model.

(over)

TABLE III. Ratios of inelastic scattering cross sections to $Z^2\sigma_{Mott}$.

E_i (MeV)	θ (deg)	1.43 MeV, 2^+ state	3.16 MeV, 2^+ state
		^{52}Cr	
39.38	127.74	(0.90 ± 0.04)-03	(0.55 ± 0.55)-05
49.44	127.74	(0.159± 0.006)-02	(0.29 ± 0.07)-04
59.84	127.71	(0.26 ± 0.02)-02	(0.89 ± 0.30)-04
75.22	127.71	(0.265± 0.007)-02	(0.842± 0.012)-04
92.73	127.74	(0.222± 0.005)-02	(0.428± 0.052)-04
110.20	127.69	(0.97 ± 0.02)-03	(0.222± 0.044)-04

E_i (MeV)	θ (deg)	0.374 MeV, 2_1^+ state	0.81 MeV, 2_2^+ state
		^{110}Pd	
39.38	127.74	(0.35 ± 0.03)-02	(0.45± 0.14)-04
49.44	127.74	(0.40 ± 0.02)-02	(0.10± 0.01)-03
59.84	127.71	(0.40 ± 0.02)-02	(0.10± 0.01)-03
75.22	127.71	(0.233± 0.003)-02	(0.86± 0.07)-04
92.73	127.74	(0.40 ± 0.05)-03	(0.48± 0.06)-04
110.20	127.69	(0.23± 0.01)-03	(0.17± 0.17)-05

E_i (MeV)	θ (deg)	0.558 MeV, 2_1^+ state	1.208 MeV, 2_2^+ state
		^{114}Cd	
39.38	127.74	(0.20 ± 0.02)-02	(0.46± 0.07)-04
49.44	127.74	(0.28 ± 0.02)-02	(0.40± 0.06)-04
59.84	127.71	(0.220± 0.014)-02	(0.58± 0.11)-04
75.22	127.71	(0.118± 0.005)-02	(0.34± 0.04)-04
92.73	127.74	(0.204± 0.007)-03	(0.11± 0.04)-04
110.20	127.69	(0.155± 0.007)-03	(0.61± 0.35)-05

E_i (MeV)	θ (deg)	1.294 MeV, 2_1^+ state	2.112 MeV, 2_2^+ state	2.266 MeV, 3^- state
		^{116}Sn		
39.38	127.74	(0.65± 0.04)-03	(0.68± 1.05)-05	(0.18± 0.02)-03
49.44	127.74	(0.88± 0.04)-03	(0.26± 0.69)-05	(0.40± 0.01)-03
59.84	127.71	(0.84± 0.03)-03	(0.21± 0.06)-04	(0.63± 0.02)-03
75.22	127.71	(0.36± 0.02)-03	(0.5 ± 7.4)-06	(0.84± 0.02)-03
75.02	127.81	(0.34± 0.02)-03	(0.47± 0.39)-05	(0.82± 0.01)-03
92.73	127.74	(0.50± 0.09)-04	(0± 0.19)-04	(0.60± 0.01)-03
110.20	127.69	(0.85± 0.10)-04	(0± 0.8)-05	(0.14± 0.01)-03

DEFINITIONS OF ABBREVIATIONS AND SYMBOLS

Note: In this list definitions are given for various photoneutron reactions in which the following symbols are used: N, NL, nN, SN and XN. Corresponding definitions apply for reactions involving other nuclear particles where the symbols N (neutron) is replaced by, e.g. P, D, T, HE, A etc. Where unknown reactions result in the production of a specific radionuclide, the chemical symbol and mass number is listed as the reaction product, e.g. a G,NA22 reaction in ^{59}Co.

A	alpha particle
ANAL	analysis
ABI	absolute integrated cross-section data
ABX	absolute cross-section data
ABY	absolute yield data. Often means cross-section per equivalent quantum is listed.
ACT	measurement of induced radioactivity of the target
ASM	asymmetric, asymmetry
AVG	average
BBL	bubble chamber
BEL B(EL)	reduced electric radiative transition probability
BF3	BF_3 neutron counter with moderator e.g., Halpern detector, long counter
BML	reduced magnetic radiative transition probability, B(ML)
BREAKS	levels located by "breaks" in the yield curve
BRKUP	breakup
BRMS	bremsstrahlung
BTW	between
C	continuous. Used to describe a photon source or a detector response function. Contrast with D = discrete.
CCH	cloud chamber
CF	compared with
CHRGD	charged
CMPT	Compton
COIN COINC	coincidence, coincide
COH	coherent
CK	Cerenkov
D	deuteron or discrete. When discrete, it is used to describe a photon source or a detector response function. Contrast with C = continuous.
DLTE	energy loss
DLTQ	momentum transfer
DST	distribution
DT BAL	detailed balance
E	electron
E/	inelastically scattered electron
E+	positron
EDST	energy distribution or spectrum
E/N	used only to indicate a coincidence experiment as in (E,E/N).

	N stands for any outgoing particle measured in coincidence with an inelastically scattered electron. Distinguish from eg., (E,N) which is used to represent an electron induced reaction when only the outgoing particle N is detected.
EMU	emulsions (photographic plates)
EXCIT	excited
F	fission
FMF	form factor
FM-1	inverse femtometers
FRAG	fragment
G	photon
G/	inelastically scattered photon
G-WIDTH	gamma-ray transition width
HAD	hadrons, hadron production
HE He3	^{3}He particle
INT	interaction, integral, intensity
INC	includes
ION	ionization chamber
ISOB	isobaric
ISM	isomer
J	multiplicity of particle defined by following symbol e.g. (G,PJN) with remark J = 2,3,5,7
JPI J-PI	spin and parity of a nuclear state
K	second multiplicity index, e.g. (G,JPKN) with both J & K positive integers greater than 1
KE	kinetic energy
L	may be an integer or zero that always follows a reaction product symbol. This is used to indicate transitions to specific states in the residual nuclide. When the letter is used as in (G,NL) the cross section given is that for the sum of transitions to two or more specific final states.
LFT	excited state lifetime
LIM	limit
LV,LVS	level, levels
LQD	liquid
MAG	magnetic spectrometer
MEAS	measurement(s)
MGC	magnetic Compton spectrometer
MGP	magnetic pair spectrometer
MOD	moderated neutron detector not employing a BF_3 counter, e.g. rhodium foil, Szilard-Chalmers reaction, ^{3}He, ^{6}Li reactions, GD loaded liquid scintillator, etc.
MSP	mass spectrometer
MULT	multiple, multipole, multiplicity
MU-T	used only in combination with G to indicate a total photon absorption cross section measurement, i.e. (G,MU-T)
N	neutron (see also XN and SN). The notation (G,N) is used to indicate a reaction in which only a single neutron is emitted, i.e. the reaction that can, in many cases, be measured by observing the radioactive decay of the residual nuclide.

nN	where n is any integer. (G,nN) indicates the sum over all reaction cross sections in which n neutrons are emitted.
NAI	NaI(Tl) spectrometer
NEUT	neutron(s)
NOX	no cross-section data
P	proton (see also XP)
PART	particle(s)
PHOT	photon(s)
PI	pion, usually written as PI+, PI-, PIO to indicate charge
POL	polarized or polarization
Q-SQUAR	momentum transfer squared (q^2)
RCL	recoil
REL	relative
RLI	relative integrated cross-section data
RLX	relative cross-section data
RSP	reaction spectrometer
RLY	relative yield data
SCTD	scattered
SCD	semiconductor (solid state) detector
SCI	scintillator detector other than NaI, e.g., CsI, KI, organic (liquid or solid), stilbene, He
SEP	separation
SEP ISOTP	separated isotope used
SIG	SIGMA (cross section)
SN	sum of neutron producing reactions, $\sigma(\gamma,SN)=\sigma(\gamma,N) + \sigma(\gamma,NP) + \sigma(\gamma,2N) + \sigma(\gamma,3N)$ + etc.
SPC	photon or particle energy spectrum
SPK	spark chamber
SPL	spallation
STAT	statistical
SYM	symetric, symmetry
T	triton
TEL	counter telescope
THR	threshold for reaction or threshold detector, e.g., $^{29}Si(n,p)^{29}Al$.
TOF	time-of-flight detector
TRK	tracks of particles or fragments observed in solid materials (glass, mylar, etc.)
TRNS	transition
UKN UNK	unknown
VIB	vibrational
VIR PHOT	virtual photon(s)
XN	all neutrons, total neutron yield, $\sigma(\gamma,XN) = \sigma(\gamma,N) + 2\sigma(\gamma,2N) + 3\sigma(\gamma,3N) + \sigma(\gamma,NP)$ + etc.
XP	all protons, total proton yield $\sigma(\gamma,XP) = \sigma(\gamma,P) + \sigma(\gamma,NP) + 2\sigma(\gamma,2P)$ + etc.
XX XXX	reaction products defined in REMARKS
YLD	yield

4PI	a 4π geometry was used or a method like radioactivity or a total absorption measurement
999	energy defined in REMARKS
$	indicates the measurement involved beams or targets that were either polarized or aligned, or that the polarization of the reaction products was determined. The polarized particle is indicated in REMARKS.
* or @	symbols used to indicate that the units associated with the numerals on one or both sides of the symbol in a specific column are not MeV. The units are defined in REMARKS.

NBS-114A (REV. 2-8C)

U.S. DEPT. OF COMM. BIBLIOGRAPHIC DATA SHEET (See instructions)	1. PUBLICATION OR REPORT NO.	2. Performing Organ. Report No.	3. Publication Date

4. TITLE AND SUBTITLE

Photonuclear Data-Abstract Sheets
1955-1982

5. AUTHOR(S)

E.G. Fuller and Henry Gerstenberg

6. PERFORMING ORGANIZATION (If joint or other than NBS, see instructions)

NATIONAL BUREAU OF STANDARDS
DEPARTMENT OF COMMERCE
WASHINGTON, D.C. 20234

7. Contract/Grant No.

8. Type of Report & Period Covered

9. SPONSORING ORGANIZATION NAME AND COMPLETE ADDRESS (Street, City, State, ZIP)

10. SUPPLEMENTARY NOTES

☐ Document describes a computer program; SF-185, FIPS Software Summary, is attached.

11. ABSTRACT (A 200-word or less factual summary of most significant information. If document includes a significant bibliography or literature survey, mention it here)

These abstract sheets cover most classes of experimental photonuclear data leading to information of the electromagnetic matrix element between the ground and excited states of a given nucleus. This fifteen volume work contains nearly 7200 abstract sheets and covers 89 chemical elements from hydrogen through americium. It represents a twenty-seven year history of the study of electromagnetic interactions. The sheets are ordered by target element, target isotope, and by an assigned bibliographic reference code. Information is given on the type of measurement, excitation energies studied, source type and energies, detector type, and angular ranges covered in the measurement. For a given reference, the relevant figures and tables are mounted on a separate sheet for each nuclide studied.

12. KEY WORDS (Six to twelve entries; alphabetical order; capitalize only proper names; and separate key words by semicolons)

data-abstract sheets, elements, experimental, isotopes, nuclear physics, photonuclear reactions

13. AVAILABILITY

☐ Unlimited

☒ For Official Distribution. Do Not Release to NTIS

☐ Order From Superintendent of Documents, U.S. Government Printing Office, Washington, D.C. 20402.

☐ Order From National Technical Information Service (NTIS), Springfield, VA. 22161

14. NO. OF PRINTED PAGES

15. Price

USCOMM-DC 6043-P80